Unconventional and topological superconductivity in correlated non-centrosymmetric systems with spin-orbit coupling

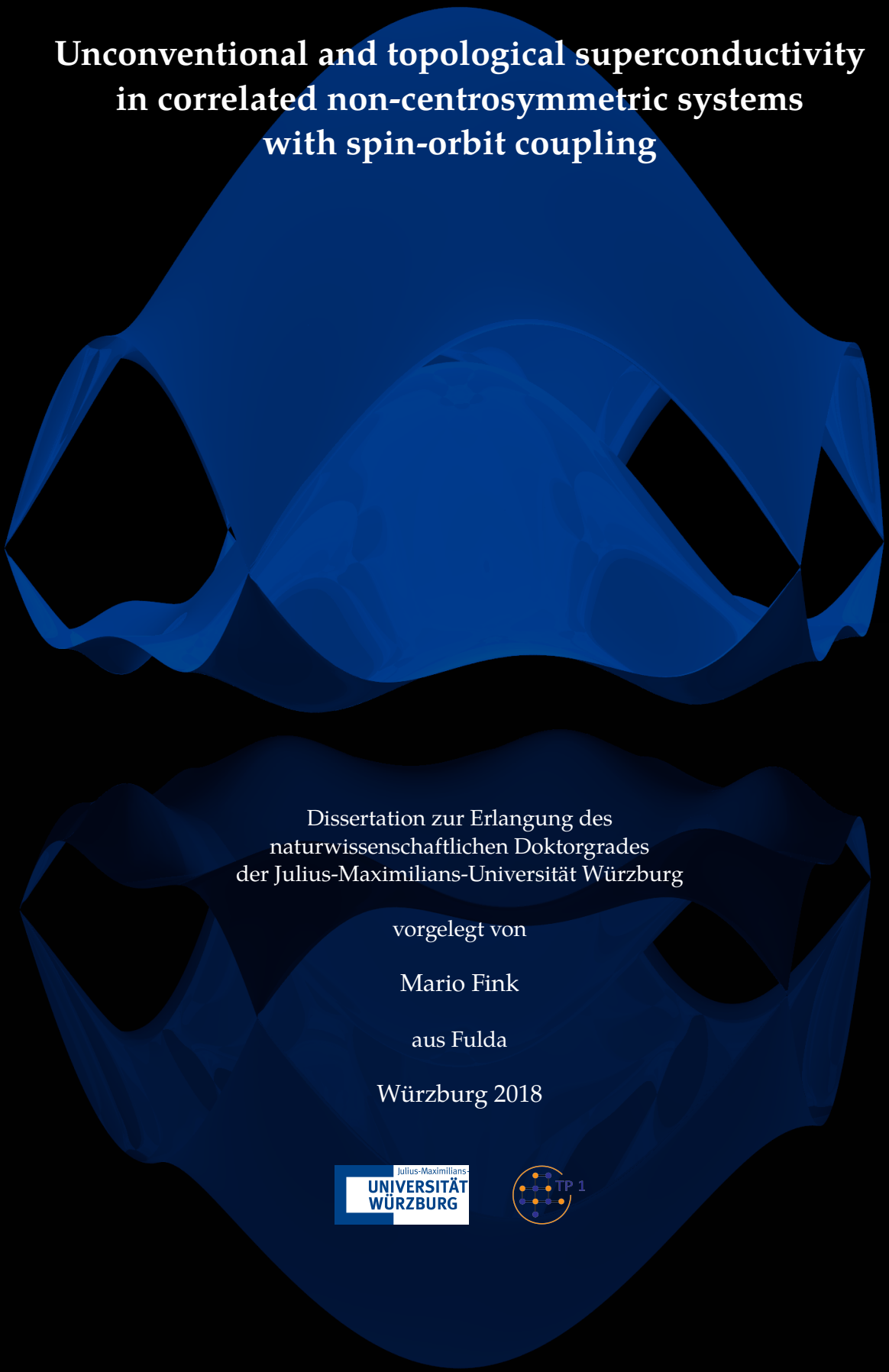

Dissertation zur Erlangung des
naturwissenschaftlichen Doktorgrades
der Julius-Maximilians-Universität Würzburg

vorgelegt von

Mario Fink

aus Fulda

Würzburg 2018

Julius-Maximilians-
UNIVERSITÄT
WÜRZBURG

TP 1

Unconventional and topological superconductivity in correlated non-centrosymmetric systems with spin-orbit coupling

Dissertation zur Erlangung des
naturwissenschaftlichen Doktorgrades
der Julius-Maximilians-Universität Würzburg

vorgelegt von

Mario Fink

aus Fulda

Würzburg 2018

Eingereicht am 2. August 2018
bei der Fakultät für Physik und Astronomie

1. Gutachter: Prof. Dr. Ronny Thomale
2. Gutachter: Prof. Dr. Björn Trauzettel
3. Gutachter:
der Dissertation

Vorsitzender: Prof. Dr. Jean Geurts

1. Prüfer: Prof. Dr. Ronny Thomale
2. Prüfer: Prof. Dr. Björn Trauzettel
3. Prüfer: Prof. Dr. Matthias Bode
im Promotionskolloquium

Tag des Promotionskolloquiums: 7. Dezember 2018

Doktorurkunde ausgehändigt am:

typeset using LuaLaTeX AMS-LaTeX BibLaTeX biber PGFPLOTS TikZ

compiled: Monday 17th December, 2018 11:45

cover: Bogoliubov-de Gennes spectrum of a chiral "d+id" superconductor

Abstract

Despite its history of more than one hundred years, the phenomenon of superconductivity has not lost any of its allure. During that time the concept and perception of the superconducting state - both from an experimental and theoretical point of view - has evolved in way that has triggered increasing interest. What was initially believed to simply be the disappearance of electrical resistivity, turned out to be a universal and inevitable result of quantum statistics, characterized by many more aspects apart from its zero resistivity. The insights of BCS-theory eventually helped to uncover its deep connection to particle physics and consequently led to the formulation of the Anderson-Higgs-mechanism. The very core of this theory is the concept of gauge symmetry (breaking). Within the framework of condensed-matter theory, gauge invariance is only one of several symmetry groups which are crucial for the description and classification of superconducting states.

In this thesis, we employ time-reversal, inversion, point group and spin symmetries to investigate and derive possible Hamiltonians featuring spin-orbit interaction in two and three spatial dimensions. *In particular, this thesis aims at a generalization of existing numerical concepts to open up the path to spin-orbit coupled (non)centrosymmetric superconductors in multi-orbital models*. This is done in a two-fold way: On the one hand, we formulate - based on the Kohn-Luttinger effect - the perturbative renormalization group in the weak-coupling limit. On the other hand, we define the spinful flow equations of the effective action in the framework of functional renormalization, which is valid for finite interaction strength as well. Both perturbative and functional renormalization groups produce a low-energy effective (spinful) theory that eventually gives rise to a particular superconducting state, which is investigated on the level of the irreducible two-particle vertex. The symbiotic relationship between both perturbative and functional renormalization can be traced back to the fact that, while the perturbative renormalization at infinitesimal coupling is only capable of dealing with the Cooper instability, the functional renormalization can investigate a plethora of instabilities both in the particle-particle and particle-hole channels.

Time-reversal and inversion are the two key symmetries, which are being used to discriminate between two scenarios. If both time-reversal and inversion symmetry are present, the Fermi surface will be two-fold degenerate and characterized by a pseudospin degree of freedom. In contrast, if inversion symmetry is broken, the Fermi surface will be spin-split and labeled by helicity. In both cases, we construct the symmetry allowed states in the particle-particle as well as the particle-hole channel. The methods presented are formally unified and implemented in a modern object-oriented

reusable and extendable C++ code. This methodological implementation is employed to one member of both families of pseudospin and helicity characterized systems. For the pseudospin case, we choose the intriguing matter of strontium ruthenate, which has been heavily investigated for already twenty-four years, but still keeps puzzling researchers. Finally, as the helicity based application, we consider the oxide heterostructure $LaAlO_3/SrTiO_3$, which became famous for its highly mobile two- dimensional electron gas and is suspected to host topological superconductivity.

Zusammenfassung

Trotz seiner über hundertjährigen Geschichte seit seiner Entdeckung hat das Phänomen der Supraleitung nichts von seiner ursprünglichen Faszination eingebüßt. Vielmehr hat sich in der Zwischenzeit der Begriff und das Verständnis des supraleitenden Zustandes in einer Weise weiterentwickelt, die das Interesse daran eher hat zunehmen lassen. Was anfänglich ausschließlich für ein Verschwinden des elektrischen Widerstands gehalten wurde, ist tatsächlich ein universelles und unvermeidliches Resultat der Quantenstatistik und besitzt viel mehr bemerkenswerte Eigenschaften als nur den widerstandslosen elektrischen Transport. Die Erkenntnisse der BCS-Theorie haben schließlich dazu geführt die tiefe Verbindung zur Teilchenphysik zu offenbaren und trugen entscheidend zur Formulierung des Anderson-Higgs-Mechanismus bei. Der wichtigste Baustein dieser Theorie ist das Konzept der (Brechung der) Eichsymmetrie. Im Rahmen der Festkörperphysik ist die Eichsymmetrie nur eine von mehreren Symmetrien, die eine essentielle Rolle für die Beschreibung und Einordnung von Phänomenen der Supraleitung spielen.

In dieser Arbeit wenden wir Zeitumkehr-, (räumliche) Inversions-, Punktgruppen- und Spin-Symmetrien an, um mögliche Hamilton-Operatoren in zwei und drei räumlichen Dimensionen, welche Spin-Bahn-Kopplung enthalten, herzuleiten und zu untersuchen. Diese Arbeit zielt auf eine Verallgemeinerung von existierenden numerischen Konzepten ab und erschließt den Weg die supraleitenden Eigenschaften von Modellen mit starker Spin-Bahn-Kopplung und mit oder ohne Inversionszentrum zu untersuchen. Dies geschieht mit Hilfe zweier methodischer Ansätze. Erstens formulieren wir aufbauend auf dem Kohn-Luttinger Effekt die störungstheoretische Renormierungsgruppe im Limes schwacher Kopplung. Zweitens verwenden wir die spinaufgelösten Flussgleichungen der effektiven Wirkung im Rahmen der funktionalen Renormierungsgruppe, die auch für endliche Wechselwirkungsstärke gültig sind. Die symbiotische Ergänzung der perturbativen und funktionalen Renormierungsgruppen ist darauf zurückzuführen, dass es mit der perturbativen Methode zwar möglich ist die Cooper Instabilität bei infinitesimaler Wechselwirkung numerisch exakt zu berechnen, aber nur die funktionale Renormierungsgruppe auch Teilchen-Loch Kondensate zugänglich macht.

Zeitumkehr- und Inversionssymmetrie sind die beiden Schlüsselsymmetrien, die verwendet werden, um zwei Szenarien zu unterscheiden. Falls sowohl Zeitumkehr- als auch Inversionssymmetrie gültig sind, sind die Fermiflächen zweifach entartet und durch einen Pseudospin-Freiheitsgrad charakterisiert. Im Gegensatz dazu führt der Verlust der Inversionssymmetrie zur Spinaufspaltung der Fermiflächen, die dann durch die sogenannte Helizität gekennzeichnet sind. In beiden Fällen leiten wir alle symmetrieerlaubten Zustände her, welche die entsprechenden Teilchen-Teilchen und Teilchen-Loch

Kondensate beschreiben. Die vorstellten und verallgemeinerten Methoden sind im Rahmen dieser Arbeit formal miteinander verbunden und in einem modernen objektorientierten C++ Quellcode implementiert worden.

Als erste vorläufige Anwendungen für diese methodische Implementierung betrachten wir zwei Systeme, die jeweils einer der beiden Familien zugeordnet werden können. Zum einen berechnen wir in der Pseudospin-Formulierung der perturbativen und funktionalen Renormierungsgruppen die Instabilitäten eines Dreiorbital-Modells für Strontiumruthenat, das seit seiner erstmaligen Synthese trotz intensiver Forschung immer noch Rätsel aufgibt. Zum anderen betrachten wir das zweidimensionale Elektronengas, das sich an der Schnittstelle zwischen $LaAlO_3$ und $SrTiO_3$ bildet und welches durch seine hohe Ladungsträgermobilität bekannt geworden ist.

Contents

List of Symbols

Symbol	Meaning
$\mathbf{r}$, $\mathbf{k}$	position in real space, momentum in reciprocal space
$\psi(\mathbf{r})$	single particle wavefunction in real space
$\mathbf{R}$	real space Bravais lattice vector
$\mathbf{G}$	reciprocal space lattice vector
Ω	volume of the first Brillouin zone
V, ν	volume of crystal, volume of real space unit cell
$f(\varepsilon_{\mathbf{k},\sigma})$	Fermi-Dirac function
$c^\dagger_\alpha$, c_α	creation and annihilation operator of particle α
$\bar{\psi}_\alpha$, ψ_α and $\bar{\phi}_{\tilde{\alpha}}$, $\phi_{\tilde{\alpha}}$	fermionic Grassmann fields in orbital and band space
σ	electron spin, takes the values $\sigma \in \{\uparrow,\downarrow\} = \{0,1\} = \{+\frac{1}{2},-\frac{1}{2}\}$
$\tilde{\sigma}$, λ	pseudospin/helical degree of freedom, $\tilde{\sigma} \in \{\tilde{\uparrow},\tilde{\downarrow}\}$, $\lambda \in \{+,-\}$
Σ	self-energy
$i\omega$	(fermionic) Matsubara frequency
$K = (i\omega, \mathbf{k})$	collective label for Matsubara frequency and momentum
α	superindex/multiindex collecting multiple quantum numbers
$U^\Lambda_{\alpha_1,\alpha_2,\alpha'_1,\alpha'_2}$	spinful two-particle vertex at cutoff Λ with $\alpha = (\mathbf{k}, b, \tilde{\sigma})$
V	(spinless) two-particle vertex, two-particle interaction
T, Λ	temperature, (temperature-, energy-) cutoff
ξ	single-particle energy including chemical potential
$\langle \ldots \rangle$	expectation value or correlation function
$\langle \ldots \rangle_{0/I}$	non-interacting/interacting correlation function
g	point group element
$\mathcal{P}(g)$	(reducible) representation of g in real/reciprocal space
$\mathcal{L}(g)$, $\mathcal{A}(g)$	(reducible) representation of g in orbital, sublattice space
$\mathcal{S}(g)$	(double-group) representation of g in spin space
$\mathcal{D}(g)$	(reducible) representation of g in sublattice/orbital/spin space
$\mathcal{B}_\mathbf{k}(g)$	transformation of $\mathcal{D}(g)$ to band/pseudospin/helical-spin space
$\hat{S}(\hat{n},\varphi) = e^{-i\hat{n}\sigma\varphi/2}$	SU(2) spin rotation about axis $\hat{n}$ by angle φ
$\hat{\Theta} = -i\sigma_y\hat{\mathcal{K}}$	time-reversal operator for spinful particles ($\hat{\mathcal{K}}$ complex conj.)
$\hat{I}$, $\hat{P}$	operator of spatial inversion
Γ_i	irreducible representation of a point group
$\chi^{C(g)}(\Gamma_i)$	character of class $C(g)$ for irred. repres. Γ_i

List of Figures

List of Tables

1. Introduction/Preface

Symmetry and superconductivity The concept of symmetry prevails in almost every branch of modern physics [Mic80; Gel07]. Symmetries do not only provide a notion of beauty [EA+94; Mol92; Rho06] but also a mathematical language that paves the way for a convenient and elegant description of a plethora of physical phenomena [Wey27; Wig12]. The benefits of a language that makes use of underlying symmetries has not only been appreciated in natural science but has even found its way into music theory [Tym06; Tym10; Maz12]. The appeal of a theory may often be characterized from the perspective of simplicity, which originates from an underlying symmetry. Landau established his theory of *phase transitions* based on *broken symmetries* and associated *order parameters* [Lan37a; Lan37b; Lan57]. One particular phenomenon that is well-described by Landau's idea of phase transitions is the *superconducting state*. In the framework of a *Ginzburg-Landau* theory [Gin50], the order-parameter of a superconductor is given by a complex field $\psi(\mathbf{r}) = |\psi(\mathbf{r})|e^{i\varphi}$ that turns out to be closely related to the Cooper pair wave function [Gor59]. In fact, this order-parameter is sufficient to describe the entire many-particle system since the Cooper pairs are able to form a coherent superposition being characterized by a macroscopic wave function [Ann11] Therefore, superconductivity is also one rare example of a quantum phenomenon exhibiting macroscopic consequences. An exception to the paradigm of symmetry breaking as an indication for a phase transition is *topological order* that neither shows a broken symmetry nor a local order parameter [Wen02b; Wen02a]. Henceforth, a valid classification of order is the distinction of *symmetry breaking* and *non-symmetry breaking* order [Wen04] (Figure 1.1). Well-known phenomena like (anti-)ferromagnetism, charge- and spin-density waves as well as superconductors all belong to the category of symmetry breaking order, making it advantageous to distinguish them by means of the particular symmetries they break.

While a *conventional superconductor* only breaks global $U(1)$*-gauge symmetry*, an *unconventional superconductor* breaks additional (spatial) symmetries. The "full" symmetry group is denoted by $\mathcal{G}_0 = \mathcal{G} \times \hat{T} \times \mathcal{U}$, where $\mathcal{G}$ is the point group of the underlying lattice, $\hat{T}$ is the time-reversal operation and $\mathcal{U}$ the gauge-group [MS94]. More precisely, the symmetry group of a superconductor is the one that comprises all operations under which the Cooper pair wave function or order parameter is invariant [VG85]. Therefore, the groups of both conventional and unconventional superconductors must obviously be subgroups of $\mathcal{G}_0$. The most general Cooper pair wave function must take spatial or momentum $\mathbf{k}$ (assuming the system is invariant under translations), spin, sublattice and orbital or band degrees of freedom of two electrons into account. Hence, the Cooper pair wave function may be denoted by the entity $\Delta^{b}_{\sigma\sigma'}(\mathbf{k}) = \left\langle c^{\dagger}_{\mathbf{k}b\sigma} c^{\dagger}_{-\mathbf{k}b\sigma'} \right\rangle$ with band index b, spins σ and σ' and momentum $\mathbf{k}$. While a conventional superconductor breaks

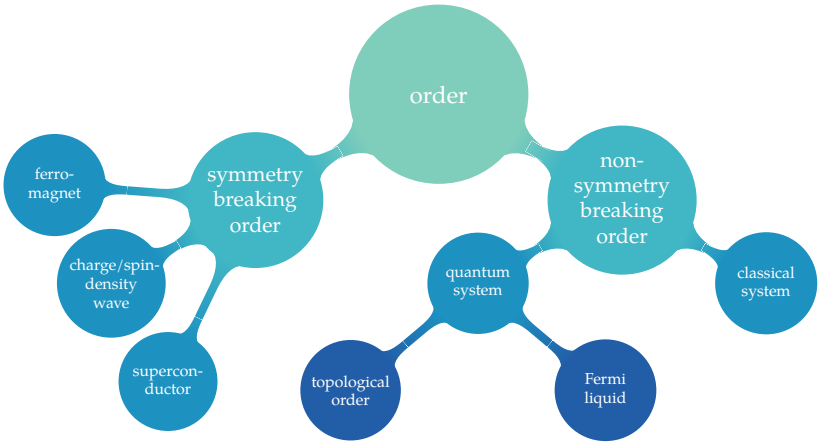

Figure 1.1.: The classification of order into symmetry-breaking and non-symmetry breaking order goes beyond Landau's theory of phase transition and opens up the path to a whole new class of phenomena (see [Wen04]) that are characterized by topological order. In contrast, well-known concepts like ferromagnetism, charge- and spin-density waves as well as superconductors fall into the paradigm of symmetry breaking order.

only $U(1)$-gauge symmetry, the concept of unconventional superconductivity opens up the pathway to a myriad of pairing states characterized by their (broken) symmetries in momentum, orbital and spin space. In mathematical terms, any possible subgroup of $\mathcal{G}_0$ may be realized as a Cooper pair. This zoo of unconventional pairing states hosts a competition for the most stable energy balance between energy gain due to pairing and repulsion being highly susceptible to material specific parameters like i.a. doping, interaction strength and spin-orbit coupling.

From an experimental point of view, the discrimination between conventional and unconventional states can be done by looking at the low-temperature behavior of various physical quantities like specific heat. On the one hand, a conventional superconductor possessing a fully gapped quasiparticle spectrum shows exponential temperature dependence. On the other hand, an unconventional superconducting state, which has symmetry protected nodes in its gap function, leads to power law dependencies in the low-temperature regime. However, even a conventional fully gapped superconductor may exhibit accidental nodes. Therefore, power law dependency in the low-temperature regime is a necessary but not sufficient criterion for unconventional superconductivity.

Milestones of superconductivity Superconductivity has been a fascinating phenomenon ever since [Onn11] and nevertheless it took nearly fifty years to produce a theory capable of correctly reproducing the experimentally observed phenomena of a second order phase transition, the exponential dependence of the specific heat, the Meissner-Ochsenfeld effect, the infinite conductivity and the dependency of the critical tempera-

ture on the isotope mass [BCS57]. The very core of this theory is the concept of *Cooper pairs* , i.e. electrons that are related by time-reversal symmetry (traditionally electrons with opposite momentum $\mathbf{k}$, $-\mathbf{k}$ and spin $\uparrow, \downarrow$) that pair up to form a new state with total spin zero. As a consequence, a macroscopic number of Cooper pairs are allowed to condense in the same quantum state as a coherent superposition (at sufficiently low temperatures) [FS05]. Furthermore, the superconducting (BCS) wave-function appears to be a superposition of states with an *even* number of electrons and hence violates particle number conservation. The quasiparticle dispersion relation of the Cooper pairs shows a characteristic *energy gap* Δ that defines the amount of energy required to break up a single Cooper pair. *Conventional superconductivity* covers all cases where the gap function $\Delta(\mathbf{k}) = \Delta$ is independent of momentum $\mathbf{k}$. A characteristic feature of BCS-theory is its *universality*, which extraordinarily applies to many elemental metals. In contrast, this means that BCS-theory is insensitive to any material specific parameters to account for different critical temperatures (expect for the electron-phonon coupling strength g_{eff}). An improvement towards strong-coupling was provided by *Eliasberg theory*. It uses an electron-phonon interaction that is local in space and retarded in time [Eli60], opposed to the non-local, non-retarded coupling parameter g_{eff} of BCS-theory [Umm13]. McMillan used Eliashberg theory to predict a maximum transition temperature for phonon-driven pairing in different classes of material [McM68]. Shortly after the formulation of the *BCS-theory*, the idea of an anisotropic gap function came up [BW63], in particular a gap function with odd parity $\Delta(-\mathbf{k}) = -\Delta(\mathbf{k})$ associated to a spin triplet state. Later, more generalizations of the BCS-gap function with even higher relative angular momentum or odd frequency dependency were developed [SSW66; Ber74]. Soon, the first experimental evidence for exotic superconducting states was found in the form of heavy-fermion superconductors [Ste84; Gor87].

The first experimental signature of a *d*-wave superconductor was encountered in 1986 in copper-oxide compounds [BM86; BMT87], which showed a much higher critical temperature than any elemental superconductor. This finding triggered activity for the search of superconductors with even higher critical temperatures, the highest so far being $YBa_2Cu_3O_7$ with $T_c \approx 92\,\mathrm{K}$ [BM88]. This line of research eventually led to the discovery of superconductivity in strontium ruthenate (Sr_2RuO_4) [Mae+94] which was latter assumed to be the "first" spin-triplet superconductor [Ish+98] and suspected to break *time-reversal symmetry* [Luk+98]. The next experimental milestone dates back to 2008 when a critical temperature of about 26 K was found in the iron-based compound $LaO_{1-x}F_xFeAs$ [Kam+08] and evidence for unconventional superconductivity in FeSe [Kot+08]. This discovery established a whole new branch of research that continues to bring forward new exciting results until today [Spr+17] (cf. (Figure 1.2)). Apart from superconductivity itself, a new field has been emerging in the area of condensed matter research based on the beforementioned notion of non-symmetry breaking and *topological order*. The experimental investigations along these lines started with the verification of the *quantum spin Hall effect* [Kön+07]. A unique way to combine and reunite both topological order and symmetry-breaking order in the form of superconductivity is represented by (the idea of) *topological superconductivity* [Qi+09].

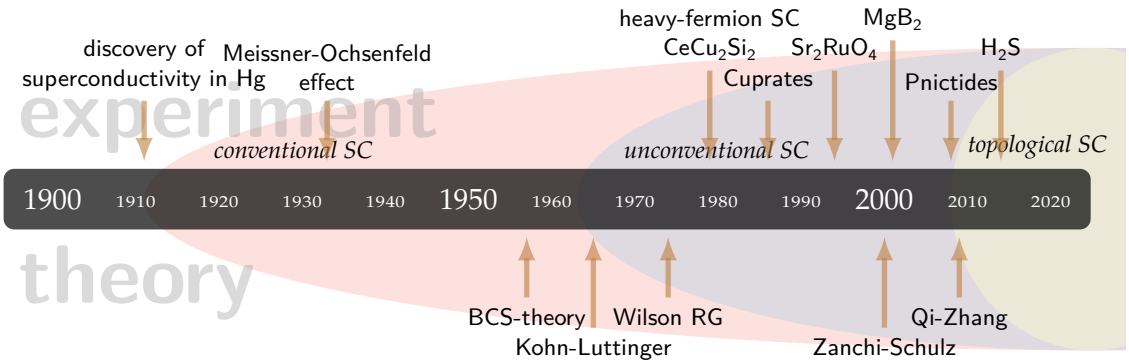

Figure 1.2.: The epoch of forty-seven years after the discovery of (conventional) superconductivity [Onn11] is characterized by a plethora of failed attempts to explain superconductivity that eventually led to the formulation of the BCS-theory [BCS57]. Kohn and Luttinger were the first to realize that Cooper pairing can emanate from a purely electronic mechanism [KL65]. More than twenty years after its publication, Zanchi and Schulz [ZS00] employed Wilson's renormalization group idea [WK74] to the dimensional weakly-correlated electron gas. In 2009, the pioneering work of Qi and Zhang [Qi+09] layed the ground for the field of topological superconductors.

Quantum many-body effects Condensed matter physics is the subject concerned with many quantum particles at finite density and temperature and their collective behavior. Quantum many-particle systems have already been in the focus of intensive research since shortly after the development of the foundation of quantum mechanics [Tho27; Fer27]. The quest for understanding the quantum effects in multi-particle models started with the investigations in simple molecules and led to the concepts of Heitler-London and Mulliken [HL27; Mul28]. Until today, the research is guided by the belief that the (many-particle) Schrödinger equation [Sch26] governs the dynamics of a quantum many-body system. However, the derivation of macroscopic properties on the basis of the Schrödinger equation turns out to be unfeasible. Consider a single-particle Hamiltonian $\mathcal{H}_0 = -\frac{\nabla^2}{2m} + V(\mathbf{r})$ and the corresponding stationary Schrödinger equation $\mathcal{H}_0\psi = E\psi$. Confining the particle to a cubic box of dimension L and employing a three-dimensional discretization mesh of N^3 points in real space, the numerical solution is obviously given by a vector comprising N^3 complex values [Tho13; Ful12]. Adding a second (identical) particle to the box, increases the size of the vector representing the two-particle wave function $\psi(\mathbf{r}_1, \mathbf{r}_2)$ to $\left(N^3\right)^2 = N^6$. Henceforth, an n-particle wave function requires at least memory of size $\left(N^3\right)^n = N^{3n} = e^{\log(N)3n}$ (ignoring the computational cost to solve the system of N coupled differential equations), which means the memory necessary to store the wave function of a quantum mechanical n-body systems, i.e. the complexity of the Hilbert space, scales exponentially. For example, taking the mesh to comprise a moderate number of $100^3 = 1 \times 10^6$ points, the wave function for only two particles already occupies $100^6 \times 16\,\mathrm{B} \approx 16\,\mathrm{TB}$ of memory (assuming a sin-

gle complex number to be of size 16 B) (cf. [Fou+01]) The (apparent) impossibility to calculate the wave functions of quantum many-body Hamiltonians comprising a critical number of particles, is known as the *exponential wall* [Koh99; FS17]. Another example is given by a spin-$\frac{1}{2}$ chain, where every particle can only be found in two different states. The computational complexity of this problem merely scales as 2^n with the number of particles n [Wen04] [Pen04, Chapter 23]. In contrast, a classical many-particle system is a much less intractable problem, since at a fixed time t the system is completely specified by $6n$ coordinates in phase space $(\mathbf{r}_i, \mathbf{p}_i)$, i.e. the problem scales linearly. Hence, the development of algorithms and efficient code for classical many-body systems has a (relatively) long history that dates back to the advent of the first modern computers during the 1940's [Zal] and found its application mainly in astrophysics [Hol41; Pee70; PS74; Whi76]. The invention of *tree algorithms* reduced the computational complexity to $O(n \log n)$ [App85] and claimed its hitherto climax in the "Millennium run", a simulation comprising up to 7.5×10^7 particles subject to the gravitational forces within a three-dimensional cross-section of the universe of about 650 Mpc or 2 Gly [SYW01; Spr05; Spr+05]. In contrast, the overall length scale of a typical quantum many-body system is 1×10^{-3} m to 1×10^{-2} m, while it contains about 10×10^{23} particles. In particular, superconductivity is an inherent quantum many-body effect whose mechanism can only be understood in an *effective* single particle picture. Therefore, we have to rely on approximative methods that are supposed to capture the "important" information.

Methodological overview While the numerical methods and ab-initio approaches to electronic structure calculations have been developed and advanced over several decades culminating in elaborate formulations of density-functional theory (DFT) [HK64; KS65], dynamical mean-field theory (DMFT) [Geo04; Kot+06; Hel07a], the *GW*-approximation (GWA) [Hed65; ORR02; Hed99] and combinations thereof (like i.a. LDA+U [Ani+92], LDA+DMFT [KV04; Hel07b] and GW+DMFT [BAG03]), the numerical approaches to superconductivity lack a substantial amount of development compared to electronic structure calculations in the sense that quantitative predictions still pose a severe challenge. On the one hand, there are ab-initio methods that start from the full many-body Hamiltonian of the crystal featuring nuclei and electrons without relying on any preliminary approximations. In order to solve the corresponding time-independent Schrödinger equation the concepts of density functional theory are reused, modified and extended to account for both electron-electron and electron-phonon interactions as well as anomalous expectation values of the density-operators. [OGK88; CG97; Lüd+05; Mar+05]. Although this kind of *density functional theory for superconductivity* (*SCDFT*) predicts critical temperatures and gap amplitudes with good experimental agreement for simple metals [Lat+04], it suffers from its limitations regarding anisotropic band structures and strong spin fluctuations. Hence, it is usually well-suited for phonon-driven superconductors. On the other hand, there are methods that are based on the formalism of Green's functions and many-body perturbation theory. These methods, however, rely on a set of phenomenological parameters describing the non-interacting one-particle spectrum and two-particle interactions. As the most simple one of these

Green's function based methods, we have the *mean-field theory*, which takes the bare interaction in band representation as the pairing potential to calculate the Cooper pair properties [Inu+88; Ann90]. Although mean-field theory can often be done analytically and provides important insights, it suffers from the fact that the interaction assumed corresponds to a high-energy theory that does not agree with the actual effective low-energy theory at the critical temperature that makes up the *pairing potential* and is a result of *emergent* quantum many-body effects. Another Green's function approach is the *random phase approximation* (*RPA*), which was originally introduced by Pines [PB53] and formulated and justified in a diagrammatic fashion by Gell-Mann and Bruckner [GB57]. Shortly after that, Anderson employed this method to superconductivity [And58a]. In diagrammatic language, the RPA amounts to a summation of all particle-hole bubbles up to infinite order of the perturbative expansion. Due to the simple topology of the involved diagrams, the series allows for an analytical solution. Extensions of the random phase approximation to three spatial dimensions [Gra+10] and the inclusion of spin-orbit coupling in multiple orbitals [Kor17; Nis+17] have been successfully employed. A modification and extension of RPA that features an improved inclusion of orbital and spin fluctuations is the *fluctuation exchange approximation* (FLEX) [BS66; BSW89]. It has been employed in two and three spatial dimensions [AKA99] and is particularly popular in the investigation of superconducting order parameters in multi-orbital Hubbard models [MYO05; Mai+11b].

Among all these methodological approaches, a special position is held by *determinant quantum monte carlo*, which evaluates an observable $\hat{A}$ by $\mathrm{Tr}\left(\hat{A}e^{-\beta\hat{H}}\right)/\mathrm{Tr}\left(e^{-\beta\hat{H}}\right)$. Here, the partition function is rewritten as a functional integral and a Hubbard-Stratonovich field is introduced into the interacting part of the Hamiltonian, which allows for the fermions to be integrated out analytically. The results appear in terms of fermionc determinants that play the role of the weights for the Hubbard-Stratonovich field to be sampled [Yin+14; Whi+89a; Whi+89b; Sca+91; Est+18]. Another whole class of methods is based on the idea of *renormalization*. In the context of condensed matter physics, it has been pioneered by Wilson in his attempt to gain more insight into the universality of phase transitions [Wil71a; Wil71b; WK74]. In particular, since the superconducting state is impossible to obtain by means of perturbative means due to the logarithmic divergence of the particle-particle diagrams, the renormalization group offers the particular tempting possibility to introduce a cutoff to avoid these divergences. This is the punchline of the *perturbative renormalization group* (*PRG*), whose foundations are the work by Kohn and Luttinger [KL65]. The perturbative treatment of the repulsive electron-electron interactions are supplemented by an logarithmic renormalization flow [Pol92; Sha94a] by feeding the effective interaction resulting from second order perturbation theory into the flow equations [RKS10]. Although, it is asymptotically exact, the perturbative renormalization suffers from its need to assume (in general) unrealistic infinitesimal small interaction strength. The most modern version of Wilson's idea of renormalization is represented by the *functional renormalization group* (*FRG*) [ZS00; HS01; KBS10]. The FRG integrates out the single-particle degrees of freedom by in-

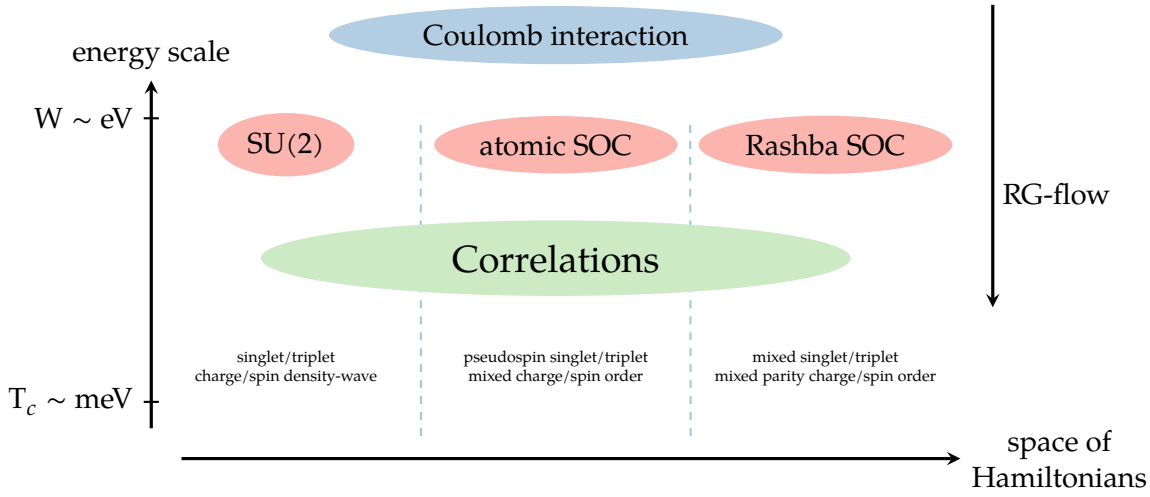

Figure 1.3.: At high energy scales about the bandwidth W the interacting theory only features the bare Coulomb repulsion. We consider three cases that subdivide the space of Hamiltonians into three sectors depending on which symmetries are or aren't *explicitly* broken. The left column features Hamiltonians fully invariant under SU(2) and spatial inversion, while the center column breaks spin rotation symmetry but keeps spatial inversion. Finally, the right column abandons both spin and spatial inversion symmetry. Correlations dominated by the microscopic details of the considered system lead to effective low-energy theories that give rise to ordering tendencies corresponding to phases of additional *spontaneously* broken symmetries.

troducing a cutoff that is successively lowered to finally obtain an effective theory of n-particle correlation functions. Its strength is its account for the unbiased interplay of particle and hole fluctuation on different energy scale and its applicability to intermediate and finite interactions. Unfortunately, the hierarchy of flow equations can only be treated up to finite order to guarantee numerical feasibility.

As a side remark, we mention the *parquet renormalization group* and *ladder renormalization group* approaches, which are well-controlled but have limited range of applicability depending on which logarithmic divergences occur in the system to be studied [MC10][Xin+17; Cla+17]. More recent developments, which are mainly (non-local) extensions of dynamical mean-field theory are the *dynamical vertex approximation* DΓA [HKT08; Hel14; Kit+18], the *one-particle irreducible approach* (1PI) [Roh+13], and the *dynamical mean-field theory to functional renormalization group* (DMF^{2}RG) [Tar+14]. In spite of all these important contributions, the calculation of superconducting properties in strongly correlated systems still pose a significant challenge and universal numerical approaches to predict the Cooper pair mechanism in a variety of systems are still not available. A general obstacle for all methods to access superconductivity is the involvement of very different energy scales. While the properties of the band structure are characterized by the order of several eV, the critical temperature of most (elemental) superconductors is about the order of meV (cf. (Figure 1.3)).

Outline In the framework of this thesis a weak-coupling to intermediate coupling renormalization group approach (and code) is developed, which is capable of identifying not only superconducting phases in the presence of centro- and noncentrosymmetric spin-orbit coupling, i.a. giving rise to mixed singlet-triplet pairing, but also their interplay with particle-hole condensates including such exotic types as mixed spin-charge density waves in systems with broken spin and/or inversion symmetries. The thesis is comprised of two parts. The first part serves as an introduction to unconventional Cooper pairing states and the methodological novelties necessary to investigate them, while the second part considers several prototypical models, whose electronic instabilities are investigated by means of the presented methods. (Chapter 2) motivates the concepts that give rise to Cooper pairing and superconducting states and briefly reviews "traditional" BCS-theory. The Kohn-Luttinger effect is presented as one of the first ideas on how to obtain superconductivity from purely electronic, repulsive interactions. It turns out, that the associated pairing states are anisotropic in momentum space. This is used as the starting point to generalize BCS-theory to incorporate both singlet and triplet states in arbitrary angular momentum channels only restricted by parity and the Pauli principle. We set up a formalism in terms of the d-vector making the associated symmetries more transparent and analyze its transformation properties with respect to spatial inversion, spin rotations, time-reversal and point group operations. (Chapter 3) leaves the realm of spin rotation symmetric single-particle terms by deriving and classifying various types of spin-orbit interaction in centro- and noncentrosymmetric models. A particular emphasis is put on the definition of appropriate basis states, which enable quantum-many body calculations. These calculations mostly involve the two-particle vertex function, whose symmetry properties with respect to spin rotation, time-reversal, point group operations and spatial inversion are described in a numerically accessible formalism. To analyze possible exotic pairing instabilities that go beyond the paradigm of singlet versus triplet Cooper pair states, mean-fields with broken $SU(2)$-symmetry (and broken inversion symmetry) are introduced, classified and constructed for prototypical crystal symmetries. Since the functional renormalization group is able to keep track of particle-hole condensates as well, the analogous formalism is set up for these density-wave states, too.

(Chapter 4) sets up the Feynman path-integral formalism in terms of fermionic Grassmann fields and introduces the associated notation in order to prepare the stage for the perturbative and functional renormalization groups, which essentially depend on these concepts and make extensive use of it. In particular, the generating functionals relevant for functional renormalization are recapitulated. The perturbative series's of various n-particle correlation functions and their resummations provide a path to compare and benchmark the perturbative and functional renormalization groups to (established) methods like i.a. random-phase approximation and fluctuation exchange calculations. The perturbative renormalization group in (Chapter 5) is presented as a combination of quantum-many body perturbation theory and logarithmic renormalization. Since the perturbative part relies on infinitesimal coupling strength, the states arising from it operate in an infinitesimal shell around the Fermi surface and therefore can only give rise

to particle-particle states since the Cooper instability is the only generic one of a Fermi liquid. This restriction is remedied by the functional renormalization group presented in (Chapter 6), which introduces an explicit cutoff, given as energy/momentum, temperature or frequency, into the single-particle theory. This cutoff is used to integrate out the degrees of freedom of the interacting Hamiltonian starting from the bare interaction down to any critical scale that exhibits the low-energy effective theory. The evolution of the effective interaction as a function of the cutoff parameter is described by a hierarchy of flow equations expressing the change of the n-particle correlation function in terms of a set of non-linear integro differential equations. We work out the close analogy between the perturbative and functional renormalization group, from which we benefit in two ways: on the one hand, this similarity enables us to use the very same models and their implementations as the input and on the other hand facilitates the process of debugging. Furthermore, it is both educating and enlightening to see how different physical states and orders emerge from two methods that only differ in the formulation of the propagators they're based on.

The second part of the thesis is dedicated to the application of the methods developed in the first part to both simple toy models as well as realistic systems that are currently and have already been subject to intensive research. (Chapter 7) provides an illustrative treatment of toy models that introduces the methodological novelties in a numerical context. This includes paradigm models like the Hubbard model on the square and honeycomb lattice and including the spin degrees of freedom to prepare for the inclusion of spin-orbit interaction. During the last decade, oxide heterostructures have been investigated as promising systems for next generation of micro-electronic devices. In (Chapter 8) we setup a minimal two-orbital model for the $LaAlO_3/SrTiO_3$ interface including Rashba spin-orbit interaction to account for the presence of the heavy ion Ti^{+4} and the broken inversion symmetry. We show that the resulting low-energy fluctuations give rise to nodal and nodeless superconducting states with topological non-trivial properties. The unconventional superconducting state in strontium ruthenate Sr_2RuO_4 has been studied for more than twenty years, while a convincing explanation of the order parameter is still missing. In (Chapter 9) we use a three-orbital model including atomic spin-orbit coupling and employ both perturbative and functional renormalization to investigate its order parameters and the system's preference of singlet or triplet pairing on particular Fermi sheets. An integral part of this thesis is devoted to the development of a modern object-oriented implementation of the perturbative and functional renormalization group methods for two and three dimensional many-body problems that is capable of analyzing the relevant particle-particle and particle-hole instabilities in the presence of spin-orbit coupling and/or inversion symmetry breaking and of classifying them in terms of irreducible representations of the respective symmetry groups in spin and orbital space.

The project and its source code can be found at

`www.physik.uni-wuerzburg.de/~mfink/FPRG/`

where the acronym represents **F**untional **P**erturbative **R**enormalization **G**roup. The or-

Table 1.1.: The methodological extension of both perturbative and functional renormalization groups enables the treatment of various two- and three-dimensional systems in presence of different kinds of spin-orbit coupling.

	perturbative RG	**functional RG**
two spatial dimensions	✓	✓
three spatial dimensions	✗	✗
long-range interaction	✓	✓
particle-particle condensates	✓	✓
particle-hole condensates	✗	✓
centrosymmetric SOC	✓	✓
non-centrosymmetric SOC	✓	✓
broken time-reversal	✗	✗

der of F and P is fixed in that way to avoid any ambiguity with respect to the pseudo-fermion renormalization group (PFFRG) [RW10; RT11]. The computational possibilities of this code with respect to the method, the spatial dimensionality, the range of interactions and the possible ordering tendencies are summarized in (Table 1.1). In two spatial dimensions we are able to employ both the perturbative as well as the functional renormalization, unlike in three spatial dimension, where only perturbative RG is feasible while the computational effort of functional RG is too demanding. In contrast, due to the limitation of infinitesimal coupling in the perturbative method, particle-hole instabilities can only be accessed in the functional RG scheme. However, both of the two implemented methods are able to deal with spin-orbit coupling and spatial inversion symmetry breaking. The breaking of the beforementioned symmetries is done explicitly as already given in the microscopic Hamiltonian in contrast to spontaneous symmetry breaking.

Part I.

Methodology for superconductivity with spin-orbit coupling

2. The Cooper problem, BCS theory and the Kohn-Luttinger effect

The *microscopic* Bardeen-Cooper-Schrieffer-theory (BCS-theory) [BCS57] is considered to be one of the greatest intellectual achievements of the twentieth century [Fos14, Chapter 4.1], and the solution to one of the hardest problems in physics. It marks the (preliminary) end of a long series of failed theories formulated by the most distinct physicists (including Einstein, Bohr, Landau, Bloch, Brillouin and Feynman) led astray by their desperate attempts to formulate a *microscopic* explanation of superconductivity [Sch10]. Although the BCS-theory was the first microscopic theory, some *phenomenological* descriptions already came about (shortly) after the discovery of the *Meissner-Ochsenfeld effect* [MO33]. These include (among others) the work of Gorter and Casimir [GC34], the *London equations* [LL35] and the *Ginzburg-Landau theory* [GL50]. One of the most interesting "failures" to derive a theory of superconductivity is probably the one by Feynman, who correctly pointed out that the superconducting state is impossible to derive by means of *perturbation theory* [Fey57]. Ironically enough, we will make extensive use of perturbative formulations in (Chapter 5) and (Chapter 6) that are, however, supplemented by the idea of *renormalization* that was only employed to quantum many-body problems starting from the early seventieth [Wil71a; Wil71b; WK74]. A valid theory of (conventional) superconductivity is required to explain five properties [BCS57] :

- second-order phase transition at the critical temperature T_c
- exponential temperature dependency of the electronic specific heat for $T < T_c$ [Cor+54]
- Meissner-Ochsenfeld effect [MO33]
- infinite conductivity
- dependence of T_c on the isotopic mass [Max50; Rey+50]

Bardeen, Cooper and Schrieffer succeeded in formulating such a theory based on the concept of *Cooper pairs* . A Cooper pair is a bound state of two electrons in a singlet $(\uparrow, \downarrow)$ with opposite momenta $(\mathbf{k}, -\mathbf{k})$. Leon Cooper showed in an earlier paper that such a bound state arises in a *Fermi gas* with arbitrarily weak attractive interactions between electrons [Coo56]. Schrieffer was then able to write down a product wave function of Cooper pairs for the superconducting *ground state* by giving up the requirement of having a system with a fixed number of particles. The chapter is comprised of three sections. The (Section 2.1) about the *Cooper problem* shows how two electrons above a quiescent

Fermi sea can lower their total energy and form a bound state. This is the basis for the conventional BCS-theory in (Section 2.2) that builds up the superconducting ground state by a coherent superposition of Cooper pairs. (Section 2.3) introduces the concept of purely electronically mediated pairing in absence of any attractive phonon-electron interaction by having Cooper pairs with finite angular momentum in singlet as well as triplet spin states. Finally, (Section 2.4) analyzes the structure of these generalized Cooper pairs and prepares the foundations for pairing in absence of spin rotation symmetry.

2.1. Cooper problem

Consider two electrons in the continuum with positions $\mathbf{r}_1$ and $\mathbf{r}_2$, which interact via the potential $V(|\mathbf{r}_1 - \mathbf{r}_2|)$ that only depends on their relative distance. The time-independent Schrödinger equation for that problem yields

$$\mathcal{H}\psi(\mathbf{r}_1, \sigma_1, \mathbf{r}_2, \sigma_2) = E\psi(\mathbf{r}_1, \sigma_1, \mathbf{r}_2, \sigma_2) \quad , \tag{2.1.1}$$

where the two-particle wave function can be split into orbital and spin part (since the Hamiltonian is spinless and commutes with both the spin and orbital angular momentum operators $\mathbf{S}^2$ and $\mathbf{L}^2$, respectively), i.e.

$$\psi(\mathbf{r}_1, \sigma_1, \mathbf{r}_2, \sigma_2) = \phi(\mathbf{r}_1, \mathbf{r}_2) \otimes \chi(\sigma_1, \sigma_2) \quad . \tag{2.1.2}$$

Since ψ must be antisymmetric with respect to exchange of the electrons, the orbital part must be symmetric and the spin part antisymmetric or vice versa. However, if we limit our discussion to the case of an antisymmetric spin singlet (symmetric triplet) part, the orbital wave function must be symmetric (antisymmetric). The Hamiltonian may be simplified by transforming to the *center of mass* reference frame: [1]

$$\mathcal{H} = \frac{p^2}{2\mu} + V(\mathbf{r}) \quad \Rightarrow \left(\frac{p^2}{2\mu} + V(\mathbf{r})\right)\phi(\mathbf{r}) = E\phi(\mathbf{r}) \quad , \tag{2.1.3}$$

with $\mathbf{r} = \mathbf{r}_1 - \mathbf{r}_2$ and $\mu = \frac{m}{2}$. We can further simplify the Hamiltonian by going to momentum space via

[1] The original two-particle Hamiltonian $\mathcal{H} = \frac{\mathbf{p}_1^2}{2m} + \frac{\mathbf{p}_2^2}{2m} + V(|\mathbf{r}_1 - \mathbf{r}_2|)$ can be written in terms of the equivalent effective one-particle problem $\mathcal{H} = \frac{p^2}{2\mu} + V(r)$ with the relative coordinate $\mathbf{r} = \mathbf{r}_1 - \mathbf{r}_2$ and the *reduced mass* $\mu = \frac{m_1 m_2}{m_1 + m_2} \overset{m_1 = m_2}{=} \frac{m}{2}$ [GPS01], which makes sure the commutator $[\mathbf{r}, \mathbf{p}] = i\hbar$ is still valid.

$$\phi(\mathbf{k}) = \frac{1}{(2\pi)^{3/2}} \int \mathrm{d}\mathbf{k}\, e^{-i\mathbf{k}\mathbf{r}} \phi(\mathbf{r}) \quad \text{and} \quad \phi(\mathbf{r}) = \frac{1}{(2\pi)^{3/2}} \int \mathrm{d}\mathbf{k}\, e^{i\mathbf{k}\mathbf{r}} \phi(\mathbf{k}) \quad . \tag{2.1.4}$$

The limitation to a singlet state requires $\phi(\mathbf{k}) = \phi(-\mathbf{k})$ to ensure a symmetric orbital wave function w.r.t. particle exchange, i.e. $\phi(\mathbf{r}_1 - \mathbf{r}_2) = +\phi(\mathbf{r}_2 - \mathbf{r}_1)$. The transformation of $V(\mathbf{r})\phi(\mathbf{r})$ is most conveniently taken care of by the *convolution theorem* [Arf85; BB86] resulting in the Schrödinger equation in momentum space

$$\left(\frac{(\hbar\mathbf{k})^2}{2\mu} - E \right) \phi(\mathbf{k}) = -\frac{1}{(2\pi)^{3/2}} \int \mathrm{d}\mathbf{k}'\, V(\mathbf{k} - \mathbf{k}')\, \phi(\mathbf{k}') \quad . \tag{2.1.5}$$

The interaction apparently only depends on the momentum transfer of the scattering process. It is reasonable to assume that the overall direction of $\mathbf{k}$ and $\mathbf{k}'$ does not matter for the value of $V(\mathbf{k} - \mathbf{k}')$ but only the angle between both momenta. [2] Since only the inner product is invariant w.r.t. rotations, we have $|\mathbf{k} - \mathbf{k}'| = \sqrt{k^2 + (k')^2 - 2\cos(\gamma)\, kk'}$ with $\gamma = \measuredangle(\mathbf{k}, \mathbf{k}')$ and $k = |\mathbf{k}|$ and $k' = |\mathbf{k}'|$. Therefore, the interaction may only depend on k, k' and the angle γ, i.e. $V(\mathbf{k} - \mathbf{k}') = V(k, k', \gamma)$. Hence, we can expand the interaction in terms of *Legendre polynomials* $P_l(x)$:

$$V(\mathbf{k} - \mathbf{k}') = \sum_{l=0}^{\infty} (2l+1)\, V_l(k, k')\, P_l(\cos(\gamma)) \quad , \tag{2.1.6}$$

where the index l serves as a label for the different angular momentum contributions [3]. Later, when inserting the above back in the Schrödinger equation it will turn out the be advantageous to express the Legendre polynomials in terms of *spherical harmonics* $Y_m^l(\theta, \phi)$, splitting further up the angular momentum contributions into different projection indices m. This can be done by means of the *spherical harmonic addition theorem* resulting in (cf. [MS99]) [4]

[2] Suppose we had e.g. the momenta $\mathbf{k} = (5, 3, -1)$ and $\mathbf{k}' = (-3, 2, 2)$, which results in $V(8, 1, -3)$. If we further assume an interaction of the form $V(\mathbf{q}) = q_x^2 - 2q_y + q_z$ it would indeed matter what the overall direction of momenta is, since $V(\mathbf{q}) = 59 \neq V(-\mathbf{q}) = 69$. However, this represents a highly unphysical form of an interaction.

[3] The angular momentum coefficients (and correct normalization in terms of angular momentum indices l in the expansion can be derived by means of the orthogonality $\int_{-1}^{1} P_n(x) P_m(x) = \frac{2}{2n+1}\delta_{nm}$ and the integration over polar and azimuth angles $\int \mathrm{d}\Omega = \int_0^{2\pi} \mathrm{d}\phi \int_0^{\pi} \mathrm{d}\theta \sin(\theta)$ (using the substitution $u = \cos(\theta)$). A simple calculation determines the coefficients to be $V_l(k, k') = \frac{1}{4\pi} \int \mathrm{d}\Omega\, V(\mathbf{k} - \mathbf{k}')\, P_l(\cos(\gamma))$.

[4] The spherical harmonics are defined by $Y_m^l(\theta, \phi) = \sqrt{\frac{2l+1}{4\pi} \frac{(l-m)!}{(l+m)!}} P_l^m(\cos(\theta)) e^{im\phi}$ with $P_l^m(\cos(\theta))$ being the *associated Legendre polynomials* [CS51]. They satisfy the *spherical harmonic addition theorem* [Edm96] , i.e. $P_l(\cos(\gamma)) = \frac{4\pi}{2l+1} \sum_{m=-l}^{+l} \overline{Y_m^l(\theta', \phi')} Y_m^l(\theta, \phi)$ where γ being the angle between two vectors whose direction are given by (θ, ϕ) and (θ', ϕ'). In general $\cos(\gamma) = \cos(\theta)\cos(\theta') + \sin(\theta)\sin(\theta')\cos(\phi - \phi')$, which simplifies to $\cos(\gamma) = \cos(\theta)$ when assuming that the second vector coincides with the z-axis, i.e. $\theta' = 0$.

$$V(\mathbf{k}-\mathbf{k}') = 4\pi \sum_{l=0}^{\infty} V_l(k,k') \sum_{m=-l}^{+l} \overline{Y_m^l(\theta,\phi)} Y_m^l(\theta',\phi') \quad , \tag{2.1.7}$$

where we defined $\theta = \theta_{\mathbf{k}}$, $\phi = \phi_{\mathbf{k}}$ and $\theta' = \theta_{\mathbf{k}'}$, $\phi' = \phi_{\mathbf{k}'}$. The two-particle wave function in momentum space can be expanded by [Jac99, Chapter 3.5]

$$\phi(\mathbf{k}) = \sum_{l=0}^{\infty} \sum_{m=-l}^{+l} \phi_{lm}(k) Y_m^l(\theta,\phi) \quad . \tag{2.1.8}$$

We are now in the position to insert the representations of the interaction and wave function in terms of spherical harmonics into (Equation 2.1.5). The integration over $\mathbf{k}'$ is written in terms of spherical coordinates $\int \mathrm{d}\mathbf{k}' = \int \mathrm{d}k' \int \Omega = \int_0^{\infty} \mathrm{d}k' \int_0^{2\pi} \mathrm{d}\phi \int_0^{\pi} \mathrm{d}\theta (k')^2 \sin(\theta)$, which enables us to employ the *orthonormality* of the spherical harmonics [5] and obtain

$$(2\varepsilon_{\mathbf{k}} - E) \sum_{l=0}^{\infty} \sum_{m=-l}^{l} \phi_{lm}(k) Y_m^l(\theta,\phi) = -\frac{1}{(2\pi)^{3/2}} \int_0^{\infty} \mathrm{d}k'\, 4\pi (k')^2 \sum_{l=0}^{\infty} V_l(k,k') \sum_{m=-l}^{l} \phi_l(k') Y_m^l(\theta,\phi) \quad , \tag{2.1.9}$$

where the kinetic energy of two free particles $2\varepsilon_{\mathbf{k}} = \frac{(\hbar\mathbf{k})^2}{2\mu}$ is used. Since we are only interested in the different orbital angular momentum channels but not the resolution into the projections, we define the wave function component associated to a particular channel l by $\phi_l(k,\theta,\phi) = \sum_{m=-l}^{l} \phi_{lm}(k) Y_m^l(\theta,\phi)$. Hence, we get

$$(2\varepsilon_{\mathbf{k}} - E) \sum_{l=0}^{\infty} \phi_l(k,\theta,\phi) = -\frac{1}{(2\pi)^{3/2}} \int_0^{\infty} \mathrm{d}k'\, 4\pi (k')^2 \sum_{l=0}^{\infty} V_l(k,k')\, \phi_l(k',\theta,\phi) \quad , \tag{2.1.10}$$

Due to the spherical harmonics being a basis with orthonormal properties the (Equation 2.1.10) must be valid for every single component l as well (where we may omit the remaining angular dependencies for now). Therefore, we obtain (cf. [Leg75])

$$(2\varepsilon_{\mathbf{k}} - E)\, \phi_l(k) = -\frac{1}{(2\pi)^{3/2}} \int_0^{\infty} \mathrm{d}k'\, 4\pi (k')^2 V_l(k,k')\, \phi_l(k') \quad , \tag{2.1.11}$$

which is an eigenvalue equation determining the wave function for a particular orbital angular momentum l and the energy E of the two electron system. We are looking for any solutions of this equation that feature $E < 0$ and therefore correspond to a *bound*

[5] The orthonormality of the spherical harmonics with respect to l and m is given by $\int \mathrm{d}\Omega\, \overline{Y_m^l(\theta,\phi)} Y_{m'}^{l'}(\theta,\phi) = \delta_{l,l'}\delta_{m,m'}$ [San04].

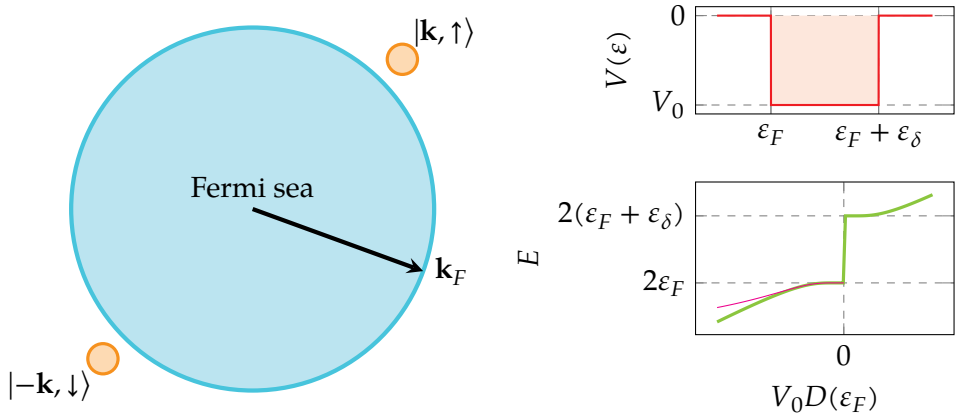

Figure 2.1.: (Figure 2.1a) Illustration of the Cooper problem featuring two electrons with opposite momenta and a net attractive interaction due to phonon exchange within a narrow energy shell above the Fermi level. (Figure 2.1b) The "traditional" BCS-interaction is given by a rectangular potential well of depth V_0 in energy space located at the Fermi level. The energy E of the two-electron system exhibits a sharp change of behavior at $V_0 D(\varepsilon_F) = 0$ that is responsible for the Cooper instability. The green graph shows the "exact" dependency in (Equation 2.1.17) while the magenta curve is the approximation for a small negative (attractive) interaction. A net attractive interaction between the electrons $V_0 < 0$ - no matter how small - will ultimately result in an energy eigenvalue $E < 0$ and the formation of a bound state.

state of the system. Let's consider a (uniformly) repulsive interaction V_0 in real space, transforming to $V_0\delta(\mathbf{k} - \mathbf{k}')$ in reciprocal space, which is itself expanded in terms of Legendre polynomials with the coefficients $V_l(k,k') = \frac{V_0}{2}\delta(k-k')P_l(0)$ with $P_l(0)$ being the l-th Legendre polynomial at abscissa $x = 0$. Inserting into (Equation 2.1.11) we find that there cannot be any bound state with $E < 0$ and even for a small attractive interaction below a certain limit there won't be any negative energy eigenvalue.

So far we exclusively considered two free particles in vacuum. We will now introduce a filled and unimpeded *Fermi sea* into the presence of the two electrons. As a consequence, the two original particles have to be positioned above the Fermi energy. However, we won't consider any interaction between the electrons in the Fermi sea and the two original ones but retain the interaction between the two electrons themselves (cf. (Figure 2.1a)). The eigenvalue equation (Equation 2.1.11) is still valid, but, however, we have to limit all momentum summations to momenta larger than the Fermi momentum. The energy of the two electron system in its new environment seems to have the lower bound $2\varepsilon_F$. Referring back to (Equation 2.1.11) we now have (cf. [AM61])

$$(2\varepsilon_{\mathbf{k}} - E)\,\phi_l(k) = -\frac{1}{(2\pi)^{3/2}} \int_{k_F}^{\infty} \mathrm{d}k'\; 4\pi (k')^2 V_l\,(k,k')\,\phi_l(k') \quad , \tag{2.1.12}$$

with the integration restricted to momenta above the Fermi level. We assume a constant interaction between the two electrons, that may arise due to exchange of *phonons* (see [Frö50; BP55; Mig58; Eli60]) and is assumed to be present in a narrow energy shell near the Fermi surface:

$$V\,(\mathbf{k} - \mathbf{k}') = \begin{cases} V_0 & , \quad k_F < k, k' < k_F + k_\delta \\ 0 & , \quad \text{otherwise} \end{cases} \quad , \tag{2.1.13}$$

with the width of the shell being very small compared to the Fermi level, i.e. $k_\delta \ll k_F$. It has been shown that this interaction can be attractive as a net result of phonon exchange and *screened Coulomb* repulsion when the energy difference between the electrons involved is small, i.e. $|\varepsilon_{\mathbf{k}} - \varepsilon_{\mathbf{k}'}| \sim k_B T$ [BCS57]. In a normal state metal with *time-reversal symmetry* the associated momentum states are always given by $|\mathbf{k}\rangle$ and $|-\mathbf{k}\rangle$. However, we may note that an interaction of this exact mathematical form implies an highly oscillatory behavior in real space because of the Fourier expansion of the *rectangle function*Assuming an interaction of this form in (Equation 2.1.12), will restrict the solutions to the $l = 0$ channel and cancel most of the integral but the thin momentum shell above k_F. The integration over the orbital angular momentum wave function produces a constant that may be canceled by doing the same integral for the wave function on the left hand side as well, i.e.

$$\begin{aligned} &\int_{k_F}^{k_F+k_\delta} \mathrm{d}k\, k^2 \phi_l(k) = -\int_{k_F}^{k_F+k_\delta} \mathrm{d}k\, \frac{4\pi k^2}{(2\pi)^{3/2}} \frac{V_0}{2\varepsilon_{\mathbf{k}} - E} \int_{k_F}^{k_F+k_\delta} \mathrm{d}k'\; (k')^2 \phi_l(k') \\ \Leftrightarrow \quad &1 = -\int_{k_F}^{k_F+k_\delta} \mathrm{d}k\, \frac{4\pi k^2}{(2\pi)^{3/2}} \frac{V_0}{2\varepsilon_{\mathbf{k}} - E} \quad . \end{aligned} \tag{2.1.14}$$

Due to the presence of normalization factors is turns out to be convenient to use an energy instead of an momentum integration, i.e. [6]

$$1 = -\,(2\pi)^{3/2}\,\frac{V_0}{2} \int_{\varepsilon_F}^{\varepsilon_F+\varepsilon_\delta} \mathrm{d}\varepsilon\; \frac{D(\varepsilon)}{2\varepsilon_{\mathbf{k}} - E} \quad . \tag{2.1.15}$$

The density of states at the Fermi level is finite and can be approximately assumed to

[6] The energy vs. momentum integration substitution produces the differential $\mathrm{d}\mathbf{k} = \sqrt{\frac{2m}{\hbar^2}} \frac{1}{2\sqrt{\varepsilon}} \mathrm{d}\varepsilon$, which gives $\frac{4\pi k^2}{(2\pi)^3} \mathrm{d}\mathbf{k} = \frac{1}{2} D(\varepsilon) \mathrm{d}\varepsilon$ with the density of states (taking into account both spin states) $D(\varepsilon) = \left(\frac{2m}{\hbar^2}\right)^{3/2} \frac{\sqrt{\varepsilon}}{2\pi^2}$

be constant. This is in contrast to the case of two free electrons that had zero density of states at the lowest possible energy due to the $\sqrt{\varepsilon}$-dependence of free particles in three dimensions. Performing the integration we obtain

$$1 = -(2\pi)^{3/2} \frac{V_0 D(\varepsilon_F)}{2} \ln\left(1 + \frac{2\varepsilon_\delta}{2\varepsilon_F - E}\right) \quad , \tag{2.1.16}$$

and finally find the energy eigenvalue to be

$$E = 2\varepsilon_F - \frac{2\varepsilon_\delta}{e^{-\frac{2}{(2\pi)^{3/2}}\frac{1}{V_0 D(\varepsilon_F)}} - 1} \overset{V_0 \to 0_-}{\approx} 2\left(\varepsilon_F - \varepsilon_\delta \exp\left[-\frac{2}{(2\pi)^{3/2}} \frac{1}{|V_0| D(\varepsilon_F)}\right]\right) \quad , \tag{2.1.17}$$

with the curious dependency on $V_0 D(\varepsilon_F)$ that is shown in (Figure 2.1b). At zero interaction $V_0 = 0$ the energy eigenvalue exhibits a distinct cusp, where it jumps from $2(\varepsilon_F + \varepsilon_\delta)$ to a value slightly below twice the Fermi energy. Therefore, already a tiny attractive interaction will lead to a bound state of the two-electron system. This phenomenon is known as the *Cooper instability*. Apparently, it is possible to construct a two-particle state with an energy that makes this state favorable compared to putting the two electrons in the lowest available states above the Fermi energy. Furthermore, if it is energetically favorable to create such a state from two electrons, it appears to be even more favorable, to let more electron pairs condense into this state. So far, we focused on the case $l = 0$, but we may easily generalize the above result to channels with $l = 1, 2$ by introducing an appropriate interaction that produces non-zero components in respective expansion coefficients $V_l(k, k')$ (cf. [AM61]). However, we should keep in mind what kind of approximations and restrictions we introduced to obtain this result: i) assuming zero temperature ii) neglecting any interactions between the two electron and the Fermi sea. Therefore, we have to find a new ansatz to get rid of these restrictions.

2.2. BCS-theory

The "traditional" BCS-theory explains superconductivity and its associated phenomena by introducing the concept of Cooper pairs that form a coherent condensate due to an effective attractive interaction mediated by phonons [Mig58; De 89]. Like in the previous section discussing the *Cooper problem* we assume a constant interaction between electrons that is present in a small energy shell above the Fermi level. The Hamiltonian yields

$$\mathcal{H} = \sum_{\mathbf{k},\sigma} \varepsilon_{\mathbf{k}} c^\dagger_{\mathbf{k},\sigma} c_{\mathbf{k},\sigma} - g \sum_{\mathbf{k},\mathbf{k}'} c^\dagger_{\mathbf{k},\downarrow} c^\dagger_{-\mathbf{k},\uparrow} c_{-\mathbf{k}',\uparrow} c_{\mathbf{k}',\downarrow} \quad , \tag{2.2.1}$$

where we denoted the attractive, isotropic coupling constant by $g > 0$. We are allowed

to neglect all interaction except the one in the Cooper channel because the available phase space (for a low-energy theory) is much larger for $\mathbf{k} = -\mathbf{k}$ than for all other states with $\mathbf{k} \neq -\mathbf{k}$. In order to calculate the resulting one-particle spectrum we apply mean-field theory . The essential idea of *BCS-theory* is to introduce the "off-diagonal" expectation value

$$b_{\mathbf{k}} = \left\langle c_{-\mathbf{k},\uparrow} c_{\mathbf{k},\downarrow} \right\rangle \qquad b_{\mathbf{k}}^{\dagger} = \left\langle c_{\mathbf{k},\downarrow}^{\dagger} c_{-\mathbf{k},\uparrow}^{\dagger} \right\rangle \quad , \tag{2.2.2}$$

which is defined with respect to the (unknown) eigenstates of (Equation 2.2.1) and which is usually zero in the normal state since the normal state Hamiltonian commutes with the particle number operator. However, in the superconducting phase this mean-field acquires a non-zero expectation value, since the superconducting state is a coherent superposition of Cooper pairs [BCS57]

$$|\psi_{BCS}\rangle = \prod_{k} \left(u_{\mathbf{k}} + v_{\mathbf{k}} c_{\mathbf{k},\uparrow}^{\dagger} c_{-\mathbf{k},\downarrow}^{\dagger} \right) |0\rangle \quad , \tag{2.2.3}$$

where the normalization fixes the coefficients $\langle \psi_{BCS} | \psi_{BCS} \rangle \stackrel{!}{=} 1 \Leftrightarrow |u_{\mathbf{k}}|^2 + |v_{\mathbf{k}}|^2 = 1$ and we get $\langle \psi_{BCS} | c_{\mathbf{k},\downarrow}^{\dagger} c_{-\mathbf{k},\uparrow}^{\dagger} | \psi_{BCS} \rangle = u_{\mathbf{k}} \overline{v}_{\mathbf{k}}$ Using the definition $\delta_{\mathbf{k}} := \left(c_{-\mathbf{k},\uparrow} c_{\mathbf{k},\downarrow} - b_{\mathbf{k}} \right)$ the interaction term in (Equation 2.2.1) can be written [Wei07]

$$\begin{aligned} c_{\mathbf{k},\downarrow}^{\dagger} c_{-\mathbf{k},\uparrow}^{\dagger} c_{-\mathbf{k}',\uparrow} c_{\mathbf{k}',\downarrow} &= \left(b_{\mathbf{k}}^{\dagger} + \delta_{\mathbf{k}}^{\dagger} \right) \left(b_{\mathbf{k}'} + \delta_{\mathbf{k}'} \right) = b_{\mathbf{k}}^{\dagger} b_{\mathbf{k}'} + b_{\mathbf{k}}^{\dagger} \delta_{\mathbf{k}'} + \delta_{\mathbf{k}}^{\dagger} b_{\mathbf{k}'} + \delta_{\mathbf{k}}^{\dagger} \delta_{\mathbf{k}'} \\ &\approx b_{\mathbf{k}}^{\dagger} b_{\mathbf{k}'} + b_{\mathbf{k}}^{\dagger} \delta_{\mathbf{k}'} + \delta_{\mathbf{k}}^{\dagger} b_{\mathbf{k}'} = -b_{\mathbf{k}}^{\dagger} b_{\mathbf{k}'} + b_{\mathbf{k}}^{\dagger} c_{-\mathbf{k}',\uparrow} c_{\mathbf{k}',\downarrow} + b_{\mathbf{k}'} c_{\mathbf{k},\downarrow}^{\dagger} c_{-\mathbf{k},\uparrow}^{\dagger} \quad , \end{aligned} \tag{2.2.4}$$

in which we assume the fluctuations $\delta_{\mathbf{k}}$ to be small and therefore justifying the neglection of terms quadratic in the fluctuations, i.e. $\delta_{\mathbf{k}}^{\dagger} \delta_{\mathbf{k}'} \approx 0$. By defining another - which will later become an important entity - "short-hand notation", i.e. $\Delta := -g \sum_{\mathbf{k}} b_{\mathbf{k}}$ we squeeze the (interacting) Hamiltonian into its final (non-interacting) shape (rename $\mathbf{k} \leftrightarrow \mathbf{k}'$ in the second term of the last equality of (Equation 2.2.4))

$$\mathcal{H} = \sum_{\mathbf{k},\sigma} \varepsilon_{\mathbf{k}} c_{\mathbf{k},\sigma}^{\dagger} c_{\mathbf{k},\sigma} + \Delta^{\dagger} c_{-\mathbf{k},\uparrow} c_{\mathbf{k},\downarrow} + \Delta c_{\mathbf{k},\downarrow}^{\dagger} c_{-\mathbf{k},\uparrow}^{\dagger} - g \sum_{\mathbf{k},\mathbf{k}'} b_{\mathbf{k}}^{\dagger} b_{\mathbf{k}'} \quad . \tag{2.2.5}$$

The resulting Hamiltonian is comprised of single-particle terms only and maybe diagonalized by employing the Nambu spinor notation $C_{\mathbf{k}} := \left(c_{\mathbf{k},\downarrow}, c_{-\mathbf{k},\uparrow}^{\dagger} \right)$ [Nam60; And58b] (and fermionic antisymmetry $\{ c_{\alpha}^{(\dagger)} c_{\alpha'}^{(\dagger)} \} = \delta_{\alpha,\alpha'}$) and implying degeneracy and inversion symmetry on the single-particle spectrum $\varepsilon_{\mathbf{k},\uparrow} = \varepsilon_{\mathbf{k},\downarrow} = \varepsilon_{-\mathbf{k},\uparrow}$

$$\mathcal{H}_{\mathrm{BCS}} = \sum_{\mathbf{k}} \left(c^{\dagger}_{\mathbf{k},\downarrow}, c_{-\mathbf{k},\uparrow}\right) \begin{pmatrix} \varepsilon_{\mathbf{k}} & \Delta \\ \Delta^{\dagger} & -\varepsilon_{\mathbf{k}} \end{pmatrix} \begin{pmatrix} c_{\mathbf{k},\downarrow} \\ c^{\dagger}_{-\mathbf{k},\uparrow} \end{pmatrix} \quad . \tag{2.2.6}$$

The new *quasiparticle* energy is obviously given by $E_{\mathbf{k}} = \pm\sqrt{\varepsilon^2_{\mathbf{k}} + |\Delta|^2}$, whereas the new eigenstates $\gamma_{\mathbf{k}}$ that diagonalize (Equation 2.2.6) are a superposition of electrons and holes, i.e.

$$\begin{pmatrix} \gamma_{\mathbf{k},+} \\ \gamma^{\dagger}_{\mathbf{k},-} \end{pmatrix} := U_{\mathbf{k}} C_{\mathbf{k}} = \begin{pmatrix} u_{\mathbf{k}} & v_{\mathbf{k}} \\ -\overline{v}_{\mathbf{k}} & \overline{u}_{\mathbf{k}} \end{pmatrix} \begin{pmatrix} c_{\mathbf{k},\downarrow} \\ c^{\dagger}_{-\mathbf{k},\uparrow} \end{pmatrix} \quad \text{with} \quad \begin{cases} u_{\mathbf{k}} = \frac{\Delta}{\sqrt{2E_{\mathbf{k}}(E_{\mathbf{k}} - \varepsilon_{\mathbf{k}})}} \\ v_{\mathbf{k}} = \frac{E_{\mathbf{k}} - \varepsilon_{\mathbf{k}}}{\sqrt{2E_{\mathbf{k}}(E_{\mathbf{k}} - \varepsilon_{\mathbf{k}})}} \end{cases} \quad , \tag{2.2.7}$$

where the normalization is fixed by the requirement $|u_{\mathbf{k}}|^2 + |v_{\mathbf{k}}|^2 \stackrel{!}{=} 1$ and we chose an arbitrary (but simple) phase for the coefficients. We take the single-orbital Hubbard model on the square lattice

$$\mathcal{H} = t \sum_{\langle i,j \rangle} c^{\dagger}_i c_j = \sum_{\mathbf{k}} \underbrace{-2t\left(\cos(k_x) + \cos\left(k_y\right)\right)}_{\equiv \varepsilon_{\mathbf{k}}} c^{\dagger}_{\mathbf{k}} c_{\mathbf{k}} \quad , \tag{2.2.8}$$

as an example to illustrate the implications of the calculations above. (Figure 2.2) shows the normal ($\varepsilon_{\mathbf{k}}$) vs. the superconducting ($E_{\mathbf{k}}$) state dispersion and the momentum dependence of the eigenstate components $u_{\mathbf{k}}$ and $v_{\mathbf{k}}$. For example, at the Γ point the new quasiparticles $\gamma_{\mathbf{k},+}$ are of pure hole character $u_{\mathbf{k}} = 0$, while at X we have equal electron and hole contribution and at M the quasiparticles have sole electron character (cf. (Figure 2.2b)). In order to justify the introduction of the mean-field parameter (Equation 2.2.2) *a posteriori* we have to actually calculate the corresponding expectation value w.r.t. $\mathcal{H}_{\mathrm{BCS}}$ (Equation 2.2.6), which is

$$\left\langle c_{\mathbf{k},\downarrow} c_{-\mathbf{k},\uparrow} \right\rangle = \frac{\left\langle c_{\mathbf{k},\downarrow} c_{-\mathbf{k},\uparrow} e^{-\beta \mathcal{H}_{\mathrm{BCS}}} \right\rangle}{\left\langle e^{-\beta \mathcal{H}_{\mathrm{BCS}}} \right\rangle} \quad . \tag{2.2.9}$$

This is most conveniently solved by rewriting the expectation value in terms of the eigenstates of $\mathcal{H}_{\mathrm{BCS}}$, i.e. the new quasiparticles by means of (Equation 2.2.7) and their inverse [Tim12]

$$\begin{pmatrix} c_{\mathbf{k},\downarrow} \\ c^{\dagger}_{-\mathbf{k},\uparrow} \end{pmatrix} = \begin{pmatrix} \overline{u}_{\mathbf{k}} & -v_{\mathbf{k}} \\ \overline{v}_{\mathbf{k}} & u_{\mathbf{k}} \end{pmatrix} \begin{pmatrix} \gamma_{\mathbf{k},\uparrow} \\ \gamma^{\dagger}_{\mathbf{k},\downarrow} \end{pmatrix} \tag{2.2.10}$$

transforming the expectation value to

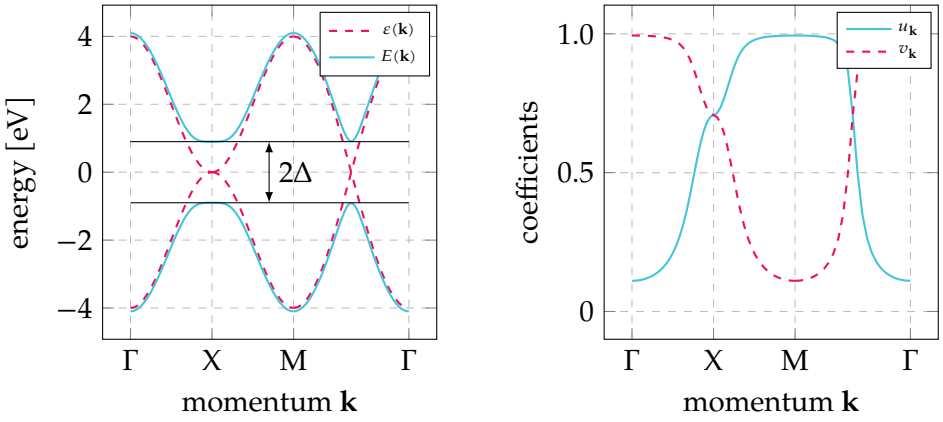

(a) (b)

Figure 2.2.: (Figure 2.2a) The hubbard model 2.2.8 with its dispersion in the normal state ($\Delta = 0$ and $E_{\mathbf{k}} \to \varepsilon_{\mathbf{k}}$) and the superconducting state ($\Delta = \text{const} > 0$ and $E_{\mathbf{k}}$). We set the constants $t = 1.0$ and $\Delta = 0.9$. (Figure 2.2b) The squares of the components $u_{\mathbf{k}}$, $v_{\mathbf{k}}$ of the eigenstates always add up to one and we see how the mixture of electron and hole states in the quasiparticle states depends on the momentum. Particularly at the (normal state) Fermi momenta we see exactly the same electron and hole contribution to the quasiparticle state (which is the case for e.g. X and the center between Γ and M). The quasiparticle at Γ and M has pure hole and electron character, respectively.

$$\begin{aligned}\left\langle c_{\mathbf{k},\downarrow} c_{-\mathbf{k},\uparrow}\right\rangle &= \left\langle \left(\overline{u}_{\mathbf{k}}\gamma_{\mathbf{k},\uparrow} - v_{\mathbf{k}}\gamma^{\dagger}_{\mathbf{k},\downarrow}\right)\left(v_{\mathbf{k}}\gamma^{\dagger}_{\mathbf{k},\uparrow} + \overline{u}_{\mathbf{k}}\gamma_{\mathbf{k},\downarrow}\right)\right\rangle \\ &= \left\langle \overline{u}_{\mathbf{k}} v_{\mathbf{k}}\gamma_{\mathbf{k},\uparrow}\gamma^{\dagger}_{\mathbf{k},\uparrow}\right\rangle + \left\langle |u_{\mathbf{k}}|^2\gamma_{\mathbf{k},\uparrow}\gamma_{\mathbf{k},\downarrow}\right\rangle - \left\langle |v_{\mathbf{k}}|^2\gamma^{\dagger}_{\mathbf{k},\downarrow}\gamma^{\dagger}_{\mathbf{k},\uparrow}\right\rangle - \left\langle \overline{u}_{\mathbf{k}} v_{\mathbf{k}}\gamma^{\dagger}_{\mathbf{k},\downarrow}\gamma_{\mathbf{k},\downarrow}\right\rangle \\ &= \overline{u}_{\mathbf{k}} v_{\mathbf{k}}\left(\left\langle \gamma_{\mathbf{k},\uparrow}\gamma^{\dagger}_{\mathbf{k},\uparrow}\right\rangle - \left\langle \gamma^{\dagger}_{\mathbf{k},\downarrow}\gamma_{\mathbf{k},\downarrow}\right\rangle\right) \end{aligned} \tag{2.2.11}$$

Using the thermal expectation value for the number operator $\left\langle \gamma^{\dagger}_{-\mathbf{k},\uparrow}\gamma_{-\mathbf{k},\uparrow}\right\rangle = n\left(E_{\mathbf{k}}\right)$ and $\left\langle \gamma_{\mathbf{k},\downarrow}\gamma^{\dagger}_{\mathbf{k},\downarrow}\right\rangle = \left\langle 1 - \gamma^{\dagger}_{\mathbf{k},\downarrow}\gamma_{\mathbf{k},\downarrow}\right\rangle = 1 - \mathrm{n_F}\left(E_{\mathbf{k}}\right)$ of the new quasiparticle (where $\mathrm{n_F}\left(E_{\mathbf{k}}\right)$ is the Fermi-Dirac distribution), we find

$$\left\langle c_{\mathbf{k},\downarrow} c_{-\mathbf{k},\uparrow}\right\rangle = \overline{u}_{\mathbf{k}} v_{\mathbf{k}}\left(1 - 2\mathrm{n_F}\left(E_{\mathbf{k}}\right)\right) \quad . \tag{2.2.12}$$

Herewith, we are able to express the *self-consistency* condition of the *gap function* (that was introduced before (Equation 2.2.5)), i.e. [7]

[7] The Fermi-Dirac function may be expressed by $1 - 2\mathrm{n_F}(E) = 1 - 2\frac{1}{1+e^{-\beta E}} = \frac{-1+e^{-\beta E}}{1+e^{-\beta E}} = \frac{-e^{\beta\frac{E}{2}}+e^{-\beta\frac{E}{2}}}{e^{\beta\frac{E}{2}}+e^{-\beta\frac{E}{2}}} = \tanh\left(\beta\frac{E}{2}\right)$ where $\beta = \frac{1}{k_B T}$

$$\Delta = -g \sum_{\mathbf{k}} \overline{u}_{\mathbf{k}} v_{\mathbf{k}} \left(1 - 2\mathrm{n_F}\left(E_{\mathbf{k}}\right)\right) = -g \sum_{\mathbf{k}} \frac{\Delta \left(1 - 2\mathrm{n_F}\left(E_{\mathbf{k}}\right)\right)}{2E_{\mathbf{k}}}$$
$$= -g \sum_{\mathbf{k}} \frac{\Delta}{2E_{\mathbf{k}}} \tanh\left(\frac{\beta E_{\mathbf{k}}}{2}\right) \quad . \tag{2.2.13}$$

For a momentum dependent Cooper pair interaction we have (using the abbreviation $V_{\mathbf{k},-\mathbf{k},\mathbf{k}',-\mathbf{k}'} = V_{\mathbf{k},\mathbf{k}'}$)

$$\Delta_{\mathbf{k}} = -\sum_{\mathbf{k}'} \frac{V_{\mathbf{k},\mathbf{k}'}\Delta_{\mathbf{k}'}}{2E_{\mathbf{k}'}} \tanh\left(\frac{\beta E_{\mathbf{k}'}}{2}\right) \quad . \tag{2.2.14}$$

We take a look at certain physical limits that provide a considerable simplification of the gap equation, e.g. in the zero temperature limit $T \to 0$ we have ($\lim_{T\to 0} \tanh\left(\frac{\beta E_{\mathbf{k}'}}{2}\right) = 1$)

$$\Delta_{\mathbf{k}} = -\sum_{\mathbf{k}'} \frac{V_{\mathbf{k},\mathbf{k}'}\Delta_{\mathbf{k}'}}{2E_{\mathbf{k}'}} = -\sum_{\mathbf{k}'} \frac{V_{\mathbf{k},\mathbf{k}'}\Delta_{\mathbf{k}'}}{2\sqrt{\varepsilon_{\mathbf{k}'}^2 + |\Delta_{\mathbf{k}}|^2}} \quad . \tag{2.2.15}$$

or the limit of infinitesimal gap amplitude $\Delta \to 0$ with $\lim_{\Delta\to 0} E_{\mathbf{k}} = \varepsilon_{\mathbf{k}}$ and we get the "linearized" gap equation

$$\Delta_{\mathbf{k}} = -\sum_{\mathbf{k}'} \frac{V_{\mathbf{k},\mathbf{k}'} \tanh\left(\frac{\beta\varepsilon_{\mathbf{k}'}}{2}\right)}{2\varepsilon_{\mathbf{k}'}} \Delta_{\mathbf{k}'} \quad . \tag{2.2.16}$$

that reduces the upcoming task to solve the gap equation to a simple eigenvector problem. We try further evaluate the gap equation with constant interaction. In (Equation 2.2.13) the sum/integral only depends on the momentum through the quasiparticle energy, which makes it advantageous to rewrite it as energy integral (where we use the Debye frequency ω_D as physical cutoff that represents the energy domain of attractive interaction $g < 0$ and $V_0 := -|g| > 0$) by means of the (normal state) density of states $D(\varepsilon)$ (that is assumed to be constant in the considered energy window, i.e. $D(\varepsilon_F)$ at the Fermi energy)

$$\Delta = \frac{V_0}{\Omega_{BZ}} \int_{-\omega_D}^{+\omega_D} \mathrm{d}\varepsilon \, \frac{\Delta D(E(\varepsilon))}{2E(\varepsilon)} \tanh\left(\frac{\beta E(\varepsilon)}{2}\right) = \Delta \frac{V_0 D(\varepsilon_F)}{\Omega_{BZ}} \int_{-\omega_D}^{+\omega_D} \mathrm{d}\varepsilon \, \frac{\tanh\left(\frac{\beta E(\varepsilon)}{2}\right)}{2E(\varepsilon)} \quad , \tag{2.2.17}$$

with $E(\varepsilon) = \sqrt{\varepsilon^2 + \Delta^2}$. This form of the gap equation can be used to approximate the critical temperature T_c that defines the transition from the normal to the superconducting state, i.e. the temperature with $\Delta(T_c) = 0$ which also simplifies $\lim_{T \nearrow T_c} E = |\varepsilon|$ (note that $\beta_C := (k_B T_C)^{-1}$)

$$\frac{\Omega_{BZ}}{V_0 D(\varepsilon_F)} = \int_{-\omega_D}^{+\omega_D} \mathrm{d}\varepsilon \, \frac{\tanh\left(\frac{\beta_C|\varepsilon|}{2}\right)}{2|\varepsilon|} \overset{|\varepsilon|=|-\varepsilon|}{=} \int_0^{+\omega_D} \mathrm{d}\varepsilon \, \frac{\tanh\left(\frac{\beta_C|\varepsilon|}{2}\right)}{|\varepsilon|} \overset{u:=\frac{\beta|\varepsilon|}{2}}{=} \int_0^{\beta_C\omega_D/2} \mathrm{d}u \, \frac{\tanh(u)}{u} \quad . \tag{2.2.18}$$

The last equation may be tackled by integration by parts where we note that $\frac{\mathrm{d}}{\mathrm{d}x}\tanh x = 1 - (\tanh(x))^2 = \frac{1}{(\cosh(x))^2}$ and we get ($\beta\omega_D \gg 1$)

$$\frac{\Omega_{BZ}}{V_0 D(\varepsilon_F)} = \left[\ln(\beta_C\omega_D/2) \underbrace{\tanh(\beta\omega_D/2)}_{=1} - \int_0^{\beta_C\omega_D/2} \mathrm{d}u \, \frac{\ln(u)}{(\cosh(u))^2}\right] \quad . \tag{2.2.19}$$

The integrand of the remaining integral decays exponentially and therefore justifying to send the upper limit to infinity, which results in a definite integral that is

$$\int_0^{\infty} \mathrm{d}u \, \frac{\ln(u)}{(\cosh(u))^2} = -\gamma + \ln\frac{\pi}{4} \quad , \tag{2.2.20}$$

with the Euler constant γ [8]. Using it gives

$$\frac{\Omega_{BZ}}{V_0 D(\varepsilon_F)} = \ln(\beta_C\omega_D/2) + \gamma - \ln\frac{\pi}{4} = \ln\left(\frac{2\beta_C\omega_D}{\pi}\right) + \gamma \quad , \tag{2.2.21}$$

the estimate for the critical temperature in the *weak-coupling limit*

$$k_B T_C = \frac{2e^{\gamma}}{\pi}\omega_D \exp\left(-\frac{\Omega_{BZ}}{V_0 D(\varepsilon_F)}\right) \approx 1.133\,87\,\omega_D \exp\left(-\frac{\Omega_{BZ}}{V_0 D(\varepsilon_F)}\right) \quad . \tag{2.2.22}$$

By doing some numerics we may also determine the temperature dependency $\Delta(T)$ of the gap amplitude derived from (Equation 2.2.17), i.e. using

[8] The Euler γ-constant is defined by $\gamma = \lim_{n\to\infty}\left[\sum_{k=1}^{n}\left(\frac{1}{k}\right) - \ln(n)\right] \approx 0.577\,21$

$$1 = \frac{V_0 D(\varepsilon_F)}{\Omega_{BZ}} \int_{-\omega_D}^{+\omega_D} \mathrm{d}\varepsilon \, \frac{\tanh\left(\frac{\beta\sqrt{\varepsilon^2+\Delta^2}}{2}\right)}{2\sqrt{\varepsilon^2+\Delta^2}} \overset{\text{sym.w.r.t.}\varepsilon\to-\varepsilon}{\downarrow =} \frac{V_0 D(\varepsilon_F)}{\Omega_{BZ}} \int_0^{\omega_D} \mathrm{d}\varepsilon \, \frac{\tanh\left(\frac{\beta\sqrt{\varepsilon^2+\Delta^2}}{2}\right)}{\sqrt{\varepsilon^2+\Delta^2}} \quad . \tag{2.2.23}$$

and solving for Δ through a range of temperatures. It turns out, that the gap exhibits a dependency on the temperature that is in the literature (poorly) approximated by $\frac{\Delta(T)}{\Delta(0)} \approx \sqrt{1-\frac{T}{T_c}}$ [Tin96, Chapter 3.6], which is shown in (Figure 2.3b). First of all, let's check out the gap at zero temperature $T \to 0 \Leftrightarrow \beta \to \infty$

$$\begin{aligned} 1 &= \frac{V_0 D(\varepsilon_F)}{\Omega_{BZ}} \int_0^{\omega_D} \frac{\mathrm{d}\varepsilon}{\Delta} \frac{1}{\sqrt{1+\frac{\varepsilon^2}{\Delta^2}}} \overset{x=\frac{\varepsilon}{\Delta}}{\downarrow =} \frac{V_0 D(\varepsilon_F)}{\Delta\Omega_{BZ}} \int_0^{\omega_D/\Delta} \mathrm{d}x \, \frac{1}{\sqrt{1+x^2}} \\ &= \frac{V_0 D(\varepsilon_F)}{\Omega_{BZ}} \operatorname{arcsinh}(x)\Big|_0^{\omega_D/\Delta} = \frac{V_0 D(\varepsilon_F)}{\Omega_{BZ}} \operatorname{arcsinh}\left(\omega_D/\Delta\right) \quad . \end{aligned} \tag{2.2.24}$$

Henceforth, the gap amplitude at zero temperature is

$$\Delta(T=0) = \frac{\omega_D}{\sinh\left(\frac{\Omega_{BZ}}{V_0 D(\varepsilon_F)}\right)} = \omega_D \operatorname{csch}\left(\frac{\Omega_{BZ}}{V_0 D(\varepsilon_F)}\right) \overset{V_0 D(\varepsilon_F)\gg 1}{\downarrow \approx} 2\omega_D \exp\left(-\frac{\Omega_{BZ}}{V_0 D(\varepsilon_F)}\right) \quad . \tag{2.2.25}$$

Although it suffered from a lot of flaws and (crude) approximations, the Cooper problem calculation already correctly predicted the exponential dependency of the binding energy on the interaction and density of states at the Fermi level (cf. (Equation 2.1.17)), apart from the factor 2 that only arises in the Cooper calculation. Comparison with (Equation 2.2.22) provides a universal ratio of zero temperature gap to critical temperature, i.e.

$$\frac{\Delta(T=0)}{k_B T_C} = \frac{\pi}{e^\gamma} \approx 1.763\,88 \quad . \tag{2.2.26}$$

The behavior of the integrand in the gap equation in (Equation 2.2.23) and its dependency on temperature is shown in (Figure 2.3a). The temperature dependency of the gap amplitude on temperature and the illustration the zero temperature gap $\Delta(T=0)$ and the critical temperature T_C is displayed in (Figure 2.3b).

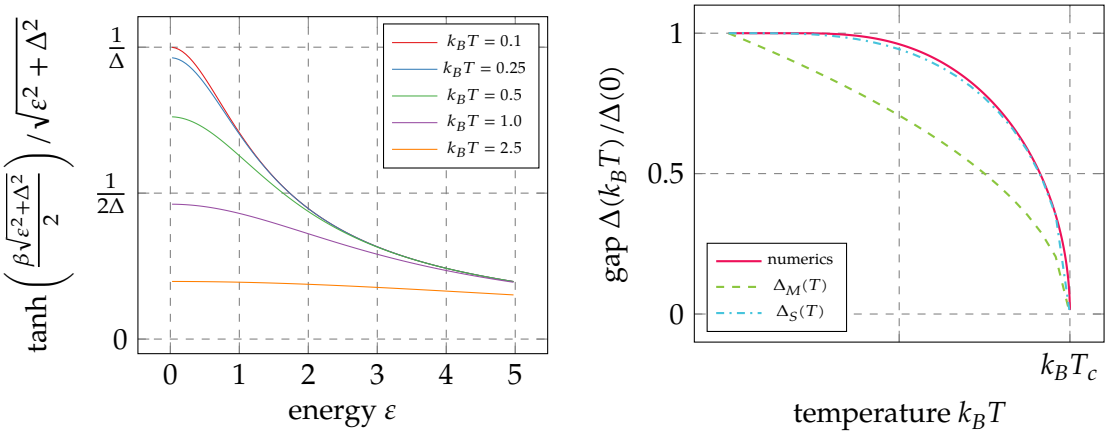

Figure 2.3.: (Figure 2.3a) The behavior of the integrand of the gap equation in (Equation 2.2.23) in terms of the energy is bell-shaped like and the integrand goes to zero for $\varepsilon \to \infty$. Increasing temperature renders the bell-shape more flat. This already suggests what $\Delta(T)$ must look like. (Figure 2.3b) The temperature dependency of the gap amplitude exhibits a zero derivative at zero temperature gap and an vertical tangent at the critical temperature T_C. While most literature uses a square root $\Delta_M(T) = \sqrt{1 - T/T_c}$ fit for the curve [Tin96, Chap. 3.6.2], the interpolation $\Delta_S(T) = \tanh\left(\frac{\pi}{e^\gamma}\sqrt{T_c/T - 1}\right)\Delta(0)$ provide a much better agreement [Fra].

2.3. Pairing due to repulsive interactions/Kohn-Luttinger effect

After having discussed the origin of the idea of *Cooper pairs* and the implications of the *conventional BCS-theory* on the superconducting state in (Section 2.1) and (Section 2.2), we proceed with pairing instabilities that are not due to *phonon exchange* and uniform effective interactions but due to purely electronic interactions. In contrast to the "phenomenological" BCS-theory that makes use of a "nonphysical effective potential to describe the complex Coulomb and phonon-induced interactions between electrons" [MA62], we will derive the exact form of the effective interactions of electronic origin from first principles. In particular, we will review the *Kohn-Luttinger effect* and see how pairing may arise from short-range repulsive interaction between electrons [KL65]. It was already noted by Anderson and Morel, who calculated the *critical temperature* including both phonon exchange and *Coulomb interaction*, that essentially all metals should become superconducting at sufficiently low temperatures [MA62]. However, the Kohn-Luttinger effect is independent of any phonon-electron interaction and shows that generically any *Fermi liquid* must become superconducting eventually when approaching zero temperature.
An isolated pair of electrons in the vacuum will naturally interact via a repulsive Coulomb potential of the form $\phi \sim +e^2/r$ with r being the distance between them. If we place an electron in a metal, the Coulomb potential will be strongly modified by *screening effects*

in the Fermi gas. This *linear response* of the electron gas to the (weak) disturbance by the electron charge can be described by the *Lindhard function* in the *static limit* [GV05; Lin54]

$$\lim_{\omega\to 0} \chi_\sigma(\mathbf{q},\omega) = -\int \mathrm{d}\mathbf{k}\, \frac{f(\varepsilon_{\mathbf{k}\sigma}) - f\left(\varepsilon_{\mathbf{k}+\mathbf{q}\sigma}\right)}{\varepsilon_{\mathbf{k}\sigma} - \varepsilon_{\mathbf{k}+\mathbf{q}\sigma}} \quad , \tag{2.3.1}$$

where $f(\varepsilon)$ is the *Fermi-Dirac function* and ε the single-particle energy of the electrons. The Lindhard function is most conveniently calculated by introducing a change of variables in the second term of (Equation 2.3.1) and making use of the rotational invariance for free electrons. [9]. The integration can be done analytically and results in the Lindhard functions

$$\chi_\sigma^{\mathrm{2D}}(|\mathbf{q}|) \sim 1 - \frac{\Theta(q-2k_F)}{q}\sqrt{q^2-(2k_F)^2} \qquad \chi_\sigma^{\mathrm{3D}}(|\mathbf{q}|) \sim k_F + \frac{k_F^2 - \left(\frac{q}{2}\right)^2}{q} \ln\frac{|q+2k_F|}{|q-2k_F|} \quad , \tag{2.3.2}$$

for free electrons in two and three dimensions at zero temperature. Their momentum dependency is shown in (Figure 2.4a). Since the Fermi surface is spherical, only the absolute value of $\mathbf{q}$ matters. Obviously, the Lindhard function in one, two and three dimensions shows a characteristic change of behavior at the momentum $|\mathbf{q}| = 2k_F$. However, we are interested in the real space structure of $\chi_\sigma(\mathbf{q})$, i.e. its Fourier transform $\chi_\sigma(\mathbf{r}) = (2\pi)^{-d/2}\int \mathrm{d}\mathbf{q}\; e^{-i\mathbf{q}\mathbf{r}}\chi_\sigma(\mathbf{q})$ with d being the dimension. $\chi_\sigma(\mathbf{r})$ exhibits a long-range oscillatory behavior that is referred to as *Friedel oscillations*. So far, we only considered the cloud of free electrons with spherical Fermi surface and ignored any lattice effects. Taking into account electrons living on a lattice will render the Fermi surface non-spherical and turn the continuous symmetry of the Lindhard function w.r.t. to rotations around the origin into a discrete symmetry that is determined by the lattice point group (cf. (Figure 2.4b)). Although we introduced the *susceptibility* $\chi_\sigma(\mathbf{q})$ as a result of linear response theory, it can as well be interpreted as one *particle-hole term* of the perturbative expansion of the two-particle vertex up to second order. Hence, $\chi_\sigma(\mathbf{q})$ also functions as a diagram contributing to the effective interaction between two electrons in the normal state. Assuming the only finite contribution to the two-particle interaction Γ to be the Lindhard function, we find $\Gamma_{\mathbf{k},-\mathbf{k};\mathbf{k}',-\mathbf{k}'} = U^2\chi(\mathbf{k}-\mathbf{k}')$ with U being the bare Coulomb repulsion. By making use of the attractive regions of the long-range oscillatory interaction, we may expect to obtain a pairing instability at sufficiently low temperatures. For a realistic normal state interaction the long-range oscillatory tail of the

[9] Renaming the summation variable $\mathbf{k} \to \mathbf{k}+\mathbf{q}$ in the second Fermi function, we find $-\int \mathrm{d}\mathbf{k}\; \frac{f(\varepsilon_{\mathbf{k}\sigma})-f(\varepsilon_{\mathbf{k}+\mathbf{q}\sigma})}{\varepsilon_{\mathbf{k}\sigma}-\varepsilon_{\mathbf{k}+\mathbf{q}\sigma}} = \int \mathrm{d}\mathbf{k}\; \left(\frac{f(\varepsilon_{\mathbf{k}\sigma})}{\varepsilon_{\mathbf{k}+\mathbf{q}\sigma}-\varepsilon_{\mathbf{k}\sigma}} - \frac{f(\varepsilon_{\mathbf{k}\sigma})}{\varepsilon_{\mathbf{k}\sigma}-\varepsilon_{\mathbf{k}-\mathbf{q}\sigma}}\right)$. For free electrons we have $\varepsilon_{\mathbf{k}} = \frac{\hbar^2}{2m}\mathbf{k}^2$ and get $\varepsilon_{\mathbf{k}\pm\mathbf{q}\sigma} - \varepsilon_{\mathbf{k}\sigma} = \frac{\hbar^2}{2m}\left(\pm 2\mathbf{k}\mathbf{q} + \mathbf{q}^2\right)$. At zero temperature, we are left with $\chi_\sigma(\mathbf{q},0) = \frac{2m}{\hbar^2}\int_{|\mathbf{k}|<k_F}\mathrm{d}\mathbf{k}\left(\frac{1}{\mathbf{q}^2+2\mathbf{k}\mathbf{q}} + \frac{1}{\mathbf{q}^2-2\mathbf{k}\mathbf{q}}\right) = \frac{2m}{\hbar^2}\int_{|\mathbf{k}|<k_F}\mathrm{d}\mathbf{k}\frac{2q^2}{q^4-4(\mathbf{k}\mathbf{q})^2}$, which reduces to an integration over $k = |\mathbf{k}|$ and the angle between $\mathbf{k}$ and $\mathbf{q}$, that is $\cos(\theta(\mathbf{k},\mathbf{q}))$ (cf. [Mih11]).

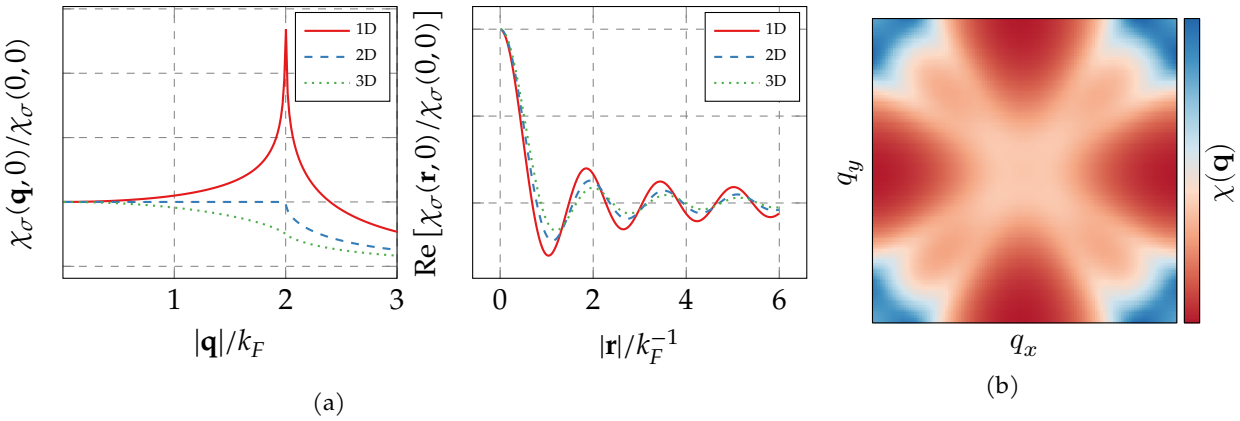

(a) (b)

Figure 2.4.: (Figure 2.4a) The Lindhard function $\chi_\sigma(\mathbf{q})$ for free electrons exhibits a characteristic cusp at the momentum $2k_F$ in all dimensions. Its Fourier transform $\chi_\sigma(\mathbf{r})$ has a long-range oscillatory behavior that is referred to as *Friedel oscillations* [SG05]. (Figure 2.4b) The Lindhard function of the extended two-dimensional Hubbard model on the square lattice with $\varepsilon_{\mathbf{k}} = -2t\left(\cos(k_x) + \cos\left(k_y\right)\right) - 4t' \cos(k_x)\cos\left(k_y\right) - \mu$ and the parameters $t = 1.0$, $t' = -0.1$, $\mu = -0.25$ for nearest, next nearest neighbor hopping and chemical potential demonstrates how the *continuous symmetry* of $\chi(\mathbf{q})$ w.r.t. to the polar angle breaks down to a *discrete symmetry* given by the lattice point group.

interaction is expected to decay more slowly than the bare direct Coulomb repulsion. Therefore, it seems reasonable to assume that a pairing instability arises in a angular momentum channel with $L > 0$.

After having captured the general idea we want to proceed to some more detailed statements about the superconducting instabilities arising from repulsive short range interaction in particular in two dimensions. The original treatment of Kohn and Luttinger calculated and found the *logarithmic divergence* of the effect exclusively in three dimensions. About twenty years later, after the rise of the high temperature superconductors, the interest in the two dimensional version came about. Although, the effect was believed to be absent in two dimension (due to the fact that the Lindhard function is constant for momentum transfers smaller than twice the Fermi momentum $q < 2k_F$, which can only give rise to s-wave symmetry pairing with $L = 0$), it was shown that higher order terms actually can generate attractive regions in the effective interaction giving rise to pairing instabilities with higher orbital angular momentum [Chu93]. The general procedure is to calculate the diagrams up to second order contributing to the interaction and to analyze the resulting effective two-particle vertex by expanding it in terms of orbital angular momentum eigenfunctions. Kohn and Luttinger only claimed that the coefficients of this expansion corresponding to odd angular momentum L must be negative and therefore trigger an instability. However, it has been shown that the scattering amplitudes may be attractive independent of L, where L can be any (higher) angular momentum. In (Chapter 5) we will return to this idea in a more formal way by explicitly finding and calculating all contributing diagrams as well as generalizing the

approach to multiple orbitals and the spin degree of freedom. By introducing the idea of *logarithmic renormalization* to this perturbative treatment, we are able to give explicit expressions for the *critical temperature*. On the contrary, one has to keep in mind, that these calculations may only be employed to infinitesimal weak bare interactions, which is mostly not the case for modern strongly correlated electrons systems of current interest.

2.4. Generalized multi-band BCS-theory

Hitherto, we introduced Cooper pairing in the two-particle angular momentum channel $L = 0$ (s-wave) (Section 2.1), worked out the corresponding BCS-theory (Section 2.2) and motivated the extension to higher angular momentum pairing $L > 0$ by the idea of Kohn-Luttinger, which may provide the microscopic mechanism for such Cooper states (Section 2.3). In order to unify and generalize these concepts we introduce an *effective interaction* that depends on momentum and band indices, since an $L = 1$ state requires antisymmetry in the spatial domain, making k-dependency inevitable (assuming intra-band pairing). BCS-theory relies on the validity of the approximation that the effective interaction that is responsible for the formation of Cooper pairs is the only relevant interaction of the Fermi liquid [And84b]. Therefore, the corresponding Hamiltonian is denoted by

$$\mathcal{H} = \sum_{\mathbf{k},b,\tilde{\sigma}} \underbrace{(\varepsilon_{\mathbf{k}b\tilde{\sigma}} - \mu)}_{:=\xi_{\mathbf{k}b\tilde{\sigma}}} c^{\dagger}_{\mathbf{k}b\tilde{\sigma}} c_{\mathbf{k}b\tilde{\sigma}} + \sum_{\mathbf{k},\mathbf{k}'} \sum_{b,b'} \sum_{\substack{\tilde{\sigma}_1,\tilde{\sigma}_2 \\ \tilde{\sigma}'_1,\tilde{\sigma}'_2}} U^{b,\tilde{\sigma}_1,b,\tilde{\sigma}_2,b',\tilde{\sigma}'_1,b',\tilde{\sigma}'_2}_{\mathbf{k},-\mathbf{k},\mathbf{k}',-\mathbf{k}'} c^{\dagger}_{\mathbf{k}b\tilde{\sigma}_1} c^{\dagger}_{-\mathbf{k}b\tilde{\sigma}_2} c_{-\mathbf{k}'b'\tilde{\sigma}'_2} c_{\mathbf{k}'b'\tilde{\sigma}'_1} \quad , \tag{2.4.1}$$

where the quantum numbers $\mathbf{k}$, b and $\tilde{\sigma}$ refer to momentum, band and (pseudo)spin. For the definition of *pseudospin* we refer to the case of centrosymmetric spin-orbit coupling and (Section 3.2). Introducing the concept of pseudospin allows us to employ the following results for spin-rotation symmetric as well as centrosymmetric spin-orbit models by simply replacing spin σ with the pseudospin label $\tilde{\sigma}$ and vice versa. In both cases, we can actually drop the (pseudo)spin index in the single-particle term, i.e. $\varepsilon_{\mathbf{k}b\tilde{\sigma}} = \varepsilon_{\mathbf{k}b}$, since we assume spin degeneracy. Although we start from a band basis we could equally well employ an orbital basis, that, however, would disguise equal-energy pairs, which we want to restrict our analysis to. Note that, although we have only two different momenta we may have all kinds of (pseudo)spin combinations arising in the interaction term in contrast to *conventional BCS-theory* as this only takes into account *time-reversal* partner states. As long as we restrict our analysis to *equal energy pairing*, a single Cooper pair must be hosted by a single band in order to make sure that the Cooper pair's constituents are energetically degenerate. Therefore, only two different band indices b and b' arise in the interaction term (Equation 2.4.1). Later within this section, we will briefly discuss the possibility of interband pairing and the exotic symmetries it gives rise to (see (Table 2.1)). The (effective) interaction must satisfy the

constraints of *fermionic antisymmetry*

$$U^{b,\tilde{\sigma}_1,b,\tilde{\sigma}_2,b',\tilde{\sigma}'_1,b',\tilde{\sigma}'_2}_{\mathbf{k},-\mathbf{k},\mathbf{k}',-\mathbf{k}'} = -U^{b,\tilde{\sigma}_2,b,\tilde{\sigma}_1,b',\tilde{\sigma}'_1,b',\tilde{\sigma}'_2}_{-\mathbf{k},\mathbf{k},\mathbf{k}',-\mathbf{k}'} = -U^{b,\tilde{\sigma}_1,b,\tilde{\sigma}_2,b',\tilde{\sigma}'_2,b',\tilde{\sigma}'_1}_{\mathbf{k},-\mathbf{k},-\mathbf{k}',\mathbf{k}'} = +U^{b,\tilde{\sigma}_2,b,\tilde{\sigma}_1,b',\tilde{\sigma}'_2,b',\tilde{\sigma}'_1}_{-\mathbf{k},\mathbf{k},-\mathbf{k}',\mathbf{k}'} \quad , \tag{2.4.2}$$

and *self-adjointness*

$$U^{b,\tilde{\sigma}_1,b,\tilde{\sigma}_2,b',\tilde{\sigma}'_1,b',\tilde{\sigma}'_2}_{\mathbf{k},-\mathbf{k},\mathbf{k}',-\mathbf{k}'} = \overline{U^{b',\tilde{\sigma}'_1,b',\tilde{\sigma}'_2,b,\tilde{\sigma}_1,b,\tilde{\sigma}_2}_{\mathbf{k}',-\mathbf{k}',\mathbf{k},-\mathbf{k}}} \quad . \tag{2.4.3}$$

where we exchanged the pair of "outgoing" with the pair of "incoming" particles. The bar denotes complex conjugation $z = a + ib \to \bar{z} = a - ib$. Note, that these requirements for the interaction vertex must be satisfied independent a single or multi-band model, spin rotation symmetry or the specific basis the Hamiltonian is given in.

2.4.1. Self-consistent BCS mean-field theory

In the spirit of finite "off-diagonal" expectation values we define the *mean-fields*

$$f_{\mathbf{k}b\tilde{\sigma}\tilde{\sigma}'} := \langle c_{-\mathbf{k}b\tilde{\sigma}} c_{\mathbf{k}b\tilde{\sigma}'} \rangle \qquad \overline{f_{\mathbf{k}b\tilde{\sigma}\tilde{\sigma}'}} := \left\langle c^\dagger_{\mathbf{k}b\tilde{\sigma}} c^\dagger_{-\mathbf{k}b\tilde{\sigma}'} \right\rangle \quad , \tag{2.4.4}$$

that feature arbitary (pseudo)spin combinations of $\tilde{\sigma}$ and $\tilde{\sigma}'$ and are used to approximate the interaction term (in (Equation 2.4.1)) by neglecting all terms quadratic in the fluctuations $\delta_{\mathbf{k}b\tilde{\sigma}\tilde{\sigma}'} := c_{-\mathbf{k}b\tilde{\sigma}} c_{\mathbf{k}b\tilde{\sigma}'} - f_{\mathbf{k}b\tilde{\sigma}\tilde{\sigma}'}$ (and its adjoint $\delta^\dagger_{\mathbf{k}b\tilde{\sigma}\tilde{\sigma}'} := c^\dagger_{\mathbf{k}b\tilde{\sigma}} c^\dagger_{-\mathbf{k}b\tilde{\sigma}'} - \overline{f_{\mathbf{k}b\tilde{\sigma}'\tilde{\sigma}}}$) that are assumed to be small, i.e.

$$\begin{aligned} c^\dagger_{\mathbf{k}b\tilde{\sigma}_1} c^\dagger_{-\mathbf{k}b\tilde{\sigma}_2} c_{-\mathbf{k}'b'\tilde{\sigma}'_2} c_{\mathbf{k}'b'\tilde{\sigma}'_1} &= \left(\overline{f_{\mathbf{k}b\tilde{\sigma}_2\tilde{\sigma}_1}} + \delta^\dagger_{\mathbf{k}b\tilde{\sigma}_1\tilde{\sigma}_2}\right)\left(f_{\mathbf{k}'b'\tilde{\sigma}'_2\tilde{\sigma}'_1} + \delta_{\mathbf{k}'b'\tilde{\sigma}'_2\tilde{\sigma}'_1}\right) \\ &= \overline{f_{\mathbf{k}b\tilde{\sigma}_2\tilde{\sigma}_1}} f_{\mathbf{k}'b'\tilde{\sigma}'_2\tilde{\sigma}'_1} + \overline{f_{\mathbf{k}b\tilde{\sigma}_2\tilde{\sigma}_1}} \delta_{\mathbf{k}'b'\tilde{\sigma}'_2\tilde{\sigma}'_1} + \delta^\dagger_{\mathbf{k}b\tilde{\sigma}_1\tilde{\sigma}_2} f_{\mathbf{k}'b'\tilde{\sigma}'_2\tilde{\sigma}'_1} + \underbrace{\delta^\dagger_{\mathbf{k}b\tilde{\sigma}_1\tilde{\sigma}_2} \delta_{\mathbf{k}'b'\tilde{\sigma}'_2\tilde{\sigma}'_1}}_{\ll 1} \\ &\approx \underbrace{-\overline{f_{\mathbf{k}b\tilde{\sigma}_2\tilde{\sigma}_1}} f_{\mathbf{k}'b'\tilde{\sigma}'_2\tilde{\sigma}'_1}}_{\in\mathbb{C}} + \overline{f_{\mathbf{k}b\tilde{\sigma}_2\tilde{\sigma}_1}} c_{-\mathbf{k}'b'\tilde{\sigma}'_2} c_{\mathbf{k}'b'\tilde{\sigma}'_1} + c^\dagger_{\mathbf{k}b\tilde{\sigma}_1} c^\dagger_{-\mathbf{k}b\tilde{\sigma}_2} f_{\mathbf{k}'b'\tilde{\sigma}'_2\tilde{\sigma}'_1} \end{aligned} \tag{2.4.5}$$

While (Equation 2.4.5) provides a fairly intuitive derivation of the mean-field approximation to the interaction term, a mathematically more rigorous solution is to rewrite the theory in terms of a *path integral* formulation, employ a *Hubbard-Stratonovich* transformation and use the *saddle-point approximation* to find the mean-fields [Kar07]. This then shows, that the fluctuations around the mean-fields actually scale intensively with the volume and therefore vanish in the thermodynamic limit [Col15, Chapter 14.3]. We insert (Equation 2.4.5) in (Equation 2.4.1) to get rid of the two-particle term and end up with the mean-field *BCS Hamiltonian* [10]

[10] In particular, we took (Equation 2.4.1) and did

$$\mathcal{H}_{BCS} = \sum_{\mathbf{k},b,\tilde{\sigma}} \xi_{\mathbf{k}b\tilde{\sigma}}\, c^{\dagger}_{\mathbf{k}b\tilde{\sigma}} c_{\mathbf{k}b\tilde{\sigma}} + \frac{1}{2}\sum_{\mathbf{k},b}\sum_{\tilde{\sigma},\tilde{\sigma}'} \left(\overline{\Delta_{\mathbf{k}b\tilde{\sigma}'\tilde{\sigma}}}\, c_{-\mathbf{k}b\tilde{\sigma}} c_{\mathbf{k}b\tilde{\sigma}'} + \Delta_{\mathbf{k}b\tilde{\sigma}\tilde{\sigma}'}\, c^{\dagger}_{\mathbf{k}b\tilde{\sigma}} c^{\dagger}_{-\mathbf{k}b\tilde{\sigma}'} \right) \quad , \tag{2.4.7}$$

where we neglected the complex number and defined the *gap function*

$$\Delta_{\mathbf{k}b\tilde{\sigma}_1\tilde{\sigma}_2} := -2\sum_{\mathbf{k}',b'}\sum_{\tilde{\sigma}'_1,\tilde{\sigma}'_2} U^{b,\tilde{\sigma}_1,b,\tilde{\sigma}_2,b',\tilde{\sigma}'_2,b',\tilde{\sigma}'_1}_{\mathbf{k},-\mathbf{k},-\mathbf{k}',\mathbf{k}'} f_{\mathbf{k}'b'\tilde{\sigma}'_2\tilde{\sigma}'_1} \overset{\text{(Equation 2.4.2)}}{\underset{\downarrow}{=}} 2\sum_{\mathbf{k}',b'}\sum_{\tilde{\sigma}'_1,\tilde{\sigma}'_2} U^{b,\tilde{\sigma}_1,b,\tilde{\sigma}_2,b',\tilde{\sigma}'_1,b',\tilde{\sigma}'_2}_{\mathbf{k},-\mathbf{k},\mathbf{k}',-\mathbf{k}'} f_{\mathbf{k}'b'\tilde{\sigma}'_2\tilde{\sigma}'_1} \quad , \tag{2.4.8}$$

and its adjoint

$$\begin{aligned}\overline{\Delta_{\mathbf{k}b\tilde{\sigma}_1\tilde{\sigma}_2}} &= -2\sum_{\mathbf{k}',b'}\sum_{\tilde{\sigma}'_1,\tilde{\sigma}'_2} \overline{U^{b,\tilde{\sigma}_1,b,\tilde{\sigma}_2,b',\tilde{\sigma}'_2,b',\tilde{\sigma}'_1}_{\mathbf{k},-\mathbf{k},-\mathbf{k}',\mathbf{k}'}}\, \overline{f_{\mathbf{k}'b'\tilde{\sigma}'_2\tilde{\sigma}'_1}} \\ &\overset{\text{(Equation 2.4.2) and (Equation 2.4.3)}}{\underset{\downarrow}{=}} 2\sum_{\mathbf{k}',b'}\sum_{\tilde{\sigma}'_1,\tilde{\sigma}'_2} U^{b',\tilde{\sigma}'_1,b',\tilde{\sigma}'_2,b,\tilde{\sigma}_1,b,\tilde{\sigma}_2}_{\mathbf{k}',-\mathbf{k}',\mathbf{k},-\mathbf{k}} \overline{f_{\mathbf{k}'b'\tilde{\sigma}'_2\tilde{\sigma}'_1}} \quad . \end{aligned} \tag{2.4.9}$$

We introduced the seemingly arbitrary factor -2 to allow for a more convenient notation in terms of *Nambu spinors* . Since $\Delta_{\mathbf{k},b,\tilde{\sigma}_1,\tilde{\sigma}_2}$ will become the main focus of our discussion we will make some remarks about its definition. In contrast to the gap function of the conventional BCS-theory (Equation 2.4.8), it has additional indices that not only introduce a (possible) momentum dependency but also a dependency on band and (pseudo)spin indices. Furthermore, the gap function may even not be diagonal in (pseudo)spin space which allows for the occurrence of any singlet or triplet state (but *not* a mixture of both, since we keep inversion symmetry, so far (see (Section 3.4))). In order to diagonalize the BCS-Hamiltonian and determine the its eigenmodes we employ

---

$$\begin{aligned}&\sum_{\substack{\mathbf{k},b\\ \tilde{\sigma}_1,\tilde{\sigma}_2}}\sum_{\substack{\mathbf{k}',b'\\ \tilde{\sigma}'_1,\tilde{\sigma}'_2}} U^{b,\tilde{\sigma}_1,b,\tilde{\sigma}_2,b',\tilde{\sigma}'_1,b',\tilde{\sigma}'_2}_{\mathbf{k},-\mathbf{k},\mathbf{k}',-\mathbf{k}'} \left(-\overline{f_{\mathbf{k}b\tilde{\sigma}_2\tilde{\sigma}_1}} f_{\mathbf{k}'b'\tilde{\sigma}'_2\tilde{\sigma}'_1} + \overline{f_{\mathbf{k}b\tilde{\sigma}_2\tilde{\sigma}_1}} c_{-\mathbf{k}'b'\tilde{\sigma}'_2} c_{\mathbf{k}'b'\tilde{\sigma}'_1} + c^{\dagger}_{\mathbf{k}b\tilde{\sigma}_1} c^{\dagger}_{-\mathbf{k}b\tilde{\sigma}_2} f_{\mathbf{k}'b'\tilde{\sigma}'_2\tilde{\sigma}'_1} \right) \\ &\quad = \underbrace{-\sum_{\substack{\mathbf{k},b\\ \tilde{\sigma}_1,\tilde{\sigma}_2}}\sum_{\substack{\mathbf{k}',b'\\ \tilde{\sigma}'_1,\tilde{\sigma}'_2}} U^{b,\tilde{\sigma}_1,b,\tilde{\sigma}_2,b',\tilde{\sigma}'_1,b',\tilde{\sigma}'_2}_{\mathbf{k},-\mathbf{k},\mathbf{k}',-\mathbf{k}'} \overline{f_{\mathbf{k}b\tilde{\sigma}_2\tilde{\sigma}_1}} f_{\mathbf{k}'b'\tilde{\sigma}'_2\tilde{\sigma}'_1}}_{:=\mathcal{K}\in\mathbb{C}} + \sum_{\substack{\mathbf{k}',b'\\ \tilde{\sigma}'_1,\tilde{\sigma}'_2}} \underbrace{\sum_{\substack{\mathbf{k},b\\ \tilde{\sigma}_1,\tilde{\sigma}_2}} U^{b,\tilde{\sigma}_1,b,\tilde{\sigma}_2,b',\tilde{\sigma}'_1,b',\tilde{\sigma}'_2}_{\mathbf{k},-\mathbf{k},\mathbf{k}',-\mathbf{k}'} \overline{f_{\mathbf{k}b\tilde{\sigma}_2\tilde{\sigma}_1}}}_{=\frac{1}{2}\overline{\Delta_{\mathbf{k}'b'\tilde{\sigma}'_1\tilde{\sigma}'_2}}} c_{-\mathbf{k}'b'\tilde{\sigma}'_2} c_{\mathbf{k}'b'\tilde{\sigma}'_1} \\ &\quad + \sum_{\substack{\mathbf{k},b\\ \tilde{\sigma}_1,\tilde{\sigma}_2}} \underbrace{\sum_{\substack{\mathbf{k}',b'\\ \tilde{\sigma}'_1,\tilde{\sigma}'_2}} U^{b,\tilde{\sigma}_1,b,\tilde{\sigma}_2,b',\tilde{\sigma}'_1,b',\tilde{\sigma}'_2}_{\mathbf{k},-\mathbf{k},\mathbf{k}',-\mathbf{k}'} f_{\mathbf{k}'b'\tilde{\sigma}'_2\tilde{\sigma}'_1}}_{=\frac{1}{2}\Delta_{\mathbf{k}b\tilde{\sigma}_1\tilde{\sigma}_2}} c^{\dagger}_{\mathbf{k}b\tilde{\sigma}_1} c^{\dagger}_{-\mathbf{k}b\tilde{\sigma}_2} \quad , \end{aligned} \tag{2.4.6}$$

where we note that in the second term of the right hand side the (pseudo)spin indices of the gap function $\overline{\Delta_{\mathbf{k}'b'}}$ have the reversed order w.r.t. their operator basis to ensure the Hermiticity of the Hamiltonian.

the Nambu formalism and get

$$\mathcal{H}_{BCS} = \frac{1}{2}\sum_{\mathbf{k},b} \mathbf{C}^{\dagger}_{\mathbf{k}b} \begin{pmatrix} \xi_{\mathbf{k}b\tilde{\uparrow}} & 0 & \Delta_{\mathbf{k}b\tilde{\uparrow}\tilde{\uparrow}} & \Delta_{\mathbf{k}b\tilde{\uparrow}\tilde{\downarrow}} \\ 0 & \xi_{\mathbf{k}b\tilde{\downarrow}} & \Delta_{\mathbf{k}b\tilde{\downarrow}\tilde{\uparrow}} & \Delta_{\mathbf{k}b\tilde{\downarrow}\tilde{\downarrow}} \\ \Delta_{\mathbf{k}b\tilde{\uparrow}\tilde{\uparrow}} & \Delta_{\mathbf{k}b\tilde{\downarrow}\tilde{\uparrow}} & -\xi_{\mathbf{k}b\tilde{\uparrow}} & 0 \\ \Delta_{\mathbf{k}b\tilde{\uparrow}\tilde{\downarrow}} & \Delta_{\mathbf{k}b\tilde{\downarrow}\tilde{\downarrow}} & 0 & -\xi_{\mathbf{k}b\tilde{\downarrow}} \end{pmatrix} \mathbf{C}_{\mathbf{k}b} - \mathcal{K} \quad , \tag{2.4.10}$$

where we defined

$$\mathbf{C}^{\dagger}_{\mathbf{k}b} := \left(c^{\dagger}_{\mathbf{k}b\tilde{\uparrow}}, c^{\dagger}_{\mathbf{k}b\tilde{\downarrow}}, c_{-\mathbf{k}b\tilde{\uparrow}}, c_{-\mathbf{k},b\tilde{\downarrow}}\right)^{T} \quad . \tag{2.4.11}$$

and the constant complex number (cf. (Equation 2.4.6))

$$\mathcal{K} := \sum_{\substack{\mathbf{k},b \\ \tilde{\sigma}_1,\tilde{\sigma}_2}} \sum_{\substack{\mathbf{k}',b' \\ \tilde{\sigma}'_1,\tilde{\sigma}'_2}} U^{b,\tilde{\sigma}_1,b,\tilde{\sigma}_2,b',\tilde{\sigma}'_1,b',\tilde{\sigma}'_2}_{\mathbf{k},-\mathbf{k},\mathbf{k}',-\mathbf{k}'} \overline{f_{\mathbf{k}b\tilde{\sigma}_2\tilde{\sigma}_1}} f_{\mathbf{k}'b'\tilde{\sigma}'_2\tilde{\sigma}'_1} \quad , \tag{2.4.12}$$

which eventually vanishes for particular symmetries and structures of the gap function. We denoted the particular (pseudo)spin degrees of freedom by $\tilde{\sigma} \in \{\tilde{\uparrow}, \tilde{\downarrow}\}$ instead of the purely "natural" spin $\sigma \in \{\uparrow, \downarrow\}$ as the single-particle Hamiltonian may feature off-diagonal elements in spin space. For the sake of simplicity in (Equation 2.4.10) and to more conveniently discuss the gap function we introduce the notation

$$\Delta_{\mathbf{k}b} := \begin{pmatrix} \Delta_{\mathbf{k}b\tilde{\uparrow}\tilde{\uparrow}} & \Delta_{\mathbf{k}b\tilde{\uparrow}\tilde{\downarrow}} \\ \Delta_{\mathbf{k}b\tilde{\downarrow}\tilde{\uparrow}} & \Delta_{\mathbf{k}b\tilde{\downarrow}\tilde{\downarrow}} \end{pmatrix} \qquad \xi_{\mathbf{k}b} := \begin{pmatrix} \xi_{\mathbf{k}b\tilde{\uparrow}} & 0 \\ 0 & \xi_{\mathbf{k}b\tilde{\downarrow}} \end{pmatrix} \quad , \tag{2.4.13}$$

for the spinful gap function and the single-particle dispersion relation. Therefore, (Equation 2.4.10) becomes

$$\mathcal{H}_{BCS} = \frac{1}{2}\sum_{\mathbf{k},b} \mathbf{C}^{\dagger}_{\mathbf{k}b} \begin{pmatrix} \xi_{\mathbf{k}b} & \Delta_{\mathbf{k}b} \\ \Delta^{\dagger}_{\mathbf{k}b} & -\xi_{\mathbf{k}b} \end{pmatrix} \mathbf{C}_{\mathbf{k}b} - \mathcal{K} \quad . \tag{2.4.14}$$

Now, we are able to establish a proper definition of the expectation value for the mean-fields introduced in (Equation 2.4.4),

$$f_{\mathbf{k}b\tilde{\sigma}\tilde{\sigma}'} = \langle c_{-\mathbf{k}b\tilde{\sigma}} c_{\mathbf{k}b\tilde{\sigma}'} \rangle := \frac{\mathrm{Tr}\left(c_{-\mathbf{k}b\tilde{\sigma}} c_{\mathbf{k}b\tilde{\sigma}'} e^{-\beta\mathcal{H}_{BCS}}\right)}{\mathrm{Tr}\left(e^{-\beta\mathcal{H}_{BCS}}\right)} \quad , \tag{2.4.15}$$

which was evaluated in (Section 2.2) in the context of conventional BCS-theory by (analytically) calculating the eigenstates of the Bogoliubov-de Gennes Hamiltonian (Equa-

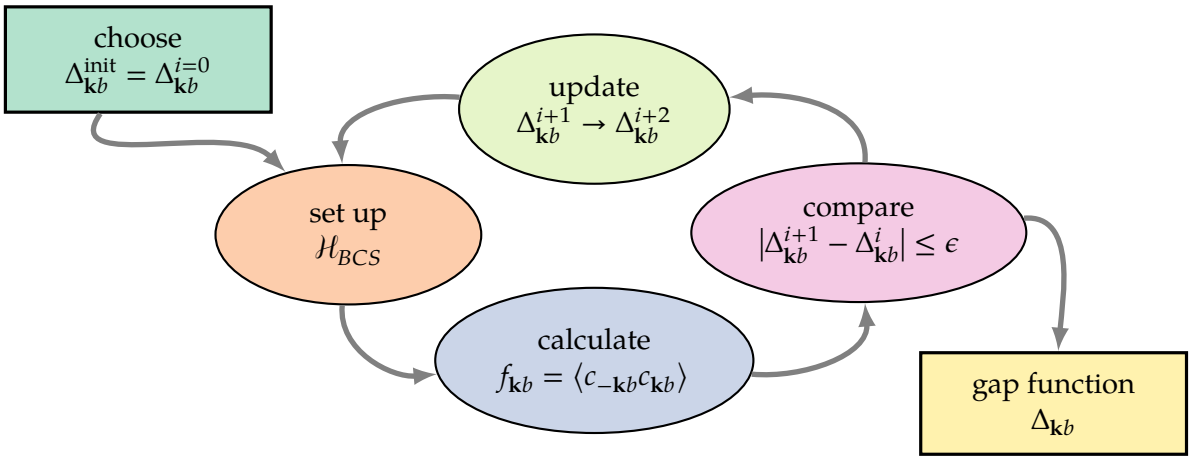

Figure 2.5.

Figure 2.6.: In order to find the gap function $\Delta_{\mathbf{k},b}$ we set up a *self-consistent* loop that makes sure that the BCS-Hamiltonian built from the gap function actually produces the exact same gap function as its off-diagonal expectation value. In principle, we may choose an arbitary initial gap function. However, by chosing an eigenvector of the Cooper pair interaction the convergence process is greatly accelerated. This gap function is used to set up the BCS-Hamiltonian (Equation 2.4.14) and to determine the actual expectation value (Equation 2.4.15) from it, which is compared to the initial gap function. Depending on its derivation from the previous one, it is adjusted and reinserted in the BCS-Hamiltonian until the deviation between two succeeding gap functions drops below some threshold ϵ.

tion 2.4.10) and expressing the off-diagonal expectation value (Equation 2.4.15) in terms of eigenstate operators that can be combined to number operators of the new quasiparticles.

2.4.2. Quasiparticle states

Although, we can evaluate the expectation value (Equation 2.4.15) numerically in a straightforward fashion in terms of the fermionic particle basis $c^\dagger_{\mathbf{k}b\tilde{\sigma}}$, $c^\dagger_{-\mathbf{k}b\tilde{\sigma}'}$, it is more stable and elegant to employ the eigenstates of $\mathcal{H}_{BCS}$, i.e. the new quasiparticle operators. Following up on (Equation 2.4.14), we denote the energy of the quasiparticles by $E_{\mathbf{k}b}$ and use

$$h_{\text{BCS}} := \begin{pmatrix} \xi_{\mathbf{k}b} & \Delta_{\mathbf{k}b} \\ \Delta^\dagger_{\mathbf{k}b} & -\xi_{\mathbf{k}b} \end{pmatrix} \quad (h_{\text{BCS}} - E_{\mathbf{k}b}\mathbb{1}_{4\times4}) = \begin{pmatrix} \xi_{\mathbf{k}b} - E_{\mathbf{k}b}\sigma_0 & \Delta_{\mathbf{k}b} \\ \Delta^\dagger_{\mathbf{k}b} & -\xi_{\mathbf{k}b} - E_{\mathbf{k}b}\sigma_0 \end{pmatrix} \quad , \quad (2.4.16)$$

where σ_0 is the zeroth Pauli matrix. The determinant of a block matrix $M = \begin{pmatrix} A & B \\ C & D \end{pmatrix}$

can be evaluated to $\det M = \det(AD - BC)$ as long as C and D commute, i.e. $[C, D] = 0$ [Sil00]. Since the single particle spectrum $\xi_{\mathbf{k}b}$ is spin-degenerate, $\xi_{\mathbf{k}b\tilde{\uparrow}} = \xi_{\mathbf{k}b\tilde{\downarrow}}$, we have $\xi_{\mathbf{k}b} \sim \sigma_0$ and therefore $\xi_{\mathbf{k}b}$ commutes with the gap function $\Delta_{\mathbf{k}b}$. Henceforth, the *characteristic polynomial* is given by (in the following we use $\xi_{\mathbf{k}b}$ interchangeable to denote both the 2×2-matrix and the scalar quantity $\xi_{\mathbf{k}b\tilde{\uparrow}} = \xi_{\mathbf{k}b\tilde{\downarrow}}$)

$$\begin{aligned}
&\det\left(h_{\mathrm{BCS}} - E_{\mathbf{k}b}\mathbb{1}_{4\times4}\right) = \det\left[\left(\xi_{\mathbf{k}b} - E_{\mathbf{k}b}\sigma_0\right)\left(-\xi_{\mathbf{k}b} - E_{\mathbf{k}b}\sigma_0\right) - \Delta_{\mathbf{k}b}\Delta_{\mathbf{k}b}^{\dagger}\right] \\
&= \det\left[\left(-\xi_{\mathbf{k}b}^2 + E_{\mathbf{k}b}^2\right)\sigma_0 - \begin{pmatrix} \left|\Delta_{\mathbf{k}b\tilde{\uparrow}\tilde{\uparrow}}\right|^2 - \left|\Delta_{\mathbf{k}b\tilde{\uparrow}\tilde{\downarrow}}\right|^2 & \Delta_{\mathbf{k}b\tilde{\uparrow}\tilde{\uparrow}}\overline{\Delta_{\mathbf{k}b\tilde{\downarrow}\tilde{\uparrow}}}\Delta_{\mathbf{k}b\tilde{\uparrow}\tilde{\downarrow}}\overline{\Delta_{\mathbf{k}b\tilde{\downarrow}\tilde{\downarrow}}} \\ \Delta_{\mathbf{k}b\tilde{\downarrow}\tilde{\uparrow}}\overline{\Delta_{\mathbf{k}b\tilde{\uparrow}\tilde{\uparrow}}}\Delta_{\mathbf{k}b\tilde{\downarrow}\tilde{\downarrow}}\overline{\Delta_{\mathbf{k}b\tilde{\uparrow}\tilde{\downarrow}}} & \left|\Delta_{\mathbf{k}b\tilde{\downarrow}\tilde{\uparrow}}\right|^2 - \left|\Delta_{\mathbf{k}b\tilde{\downarrow}\tilde{\downarrow}}\right|^2 \end{pmatrix}\right] \\
&= \left(-\xi_{\mathbf{k}b}^2 + E_{\mathbf{k}b}^2\right)^2 - \left(-\xi_{\mathbf{k}b}^2 + E_{\mathbf{k}b}^2\right)\mathrm{Tr}\left(\Delta_{\mathbf{k}b}\Delta_{\mathbf{k}b}^{\dagger}\right) + \det\left(\Delta_{\mathbf{k}b}\Delta_{\mathbf{k}b}^{\dagger}\right) \\
&\stackrel{!}{=} 0 \quad ,
\end{aligned} \tag{2.4.17}$$

where the trace Tr refers to the sum of diagonal elements. Note, that this equation has four algebraic solutions, in general. Solving successively for $\left(-\xi_{\mathbf{k}b}^2 + E_{\mathbf{k}b}^2\right)$ and the quasiparticle energy $E_{\mathbf{k}b}$ provides (inserting the factor $1/2$ from (Equation 2.4.14) by rescaling $E_{\mathbf{k}b}$)

$$E_{\mathbf{k}b} = \pm\frac{1}{2}\sqrt{\xi_{\mathbf{k}b}^2 + \frac{1}{2}\mathrm{Tr}\left(\Delta_{\mathbf{k}b}\Delta_{\mathbf{k}b}^{\dagger}\right) \pm \sqrt{\left(\frac{1}{2}\mathrm{Tr}\left(\Delta_{\mathbf{k}b}\Delta_{\mathbf{k}b}^{\dagger}\right)\right)^2 - \det\left(\Delta_{\mathbf{k}b}\Delta_{\mathbf{k}b}^{\dagger}\right)}} \quad . \tag{2.4.18}$$

In the theory of unconventional superconductivity one distinguishes two types of gap functions: *unitary* and *non-unitary* gaps [SAM05]. In the case of a *unitary gap function* we have $\Delta_{\mathbf{k}b}\Delta_{\mathbf{k}b}^{\dagger} \propto \sigma_0$, the matrix $\Delta_{\mathbf{k}b}\Delta_{\mathbf{k}b}^{\dagger}$ has no off-diagonal elements and consequently $\left(\frac{1}{2}\mathrm{Tr}\left(\Delta_{\mathbf{k}b}\Delta_{\mathbf{k}b}^{\dagger}\right)\right)^2 = \det\left(\Delta_{\mathbf{k}b}\Delta_{\mathbf{k}b}^{\dagger}\right)$. Therefore, (Equation 2.4.18) simplifies to the two quasiparticle energy eigenvalues

$$E_{\mathbf{k}b} = \pm\frac{1}{2}\sqrt{\xi_{\mathbf{k}b}^2 + \frac{1}{2}\mathrm{Tr}\left(\Delta_{\mathbf{k}b}\Delta_{\mathbf{k}b}^{\dagger}\right)} \quad . \tag{2.4.19}$$

While the unitary superconductor has only two branches of quasiparticle energies like in the conventional BCS-theory (Section 2.2), the non-unitary gap splits these eigenvalues further into two more bands.

For a unitary gap, we can determine the analytical eigenstates associated to (Equation 2.4.19) by making the ansatz

$$U_{\mathbf{k}b} = \begin{pmatrix} u_{\mathbf{k}b} & v_{\mathbf{k}b} \\ \overline{v}_{-\mathbf{k}b} & \overline{u}_{-\mathbf{k}b} \end{pmatrix} \quad \in \mathbb{C}^{4\times4} \quad \text{where} \quad u_{\mathbf{k}b}, v_{\mathbf{k}b} \in \mathbb{C}^{2\times2} \quad , \tag{2.4.20}$$

with the requirement $U_{\mathbf{k}b}^{\dagger}U_{\mathbf{k}b} = \mathbb{1}_{4\times4}$ that ensures that the new quasiparticles fulfill

fermionic anticommutation relations. The 2×2-matrices in the second row are associated to momentum $-\mathbf{k}$ since $U_{\mathbf{k}b}$ is supposed to transform the vector of operators $\mathbf{C}^\dagger_{\mathbf{k}b} = \left(c^\dagger_{\mathbf{k}b\tilde{\uparrow}}, c^\dagger_{\mathbf{k}b\tilde{\downarrow}}, c_{-\mathbf{k}b\tilde{\uparrow}}, c_{-\mathbf{k},b\tilde{\downarrow}}\right)^T$ in (Equation 2.4.11) to the new basis $\mathbf{D}_{\mathbf{k}b} \coloneqq U_{\mathbf{k}b}\mathbf{C}_{\mathbf{k}b}$ with $\mathbf{D}^\dagger_{\mathbf{k}b} = \left(d^\dagger_{\mathbf{k}b\tilde{\uparrow}}, d^\dagger_{\mathbf{k}b\tilde{\downarrow}}, d_{-\mathbf{k}b\tilde{\uparrow}}, d_{-\mathbf{k},b\tilde{\downarrow}}\right)^T$. In contrast, when finding the eigenmodes of the simple spinless BCS Hamiltonian (cf. (Equation 2.2.7)) we don't have to care about $\mathbf{k}$ versus $-\mathbf{k}$ assuming a trivial momentum independent state. While the single particle dispersion $\xi_{\mathbf{k}b} = \xi_{-\mathbf{k}b}$ and the quasiparticle energy $E_{\mathbf{k}b} = E_{-\mathbf{k}b}$ are symmetric with respect to $\mathbf{k}$, the gap function satisfies $\Delta_{\mathbf{k}b} = \left(\Delta_{-\mathbf{k}b}\right)^T$ (anticipating the result in (Equation 2.4.24)). For a unitary gap, we choose the 2×2 blocks of the (normalized) eigenstates of h_{BCS} to be

$$u_{\mathbf{k}b} = \frac{\Delta_{\mathbf{k}b}}{\sqrt{2E_{\mathbf{k}b}\left(E_{\mathbf{k}b} - \xi_{\mathbf{k}b}\right)}} \quad v_{\mathbf{k}b} = \frac{\left(E_{\mathbf{k}b} - \xi_{\mathbf{k}b}\right)\sigma_0}{\sqrt{2E_{\mathbf{k}b}\left(E_{\mathbf{k}b} - \xi_{\mathbf{k}b}\right)}} \quad . \tag{2.4.21}$$

Note, that the new quasiparticle states in $\mathbf{D}_{\mathbf{k},b}$ are in general a superposition of two electrons and one hole *or* one electron and two holes. [11] The symmetry of $v_{\mathbf{k}b}$ is determined by the single particle and quasiparticle dispersions $\xi_{\mathbf{k}b}$ and $E_{\mathbf{k}b}$ and therefore always transforms trivial, i.e. according to the A_1 representation of the underlying point group. In contrast, the symmetries of $u_{\mathbf{k}b}$ are fully inherited from the gap function itself. For the sake of brevity (and since we'll calculate them numerically, anyway) we omit the determination of the eigenstates for a non-unitary gap, which can be found in [SU91, Appendix A, 305f.].

2.4.3. Parametrization of gap function and d-vector

The spinful gap function $\Delta_{\mathbf{k}b}$ in (Equation 2.4.13) takes into account all (pseudo)spin channels. In this subsection, we will formulate another (more transparent) representation of the gap function by making use of the (*pseudo-*) *SU(2) invariance*, i.e. the invariance of the Hamiltonian under any transformation $e^{-i\varphi\hat{n}\tilde{\sigma}}$ with $\tilde{\sigma}$ being the vector of (pseudospin) Pauli matrices (pseudospin and its associated transformation will be introduced in (Section 3.3.2)). The possible two-particle states arising from the addition of two spin-$\frac{1}{2}$ particles with momenta $\mathbf{k}_1$, $\mathbf{k}_2$ and (pseudo)spins $\tilde{\sigma}_1$,$\tilde{\sigma}_2$ are given in *product basis* by

[11] For example, the third eigenstate, i.e. third column of (Equation 2.4.20) is given by

$$h_{\mathrm{BCS}}\mathbf{U}^{(3)}_{\mathbf{k}b} = \begin{pmatrix} \xi_{\mathbf{k}b} & 0 & \Delta_{\mathbf{k}b\tilde{\uparrow}\tilde{\uparrow}} & \Delta_{\mathbf{k}b\tilde{\uparrow}\tilde{\downarrow}} \\ 0 & \xi_{\mathbf{k}b} & \Delta_{\mathbf{k}b\tilde{\downarrow}\tilde{\uparrow}} & \Delta_{\mathbf{k}b\tilde{\downarrow}\tilde{\downarrow}} \\ \overline{\Delta_{\mathbf{k}b\tilde{\uparrow}\tilde{\uparrow}}} & \overline{\Delta_{\mathbf{k}b\tilde{\downarrow}\tilde{\uparrow}}} & -\xi_{\mathbf{k}b} & 0 \\ \overline{\Delta_{\mathbf{k}b\tilde{\uparrow}\tilde{\downarrow}}} & \overline{\Delta_{\mathbf{k}b\tilde{\downarrow}\tilde{\downarrow}}} & 0 & -\xi_{\mathbf{k}b} \end{pmatrix} \begin{pmatrix} E_{\mathbf{k}b} - \xi_{\mathbf{k}b} \\ 0 \\ \overline{\Delta_{-\mathbf{k}b\tilde{\uparrow}\tilde{\uparrow}}} \\ \overline{\Delta_{-\mathbf{k}b\tilde{\downarrow}\tilde{\uparrow}}} \end{pmatrix} = \begin{pmatrix} \xi_{\mathbf{k}b}\left(E_{\mathbf{k}b} - \xi_{\mathbf{k}b}\right) - \left(\Delta_{\mathbf{k}b}\Delta^\dagger_{\mathbf{k}b}\right)_{\tilde{\uparrow}\tilde{\uparrow}} \\ \left(\Delta_{\mathbf{k}b}\Delta^\dagger_{\mathbf{k}b}\right)_{\tilde{\uparrow}\tilde{\downarrow}} \\ \overline{\Delta_{\mathbf{k}b\tilde{\uparrow}\tilde{\uparrow}}}\left(E_{\mathbf{k}b} - \xi_{\mathbf{k}b} + \xi_{\mathbf{k}b}\right) \\ \overline{\Delta_{\mathbf{k}b\tilde{\uparrow}\tilde{\downarrow}}}\left(E_{\mathbf{k}b} - \xi_{\mathbf{k}b} + \xi_{\mathbf{k}b}\right) \end{pmatrix} = \begin{pmatrix} -E_{\mathbf{k}b}\left(E_{\mathbf{k}b} - \xi_{\mathbf{k}b}\right) \\ 0 \\ -E_{\mathbf{k}b}\overline{\Delta_{-\mathbf{k}b\tilde{\uparrow}\tilde{\uparrow}}} \\ -E_{\mathbf{k}b}\overline{\Delta_{-\mathbf{k}b\tilde{\downarrow}\tilde{\uparrow}}} \end{pmatrix} ,$$

using the eigenvalues $E^2 = \xi^2_{\mathbf{k}b} + \frac{1}{2}\,\mathrm{Tr}\left(\Delta_{\mathbf{k}b}\Delta^\dagger_{\mathbf{k}b}\right) = \xi^2_{\mathbf{k}b} + \left(\Delta_{\mathbf{k}b}\Delta^\dagger_{\mathbf{k}b}\right)_{\tilde{\uparrow}\tilde{\uparrow}}$ for the third equality.

$$\Psi\left(\mathbf{k}_1, \tilde{\sigma}_1; \mathbf{k}_2, \tilde{\sigma}_2\right) = \frac{1}{\sqrt{2}}\left(\left|\mathbf{k}_1, \tilde{\sigma}_1\right\rangle \otimes \left|\mathbf{k}_2, \tilde{\sigma}_2\right\rangle - \left|\mathbf{k}_2, \tilde{\sigma}_2\right\rangle \otimes \left|\mathbf{k}_1, \tilde{\sigma}_1\right\rangle\right) \quad , \tag{2.4.22}$$

where the antisymmetrization ensures fermionic anticommutation $\Psi\left(\mathbf{k}_2, \tilde{\sigma}_2; \mathbf{k}_1, \tilde{\sigma}_1\right) = -\Psi\left(\mathbf{k}_1, \tilde{\sigma}_1; \mathbf{k}_2, \tilde{\sigma}_2\right)$. In (pseudo)spin space, we obviously have the four possible states $|\tilde{\sigma}_1, \tilde{\sigma}_2\rangle \in \{|\tilde{\uparrow}, \tilde{\uparrow}\rangle, |\tilde{\uparrow}, \tilde{\downarrow}\rangle, |\tilde{\downarrow}, \tilde{\uparrow}\rangle, |\tilde{\downarrow}, \tilde{\downarrow}\rangle\}$. Assuming spin rotation symmetry, the total spin $S \in \{0, 1\}$ is a "good quantum number" and may be used to classify these four states by *singlet* $S = 0$ associated to $\frac{1}{\sqrt{2}}\left(|\tilde{\uparrow}, \tilde{\downarrow}\rangle - |\tilde{\downarrow}, \tilde{\uparrow}\rangle\right)$ and *triplet* $S = 1$ associated to $|\tilde{\uparrow}, \tilde{\uparrow}\rangle$, $\frac{1}{\sqrt{2}}\left(|\tilde{\uparrow}, \tilde{\downarrow}\rangle + |\tilde{\downarrow}, \tilde{\uparrow}\rangle\right)$ and $|\tilde{\downarrow}, \tilde{\downarrow}\rangle$ with projected angular momentum $m = +1$, $m = 0$ and $m = -1$. These states are obtained by going from product basis to total angular momentum basis by means of *Clebsch-Gordan coefficients* [Wei12]. Note, that the triplet states are *even* while the singlet state is *odd* under exchange of both particles. Consequently, when looking at the entire two-particle wave-function (Equation 2.4.22) (note the "natural" spins $\sigma_i \neq \tilde{\sigma}_i$)

$$\Psi\left(\mathbf{k}_1, \sigma_1; \mathbf{k}_2, \sigma_2\right) = \left|\mathbf{k}_1, \mathbf{k}_2\right\rangle \otimes \left|\psi_{\mathrm{SGT/TPT}}\right\rangle \quad , \tag{2.4.23}$$

we see that the spin triplet (TPT) state has to feature an odd spatial part $|\mathbf{k}_1, \mathbf{k}_2\rangle = -|\mathbf{k}_2, \mathbf{k}_1\rangle$ while the spin singlet state (SGT) involves an even spatial part, i.e. $|\mathbf{k}_1, \mathbf{k}_2\rangle = +|\mathbf{k}_2, \mathbf{k}_1\rangle$, in order to satisfy the fermionic statistics of the total wave function. Taking into account further degrees of freedom like orbital or band index can give rise to exotic pairing states with spin and momentum wave functions that are both odd or both even (cf. (Table 2.1)). However, note that the factorization into spatial and spin part in (Equation 2.4.23) is not generally applicable. As soon as we switch on any spin-orbit coupling, we will couple spin and spatial degrees of freedom and promote the total angular momentum $J = L + S$ to be the new "good quantum number". Spin-rotation invariance is still preserved with respect to pseudospin transformations (cf. (Section 3.3.2)). These symmetry requirements have implications on the gap function (Equation 2.4.13) that corresponds to a two-particle state with zero net momentum $\mathbf{k}_1 = \mathbf{k}$, $\mathbf{k}_2 = -\mathbf{k}$. As a consequence, the transformation $\mathbf{k} \to -\mathbf{k}$ corresponds to particle exchange. Treating the gap function as the total two-particle wave-function we have

$$\Delta_{-\mathbf{k}b} = \begin{pmatrix} \Delta_{-\mathbf{k}b\tilde{\uparrow}\tilde{\uparrow}} & \Delta_{-\mathbf{k}b\tilde{\uparrow}\tilde{\downarrow}} \\ \Delta_{-\mathbf{k}b\tilde{\downarrow}\tilde{\uparrow}} & \Delta_{-\mathbf{k}b\tilde{\downarrow}\tilde{\downarrow}} \end{pmatrix} \overset{\text{particle exch.}}{\underset{\downarrow}{=}} -\begin{pmatrix} \Delta_{\mathbf{k}b\tilde{\uparrow}\tilde{\uparrow}} & \Delta_{\mathbf{k}b\tilde{\downarrow}\tilde{\uparrow}} \\ \Delta_{\mathbf{k}b\tilde{\uparrow}\tilde{\downarrow}} & \Delta_{\mathbf{k}b\tilde{\downarrow}\tilde{\downarrow}} \end{pmatrix} = -\left(\Delta_{\mathbf{k}b}\right)^T \quad . \tag{2.4.24}$$

Since the set of Pauli matrices $\boldsymbol{\sigma} = \{\sigma_0, \sigma_x, \sigma_y, \sigma_z\} = \{\sigma_0, \sigma_1, \sigma_2, \sigma_3\} = \boldsymbol{\sigma}$ [Pau88] forms a complete basis of $\mathbb{C}^{2\times 2}$ space, we can exploit this property to parameterize the gap matrix $\Delta_{\mathbf{k}b}$. To this end we introduce the four-vector $d^\mu(\mathbf{k}) \in \mathbb{C}^4$ providing the coefficients for the Pauli matrices [BW63; Sam11]. We choose the singlet part to be described by the d^0 element. Since the singlet part is $\propto \left(\Delta_{\mathbf{k}b\tilde{\uparrow}\tilde{\downarrow}} - \Delta_{\mathbf{k}b\tilde{\downarrow}\tilde{\uparrow}}\right)$ we require

Table 2.1.: We take into account Cooper pair wave functions with three degrees of freedom, i.e. momentum $\mathbf{k}$, spin σ and orbital or band index b. In order to satisfy the overall antisymmetry required by the Pauli principle we can choose one degree of freedom to be odd and the other two to behave even or all three to be odd. Note, that this classification is (fully) valid only in the absence of spin-orbit coupling. In the presence of centrosymmetric spin-orbit interaction, inversion symmetry introduces a definite parity of the gap function but we cannot separately transform spin and orbital degrees of freedom, anymore. While the "usual" even parity singlet and odd parity triplet solutions are mostly realized, the "exotic" possibilities of even parity triplet and odd parity singlet are energetically disfavored (cf. [Hir; Hir16]). Starting from an orbital basis perspective, it is the specific structure of the non-interacting microscopic Hamiltonian and its eigenstates, which decide if the paired orbital states actually correspond to equal energies and whether these exotic Cooper pairs are suppressed (cf. [Fis13, Section 4.2]). The zoo of possible Cooper states may be further enlarged by considering odd frequency pairing [Ber74; BB13; LB17].

momentum $\mathbf{k}$	spin σ	orbital o or band b	name
even	odd	even	even L singlet
odd	even	even	odd L triplet
even	even	odd	even L triplet
odd	odd	odd	odd L singlet

$$i\sum_{\mu=0}^{3} d^{\mu}_{\mathbf{k}b}\sigma_{\mu}\sigma_{2} \stackrel{!}{=} \Delta_{\mathbf{k}b} \quad \Leftrightarrow \quad i\left(d_{\mathbf{k}b}\cdot\boldsymbol{\sigma}\right)\sigma_{y} = \begin{pmatrix} -d^{x}_{\mathbf{k}b} + id^{y}_{\mathbf{k}b} & d^{0}_{\mathbf{k}b} + d^{z}_{\mathbf{k}b} \\ -d^{0}_{\mathbf{k}b} + d^{z}_{\mathbf{k}b} & d^{x}_{\mathbf{k}b} + id^{y}_{\mathbf{k}b} \end{pmatrix} \stackrel{!}{=} \Delta_{\mathbf{k}b} \quad . \tag{2.4.25}$$

Comparison with (Equation 2.4.13) provides

$$\begin{aligned} d^{0}_{\mathbf{k}b} &= \frac{1}{2}\left(\Delta_{\mathbf{k}b\tilde{\uparrow}\tilde{\downarrow}} - \Delta_{\mathbf{k}b\tilde{\downarrow}\tilde{\uparrow}}\right) \quad d^{x}_{\mathbf{k}b} = -\frac{1}{2}\left(\Delta_{\mathbf{k}b\tilde{\uparrow}\tilde{\uparrow}} - \Delta_{\mathbf{k}b\tilde{\downarrow}\tilde{\downarrow}}\right) \\ d^{y}_{\mathbf{k}b} &= \frac{1}{2i}\left(\Delta_{\mathbf{k}b\tilde{\uparrow}\tilde{\uparrow}} + \Delta_{\mathbf{k}b\tilde{\downarrow}\tilde{\downarrow}}\right) \quad d^{z}_{\mathbf{k}b} = \frac{1}{2}\left(\Delta_{\mathbf{k}b\tilde{\uparrow}\tilde{\downarrow}} + \Delta_{\mathbf{k}b\tilde{\downarrow}\tilde{\uparrow}}\right) \quad . \end{aligned} \tag{2.4.26}$$

Employing the antisymmetry of the gap with respect to inversion of momentum and transposition (Equation 2.4.24) yields

$$d^{0}_{-\mathbf{k}b} = d^{0}_{\mathbf{k}b} \quad \text{and} \quad d^{x,y,z}_{-\mathbf{k}b} = -d^{x,y,z}_{\mathbf{k}b} \quad , \tag{2.4.27}$$

which reflects the symmetry and antisymmetry of the spatial part of the singlet and triplet gap function, respectively. Note, that we denote the total four-component d-

vector by $d_{\mathbf{k}b}$ while the zeroth component is $d^0_{\mathbf{k}b}$ and the x, y, z components are indicated by a bold letter $\mathbf{d}_{\mathbf{k}b}$. Now, that we have a more transparent notation of the gap function we reformulate the expression $\Delta_{\mathbf{k}b}\Delta^\dagger_{\mathbf{k}b}$ in order to see what the difference between a unitary and non-unitary gap is in terms of the d-vector. Using (Equation 2.4.25) and assuming a pure spin singlet (SGT) gap we find

$$\Delta_{\mathbf{k}b}\Delta^\dagger_{\mathbf{k}b} = \begin{pmatrix} |d^0|^2 & 0 \\ 0 & |d^0|^2 \end{pmatrix} = |d^0|^2\sigma_0 \quad . \tag{2.4.28}$$

In contrast, for a pure spin triplet (TPT) gap we obtain

$$\begin{aligned}\Delta_{\mathbf{k}b}\Delta^\dagger_{\mathbf{k}b} &= \begin{pmatrix} |d^x|^2 + |d^y|^2 + |d^z|^2 + id^x\overline{d^y} - id^y\overline{d^x} & -d^x\overline{d^z} + id^y\overline{d^z} + d^z\overline{d^x} - id^z\overline{d^y} \\ -d^z\overline{d^x} - id^z\overline{d^y} + d^x\overline{d^z} + id^y\overline{d^z} & |d^x|^2 + |d^y|^2 + |d^z|^2 - id^x\overline{d^y} + id^y\overline{d^x} \end{pmatrix} \\ &= |\mathbf{d}_{\mathbf{k}b}|^2\sigma_0 + i\left(\mathbf{d}_{\mathbf{k}b} \times \overline{\mathbf{d}}_{\mathbf{k}b}\right)\cdot\sigma \quad ,\end{aligned} \tag{2.4.29}$$

where we omitted the momentum and band index for compactness. Apparently, only triplet pairing can represent a non-unitary gap function while the singlet part is always unitary. For a triplet gap function to be non-unitary the entity $\left(\mathbf{d}_{\mathbf{k}b} \times \overline{\mathbf{d}}_{\mathbf{k}b}\right)$ must be non-zero which necessarily requires a complex valued d-vector [SAM09]. In order to provide a physical intuition about a non-unitary state we consider the spin expectation value (at zero temperature) $\left\langle \hat{S} \right\rangle = \langle \Delta_{\mathbf{k}b}|\hat{S}|\Delta_{\mathbf{k}b}\rangle$ where $\hat{S}$ is the two-particle operator $\hat{S} := \hat{s}_1 \otimes \sigma_0 + \sigma_0 \otimes \hat{s}_2$ and the state $|\Delta_{\mathbf{k}b}\rangle$ is expressed in terms of a four-vector $|\Delta_{\mathbf{k}b}\rangle = \left(\Delta_{\tilde{\uparrow}\tilde{\uparrow}}, \Delta_{\tilde{\uparrow}\tilde{\downarrow}}, \Delta_{\tilde{\downarrow}\tilde{\uparrow}}, \Delta_{\tilde{\downarrow}\tilde{\downarrow}}\right)$. The two-particle spin operator for e.g. the x-component is given by

$$\hat{S}_x = \frac{\sigma_x \otimes \sigma_0 + \sigma_0 \otimes \sigma_x}{2} = \frac{1}{2}\begin{pmatrix} 0 & 0 & 1 & 0 \\ 0 & 0 & 0 & 1 \\ 1 & 0 & 0 & 0 \\ 0 & 1 & 0 & 0 \end{pmatrix} + \frac{1}{2}\begin{pmatrix} 0 & 1 & 0 & 0 \\ 1 & 0 & 0 & 0 \\ 0 & 0 & 0 & 1 \\ 0 & 0 & 1 & 0 \end{pmatrix} = \frac{1}{2}\begin{pmatrix} 0 & 1 & 1 & 0 \\ 1 & 0 & 0 & 1 \\ 1 & 0 & 0 & 1 \\ 0 & 1 & 1 & 0 \end{pmatrix} \quad , \tag{2.4.30}$$

With these prerequisites the spin expectation value for e.g. $\hat{S}_x$ of the two-particle state given by the gap function $\Delta_{\mathbf{k}b}$ is

$$\begin{aligned}\langle \Delta_{\mathbf{k}b}|\hat{S}_x|\Delta_{\mathbf{k}b}\rangle &= \frac{1}{2}\left[\left(\overline{\Delta}_{\tilde{\uparrow}\tilde{\uparrow}} + \overline{\Delta}_{\tilde{\downarrow}\tilde{\downarrow}}\right)\left(\Delta_{\tilde{\uparrow}\tilde{\downarrow}} + \Delta_{\tilde{\downarrow}\tilde{\uparrow}}\right) + \left(\overline{\Delta}_{\tilde{\uparrow}\tilde{\downarrow}} + \overline{\Delta}_{\tilde{\downarrow}\tilde{\uparrow}}\right)\left(\Delta_{\tilde{\uparrow}\tilde{\uparrow}} + \Delta_{\tilde{\downarrow}\tilde{\downarrow}}\right)\right] \\ &\overset{(Equation\ 2.4.26)}{\overset{\downarrow}{=}} \quad 2\left(-id^z\overline{d^y} + id^y\overline{d^z}\right) = 2i\left(\mathbf{d}_{\mathbf{k}b} \times \overline{\mathbf{d}}_{\mathbf{k}b}\right)_x \quad .\end{aligned} \tag{2.4.31}$$

For the remaining y and z components we get analogous results that can be expressed by means of the vector $\mathbf{d}_{\mathbf{k}b} \times \overline{\mathbf{d}}_{\mathbf{k}b}$. Therefore, the spin expectation value for a some gap function $\Delta_{\mathbf{k}b}$ is proportional to $\mathbf{d}_{\mathbf{k}b} \times \overline{\mathbf{d}}_{\mathbf{k}b}$ and obviously is only finite for a *non-*

unitary gap. As a consequence, a non-unitary pairing state features some finite "internal magnetization". Any finite spin expectation value is associated to a particular momentum $\mathbf{k}$ (and band index b) while the net magnetization (averaged over the Fermi surface) may still be zero. By means of the d-vector, the expression for the quasiparticle energy $E_{\mathbf{k}b}$ in (Equation 2.4.18) can be reformulated in a much more transparent fashion. The gap matrix with both finite singlet and triplet contributions results in $\Delta_{\mathbf{k}b}\Delta_{\mathbf{k}b}^{\dagger} = |d_{\mathbf{k}b}|^2\sigma_0 + i\left(\mathbf{d}_{\mathbf{k}b} \times \overline{\mathbf{d}_{\mathbf{k}b}}\right) \cdot \boldsymbol{\sigma}$ by combining (Equation 2.4.28) and (Equation 2.4.29), where the absolute square of the d-vector contains all four components. The trace and determinants occurring in the quasiparticle energy $E_{\mathbf{k}b}$ are hence given by

$$\mathrm{Tr}\left(\Delta_{\mathbf{k}b}\Delta_{\mathbf{k}b}^{\dagger}\right) = 2|d_{\mathbf{k}b}|^2 \quad \text{and} \quad \det\left(\Delta_{\mathbf{k}b}\Delta_{\mathbf{k}b}^{\dagger}\right) = |d_{\mathbf{k}b}|^4 - \left|\mathbf{d}_{\mathbf{k}b} \times \overline{\mathbf{d}_{\mathbf{k}b}}\right|^2 \quad . \tag{2.4.32}$$

Putting these results together, the energy $E_{\mathbf{k}b}$ describing the quasiparticle spectra for both unitary and non-unitary gaps, reduces to the neat expression

$$E_{\mathbf{k}b} = \pm\frac{1}{2}\sqrt{\xi_{\mathbf{k}b}^2 + |d_{\mathbf{k}b}|^2 \pm \left|\mathbf{d}_{\mathbf{k}b} \times \overline{\mathbf{d}_{\mathbf{k}b}}\right|} \quad , \tag{2.4.33}$$

where $\left|\mathbf{d}_{\mathbf{k}b} \times \overline{\mathbf{d}_{\mathbf{k}b}}\right|$ vanishes for a unitary gap.

2.4.4. Symmetries and d-vector transformations

In order to identify possible candidate d-vectors for certain models, it is advantageous to consider symmetries and the (possible) restrictions they impose on the structure of the d-vector. Therefore, we take four types of transformations into account, that are *time-reversal*, *spatial inversion*, (*pseudo*)*spin rotation* and *point group transformations*. To be able to perform the transformation more transparently, the d-vector is written as

$$d_{\mathbf{k}b} = \left(d_{\mathbf{k}b}^0, d_{\mathbf{k}b}^x, d_{\mathbf{k}b}^y, d_{\mathbf{k}b}^z\right)^T = d_{\mathbf{k}b}^0\,\hat{x}^0 + d_{\mathbf{k}b}^x\,\hat{x} + d_{\mathbf{k}b}^y\,\hat{y} + d_{\mathbf{k}b}^z\,\hat{z} \quad , \tag{2.4.34}$$

where the basis of the d-vector is explicitly introduced in order to distinguish the transformation of components and basis. The components incorporate the momentum degree of freedom, while the basis represents the (pseudo)spin degrees of freedom. The time-reversal operation for spin-$\frac{1}{2}$ particles is given by $\hat{\Theta} = -i\sigma_y\mathcal{K}$ [12] and its inverse is $\hat{\Theta}^{-1} = i\sigma_y\mathcal{K}$. Hence, the gap matrix transforms by (cf. appendix D)

[12] Due to the complex conjugation $\mathcal{K}$ the operator $\hat{\Theta} = -i\sigma_y\mathcal{K}$ is non-unitary [Wig12; SN11] [Sch05b, Chap. 11.4, p.228]. Thus, we have to take care of the fact that $\hat{\Theta}^{-1} \neq \hat{\Theta}^{\dagger}$ and use $\hat{\Theta}^{-1} = +i\sigma_y\mathcal{K}$ for all transformations, since $\hat{\Theta}^{-1}\hat{\Theta} = +i\sigma_y\mathcal{K}\left(-i\sigma_y\mathcal{K}\right) = i\sigma_y(+i)(-\sigma_y) = \sigma_0$.

$$\sum_{\tilde{\sigma},\tilde{\sigma}'} \left(\Delta_{\mathbf{k}b}\right)_{\tilde{\sigma}\tilde{\sigma}'} c^{\dagger}_{\mathbf{k}b\tilde{\sigma}} c^{\dagger}_{-\mathbf{k}b\tilde{\sigma}'} \xrightarrow{\mathrm{TR}} \sum_{\tilde{\sigma},\tilde{\sigma}'} \left(\hat{\Theta}^{-1}\Delta_{\mathbf{k}b}\hat{\Theta}\right)_{\tilde{\sigma}\tilde{\sigma}'} c^{\dagger}_{\mathbf{k}b\tilde{\sigma}} c^{\dagger}_{-\mathbf{k}b\tilde{\sigma}'}$$
$$= \sum_{\tilde{\sigma},\tilde{\sigma}'} \begin{pmatrix} \overline{\Delta_{-\mathbf{k}b\tilde{\downarrow}\tilde{\downarrow}}} & -\overline{\Delta_{-\mathbf{k}b\tilde{\downarrow}\tilde{\uparrow}}} \\ -\overline{\Delta_{-\mathbf{k}b\tilde{\uparrow}\tilde{\downarrow}}} & \overline{\Delta_{-\mathbf{k}b\tilde{\uparrow}\tilde{\uparrow}}} \end{pmatrix} c^{\dagger}_{\mathbf{k}b\tilde{\sigma}} c^{\dagger}_{-\mathbf{k}b\tilde{\sigma}'} \quad . \tag{2.4.35}$$

Inserting the transformed gap matrix elements into the definition of the d-vector in terms of $\Delta_{\mathbf{k}b}$ (Equation 2.4.26) yields the behavior of $d_{\mathbf{k}b}$ under time-reversal. A more elegant solution is to take the d-vector directly into account and considering that the vector of (pseudospin) Pauli matrices, as being an operator of angular momentum, must be odd under time-reversal, i.e. $\boldsymbol{\sigma} \xrightarrow{\mathrm{TR}} -\boldsymbol{\sigma}$, while the zeroth Pauli matrix is invariant, of course. Note, that the transformation of Pauli matrices only affects the basis but not the components in (Equation 2.4.34). Therefore, the d-vector must transform according to

$$i\left[d_{\mathbf{k}b}\cdot\boldsymbol{\sigma}\right]\sigma_y = i\left[\left(d^0_{\mathbf{k}b},\mathbf{d}_{\mathbf{k}b}\right)^T\cdot\left(\sigma_0,\boldsymbol{\sigma}\right)^T\right]\sigma_y \xrightarrow{\mathrm{TR}} i\left[\left(\overline{d^0_{-\mathbf{k}b}},\overline{\mathbf{d}_{-\mathbf{k}b}}\right)^T\cdot\left(\sigma_0,-\boldsymbol{\sigma}\right)^T\right]\sigma_y \quad . \tag{2.4.36}$$

Summarizing the above, we have $d^0_{\mathbf{k}b} \xrightarrow{\mathrm{TR}} \overline{d^0_{-\mathbf{k}b}}$ and $\mathbf{d}_{\mathbf{k}b} \xrightarrow{\mathrm{TR}} -\overline{\mathbf{d}_{-\mathbf{k}b}}$. Concerning the spatial inversion $\hat{I}$, we know that the momentum behaves odd, $\mathbf{k} \xrightarrow{\hat{I}} -\mathbf{k}$ and the (pseudo)spin (as being a pseudo/axial vector) must be even under spatial inversion, i.e. $\boldsymbol{\sigma} \xrightarrow{\hat{I}} \boldsymbol{\sigma}$. While the momentum determines the behavior of the components, the Pauli matrices only affect the basis in (Equation 2.4.34), i.e. the basis is invariant w.r.t. spatial inversion. Therefore, the properties of the d-vector under inversion are already entirely given by (Equation 2.4.24), i.e $\left(d^0_{\mathbf{k}b},\mathbf{d}_{\mathbf{k}b}\right)^T \xrightarrow{\hat{I}} \left(d^0_{\mathbf{k}b},-\mathbf{d}_{\mathbf{k}b}\right)^T$. In contrast, the transformation properties of the d-vector with respect to (pseudo)spin rotations require a more extended analysis. An SU(2) transformation and spin rotation, respectively, is defined by the operator

$$\hat{S}\left(\hat{n},\varphi\right) = e^{-i\hat{n}\boldsymbol{\sigma}\varphi/2} = \sigma_0\cos\left(\varphi/2\right) - i\hat{n}\cdot\boldsymbol{\sigma}\sin\left(\varphi/2\right) \quad , \tag{2.4.37}$$

where $\hat{n}$ (with $|\hat{n}| = \sqrt{\sum_{j=1}^{3}\hat{n}_j^2} = 1$) is the axis of rotation and φ is the angle of rotation. Note, that this transformation has the well-known property of introducing a minus sign on rotation by 2π about any axis, which usually requires the use of *double groups* [Bet29]. Instead of proceeding straightforwardly with the transformation $\Delta_{\mathbf{k}b} \xrightarrow{\hat{S}} \hat{S}^{-1}\Delta_{\mathbf{k}b}\hat{S}$, we first determine the transformation behavior of every single Pauli matrix under spin rotation. The i-th (pseudospin) Pauli matrix σ_i transforms like

$$\sigma_i \xrightarrow{\hat{S}} \left(\hat{S}\left(\hat{n},\varphi\right)\right)^{-1}\sigma_i\hat{S}\left(\hat{n},\varphi\right) = \sigma_i\left(\cos\left(\varphi/2\right)\right)^2 + 2\cos\left(\varphi/2\right)\sin\left(\varphi/2\right)\left[\sum_{j,k=1}^{3}\epsilon_{ijk}\hat{n}_j\sigma_k\right] + \left(\sin\left(\varphi/2\right)\right)^2\left[\sigma_i\left(2\hat{n}_i^2-1\right)+2\hat{n}_i\sum_{j=1}^{3}\left(1-\delta_{ij}\right)\sigma_j\hat{n}_j\right] \quad . \tag{2.4.38}$$

By inserting the transformed Pauli matrices into the definition of the d-vector $i\left[d_{\mathbf{k}b}\cdot\boldsymbol{\sigma}\right]\sigma_2$ (insert components of $\boldsymbol{\sigma}$, but don't substitute σ_y since σ_y is only part of the notation) and collecting terms with respect to Pauli matrices we find the transformed components of the d-vector. The i-th component of the transformed d-vector is then given by

$$d^i_{\mathbf{k}b} \xrightarrow{\hat{S}} d^i_{\mathbf{k}b}\left(\left(\cos\left(\varphi/2\right)\right)^2+\left(\sin\left(\varphi/2\right)\right)^2\left(2\hat{n}_i^2-1\right)\right) + \sum_{j=1}^{3}\left(1-\delta_{ij}\right)d^j_{\mathbf{k}b}\left(2\left(\sin\left(\varphi/2\right)\right)^2\hat{n}_i\hat{n}_j+2\cos\left(\varphi/2\right)\sin\left(\varphi/2\right)\sum_{k=1}^{3}\epsilon_{ijk}n_k\right) \quad . \tag{2.4.39}$$

The identities $\left(\cos\left(\varphi/2\right)\right)^2-\left(\sin\left(\varphi/2\right)\right)^2=\cos\left(\varphi\right)$, $2\cos\left(\varphi/2\right)\sin\left(\varphi/2\right)=\sin\left(\varphi\right)$ and $2\left(\sin\left(\varphi/2\right)\right)^2=1-\cos\left(\varphi\right)$ simplify this result to the transformed, for instance, x-component of the d-vector

$$d^x_{\mathbf{k}b} \xrightarrow{\hat{S}} d^x_{\mathbf{k}b}\left[\cos\left(\varphi\right)+\hat{n}_x^2\left(1-\cos\left(\varphi\right)\right)\right]+d^y_{\mathbf{k}b}\left[\hat{n}_x\hat{n}_y\left(1-\cos\left(\varphi\right)\right)+\hat{n}_z\sin\left(\varphi\right)\right] + d^z_{\mathbf{k}b}\left[\hat{n}_x\hat{n}_z\left(1-\cos\left(\varphi\right)\right)-\hat{n}_y\sin\left(\varphi\right)\right] \quad , \tag{2.4.40}$$

which is exactly the first row of the SO(3) rotation matrix $\mathcal{R}(\hat{n},\varphi)$ that rotates a *true/polar vector* $\mathbf{r}\in\mathbb{R}^3$ about the axis $\hat{n}$ by angle φ. Henceforth, the d-vector describing the gap function transforms according to

$$\left(d^0_{\mathbf{k}b},\mathbf{d}_{\mathbf{k}b}\right)^T \xrightarrow{\hat{S}} \left(d^0_{\mathbf{k}b},\mathcal{R}(\hat{n},\varphi)\mathbf{d}_{\mathbf{k}b}\right)^T \quad , \tag{2.4.41}$$

under any SU(2) rotation. This transformation is exclusively a transformation of basis, i.e. the Pauli matrices, while the components (momentum dependency) is not affected at all. Although, the d-vector transforms like a polar vector under rotation, it behaves unlike a polar vector w.r.t. to reflections. A reflection may be composed of a spatial inversion followed or preceded by a rotation about the normal vector of the plane by π. As already noted, the spatial inversion doesn't affect the basis of the d-vector, i.e. the Pauli matrices. For instance, a reflection in the x-z plane therefore only involves a rotation by π about the y-axis, that is given by (Equation 2.4.38), the Pauli matrices transform according to $\left(\sigma_x,\sigma_y,\sigma_z\right)\longrightarrow\left(-\sigma_x,\sigma_y,-\sigma_z\right)$. A further consequence of (Equation 2.4.39) is, that the d-vector does not obey any *double group* properties like the SU(2) spin de-

Table 2.2.: When transforming the d-vector, one has to distinguish the behavior of the basis (spin degrees of freedom) and the behavior of its components (momentum degree of freedom). The properties given below are the result of the combined transformation of both basis (spin) and components (momentum) (except for spin and orbital rotation, respectively). Time-reversal affects both spin, introducing the overall minus in the triplet part and momentum, which is inverted in both singlet and triplet part. The spatial inversion only has an effect on momentum since (pseudo)spin represents an pseudo/axial vector. Note, that spatial inversion corresponds to fermionic exchange of the Cooper pair (Equation 2.4.24), which may be used to simplify the given results. Unlike the SU(2) spin degrees of freedom the d-vector originates from, it rather behaves like a polar vector in real space, which becomes apparent for the spin-rotation. The entity $\mathcal{R}(\hat{n},\varphi) \in \mathbb{R}^3$ is the SO(3) rotation matrix for a polar vector about an axis $\hat{n}$ by angle φ (cf. [SAM05] and [SU91, p.244]). Remarkably, the d-vector therefore doesn't exhibit any double group properties and maps onto itself under a rotation by 2π about any axis, which is, however, a consequence of the d-vector carrying total spin $S = 1$.

transformation	operator	singlet (SGT) $d^0_{\mathbf{k}b}$	triplet (TPT) $\mathbf{d}_{\mathbf{k}b}$
time-reversal	$\hat{\Theta}$	$\overline{d^0_{-\mathbf{k}b}}$	$-\overline{\mathbf{d}_{-\mathbf{k}b}}$
inversion/fermionic exchange	$\hat{I}$	$d^0_{-\mathbf{k}b}$	$\mathbf{d}_{-\mathbf{k}b}$
spin rotation	$\hat{S}(\hat{n},\varphi)$	$d^0_{\mathbf{k}b}$	$\mathcal{R}(\hat{n},\varphi)\mathbf{d}_{\mathbf{k}b}$
real space/orbital rotation	$\mathcal{R}(\hat{n},\varphi)$	$d^0_{\mathcal{R}(\hat{n},\varphi)\mathbf{k}b}$	$\mathbf{d}_{\mathcal{R}(\hat{n},\varphi)\mathbf{k}b}$

grees it originates from, but the simple group behavior of the real space entities. The transformation properties of the d-vector are summarized in (Table 2.2).

When dealing with Hamiltonians corresponding to models on certain lattice types, the *crystal field* will break down the continuous SO(3) transformations of the orbital/momentum part of the d-vector to the discrete operations of the corresponding *finite groups*. The point groups provide a set of symmetry allowed basis functions representing the momentum dependency of the d-vector up to any order. These will be worked out in (Section 3.4). Since the transformations of *orbital rotation* and (*pseudo*)*spin rotations* may be performed independently the sets of possible d-vectors are usually subject to degeneracy. For instance, in the environment of a crystal with D_{4h}symmetry, possible d-vectors for triplet pairing must feature odd basis functions and are given by i.a. the two-dimensional E_u representation featuring the basis functions $\sin k_x \cos k_z$ and $\sin k_y \cos k_z$. Assuming a "natural" spin degree of freedom with SU(2) invariance the total spin $S = 1$ of the triplet wave function may point anywhere, i.e. we are allowed to freely rotate the d-vector in any direction according to (Equation 2.4.39). Therefore, by combining the two basis functions with the three components of the d-vector, one ends up with a

six-fold degeneracy of possible triplet states. For instance, the allowed d-vectors may be given as linear combinations of the basis functions by $\mathbf{d}_{\mathbf{k}b}^{(1,2)} = \left(\hat{x}\sin k_x \pm \hat{y}\sin k_y\right)\cos k_z$, $\mathbf{d}_{\mathbf{k}b}^{(3,4)} = \left(\hat{x}\sin k_y \pm \hat{y}\sin k_x\right)\cos k_z$ and $\mathbf{d}_{\mathbf{k}b}^{(5,6)} = \left(\sin k_x \pm (i)\sin k_y\right)\cos k_z\,\hat{z}$. The first two states are aligned in the x-y-plane while the third state points along the z-direction. Following (Equation 2.4.29), we find that all of these states apparently exhibit the same gap magnitude $\Delta_{\mathbf{k}b}\Delta_{\mathbf{k}b}^{\dagger} = \sin^2 k_x + \sin^2 k_y = |\mathbf{d}_{\mathbf{k}b}|^2$. (cf. [Sig05; NS00]). As long as the Hamiltonian doesn't feature any spin off-diagonal terms all SU(2) rotations are symmetry operations, i.e. $\left[\hat{S}, \mathcal{H}_0\right] = 0$, since the spin doesn't "feel" the crystal field. Hence, we may arbitrarily transform the spin (hence the basis $\hat{x}$, $\hat{y}$ and $\hat{z}$) such that all d-vectors $\mathbf{d}^{(1,\ldots,6)}$ are simply connected by a spin rotation. Note, that under operations of the point group $\mathrm{D_{4h}}$ the basis vectors $\hat{x}$, $\hat{y}$ (Pauli matrices σ_x, σ_z) transform according to the $\mathrm{E_g}$ and $\hat{z}$ (σ_z) like the $\mathrm{A_{2g}}$ representation. (cf. (Table A.1)). However, as soon as spin-orbit coupling is introduced the orbital and (pseudo)spin degrees of freedom are coupled. Therefore, we are not allowed to employ the corresponding transformations in (Table 2.2) separately, anymore [And84a]. As a consequence, the degeneracy of several pairing wave functions is lifted. Mathematically, the coupling of orbital/momentum and spin degrees of freedom and their simultaneous transformation is expressed by [Gos]

$$\mathrm{E_u} \otimes \left(\mathrm{E_g} \oplus \mathrm{A_{2g}}\right) = \mathrm{A_{1u}} \oplus \mathrm{A_{2u}} \oplus \mathrm{B_{1u}} \oplus \mathrm{B_{2u}} \oplus \mathrm{E_u} \quad . \tag{2.4.42}$$

Hence, the six-fold degeneracy of possible triplet d-vectors splits up into four one dimensional and one two dimensional representation. By employing combined spin and orbital transformation, i.e. transforming both components and basis, it is impossible to transform any of the states $\mathbf{d}^{(1,\ldots,6)}$ into another one. The classification of singlet and triplet in the presence of *spin-orbit coupling* will be discussed in more detail in (Section 3.4) and employed to a realistic Hamiltonians in (Chapter 9). We note, that the d-vector as a smart parametrization and auxiliary entity may also be employed for the characterization and classification of *unconventional particle-hole states* in the sense that they feature nonzero angular momentum (cf. [Nay00; GC10]). Most of the properties of the d-vector discussed in the previous two sections may be straightforwardly employed, except for the fermionic exchange (Equation 2.4.24). In contrast, to the particle-particle states the particle-hole condensates are characterized by an additional parameter $\mathbf{Q}$, which specifies the momentum transfer and usually lowers the full symmetry of the point group (Section 3.5).

Summary and preview

In this chapter we motivated the concept of Cooper pairs in correlated electron systems and reviewed the basics of BCS-theory. The Kohn-Luttinger effect was discussed as one possible mechanism for the emergence of unconventional pairing as a result of repulsive electron-electron interactions. We provided a generalization of BCS-theory

to multiband (-orbital) systems for gap functions with non trivial momentum dependencies and introduced the basics for the description of pairing states in models with (centrosymmetric) spin-orbit coupling. The following chapter will provide a characterization and classification of spin-orbit interaction in (non-)centrosymmetric models. Based on the possible spin-orbit terms and the symmetries that are conserved or broken, we will define the concepts of pseudospin and helical spin degree of freedom and analyze the structure of the corresponding effective interaction in orbital and band basis. These generalized two-particle vertices will serve as an input for mean-field theories that allow for singlet and triplet instabilities in terms of the pseudospin degree of freedom as well as mixed singlet-triplet states. The chapter will be concluded by constructing basis functions for unconventional particle-particle and particle-hole states that interweave momentum and pseudospin or helical spin degrees of freedom.

3. Mean-field theory in absence of spin rotation invariance

In (Chapter 5) and (Chapter 6) we will formulate the perturbative and functional renormalization groups for fermionic systems and (in particular) for the corresponding irreducible two-particle vertices with broken SU(2)-symmetry. In order to analyze the occurring ordering tendencies and instabilities, we have to work out a mean-field theory that takes into account the broken spin symmetry. *Two* different scenarios are distinguished depending on which additional symmetries are broken. On the one hand, we will discuss the mean-field theory for Hamiltonians with *time-reversal* and *inversion* symmetry, which ensure the two-fold spin degeneracy of the bands involved. On the other hand, we will have systems where either *inversion* or *time-reversal* symmetry is lost, which results in the spin-splitting of the corresponding Fermi surfaces. In the former case, spin symmetry is spoiled by atomic spin-orbit coupling $\mathbf{L} \cdot \mathbf{S}$ [Win03], and the considerations of (Section 2.4) apply. Hence, we are still able to classify the pairing states and gap functions by singlet and triplet states (and therefore by the d-vector) as inversion symmetry requires a definite parity [VG84; Ell54]. Broken inversion symmetry at the surface, at a heterointerface or in a non-centrosymmetric crystal supports the presence of exotic spin-orbit interactions like Rashba [BR84a; RS88], Dresselhaus [Dre55] or Kane-Mele terms [KM05b] (which is the time-reversal invariant doublet of Haldane's model for the *quantum anomalous Hall effect* [Hal88; ZLW14]). These terms lift the spin degeneracy and can in principle induce a mixture of spin singlet and triplet states [GR01]. An exception to this paradigm is given by the so-called *in-plane-Rashba* Hamiltonian that preserves inversion symmetry and is realized in buckled honeycomb structures, where the in-plane mirror symmetry is broken [LJY11; Mar+18].

3.1. Origin and classification of spin-orbit interaction

It was first noted in the context of relativistic quantum mechanics, i.e. the unification of quantum mechanics and special relativity that a fermionic wave function must incorporate an intrinsic degree of freedom [Dir28; FP39], that is nowadays called spin. Therefore, we cannot rely on non-relativistic methods to derive spin-orbit interaction. The proper description of the electron (including its spin) is given by the *Dirac equation* [Dir81; Dir36], that yields

$$i\hbar \frac{\partial}{\partial t} |\Psi\rangle = \left(c\, \boldsymbol{\alpha} \cdot \hat{\mathbf{p}} + \beta\, mc^2 \right) |\Psi\rangle \quad , \tag{3.1.1}$$

where the momentum operator is $\hat{p}_j = -i\hbar\frac{\partial}{\partial x_j}$. The state $|\Psi\rangle$ is actually a two component state (bispinor) that we denote by $|\Psi\rangle = (\psi_A, \psi_B)^T$. Using the standard convention for $\boldsymbol{\alpha}$ and β matrices (cf. γ matrices) that is [Sha12]

$$\alpha_j = \sigma_x \otimes \sigma_j \quad j \in \{1,2,3\} \quad \text{and} \quad \beta = \sigma_z \otimes \sigma_0 \quad , \tag{3.1.2}$$

where $\boldsymbol{\sigma} = \left(\sigma_x, \sigma_y, \sigma_z\right)$ are the Pauli matrices with $\sigma_0 = \mathbb{1}_{2\times 2}$. Therefore, we can express the Dirac equation in terms of a 2×2 matrix by

$$i\hbar\frac{\partial}{\partial t}|\Psi\rangle = \underbrace{\begin{pmatrix} mc^2 & c\,\boldsymbol{\sigma}\cdot\hat{\mathbf{p}} \\ c\,\boldsymbol{\sigma}\cdot\hat{\mathbf{p}} & -mc^2 \end{pmatrix}}_{=\mathcal{H}_D}|\Psi\rangle \quad . \tag{3.1.3}$$

In order to see, how spin-orbit coupling originates from this equation, we have to include an external potential (due to the atomic core or the lattice) $V(\mathbf{r})$ whose symmetries are crucial for the types of spin-orbit interaction arising from it. For instance, in the hydrogen atom, $V(\mathbf{r})$ possesses spherical symmetry, in the perfect lattice we have $V(\mathbf{r}+\mathbf{R}) = V(\mathbf{r})$, while in a non-centrosymmetric crystal or at an heterostructure interface, we have $V(-\mathbf{r}) \neq V(\mathbf{r})$. Hence, the Dirac Hamiltonian is

$$\mathcal{H}_D = c\,\boldsymbol{\alpha}\cdot\hat{\mathbf{p}} + \beta\, mc^2 + V(\mathbf{r}) \quad . \tag{3.1.4}$$

The time-dependency of the bispinor may be split off by the ansatz $|\Psi\rangle = e^{-iE_\Psi/\hbar t}|\Psi_0\rangle$ resulting in

$$i\hbar\frac{\partial}{\partial t}|\Psi\rangle = E_\Psi|\Psi\rangle = \mathcal{H}_D|\Psi\rangle \quad . \tag{3.1.5}$$

This stationary version of the Dirac equation represents a coupled linear system in terms of the components ψ_A and ψ_B, i.e.

$$\begin{pmatrix} mc^2 + V(\mathbf{r}) - E_\Psi & c\,\boldsymbol{\sigma}\cdot\hat{\mathbf{p}} \\ c\,\boldsymbol{\sigma}\cdot\hat{\mathbf{p}} & -mc^2 + V(\mathbf{r}) - E_\Psi \end{pmatrix}\begin{pmatrix}\psi_A \\ \psi_B\end{pmatrix} = 0 \quad . \tag{3.1.6}$$

Solving for part ψ_A of the bispinor provides

$$\begin{cases} \left(mc^2 + V(\mathbf{r}) - E_\Psi\right)\psi_A + c\,\boldsymbol{\sigma}\cdot\hat{\mathbf{p}}\left(E_\Psi + mc^2 - V(\mathbf{r})\right)^{-1} c\,\boldsymbol{\sigma}\cdot\hat{\mathbf{p}}\,\psi_A = 0 \\ \psi_B = -\left(-mc^2 + V(\mathbf{r}) - E_\Psi\right)^{-1} c\,\boldsymbol{\sigma}\cdot\hat{\mathbf{p}}\,\psi_A \end{cases} . \tag{3.1.7}$$

We introduce the notation $E := E_\Psi - mc^2$, where E corresponds to the non-relativistic

energy that lacks the energy due to the rest mass. The first equation that determines ψ_A may be simplified to

$$\boldsymbol{\sigma}\cdot\hat{\mathbf{p}}\frac{c^2}{E+2mc^2-V(\mathbf{r})}\boldsymbol{\sigma}\cdot\hat{\mathbf{p}}\,\psi_A=(E-V(\mathbf{r}))\,\psi_A \quad . \tag{3.1.8}$$

Since the non-relativistic energy E appears on the left and right hand side of (Equation 3.1.8) we employ the expansion [1] (in terms of $\frac{v^2}{c^2}$ [2])

$$\begin{aligned}\frac{1}{E+2mc^2-V(\mathbf{r})}&=\frac{1}{2mc^2}\frac{1}{1+\frac{E-V(\mathbf{r})}{2mc^2}}=\frac{1}{2mc^2}\left(1+\frac{E-V(\mathbf{r})}{2mc^2}\right)^{-1}\\&\approx\frac{1}{2mc^2}\left(1-\frac{E-V(\mathbf{r})}{2mc^2}+\frac{(E-V(\mathbf{r}))^2}{4m^2c^4}\right) \quad .\end{aligned} \tag{3.1.9}$$

By remembering the identity $(\boldsymbol{\sigma}\cdot\hat{\mathbf{p}})^2=\hat{\mathbf{p}}^2$, [3] we simply get the Schrödinger equation in zeroth order of the expansion when employed to (Equation 3.1.8). However, the interesting terms come up in the first order of the expansion. When inserting the first order of (Equation 3.1.9) into (Equation 3.1.8) we get i.a.

$$\begin{aligned}(E-V(\mathbf{r}))\boldsymbol{\sigma}\cdot\hat{\mathbf{p}}\,\psi_A&=\boldsymbol{\sigma}\cdot\hat{\mathbf{p}}\,(E-V(\mathbf{r}))\,\psi_A+[E-V(\mathbf{r}),\boldsymbol{\sigma}\cdot\hat{\mathbf{p}}]\;\psi_A\\&=\boldsymbol{\sigma}\cdot\hat{\mathbf{p}}\,\frac{\hat{\mathbf{p}}^2}{2m}\psi_A+\boldsymbol{\sigma}\cdot[\hat{\mathbf{p}}\,,V(\mathbf{r})]\,\psi_A \quad ,\end{aligned} \tag{3.1.10}$$

where we used the zeroth order result on the first term and the commutator $[E,\hat{\mathbf{p}}]=0$. Summarizing the hitherto results by using (Equation 3.1.9) and (Equation 3.1.10) in (Equation 3.1.8) we have

$$E\psi_A=\left[\frac{\hat{\mathbf{p}}^2}{2m}+V(\mathbf{r})-\frac{\hat{\mathbf{p}}^4}{8m^3c^2}-\frac{(\boldsymbol{\sigma}\cdot\hat{\mathbf{p}})\,(\boldsymbol{\sigma}\cdot[\hat{\mathbf{p}},V(\mathbf{r})])}{4m^2c^2}\right]\psi_A \quad . \tag{3.1.11}$$

The last term in (Equation 3.1.11) may be split into two by employing the identity $(\boldsymbol{\sigma}\cdot\mathbf{a})\,(\boldsymbol{\sigma}\cdot\mathbf{b})=\mathbf{a}\cdot\mathbf{b}+i\boldsymbol{\sigma}\,(\mathbf{a}\times\mathbf{b})$ [4]. Note, that the first term resulting from this identity,

[1] We simply use the Taylor expansion of $(1+x)^{-1}$ that is $\frac{1}{1+x}\overset{x\approx 0}{\approx}1-x+x^2+....$

[2] The expansion is justified by considering that $E-V(\mathbf{r})\approx mv^2$ by virtue of the *virial theorem* [Foc30; Kal76] and therefore $\frac{E-V(\mathbf{r})}{2mc^2}\approx\frac{v^2}{c^2}\ll 1$.

[3] The identity is shown by dividing in pure and mixed terms of $(\boldsymbol{\sigma}\cdot\hat{\mathbf{p}})^2=\sum_{i=1}^3\sigma_i\hat{p}_i\sum_{j=1}^3\sigma_j\hat{p}_j$ which gives $\sum_{i,j}\sigma_i\sigma_j\hat{p}_i\hat{p}_j\left(\delta_{ij}+(1-\delta_{ij})\right)$ and only the pure terms survive due to the anticommutation of the Pauli matrices, i.e. $\sigma_i\sigma_j=-\sigma_i\sigma_j$ for $i\neq j$.

[4] We can prove this by collecting the pure and mixed terms w.r.t. the Pauli matrices, i.e. $(\boldsymbol{\sigma}\cdot\mathbf{a})\,(\boldsymbol{\sigma}\cdot\mathbf{b})=\sum_{i,j=1}^3 a_ib_j\left(\delta_{ij}\sigma_i\sigma_j+(1-\delta_{ij})\sigma_i\sigma_j\right)=\sum_{i,j=1}^3 a_ib_j\left(\mathbb{1}_{2\times2}+i\sum_k\epsilon_{ijk}\sigma_k\right)$. Using the cyclic invariance $\epsilon_{ijk}=$

i.e. $-\frac{\hat{\mathbf{p}}\cdot[\hat{\mathbf{p}},V(\mathbf{r})]}{4m^2c^2}$ is not Hermitian since $(\hat{\mathbf{p}}\cdot[\hat{\mathbf{p}},V(\mathbf{r})])^\dagger = \hat{\mathbf{p}}\cdot[\hat{\mathbf{p}},V(\mathbf{r})] - \underbrace{[\hat{\mathbf{p}}\cdot\hat{\mathbf{p}},V(\mathbf{r})]}_{\neq 0}$. If $\mathcal{H}_D$ is not Hermitian, $e^{-i\mathcal{H}_D/\hbar t}$ is not unitary which means that the probability is not conserved and is time dependent. Obviously, this was caused by having neglected the second bispinor component ψ_B, so far. Taking it into account will fix the non-Hermiticity and results in a correction term [Sha12, Chap. 20, p. 573] that is included into the "effective" Dirac Hamiltonian that yields (cf. (Equation 3.1.11))

$$\mathcal{H}_{DS} = \frac{\hat{\mathbf{p}}^2}{2m} + V(\mathbf{r}) - \frac{\hat{\mathbf{p}}^4}{8m^3c^2} - \frac{i\boldsymbol{\sigma}\cdot(\hat{\mathbf{p}}\times[\hat{\mathbf{p}},V(\mathbf{r})])}{4m^2c^2} - \frac{[\hat{\mathbf{p}},[\hat{\mathbf{p}},V(\mathbf{r})]]}{8m^2c^2} \quad . \tag{3.1.12}$$

Our interest, however, is focused on the fourth term of the Hamiltonian, that is simplified by computing the commutator $[\hat{\mathbf{p}},V(\mathbf{r})] = [-i\hbar\nabla,V(\mathbf{r})] = -i\hbar\nabla V(\mathbf{r})$. This term represents the *spin-orbit interaction* correction to the one-particle Hamiltonian and is finally given by (cf. [Sch68])

$$\mathcal{H}_{SOC} = -\frac{i\boldsymbol{\sigma}\cdot(\hat{\mathbf{p}}\times(-i\hbar\nabla V(\mathbf{r})))}{4m^2c^2} = \frac{\hbar}{4m^2c^2}\boldsymbol{\sigma}\cdot(\nabla V(\mathbf{r})\times\hat{\mathbf{p}}) \quad . \tag{3.1.13}$$

For example, if we consider the spherically symmetric potential (e.g. the potential of the hydrogen atom) $V(\mathbf{r}) = -\frac{1}{4\pi\epsilon_0}\frac{e^2}{r}$ we get

$$\mathcal{H}^H_{SOC} = \frac{e^2\hbar}{16m^2c^2\pi\epsilon_0|\mathbf{r}|^3}\boldsymbol{\sigma}\cdot(\mathbf{r}\times\hat{\mathbf{p}}) = \frac{e^2}{8m^2c^2\pi\epsilon_0 r^3}\mathbf{S}\cdot\mathbf{L} \quad , \tag{3.1.14}$$

which is the well known atomic $\mathbf{L}\cdot\mathbf{S}$ term. The evaluation of specific matrix elements of $\mathbf{L}\cdot\mathbf{S}$ for the p and d-orbitals is given in appendix B. Apart from the atomic spin-orbit coupling, a lot of important effects arise from (Equation 3.1.13), if we depart from the spherical symmetry of $V(\mathbf{r})$. As a side remark, we mention that spin-orbit coupling may not only be the result of relativistic quantum mechanics, but may also occur in strongly correlated, non-relativistic systems as *dynamically generated spin-orbit coupling* due to Fermi surface instabilities with higher angular momentum [WZ04]. In particular, we are interested in the spin-orbit coupling of the (itinerant) electrons on the lattice. Consequently, $V(\mathbf{r})$ inherits the symmetry of the lattice, i.e. $V(\mathbf{r}) = V(\mathbf{r}+\mathbf{R})$ with $\mathbf{R}$ being a real space lattice vector. On the one hand, we can proceed in the spirit of $\mathbf{k}\cdot\mathbf{p}$-*theory* and derive the spin-orbit terms in a (time-independent) perturbative way [Sho50; DKK55]. Treating spin-orbit coupling as a perturbation in the $\mathbf{k}\cdot\mathbf{p}$ framework is a method that was extensively used to investigate semiconductor band structures [Kan56; Kan57; Kan66; Kan82]. It has been employed to derive model Hamiltonians for the *quantum spin Hall effect* and *topological insulators* [BHZ06; QZ10]. More recently, the method was extended and applied to two-dimensional nanostructures [Gal05], car-

ϵ_{kij} of the Levi-Civita symbol we find $\sum_{i=1}^3 a_i b_i + i\sum_{kij}\sigma_k\epsilon_{kij}a_i b_j = \mathbf{a}\cdot\mathbf{b} + i\boldsymbol{\sigma}\cdot(\mathbf{a}\times\mathbf{b})$.

bon nanotubes and graphene nanoribbons [MM11]. Even more, $\mathbf{k}\cdot\mathbf{p}$-theory proved to be useful for the derivation of models for topological insulators [QZ10, Appendix A] and the *quantum anomalous Hall effect* [ZLW14]. On the other hand, we can - based on the point group of the underlying lattice - simply write down all invariant terms in orbital, spin and momentum space [LK55; Lut56]. As the *theory of invariant* or *invariant expansion* [BP74; TRR79; Win03] this has been applied to i.a. graphene [WZ10; KIF17] and silicene [GBT13].

3.1.1. $\mathbf{k}\cdot\mathbf{p}$-theory

The $\mathbf{k}\cdot\mathbf{p}$-theory is a well-established method in semiconductor physics and a variant of perturbation theory for the calculation of band energies and wave function in the vicinity of high symmetry points e.g. Γ, where the deviation $\mathbf{k}$ from Γ in k-space is treated as a small perturbation to the Hamiltonian at Γ [DKK55; Kan56; Kan66]. Consider the Bloch wave function with spin dependency given by the spinor χ_σ [WR28; Blo29] [Mah11, Chap. 3.1, p.32]

$$\psi_{\mathbf{k}b\sigma}(\mathbf{r}) = u_{\mathbf{k}b}(\mathbf{r})e^{i\mathbf{kr}}\chi_\sigma \quad , \tag{3.1.15}$$

with momentum $\mathbf{k}$, real space vector $\mathbf{r}$ and band index b. The cell periodic part $u_{\mathbf{k}b}(\mathbf{r})$ of the Bloch wave function satisfies $u_{\mathbf{k}b}(\mathbf{r}+\mathbf{R}) = u_{\mathbf{k}b}(\mathbf{r})$ with $\mathbf{R}$ being a real space Bravais lattice vector [Bra66]. The wave function is an eigenstate of the non-interacting Hamiltonian $\mathcal{H}_0 = \frac{\hat{\mathbf{p}}^2}{2m} + V(\mathbf{r})$ given that $\mathcal{H}_0\psi_{\mathbf{k}b\sigma}(\mathbf{r}) = \varepsilon_{\mathbf{k}b\sigma}\psi_{\mathbf{k}b\sigma}(\mathbf{r})$ with $\varepsilon_{\mathbf{k}b\sigma}$ being the single particle energy of band b and spin σ at momentum $\mathbf{k}$. In order to determine the matrix elements $\langle \mathbf{k}'b'\sigma'|\,\mathcal{H}_0 + \mathcal{H}_{SOC}\,|\mathbf{k}b\sigma\rangle$ of the total Hamiltonian we have to find the action of $\mathcal{H}_{SOC}$ (Equation 3.1.13) as well as $\mathcal{H}_0$ on the Bloch states. The non-interacting Hamiltonian acts on the Bloch state as (cf. [MM11])

$$\begin{aligned}\hat{\mathbf{p}}^2\psi_{\mathbf{k}b\sigma}(\mathbf{r}) &= (-i\hbar\nabla)^2 u_{\mathbf{k}b}(\mathbf{r})e^{i\mathbf{kr}}\chi_\sigma = (-i\hbar\nabla)e^{i\mathbf{kr}}\left(\hat{\mathbf{p}}+\hbar\mathbf{k}\right)u_{\mathbf{k}b}(\mathbf{r})\chi_\sigma \\ &= e^{i\mathbf{kr}}\chi_\sigma\left(\hat{\mathbf{p}}^2 + 2\hbar\mathbf{k}\cdot\hat{\mathbf{p}} + (\hbar\mathbf{k})^2\right)u_{\mathbf{k}b}(\mathbf{r})\chi_\sigma \quad .\end{aligned} \tag{3.1.16}$$

The spin-orbit part of the Hamiltonian $\mathcal{H}_{SOC} \propto \boldsymbol{\sigma}\cdot(\nabla V(\mathbf{r})\times\hat{\mathbf{p}})$ has the effect

$$\sum_{mn}\epsilon_{lmn}\left(\nabla V(\mathbf{r})\right)_m\hat{\mathbf{p}}_n u_{\mathbf{k}b}(\mathbf{r})e^{i\mathbf{kr}}\chi_\sigma = \sum_{mn}\left(\nabla V(\mathbf{r})\right)_m e^{i\mathbf{kr}}\left(\hat{\mathbf{p}}+\hbar\mathbf{k}\right)_n u_{\mathbf{k}b}(\mathbf{r})\chi_\sigma \quad . \tag{3.1.17}$$

Therefore, the Schrödinger equation of the total Hamiltonian yields

$$\frac{e^{i\mathbf{kr}}}{2m}\left[\hat{\mathbf{p}}^2 + 2\hbar\mathbf{k}\cdot\hat{\mathbf{p}} + \frac{\hbar^2}{2mc^2}\boldsymbol{\sigma}_{\sigma\sigma'}\cdot(\nabla V(\mathbf{r})\times(\hat{\mathbf{p}}+\hbar\mathbf{k}))\right]u_{\mathbf{k}b}(\mathbf{r})\chi_{\sigma'} = \left(\varepsilon_{\mathbf{k}b\sigma} - \frac{(\hbar\mathbf{k})^2}{2m}\right)u_{\mathbf{k}b}(\mathbf{r})\chi_\sigma \quad , \tag{3.1.18}$$

which is exactly valid only in the limit $\mathbf{k} \to 0$ at the Γ-point. Hence, we can treat $\mathbf{k}$ as a small perturbation to find the band energies in the vicinity of the Γ-point. The second term is called the "$\mathbf{k} \cdot \hat{\mathbf{p}}$-interaction", the third term with $\hat{\mathbf{p}}$ is the atomic like spin-orbit interaction, while the third term with $\mathbf{k}$ is responsible for the momentum dependent spin-orbit coupling [Kan57]. However, we are interested in the matrix elements of the spin-orbit interaction with respect to the Bloch states. These are extracted by multiplying the spin-orbit part of the equation with another Bloch state and integrating over the Wigner-Seitz cell, i.e. (cf. [Sam09, Section II.])

$$\begin{aligned}\langle \mathbf{k}' b' \sigma' | \, \mathcal{H}_{SOC} \, | \mathbf{k} b \sigma \rangle &= \frac{\hbar^2}{4m^2c^2} \int_{WS} \mathrm{d}\mathbf{r} \, \overline{u_{\mathbf{k}'b'}(\mathbf{r})} \overline{\chi_{\sigma'}} \, \boldsymbol{\sigma}_{\sigma'\sigma} \cdot (\nabla V(\mathbf{r}) \times (\hat{\mathbf{p}} + \hbar\mathbf{k})) \, u_{\mathbf{k}b}(\mathbf{r}) \chi_\sigma \\ &:= \mathbf{L}_{bb'}^{\sigma\sigma'}(\mathbf{k}) \cdot \boldsymbol{\sigma}_{\sigma'\sigma} \quad . \end{aligned} \tag{3.1.19}$$

There are apparently two terms that arise from the action of the spin-orbit operator on the Bloch wave function. The second one is usually neglected since it becomes very small in the vicinity of the center of the Brillouin zone, but gives, however, rise to momentum dependent spin-orbit coupling. The corresponding second quantized Hamiltonian can be written as

$$\mathcal{H}_0 = \sum_{\mathbf{k}} \sum_{b,b'} \sum_{\sigma,\sigma'} \left(\varepsilon_{\mathbf{k}b\sigma} \, \delta_{b,b'} \delta_{\tilde{\sigma},\tilde{\sigma}'} + \mathbf{L}_{bb'}^{\sigma\sigma'}(\mathbf{k}) \cdot \boldsymbol{\sigma}_{\sigma'\sigma} \right) c_{\mathbf{k},b,\sigma}^\dagger c_{\mathbf{k},b',\sigma'} \quad . \tag{3.1.20}$$

This equations provides a basis to calculate not only the matrix elements but also the absolute strength of the spin-orbit coupling terms by numerical evaluation of the Bloch states and integrals [KM05a; Min+06]. Apart from (trying to) straightforwardly evaluating the integral in (Equation 3.1.19) (over unknown Bloch wave functions), one can already derive a lot of constraints on $\mathbf{L}_{bb'}^{\sigma\sigma'}(\mathbf{k})$ if we require the Hamiltonian to be self-adjoint and symmetric with respect to time-reversal and/or spatial inversion, which will, however, be done in detail in (Section 3.1.2). $\mathbf{k} \cdot \mathbf{p}$-theory is in particular useful to provide estimates for the absolute strength of spin-orbit terms. However, it can only calculate the Hamiltonian in the vicinity of high symmetry points, while we are in need of the Hamiltonian in the overall Brillouin zone. Therefore, we have to rely on the *invariant expansion* as a complementary method to find $\mathcal{H}_{SOC}$.

3.1.2. Invariant expansion

Apart from deriving spin-orbit coupling from the action and the perturbative influence of the spin-orbit operator on the Bloch wave function and the corresponding band energies, we may also start from a generic point of view that only uses the lattice symmetries and additional constraints given by Hermiticity, time-reversal and inversion symmetry. Hence, we will also try to determine and classify spin-orbit coupling terms that emerge from a theory of invariants . Note, that we have to entangle three different spaces with each other, i.e.

momentum × orbital × spin

given by the direct product of their respective representations. When constructing a spin-orbit Hamiltonian from scratch, there are four key symmetries that have to be taken into account

- Hermiticity
- time-reversal symmetry
- odd/even parity, i.e. (anti-)symmetry w.r.t. spatial inversion
- point group symmetry

A general non-interacting multi-orbital Hamiltonian is given by the ansatz

$$\mathcal{H}_0 = \sum_{\mathbf{k}} \sum_{\alpha,\alpha'} \sum_{\sigma,\sigma'} \left[t^{\sigma\sigma'}_{\alpha\alpha'}(\mathbf{k})\delta_{\sigma\sigma'} + \lambda^{\sigma\sigma'}_{\alpha\alpha'}(\mathbf{k}) \right] a^\dagger_{\mathbf{k}\alpha\sigma} a_{\mathbf{k}\alpha'\sigma'} \quad , \tag{3.1.21}$$

where $\alpha = (s, o)$ is a multiindex for sublattice s and orbital o and σ, σ' are the "natural" spin degrees of freedom. While the first term $t(\mathbf{k})$ represents the usual tight-binding dispersion matrix elements and is diagonal in spin space, the second one ($\lambda(\mathbf{k})$) hosts spin-orbit coupling and may contain any off-diagonal elements in spin space. We focus on the second spin-dependent term, for which we make the ansatz

$$\lambda^{\sigma\sigma'}_{\alpha\alpha'}(\mathbf{k}) = \sum_{i=0}^{3} M_i^{\alpha\alpha'}(\mathbf{k}) \sigma_i^{\sigma\sigma'} \qquad , \quad M_i^{\alpha\alpha'}(\mathbf{k}) \in \mathbb{C} \quad , \tag{3.1.22}$$

where the $\sigma_i \quad i \in \{0, 1, 2, 3\}$ represent the Pauli matrices $\sigma_x, \sigma_y, \sigma_z$ including the unity matrix σ_0, since these comprise a complete basis of $\mathbb{C}^{2\times 2}$. Later it will turn out to be convenient to use the notation $M := (M_0, \mathbf{M})$ as a abbreviation for the zeroth and first to third components of M. Although, we are interested in the spin-dependent matrix elements of the single-particle Hamiltonian we keep σ_0 since there may be spin-diagonal terms arising from (Equation 3.1.13) (cf. [Sam09, Section II. B., Eq.(18)]). Of course, we require $\mathcal{H}_0$ to be Hermitian and the spin-dependent part $\lambda^{\sigma\sigma'}_{\alpha\alpha'}(\mathbf{k})$ to be Hermitian on its own, as well. From the condition $\mathcal{H}_0^\dagger \stackrel{!}{=} \mathcal{H}_0$ we get

$$\left(\lambda^{\sigma\sigma'}_{\alpha\alpha'}(\mathbf{k})\right)^\dagger = \overline{\lambda^{\sigma'\sigma}_{\alpha'\alpha}(\mathbf{k})} = \sum_{i=0}^{3} \overline{M_i^{\alpha'\alpha}(\mathbf{k})} \sigma_i^{\sigma\sigma'} \stackrel{!}{=} \sum_{i=0}^{3} M_i^{\alpha\alpha'}(\mathbf{k}) \sigma_i^{\sigma\sigma'} \quad , \tag{3.1.23}$$

where we used that the Pauli matrices are self-adjoint. Since the Pauli matrices are linear-independent, we can infer the requirement for *Hermiticity*

$$\overline{M_i^{\alpha'\alpha}(\mathbf{k})} = M_i^{\alpha\alpha'}(\mathbf{k}) \quad i \in \{0, 1, 2, 3\} \quad . \tag{3.1.24}$$

Next, we will implement *time-reversal symmetry* into our spin-orbit Hamiltonian. Since we are dealing with spin-$\frac{1}{2}$ fermions the time-reversal operator is given by $\hat{\Theta} = -i\sigma_y\mathcal{K}$ with $\mathcal{K}$ being the operator of complex conjugation [Wig12] [Sch05b, Chap. 11.4, p.228]. However, for a multi-orbital Hamiltonian the time-reversal operator is

$$\hat{\Theta}_o := \mathbb{1}_{n_o\times n_o} \otimes \hat{\Theta} = \mathbb{1}_{n_o\times n_o} \otimes \left(-i\sigma_y\mathcal{K}\right) \quad , \tag{3.1.25}$$

where n_o is the number of orbitals. Note, that time-reversal has indeed a non-trivial effect on orbitals, as well, since $\hat{\Theta}$ affects the spherical harmonics by $Y_l^m(\theta,\phi) \overset{\text{TR}}{\to} \overline{Y_l^m(\theta,\phi)} = (-1)^m Y_l^{-m}(\theta,\phi)$ [SN11, Chap. 4.4, p. 276]. However, we assume to be using *real* orbital basis that combines spherical harmonics with $+m$ and $-m$ and thereby canceling the effect of time-reversal (cf. appendix B). Thus, the time-reversed spin-orbit Hamiltonian is given by (momentum is odd with respect to time-reversal, $\mathbf{k} \to -\mathbf{k}$)

$$\begin{aligned}\hat{\Theta}_o^{-1}\mathcal{H}(\mathbf{k})\hat{\Theta}_o \quad \Rightarrow \quad \hat{\Theta}_o^{-1}\lambda_{\alpha\alpha'}^{\sigma\sigma'}(\mathbf{k})\hat{\Theta}_o &= \overline{M_0^{\alpha\alpha'}(-\mathbf{k})}\sigma_0 + \overline{\mathbf{M}^{\alpha\alpha'}(-\mathbf{k})}\cdot(-\boldsymbol{\sigma}) \\ &\overset{!}{=} M_0^{\alpha\alpha'}(\mathbf{k})\sigma_0 + \mathbf{M}^{\alpha\alpha'}(\mathbf{k})\cdot\boldsymbol{\sigma} \quad .\end{aligned} \tag{3.1.26}$$

where we used that the spin (as being governed by angular momentum algebra) is odd under time-reversal, i.e. $\hat{\Theta}^{-1}\hat{\boldsymbol{\sigma}}\hat{\Theta} = -\hat{\boldsymbol{\sigma}}$ [SN11, Chap. 4.4, p. 275] [Wig32] [5]. Consequently, the condition time-reversal invariance imposes on $M(\mathbf{k})$ is

$$M_0^{\alpha\alpha'}(\mathbf{k}) = \overline{M_0^{\alpha\alpha'}(-\mathbf{k})} \qquad \text{and} \qquad \mathbf{M}^{\alpha\alpha'}(\mathbf{k}) = -\overline{\mathbf{M}^{\alpha\alpha'}(-\mathbf{k})} \quad . \tag{3.1.27}$$

Details and an alternative derivation are given in appendix D. As an example, let's consider the $\mathbf{L}\cdot\mathbf{S}$ term in the three d-orbitals d_{xz}, d_{yz} and d_{xy}. In terms of the basis $\mathbf{c}_{o\sigma}^\dagger = \left(c_{d_{xz}}^\dagger, c_{d_{yz}}^\dagger, c_{d_{xy}}^\dagger\right)^T \otimes \left(c_\uparrow^\dagger, c_\downarrow^\dagger\right)^T$ it is given by (see its alternative derivation in appendix B)

$$\hat{\mathbf{L}}\cdot\hat{\mathbf{S}} = \frac{1}{2}\mathbf{c}_{o\sigma}^\dagger \begin{pmatrix} 0 & -i\sigma_z & -i\sigma_x \\ i\sigma_z & 0 & i\sigma_y \\ i\sigma_x & -i\sigma_y & 0 \end{pmatrix} \mathbf{c}_{o\sigma} \quad . \tag{3.1.28}$$

If we express this operator in terms of the entities introduced above we get (cf. (Equation 3.1.39))

$$M_0^{\alpha\alpha'}(\mathbf{k}) = 0 \qquad \text{and} \qquad \mathbf{M}^{\alpha\alpha'}(\mathbf{k}) = \begin{pmatrix} 0 & -i\hat{z} & -i\hat{x} \\ i\hat{z} & 0 & i\hat{y} \\ i\hat{x} & -i\hat{y} & 0 \end{pmatrix} \quad , \tag{3.1.29}$$

[5] Note, that time-reversal is non-unitary, therefore we have $\Theta^{-1} \neq \Theta^\dagger$ with $\Theta^{-1} = +i\sigma_y\mathcal{K}$.

with $\hat{x}, \hat{y}, \hat{z}$ being the unit vectors in Cartesian coordinates. Hermiticity (Equation 3.1.24) is obviously fulfilled and time-reversal symmetry (Equation 3.1.27) is intact as well, since apparently $\mathbf{M}^{\alpha\alpha'} = -\overline{\mathbf{M}^{\alpha\alpha'}}$ due to $\mathbf{M}$ being momentum independent. In order to check out the implications of parity, i.e. the behavior of the Hamiltonian w.r.t. to spatial inversion, we split it into an inversion symmetric (gerade) and antisymmetric (ungerade) part, which amounts to the definition

$$\mathbf{M}_g(\mathbf{k}) \coloneqq \frac{\mathbf{M}(\mathbf{k}) + \mathbf{M}(-\mathbf{k})}{2} \qquad \text{and} \qquad \mathbf{M}_u(\mathbf{k}) \coloneqq \frac{\mathbf{M}(\mathbf{k}) - \mathbf{M}(-\mathbf{k})}{2} \quad , \tag{3.1.30}$$

that implies for the non-interacting Hamiltonian the form

$$\mathcal{H}_0 = \sum_{\mathbf{k}} \sum_{\alpha,\alpha'} \sum_{\sigma,\sigma'} \left[t^{\sigma\sigma'}_{\alpha\alpha'}(\mathbf{k}) \delta_{\sigma\sigma'} + \left(\mathbf{M}_g^{\alpha\alpha'}(\mathbf{k}) + \mathbf{M}_u^{\alpha\alpha'}(\mathbf{k}) \right) \cdot \boldsymbol{\sigma}_{\sigma\sigma'} \right] a^\dagger_{\mathbf{k}\alpha\sigma} a_{\mathbf{k}\alpha'\sigma'} \quad . \tag{3.1.31}$$

Physically, this symmetry or antisymmetry of the Hamiltonian is related to the symmetry of the potential $V(\mathbf{r})$ in (Equation 3.1.13), which may similarly split up into symmetric and antisymmetric part. This enables us to even deal with arbitrary potentials comprising parts of both symmetry. Let's denote the parity operator or operator of spatial inversion by $\hat{I}$. Apparently, the symmetry of the Hamiltonian is inherited by $\mathbf{M}^{\alpha\alpha'}(\mathbf{k})$ since $\hat{I}^{-1}\lambda^{\sigma\sigma'}_{\alpha\alpha'}(\mathbf{k})\hat{I} = \lambda^{\sigma\sigma'}_{\alpha\alpha'}(-\mathbf{k}) = \pm\lambda^{\sigma\sigma'}_{\alpha\alpha'}(\mathbf{k})$ and the spin is a pseudo/axial-vector that doesn't transform under spatial inversion, i.e. $\hat{I}^{-1}\boldsymbol{\sigma}\hat{I} = \boldsymbol{\sigma}$. For simplicity, we assume in the following the spin-orbit part of the Hamiltonian to be either fully symmetric or antisymmetric (of course, $t^{\sigma\sigma'}_{\alpha\alpha'}(\mathbf{k})$ is always symmetric). However, we may always get back to an arbitrary potential $V(\mathbf{r})$ by taking into account both finite symmetric and antisymmetric parts. By summarizing the requirements and conditions for Hermiticity, time-reversal and parity, for the symmetric case $\mathbf{M}(\mathbf{k}) = \mathbf{M}(-\mathbf{k})$, starting from (Equation 3.1.27), we get

$$\begin{aligned} \mathbf{M}^{\alpha\alpha'}(\mathbf{k}) = -\overline{\mathbf{M}^{\alpha\alpha'}(-\mathbf{k})} &\overset{(Equation\ 3.1.30)}{\downarrow =} -\overline{\mathbf{M}^{\alpha\alpha'}(\mathbf{k})} \\ &\overset{(Equation\ 3.1.24)}{\downarrow =} -\mathbf{M}^{\alpha'\alpha}(\mathbf{k}) = -\left[\mathbf{M}^{\alpha\alpha'}(\mathbf{k})\right]^T \quad . \end{aligned} \tag{3.1.32}$$

Hence, the orbital matrix (with indices α, α') is antisymmetry and all diagonal terms must vanish. Thus, there's no single band model with symmetric spin-orbit interaction. Besides, the first equality states that $\mathbf{M}^{\alpha\alpha'}(\mathbf{k}) \coloneqq i\mathbf{N}^{\alpha\alpha'}(\mathbf{k}), \mathbf{N} \in \mathbb{R}^3$ must be purely imaginary. Note, that this is indeed the case for our example (Equation 3.1.29). Analogously, $M_0^{\alpha\alpha'}(\mathbf{k}) \in \mathbb{R}$ is real and must be symmetric in the orbital indices. Let's turn to the antisymmetric case $\mathbf{M}(\mathbf{k}) = -\mathbf{M}(-\mathbf{k})$. Here, we get (starting from (Equation 3.1.27))

Table 3.1.: The classification of spin-orbit interaction Hamiltonians that are subject to Hermiticity, time-reversal symmetry and definite parity shows that all matrix elements must be real or purely imaginary. The (anti-)symmetry of terms in orbital indices ensures that in a single band model there's only antisymmetric spin-orbit coupling and it requires at least two orbitals to have finite spin-orbit interaction in a centrosymmetric system. For the definition of $M^{\alpha\alpha}(\mathbf{k})$ we refer to (Equation 3.1.22).

	centrosymmetric		non-centrosymmetric	
	$M_0^{\alpha\alpha'}(\mathbf{k})$	$\mathbf{M}^{\alpha,\alpha'}(\mathbf{k})$	$M_0^{\alpha\alpha'}(\mathbf{k})$	$\mathbf{M}^{\alpha,\alpha'}(\mathbf{k})$
parity	even	even	odd	odd
number	real	imaginary	imaginary	real
orbital matrix	symmetric	antisymmetric	antisymmetric	symmetric

$$\mathbf{M}^{\alpha\alpha'}(\mathbf{k}) = -\overline{\mathbf{M}^{\alpha\alpha'}(-\mathbf{k})} \overset{(Equation\ 3.1.30)}{\overset{\downarrow}{=}} \overline{\mathbf{M}^{\alpha\alpha'}(\mathbf{k})} \overset{(Equation\ 3.1.24)}{\overset{\downarrow}{=}} \mathbf{M}^{\alpha'\alpha}(\mathbf{k}) = \left[\mathbf{M}^{\alpha\alpha'}(\mathbf{k})\right]^T \quad . \tag{3.1.33}$$

First, this tells us that $\mathbf{M}^{\alpha\alpha'}(\mathbf{k}) \in \mathbb{R}^3$ is real. Second, its orbital matrix is symmetric, which opens up the possibility for finite spin-orbit interaction in a single band $\alpha = \alpha'$. Like expected, the antisymmetric zeroth component $M_0^{\alpha\alpha'}(\mathbf{k}) = iN_0^{\alpha\alpha'}(\mathbf{k})$, $N_0 \in \mathbb{R}$ is purely imaginary and antisymmetric w.r.t. to its orbital indices, i.e. $M_0^{\alpha\alpha'}(\mathbf{k}) = -\left[M_0^{\alpha\alpha'}(\mathbf{k})\right]^T$. For the single band case $\alpha = \alpha' = 1$ with finite antisymmetric spin-orbit interaction, $\mathbf{M}^{\alpha\alpha'}(\mathbf{k})$ is denoted by $\boldsymbol{\gamma}(\mathbf{k}) \in \mathbb{R}^3$ with $\boldsymbol{\gamma}(-\mathbf{k}) = -\boldsymbol{\gamma}(\mathbf{k})$ most commonly in the literature [Gmi+09; Smi+17a; BS12]. Please note, that due to its antisymmetric property $\boldsymbol{\gamma}(-\mathbf{k})$ is zero not only at $\mathbf{k} = 0$ but at some high-symmetry points with $\mathbf{k} + \mathbf{G} = -\mathbf{k}$ as well, where $\mathbf{G}$ is some reciprocal lattice vector.

After fixing and classifying most of the constraints that must be imposed on a physical reasonable spin-orbit interaction we have to focus on the point group and lattice symmetry at last, that also enable us to derive particular Hamiltonians featuring phenomenological parameters. Let's introduce some nomenclature for the transformation of real space and reciprocal space vectors (momenta), spin transformations and sublattice/orbital transformations w.r.t. to point group $\mathcal{G}$ with element $g \in \mathcal{G}$ and $g \in \mathcal{G}^D$ for the spinor transformation, where $\mathcal{G}^D$ is the corresponding *double group* . We define

$$\mathbf{k} \in \mathbb{R}^3 \quad \rightarrow \quad \mathbf{k}' = \mathcal{P}(g)\mathbf{k} \qquad \text{with} \quad \mathcal{P}(g) \in \mathbb{R}^{3\times 3} \tag{3.1.34}$$

$$\chi \in \mathbb{C}^2 \quad \rightarrow \quad \chi' = \mathcal{S}(g)\chi \qquad \text{with} \quad \mathcal{S}(g) \in \mathbb{C}^{2\times 2} \tag{3.1.35}$$

$$\mathbf{a}_o \in \mathbb{C}^{n_o n_s} \quad \rightarrow \quad \mathbf{a}_o' = \mathcal{L}(g)\mathbf{a}_o \qquad \text{with} \quad \mathcal{L}(g) \in \mathbb{C}^{n_o n_s \times n_o n_s} \quad , \tag{3.1.36}$$

with $\mathbf{a}_o$ being an "orbital spinor" whose size is determined by the number of sublattices n_s times the number of orbitals n_o in the Hamiltonian. The reducible representations $\mathcal{P}(g)$ and $\mathcal{L}(g)$ are associated to a subgroup of the full continuous rotation group SO(3). The SU(2) transformation representation $\mathcal{S}(g)$ consists of twice the number of elements compared to the group $\mathcal{G}$. The rotations are given by $\mathcal{S}(\hat{n}, \varphi) = e^{-i\hat{n}\sigma\varphi/2} = \mathbb{1}\cos(\varphi/2) - i\hat{n}\sigma\sin(\varphi/2)$ where the rotation is about the axis $\hat{n}$ by angle φ. The reflection in the plane given by its normal vector $\hat{n}$ is constructed by a inversion (whose representation is unity due to spin being a pseudovector) followed by a rotation about the axis $\hat{n}$ by π, i.e. $\mathcal{S}(\hat{n}) = -i\hat{n}\sigma$ [Mer98]. The (reducible) transformation $\mathcal{D}(g)$ of the spinful Hamiltonian necessarily features an element $g \in \mathcal{G}^D$ of the double group and is given by

$$\mathcal{D}(g) = \mathcal{L}(g) \otimes \mathcal{S}(g) \qquad \text{with} \quad \mathcal{D}(g) \in \mathbb{C}^{2n_o n_s \times 2n_o n_s} \quad . \tag{3.1.37}$$

Analogously to the *invariant expansion* or *theory of invariants* we require the Hamiltonian $\mathcal{H}_0(\mathbf{k})$ (cf. (Equation 3.1.21)) to satisfy [BP74; LK55; Lut56; Win03]

$$\mathcal{D}(g)^\dagger \mathcal{H}_0(\mathbf{k}) \mathcal{D}(g) = \mathcal{H}_0(\mathcal{P}(g)\mathbf{k}) \qquad \forall g \in \mathcal{G}^{(D)} \quad . \tag{3.1.38}$$

By exploring the transformation behavior of the sublattices/orbitals involved we are able to classify subspaces of these sublattice/orbitals according to irreducible representations of $\mathcal{G}$ and to split the Hamiltonian into blocks of size $n_{\Gamma_i} \times n_{\Gamma_j}$ where $n_{\Gamma_{i,j}}$ are the dimensions of the irreducible representations. Every block may then be expanded in terms of products of basis functions of $\mathbf{k}$ and invariant matrices that transform like the irreducible representations Γ_k that are contained in the product $\Gamma_i \times \Gamma_j$. [TRR79; Win03]. The details of this treatment for d-orbitals on a tetragonal lattice are given in appendix C.

Centrosymmetric spin-orbit coupling

After having assembled all necessary tools and prerequisites, we will continue by trying to reconstruct the $\mathbf{L}\cdot\mathbf{S}$ term in (Equation 3.1.29). We have to stick to the centrosymmetric case in (Table 3.1). Since we are not allowed to have finite diagonal elements in the orbital matrix we can already exclude the representations A_{1g} and B_{1g} in the upper left 2×2 block as basis in orbital space as these correspond to the τ_0 and τ_z orbital Pauli matrices. We also learned from (Table 3.1) that $\mathbf{M}^{\alpha\alpha'}(\mathbf{k})$ has to be purely imaginary, which excludes B_{2g}, too and leaves us with A_{2g} and τ_y corresponding to σ_z in spin space. The

block with $B_{2g} \otimes B_{2g} = A_{1g}$ has to be zero as well, which means that we are left with the 4×2 block of the $E_g \otimes B_{2g} = E_g$ representation. As mentioned above, the Pauli matrices σ_x, σ_y behave according to the E_g representation. To fix the order of the two components, we look, for instance, at the σ_x operation. We find that σ_x must be associated to d_{xz} and σ_y must be associated to the d_{yz} since $\sigma_x a^\dagger_{xz} a_{xy}$ transforms into $(-\sigma_x) a^\dagger_{xz} (-a_{xy})$ under σ_x. This choice renders the Hamiltonian invariant with respect to the point group in the sense (Equation 3.1.38). The operation e.g. C_4^+ fixes the opposite sign while the overall sign is arbitrary, i.e. given by the associated phenomenological coefficient. Therefore, we end up with the spin-orbit matrix for a centrosymmetric, momentum-independent model with d_{xz}, d_{yz} and d_{xy} that yields

$$\mathbf{M}^{\alpha\alpha'}(\mathbf{k}) = \begin{pmatrix} 0 & -i\hat{z} & -i\hat{x} \\ i\hat{z} & 0 & i\hat{y} \\ i\hat{x} & -i\hat{y} & 0 \end{pmatrix} \quad , \tag{3.1.39}$$

and fully agrees with the $\mathbf{L} \cdot \mathbf{S}$ term given in (Equation 3.1.29) (up to prefactors) that was calculated by evaluating the matrix elements explicitly by considering the action of the angular momentum operator on the d-orbitals. We now proceed by exploring the possibility of momentum dependent spin-orbit interaction in centrosymmetric crystals. (Table 3.1) shows that this is possible only in a *multi-orbital model* . We begin with the three orbital case that leads to (Equation 3.1.39) for momentum-independent terms and try to take into account momentum dependent basis functions. Firstly, the associated basis functions in $\mathbf{k}$-space must be even and therefore can only be one-dimensional representations of D_{4h}. Secondly, the orbital matrix $\mathbf{M}^{\alpha\alpha'}$ must be antisymmetric in the orbital indices. Thirdly, $\mathbf{M}^{\alpha\alpha'}$ must be purely imaginary. In contrast to the momentum independent case before, where we simply used the same representation in both orbital and spin space to make sure that the entire block is invariant (transforms as A_{1g}), we now have to "entangle" all *three* different spaces:

$$\textbf{momentum} \times \textbf{orbital} \times \textbf{spin}$$

It turns out to be most convenient to work out the product representations successively, which may be done in three ways. Here, we first couple orbital and spin space and use their product representation to be merged with the one in momentum space. We start with the upper left 2×2 block of the d_{xz} and d_{yz} orbitals, where we already proved that the only valid orbital basis matrix is τ_y associated to A_{2g}. Hence, the direct product of A_{2g} (orbital space) and the representation in spin space must consist of one-dimensional representations, which excludes E_g with σ_x and σ_y. The remaining Pauli matrix σ_z transforms like A_{2g} and fixes the representation in momentum space to be $\Gamma_{\text{orbital}} \otimes \Gamma_{\text{spin}} = A_{2g} \otimes A_{2g} = A_{1g}$. Consequently, in d_{xz} and d_{yz} space we get for first nearest neighbors:

$$\mathcal{H}^{xz,yz}_{SOC} = \left(\cos(k_x) + \cos\left(k_y\right)\right) \tau_y \otimes \sigma_z \quad . \tag{3.1.40}$$

The remaining derivation and final result of non-local spin-orbit terms in the five-d-orbital Hamiltonian are given in appendix C.1. As we respected both time-reversal and inversion symmetry for the spin-orbit coupling terms in centrosymmetric models, we expect the bands to be doubly degenerate. However, due to the spin-off-diagonal terms the SU(2) spin rotation symmetry is obviously broken. Therefore, we will introduce the *pseudospin* degree of freedom in (Section 3.2) to describe centrosymmetric spin-orbit coupled models in band basis.

Non-centrosymmetric spin-orbit coupling

The simplest non-centrosymmetric spin-orbit coupling Hamiltonian is actually a single band model (in contrast to centrosymmetric spin-orbit coupling that does only exist for multi-orbital Hamiltonians). Hence, we introduce the notation [BS12, Chap. 4.2.1, p.131]

$$\gamma(\mathbf{k}) \coloneqq \mathbf{M}^{\alpha\alpha'}(\mathbf{k}) \quad \text{with} \quad \alpha = \alpha' = 1 \quad , \tag{3.1.41}$$

for the antisymmetric $\gamma(-\mathbf{k}) = -\gamma(-\mathbf{k})$ and real $\gamma(\mathbf{k}) \in \mathbb{R}^3$ *spin-orbit field* $\gamma(\mathbf{k})$ (cf. (Table 3.1)). $\gamma(\mathbf{k})$ introduces a momentum dependent spin quantization axis that lifts the spin degeneracy. We refer back to the Hamiltonian (Equation 3.1.21) that yields

$$\mathcal{H}_0 = \sum_{\mathbf{k}} \sum_{\sigma,\sigma'} \left[\varepsilon(\mathbf{k}) \delta_{\sigma\sigma'} + \gamma(\mathbf{k}) \cdot \boldsymbol{\sigma}^{\sigma\sigma'} \right] a^\dagger_{\mathbf{k}\sigma} a_{\mathbf{k}\sigma'} \quad , \tag{3.1.42}$$

in our specific case of a single-orbital Hamiltonian with broken inversion symmetry where the spinless term $t_{\alpha,\alpha'} \coloneqq \varepsilon$ is already diagonal in orbital and spin indices. While the spinless term is invariant under spin-rotations, of course, $\gamma(\mathbf{k})$ transforms like a polar vector, i.e. a spin rotation about the axis $\hat{n}$ by angle φ affects γ by $\gamma(\mathbf{k}) \longrightarrow \mathcal{R}(\hat{n}, \varphi)\gamma(\mathbf{k})$, where $\mathcal{R}(\hat{n}, \varphi)$ is the SO(3) rotation matrix (for details, see analogous case of d-vector in (Section 2.4.4)) The eigenvalues $\xi(\mathbf{k})$ of (Equation 3.1.42) are straightforwardly calculated

$$\begin{aligned} &\mathcal{H}_0 \mathbf{u}_\mathbf{k} = \xi(\mathbf{k}) \mathbf{u}_\mathbf{k} \qquad \Rightarrow \qquad \begin{pmatrix} \varepsilon + \gamma^z - \xi & \gamma^x - i\gamma^y \\ \gamma^x + i\gamma^y & \varepsilon - \gamma^z - \xi \end{pmatrix} \mathbf{u}_\mathbf{k} = 0 \\ &\Rightarrow (\varepsilon - \xi)^2 - (\gamma^z)^2 - (\gamma^x)^2 - (\gamma^y)^2 = (\varepsilon - \xi)^2 - |\gamma|^2 \stackrel{!}{=} 0 \quad , \end{aligned} \tag{3.1.43}$$

and therefore given by

$$\xi(\mathbf{k})_\pm = \varepsilon(\mathbf{k}) \pm |\gamma(\mathbf{k})| \quad . \tag{3.1.44}$$

The new spin-like degree of freedom characterizing the spin-split states is called the

helicity $\lambda = \pm$ of the bands [SAM09; Sam09]. The eigenvectors of (Equation 3.1.42), we label with helicity λ, are determined by

$$(\mathcal{H}_0 - \xi_{\mathbf{k}\lambda}\sigma_0)\,\mathbf{u}_{\mathbf{k}\lambda} = 0 \quad \Rightarrow \quad \begin{pmatrix} \varepsilon + \gamma^z - \xi & \gamma^x - i\gamma^y \\ \gamma^x + i\gamma^y & \varepsilon - \gamma^z - \xi \end{pmatrix} \begin{pmatrix} u^{\uparrow}_{\mathbf{k}\lambda} \\ u^{\downarrow}_{\mathbf{k}\lambda} \end{pmatrix} = 0 \quad , \tag{3.1.45}$$

and therefore given by (cf. [SAM09, p. 7, eq. (15)])

$$\mathbf{u}_{\mathbf{k}\lambda} = \begin{pmatrix} u^{\uparrow}_{\mathbf{k}\lambda} \\ u^{\downarrow}_{\mathbf{k}\lambda} \end{pmatrix} \propto \begin{pmatrix} -\gamma^x + i\gamma^y \\ \gamma^z + \lambda|\boldsymbol{\gamma}| \end{pmatrix} \quad . \tag{3.1.46}$$

In order to write the eigenstate in a clearly arranged form we introduce the momentum-dependent phase

$$e^{i\phi_{\mathbf{k}}} = \frac{-\gamma^x + i\gamma^y}{\sqrt{(\gamma^x)^2 + (\gamma^y)^2}} \quad . \tag{3.1.47}$$

Expressing (Equation 3.1.46) in terms of that phase, we find

$$\begin{pmatrix} e^{i\phi_{\mathbf{k}}} \\ \frac{\gamma^z + \lambda|\boldsymbol{\gamma}|}{\sqrt{(\gamma^x)^2 + (\gamma^y)^2}} \end{pmatrix} = \begin{pmatrix} e^{i\phi_{\mathbf{k}}} \\ \frac{\gamma^z + \lambda|\boldsymbol{\gamma}|}{\sqrt{(|\boldsymbol{\gamma}| + \gamma^z)(|\boldsymbol{\gamma}| - \gamma^z)}} \end{pmatrix} = \begin{pmatrix} e^{i\phi_{\mathbf{k}}} \\ \sqrt{\frac{|\boldsymbol{\gamma}| + \lambda\gamma^z}{|\boldsymbol{\gamma}| - \lambda\gamma^z}} \end{pmatrix} \to \begin{pmatrix} \sqrt{|\boldsymbol{\gamma}| - \lambda\gamma^z}\, e^{i\phi_{\mathbf{k}}} \\ \sqrt{|\boldsymbol{\gamma}| + \lambda\gamma^z} \end{pmatrix} \quad . \tag{3.1.48}$$

The corresponding norm is given by

$$\left|\sqrt{|\boldsymbol{\gamma}| - \lambda\gamma^z}\, e^{i\phi_{\mathbf{k}}}\right|^2 + \left|\sqrt{|\boldsymbol{\gamma}| + \lambda\gamma^z}\right|^2 = (|\boldsymbol{\gamma}| - \lambda\gamma^z) + (|\boldsymbol{\gamma}| + \lambda\gamma^z) = 2|\boldsymbol{\gamma}| \quad . \tag{3.1.49}$$

Therefore, the normalized eigenstates are given by

$$\mathbf{u}_{\mathbf{k}\lambda} = \begin{pmatrix} u^{\uparrow}_{\mathbf{k}\lambda} \\ u^{\downarrow}_{\mathbf{k}\lambda} \end{pmatrix} = \begin{pmatrix} \sqrt{\frac{1 - \lambda\gamma^z/|\boldsymbol{\gamma}|}{2}}\, e^{i\phi_{\mathbf{k}}} \\ \sqrt{\frac{1 + \lambda\gamma^z/|\boldsymbol{\gamma}|}{2}} \end{pmatrix} \quad \text{with} \quad e^{i\phi_{\mathbf{k}}} = \frac{-\gamma^x + i\gamma^y}{\sqrt{(\gamma^x)^2 + (\gamma^y)^2}} \quad , \tag{3.1.50}$$

where the phase satisfies $e^{i\phi_{-\mathbf{k}}} = -e^{i\phi_{\mathbf{k}}}$ due to the antisymmetry $\boldsymbol{\gamma}(-\mathbf{k}) = -\boldsymbol{\gamma}(\mathbf{k})$. These eigenvectors are used to define new quasiparticle states in terms of which the Hamiltonian assumes the compact form

$$\mathcal{H}_0 = \sum_{\mathbf{k}} \sum_{\lambda} \xi_{\mathbf{k}\lambda} b^{\dagger}_{\mathbf{k}\lambda} b_{\mathbf{k}\lambda} \quad , \tag{3.1.51}$$

with the eigenvalues (Equation 3.1.44) and the new helical quasiparticle operators that are given by the unitary transformation

$$\begin{pmatrix} b_{\mathbf{k}+} \\ b_{\mathbf{k}-} \end{pmatrix} := \begin{pmatrix} \sqrt{\frac{1-\gamma^z/|\gamma|}{2}} e^{i\phi_{\mathbf{k}}} & \sqrt{\frac{1+\gamma^z/|\gamma|}{2}} \\ -\sqrt{\frac{1+\gamma^z/|\gamma|}{2}} & \sqrt{\frac{1-\gamma^z/|\gamma|}{2}} e^{-i\phi_{\mathbf{k}}} \end{pmatrix} \begin{pmatrix} a_{\mathbf{k}\uparrow} \\ a_{\mathbf{k}\downarrow} \end{pmatrix} = \underbrace{\begin{pmatrix} u_{\mathbf{k}} & v_{\mathbf{k}} \\ -\overline{v}_{\mathbf{k}} & \overline{u}_{\mathbf{k}} \end{pmatrix}}_{:=U_{\mathbf{k}}} \begin{pmatrix} a_{\mathbf{k}\uparrow} \\ a_{\mathbf{k}\downarrow} \end{pmatrix} \quad . \tag{3.1.52}$$

The matrix elements of the Bogoliubov transformation defining the helical states in terms of the "natural" spin states satisfy the relations $\overline{u}_{\mathbf{k}} = e^{-2i\phi_{\mathbf{k}}} u_{\mathbf{k}}$, $\overline{v}_{\mathbf{k}} = v_{\mathbf{k}}$, $u_{-\mathbf{k}} = -e^{i\phi_{\mathbf{k}}} v_{\mathbf{k}}$ and $v_{-\mathbf{k}} = e^{-i\phi_{\mathbf{k}}} u_{\mathbf{k}}$. Therefore, the new quasiparticle states fulfill

$$\begin{pmatrix} b_{\mathbf{k}+} \\ b_{\mathbf{k}-} \end{pmatrix} \to \begin{pmatrix} b_{-\mathbf{k}+} \\ b_{-\mathbf{k}-} \end{pmatrix} = \begin{pmatrix} b_{\mathbf{k}-} e^{i\phi_{\mathbf{k}}} \\ -b_{\mathbf{k}+} e^{-i\phi_{\mathbf{k}}} \end{pmatrix} \quad , \tag{3.1.53}$$

under inversion of $\mathbf{k}$ and do, like expected, not yield a degenerate state. The behavior of the new quasiparticle states $b_{\mathbf{k}\lambda}$ under time-reversal is given by $b_{\mathbf{k}\lambda} \longrightarrow U_{-\mathbf{k}} \hat{\Theta} U_{\mathbf{k}}^{-1} \mathbf{b}_{\mathbf{k}\lambda} = \mathrm{diag}(e^{i\phi_{\mathbf{k}}}, e^{-i\phi_{\mathbf{k}}})\, \mathbf{b}_{\mathbf{k}\lambda}$ with $\Theta = -i\sigma_y \mathcal{K}$ [6]. Hence, the operator of time-reversal in helical basis $\Omega := U_{-\mathbf{k}} \hat{\Theta} U_{\mathbf{k}}^{-1}$ is diagonal and the helical quasiparticle states are invariant under time-reversal up to a k-dependent phase $\phi(\mathbf{k})$ and the inversion of momentum. In contrast, time-reversal for "natural spin" states, usually exchanges both spin states. As a consequence of the broken spin symmetry and the $\mathbf{k}$-dependent quantization axis, we have a momentum dependent spin expectation value that is

$$\begin{aligned} \langle \boldsymbol{\sigma} \rangle_\lambda &= \langle \mathbf{k}, \lambda | \, \boldsymbol{\sigma} \, | \mathbf{k}, \lambda \rangle \\ &= \lambda \left(\overline{u}_{\mathbf{k}} v_{\mathbf{k}} + \overline{v}_{\mathbf{k}} u_{\mathbf{k}}, -i\overline{u}_{\mathbf{k}} v_{\mathbf{k}} + i\overline{v}_{\mathbf{k}} u_{\mathbf{k}}, \overline{u}_{\mathbf{k}} u_{\mathbf{k}} - \overline{v}_{\mathbf{k}} v_{\mathbf{k}} \right) = -\lambda \frac{\boldsymbol{\gamma}_{\mathbf{k}}}{|\boldsymbol{\gamma}_{\mathbf{k}}|} \quad . \end{aligned} \tag{3.1.55}$$

The spin expectation value points opposite to the momentum dependent direction of $\boldsymbol{\gamma}(\mathbf{k})$ for helicity $+$. Therefore, the normal non-interacting state of the Hamiltonian with antisymmetric spin-orbit coupling already exhibits a highly non-trivial spin structure. Note that the physical origin of the antisymmetric spin-orbit field (SOF) [Gmi+09] is very diverse. Here, we mainly distinguish two situations. On the one hand, we have *bulk inversion asymmetry* (*BIA*) originating from the intrinsic lack of an inversion center in a crystal that gives rise to the *Dresselhaus term*. On the other hand, one encounters *structure inversion asymmetry* (*SIA*) that can be traced back to a heterostructure-interface that breaks inversion symmetry along a specifically engineered crystal direction and is linked to *Rashba* spin-orbit interaction [BR84a; BR84b]. Note that there's also the effect

[6] In detail we have:

$$U_{-\mathbf{k}} \hat{\Theta} U_{\mathbf{k}}^{-1} \, \mathbf{b}_{\mathbf{k}\lambda} = U_{-\mathbf{k}} \left(-i\sigma_y \right) U_{\mathbf{k}}^T = \begin{pmatrix} u_{-\mathbf{k}} & v_{-\mathbf{k}} \\ -\overline{v}_{-\mathbf{k}} & \overline{u}_{-\mathbf{k}} \end{pmatrix} \begin{pmatrix} 0 & -1 \\ 1 & 0 \end{pmatrix} \begin{pmatrix} u_{\mathbf{k}} & -\overline{v}_{\mathbf{k}} \\ v_{\mathbf{k}} & \overline{u}_{\mathbf{k}} \end{pmatrix} = \begin{pmatrix} e^{i\phi(\mathbf{k})} & 0 \\ 0 & e^{-i\phi(\mathbf{k})} \end{pmatrix} \tag{3.1.54}$$

of *Interface Inversion Asymmetry* (*IIA*) that results from the different kinds of atoms on both sides of the interface [Fab+07, Section III. G.].

We didn't take any point group symmetries of the underlying lattice into account so far to determine the momentum structure of the spin-orbit field $\boldsymbol{\gamma}(\mathbf{k})$, since our single-band model was generic. We will catch up on this by using a two-orbital d_{xz}, d_{yz} model on the tetragonal lattice with inversion symmetry breaking induced by e.g. a heterostructure-interface along the [0 0 1] direction. Therefore, the point group to be considered is C_{4v} that has the five irreducible representations A_1, A_2, B_1, B_2 and E, whereas the d_{xz}, d_{yz} orbitals transform according to E. Only the two-dimensional dispersion along the k_x, k_y planes for fixed k_z are calculated. Henceforth, basis functions of the representation E are the only antisymmetric ones, where we have $\sin(k_x)$ and $\sin\left(k_y\right)$ in first order. In contrast, to a purely orbital Hamiltonian we have to entangle orbital and spin spaces with each other. The Pauli matrices τ_0, τ_x, τ_y and τ_z in orbital space are used again to construct the invariant in terms of orbitals. However, τ_y may be excluded since the non-centrosymmetric matrix $\mathbf{M}^{\alpha,\alpha'}$ must be real (cf. (Table 3.1)). Since the basis functions are E representation like, the combined orbital-spin space direct product representation (or irreducible representations contained therein) must transform like E, as well. Since the remaining Pauli matrices τ_0, τ_x and τ_z transform like A_1, B_1 and B_2, the Pauli matrices used in spin space must consequently be of E character, too, being σ_x and σ_y. This is the result of the product representations of $A_1 \otimes E = E$, $B_1 \otimes E = E$ and $B_2 \otimes E = E$. To sum it up, we can expand the spin-orbit Hamiltonian in d_{xz}, d_{yz} orbitals in terms of the invariants

$$\begin{aligned}\mathcal{H}_{SOC}^{xz,yz} = &+ \sin\left(k_y\right)\tau_0 \otimes \sigma_x - \sin\left(k_x\right)\tau_0 \otimes \sigma_y \\ &+ \sin\left(k_x\right)\tau_x \otimes \sigma_x - \sin\left(k_y\right)\tau_x \otimes \sigma_y \\ &+ \sin\left(k_y\right)\tau_z \otimes \sigma_x + \sin\left(k_x\right)\tau_z \otimes \sigma_y \quad . \end{aligned} \tag{3.1.56}$$

To determine, if we have to connect k_x and to σ_x or to σ_y (in any of the three invariants) and what the relative sign is, we consider, for instance, the operations C_4^+ and σ_x. (Equation 3.1.56) being first order in the basis functions may be arbitrarily expanded to higher orders involving e.g. $\sin\left(k_x\right)\cos\left(k_y\right)$ and $\sin\left(k_y\right)\cos\left(k_x\right)$ in second order. For completeness, we assemble the remaining terms for the full five d-orbital model with non-centrosymmetric spin-orbit interaction. We split the Hamiltonian into the sectors involving the d_{xz}, d_{yz} orbitals combined with d_{xy}, $d_{x^2-y^2}$ and d_{z^2} and the 3×3 block containing all one-dimensional representations. The one-dimensional orbital blocks may be easily composed by firstly entangling momentum and spin space, corresponding to a product of $E \otimes E$ with basis terms $\sin(k_x)$, $\sin\left(k_y\right)$ and σ_x, σ_y. Since $E \otimes E = A_1 \oplus A_2 \oplus B_1 \oplus B_2$, we expect to get all four one-dimensional representations by combining these terms. Indeed, we find that $\sin\left(k_x\right)\sigma_y - \sin\left(k_y\right)\sigma_x$ behaves like A_1, $\sin\left(k_x\right)\sigma_x + \sin\left(k_y\right)\sigma_y$ transforms like A_2, $\sin\left(k_x\right)\sigma_y + \sin\left(k_y\right)\sigma_x$ is associated to

Table 3.2.: We summarize the most common types of spin-orbit coupling classified with respect to inversion symmetry. On the one hand, centrosymmetric crystals only exhibit the well-known atomic $\mathbf{L}\cdot\mathbf{S}$ spin-orbit coupling, which is momentum independent (in zeroth order). On the other hand, non-centrosymmetric crystals may show numerous types of spin-orbit interaction like *Rashba* and *Dresselhaus terms*. These are bound to exhibit spin-momentum locking due to symmetry requirements.

SOC	**atomic**	**Rashba**	**Dresselhaus**	**Kane-Mele**
Hamiltonian	$\mathbf{L}\cdot\mathbf{S}$	$(\mathbf{k}\otimes\sigma)_z$	$k_x\sigma_y + k_y\sigma_x$	$i\,(\mathbf{d}_1\otimes\mathbf{d}_2)\cdot\sigma$
inversion symmetry	✓	✗	✗	✗
momentum dependency	✓/✗	✓	✓	✓
spatial dimension	3	2	3	2

B_1 and $\sin(k_x)\,\sigma_x - \sin\left(k_y\right)\sigma_y$ corresponds to B_2. In the sectors involving the d_{xz}, d_{yz} orbitals we observe that the product of E in momentum space and E in orbital space requires a one-dimensional representation in spin space, leaving us with σ_0 and σ_z. The non-centrosymmetric spin-orbit matrix $\mathbf{M}^{\alpha\alpha'}(\mathbf{k})$ for the five d-orbitals is therefore given by (up to first order)

$$\mathbf{M}^{\alpha\alpha'}(\mathbf{k}) = \begin{pmatrix} 2k_y\hat{x} & k_x\hat{x}-k_y\hat{y} & k_x\hat{z} & k_y\hat{z} & k_y\hat{z} \\ k_x\hat{x}-k_y\hat{y} & -2k_x\hat{y} & -k_y\hat{z} & k_x\hat{z} & -k_x\hat{z} \\ k_x\hat{z} & -k_y\hat{z} & k_x\hat{y}-k_y\hat{x} & k_x\hat{x}+k_y\hat{y} & k_x\hat{x}-k_y\hat{y} \\ k_y\hat{z} & k_x\hat{z} & k_x\hat{x}+k_y\hat{y} & k_x\hat{y}-k_y\hat{x} & k_x\hat{y}+k_y\hat{x} \\ k_y\hat{z} & -k_x\hat{z} & k_x\hat{x}-k_y\hat{y} & k_x\hat{y}+k_y\hat{x} & k_x\hat{y}-k_y\hat{x} \end{pmatrix}, \tag{3.1.57}$$

where $(\alpha,\alpha') = (xz, yz, xy, x^2-y^2, z^2)$. For the sake of simplicity we abbreviated $\sin\left(k_{x,y}\right)$ by $k_{x,y}$ throughout. Note, that there are different phenomenological constants corresponding to every orbital block and representation (which are, however, not distinguished in (Equation 3.1.57)) We find some well-known models in the Hamiltonian, in particular the Rashba term $k_x\hat{y} - k_y\hat{x}$ the Dresselhaus term $k_x\hat{y} + k_y\hat{x}$ and some unfamiliar terms $k_x\hat{x} + k_y\hat{y}$ and $k_x\hat{x} - k_y\hat{y}$ as well as the $k_y\hat{z}$, $k_x\hat{z}$ terms in the two-dimensional representation sectors. The resulting non-trivial spin structures arising from these non-centrosymmetric spin-orbit terms are shown in (Figure 3.1). A summary and classification of different types of spin-orbit interaction in centrosymmetric and non-centrosymmetric models is given in (Table 3.2).

3.2. Pseudospin and definition of Bloch states

A spinful single-particle Hamiltonian $\mathcal{H}_0$ that *doesn't* feature any spin-orbit coupling is denoted by

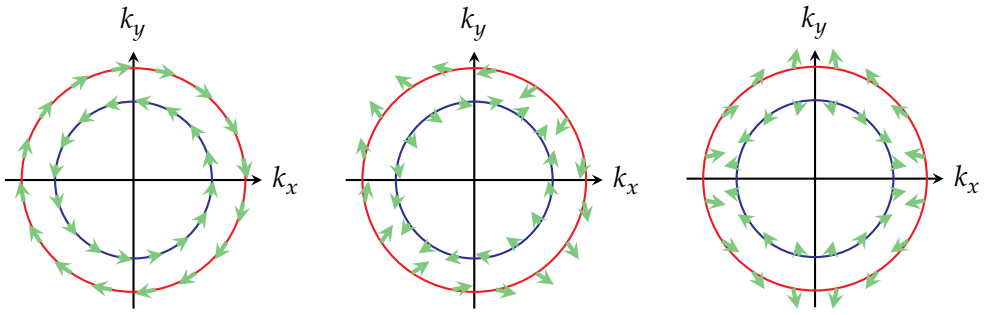

Figure 3.1.: (Figure 3.1a) illustrates the Rashba term $\gamma_{\mathbf{k}} = \left(k_y, -k_x, 0\right)$ resulting in a spin-split Fermi surface with momentum dependent spin expectation values $\langle\sigma\rangle_\lambda = -\lambda\frac{\gamma_{\mathbf{k}}}{|\gamma_{\mathbf{k}}|}$ (cf. (Equation 3.1.55)). In particular, the spin expectation value is aligned in the x-y-plane and is perpendicular to the Fermi momentum in the case of Rashba spin-orbit interaction (evolving counter clock-wise). Note that the length of arrows does not reflect the actual magnitude of the spin expectation value. The Rashba term appears on the diagonals of (Equation 3.1.57). (Figure 3.1b) shows the *Dresselhaus term* $\gamma_{\mathbf{k}} = \left(k_y, k_x, 0\right)$ resulting in a spin-split Fermi surface with spins rotating clock-wise around the Fermi surface (in contrast, to the Rashba spin structure). The Dresselhaus term shows up in the $x^2 - y^2, z^2$ orbital matrix elements in (Equation 3.1.57). In (Figure 3.1c), the spin structure of the unnamed term $\gamma_{\mathbf{k}} = \left(k_x, -k_y, 0\right)$ is shown, which reassembles the one of the Dresselhaus up to a shift $\pi/4$ along the Fermi surface.

$$\mathcal{H}_0 = \sum_{\mathbf{k}} \sum_{\alpha,\alpha'} \sum_{\sigma,\sigma'} \left(t_{\alpha\alpha'}(\mathbf{k}) \otimes \sigma_0\right) c^\dagger_{\mathbf{k}\alpha\sigma} c_{\mathbf{k}\alpha'\sigma'} \quad , \tag{3.2.1}$$

where $\alpha = (s, o)$ represents the sublattice and orbital degrees of freedom and σ_0 is the 2×2 identity matrix. Since the Hamiltonian is diagonal in spin space we can easily write down a set of eigenstates, i.e.

$$\mathbf{u}_{\mathbf{k}\alpha\uparrow} = \mathbf{u}_{\mathbf{k}\alpha} \otimes \begin{pmatrix} 1 \\ 0 \end{pmatrix} \qquad \mathbf{u}_{\mathbf{k}\alpha\downarrow} = \mathbf{u}_{\mathbf{k}\alpha} \otimes \begin{pmatrix} 0 \\ 1 \end{pmatrix} \quad , \tag{3.2.2}$$

with $\left(t_{\alpha\alpha'} \otimes \sigma_0\right) \mathbf{u}_{\mathbf{k}\alpha\uparrow} = \xi_{\mathbf{k}\alpha\uparrow} \mathbf{u}_{\mathbf{k}\alpha\uparrow}$ and $\left(t_{\alpha\alpha'} \otimes \sigma_0\right) \mathbf{u}_{\mathbf{k}\alpha\downarrow} = \xi_{\mathbf{k}\alpha\uparrow} \mathbf{u}_{\mathbf{k}\alpha\downarrow}$ with the eigenvalues $\xi_{\mathbf{k}\alpha\uparrow}, \xi_{\mathbf{k}\alpha\downarrow} \in \mathbb{R}$. Due to the two-fold degeneracy, this definition of eigenstates is arbitrary and there is an infinite number of equally valid choices given by

$$\begin{aligned} \mathbf{u}'_{\mathbf{k}\alpha\tilde{\uparrow}} &:= a\, \mathbf{u}_{\mathbf{k}\alpha\uparrow} + b\, \mathbf{u}_{\mathbf{k}\alpha\downarrow} \\ \mathbf{u}'_{\mathbf{k}\alpha\tilde{\downarrow}} &:= -\bar{b}\, \mathbf{u}_{\mathbf{k}\alpha\uparrow} + \bar{a}\, \mathbf{u}_{\mathbf{k}\alpha\downarrow} \end{aligned} \qquad a, b \in \mathbb{C} \qquad |a|^2 + |b|^2 = 1 \quad , \tag{3.2.3}$$

in terms of the original eigenstates (Equation 3.2.2). We denote the new spin degree of freedom by $\tilde{\sigma} \in \{\tilde{\uparrow}, \tilde{\downarrow}\}$ and call it *pseudospin* since it corresponds to a superposition of both eigenstates of the σ_z operator. Here, we will stick to the convention of expressing SU(2)-symmetric eigenstates in terms of the "pure" σ_z-eigenstates

$$|\uparrow\rangle = \begin{pmatrix} 1 \\ 0 \end{pmatrix} \qquad |\downarrow\rangle = \begin{pmatrix} 0 \\ 1 \end{pmatrix} \quad . \tag{3.2.4}$$

In this context, the distinction between "natural" spin $|\uparrow, \downarrow\rangle$ and pseudospin $|\tilde{\uparrow}, \tilde{\downarrow}\rangle$ is artificial since both definitions are simply related by a spin rotation (Equation 3.2.3). This applies for multi-orbital systems with SU(2) as well since we can always choose the superposition of degenerate eigenstates that corresponds to the σ_z states in the particular band. As long as we treat both orbital- and spin- angular momentum separately, we have a convenient description in terms of the orbital and spin operator eigenstates at hand. In contrast, a non-interacting Hamiltonian including (centrosymmetric) spin-orbit interaction is given by (cf. (Section 3.1.2))

$$\mathcal{H}_0 + \hat{\mathbf{L}}\cdot\hat{\mathbf{S}} = \sum_{\mathbf{k}} \sum_{\alpha,\alpha'} \sum_{\sigma,\sigma'} \underbrace{\left(t_{\alpha\alpha'} \otimes \sigma_0 + \langle \alpha, \sigma | \, \hat{\mathbf{L}}\cdot\hat{\mathbf{S}} \, | \alpha', \sigma' \rangle\right)}_{:= h^{\sigma\sigma'}_{\alpha\alpha'}(\mathbf{k})} c^\dagger_{\mathbf{k}\alpha\sigma} c_{\mathbf{k}\alpha'\sigma'} \quad , \tag{3.2.5}$$

Spin-orbit interaction intertwines orbital and spin space such that we have to rely on a new description in terms of the total angular momentum $\mathbf{J} = \mathbf{L} + \mathbf{S}$ that serves as the new "good quantum number". As a consequence, the Hamiltonian neither exhibits symmetry with respect to neither spin rotations nor to orbital transformation but only w.r.t. to a combined transformation of spin and orbital degrees of freedom, whose generators are given by the total angular momentum, i.e. $\mathcal{D} = e^{-i\mathbf{J}\hat{n}\varphi}$. Henceforth, in contrast to (Equation 3.2.4) a description in pure σ_z state is impossible and we have to rely on a new definition. In the former case, the requirement of using pure σ_z states made the definition of the (pseudo)spin degree of freedom unique. But how do we get rid of this ambiguity for a Hamiltonian with finite λ $\mathbf{L} \cdot \mathbf{S}$? The idea is to switch on the spin-orbit coupling *adiabatically* in λ (and therefore introducing spin off-diagonal terms) and continuously connect the new pseudospin states with the pure σ_z states [UR85, Section II. A.]. This is illustrated by some exemplary three band model and the definition of its pseudospin $\tilde{\uparrow}$ state, i.e.

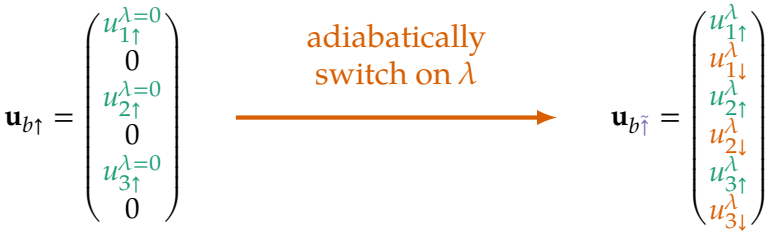

The adiabatic process of switching on the spin-orbit coupling implies that *all* components of the respective eigenvector $\mathbf{u}_{b\tilde{\uparrow}}$ behave *continuously and smooth* as a function of λ. The condition for unambiguous, *adiabatic definition of pseudospin* may be expressed by

$$\begin{cases} \lim\limits_{\lambda\to 0} \mathbf{u}_{b\tilde{\uparrow}} = \mathbf{u}_{b\uparrow} \\ \lim\limits_{\lambda\to 0} \mathbf{u}_{b\tilde{\downarrow}} = \mathbf{u}_{b\downarrow} \end{cases}, \tag{3.2.6}$$

where b is some band index. This definition relies on the definition of the "natural" spin state (cf. (Equation 3.2.4)) and amounts to finding the linear combination of "intrinsic" (e.g. numerically given) eigenstates that helps to satisfy this condition (cf. (Equation 3.2.3)). The required set of coefficients $a, b \in \mathbb{C}$ generally depends on the specific value of the spin-orbit strength λ, i.e. the coefficients $a = a_\lambda$ and $b = b_\lambda$ are a (discontinuous) function of λ (cf. (Equation 3.2.3)). Note, that the *pseudospin* degree of freedom $\tilde{\sigma}$ is used for Hamiltonians including the centrosymmetric spin-orbit coupling only (cf. (Section 3.1.2)) while the *helical* spin degree of freedom λ (not to be confused with the phenomenological parameter λ controlling the strength of atomic spin-orbit coupling) is used for non-centrosymmetric Hamiltonians (cf. (Section 3.1.2)). In the latter case, the definition of the spin degree of freedom is unambiguous since there is no degeneracy that allows for a superposition of spin states. However, both spin degrees of freedom, the pseudospin as well as the helical spin, still suffer from some vagueness in their definitions due to the *gauge symmetry* of the corresponding eigenstates. No matter, if we determine the (pseudospin or helical) eigenstates $\mathbf{u}_{\mathbf{k}b(\lambda,\tilde{\sigma})}$ of a generic one-particle Hamiltonian $h^{\sigma\sigma'}_{\alpha\alpha'}(\mathbf{k})$ including orbital and spin degrees of freedom numerically or analytically, we will find that the phases of the eigenstates are arbitrary in the sense that the redefinition $\mathbf{u}_{\mathbf{k}b(\lambda,\tilde{\sigma})} \to e^{-i\varphi(\mathbf{k},b,(\lambda,\tilde{\sigma}))}\mathbf{u}_{\mathbf{k}b(\lambda,\tilde{\sigma})}$ still yields a valid set of eigenvectors. In particular, in the former numerical case, the phases of the eigenvectors along a closed and continuous path through the Brillouin zone are varying in a random and messy way. This intricacy was also noted in the context of *topological insulators* and the definition of the *Berry phase* [BH13, chap. 2.2]. However, in contrast, to our case, the Berry phase can be computed gauge independent circumventing the problem of the chaotic phases. But this is possible only since the Berry phase is a scalar entity, while we are to deal with vertex functions that essentially depend on their basis and their phases.

The solution is to regauge the eigenstates in such a way that the phases behave *smooth and continuous* along a closed path through the Brillouin zone [BH13, chap. 2.1]. It turns out, that for particular Hamiltonians, it is actually impossible to find a continuous phase that is also single-valued. This lack of single-valuedness indicates a non-zero Hall conductance [HK10]. To emphasize and confirm this result we have a look at the Hamiltonian of the single-band Hubbard model

$$\mathcal{H} = \sum_{\mathbf{k}} \sum_{\sigma,\sigma'} \left(\cos(k_x) + \cos\left(k_y\right)\right) \delta_{\sigma\sigma'} c^{\dagger}_{\mathbf{k}\sigma} c_{\mathbf{k}\sigma'} \quad , \tag{3.2.7}$$

whose $\mathbf{k}$-independent eigenstates can obviously be chosen to be the σ_z eigenstates $|\uparrow\rangle = (1,0)^T$ and $|\downarrow\rangle = (0,1)^T$. Another set of eigenstates is given by $|\uparrow\rangle = e^{-i\nu(\mathbf{k})}(1,0)^T$ and $|\uparrow\rangle = e^{-i\mu(\mathbf{k})}(1,0)^T$ where $\nu(\mathbf{k})$ and $\mu(\mathbf{k})$ may represent any discontinuous and exotic function you can think of. Although, these are valid eigenvectors, the interaction that is rewritten in terms of this basis is not the one corresponding to the original model, anymore. Even in this simple example, we are destined to employ a smooth and continuous (and even more constant, in this case) phase along a closed path through the Brillouin zone. Up to a global $\mathbf{k}$-independent phase the requirement of *smoothness and continuousness* is sufficient to remove the arbitrariness of the phase. This requirement rules out the possibility of employing the Bloch states in an irreducible (asymmetric) part of the Brillouin zone and implying the remaining ones by means of point group symmetries since this introduces some unwanted and unphysical discontinuities in the phase of eigenvectors and therefore in the Bloch wave functions across the border of the irreducible units (cf. [SC04, V. Discussion] and [MHW13, Summary and Outlook]). More technically, after fixing the global phase at a randomly chosen $\mathbf{k}$-point one may proceed by determining the phase at a neighboring $\mathbf{k}$-point by minimizing the overall phase difference between the eigenvectors at the respective momenta. In particular, we shift the phase of the subsequent eigenvector such that the overlap (inner product) of both eigenstates has the phase $\varphi = 0$, i.e. the inner product is real. Consider the two subsequent momenta, along a closed path e.g. the Fermi surface in two dimensions, and their associated eigenvectors denoted by $\mathbf{k}_\kappa$, $\mathbf{k}_{\kappa+1}$ and $\mathbf{u}_\kappa$, $\mathbf{u}_{\kappa+1}$. Their overlap is given by $\langle \mathbf{u}_\kappa | \mathbf{u}_{\kappa+1} \rangle = re^{i\varphi}$. Thus, in order to ensure the smoothness of the given eigenvectors, we shift the phase of the second (at $\mathbf{k}_{\kappa+1}$) state by $\mathbf{u}_{\kappa+1} \to e^{-i\varphi}\mathbf{u}_{\kappa+1}$ where $\varphi = \arg\langle \mathbf{u}_\kappa | \mathbf{u}_{\kappa+1} \rangle$. This is illustrated in (Figure 3.2), which shows the two-component eigenstates of a p_z-orbital tight-binding model on the honeycomb lattice before and after the smoothing procedure. For clarity, we simply chose the Fermi surface as the closed path through the Brillouin zone. However, in general, we require the phase of eigenstates to be continuous throughout the Brillouin zone. Furthermore, we only included the eigenstates of the lower band with the Fermi surface. To get some insight into the structure of the phase of eigenstates, we consider the analytical solution of the first nearest neighbor tight-binding Hamiltonian

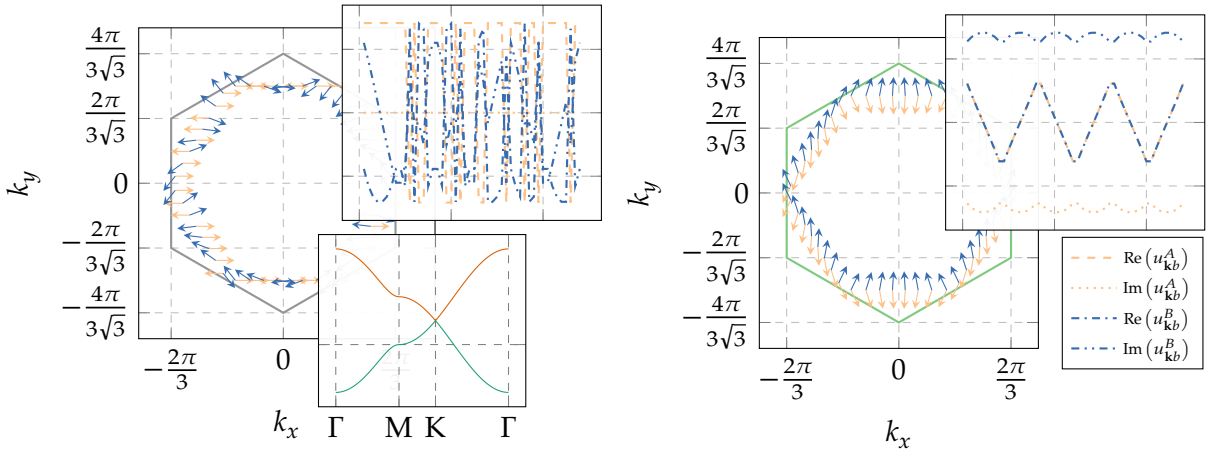

(a) (b)

Figure 3.2.: As an example for the definition of the proper phase of eigenstates we provide the Hubbard model on the honeycomb lattice featuring p_z orbitals. The Hamiltonian is given by (Equation 3.2.8) with the chemical potential set to $\mu = -t$. (Figure 3.2a) shows the numerically given eigenstates as produced by any linear algebra package, i.a. [And+90; San10; GJ+10]. An arrow represents a single complex component of the eigenvector in the complex plane, where the yellow arrows indicate the weight of the A sublattice and the blue arrows the weights of sublattice B. Going along the Fermi surface, the arrows, i.e. the phases of the eigenvectors are uncorrelated and change randomly. The inset in the upper right shows the real and complex parts of both sublattice components in the respective eigenstates along the Fermi surface in counter-clockwise direction. In contrast, the arrows in (Figure 3.2b) change smoothly and continuously along the Fermi surface, which becomes apparent, in particular, in the corresponding inset.

$$\begin{aligned}\mathcal{H}_0(\mathbf{k}) &= t\sum_{\alpha,\alpha'}\sum_{\mathbf{k}}\underbrace{\left(e^{-i\mathbf{k}(\boldsymbol{\tau}_B-\boldsymbol{\tau}_A)}+e^{-i\mathbf{k}(-\mathbf{a}_1+\boldsymbol{\tau}_B-\boldsymbol{\tau}_A)}+e^{-i\mathbf{k}(-\mathbf{a}_2+\boldsymbol{\tau}_B-\boldsymbol{\tau}_A)}\right)}_{:=h(\mathbf{k})} c^\dagger_{\alpha\mathbf{k}}c_{\alpha'\mathbf{k}} \\ &= t\sum_{\mathbf{k}}\left(c^\dagger_{A\mathbf{k}},c^\dagger_{B\mathbf{k}}\right)^T\begin{pmatrix}0 & h(\mathbf{k})\\ \overline{h}(\mathbf{k}) & 0\end{pmatrix}\begin{pmatrix}c_{A\mathbf{k}}\\ c_{B\mathbf{k}}\end{pmatrix}\quad,\end{aligned} \tag{3.2.8}$$

where $\boldsymbol{\tau}_A = (0,0)^T$ and $\boldsymbol{\tau}_B = (a,0)^T$ are the positions of the sites of sublattices A and B in the unit cell. The real space basis vectors are given by $\mathbf{a}_1 = \left(3,\sqrt{3}\right)\frac{a}{2}$ and $\mathbf{a}_1 = \left(3,-\sqrt{3}\right)\frac{a}{2}$. The eigenvalues $\varepsilon_{\mathbf{k}}$ and eigenvectors $\mathbf{u}_{\mathbf{k}}$ may be straightforwardly calculated to be $\varepsilon_{\mathbf{k}} = \pm|h(\mathbf{k})|$ and $\mathbf{u}_{\mathbf{k}} = \frac{1}{\sqrt{2}}\left(\pm h(\mathbf{k})/\varepsilon_{\mathbf{k}},1\right)^T$. The k-dependency of $h(\mathbf{k})$ suggests that the eigenvectors are expected to transform according to the B_1 representation of the point group, which is confirmed in the plot of the smoothed phases in (Figure 3.2). Note, that the plot of smoothed phases may still look differently depending on the global

phase, that may be chosen freely. By adjusting the phases of eigenvectors smoothly along a closed path through the Brillouin zone, the phases are usually even continuous across the border of the Brillouin zone. Therefore, one may as well choose the Fermi surfaces in the extended zone scheme as the closed path, since eigenvectors at k-points related by a reciprocal lattice $\mathbf{G} = n_1\mathbf{b}_1 + n_2\mathbf{b}_2$ are the same. An exception, however, is given by a Hamiltonian on a lattice with multiple sites in the unit cell, e.g. the tight-binding Hamiltonian on the honeycomb lattice. Setting up the Hamiltonian (Equation 3.2.8) at a momentum $\mathbf{k} + \mathbf{G}$ we find

$$\mathcal{H}_0(\mathbf{k}) = t \sum_{\mathbf{k}} \left(c^\dagger_{A\mathbf{k}}, c^\dagger_{B\mathbf{k}}\right)^T \begin{pmatrix} 0 & e^{-i\mathbf{G}(\boldsymbol{\tau}_B - \boldsymbol{\tau}_A)} h(\mathbf{k}) \\ e^{i\mathbf{G}(\boldsymbol{\tau}_B - \boldsymbol{\tau}_A)} \overline{h}(\mathbf{k}) & 0 \end{pmatrix} \begin{pmatrix} c_{A\mathbf{k}} \\ c_{B\mathbf{k}} \end{pmatrix} \quad , \tag{3.2.9}$$

where we used $\mathbf{G} \cdot \mathbf{a}_{1,2} = 2\pi n$ with $n \in \mathbb{Z}$. While the additional phase cancels in the expression for the eigenvalues, the eigenstates at a momentum shifted by a reciprocal lattice vector are given by $\mathbf{u}_{\mathbf{k}+\mathbf{G}} = \frac{1}{\sqrt{2}} \left(\pm e^{-i\mathbf{G}(\boldsymbol{\tau}_B - \boldsymbol{\tau}_A)} h(\mathbf{k})/\varepsilon_{\mathbf{k}}, 1\right)^T$. Henceforth, one has to take special care of how the eigenvectors are (continuously) connected to the next zone, which is of particular importance for the calculation of scattering processes and the *back-folding* of quasiparticle states. Finally, we comment on the relationship of the presented definition of eigenstates to previous works on this topic. [Fu15; KF15] present a definition of basis states in the presence of inversion and time-reversal symmetry for spin-orbit coupled metals. The combined application of inversion and time-reversal symmetry enables the definition of a *Kramers doublet*. The orthogonality of the two states belonging to the doublet allows for a unitary U(2) transformation. This transformation can be used to redefines both states in order to satisfy the condition for the "manifestly covariant Bloch basis" (MCBB). This condition requires the Bloch wave function spinor at the origin of real space, i.e. $\mathbf{r} = 0$ (where the Bloch theorem (Equation 3.1.15) assumes the simple form $\psi_{\mathbf{k}b\sigma}(\mathbf{r} = 0) = u_{\mathbf{k}b}(\mathbf{r} = 0)\chi_\sigma$) to be fully spin-polarized along a global spin-quantization axis, which is employed for all k-points in the entire Brillouin zone. As a consequence, the *MCBB* exhibits a particular simple transformation behavior with respect to point group operations, which is in contrast, to a generic basis choice that only respects the point group operations on basis states only up to a complicated and random phase along the Fermi surface (cf. [Blo85]). However, this definition contradicts the requirement of a continuous phase since it exhibits discontinuities of the eigenvector components at the borders of the sectors of the Brillouin, which define the star of $\mathbf{k}$ (cf. previous discussion and [SC04, V. Discussion]). These discontinuities can be abandoned at the prize of introducing $\mathbf{k}$-dependent representation matrices in orbital-spin space, which, unfortunately, don't reflect the physical symmetries of orbital and spin degrees of freedom, anymore [MHW13] (see appendix E). We will, however, make use of and assume momentum independent representation matrices (as introduced in (Section 3.3.1)) in orbital-spin space that directly stem from the transformation behavior of spherical harmonics and the SU(2)-spin degree of freedom. In contrast, the definition of basis states we presented (for k-independent representation matrices, as well) not

only removes the apparent "arbitrariness" of phases (which are actually not arbitrary but part of the Hamiltonian (cf. (Figure 3.2b))), but also respects the condition of continuity resulting in an equally unique set of basis states (up to a global phase). More about the issues associated to this "gauge freedom" and other choices of Bloch states is found in appendix E.

3.3. Structure and symmetries of the two-particle vertex

Before we embark on the endeavor of a mean-field theory in absence of spin rotation symmetry (and inversion symmetry), we will try to gain more insight into the structure of the two-particle interaction to be analyzed. The presence or absence of *time-reversal*, *spin-rotation* and *inversion* symmetries determines the specific form of the interaction to a great extend. We will derive the effect of the corresponding transformations on two-particle vertices in both orbital and band space. In orbital space, the spinful interaction is denoted by $U^{\sigma_1\sigma_2\sigma_1'\sigma_2'}_{\alpha_1\alpha_2\alpha_1'\alpha_2'}$ (with σ being the "natural" spin degree of freedom and α representing all other quantum numbers). The interaction is apparently comprised of $2^4 = 16$ spin sectors. In particular, in a numerical context it is important to distinguish between the entire object of the two-particle vertex (denoted by $\Gamma^{(4)}$, being an operator, and the rank four tensor $U^{\sigma_1\sigma_2\sigma_1'\sigma_2'}_{\alpha_1\alpha_2\alpha_1'\alpha_2'} \in \mathbb{C}^{n\times n\times n\times n}$ (which is all we deal with numerically). Their relation is given by

$$\Gamma^{(4)} = \sum_{\substack{\alpha_1,\alpha_2,\\ \alpha_1',\alpha_2'}} \sum_{\substack{\sigma_1,\sigma_2\\ \sigma_1',\sigma_2'}} U^{\sigma_1\sigma_2\sigma_1'\sigma_2'}_{\alpha_1\alpha_2\alpha_1'\alpha_2'}\, a^\dagger_{\alpha_1'\sigma_1'} a^\dagger_{\alpha_2'\sigma_2'} a_{\alpha_2\sigma_2} a_{\alpha_1\sigma_1} \quad , \tag{3.3.1}$$

with $a^\dagger_{\alpha\sigma}/a_{\alpha\sigma}$ creating/annihilating a fermion with spin σ and collected quantum numbers α. We introduce the basis

$$\mathbf{A}^\dagger_\alpha = \left(a^\dagger_{\alpha\uparrow}a^\dagger_{\alpha\uparrow}, a^\dagger_{\alpha\uparrow}a^\dagger_{\alpha\downarrow}, a^\dagger_{\alpha\downarrow}a^\dagger_{\alpha\uparrow}, a^\dagger_{\alpha\downarrow}a^\dagger_{\alpha\downarrow}\right) \quad , \tag{3.3.2}$$

where α represents all quantum numbers except spin. On the one hand, in *orbital basis*, these are $\alpha = (\mathbf{k}, s, o, \sigma)$ momentum $\mathbf{k}$, sublattice s, orbital o and spin σ. On the other hand, in *band basis*, the quantum numbers are $\tilde{\alpha} = (\mathbf{k}, b, \tilde{\sigma})$ momentum $\mathbf{k}$, band b and pseudospin $\tilde{\sigma}$. Using any of these bases the two-particle vertex can be written as

$$\begin{pmatrix} U^{\uparrow\uparrow\uparrow\uparrow}_{\alpha_1\alpha_2\alpha_1'\alpha_2'} & U^{\uparrow\uparrow\uparrow\downarrow}_{\alpha_1\alpha_2\alpha_1'\alpha_2'} & U^{\uparrow\uparrow\downarrow\uparrow}_{\alpha_1\alpha_2\alpha_1'\alpha_2'} & U^{\uparrow\uparrow\downarrow\downarrow}_{\alpha_1\alpha_2\alpha_1'\alpha_2'} \\ U^{\downarrow\uparrow\uparrow\uparrow}_{\alpha_1\alpha_2\alpha_1'\alpha_2'} & U^{\uparrow\downarrow\uparrow\downarrow}_{\alpha_1\alpha_2\alpha_1'\alpha_2'} & U^{\uparrow\downarrow\downarrow\uparrow}_{\alpha_1\alpha_2\alpha_1'\alpha_2'} & U^{\uparrow\downarrow\downarrow\downarrow}_{\alpha_1\alpha_2\alpha_1'\alpha_2'} \\ U^{\downarrow\uparrow\uparrow\uparrow}_{\alpha_1\alpha_2\alpha_1'\alpha_2'} & U^{\downarrow\uparrow\uparrow\downarrow}_{\alpha_1\alpha_2\alpha_1'\alpha_2'} & U^{\downarrow\uparrow\downarrow\uparrow}_{\alpha_1\alpha_2\alpha_1'\alpha_2'} & U^{\downarrow\uparrow\downarrow\downarrow}_{\alpha_1\alpha_2\alpha_1'\alpha_2'} \\ U^{\downarrow\downarrow\uparrow\uparrow}_{\alpha_1\alpha_2\alpha_1'\alpha_2'} & U^{\downarrow\downarrow\uparrow\downarrow}_{\alpha_1\alpha_2\alpha_1'\alpha_2'} & U^{\downarrow\downarrow\downarrow\uparrow}_{\alpha_1\alpha_2\alpha_1'\alpha_2'} & U^{\downarrow\downarrow\downarrow\downarrow}_{\alpha_1\alpha_2\alpha_1'\alpha_2'} \end{pmatrix} \quad , \tag{3.3.3}$$

The vertex function is required to satisfy *fermionic antisymmetry* upon particle exchange, *self-adjointness* and eventually *time-reversal symmetry* . Mathematically, we have

- fermionic particle exchange

$$U^{\sigma_1\sigma_2\sigma_1'\sigma_2'}_{\alpha_1\alpha_2\alpha_1'\alpha_2'} = -U^{\sigma_2\sigma_1\sigma_1'\sigma_2'}_{\alpha_2\alpha_1\alpha_1'\alpha_2'} = -U^{\sigma_1\sigma_2\sigma_2'\sigma_1'}_{\alpha_1\alpha_2\alpha_2'\alpha_1'} = +U^{\sigma_2\sigma_1\sigma_2'\sigma_1'}_{\alpha_2\alpha_1\alpha_2'\alpha_1'} \tag{3.3.4}$$

- self-adjointness

$$\overline{U^{\sigma_1\sigma_2\sigma_1'\sigma_2'}_{\alpha_1\alpha_2\alpha_1'\alpha_2'}} = U^{\sigma_1'\sigma_2'\sigma_1\sigma_2}_{\alpha_1'\alpha_2'\alpha_1\alpha_2} \tag{3.3.5}$$

as a natural consequence of fermionic exchange statistics of the operators in (Equation 3.3.2) and the requirement $\left(\Gamma^{(4)}_{\Lambda}\right)^{\dagger} = \Gamma^{(4)}_{\Lambda}$. More precisely, the "self-adjointness" amounts to the *Osterwalder-Schrader positivity* of the action in imaginary time functional integral formalism [OS73; Wet07; Ebe14]. Although, the two-particle vertex in (Equation 3.3.4) and (Equation 3.3.5) is given in orbital-spin basis, analogous relations apply to any other basis, e.g. band-pseudospin basis, which is related to orbital-spin basis by a unitary transformation. The antisymmetry with respect to fermionic particle exchange and the Hermiticity of the two-particle vertex impose constraints on the structure of the vertex that significantly reduces the number of independent elements. In particular, the sixteen "spin sectors" in (Equation 3.3.3) are reduced to six independent tensors. A two-particle vertex, which satisfies Hermiticity and fermionic antisymmetry must have the structure (the pseudospin indices $\{\tilde{\sigma}\}$ indicates the general validity of the statements below)

$$U^{\tilde{\sigma}_1\tilde{\sigma}_2\tilde{\sigma}_1'\tilde{\sigma}_2'}_{\alpha_1\alpha_2\alpha_1'\alpha_2'} = \begin{pmatrix} A_{\alpha_1\alpha_2\alpha_1'\alpha_2'} & B_{\alpha_1\alpha_2\alpha_1'\alpha_2'} & -B_{\alpha_1\alpha_2\alpha_2'\alpha_1'} & C_{\alpha_1\alpha_2\alpha_1'\alpha_2'} \\ \overline{B_{\alpha_1'\alpha_2'\alpha_1\alpha_2}} & D_{\alpha_1\alpha_2\alpha_1'\alpha_2'} & -D_{\alpha_1\alpha_2\alpha_2'\alpha_1'} & E_{\alpha_1\alpha_2\alpha_1'\alpha_2'} \\ -\overline{B_{\alpha_2'\alpha_1'\alpha_1\alpha_2}} & -D_{\alpha_2\alpha_1\alpha_1'\alpha_2'} & D_{\alpha_2\alpha_1\alpha_2'\alpha_1'} & -E_{\alpha_2\alpha_1\alpha_1'\alpha_2'} \\ \overline{C_{\alpha_1'\alpha_2'\alpha_1\alpha_2}} & \overline{E_{\alpha_1'\alpha_2'\alpha_1\alpha_2}} & -\overline{E_{\alpha_1'\alpha_2'\alpha_2\alpha_1}} & F_{\alpha_1\alpha_2\alpha_1'\alpha_2'} \end{pmatrix} , \tag{3.3.6}$$

where the introduced tensors $\{A, B, C, D, E, F\}$ must satisfy the constraints

$$\begin{cases} X_{\alpha_1\alpha_2\alpha_1'\alpha_2'} = -X_{\alpha_2\alpha_1\alpha_1'\alpha_2'} = -X_{\alpha_1\alpha_2\alpha_2'\alpha_1'} = X_{\alpha_2\alpha_1\alpha_2'\alpha_1'} & \text{where} \quad X \in \{A, C, F\} \\ X_{\alpha_1\alpha_2\alpha_1'\alpha_2'} = \overline{X_{\alpha_1'\alpha_2'\alpha_1\alpha_2}} & \text{where} \quad X \in \{A, D, F\} \\ X_{\alpha_1\alpha_2\alpha_2'\alpha_1'} = \overline{X_{\alpha_1'\alpha_2'\alpha_2\alpha_1}} & \text{where} \quad X \in \{D\} \end{cases} . \tag{3.3.7}$$

Hence, A, C, F satisfy antisymmetric conditions under particle exchange with respect to the residual indices and A, D, F have to be self-adjoint. Combining both constraints on D, we obtain $D_{\alpha_1\alpha_2\alpha_1'\alpha_2'} = D_{\alpha_2\alpha_1\alpha_2'\alpha_1'}$, as well. Note, that B and E are restricted by the antisymmetry with respect to exchange of unprimed (for B) and primed indices

(for E), only (in contrast to A, C and F, that are antisymmetric with respect to both unprimed and primed), while they are both symmetric with respect to exchange of both pairs of indices at a time. As a final remark, we mention that a similar parametrization of the two-particle vertex was introduced in [EM10] for the *Nambu vertex* of a singlet superconductor.

3.3.1. Orbital space

Both single-particle and interaction term of a multi-orbital Hamiltonian describing strongly correlated electrons on a lattice are naturally given in orbital-spin basis. Henceforth, we will analyze the two-particle vertex with respect to a basis (Equation 3.3.2) whose quantum numbers (α, σ) refer to $\alpha = (s, o, \mathbf{k})$ sublattice s, orbital o, momentum $\mathbf{k}$ and "natural" spin indices first. The fermionic Grassmann fields $\bar{\psi}_{\mathbf{k}\alpha\sigma}$, $\psi_{\mathbf{k}\alpha\sigma}$ are more convenient to work with than the corresponding fermion operators $a^\dagger_{\mathbf{k}\alpha\sigma}$, $a_{\mathbf{k}\alpha\sigma}$ and will be used throughout the methodological development of the renormalization group techniques in (Chapter 4), (Chapter 5) and (Chapter 6). Note that, in general there's no complex conjugated version of $\psi_{\mathbf{k},\alpha,\sigma}$ being $\bar{\psi}_{\mathbf{k},\alpha,\sigma}$ since both are simply different generators of the Grassman algebra. [7]

Time-reversal

To see what the implications of *time-reversal symmetry* on the spinful two-particle vertex in orbital-spin basis are, firstly we have a look at the transformation of a spinful single-particle state, i.e. [SN11; Sch05b]

$$\psi_{\mathbf{k}\alpha\sigma} \xrightarrow{\text{TR}} \hat{\Theta}\, \psi_{-\mathbf{k}\alpha\sigma} = \sum_{\sigma'} \left(-i\sigma_y\right)_{\sigma\sigma'} \bar{\psi}_{-\mathbf{k}\alpha\sigma'} \tag{3.3.8}$$

$$\bar{\psi}_{\mathbf{k}\alpha\sigma} \xrightarrow{\text{TR}} \hat{\Theta}^{-1}\, \bar{\psi}_{-\mathbf{k}\alpha\sigma} = \sum_{\sigma'} \psi_{-\mathbf{k}\alpha\sigma'} \left(+i\sigma_y\right)_{\sigma'\sigma} = \sum_{\sigma'} \psi_{-\mathbf{k}\alpha\sigma'} \left(i\sigma_y\right)_{\sigma'\sigma} \quad , \tag{3.3.9}$$

where the multiindex α is resolved into momentum $\mathbf{k}$ and any residual indices α and σ. It was taken into account in (Equation 3.3.9) that momentum is odd under time-reversal. Using (Equation 3.3.1) in its functional integral formulation featuring Grassmann fields we can apply the passive time-reversal transformation given by (Equation 3.3.9) and obtain (a detailed calculation for single particle Hamiltonian is given in appendix D)

[7] Although, $\bar{\psi}_\alpha$ and ψ_α are two different generators of the Grassmann algebra one can define a bijective mapping relating $\bar{\psi}_\alpha$ and ψ_α with each other by conjugation. This is possible only for an algebra with an even number of generators divided into two sets of generators. Hence, the conjugation is $\overline{c\psi_\alpha} = \bar{c}\bar{\psi}_\alpha$, $c \in \mathbb{C}$ [NO88b, chap 1.5] and $\overline{\psi_\alpha \psi_{\alpha'}} = \bar{\psi}_{\alpha'}\bar{\psi}_\alpha$ in order to satisfy the "superreal" condition $\overline{\psi\bar{\psi}} = \psi\bar{\psi}$ [Nak03, chap. 1.5.8]. However, the operators $c^\dagger_{\mathbf{k}}$ and $c_{\mathbf{k}}$ behave according to $c^\dagger_{\mathbf{k}} \xrightarrow{\text{TR}} c^\dagger_{-\mathbf{k}}$ and $c_{\mathbf{k}} \xrightarrow{\text{TR}} c_{-\mathbf{k}}$ under time-reversal.

$$\Gamma^{(4)}_{\Lambda} \xrightarrow{\text{TR}} \tilde{\Gamma}^{(4)}_{\Lambda} = \sum_{\substack{\alpha_1,\alpha_2,\\ \alpha_1',\alpha_2'}} \sum_{\substack{\mathbf{k}_1,\mathbf{k}_2,\\ \mathbf{k}_1',\mathbf{k}_2'}} \sum_{\substack{\tau_1,\tau_2,\\ \tau_1',\tau_2'}} \times \left[\sum_{\substack{\sigma_1,\sigma_2,\\ \sigma_1',\sigma_2'}} U^{\sigma_1\sigma_2\sigma_1'\sigma_2'}_{\alpha_1\alpha_2\alpha_1'\alpha_2'} (\mathbf{k}_1,\mathbf{k}_2,\mathbf{k}_1',\mathbf{k}_2') \left(-i\sigma_y\right)_{\tau_1'\sigma_1'} \left(-i\sigma_y\right)_{\tau_2'\sigma_2'} \left(-i\sigma_y\right)_{\sigma_2\tau_2} \left(-i\sigma_y\right)_{\sigma_1\tau_1} \right] \times \psi_{-\mathbf{k}_1'\alpha_1'\tau_1'} \psi_{-\mathbf{k}_2'\alpha_2'\tau_2'} \bar{\psi}_{-\mathbf{k}_2\alpha_2\tau_2} \bar{\psi}_{-\mathbf{k}_1\alpha_1\tau_1} \quad . \tag{3.3.10}$$

The vertex function inside the brackets in (Equation 3.3.10) denoted by $\tilde{U}$ evaluates to (using the basis (Equation 3.3.2) in terms of spin indices $\{\tau_1, \tau_2, \tau_1', \tau_2'\}$)

$$\begin{pmatrix} U^{\downarrow\downarrow\downarrow\downarrow}_{\alpha_1\alpha_2\alpha_1'\alpha_2'} & -U^{\downarrow\downarrow\downarrow\uparrow}_{\alpha_1\alpha_2\alpha_1'\alpha_2'} & -U^{\downarrow\downarrow\uparrow\downarrow}_{\alpha_1\alpha_2\alpha_1'\alpha_2'} & U^{\downarrow\downarrow\uparrow\uparrow}_{\alpha_1\alpha_2\alpha_1'\alpha_2'} \\ -U^{\downarrow\uparrow\downarrow\downarrow}_{\alpha_1\alpha_2\alpha_1'\alpha_2'} & U^{\downarrow\uparrow\downarrow\uparrow}_{\alpha_1\alpha_2\alpha_1'\alpha_2'} & U^{\downarrow\uparrow\uparrow\downarrow}_{\alpha_1\alpha_2\alpha_1'\alpha_2'} & -U^{\downarrow\uparrow\uparrow\uparrow}_{\alpha_1\alpha_2\alpha_1'\alpha_2'} \\ -U^{\uparrow\downarrow\downarrow\downarrow}_{\alpha_1\alpha_2\alpha_1'\alpha_2'} & U^{\uparrow\downarrow\downarrow\uparrow}_{\alpha_1\alpha_2\alpha_1'\alpha_2'} & U^{\uparrow\downarrow\uparrow\downarrow}_{\alpha_1\alpha_2\alpha_1'\alpha_2'} & -U^{\uparrow\downarrow\uparrow\uparrow}_{\alpha_1\alpha_2\alpha_1'\alpha_2'} \\ U^{\uparrow\uparrow\downarrow\downarrow}_{\alpha_1\alpha_2\alpha_1'\alpha_2'} & -U^{\uparrow\uparrow\downarrow\uparrow}_{\alpha_1\alpha_2\alpha_1'\alpha_2'} & -U^{\uparrow\uparrow\uparrow\downarrow}_{\alpha_1\alpha_2\alpha_1'\alpha_2'} & U^{\uparrow\uparrow\uparrow\uparrow}_{\alpha_1\alpha_2\alpha_1'\alpha_2'} \end{pmatrix} (\mathbf{k}_1,\mathbf{k}_2,\mathbf{k}_1',\mathbf{k}_2') \quad . \tag{3.3.11}$$

i.e. the spin structure of the two-particle vertex is significantly altered. To find the complete transformation behavior of the two-particle vertex elements, we have to compare the indices of the basis in (Equation 3.3.10) with the ones in the original vertex function (Equation 3.3.3). Comparing "coefficients" in terms of Grassmann fields, implies the transformation behavior of the tensor elements:

$$\begin{aligned} U^{\sigma_1\sigma_2\sigma_1'\sigma_2'}_{\alpha_1\alpha_2\alpha_1'\alpha_2'} (\mathbf{k}_1\mathbf{k}_2\mathbf{k}_1'\mathbf{k}_2') &\xrightarrow{\text{TR}} \tilde{U}^{\sigma_1'\sigma_2'\sigma_1\sigma_2}_{\alpha_1'\alpha_2'\alpha_1\alpha_2} (-\mathbf{k}_1', -\mathbf{k}_2', -\mathbf{k}_1, -\mathbf{k}_2) \\ &= \overline{\tilde{U}^{\sigma_1\sigma_2\sigma_1'\sigma_2'}_{\alpha_1\alpha_2\alpha_1'\alpha_2'}} (-\mathbf{k}_1, -\mathbf{k}_2, -\mathbf{k}_1', -\mathbf{k}_2') \quad , \end{aligned} \tag{3.3.12}$$

where we used the Hermiticity of the vertex function (Equation 3.3.5) and the spin structure of $\tilde{U}$ is given by (Equation 3.3.11). Hence, *time-reversal invariance* of the two-particle vertex then implies i.a. the conditions (cf. [Ebe14] for two-particle vertices in Nambu representation)

$$\begin{aligned} U^{\downarrow\uparrow\uparrow\downarrow}_{\alpha_1\alpha_2\alpha_1'\alpha_2'} (\mathbf{k}_1,\mathbf{k}_2,\mathbf{k}_1',\mathbf{k}_2') &= \overline{U^{\uparrow\downarrow\downarrow\uparrow}_{\alpha_1\alpha_2\alpha_1'\alpha_2'}} (-\mathbf{k}_1,-\mathbf{k}_2,-\mathbf{k}_1',-\mathbf{k}_2') \\ U^{\uparrow\uparrow\uparrow\downarrow}_{\alpha_1\alpha_2\alpha_1'\alpha_2'} (\mathbf{k}_1,\mathbf{k}_2,\mathbf{k}_1',\mathbf{k}_2') &= -\overline{U^{\downarrow\downarrow\downarrow\uparrow}_{\alpha_1\alpha_2\alpha_1'\alpha_2'}} (-\mathbf{k}_1,-\mathbf{k}_2,-\mathbf{k}_1',-\mathbf{k}_2') \quad . \end{aligned} \tag{3.3.13}$$

We note, that the two-particle vertex $U^{\sigma_1,\sigma_2,\sigma_1',\sigma_2'}_{\alpha_1,\alpha_2,\alpha_1',\alpha_2'} (\mathbf{k}_1,\mathbf{k}_2,\mathbf{k}_1',\mathbf{k}_2')$ must obey *momentum conservation* and implicitly depends on three momenta only since the fourth one is fixed by $\mathbf{k}_2' = \mathbf{k}_1 + \mathbf{k}_2 - \mathbf{k}_1'$.

Spin-rotation

Implying any spin symmetries w.r.t to SU(2) transformations or a subgroup thereof, will introduce dependencies between the spin sectors and eventually requires some elements to be zero. To see the consequences of these symmetries on the level of the two-particle vertex, we first introduce the general SU(2) transformation $\hat{S}(\hat{n},\varphi) = e^{-i\hat{n}\sigma\varphi/2} = \sigma_0\cos(\varphi/2) - i(\hat{n}\cdot\boldsymbol{\sigma})\sin(\varphi/2)$ of the fields/operators corresponding to a rotation by φ about the axis given by $\hat{n}$ ($\boldsymbol{\sigma} = \left(\sigma_0, \sigma_x, \sigma_y, \sigma_z\right)$ is the vector of Pauli matrices)

$$\psi_{\alpha\sigma} \to \hat{S}(\hat{n},\varphi)\psi_{\alpha\sigma} = \sum_{\sigma'} \hat{S}_{\sigma\sigma'}(\hat{n},\varphi)\psi_{\alpha\sigma'} \tag{3.3.14}$$

$$\bar{\psi}_{\alpha\sigma} \to \sum_{\sigma'} \bar{\psi}_{\alpha\sigma'}\hat{S}^{\dagger}_{\sigma'\sigma}(\hat{n},\varphi) = \sum_{\sigma'} \overline{\hat{S}}_{\sigma\sigma'}(\hat{n},\varphi)\bar{\psi}_{\alpha\sigma'} \quad , \tag{3.3.15}$$

where $\hat{S}^{\dagger}(\hat{n},\varphi)\hat{S}(\hat{n},\varphi) = \sigma_0$ and $\sum_\tau \hat{S}^{\dagger}(\hat{n},\varphi)_{\sigma\tau}\hat{S}(\hat{n},\varphi)_{\tau\sigma'} = \delta_{\sigma\sigma'}$, respectively, due to unitarity. Applying this transformation to each of the four fermionic fields of the two-particle vertex, results in a transformed vertex, whose elements are given by

$$U^{\sigma_1\sigma_2\sigma_1'\sigma_2'}_{\alpha_1\alpha_2\alpha_1'\alpha_2'} \to \sum_{\substack{\sigma_1,\sigma_2\\ \sigma_1',\sigma_2'}} U^{\sigma_1\sigma_2\sigma_1'\sigma_2'}_{\alpha_1\alpha_2\alpha_1'\alpha_2'} \overline{S}_{\tau_1'\sigma_1'}\overline{S}_{\tau_2'\sigma_2'}S_{\tau_2\sigma_2}S_{\tau_1\sigma_1} \quad . \tag{3.3.16}$$

In particular, under spin rotations about the z-axis, i.e. $\hat{S}(\hat{z},\varphi) = e^{-i\sigma_z\varphi/2}$, the vertex transforms to

$$\begin{pmatrix} U^{\uparrow\uparrow\uparrow\uparrow}e^{i\left(\frac{\varphi}{2}+\frac{\varphi}{2}-\frac{\varphi}{2}-\frac{\varphi}{2}\right)} & U^{\uparrow\uparrow\uparrow\downarrow}e^{i\left(\frac{\varphi}{2}+\frac{\varphi}{2}-\frac{\varphi}{2}+\frac{\varphi}{2}\right)} & U^{\uparrow\uparrow\downarrow\uparrow}e^{i\left(\frac{\varphi}{2}+\frac{\varphi}{2}+\frac{\varphi}{2}-\frac{\varphi}{2}\right)} & U^{\uparrow\uparrow\downarrow\downarrow}e^{i\left(\frac{\varphi}{2}+\frac{\varphi}{2}+\frac{\varphi}{2}+\frac{\varphi}{2}\right)} \\ U^{\uparrow\downarrow\uparrow\uparrow}e^{i\left(\frac{\varphi}{2}-\frac{\varphi}{2}-\frac{\varphi}{2}-\frac{\varphi}{2}\right)} & U^{\uparrow\downarrow\uparrow\downarrow}e^{i\left(\frac{\varphi}{2}-\frac{\varphi}{2}-\frac{\varphi}{2}+\frac{\varphi}{2}\right)} & U^{\uparrow\downarrow\downarrow\uparrow}e^{i\left(\frac{\varphi}{2}-\frac{\varphi}{2}+\frac{\varphi}{2}-\frac{\varphi}{2}\right)} & U^{\uparrow\downarrow\downarrow\downarrow}e^{i\left(\frac{\varphi}{2}-\frac{\varphi}{2}+\frac{\varphi}{2}+\frac{\varphi}{2}\right)} \\ U^{\downarrow\uparrow\uparrow\uparrow}e^{i\left(\frac{-\varphi}{2}+\frac{\varphi}{2}-\frac{\varphi}{2}-\frac{\varphi}{2}\right)} & U^{\downarrow\uparrow\uparrow\downarrow}e^{i\left(\frac{-\varphi}{2}+\frac{\varphi}{2}-\frac{\varphi}{2}+\frac{\varphi}{2}\right)} & U^{\downarrow\uparrow\downarrow\uparrow}e^{i\left(\frac{-\varphi}{2}+\frac{\varphi}{2}+\frac{\varphi}{2}-\frac{\varphi}{2}\right)} & U^{\downarrow\uparrow\downarrow\downarrow}e^{i\left(\frac{-\varphi}{2}+\frac{\varphi}{2}+\frac{\varphi}{2}+\frac{\varphi}{2}\right)} \\ U^{\downarrow\downarrow\uparrow\uparrow}e^{i\left(-\frac{\varphi}{2}-\frac{\varphi}{2}-\frac{\varphi}{2}-\frac{\varphi}{2}\right)} & U^{\downarrow\downarrow\uparrow\downarrow}e^{i\left(-\frac{\varphi}{2}-\frac{\varphi}{2}-\frac{\varphi}{2}+\frac{\varphi}{2}\right)} & U^{\downarrow\downarrow\downarrow\uparrow}e^{i\left(-\frac{\varphi}{2}-\frac{\varphi}{2}+\frac{\varphi}{2}-\frac{\varphi}{2}\right)} & U^{\downarrow\downarrow\downarrow\downarrow}e^{i\left(-\frac{\varphi}{2}-\frac{\varphi}{2}+\frac{\varphi}{2}+\frac{\varphi}{2}\right)} \end{pmatrix} . \tag{3.3.17}$$

For the two-particle vertex to be invariant under such a rotation, the transformed vertex must evaluate to the original vertex. Therefore, the ten transformed vertex elements that feature an unequal number of ingoing to outgoing up and down spins must be zero. Fermionic antisymmetry furthermore requires the four "inner" elements to be interdependent, i.e. $U^{\uparrow\downarrow\uparrow\downarrow} = -U^{\downarrow\uparrow\uparrow\downarrow} = -U^{\downarrow\uparrow\downarrow\uparrow} = U^{\downarrow\uparrow\uparrow\downarrow} := V_{\alpha_1\alpha_2\alpha_1'\alpha_2'}$ while the elements $U^{\uparrow\uparrow\uparrow\uparrow} := V^{\uparrow}_{\alpha_1\alpha_2\alpha_1'\alpha_2'}$ and $U^{\downarrow\downarrow\downarrow\downarrow} := V^{\uparrow}_{\alpha_1\alpha_2\alpha_1'\alpha_2'}$ have to be antisymmetric as well. Therefore, the $e^{-i\sigma_z\varphi/2}$-symmetric two-particle vertex is given by

$$U^{\sigma_1\sigma_2\sigma_1'\sigma_2'}_{\alpha_1\alpha_2\alpha_1'\alpha_2'} = \left(V^{\uparrow}_{\alpha_1\alpha_2\alpha_1'\alpha_2'}\delta_{\sigma_1\uparrow} + V^{\downarrow}_{\alpha_1\alpha_2\alpha_1'\alpha_2'}\delta_{\sigma_1\downarrow}\right)\delta_{\sigma_1\sigma_2}\delta_{\sigma_1'\sigma_2'}\delta_{\sigma_1\sigma_1'} + V_{\alpha_1\alpha_2\alpha_1'\alpha_2'}\delta_{\sigma_1\sigma_1'}\delta_{\sigma_2\sigma_2'} - V_{\alpha_2\alpha_1\alpha_1'\alpha_2'}\delta_{\sigma_1\sigma_2'}\delta_{\sigma_2\sigma_1'} \quad , \tag{3.3.18}$$

with $V^{\uparrow,\downarrow}_{\alpha_1\alpha_2\alpha_1'\alpha_2'} = -V^{\uparrow,\downarrow}_{\alpha_2\alpha_1\alpha_1'\alpha_2'} = -V^{\uparrow,\downarrow}_{\alpha_1\alpha_2\alpha_2'\alpha_1'}$ and $V_{\alpha_1\alpha_2\alpha_1'\alpha_2'} = V_{\alpha_2\alpha_1\alpha_2'\alpha_1'}$ which means it only contains three independent spinless coupling functions (cf. [MH14, Sec. 1.3, p. 21] [MEH14; MH12]). If we require full SU(2) spin rotation symmetry, we will get even more interdependencies resulting in a single spinless coupling function $V_{\alpha_1\alpha_2\alpha_1'\alpha_2'}$. Hence, the vertex function must be invariant under the most general $\hat{S}(\hat{n},\varphi)$ (Equation 3.3.16) associated to an arbitrary axis of rotation $\hat{n}$ and an arbitrary angle φ. This is possible only, if the matrix elements of $\hat{S}$ sum up to unity by employing the unitary relation $\sum_\tau \overline{\hat{S}}(\hat{n},\varphi)_{\tau\sigma}\hat{S}(\hat{n},\varphi)_{\tau\sigma'} = \delta_{\sigma\sigma'}$. To this end, the primed and unprimed spins σ_1, σ_2 and σ_1', σ_2' have to be pairwise identical, e.g. either $\sigma_1 = \sigma_1'$ and $\sigma_2 = \sigma_2'$ or $\sigma_1 = \sigma_2'$ and $\sigma_2 = \sigma_1'$ (cf. (Equation 3.3.16)) All vertex elements that don't satisfy this condition must vanish. Hence, the fully spin symmetric two-particle vertex has the form

$$U^{\sigma_1\sigma_2\sigma_1'\sigma_2'}_{\alpha_1\alpha_2\alpha_1'\alpha_2'} = V_{\alpha_1\alpha_2\alpha_1'\alpha_2'}\delta_{\sigma_1\sigma_1'}\delta_{\sigma_2\sigma_2'} - V_{\alpha_2\alpha_1\alpha_1'\alpha_2'}\delta_{\sigma_1\sigma_2'}\delta_{\sigma_2\sigma_1'} \quad , \tag{3.3.19}$$

which may be represented in matrix form (Equation 3.3.3) by

$$\begin{pmatrix} V_{\alpha_1\alpha_2\alpha_1'\alpha_2'} - V_{\alpha_2\alpha_1\alpha_1'\alpha_2'} & 0 & 0 & 0 \\ 0 & V_{\alpha_1\alpha_2\alpha_1'\alpha_2'} & -V_{\alpha_2\alpha_1\alpha_1'\alpha_2'} & 0 \\ 0 & -V_{\alpha_2\alpha_1\alpha_1'\alpha_2'} & V_{\alpha_1\alpha_2\alpha_1'\alpha_2'} & 0 \\ 0 & 0 & 0 & V_{\alpha_1\alpha_2\alpha_1'\alpha_2'} - V_{\alpha_2\alpha_1\alpha_1'\alpha_2'} \end{pmatrix} \quad , \tag{3.3.20}$$

where the single spinless coupling function satisfies

$$V_{\alpha_1\alpha_2\alpha_1'\alpha_2'} = V_{\alpha_2\alpha_1\alpha_2'\alpha_1'} \qquad \overline{V_{\alpha_1\alpha_2\alpha_1'\alpha_2'}} = V_{\alpha_1'\alpha_2'\alpha_1\alpha_2} \quad , \tag{3.3.21}$$

which can be shown by employing the fermionic particle exchange (Equation 3.3.4) in (Equation 3.3.19) twice and using the Hermiticity (Equation 3.3.5). The relation (Equation 3.3.19) also determines how a spinful two-particle vertex describing a SU(2)-invariant spinless interaction like e.g. the Coulomb interaction U looks like. Because the spinless coupling function $V_{\alpha_1\alpha_2\alpha_1'\alpha_2'}$ equals the Coulomb interaction, we simply have $U^{\sigma_1\sigma_2\sigma_1'\sigma_2'}_{\alpha_1\alpha_2\alpha_1'\alpha_2'} = U\delta_{\sigma_1\sigma_1'}\delta_{\sigma_2\sigma_2'} - U\delta_{\sigma_1\sigma_2'}\delta_{\sigma_2\sigma_1'}$. This relation will be employed extensively for spinful (renormalization group) calculations since it extends straightforwardly to multi-orbital interactions exhibiting SU(2) invariance.

Inversion

The operation of spatial *inversion* $\hat{P}$ affects the relevant quantum numbers of momentum, sublattice, orbital and spin according to

$$\begin{aligned}
&\text{momentum} && \mathbf{k} \xrightarrow{\hat{P}} -\mathbf{k} && (3.3.22)\\
&\text{sublattice} && s \xrightarrow{\hat{P}} f(s) && (3.3.23)\\
&\text{orbital} && o \xrightarrow{\hat{P}} (-1)^l o && (3.3.24)\\
&\text{spin} && \sigma \xrightarrow{\hat{P}} \sigma \quad , && (3.3.25)
\end{aligned}$$

where $f(s)$ is a function of permutation that shuffles the sublattice indices and depends on the specific lattice geometry. The orbital degree of freedom may acquire a minus sign depending on the specific angular momentum quantum number l [Bal98]. Finally, spin σ is unaffected by spatial inversion since it is a *pseudovector/axial vector*. Hence, we find that the two-particle vertex (Equation 3.3.1) in orbital space behaves under inversion according to

$$\begin{aligned}
\Gamma^{(4)} &= \sum_{\substack{\mathbf{k}_1,\mathbf{k}_2,\\ \mathbf{k}_1',\mathbf{k}_2'}} \sum_{\substack{s_1,s_2,\\ s_1',s_2'}} \sum_{\substack{o_1,o_2,\\ o_1',o_2'}} \sum_{\substack{\sigma_1,\sigma_2,\\ \sigma_1',\sigma_2'}} U^{\sigma_1\sigma_2\sigma_1'\sigma_2'}_{(\mathbf{k}_1 s_1 o_1)(\mathbf{k}_2 s_2 o_2)(\mathbf{k}_1' s_1' o_1')(\mathbf{k}_2' s_2' o_2')}\, \bar{\psi}_{\mathbf{k}_1' s_1' o_1'} \bar{\psi}_{\mathbf{k}_2' s_2' o_2'} \psi_{\mathbf{k}_2 s_2 o_2} \psi_{\mathbf{k}_1 s_1 o_1} \\
&\xrightarrow{\hat{P}} \sum_{\substack{\mathbf{k}_1,\mathbf{k}_2,\\ \mathbf{k}_1',\mathbf{k}_2'}} \sum_{\substack{s_1,s_2\\ s_1',s_2'}} \sum_{\substack{o_1,o_2\\ o_1',o_2'}} \sum_{\substack{\sigma_1,\sigma_2\\ \sigma_1',\sigma_2'}} U^{\sigma_1\sigma_2\sigma_1'\sigma_2'}_{(\mathbf{k}_1 s_1 o_1(\mathbf{k}_2 s_2 o_2)(\mathbf{k}_1' s_1' o_1')(\mathbf{k}_2' s_2' o_2')} \\
&\qquad \times \bar{\psi}_{-\mathbf{k}_1' f(s_1')(-1)^{l_1'} o_1'} \bar{\psi}_{-\mathbf{k}_2' f(s_2')(-1)^{l_1'} o_2'} \psi_{-\mathbf{k}_2 f(s_2)(-1)^{l_2} o_2} \psi_{-\mathbf{k}_1 f(s_1)(-1)^{l_1} o_1} \quad ,
\end{aligned} \tag{3.3.26}$$

Note, that the requirement of inversion symmetry on the two-particle vertex $\Gamma^{(4)}$ which results in $\Gamma^{(4)} \xrightarrow{\hat{P}} \tilde{\Gamma}^{(4)} \overset{!}{=} \Gamma^{(4)}$, imposes constraints on the vertex structure that significantly reduces the number of independent couplings.

Point-group symmetries

An important property of any n-body correlation function for electrons on the lattice is, that it must transform according to the underlying point group symmetry. Albeit we're dealing with the irreducible two-particle vertex, its transformation behavior is essentially determined by the transformation properties of the single-particle states the vertex is based on. Let's consider the point group $\mathcal{G}$ and one of its elements denoted by $g \in \mathcal{G}$. Since we consider single-particle states involving sublattice, orbital, spin and momentum degrees of freedom, we have to establish all (reducible or irreducible) representations that operate in the respective spaces. The two- or three-dimensional momentum space representation is denoted by $\mathcal{D}(g)$. The representations in sublattice

and orbital space are given by $\mathcal{A}(g)$ and $\mathcal{L}(g)$. Finally, the most crucial transformation matrices, denoted by $\mathcal{S}(g)$ with double group element $g \in \mathcal{G}^D$ that actually form a *double group* are the ones operating in spin space. Although, its double group properties can be ignored in some cases (e.g. symmetry of the spinful Hamiltonian) it's important to keep in mind that $\mathcal{S}(g)$ behaves as a double group representation when acting on single-particle states. The fermionic single-particle basis states given by the fields $\bar{\psi}$ and ψ are therefore transformed according to

$$\psi_{\mathbf{k}so\sigma} \overset{g\in\mathcal{G}}{\longrightarrow} \sum_{s'o'\sigma'} \left(\mathcal{A}(g)\otimes\mathcal{L}(g)\otimes\mathcal{S}(g)\right)_{(so\sigma)(s'o'\sigma')} \psi_{\mathbf{k}s'o'\sigma'} = \psi_{\mathcal{P}(g^{-1})\mathbf{k}s'o'\sigma'} \tag{3.3.27a}$$

$$\bar{\psi}_{\mathbf{k}so\sigma} \overset{g\in\mathcal{G}}{\longrightarrow} \sum_{s',o',\sigma'} \left(\mathcal{A}(g)\otimes\mathcal{L}(g)\otimes\mathcal{S}(g)\right)^{\dagger}_{(so\sigma)(s'o'\sigma')} \bar{\psi}_{\mathbf{k}s'o'\sigma'} = \bar{\psi}_{\mathcal{P}(g^{-1})\mathbf{k}s'o'\sigma'} \quad , \tag{3.3.27b}$$

where the indices s, o and σ represent sublattice, orbital and spin. The collective indices $(so\sigma)$ and $(s'o'\sigma')$ refer to a single index each in direct product space. For brevity of notation, we denote $\mathcal{A}(g)\otimes\mathcal{L}(g)\otimes\mathcal{S}(g) \coloneqq \mathcal{D}(g)$. We took into account that the operation g in real space corresponds to g^{-1} in reciprocal space [DDJ08, chap. 13.3 "Symmetry of **k**-Vectors and the Group of the Wave Vector"]. For future reference and simplified notation the multiindices $\alpha, \beta \coloneqq (s-1)\, n_o 2 + (o-1)\, 2 + \sigma$ (n_o being the number of orbitals) are defined and the point group transformation of fields is summarized by

$$\psi_{\mathbf{k}so\sigma} \overset{g\in\mathcal{G}^D}{\longrightarrow} \sum_{s',o',\sigma'} \mathcal{D}(g)_{(so\sigma)(s'o'\sigma')} \psi_{\mathbf{k}s'o'\sigma'} = \sum_{\alpha'} \mathcal{D}(g)_{\alpha\alpha'} \psi_{\mathbf{k}\alpha'} = \psi_{\mathcal{P}(g^{-1})\mathbf{k}\alpha'} \tag{3.3.28a}$$

$$\bar{\psi}_{\mathbf{k}so\sigma} \overset{g\in\mathcal{G}^D}{\longrightarrow} \sum_{s',o',\sigma'} \bar{\psi}_{\mathbf{k}s'o'\sigma'} \overline{\mathcal{D}(g)}_{(s'o'\sigma')(so\sigma)} = \sum_{\alpha'} \bar{\psi}_{\mathbf{k}\alpha'} \overline{\mathcal{D}(g)}_{\alpha'\alpha} = \bar{\psi}_{\mathcal{P}(g^{-1})\mathbf{k}\alpha'} \quad , \tag{3.3.28b}$$

where g is an element of the double group $\mathcal{G}^D$. Note, that one has to distinguish the transformations associated to real space, which are given by the matrices acting on momentum, sublattice and orbital degrees of freedom and the ones operating in spin space. In general, the transformation in real space affecting the combined momentum, sublattice and orbital degrees of freedom may be performed independently from the one in spin space. However, in the presence of spin-orbit interaction, the real space and spin space degrees of freedom are coupled. Therefore, the corresponding Hamiltonian will exhibit symmetries only with respect to combined real and spin space transformations. Before we proceed to the two-particle vertices, we have a look at the transformation of the single-particle Hamiltonian, i.e. the non-interacting action $S_0[\bar{\psi}, \psi]$:

$$
\begin{aligned}
S_0\left[\bar{\psi},\psi\right] &= \sum_{i\omega_n,\mathbf{k}} \sum_{\alpha,\alpha'} \bar{\psi}_{\mathbf{k}\alpha'} \left(i\omega_n \delta_{\alpha\alpha'} - h_{\alpha\alpha'}(\mathbf{k})\right) \psi_{\mathbf{k}\alpha} \\
&\overset{g\in\mathcal{G}}{\longrightarrow} \sum_{i\omega_n,\mathbf{k}} \sum_{\alpha,\alpha'} \sum_{\beta,\beta'} \bar{\psi}_{\mathcal{P}(g^{-1})\mathbf{k}\beta'} \overline{\mathcal{D}(g)}_{\beta'\alpha'} \left(i\omega_n \delta_{\alpha\alpha'} - h_{\alpha\alpha'}(\mathbf{k})\right) \mathcal{D}(g)_{\alpha\beta} \psi_{\mathcal{P}(g^{-1})\mathbf{k}\beta} \\
&= \sum_{i\omega_n,\mathbf{k}} \sum_{\beta,\beta'} \bar{\psi}_{\mathcal{P}(g^{-1})\mathbf{k}\beta'} \left(i\omega_n \delta_{\beta'\beta} - \sum_{\alpha,\alpha'} \overline{\mathcal{D}(g)}_{\beta'\alpha'} h_{\alpha\alpha'}(\mathbf{k}) \mathcal{D}(g)_{\alpha\beta} \right) \psi_{\mathcal{P}(g^{-1})\mathbf{k}\beta} \quad , \qquad (3.3.29)
\end{aligned}
$$

where the second equality made use of the unitary property $\sum_\alpha \overline{\mathcal{D}(g)}_{\beta'\alpha} \mathcal{D}(g)_{\alpha\beta} = \delta_{\beta'\beta}$ for the first term involving the Matsubara frequency. Comparing coefficients in terms of Grassmann fields, yields the transformation rule for the single-particle matrix elements that is

$$
h_{\alpha\alpha'}(\mathbf{k}) \overset{g\in\mathcal{G}}{\longrightarrow} \sum_{\alpha,\alpha'} \overline{\mathcal{D}(g)}_{\beta'\alpha'} h_{\alpha\alpha'}(\mathbf{k}) \mathcal{D}(g)_{\alpha\beta} \overset{!}{=} h_{\alpha\alpha'}(\mathcal{P}(g^{-1})\mathbf{k}) \quad . \qquad (3.3.30)
$$

The invariance of the non-interacting action under this transformation is ensured by construction (cf. appendix A and (Section 3.1.2)). Here, it is important to note, that we can neglect the double group character of the spinful transformation because all extended group elements $\bar{g} = \bar{E}g$ don't differ from their simple counterparts g since the additional sign $\mathcal{D}\left(\bar{E}\right) = -\mathcal{D}\left(E\right)$ cancels in (Equation 3.3.30). The generalization of (Equation 3.3.29) to the transformation of the two-particle vertex is straightforward. Referring to (Equation 3.3.1) and denoting the momenta explicitly the two-particle vertex becomes

$$
\begin{aligned}
\Gamma^{(4)}\left[\bar{\psi},\psi\right] &= \sum_{\substack{\alpha_1,\alpha_2,\\ \alpha_1',\alpha_2'}} \sum_{\substack{\mathbf{k}_1,\mathbf{k}_2,\\ \mathbf{k}_1',\mathbf{k}_2'}} U^{\alpha_1\alpha_2\alpha_1'\alpha_2'}_{\mathbf{k}_1\mathbf{k}_2\mathbf{k}_1'\mathbf{k}_2'} \bar{\psi}_{\mathbf{k}_1'\alpha_1'} \bar{\psi}_{\mathbf{k}_2'\alpha_2'} \psi_{\mathbf{k}_2\alpha_2} \psi_{\mathbf{k}_1\alpha_1} \\
&\overset{g\in\mathcal{G}}{\longrightarrow} \sum_{\substack{\beta_1,\beta_2,\\ \beta_1',\beta_2'}} \sum_{\substack{\mathbf{k}_1,\mathbf{k}_2,\\ \mathbf{k}_1',\mathbf{k}_2'}} \sum_{\substack{\alpha_1,\alpha_2,\\ \alpha_1',\alpha_2'}} U^{\alpha_1\alpha_2\alpha_1'\alpha_2'}_{\mathbf{k}_1\mathbf{k}_2\mathbf{k}_1'\mathbf{k}_2'} \overline{\mathcal{D}(g)}_{\beta_1'\alpha_1'} \overline{\mathcal{D}(g)}_{\beta_2'\alpha_2'} \mathcal{D}(g)_{\alpha_2\beta_2} \mathcal{D}(g)_{\alpha_1\beta_1} \\
&\quad \times \bar{\psi}_{\mathcal{P}(g^{-1})\mathbf{k}_1'\beta_1'} \bar{\psi}_{\mathcal{P}(g^{-1})\mathbf{k}_2'\beta_2'} \psi_{\mathcal{P}(g^{-1})\mathbf{k}_2\beta_2} \psi_{\mathcal{P}(g^{-1})\mathbf{k}_1\beta_1} \quad , \qquad (3.3.31)
\end{aligned}
$$

resulting in the transformation of the tensor elements with respect to the same Grassmann fields

$$U^{\alpha_1\alpha_2\alpha_1'\alpha_2'}_{\mathbf{k}_1\mathbf{k}_2\mathbf{k}_1'\mathbf{k}_2'} \xrightarrow{g\in\mathcal{G}} U^{\alpha_1\alpha_2\alpha_1'\alpha_2'}_{\mathcal{P}(g^{-1})\mathbf{k}_1\,\mathcal{P}(g^{-1})\mathbf{k}_2\,\mathcal{P}(g^{-1})\mathbf{k}_1'\,\mathcal{P}(g^{-1})\mathbf{k}_2'}$$
$$= \sum_{\substack{\beta_1,\beta_2,\\ \beta_1',\beta_2'}} U^{\beta_1\beta_2\beta_1'\beta_2'}_{\mathbf{k}_1\mathbf{k}_2\mathbf{k}_1'\mathbf{k}_2'} \overline{\mathcal{D}(g)}_{\alpha_1'\beta_1'} \overline{\mathcal{D}(g)}_{\alpha_2'\beta_2'} \mathcal{D}(g)_{\beta_2\alpha_2} \mathcal{D}(g)_{\beta_1\alpha_1} \quad . \tag{3.3.32}$$

Let's assume, there are $n_\alpha n_\kappa$ different single-particle states (due to the number of degrees of freedom n_α in sublattice, orbital and spin space and n_κ discretized momenta in reciprocal space) described by $\psi_{\mathbf{k}\alpha}$. Hence, the two-particle vertex contains $n_\alpha^4 n_\kappa^3$ coupling constants. Denoting the order of the group $\mathcal{G}$ by $\left|\mathcal{G}\right|$, all $n_\alpha^4 n_\kappa^3$ coupling constants are already determined by a particular set of $\frac{n_\alpha^4 n_\kappa^3}{|\mathcal{G}|}$ couplings and the transformation rule (Equation 3.3.32).

So far, we dealt with the two-particle vertex in orbital-spin basis. However, in (Chapter 5) and (Chapter 6) we will see, that these quantum many-body calculations are most conveniently performed in band space, i.e. in the basis where the one-particle Hamiltonian (and therefore the single-particle propagator) assumes diagonal form. Furthermore, the band basis allows for a more transparent interpretation of the resulting physical entities. Unfortunately, the shape and spin structure of the two-particle vertex will also change due to the fact that it's expressed in terms of the new basis featuring the *pseudopsin* or *helical spin* degree of freedom. Both pseudospin and helical spin amount to a superposition of "natural" ↑ and ↓ spins eventually associated to different orbitals.

3.3.2. Band space

The correlation and vertex functions in band space are the ones, which provide conclusive information about physical properties like e.g. superconducting gap functions, low energy behavior of specific heat. The correlation functions in band space correspond to specific Fermi surfaces while the orbital space vertex functions cannot be associated to any particular Fermi sheet. Furthermore, the loop integrals occurring in the framework of perturbation theory are most conveniently evaluated in band space, because it is the basis that the non-interacting Green's functions are diagonal in (cf. (Chapter 5)). Henceforth, we need the transformation rule in band-pseudospin/helical-spin space corresponding to (Equation 3.3.32) in orbital-spin space. The path from orbital to band space is paved by the unitary basis transformation

$$\phi_{\mathbf{k}b(\tilde{\sigma},\lambda)} = \sum_{s,o,\sigma} U^{b(\tilde{\sigma},\lambda)}_{so\sigma}(\mathbf{k})\,\psi_{\mathbf{k}so\sigma} = \sum_{\alpha} U^{\tilde{\alpha}\alpha}_{\mathbf{k}}\psi_{\mathbf{k}\alpha} \coloneqq \phi_{\mathbf{k}\tilde{\alpha}} \tag{3.3.33a}$$

$$\bar{\phi}_{\mathbf{k}b(\tilde{\sigma},\lambda)} = \sum_{s,o,\sigma} \left(U^{b(\tilde{\sigma},\lambda)}_{so\sigma}(\mathbf{k})\right)^\dagger \bar{\psi}_{\mathbf{k}so\sigma} = \sum_{\alpha} \bar{\psi}_{\mathbf{k}\alpha}\overline{U}^{\alpha\tilde{\alpha}}_{\mathbf{k}} \coloneqq \bar{\phi}_{\mathbf{k}\tilde{\alpha}} \quad , \tag{3.3.33b}$$

where we again abbreviated the indices (s, o, σ) by α and the band and pseudospin/helical-

spin indices by $\tilde{\alpha} = (b, (\tilde{\sigma}, \lambda))$. We introduced the new fermionic fields $\bar{\phi}$ and ϕ representing the states in band space. Here, $U_{\mathbf{k}}$ is the matrix of eigenvectors of the single-particle Hamiltonian $\mathcal{H}_0$ at $\mathbf{k}$, which crucially depends on the gauge of phases of eigenstates and eventually on the definition of the *pseudospin* discussed in (Section 3.2). In order to find the transformation behavior of the two-particle vertex in band space, we first have to work out the transformation behavior of an eigenvector $\mathbf{u}_{\mathbf{k},\tilde{\alpha}}$ of the single-particle Hamiltonian $\mathcal{H}_0$ at $\mathbf{k}$ for band/pseudospin/helical-spin $\tilde{\alpha}$ with eigenvalue/band-energy $\xi_{\mathbf{k}\tilde{\alpha}}$. Based on how $\mathcal{H}_0$ transforms (see (Equation 3.3.30)), the eigenvalue equation reveals what the eigenvector $\mathbf{u}_{\mathcal{P}(g^{-1})\mathbf{k}\tilde{\alpha}}$ at the transformed momentum $\mathcal{P}(g^{-1})\mathbf{k}$ looks like, i.e.

$$\begin{aligned}
&\mathcal{H}_{0\mathbf{k}}\mathbf{u}_{\mathbf{k}\tilde{\alpha}} = \xi_{\mathbf{k}\tilde{\alpha}}\mathbf{u}_{\mathbf{k}\tilde{\alpha}} = \mathcal{H}_{0\mathbf{k}}\underbrace{\left(\mathcal{D}(g)\right)^{\dagger}\mathcal{D}(g)}_{=\mathbb{1}}\mathbf{u}_{\mathbf{k}\tilde{\alpha}} \\
&\Rightarrow \underbrace{\mathcal{D}(g)\mathcal{H}_{0\mathbf{k}}\left(\mathcal{D}(g)\right)^{\dagger}}_{=\mathcal{H}_{0\mathcal{P}(g^{-1})\mathbf{k}}}\mathcal{D}(g)\mathbf{u}_{\mathbf{k}\tilde{\alpha}} = \mathcal{D}(g)\xi_{\mathbf{k}\tilde{\alpha}}\mathbf{u}_{\mathbf{k}\tilde{\alpha}} = \xi_{\mathbf{k}\tilde{\alpha}}\mathcal{D}(g)\mathbf{u}_{\mathbf{k}\tilde{\alpha}} \quad . \qquad (3.3.34)
\end{aligned}$$

Consequently, in terms of the original eigenvector $\mathbf{u}_{\mathbf{k}\tilde{\alpha}}$ at $\mathbf{k}$, the eigenvector at $\mathcal{P}(g^{-1})\mathbf{k}$ is given by $\tilde{\mathbf{u}}_{\mathcal{P}(g^{-1})\mathbf{k}\tilde{\alpha}} = \mathcal{D}(g)\mathbf{u}_{\mathbf{k}\tilde{\alpha}}$. However, this eigenvector generally differs from the eigenvector $\mathbf{u}_{\mathcal{P}(g^{-1})\mathbf{k},\tilde{\alpha}}$ defined at momentum $\mathcal{P}(g^{-1})\mathbf{k}$. In case of degenerate bands characterized by pseudospin, the transformed eigenstate $\tilde{\mathbf{u}}_{\mathcal{P}(g^{-1})\mathbf{k}\tilde{\alpha}}$ equals a superposition of both pseudospin states of the specific band at the respective momentum, i.e.

$$\begin{aligned}
\mathcal{D}(g)\mathbf{u}_{\mathbf{k}b\tilde{\sigma}} &= c_{\tilde{\uparrow}}\mathbf{u}_{\mathcal{P}(g^{-1})\mathbf{k}b\tilde{\uparrow}} + c_{\tilde{\downarrow}}\mathbf{u}_{\mathcal{P}(g^{-1})\mathbf{k}b\tilde{\downarrow}} \quad , \\
&\text{where} \quad c_{\tilde{\uparrow}}, c_{\tilde{\downarrow}} \in \mathbb{C} \quad \text{and} \quad \left|c_{\tilde{\uparrow}}\right|^2 + \left|c_{\tilde{\downarrow}}\right|^2 = 1 \quad . \qquad (3.3.35)
\end{aligned}$$

Thanks to the orthonormality of eigenstates at $\mathcal{P}(g^{-1})\mathbf{k}$ the coefficients are given by $c_{\tilde{\uparrow}} = \left\langle \mathbf{u}_{\mathcal{P}(g^{-1})\mathbf{k}b\tilde{\uparrow}} \right| \mathcal{D}(g) \left| \mathbf{u}_{\mathbf{k}b\tilde{\sigma}} \right\rangle$ and $c_{\tilde{\downarrow}} = \left\langle \mathbf{u}_{\mathcal{P}(g^{-1})\mathbf{k}b\tilde{\downarrow}} \right| \mathcal{D}(g) \left| \mathbf{u}_{\mathbf{k}b\tilde{\sigma}} \right\rangle$. In contrast, if we have non-degenerate bands labeled by helicity, the eigenstate at $\mathbf{k}$ must be mapped by the point group operation onto an eigenstate at $\mathcal{P}(g^{-1})\mathbf{k}$ associated to the same energy and therefore the same helicity, i.e.

$$\mathcal{D}(g)\mathbf{u}_{\mathbf{k}b\lambda} = e^{-i\varphi}\mathbf{u}_{\mathcal{P}(g^{-1})\mathbf{k}b\lambda} \quad . \qquad (3.3.36)$$

the two states can only differ by a *phase shift*. It is important to note, that the inversion operation is not part of the point group $g \in \mathcal{G}$ for the case of helical spin by definition, since helicity arises from broken inversion symmetry. Numerically, it is most efficient to encode these phase shifts and coefficients for all bands in a matrix $\mathcal{B}_{\mathbf{k}}(g)$ that amounts to the "representation" matrix $\mathcal{D}(g)$ in band space including the momentum dependency due to the particular choice of *gauge* and eventually *pseudospin*. It it given by

$$\mathcal{B}_{\mathbf{k}}(g) = U_{\mathcal{P}(g^{-1})\mathbf{k}} \mathcal{D}(g) U_{\mathbf{k}}^{\dagger} \quad , \tag{3.3.37}$$

where $U_{\mathbf{k}}$ and $U_{\mathcal{P}(g^{-1})\mathbf{k}}$ are the matrices of eigenvectors at the respective $\mathbf{k}$-points. $\mathcal{B}_{\mathbf{k}}(g)$ describes the transformation of single-particle states $\psi_{\mathbf{k}b(\tilde{\sigma},\lambda)}$ in band space. To see this, consider (Equation 3.3.33a) at the transformed momentum $\mathcal{P}(g^{-1})\mathbf{k}$, i.e.

$$\begin{aligned} \phi_{\mathcal{P}(g^{-1})\mathbf{k}\tilde{\alpha}} = U^{\tilde{\alpha}\alpha}_{\mathcal{P}(g^{-1})\mathbf{k}} \underbrace{\psi_{\mathcal{P}(g^{-1})\mathbf{k}\alpha}}_{=\mathcal{D}(g)_{\alpha\beta}\psi_{\mathbf{k}\beta}} &= U^{\tilde{\alpha}\alpha}_{\mathcal{P}(g^{-1})\mathbf{k}} \left(\mathcal{D}(g) \underbrace{U_{\mathbf{k}}^{\dagger} U_{\mathbf{k}}}_{=\mathbb{1}} \right)_{\alpha\beta} \psi_{\mathbf{k}\beta} \\ &= \underbrace{\left(U_{\mathcal{P}(g^{-1})\mathbf{k}} \mathcal{D}(g) U_{\mathbf{k}}^{\dagger} \right)_{\tilde{\alpha}\tilde{\beta}}}_{=(\mathcal{B}_{\mathbf{k}}(g))_{\tilde{\alpha}\tilde{\beta}}} \underbrace{(U_{\mathbf{k}}\psi_{\mathbf{k}})_{\tilde{\beta}}}_{=\phi_{\mathbf{k}\tilde{\beta}}} \quad , \end{aligned} \tag{3.3.38}$$

where we used (Equation 3.3.28a). We simply wrote down the orbital to band transformation of the fields at some transformed momentum given by $\mathcal{P}(g^{-1})\mathbf{k}$. After introducing a resolution of identity in terms of matrices of eigenvectors, we can apply the one on the right hand side to the orbital field at the untransformed momentum, resulting in the field in band space at the untransformed momentum. Consequently, the matrix product of remaining entities on the right hand side must necessarily provide the desired transformation in band space. Based on these results we can summarize the transformation of single-particle states in band space associated to pseudospin or helicity by

$$\phi_{\mathbf{k}b(\sigma,\lambda)} \overset{g\in\mathcal{G}^D}{\longrightarrow} \sum_{b',(\sigma',\lambda')} \mathcal{B}_{\mathbf{k}}(g)_{(b(\sigma,\lambda))(b'(\sigma',\lambda'))} \phi_{\mathbf{k}b'(\sigma',\lambda')} = \sum_{\tilde{\alpha}'} \mathcal{B}_{\mathbf{k}}(g)_{\tilde{\alpha}\tilde{\alpha}'} \phi_{\mathbf{k}\tilde{\alpha}'} = \phi_{\mathcal{P}(g^{-1})\mathbf{k}\tilde{\alpha}} \tag{3.3.39a}$$

$$\bar{\phi}_{\mathbf{k}b(\sigma,\lambda)} \overset{g\in\mathcal{G}^D}{\longrightarrow} \sum_{b',(\sigma',\lambda')} \bar{\phi}_{\mathbf{k}b'(\sigma',\lambda')} \overline{\mathcal{B}_{\mathbf{k}}(g)}_{(b'(\sigma',\lambda'))(b(\sigma,\lambda))} = \sum_{\tilde{\alpha}'} \bar{\phi}_{\mathbf{k}\tilde{\alpha}'} \overline{\mathcal{B}_{\mathbf{k}}(g)}_{\tilde{\alpha}'\tilde{\alpha}} = \bar{\phi}_{\mathcal{P}(g^{-1})\mathbf{k}\tilde{\alpha}} \quad , \tag{3.3.39b}$$

Like already suggested above, the transformation matrices $\mathcal{B}_{\mathbf{k}}(g)$ are expected to be 2×2-block-diagonal in band-pseudospin-space and diagonal in helical-spin space. Only in the pseudospin case with degenerate bands, we may have off-diagonal elements in the spin degree of freedom (which is apparent from (Equation 3.3.34)). Note, that the entities $\mathcal{B}_{\mathbf{k}}(g)$ (Equation 3.3.37) also form a representation of the simple group $\mathcal{G}$ that is parametrized by momentum $\mathbf{k}$. We can see this by looking at the group composition rule

$$\begin{aligned}\mathcal{B}_{\mathcal{D}(g^{-1})\mathbf{k}}(\tilde{g}) \cdot \mathcal{B}_{\mathbf{k}}(g) &= U_{\mathcal{D}(\tilde{g}^{-1})\mathcal{D}(g^{-1})\mathbf{k}} \mathcal{D}(\tilde{g}) U^{\dagger}_{\mathcal{D}(g^{-1})\mathbf{k}} U_{\mathcal{D}(g^{-1})\mathbf{k}} \mathcal{D}(g) U^{\dagger}_{\mathbf{k}} \\ &= U_{\mathcal{D}((\tilde{g}\circ g)^{-1})\mathbf{k}} \mathcal{D}(\tilde{g}\circ g) U^{\dagger}_{\mathbf{k}} = \mathcal{B}_{\mathbf{k}}(\tilde{g}\circ g) \quad . \end{aligned} \tag{3.3.40}$$

Analogously to the transformation of the two-particle vertex in orbital-spin-space (Equation 3.3.32) we can by means of (Equation 3.3.39a) and (Equation 3.3.39b) work out the transformation of the two-particle vertex function in band-pseudospin/helical space. It yields

$$\begin{aligned} & U^{\tilde{\alpha}_1\tilde{\alpha}_2\tilde{\alpha}'_1\tilde{\alpha}'_2}_{\mathbf{k}_1\mathbf{k}_2\mathbf{k}'_1\mathbf{k}'_2} \overset{g\in\mathcal{G}}{\longrightarrow} U^{\tilde{\alpha}_1\tilde{\alpha}_2\tilde{\alpha}'_1\tilde{\alpha}'_2}_{\mathcal{D}(g^{-1})\mathbf{k}_1\mathcal{D}(g^{-1})\mathbf{k}_2\mathcal{D}(g^{-1})\mathbf{k}'_1\mathcal{D}(g^{-1})\mathbf{k}'_2} \\ &= \sum_{\substack{\tilde{\beta}_1,\tilde{\beta}_2,\\ \tilde{\beta}'_1,\tilde{\beta}'_2}} U^{\tilde{\beta}_1\tilde{\beta}_2\tilde{\beta}'_1\tilde{\beta}'_2}_{\mathbf{k}_1\mathbf{k}_2\mathbf{k}'_1\mathbf{k}'_2} \overline{\mathcal{B}_{\mathbf{k}}(g)}_{\tilde{\alpha}'_1\tilde{\beta}'_1} \overline{\mathcal{B}_{\mathbf{k}}(g)}_{\tilde{\alpha}'_2\tilde{\beta}'_2} \mathcal{B}_{\mathbf{k}}(g)_{\tilde{\beta}_2\tilde{\alpha}_2} \mathcal{B}_{\mathbf{k}}(g)_{\tilde{\beta}_1\alpha_1} \quad . \end{aligned} \tag{3.3.41}$$

In spite of the transformation matrices $\mathcal{B}_{\mathbf{k}}(g)$ not being a (double group) representation of the group $g \in \mathcal{G}$, the vertex function is single-valued. However, because $\mathcal{B}_{\mathbf{k}}(g)$ is derived from the orbital space transformation $\mathcal{D}(g)$ it also inherits the minus sign from its double group elements, which is essential for the single-particle states in band space and the two-particle vertex to be consistent with time-reversal, because for fermions we have $\hat{\Theta}^2 = -1$. More intuitively, for the states belonging to the first half of the (two-dimensional) Brillouin zone (corresponding to rotations around the z-axis with $\varphi \in [0, \pi]$), the time-reversal states are located in the second half of the Brillouin zone (corresponding to rotations around the z-axis with $\varphi \in [\pi, 2\pi]$). However, when time-reversal is employed to the states in the second half, the momenta are mapped back to the first half but acquire an additional minus sign due to $\hat{\Theta}^2 = -1$. This is consistent with rotations by $\varphi \in [2\pi, 3\pi]$, where the *double group* property comes into play. As a consequence, we always have to pair up time-reversal partners e.g. for helical states $|k, +\rangle$ and $|-k, +\rangle$, to get a simple point group transformation behavior of the associated correlation functions that The detailed analysis of point group operations for pseudospin and helical spin states is also used to reduce the number of states involved in numerics. However, the reduction scheme for the pseudospin degree of freedom differs from the one for helical bands as shown in (Figure 3.3).

Time-reversal

How do the single-particle states (Equation 3.3.33a) and (Equation 3.3.33b) in band space behave with respect to time-reversal? The time-reversal operator $\hat{\Theta} = -i\sigma_y\hat{\mathcal{K}}$ is only valid for "natural" spin states. For instance, this becomes evident from the fact that $\hat{\Theta}$ inverses the "natural" spin, while the helical spin state (in presence of time-reversal symmetry) must be mapped to a state with the same energy. However, since both pseudospin and helical spin can be expressed in terms of the "natural" spin degree

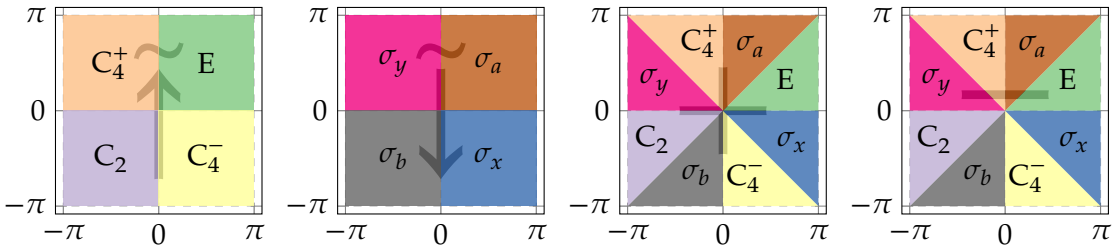

Figure 3.3.: The symmetry reduction of single-particle states by means of point group operations for e.g. a model on the square lattice with C_{4v}-symmetry works differently for pseudospin and helical states. Since the pseudospin (like the "natural" spin) is inverted by a reflection, we can limit the reduced sector of the Brillouin zone to one pseudospin state. In contrast, for helical spin there's no point group operation that mediates between both helical spin states. However, the symmetry reduction for helical bands works for pseudospin as well and the amount of phase space, i.e. the number of states in the reduced sector(s) is the same for both pseudospin and helical-spin.

of freedom, we can still apply $\hat{\Theta}$ to the fields in band space, or equivalently, transform the time-reversal operator to band space, i.e.

$$\hat{\Xi}_{\mathbf{k}} \equiv U_{-\mathbf{k}} \hat{\Theta} \left(U_{\mathbf{k}}\right)^{\dagger} \quad , \tag{3.3.42}$$

where the new time-reversal operator $\hat{\Xi}$ in band space is momentum dependent. When acting on a field in band space, $\hat{\Xi}_{\mathbf{k}}$ transforms it to orbital-spin-space, employs the usual time-reversal operator $\hat{\Theta}$ and transforms the resulting state at $-\mathbf{k}$ back to band space. Therefore, we get the transformation rule for the fields

$$\phi_{\mathbf{k}\tilde{\alpha}} = \sum_{\alpha} U^{\tilde{\alpha}\alpha}_{\mathbf{k}} \psi_{\mathbf{k}\alpha} \xrightarrow{\text{TR}} \hat{\Xi}^{\tilde{\alpha}\tilde{\beta}}_{\mathbf{k}} \phi_{\mathbf{k}\tilde{\beta}} = \tilde{\phi}_{-\mathbf{k}\tilde{\alpha}} \tag{3.3.43a}$$

$$\bar{\phi}_{\mathbf{k}\tilde{\alpha}} = \sum_{\alpha} \bar{\psi}_{\mathbf{k}\alpha} \overline{U}^{\alpha\tilde{\alpha}}_{\mathbf{k}} \xrightarrow{\text{TR}} \left(\hat{\Xi}^{\tilde{\alpha}\tilde{\beta}}_{\mathbf{k}}\right)^{-1} \bar{\phi}_{\mathbf{k}\tilde{\beta}} = \bar{\tilde{\phi}}_{-\mathbf{k}\tilde{\alpha}} \tag{3.3.43b}$$

In presence of time-reversal symmetry, this operation connects states that are degenerate, i.e. for a state in band-helical space the symmetry properties of $U_{\mathbf{k}}$ ensure that (Equation 3.3.43a) and (Equation 3.3.43b) always map a state with helicity λ to a state with the same helicity that can only differ by a phase (cf. (Section 3.1.2) and (Equation 3.1.53)). However, in contrast to the case of helicity, time-reversal maps the pseudospin at $\mathbf{k}$ to its opposite state at $-\mathbf{k}$, which still yields an equal-energy state due to inversion symmetry and *Kramers degeneracy*. Hence, the matrices $\hat{\Xi}^{\tilde{\alpha}\tilde{\beta}}_{\mathbf{k}}$ are diagonal in helical spin space and have off-diagonal elements, only, in pseudospin space. Since

time-reversal inverts the pseudospin degree of freedom (exactly like it does the "natural" spin, cf. the discussion at the beginning of (Section 3.4.1)), the requirement of time-reversal imposes strong constraints on the structure of the two-particle vertex. There, the constraints are the same as in (Equation 3.3.13) up to a phase.

Inversion

In contrast to the inversion of the two-particle vertex in orbital space (Section 3.3.1), the corresponding transformation in band space appears to be considerably simpler since only momentum and helical spin are affected, i.e.

$$\begin{aligned}
&\text{momentum} && \mathbf{k} \xrightarrow{\hat{P}} -\mathbf{k} && (3.3.44)\\
&\text{band} && b \xrightarrow{\hat{P}} b && (3.3.45)\\
&\text{pseudospin} && \tilde{\sigma} \xrightarrow{\hat{P}} \tilde{\sigma} && (3.3.46)\\
&\text{helicity} && \lambda \xrightarrow{\hat{P}} e^{-i\phi_{\mathbf{k}}}\bar{\lambda} \quad , && (3.3.47)
\end{aligned}$$

where, however, the appearance of the helical spin degree of freedom already presumes broken inversion symmetry. $\bar{\lambda}$ denotes the opposite helicity with respect to λ and the additional phase $\phi_{\mathbf{k}}$ depends on the untransformed momentum $\mathbf{k}$ (cf. (Equation 3.1.53)). Hence, an eigenstate at momentum $\mathbf{k}$ characterized by helicity λ maps to an eigenstate at $-\mathbf{k}$ with opposite helicity and a different energy, which is to be expected since the corresponding Hamiltonian breaks inversion symmetry and does not commute with $\hat{P}$. This already suggests that the inversion operation is not well suited to find Cooper states for equal energy pairing (in contrast to time-reversal, cf. (Section 3.4.2)). However, the transformation of the two-particle vertex characterized by pseudospin degrees of freedom is

$$\begin{aligned}
\Gamma^{(4)} = &\sum_{\substack{\mathbf{k}_1,\mathbf{k}_2,\\ \mathbf{k}_1',\mathbf{k}_2'}} \sum_{\substack{b_1,b_2,\\ b_1',b_2'}} \sum_{\substack{\tilde{\sigma}_1,\tilde{\sigma}_2,\\ \tilde{\sigma}_1',\tilde{\sigma}_2'}} U^{b_1\tilde{\sigma}_1 b_2\tilde{\sigma}_2 b_1'\tilde{\sigma}_1' b_2'\tilde{\sigma}_2'}_{\mathbf{k}_1\mathbf{k}_2\mathbf{k}_1'\mathbf{k}_2'} \bar{\phi}_{\mathbf{k}_1' b_1'\tilde{\sigma}_1'} \bar{\phi}_{\mathbf{k}_2' b_2'\tilde{\sigma}_2'} \phi_{\mathbf{k}_2 b_2\tilde{\sigma}_2} \phi_{\mathbf{k}_1 b_1\tilde{\sigma}_1}\\
\xrightarrow{\hat{P}} &\sum_{\substack{\mathbf{k}_1,\mathbf{k}_2,\\ \mathbf{k}_1',\mathbf{k}_2'}} \sum_{\substack{b_1,b_2\\ b_1',b_2'}} \sum_{\substack{\tilde{\sigma}_1,\tilde{\sigma}_2\\ \tilde{\sigma}_1',\tilde{\sigma}_2'}} U^{b_1\tilde{\sigma}_1 b_2\tilde{\sigma}_2 b_1'\tilde{\sigma}_1' b_2'\tilde{\sigma}_2'}_{\mathbf{k}_1\mathbf{k}_2\mathbf{k}_1'\mathbf{k}_2'} \bar{\phi}_{-\mathbf{k}_1' b_1'\tilde{\sigma}_1'} \bar{\phi}_{-\mathbf{k}_2' b_2'\tilde{\sigma}_2'} \phi_{-\mathbf{k}_2 b_2\tilde{\sigma}_2} \phi_{-\mathbf{k}_1 b_1\tilde{\sigma}_1} \quad , \qquad (3.3.48)
\end{aligned}$$

The requirement of inversion symmetry $\Gamma^{(4)} \xrightarrow{\hat{P}} \tilde{\Gamma}^{(4)} \stackrel{!}{=} \Gamma^{(4)}$ does not only restrict the number of independent couplings for pseudospin quasiparticles that exhibit inversion symmetry but also limits the possible non-zero pseudospin sectors for Cooper pairs and therefore facilitates the mean-field theory in the particle-particle channel (Section 3.4.1).

3.4. Generalized Cooper pairs

In (Section 2.2) and (Section 2.4) we discussed the mean-field theories for SU(2)-invariant and time-reversal symmetric models on lattices with inversion symmetry. Then it is possible to classify the superconducting pairing states by means of *singlet* and *triplet* part. In this section we will generalize the concept of Cooper pairs to particle-particle condensates to effective interactions in systems lacking SU(2)-symmetry (and eventually inversion symmetry). If inversion symmetry is present, the corresponding mean-fields are continuously connected to the ones with full SU(2)-symmetry (that were discussed in (Chapter 2)) with respect to the strength of spin-orbit interaction.
Let's consider the discrete symmetry operator of *parity* , denoted by $\hat{P}$. The effect of this unitary operator on some state $|\psi(\mathbf{r})\rangle$ is given by $|\psi(\mathbf{r})\rangle \longrightarrow \hat{P}\,|\psi(\mathbf{r})\rangle = e^{i\gamma}\,|\psi(-\mathbf{r})\rangle$ with $\gamma \in \mathbb{R}$ [Bal98, Chap. 13.1, p. 371]. Applying the operator twice, yields $\hat{P}^2\,|\psi(\mathbf{r})\rangle = \hat{P}e^{i\gamma}\,|\psi(-\mathbf{r})\rangle = e^{2i\gamma}\,|\psi(\mathbf{r})\rangle$. Since the phase factor has no physical implications [SN11, Chap. 4.2, p. 252] we can safely set it to unity. Hence, the operator satisfies $\hat{P}^2 = \mathbb{1}$ and its eigenvalues must be ± 1. As a consequence, the expectation value $\langle\psi(\mathbf{r})|\hat{A}|\psi(\mathbf{r})\rangle$ of any observable $\hat{A}$, that is invariant under *spatial inversion* must either feature a *symmetric* or an *antisymmetric* state $|\psi(\mathbf{r})\rangle$, since

$$\begin{aligned}\langle\psi(\mathbf{r})|\hat{A}|\psi(\mathbf{r})\rangle \overset{\text{inversion}}{\longrightarrow} \langle\psi(\mathbf{r})|\hat{P}^\dagger\hat{A}\hat{P}|\psi(\mathbf{r})\rangle &= \langle\psi(-\mathbf{r})|\hat{A}|\psi(-\mathbf{r})\rangle \\ &= \langle\pm\psi(\mathbf{r})|\hat{A}|\pm\psi(\mathbf{r})\rangle \overset{!}{=} \langle\psi(\mathbf{r})|\hat{A}|\psi(\mathbf{r})\rangle \quad . \end{aligned} \tag{3.4.1}$$

In contrast, a state $|\phi(\mathbf{r})\rangle$ with a non-specific parity, that is however expressable as a superposition of symmetric and antisymmetric parts, i.e.

$$|\phi(\mathbf{r})\rangle = \underbrace{\frac{|\phi(\mathbf{r})\rangle + |\phi(-\mathbf{r})\rangle}{2}}_{:=|\phi(\mathbf{r})\rangle_{\mathrm{g}}} + \underbrace{\frac{|\phi(\mathbf{r})\rangle - |\phi(-\mathbf{r})\rangle}{2}}_{:=|\phi(\mathbf{r})\rangle_{\mathrm{u}}} = |\phi(\mathbf{r})\rangle_{\mathrm{g}} + |\phi(\mathbf{r})\rangle_{\mathrm{u}} \quad , \tag{3.4.2}$$

where $|\phi(-\mathbf{r})\rangle_{\mathrm{g}} = +\,|\phi(\mathbf{r})\rangle_{\mathrm{g}}$ and $|\phi(-\mathbf{r})\rangle_{\mathrm{u}} = -\,|\phi(\mathbf{r})\rangle_{\mathrm{u}}$, cannot produce an expectation value $\langle\phi(\mathbf{r})|\hat{A}|\phi(\mathbf{r})\rangle$ that is invariant under spatial inversion. The presence of a *center of inversion* forbids the existence of a superconducting phase without *definite parity* and the mixing of even and odd pairing wave functions can only occur in systems without inversion symmetry [MS94]. As a reminder, that the definition of Bloch states with respect to their *gauge* and eventually their *pseudospin* discussed in (Section 3.2) is essential for the numerical evaluation of the upcoming analysis, we want to establish the connection between the "properly gauged" Bloch states and Anderson's recipe to build up pairing states using inversion and time-reversal symmetry [And84a]. To do this, we first summarize the effect of inversion and time-reversal on both pseudospin-states and helical-states (cf. (Section 3.3.2)). A properly defined pseudospin state $|\mathbf{k}\tilde{\sigma}\rangle$ and a helical state $|\mathbf{k}\lambda\rangle$ are affected by inversion $\hat{P}$ and time-reversal $\hat{\Theta}$ by (for their effect on helical

states we refer to (Equation 3.1.53))

$$|\mathbf{k}\tilde{\sigma}\rangle \xrightarrow{\hat{P}} e^{i\varphi^P_{\mathbf{k}}} |-\mathbf{k}\tilde{\sigma}\rangle \qquad |\mathbf{k}\tilde{\sigma}\rangle \xrightarrow{\hat{\Theta}} e^{i\varphi^T_{\mathbf{k}}} |-\mathbf{k}\bar{\tilde{\sigma}}\rangle \tag{3.4.3a}$$

$$|\mathbf{k}\lambda\rangle \xrightarrow{\hat{P}} e^{i\tau^P_{\mathbf{k}}} \left|-\mathbf{k}\bar{\lambda}\right\rangle \qquad |\mathbf{k}\tilde{\sigma}\rangle \xrightarrow{\hat{\Theta}} e^{i\tau^T_{\mathbf{k}}} |-\mathbf{k}\lambda\rangle \quad , \tag{3.4.3b}$$

where $\bar{\tilde{\sigma}}$ and $\bar{\lambda}$ denote the opposite state, respectively. The states $|-\mathbf{k}\tilde{\sigma}\rangle$, $|-\mathbf{k}\bar{\tilde{\sigma}}\rangle$ and $\left|-\mathbf{k}\bar{\lambda}\right\rangle$, $|-\mathbf{k}\lambda\rangle$ are the numerically determined Bloch states at the respective k-points. Hence, the inversion operation doesn't affect the pseudospin degree of freedom but inverts the helical spin. In contrast, time-reversal inverts the pseudospin and keeps the helical degree of freedom. Here, we assume the pseudospin degree of freedom to be properly defined but assume the Bloch states to have arbitrary phases (Section 3.2). Therefore, we have to take into account the phases $e^{i\varphi^{P,T}_{\mathbf{k}}}$ and $e^{i\tau^{P,T}_{\mathbf{k}}}$ for pseudospin and helicity, since the Bloch states at $\mathbf{k}$ and $-\mathbf{k}$ don't have a fixed phase relation. However, by applying inversion and time-reversal twice, we find, that $e^{i\varphi^{P,T}_{\mathbf{k}}}$ and $e^{i\tau^{P,T}_{\mathbf{k}}}$ must satisfy the following constraints:

$$\hat{P}^2 |\mathbf{k}\tilde{\sigma}\rangle = \hat{P} e^{i\varphi^P_{\mathbf{k}}} |-\mathbf{k}\tilde{\sigma}\rangle = e^{i\varphi^P_{\mathbf{k}}} e^{i\varphi^P_{-\mathbf{k}}} |\mathbf{k}\tilde{\sigma}\rangle \overset{!}{=} |\mathbf{k}\tilde{\sigma}\rangle \qquad \Rightarrow e^{i\varphi^P_{-\mathbf{k}}} = e^{-i\varphi^P_{\mathbf{k}}} \tag{3.4.4}$$

$$\hat{\Theta}^2 |\mathbf{k}\tilde{\sigma}\rangle = \hat{\Theta} e^{i\varphi^T_{\mathbf{k}}} |-\mathbf{k}\bar{\tilde{\sigma}}\rangle = e^{-i\varphi^T_{\mathbf{k}}} e^{i\varphi^{\bar{T}}_{-\mathbf{k}}} |\mathbf{k}\tilde{\sigma}\rangle \overset{!}{=} -|\mathbf{k}\tilde{\sigma}\rangle \qquad \Rightarrow e^{i\varphi^T_{-\mathbf{k}}} = -e^{i\varphi^{\bar{T}}_{\mathbf{k}}} \tag{3.4.5}$$

$$\hat{P}^2 |\mathbf{k}\lambda\rangle = \hat{P} e^{i\tau^P_{\mathbf{k}}} \left|-\mathbf{k}\bar{\lambda}\right\rangle = e^{i\tau^P_{\mathbf{k}}} e^{i\tau^{\bar{P}}_{-\mathbf{k}}} |\mathbf{k}\lambda\rangle \overset{!}{=} |\mathbf{k}\lambda\rangle \qquad \Rightarrow e^{i\tau^P_{-\mathbf{k}}} = e^{-i\tau^{\bar{P}}_{\mathbf{k}}} \tag{3.4.6}$$

$$\hat{\Theta}^2 |\mathbf{k}\lambda\rangle = \hat{\Theta} e^{i\tau^T_{\mathbf{k}}} |-\mathbf{k}\lambda\rangle = e^{-i\tau^T_{\mathbf{k}}} e^{i\tau^T_{-\mathbf{k}}} |\mathbf{k}\lambda\rangle \overset{!}{=} -|\mathbf{k}\lambda\rangle \qquad \Rightarrow e^{i\tau^T_{-\mathbf{k}}} = -e^{i\tau^T_{\mathbf{k}}} \quad , \tag{3.4.7}$$

since $\hat{P}^2 = 1$ and $\hat{\Theta}^2 = -1$. The entities $\bar{T}$ and $\bar{P}$ denote the phases $e^{i\varphi^{\bar{T}}_{\mathbf{k}}}$ and $e^{i\tau^{\bar{P}}_{\mathbf{k}}}$ associated to the opposite pseudo/helical-spin degrees of freedom. Apparently, the functions $e^{i\varphi^P_{\mathbf{k}}}$ and $e^{i\tau^P_{\mathbf{k}}}$ describing the phase difference between Bloch states related by the inversion operation, are transformed to their complex conjugate under $\mathbf{k} \to -\mathbf{k}$, while the corresponding functions $e^{i\varphi^T_{\mathbf{k}}}$ and $e^{i\tau^T_{\mathbf{k}}}$ for time-reversal must be odd in momentum $\mathbf{k}$. Apart from these constraints these functions may behave arbitrarily and discontinuous. However, for a *smooth gauge* of the Bloch states (cf. (Section 3.2)), they show an exceptionally simple behavior. For instance, in case of a smooth gauge, $e^{i\varphi^P_{\mathbf{k}}} = 1$ is constant and $e^{i\varphi^T_{\mathbf{k}}} = \pm 1$ in the first/second half of the Brillouin zone (cf. (Section 3.2) and (Figure 3.2)). Finally, we consider the Cooper pairs built from these inversion and time-reversal operation related partner states. In case of pseudospin states we can easily get rid of the relative phases by either adjusting the Bloch states or transforming the Cooper vertex appropriately. This will result in $e^{i\varphi^P_{\mathbf{k}}} = 1$ and $e^{i\varphi^T_{\mathbf{k}}} = 1 = -e^{i\varphi^{\bar{T}}_{\mathbf{k}}}$. Henceforth, a (singlet) Cooper pair in pseudospin basis comprised of time-reversal partner states is given by

$$\left\langle c^\dagger_{\mathbf{k}\tilde{\sigma}} \hat{\Theta} c^\dagger_{\mathbf{k}\tilde{\sigma}} \right\rangle = \left\langle c^\dagger_{\mathbf{k}\tilde{\sigma}} c^\dagger_{-\mathbf{k}\tilde{\bar{\sigma}}} \right\rangle \tag{3.4.8}$$

The pseudospin triplet state made up of inversion symmetry related states is expressed by (including the relative phase)

$$\left\langle c^\dagger_{\mathbf{k}\tilde{\sigma}} \hat{P} c^\dagger_{\mathbf{k}\tilde{\sigma}} \right\rangle = \left\langle c^\dagger_{\mathbf{k}\tilde{\sigma}} e^{i\varphi^P_{\mathbf{k}}} c^\dagger_{-\mathbf{k}\tilde{\sigma}} \right\rangle \tag{3.4.9}$$

Checking the parity of this pairing state, we find

$$\left\langle c^\dagger_{-\mathbf{k}\tilde{\sigma}} e^{i\varphi^P_{-\mathbf{k}}} c^\dagger_{\mathbf{k}\tilde{\sigma}} \right\rangle = -\left\langle c^\dagger_{\mathbf{k}\tilde{\sigma}} e^{-i\varphi^P_{\mathbf{k}}} c^\dagger_{-\mathbf{k}\tilde{\sigma}} \right\rangle = -e^{-i2\varphi^P_{\mathbf{k}}} \left\langle c^\dagger_{\mathbf{k}\tilde{\sigma}} e^{i\varphi^P_{\mathbf{k}}} c^\dagger_{-\mathbf{k}\tilde{\sigma}} \right\rangle \quad , \tag{3.4.10}$$

where the fermionic anticommutation of the operators and (Equation 3.4.4) were used. This shows, that for the odd parity of the pseudospin triplet state to be satisfied, we have to require a trivial phase relation of the inversion symmetry related states, i.e. $\varphi^P_{\mathbf{k}} = 0$. In contrast to pseudospin pairing states, the phase relation of time-reversal partners based on helical states must remain non-trivial because the time-reversal operation conserves helicity. This necessarily results in the even parity states discussed in (Section 3.4.2).

3.4.1. Degenerate Fermi surface and pseudospin

In this section firstly we handle the case of inversion symmetric spin-orbit coupling and a two-particle vertex satisfying both *time-reversal* and *inversion* symmetry. Therefore, all Fermi surfaces are doubly degenerated. However, since the SU(2)-symmetry may be broken - because of centrosymmetric spin-orbit coupling - we have to rely on a *pseudospin* degree of freedom accounting for the double degeneracy. Assuming that the normal-state Hamiltonian respects both inversion and time-reversal symmetry, we can construct its degenerate eigenstates by the following procedure: We start with an arbitrary eigenstate labeled by $\tilde{\sigma}$ at momentum $\mathbf{k}$, denoted by $|\mathbf{k}, \tilde{\sigma}\rangle$. By applying both inversion and time-reversal on that state, we obtain $\hat{\Theta}\hat{P}\,|\mathbf{k}, \tilde{\sigma}\rangle = \hat{P}\hat{\Theta}\,|\mathbf{k}, \tilde{\sigma}\rangle := |\mathbf{k}, \tilde{\sigma}'\rangle$, noting that parity and time- reversal commute and denoting the newly produced state by $|\mathbf{k}, \tilde{\sigma}'\rangle$. How is that state related to the original one? We know that both inversion and time-reversal transform the momentum to $\mathbf{k} \to -\mathbf{k}$, so that we end up at the original $\mathbf{k}$, but what is the new pseudospin degree of freedom? Due to the property $\hat{\Theta}^2 = -1$ for fermionic spin-$\frac{1}{2}$ particles, $|\mathbf{k}, \tilde{\sigma}'\rangle$ must be orthogonal to $|\mathbf{k}, \tilde{\sigma}\rangle$ [8]. Therefore, we have two

[8] Both unitary and antiunitary transformed states satisfy $|\langle\alpha|\beta\rangle| = |\langle\alpha'|\beta'\rangle|$, where in the unitary case we simply have $\langle\alpha'|\beta'\rangle = \langle\alpha U^\dagger U\beta\rangle = \langle\alpha|\beta\rangle$ [Wig32]. In contrast, time-reversal is an *antiunitary* operation that transforms expectation values according to $\langle\alpha|\beta\rangle \to \langle\alpha'|\beta'\rangle = \overline{\langle\alpha|\beta\rangle} = \langle\beta|\alpha\rangle$ [SN11, chap. 4.4, p. 269]. Therefore, we have $\langle\mathbf{k}, \tilde{\sigma}|\mathbf{k}, \tilde{\sigma}'\rangle = \left\langle\hat{\Theta}\hat{P}\,|\mathbf{k}, \tilde{\sigma}'\rangle\middle|\hat{\Theta}\hat{P}\,|\mathbf{k}, \tilde{\sigma}\rangle\right\rangle = \left\langle\hat{\Theta}\hat{P}\hat{\Theta}\hat{P}\,|\mathbf{k}, \tilde{\sigma}\rangle\middle|\hat{\Theta}\hat{P}\,|\mathbf{k}, \tilde{\sigma}\rangle\right\rangle = -\langle\mathbf{k}, \tilde{\sigma}|\mathbf{k}, \tilde{\sigma}'\rangle = 0$, using $\hat{P}^2 = 1$ and $\hat{\Theta}^2 = -1$.

component eigenstates at every $\mathbf{k}$-point and we are able to define $\mathbf{k}$-dependent Hermitian operators by [Yip14; Smi+17a]

$$\begin{aligned}\sigma_1(\mathbf{k}) &= |\mathbf{k},\tilde{\sigma}\rangle\langle\mathbf{k},\tilde{\sigma}'| + |\mathbf{k},\tilde{\sigma}'\rangle\langle\mathbf{k},\tilde{\sigma}| \\ \sigma_2(\mathbf{k}) &= -i|\mathbf{k},\tilde{\sigma}\rangle\langle\mathbf{k},\tilde{\sigma}'| + i|\mathbf{k},\tilde{\sigma}'\rangle\langle\mathbf{k},\tilde{\sigma}| \\ \sigma_3(\mathbf{k}) &= |\mathbf{k},\tilde{\sigma}\rangle\langle\mathbf{k},\tilde{\sigma}| - |\mathbf{k},\tilde{\sigma}'\rangle\langle\mathbf{k},\tilde{\sigma}'| \quad . \end{aligned} \tag{3.4.11}$$

Since this construction is done using a two component basis, $\sigma_1(\mathbf{k})$, $\sigma_2(\mathbf{k})$ and $\sigma_3(\mathbf{k})$ can simply be expressed as the Pauli matrices (not necessarily in this order!). This statement is based on the general fact that the form of the Pauli matrices is independent of the basis. However, for *one particular* basis $|\mathbf{k},\tilde{\sigma}\rangle$, $|\mathbf{k},\tilde{\sigma}'\rangle$ (or by applying another unitary transformation to the states in (Equation 3.4.11) that induces the change of basis), one can make $\sigma_1(\mathbf{k})$, $\sigma_2(\mathbf{k})$ and $\sigma_3(\mathbf{k})$ coincide with the usual "natural" spin Pauli matrices. This is the more intuitive and simplified statement of the more general derivation of transformation matrices in band basis for multiple bands of centrosymmetric spin-orbit coupling Hamiltonians, which are are simply comprised of Pauli matrices (cf. (Equation 3.3.39a) and (Equation 3.3.39b)). More precisely, the transformation matrices $\mathcal{B}(\mathbf{k})$ are 2×2-block-diagonal in band space and may therefore be expanded in terms of Pauli matrices. Analogously to (Equation 3.4.11), one can define the $\sigma_{1,2,3}$ matrices at $-\mathbf{k}$ by applying the parity and time-reversal operation to the states $|\mathbf{k},\tilde{\sigma}\rangle$, $|\mathbf{k},\tilde{\sigma}'\rangle$, i.e. $\hat{P}|\mathbf{k},\tilde{\sigma}^{(\prime)}\rangle = |-\mathbf{k},\tilde{\sigma}^{(\prime)}\rangle$, $\hat{\Theta}|\mathbf{k},\tilde{\sigma}\rangle = \hat{P}|\mathbf{k},\tilde{\sigma}'\rangle$ and $\hat{\Theta}|\mathbf{k},\tilde{\sigma}'\rangle = -\hat{P}|\mathbf{k},\tilde{\sigma}\rangle$. This shows that the matrices $\sigma_{1,2,3}(\mathbf{k})$ are even under inversion and odd under time-reversal in full correspondence with the "natural" Pauli matrices $\sigma_{x,y,z}$ [Yip14]. The Cooper channel of the two-particle vertex in band-pseudospin basis discussed in (Section 3.3.2) is given by the coupling constants

$$U^{bb'\tilde{\sigma}_1\tilde{\sigma}_2\tilde{\sigma}'_1\tilde{\sigma}'_2}_{\mathbf{k}\mathbf{k}'}\bar{\phi}_{\mathbf{k}'b'\tilde{\sigma}'_1}\bar{\phi}_{-\mathbf{k}'b'\tilde{\sigma}'_2}\phi_{-\mathbf{k}b\tilde{\sigma}_2}\phi_{\mathbf{k}b\tilde{\sigma}_1} := U^{b\tilde{\sigma}_1,b\tilde{\sigma}_2,b'\tilde{\sigma}'_1,b'\tilde{\sigma}'_2}_{\mathbf{k},-\mathbf{k},\mathbf{k}',-\mathbf{k}'}\bar{\phi}_{\mathbf{k}'b'\tilde{\sigma}'_1}\bar{\phi}_{-\mathbf{k}'b'\tilde{\sigma}'_2}\phi_{-\mathbf{k}b\tilde{\sigma}_2}\phi_{\mathbf{k}b\tilde{\sigma}_1} \quad . \tag{3.4.12}$$

where we took into account that - in the *weak-coupling* regime - a Cooper pair must be hosted by a single band. *Inversion symmetry* requires the two-particle vertex (Equation 3.4.12) to satisfy (cf. (Equation 3.3.48))

$$\begin{aligned} U^{bb'\tilde{\sigma}_1\tilde{\sigma}_2\tilde{\sigma}'_1\tilde{\sigma}'_2}_{\mathbf{k}\mathbf{k}'}\bar{\phi}_{\mathbf{k}'b'\tilde{\sigma}'_1}\bar{\phi}_{-\mathbf{k}'b'\tilde{\sigma}'_2}\phi_{-\mathbf{k}b\tilde{\sigma}_2}\phi_{\mathbf{k}b\tilde{\sigma}_1} &\xrightarrow{\hat{P}} U^{bb'\tilde{\sigma}_1\tilde{\sigma}_2\tilde{\sigma}'_1\tilde{\sigma}'_2}_{\mathbf{k}\mathbf{k}'}\bar{\phi}_{-\mathbf{k}'b'\tilde{\sigma}'_1}\bar{\phi}_{\mathbf{k}'b'\tilde{\sigma}'_2}\phi_{\mathbf{k}b\tilde{\sigma}_2}\phi_{-\mathbf{k}b\tilde{\sigma}_1} \\ \overset{\phi_\alpha\phi_\beta=-\phi_\beta\phi_\alpha}{\downarrow =} U^{bb'\tilde{\sigma}_1\tilde{\sigma}_2\tilde{\sigma}'_1\tilde{\sigma}'_2}_{\mathbf{k}\mathbf{k}'}\bar{\phi}_{\mathbf{k}'b'\tilde{\sigma}'_2}\bar{\phi}_{-\mathbf{k}'b'\tilde{\sigma}'_1}\phi_{-\mathbf{k}b\tilde{\sigma}_1}\phi_{\mathbf{k}b\tilde{\sigma}_2} &\overset{!}{=} U^{bb'\tilde{\sigma}_1\tilde{\sigma}_2\tilde{\sigma}'_1\tilde{\sigma}'_2}_{\mathbf{k}\mathbf{k}'}\bar{\phi}_{\mathbf{k}'b'\tilde{\sigma}'_1}\bar{\phi}_{-\mathbf{k}'b'\tilde{\sigma}'_2}\phi_{-\mathbf{k}b\tilde{\sigma}_2}\phi_{\mathbf{k}b\tilde{\sigma}_1} \quad , \end{aligned} \tag{3.4.13}$$

where the summation is implicit. Note, that the original momentum structure was restored by anticommuting twice, while the pseudospin structure changed. Assuming Hermiticity of the vertex on top of inversion symmetry and comparing the pseudospin

sectors in (Equation 3.3.6) with the corresponding ones in (Equation 3.4.13), we find that both $B_{b\mathbf{k}b-\mathbf{k}b'\mathbf{k}'b'-\mathbf{k}'} = -B_{b\mathbf{k}b-\mathbf{k}b'\mathbf{k}'b'-\mathbf{k}'} = 0$ and $E_{b\mathbf{k}b-\mathbf{k}b'\mathbf{k}'b'-\mathbf{k}'} = -E_{b\mathbf{k}b-\mathbf{k}b'\mathbf{k}'b'-\mathbf{k}'} = 0$ must be zero. Henceforth, in the pseudospin Cooper channel, there are only eight non-zero pseudospin sectors including the four independent elements A, C, D and F (cf. (Equation 3.3.6)). Note, that this is a consequence of the *weak-coupling* condition, which assumes that a Cooper pair is hosted by a single band. These prerequisites considerably simplify the *mean-field theory* derived in (Section 2.4). The *gap function* (Equation 2.4.8) for the interaction (Equation 3.4.12) yields

$$\Delta_{\mathbf{k}b\tilde{\sigma}_1\tilde{\sigma}_2} = -2\sum_{\substack{\mathbf{k}',b'\\ \tilde{\sigma}_1',\tilde{\sigma}_2'}} U^{bb'\tilde{\sigma}_1\tilde{\sigma}_2\tilde{\sigma}_1'\tilde{\sigma}_2'}_{\mathbf{k}\mathbf{k}'} f_{\mathbf{k}'b'\tilde{\sigma}_2'\tilde{\sigma}_1'} = i\left(d_{\mathbf{k}b}\cdot\boldsymbol{\sigma}\right)\sigma_y = \begin{pmatrix} -d^x_{\mathbf{k}b} + id^y_{\mathbf{k}b} & d^0_{\mathbf{k}b} + d^z_{\mathbf{k}b} \\ -d^0_{\mathbf{k}b} + d^z_{\mathbf{k}b} & d^x_{\mathbf{k}b} + id^y_{\mathbf{k}b} \end{pmatrix} \quad , \tag{3.4.14}$$

where we used the parametrization in terms of the d-vector (Equation 2.4.25). Solving for the four components of the d-vector and performing the summation over pseudospins $\tilde{\sigma}_1'$, $\tilde{\sigma}_2'$, where we get two contributions in every component since A, C, D and F are the only non-zero vertex elements, we find the gap equations:

$$d^0_{\mathbf{k}b} = -\sum_{\mathbf{k}',b'}\left[\left(U^{bb'\tilde{\uparrow}\tilde{\downarrow}\tilde{\uparrow}\tilde{\downarrow}}_{\mathbf{k}\mathbf{k}'} - U^{bb'\tilde{\downarrow}\tilde{\uparrow}\tilde{\uparrow}\tilde{\downarrow}}_{\mathbf{k}\mathbf{k}'}\right) f_{\mathbf{k}'b'\tilde{\downarrow}\tilde{\uparrow}} + \left(U^{bb'\tilde{\uparrow}\tilde{\downarrow}\tilde{\downarrow}\tilde{\uparrow}}_{\mathbf{k}\mathbf{k}'} - U^{bb'\tilde{\downarrow}\tilde{\uparrow}\tilde{\downarrow}\tilde{\uparrow}}_{\mathbf{k}\mathbf{k}'}\right) f_{\mathbf{k}'b'\tilde{\uparrow}\tilde{\downarrow}}\right] \tag{3.4.15}$$

$$d^x_{\mathbf{k}b} = -\sum_{\mathbf{k}',b'}\left[\left(U^{bb'\tilde{\downarrow}\tilde{\downarrow}\tilde{\uparrow}\tilde{\uparrow}}_{\mathbf{k}\mathbf{k}'} - U^{bb'\tilde{\uparrow}\tilde{\uparrow}\tilde{\uparrow}\tilde{\uparrow}}_{\mathbf{k}\mathbf{k}'}\right) f_{\mathbf{k}'b'\tilde{\uparrow}\tilde{\uparrow}} + \left(U^{bb'\tilde{\downarrow}\tilde{\downarrow}\tilde{\downarrow}\tilde{\downarrow}}_{\mathbf{k}\mathbf{k}'} - U^{bb'\tilde{\uparrow}\tilde{\uparrow}\tilde{\downarrow}\tilde{\downarrow}}_{\mathbf{k}\mathbf{k}'}\right) f_{\mathbf{k}'b'\tilde{\downarrow}\tilde{\downarrow}}\right] \tag{3.4.16}$$

$$d^y_{\mathbf{k}b} = i\sum_{\mathbf{k}',b'}\left[\left(U^{bb'\tilde{\downarrow}\tilde{\downarrow}\tilde{\uparrow}\tilde{\uparrow}}_{\mathbf{k}\mathbf{k}'} + U^{bb'\tilde{\uparrow}\tilde{\uparrow}\tilde{\uparrow}\tilde{\uparrow}}_{\mathbf{k}\mathbf{k}'}\right) f_{\mathbf{k}'b'\tilde{\uparrow}\tilde{\uparrow}} + \left(U^{bb'\tilde{\downarrow}\tilde{\downarrow}\tilde{\downarrow}\tilde{\downarrow}}_{\mathbf{k}\mathbf{k}'} + U^{bb'\tilde{\uparrow}\tilde{\uparrow}\tilde{\downarrow}\tilde{\downarrow}}_{\mathbf{k}\mathbf{k}'}\right) f_{\mathbf{k}'b'\tilde{\downarrow}\tilde{\downarrow}}\right] \tag{3.4.17}$$

$$d^z_{\mathbf{k}b} = -\sum_{\mathbf{k}',b'}\left[\left(U^{bb'\tilde{\uparrow}\tilde{\downarrow}\tilde{\uparrow}\tilde{\downarrow}}_{\mathbf{k}\mathbf{k}'} + U^{bb'\tilde{\downarrow}\tilde{\uparrow}\tilde{\uparrow}\tilde{\downarrow}}_{\mathbf{k}\mathbf{k}'}\right) f_{\mathbf{k}'b'\tilde{\downarrow}\tilde{\uparrow}} + \left(U^{bb'\tilde{\uparrow}\tilde{\downarrow}\tilde{\downarrow}\tilde{\uparrow}}_{\mathbf{k}\mathbf{k}'} + U^{bb'\tilde{\downarrow}\tilde{\uparrow}\tilde{\downarrow}\tilde{\uparrow}}_{\mathbf{k}\mathbf{k}'}\right) f_{\mathbf{k}'b'\tilde{\uparrow}\tilde{\downarrow}}\right] \quad . \tag{3.4.18}$$

These four coupled gap equations for singlet $d^0_{\mathbf{k}b} = d^0_{-\mathbf{k}b}$ and triplet components $d^{x,y,z}_{\mathbf{k}b} = -d^{x,y,z}_{-\mathbf{k}b}$ have to be solved self-consistently according to (Figure 2.6). In the SU(2)-symmetric case the vertex elements $U^{bb'\tilde{\uparrow}\tilde{\uparrow}\tilde{\downarrow}\tilde{\downarrow}}$ and $U^{bb'\tilde{\downarrow}\tilde{\downarrow}\tilde{\uparrow}\tilde{\uparrow}}$ must be zero (cf. (Equation 3.3.19)) and all three d-vector components are degenerate. Therefore, the pseudospin sectors $U^{bb'\tilde{\sigma}\tilde{\sigma}\bar{\tilde{\sigma}}\bar{\tilde{\sigma}}}$ (where $\bar{\tilde{\sigma}}$ denotes the opposite pseudospin state to $\tilde{\sigma}$) are essential to lift the d-vector's degeneracy and find its preferred direction. $f_{\mathbf{k}b\tilde{\sigma}\tilde{\sigma}'}$ is defined by the thermal expectation value $\langle c_{-\mathbf{k}b\tilde{\sigma}} c_{\mathbf{k}b\tilde{\sigma}'}\rangle$ (Equation 2.4.15). For a unitary gap we can express the operators $c_{-\mathbf{k}b\tilde{\sigma}}$ and $c_{\mathbf{k}b\tilde{\sigma}'}$ in terms of the new quasiparticle states $d_{-\mathbf{k}b\tilde{\sigma}}$ and $d_{\mathbf{k}b\tilde{\sigma}'}$ by $\mathbf{C}_{\mathbf{k}b} = U^\dagger_{\mathbf{k}b}\mathbf{D}_{\mathbf{k}b}$ (see (Equation 2.4.20)). For instance, the hole states $c_{\pm\mathbf{k}b\tilde{\sigma}}$ are given by

$$\begin{aligned} c_{-\mathbf{k}b\tilde{\sigma}} &= (E_{\mathbf{k}b} - \xi_{\mathbf{k}b})\, d^\dagger_{\mathbf{k}b\tilde{\sigma}} - \Delta_{\mathbf{k}b\tilde{\sigma}\tilde{\uparrow}} d_{-\mathbf{k}b\tilde{\uparrow}} - \Delta_{\mathbf{k}b\tilde{\sigma}\tilde{\downarrow}} d_{-\mathbf{k}b\tilde{\downarrow}} \\ c_{\mathbf{k}b\tilde{\sigma}} &= \Delta_{\mathbf{k}b\tilde{\sigma}\tilde{\uparrow}} d_{\mathbf{k}b\tilde{\uparrow}} + \Delta_{\mathbf{k}b\tilde{\sigma}\tilde{\downarrow}} d_{\mathbf{k}b\tilde{\downarrow}} + (E_{\mathbf{k}b} - \xi_{\mathbf{k}b})\, d^\dagger_{-\mathbf{k}b\tilde{\sigma}} \quad . \end{aligned} \tag{3.4.19}$$

We insert these operators into the expectation values $\langle c_{-\mathbf{k}b\tilde{\sigma}} c_{\mathbf{k}b\tilde{\sigma}'} \rangle$ and evaluate them with respect to the eigenstates of the Bogoliubov-de Gennes Hamiltonian. Hence, all anomalous expectation values $\left\langle d^{(\dagger)}_\alpha d^{(\dagger)}_{\alpha'} \right\rangle$ must be zero. The only terms that contribute to the expectation values are the number operators $\left\langle d^\dagger_\alpha d_{\alpha'} \right\rangle = \left\langle 1 - d_{\alpha'} d^\dagger_\alpha \right\rangle \propto \delta_{\alpha\alpha'}$ (anticommutation relations of fermion operators $c^\dagger_\alpha$, c_α are preserved by the unitary transformation). The results for all pseudospin combinations can be summarized by

$$\begin{aligned} \langle c_{-\mathbf{k}b\tilde{\sigma}} c_{\mathbf{k}b\tilde{\sigma}'} \rangle &= \frac{1}{2E_{\mathbf{k}b}\,(E_{\mathbf{k}b} - \xi_{\mathbf{k}b})} \left\langle (E_{\mathbf{k}b} - \xi_{\mathbf{k}b}) \left(\Delta_{\mathbf{k}b\tilde{\sigma}\tilde{\sigma}'} d^\dagger_{\mathbf{k}b\tilde{\sigma}} d_{\mathbf{k}b\tilde{\sigma}} - \Delta_{\mathbf{k}b\tilde{\sigma}'\tilde{\sigma}} d^\dagger_{-\mathbf{k}b\tilde{\sigma}'} d_{-\mathbf{k}b\tilde{\sigma}'} \right) \right\rangle \\ &= \frac{\Delta_{\mathbf{k}b\tilde{\sigma}'\tilde{\sigma}}}{2E_{\mathbf{k}b}} \left(n(E_{\mathbf{k}b\tilde{\sigma}}) - (1 - n(E_{\mathbf{k}b\tilde{\sigma}'})) \right) = \frac{\Delta_{\mathbf{k}b\tilde{\sigma}'\tilde{\sigma}}}{2E_{\mathbf{k}b}} \left(2n(E_{\mathbf{k}b}) - 1 \right) \quad , \end{aligned} \tag{3.4.20}$$

where the quasiparticles energies of the *Bogoliubov-de Gennes* Hamiltonian (Equation 2.4.14) for a unitary gap are given by $E_{\mathbf{k}b} = \pm\frac{1}{2}\sqrt{\xi^2_{\mathbf{k}b} + \frac{1}{2}\operatorname{Tr}\left(\Delta_{\mathbf{k}b}\Delta^\dagger_{\mathbf{k}b}\right)}$ (cf. (Equation 2.4.19)) and $n(E_{\mathbf{k}b}) = \left(1 + e^{\beta E_{\mathbf{k}b}}\right)^{-1}$ denotes the *Fermi-Dirac distribution*. Employing this result and $2n(E_{\mathbf{k}b}) - 1 = \tanh\left(\beta E_{\mathbf{k}b}/2\right)$ in (Equation 3.4.14), the *spinful unitary gap equation* yields (cf. [SU91; SAM05])

$$\Delta_{\mathbf{k}b\tilde{\sigma}_1\tilde{\sigma}_2} = -\sum_{\substack{\mathbf{k}',b' \\ \tilde{\sigma}'_1,\tilde{\sigma}'_2}} U^{bb'\tilde{\sigma}_1\tilde{\sigma}_2\tilde{\sigma}'_1\tilde{\sigma}'_2}_{\mathbf{k}\mathbf{k}'} \Delta_{\mathbf{k}'b'\tilde{\sigma}'_2\tilde{\sigma}'_1} \frac{\tanh\left(\frac{\beta E_{\mathbf{k}'b'}}{2}\right)}{E_{\mathbf{k}'b'}} \quad , \tag{3.4.21}$$

which determines the momentum and pseudospin structure of the unitary gap $\Delta_{\mathbf{k}b\tilde{\sigma}_1\tilde{\sigma}_2}$ from the *effective Cooper interaction* $U^{bb'\tilde{\sigma}_1\tilde{\sigma}_2\tilde{\sigma}'_1\tilde{\sigma}'_2}_{\mathbf{k}\mathbf{k}'}$. Although the numerically exact gap magnitude $|\Delta_{\mathbf{k}b}|$, the critical temperature $\beta_c^{-1} = k_B T_c$ and its momentum/band/pseudospin dependency can only be calculated self-consistently and iteratively from (Equation 3.4.21), it is helpful to calculate the eigenmodes of the effective interaction. The eigenvectors of $U^{bb'\tilde{\sigma}_1\tilde{\sigma}_2\tilde{\sigma}'_1\tilde{\sigma}'_2}_{\mathbf{k}\mathbf{k}'}$ provide a good starting point for the self-consistency iteration and already exhibit the symmetries of the exact solution. [9]. Since the effective interaction must be Hermitian $U^{bb'\tilde{\sigma}_1\tilde{\sigma}_2\tilde{\sigma}'_1\tilde{\sigma}'_2}_{\mathbf{k}\mathbf{k}'} = \overline{U^{b'b\tilde{\sigma}'_1\tilde{\sigma}'_2\tilde{\sigma}_1\tilde{\sigma}_2}_{\mathbf{k}'\mathbf{k}}}$ (Equation 3.3.5), we can choose a parametrization for the pseudospin indices, i.e. a mapping of both indices to a single one by writing the four possible pseudospin states as a four-vector, e.g. by means of the

[9] In the (unphysical) limit of zero gap magnitude $|\Delta| \to 0$ resulting in $\lim_{|\Delta|\to 0} E_{\mathbf{k}'b'} = \frac{\xi_{\mathbf{k}'b'}}{2}$ and infinite temperature with the consequence $\lim_{\beta\to 0} \tanh\left(\frac{\beta E_{\mathbf{k}'b'}}{2}\right) = \frac{\beta E_{\mathbf{k}'b'}}{2}$ the gap equation (Equation 3.4.21)

d-vector, represent it as a Hermitian matrix $U^{bb'\tilde{\sigma}_1\tilde{\sigma}_2\tilde{\sigma}'_1\tilde{\sigma}'_2}_{\mathbf{k}\mathbf{k}'} \in \mathbb{C}^{N_U \times N_U}$ ($N_U = 4n_b n_k$, with n_b, n_k being the number of bands and momenta), and determine its *spectral decomposition/eigen decomposition* [GG95; Mey00; Ste98]

$$U^{bb'\tilde{\sigma}_1\tilde{\sigma}_2\tilde{\sigma}'_1\tilde{\sigma}'_2}_{\mathbf{k}\mathbf{k}'} = \sum_n^{N_U} \xi_n f^n_{\mathbf{k}b\tilde{\sigma}_1\tilde{\sigma}_2} \left(f^n_{\mathbf{k}'b'\tilde{\sigma}'_1\tilde{\sigma}'_2}\right)^\dagger := U^{bb'\mu\nu}_{\mathbf{k}\mathbf{k}'} \quad . \tag{3.4.23}$$

with the eigenvalues ξ_n and eigenvectors $f^n_{\mathbf{k}b\tilde{\sigma}\tilde{\sigma}'}$ that are subject to the condition $f^n_{-\mathbf{k}b\tilde{\sigma}'\tilde{\sigma}} = -f^n_{\mathbf{k}b\tilde{\sigma}\tilde{\sigma}'}$ due to the antisymmetry of $U^{bb'\tilde{\sigma}_1\tilde{\sigma}_2\tilde{\sigma}'_1\tilde{\sigma}'_2}_{\mathbf{k}\mathbf{k}'}$ under particle exchange. The last equality defines the Cooper channel interaction as a matrix $U^{bb'\mu\nu}_{\mathbf{k}\mathbf{k}'}$ in terms of the pseudospin parametrization given by the indices $\mu, \nu \in \{0, 1, 2, 3\}$. The most transparent and convenient parametrization of the two-particle pseudospin states in the Cooper channel is defined by the bilinear in the fields [10]

$$P^\mu_{\mathbf{k}b} := \left(i\sigma_\mu\sigma_y\right)_{\tilde{\sigma}\tilde{\sigma}'} \phi_{-\mathbf{k}b\tilde{\sigma}}\phi_{\mathbf{k}b\tilde{\sigma}'} \quad , \tag{3.4.25}$$

with the Pauli matrices σ_y and $\sigma_\mu \in \{\sigma_0, \sigma_x, \sigma_y, \sigma_z\}$. The summation over pseudospin indices is implicit on the right hand side. In analogy to the d-vector (Section 2.4.3), this parametrization has the spatial symmetries $P^0_{-\mathbf{k}b} = P^0_{\mathbf{k}b}$ and $P^\mu_{-\mathbf{k}b} = -P^\mu_{\mathbf{k}b}\ \forall \mu \in \{1, 2, 3\}$. Using the parametrization (Equation 3.4.25) and including the basis in terms of fields in (Equation 3.4.23), we find

$$U^{bb'\tilde{\sigma}_1\tilde{\sigma}_2\tilde{\sigma}'_1\tilde{\sigma}'_2}_{\mathbf{k}\mathbf{k}'} \bar{\phi}_{\mathbf{k}'b'\tilde{\sigma}'_1}\bar{\phi}_{-\mathbf{k}'b'\tilde{\sigma}'_2}\phi_{-\mathbf{k}b\tilde{\sigma}_2}\phi_{\mathbf{k}b\tilde{\sigma}_1} = U^{bb'\mu\nu}_{\mathbf{k}\mathbf{k}'}\overline{P^\mu_{\mathbf{k}'b'}}P^\nu_{\mathbf{k}b} \quad . \tag{3.4.26}$$

The spatial inversion symmetry of the two-particle vertex (Equation 3.4.13) requires

becomes

$$\Delta_{\mathbf{k}b\tilde{\sigma}_1\tilde{\sigma}_2} = -\frac{\beta}{2}\sum_{\substack{\mathbf{k}',b'\\ \tilde{\sigma}'_1,\tilde{\sigma}'_2}} U^{bb'\tilde{\sigma}_1\tilde{\sigma}_2\tilde{\sigma}'_1\tilde{\sigma}'_2}_{\mathbf{k}\mathbf{k}'}\Delta_{\mathbf{k}'b'\tilde{\sigma}'_2\tilde{\sigma}'_1} = -\frac{\beta}{2}\sum_{\substack{\mathbf{k}',b'\\ \tilde{\sigma}'_1,\tilde{\sigma}'_2}}\sum_{n=0}\xi_n f_n^{\tilde{\sigma}_1\tilde{\sigma}_2}(\mathbf{k}, b)\left(f_n^{\tilde{\sigma}'_1\tilde{\sigma}'_2}(\mathbf{k}', b')\right)^\dagger \Delta_{\mathbf{k}'b'\tilde{\sigma}'_2\tilde{\sigma}'_1} \quad . \tag{3.4.22}$$

Assuming that the gap $\Delta_{\mathbf{k}b\tilde{\sigma}_1\tilde{\sigma}_2}$ is proportional to one particular eigenvector $f_0^{\tilde{\sigma}_1\tilde{\sigma}_2}(\mathbf{k}, b)$ with eigenvalue ξ_0, i.e. $\Delta_{\mathbf{k}b\tilde{\sigma}_1\tilde{\sigma}_2} = g\, f_0^{\tilde{\sigma}_1\tilde{\sigma}_2}(\mathbf{k}, b)$ with $g \in \mathbb{R}$ and taking into account that the eigenvectors are orthonormal, i.e. $f_i^\dagger f_j = \delta_{ij}$, we find $1 = -\frac{\beta}{2}\xi_0 \Rightarrow \beta^{-1} = k_B T_c = -2\xi_0$, i.e. the most negative eigenvalue determines the transition temperature.

[10] An alternative parametrization that corresponds to the product pseudospin basis, in contrast to the total angular momentum basis, is given by

$$P^\mu_{\mathbf{k}b} := \left(\frac{\sigma_\mu + (-1)^\mu\sigma_\mu\sigma_z}{2\, e^{i\frac{\pi}{2}g(\mu)}}\right)_{\tilde{\sigma}\tilde{\sigma}'} \phi_{-\mathbf{k}b\tilde{\sigma}}\phi_{\mathbf{k}b\tilde{\sigma}'} \quad \text{with} \quad g(\mu) = -\frac{\mu^3}{6} + \mu^2 - \frac{5\mu}{6} \quad , \tag{3.4.24}$$

that does, however, not exhibit, the symmetry/antisymmetry w.r.t. to spatial inversion in the zeroth and first to third components, unlike the d-vector like parametrization.

every element in the newly parametrized vertex $U^{bb'\mu\nu}_{\mathbf{k}\mathbf{k}'}$, that mixes $\mu = 0$ with $\nu \in \{1,2,3\}$ to vanish, since the right hand side of (Equation 3.4.26) can only be invariant with respect to spatial inversion, if both of the two bilinears are either even or odd under $\mathbf{k} \to -\mathbf{k}$ (cf. appendix F). Taking the spectral decomposition of the vertex matrix $U^{bb'\mu\nu}_{\mathbf{k}\mathbf{k}'}$ (Equation 3.4.23) into account, we can represent the Cooper vertex by

$$\begin{aligned} U^{bb'\tilde{\sigma}_1\tilde{\sigma}_2\tilde{\sigma}'_1\tilde{\sigma}'_2}_{\mathbf{k}\mathbf{k}'} \bar{\phi}_{\mathbf{k}'b'\tilde{\sigma}'_1} \bar{\phi}_{-\mathbf{k}'b'\tilde{\sigma}'_2} \phi_{-\mathbf{k}b\tilde{\sigma}_2} \phi_{\mathbf{k}b\tilde{\sigma}_1} &= \sum_n^{N_U} \xi_n f^n_{\mathbf{k}b\mu} \left(f^n_{\mathbf{k}'b'\nu}\right)^\dagger \overline{P^\mu_{\mathbf{k}'b'}} P^\nu_{\mathbf{k}b} \\ &= \sum_\Gamma \sum_{m=1}^{d_\Gamma} \sum_{n=1} f^{\Gamma mn}_{\mathbf{k}b\mu} \left(f^{\Gamma mn}_{\mathbf{k}'b'\nu}\right)^\dagger \overline{P^\mu_{\mathbf{k}'b'}} P^\nu_{\mathbf{k}b} \quad , \end{aligned} \tag{3.4.27}$$

where the eigenmodes $f^n_{\mathbf{k}b\mu}$ must be *irreducible representations* of the underlying point group (Section 3.3.1). Here, Γ denotes an irreducible representation of the point group $\mathcal{G}$ and d_Γ is the dimension of the representation Γ. This representation of the Cooper vertex closely resembles the decomposition of the two-particle interaction in the continuum in terms of spherical harmonics (Equation 2.1.7).

3.4.2. Non-degenerate bands and helicity

If inversion symmetry is broken, the eigenstates $|\mathbf{k}, b, \lambda\rangle$ of the single-particle Hamiltonian are characterized by momentum $\mathbf{k}$, band index b and helicity λ. The spatial inversion operation $|\mathbf{k}, b, \lambda\rangle \to \hat{P}\,|\mathbf{k}, b, \lambda\rangle$ does not yield a degenerate state anymore like in (Section 3.4.1), but a state with opposite helicity $\bar{\lambda}$ (cf. (Equation 3.1.53))

$$|\mathbf{k}, b, \lambda\rangle \to \hat{P}\,|\mathbf{k}, b, \lambda\rangle = |-\mathbf{k}, b, \lambda\rangle = e^{i\phi_{\mathbf{k}b}} \left|\mathbf{k}, b, \bar{\lambda}\right\rangle \quad , \tag{3.4.28}$$

the eigenenergies of which differ by $\left|\varepsilon_{\mathbf{k}b\lambda} - \varepsilon_{\mathbf{k}b\bar{\lambda}}\right| > 0$. Here, we restrict our analysis to *equal energy pairing* (weak-coupling limit), which is to assume that the splitting due to non-centrosymmetric spin-orbit coupling, e.g. the Rashba term $\propto \lambda_R$ is much larger than any critical temperature scale $k_B T_c$, i.e. $\lambda_R \gg k_B T_c$. Hence, we can apparently not rely on inversion to produce a degenerate state. However, we can enforce equal energy pairing by simply taking two states at opposite momenta $\mathbf{k}$ and $-\mathbf{k}$ with the same helicity λ, i.e. we pair up $|\mathbf{k}, b, \lambda\rangle$ and $|-\mathbf{k}, b, \lambda\rangle$. In (Section 3.1.2), we encountered that these two states are related by *time-reversal* up to a k-dependent phase. The recipe to pair up states that are related by time-reversal was first noted in the context of "dirty" superconductors [And59; And84c]. In order to produce the equal energy pairing states, which make up a Cooper pair, we have to use an operation that reflects a symmetry of the Hamiltonian. Before we investigate its consequences on the symmetries of the resulting pairing states, we have a look at what the corresponding structure in the helicity degree of freedom is. Since we restrict our analysis to equal energy pairing in the weak-coupling limit, we are limited to Cooper pairs with the same helicity. Therefore, we only have to

care about four helical spin sectors (out of sixteen) in the *effective two-particle vertex*, that are given by

$$U^{b\lambda b'\lambda'}_{\mathbf{k}\mathbf{k}'} := U^{b\lambda b,\lambda,b'\lambda',b'\lambda'}_{\mathbf{k},-\mathbf{k},\mathbf{k}',-\mathbf{k}'} \quad \text{with} \quad \lambda,\lambda' \in \{+,-\} \quad , \tag{3.4.29}$$

satisfying Hermiticity $\overline{U^{b\lambda b'\lambda'}_{\mathbf{k}\mathbf{k}'}} = U^{b'\lambda' b\lambda}_{\mathbf{k}'\mathbf{k}}$, like expected. The corresponding gap equation (Equation 2.4.8) in the helical degrees of freedom is greatly simplified by the weak-coupling restriction and is given by

$$\Delta_{\mathbf{k}b\lambda} = -2 \sum_{\mathbf{k}',b',\lambda'} U^{b\lambda b'\lambda'}_{\mathbf{k}\mathbf{k}'} f_{\mathbf{k}'b'\lambda'} = -2 \sum_{\mathbf{k}',b',\lambda'} U^{b\lambda b'\lambda'}_{\mathbf{k}\mathbf{k}'} \left\langle c_{-\mathbf{k}'b'\lambda'} c_{\mathbf{k}'b'\lambda'} \right\rangle \quad , \tag{3.4.30}$$

which reflects that there are only two helical spin components of the gap, opposed to the gap matrix, or d-vector, in pseudospin space. Independent of the symmetries and specific basis of the two-particle vertex, we can analysis the object $\langle c_{-\mathbf{k}b\lambda} c_{\mathbf{k}b\lambda} \rangle$. Since we require the helical states $c_{-\mathbf{k}b\lambda}$ and $c_{\mathbf{k}b\lambda}$ to be time-reversal partners, they must be related by $\hat{\Xi} c_{\mathbf{k}b\lambda} = e^{i\phi_{\mathbf{k}b\lambda}} c_{-\mathbf{k}b\lambda}$, where $\hat{\Xi} = U_{-\mathbf{k}} \hat{\Theta} \left(U_{\mathbf{k}}\right)^{-1}$ is the time-reversal operator for helical states (cf. (Section 3.3.2)) with $\hat{\Theta} = -i\sigma_y \mathcal{K}$. The matrix of eigenstates $U_{\mathbf{k}}$ of the single-particle Hamiltonian transforms between spin and helical basis. Employing the time-reversal operation twice, we find

$$\hat{\Xi}^2 c_{\mathbf{k}b\lambda} = \hat{\Xi} e^{i\phi_{\mathbf{k}b\lambda}} c_{-\mathbf{k}b\lambda} = e^{-i\phi_{\mathbf{k}b\lambda}} e^{i\phi_{-\mathbf{k}b\lambda}} c_{\mathbf{k}b\lambda} \stackrel{!}{=} -c_{\mathbf{k}b\lambda} \quad , \tag{3.4.31}$$

since the fermionic property dictates $\hat{\Xi}^2 = -1$. This shows that the additional phase $e^{i\phi_{\mathbf{k}b\lambda}}$ arising from time-reversal must be odd in momentum $e^{i\phi_{\mathbf{k}b\lambda}} = -e^{i\phi_{-\mathbf{k}b\lambda}}$, which may also understood as a result of the *double group* properties of the fermionic state involved. In the context of non-centrosymmetric spin-orbit coupling (Section 3.1.2), we analytically worked out the phase arising between time-reversal partners and showed that this phase is (at least, for a single-band model) odd in momentum (Equation 3.1.47). Taking these results into account, the pairing state between time-reversal partners

$$\tilde{\Delta}_{\mathbf{k}b\lambda} := e^{i\phi_{\mathbf{k}b\lambda}} \left\langle c_{-\mathbf{k}b\lambda} c_{\mathbf{k}b\lambda} \right\rangle \quad , \tag{3.4.32}$$

must be even in momentum

$$\Rightarrow \quad \tilde{\Delta}_{-\mathbf{k}b\lambda} = e^{i\phi_{-\mathbf{k}b\lambda}} \left\langle c_{\mathbf{k}b\lambda} c_{-\mathbf{k}b\lambda} \right\rangle = \left(-e^{i\phi_{\mathbf{k}b\lambda}}\right) \left(-\left\langle c_{-\mathbf{k}b\lambda} c_{\mathbf{k}b\lambda} \right\rangle\right) = \tilde{\Delta}_{\mathbf{k}b\lambda} \quad , \tag{3.4.33}$$

as a result of the phase being odd in momentum and the fermionic anticommutation. Hence, Cooper pairs on non-degenerate bands characterized by helicity λ always transform according to even *irreducible representations* [SC04]. Naively, one could straightfor-

wardly try to investigate the superconducting order parameter by calculating the eigenmodes of $U^{b\lambda b'\lambda'}_{\mathbf{k}\mathbf{k}'}$. However, a simple argument shows that this results in gap functions in momentum space that do not transform according to any irreducible representations due to the *branch cut* that deals with the double-valuedness of the pair wave function along the Fermi surface that is introduced by the fermionic *double group* property [Blo85; SZB04]. More precisely, if we go around the Fermi surface by more than 2π, we acquire a minus sign due the single-particle states obeying double group transformation behavior (cf. (Section 3.3.1)). Equivalently, one can look at a state at $\mathbf{k}$ that is paired with a state at $-\mathbf{k}$ of the same helicity (its time-reversal partner), which in turn has a time-reversal partner that differs from the original state by a minus sign. To resolve this contradiction, we restrict ourselves to states in the first half of the Brillouin zone and pair them up with their time-reversal partners in the second half. Hence, the non-classifiable gap function is given by $\Delta_{\mathbf{k}b\lambda}$, related to the straightforward pairing of *Bloch states*. These are related to the time-reversal paired gap functions by $\tilde{\Delta}_{\mathbf{k}b\lambda} = e^{i\phi_{\mathbf{k}b\lambda}}\Delta_{\mathbf{k}b\lambda}$, i.e. exactly the phases that arise from the time-reversal operation. In order to investigate the possibility of *singlet/triplet mixing* more closely, we have to transform the gap function obtained in helical space back to pseudospin basis. Thanks to the evenness of the gap function in helical space $\tilde{\Delta}_{\mathbf{k}b\lambda}$, we can straightforwardly write down the singlet and triplet part of the pair wave function in pseudospin space by symmetrization and antisymmetrization, i.e. [SAM09; Smi+17b]

$$d^0_{\mathbf{k}b} = \frac{\tilde{\Delta}_{\mathbf{k}b+} + \tilde{\Delta}_{\mathbf{k}b-}}{2} \qquad \mathbf{d}_{\mathbf{k}b} = \frac{\gamma_{\mathbf{k}}}{|\gamma_{\mathbf{k}}|}\frac{\tilde{\Delta}_{\mathbf{k}b+} - \tilde{\Delta}_{\mathbf{k}b-}}{2} \quad . \tag{3.4.34}$$

This relations can be inverted to yield the helical gap function in terms of singlet and triplet contributions

$$\tilde{\Delta}_{\mathbf{k}b\lambda} = d^0_{\mathbf{k}b} + \lambda\frac{\gamma_{\mathbf{k}}}{|\gamma_{\mathbf{k}}|}\cdot\mathbf{d}_{\mathbf{k}b} \quad . \tag{3.4.35}$$

From (Equation 3.4.34) we can already see that a mixing of singlet and triplet Cooper pairs occurs if the helical gaps have different amplitude on the two non-degenerate Fermi surfaces characterized by $\lambda = \pm$.

3.4.3. Construction of symmetrized particle-particle basis states

In the preceding two sections, we worked out the mean-field theories for generalized Cooper pair states in presence of time-reversal and with or without inversion symmetry. In presence of inversion symmetry, the single-particle Hamiltonian assumes its diagonal form when written in *pseudospin* basis, while in absence of inversion symmetry, the band energies are characterized by the *helical* spin degree of freedom. In both cases we found that the *effective two-particle interaction* can be most conveniently analyzed with respect to the possible particle-particle instabilities that may arise from it, by using its represen-

tation in pseudospin basis and employing the parametrization (Equation 3.4.26)

$$U^{bb'\tilde{\sigma}_1\tilde{\sigma}_2\tilde{\sigma}'_1\tilde{\sigma}'_2}_{\mathbf{k}\mathbf{k}'}\bar{\phi}_{\mathbf{k}'b'\tilde{\sigma}'_1}\bar{\phi}_{-\mathbf{k}'b'\tilde{\sigma}'_2}\phi_{-\mathbf{k}b\tilde{\sigma}_2}\phi_{\mathbf{k}b\tilde{\sigma}_1} = U^{bb'\mu\nu}_{\mathbf{k}\mathbf{k}'}\overline{P^{\mu}_{\mathbf{k}'b'}}P^{\nu}_{\mathbf{k}b} \quad , \tag{3.4.36}$$

in pseudospin basis where the bilinear $P^{\nu}_{\mathbf{k}b}$ is defined by

$$P^{\mu}_{\mathbf{k}b} = \left(i\sigma_\mu\sigma_y\right)_{\tilde{\sigma}\tilde{\sigma}'}\phi_{-\mathbf{k}b\tilde{\sigma}}\phi_{\mathbf{k}b\tilde{\sigma}'} \quad . \tag{3.4.37}$$

The *spectral decomposition* of $U^{bb'\mu\nu}_{\mathbf{k}\mathbf{k}'}$ then reveals the symmetries and *harmonic composition* of possible gap functions $\Delta_{\mathbf{k}b\tilde{\sigma}}$:

$$U^{bb'\mu\nu}_{\mathbf{k}\mathbf{k}'} = \sum_n \xi_n f^n_{\mathbf{k}b\mu}\left(f^n_{\mathbf{k}'b'\nu}\right)^\dagger \quad , \tag{3.4.38}$$

that are given by its eigenmodes $f^n_{\mathbf{k}b\mu}$. In (Section 3.3.2) we worked out the behavior of the two-particle vertex $U^{bb'\tilde{\sigma}_1\tilde{\sigma}_2\tilde{\sigma}'_1\tilde{\sigma}'_2}_{\mathbf{k}\mathbf{k}'}$ with respect to *time-reversal*, *point group* and eventually *inversion* transformations. These symmetries restrict the range of possible eigenmodes $f^n_{\mathbf{k}b\mu}$ in which the spatial $\mathbf{k}$ and pseudospin μ degrees of freedom are inherently coupled. The bilinear $P^{\mu}_{\mathbf{k}b}$ exhibits transformation behavior that is quite similar to the one of the d-vector discussed in (Section 2.4.4). In particular, we have

$$\text{inversion} \qquad P^{\mu}_{\mathbf{k}b} \xrightarrow{\hat{P}} P^{\mu}_{-\mathbf{k}b} = g^{\mu\nu}P^{\nu}_{\mathbf{k}b} \tag{3.4.39}$$

$$\text{time-reversal} \qquad P^{\mu}_{\mathbf{k}b} \xrightarrow{\hat{\Theta}} -g^{\mu\nu}\overline{P^{\nu}_{-\mathbf{k}b}} = g^{\mu\nu}\overline{P^{\nu}_{\mathbf{k}b}} \tag{3.4.40}$$

$$\text{rotation} \qquad P^{\mu}_{\mathbf{k}b} \xrightarrow{\hat{R}} \mathcal{D}^{\mu\nu}_g P^{\nu}_{\mathcal{R}(\hat{n},\varphi)\mathbf{k}b} \quad , \tag{3.4.41}$$

where $g^{\mu\nu} = \mathrm{diag}(+1,-1,-1,-1)$ and $\mathcal{D}^{\mu\nu}_g = \mathrm{diag}(1,\mathcal{R}(\hat{n},\varphi))$ with $\mathcal{R}(\hat{n},\varphi) \in \mathbb{R}^{3\times3}$ being the SO(3) rotation representation in real space. In (Equation 3.4.39) we took into account the fermionic anticommutation of fields and the fact that the singlet part is odd and the triplet part even with respect to the exchange of spin indices. (Equation 3.4.36) suggests, that the four component eigenmodes $f^n_{\mathbf{k}b\mu}$ transform conjugate to $P^{\mu}_{\mathbf{k}b}$. These properties can be employed to construct basis functions in band/pseudospin/momentum space corresponding to arbitrary *irreducible representation* of the particular point group $\mathcal{G}$. Due to the fermionic anticommutation of Grassmann fields and (Equation 3.4.39), the eigenstates must obey $f_{-\mathbf{k}b\mu} = \left(f_{\mathbf{k}b\mu=0}, -f_{\mathbf{k}b\mu=1,2,3}\right)$ (cf. (Equation 2.4.24)).

Tetragonal point group $\mathbf{D_{4h}}$ In particular, the possible pairing states governed by the tetragonal point group $\mathrm{D_{4h}}$ are inspected. The definition and notation of its group elements and irreducible representations are given in appendix H. The tetragonal point

group gives rise to ten irreducible representations, which are divided into two classes by their *even* (g) or *odd* (u) parity, each of which contains four one (A_{1g}, A_{2g}, B_{1g}, B_{2g} and A_{1u}, A_{2u}, B_{1u}, B_{2u}) and one two-dimensional (E_g and E_u) irreducible representations. Since D_{4h} contains inversion i as one of its group elements, the constraint of a definite parity forbids states $f^n_{\mathbf{k}b\mu}$ with finite components in both $\mu = 0$ and $\mu > 0$ sectors (cf. appendix F). In principle, the $\mu = 0$ component $f^n_{\mathbf{k}b0}$ of the pairing function may transform according to any of the even parity representations A_{1g}, A_{2g}, B_{1g}, B_{2g} or E_g, i.e. given by an arbitrary superposition of lattice harmonics corresponding to these representations. In contrast, the $\mu = 1,2,3$ components $f^n_{\mathbf{k}b\mu}$ must each contain an odd function in $\mathbf{k}$, i.e. one of A_{1u}, A_{2u}, B_{1u} or B_{2u}. In (Section 2.4.3) we saw that if spin-orbit interaction couples spin and spatial degrees of freedom, the Hamiltonian only exhibits symmetries with respect to the combined transformation of all degrees of freedom, which are *pseudospin*, *band* and *momentum*. Therefore, we have to consider the product representations

$$(A_{1u} \oplus A_{2u} \oplus B_{1u} \oplus B_{2u} \oplus E_u) \otimes \left(E_g \oplus A_{2g}\right) = A_{1u} \oplus A_{2u} \oplus B_{1u} \oplus B_{2u} \oplus E_u \quad . \tag{3.4.42}$$

The first bracket on the left hand side corresponds to all available momentum space functions in $f^n_{\mathbf{k}b\mu=1,2,3}$ while the second bracket on the left hand side describes the transformation behavior of the (pseudospin) Pauli matrices (cf. (Table A.1)). Note that these basis functions can only be employed in three dimensions since in two dimensions, i.e. for a fixed k_z-component at e.g. $k_z = 0$ or $k_z = \pi$, there is only one odd representation being E_u (only consider the representation basis functions featuring $\cos(k_z)$ and hence $\cos(k_z = 0) = 1$). However, this implies the same possible triplet pairing functions already obtained in (Equation 3.4.42) since $E_u \otimes \left(E_g \oplus A_{2g}\right) = A_{1u} \oplus A_{2u} \oplus B_{1u} \oplus B_{2u} \oplus E_u$. In order to explicitly construct these pairing functions, one may either consider all available constraints and play around with the residual degrees of freedom to find the form that resembles the behavior of the five possible triplet functions or one may construct them "by hand". First of all, we denote the pairing function (in analogy to the d-vector in (Section 2.4.3)) by

$$f^\mu_{\mathbf{k}b} = f^0_{\mathbf{k}b}\,\hat{x}^0 + f^1_{\mathbf{k}b}\,\hat{x} + f^2_{\mathbf{k}b}\,\hat{y} + f^3_{\mathbf{k}b}\,\hat{z} \quad \text{and} \quad f^\mu_{ib} = f^0_{ib}\,\hat{x}^0 + f^1_{ib}\,\hat{x} + f^2_{ib}\,\hat{y} + f^3_{ib}\,\hat{z} \quad , \tag{3.4.43}$$

in reciprocal space with momentum $\mathbf{k}$ and real space with lattice site i, respectively. Next, we take all lattice sites corresponding to n-th nearest neighbors into account and successively apply all group operations to $f^\mu_{\mathbf{k}b}$ and prepend their characters χ_Γ of the respective irreducible representation Γ of the point group. The transformation involves both spatial and spin degrees of freedom. In particular, the components $f^\mu_{\mathbf{k}b}$ transform according to (Equation 3.4.41) and exactly like the d-vector in (Section 2.4.4). The procedure is illustrated for the case of 4th nearest neighbors in (Figure 3.4). More precisely, we set up the sum of sixteen (number of point group elements) terms that yields

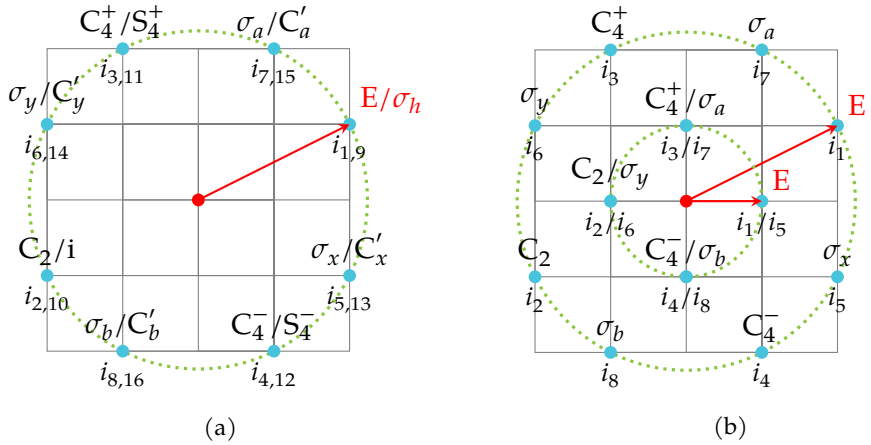

Figure 3.4.: The construction of particle-particle states governed by the point group D_{4h} in (Figure 3.4a) and C_{4v} in (Figure 3.4b) is performed by transforming and summing up f_{ib}^{μ} for all operations including their characters for the desired representation. Here, the process is illustrated for 1st and 4th nearest neighbors basis functions on the tetragonal lattice and square lattice, respectively. While inversion symmetry is present in (Figure 3.4a), the loss of inversion symmetry corresponding to (Figure 3.4b) enables the mixing of singlet and triplet states.

$$
\begin{aligned}
f_{ib}^{\mu} \longrightarrow\ & \chi_\Gamma(\mathrm{E})\left(f_{i_1b}^0\hat{x}^0 + f_{i_1b}^1\hat{x} + f_{i_1b}^2\hat{y} + f_{i_1b}^3\hat{z}\right) + \chi_\Gamma(\mathrm{C}_2)\left(f_{i_2b}^0\hat{x}^0 - f_{i_2b}^1\hat{x} - f_{i_2b}^2\hat{y} + f_{i_2b}^3\hat{z}\right) \\
& + \chi_\Gamma(\mathrm{C}_4^+)\left(f_{i_3b}^0\hat{x}^0 + f_{i_3b}^2\hat{x} - f_{i_3b}^1\hat{y} + f_{i_3b}^3\hat{z}\right) + \chi_\Gamma(\mathrm{C}_4^-)\left(f_{i_4b}^0\hat{x}^0 - f_{i_4b}^2\hat{x} + f_{i_4b}^1\hat{y} + f_{i_4b}^3\hat{z}\right) \\
& + \chi_\Gamma(\sigma_x)\left(f_{i_5b}^0\hat{x}^0 - f_{i_5b}^1\hat{x} + f_{i_5b}^2\hat{y} - f_{i_5b}^3\hat{z}\right) + \ldots + \chi_\Gamma(\mathrm{i})\left(f_{i_{10}b}^0\hat{x}^0 + f_{i_{10}b}^1\hat{x} + f_{i_{10}b}^2\hat{y} + f_{i_{10}b}^3\hat{z}\right) \\
& + \ldots + \chi_\Gamma(\mathrm{C}_b')\left(f_{i_{16}b}^0\hat{x}^0 - f_{i_{16}b}^2\hat{x} - f_{i_{16}b}^1\hat{y} + f_{i_{16}b}^3\hat{z}\right) \quad , \qquad (3.4.44)
\end{aligned}
$$

where both real space lattice coordinates (site index i) and spin degrees of freedom are transformed at once, since they are assumed to be coupled due to spin-orbit interaction. Note, that although the (pseudospin) Pauli matrices transform like the components of a polar vector under rotations, they behave unlike the components of a true vector with respect to reflections, which becomes obvious for the operation σ_x, for instance. The characters χ_Γ (given in (Table H.6)) have to be inserted into the sum (Equation 3.4.44) for the respective irreducible representation in (Equation 3.4.42). The singlet components will cancel for any odd representation since the singlet components do transform in the same way for the first eight operations (belonging to C_{4v}) and the second eight operations (taking into account the inversion and three-dimensionality for D_{4h}). After collecting terms with respect to site index and basis $\hat{x}$, $\hat{y}$ and $\hat{z}$, they are transformed to k-space to yield the desired order parameters given in (Table 3.3) and (Table 3.4).

Table 3.3.: The point group D_{4h} allows for five singlet pairing functions each. Since spin-orbit interaction is assumed to be present, the unit vectors $\hat{x}$, $\hat{y}$ and $\hat{z}$ represent the pseudospin structure of the two-particle states. Note, that combined transformation of all degrees of freedoms, i.e. momentum, band and pseudospin are implicit in this classification. However, the singlet pairing states with total spin $S = 0$ do not change under spin transformations anyway.

	singlet
irr. repr. Γ	pairing function $f^0_{\mathbf{k}b}$
A_{1g}	$\left(\cos(k_x) + \cos\left(k_y\right)\right)\cos(k_z)$
A_{2g}	$\left(\sin(x)\sin\left(2k_y\right) - \sin(2k_x)\sin\left(k_y\right)\right)\cos(k_z)$
B_{1g}	$\left(\cos(k_x) - \cos\left(k_y\right)\right)\cos(k_z)$
B_{2g}	$\sin(k_x)\sin\left(k_y\right)\cos(k_z)$
E_g	$\sin(k_x)\sin(k_z), \sin\left(k_y\right)\sin(k_z)$

Square lattice point group C_{4v} If inversion symmetry is broken, the tetragonal point group D_{4h} breaks down to the square lattice point group C_{4v} that is merely comprised of eight group elements and has only five irreducible representations A_1, A_2, B_1, B_2 and E. The singlet part that has to be even in momentum and must transform according to one of the one-dimensional representations A_1, A_2, B_1, B_2, while the triplet part has to be comprised of E in k-space. Due to the lack of the inversion operation, the system is allowed to host pairing with an order parameter that features both a finite singlet and a triplet part. Obviously, valid order parameters of *mixed parity* are not given by combining singlet and triplet parts in an arbitrary way. Rather, the entire pairing function must transform according to a specific irreducible representation as well. Including the transformation behavior of the d-vector basis, which is $(E \oplus A_2)$, we find the product representations for the triplet part:

$$E \otimes (E \oplus A_2) = A_1 \oplus A_2 \oplus B_1 \oplus B_2 \oplus E \quad . \tag{3.4.45}$$

To construct these pairing functions explicitly, we state the transformation of all singlet/triplet components with respect to the eight operations, i.e. (cf. (Figure 3.4b))

Table 3.4.: The point group D_{4h} allows for five triplet pairing states corresponding to the irreducible representations A_{1u}, A_{2u}, B_{1u} and B_{2u} in the presence of spin-orbit interaction. The unit vectors $\hat{x}$, $\hat{y}$ and $\hat{z}$ represent the pseudospin structure of the two-particle states. The second column of the table shows the general structure of the pairing states in terms of basis functions $f^{\Gamma}_{k_x k_y k_z}$ in momentum space associated to a certain irreducible representation Γ (given in (Table H.7)) and the pseudospin unit vectors. The third column gives the lowest order (mostly next nearest neighbor) contributions to the pairing states. Note, that some of these states exploit the three-dimensionality and have to vanish in the limit of two dimensions $k_z \to 0$ with k_x, k_y-dependence, only (cf. [Sig+99; ZM05; HY18]). Since the triplet pairing states carry total spin $S = 1$ and spatial and spin degree of freedom are assumed to be coupled, we always have to take combined transformations of momentum and spin into account.

triplet		
irr. repr. Γ	$\mathbf{k}/\tilde{\sigma}$-structure	pairing function $f^{\mu}_{\mathbf{k}b}$
A_{1u}	$\hat{x} f^{E_u}_{k_x k_z} + \hat{y} f^{E_u}_{k_y k_z} + \hat{z} f^{A_{2u}}_{k_x k_y k_z}$	$\left(\hat{x}\sin\left(k_y\right) - \hat{y}\sin(k_x)\right)\cos(k_z)$ $+\hat{z}\left(\sin(k_x)\sin\left(2k_y\right) - \sin(2k_x)\sin\left(k_y\right)\right)\sin(k_z)$
A_{2u}	$\hat{x} f^{E_u}_{k_y k_z} - \hat{y} f^{E_u}_{k_x k_z} + \hat{z} f^{A_{1u}}_{k_x k_y k_z}$	$\left(\hat{x}\sin(k_x) + \hat{y}\sin\left(k_y\right)\right)\cos(k_z)$ $+\hat{z}\left(\cos(k_x) + \cos\left(k_y\right)\right)\sin(k_z)$
B_{1u}	$\hat{x} f^{E_u}_{k_x k_z} - \hat{y} f^{E_u}_{k_y k_z} + \hat{z} f^{B_{2u}}_{k_x k_y k_z}$	$\left(\hat{x}\sin\left(k_y\right) + \hat{y}\sin(k_x)\right)\cos(k_z)$ $+\hat{z}\sin(k_x)\sin\left(k_y\right)\sin(k_z)$
B_{2u}	$\hat{x} f^{E_u}_{k_y k_z} + \hat{y} f^{E_u}_{k_x k_z} + \hat{z} f^{B_{1u}}_{k_x k_y k_z}$	$\left(\hat{x}\sin(k_x) - \hat{y}\sin\left(k_y\right)\right)\cos(k_z)$ $+\hat{z}\left(\cos(k_x) - \cos\left(k_y\right)\right)\sin(k_z)$
E_u	$\hat{x} f^{E_g}_{\pi k_z}, \hat{y} f^{E_g}_{\pi k_z}, \hat{z} f^{E_u}_{k_x k_z}, \hat{z} f^{E_u}_{k_y k_z}$	$\sin(k_z)\hat{x}, \sin(k_z)\hat{y}$ $\hat{z}\sin(k_x)\cos(k_z), \hat{z}\sin\left(k_y\right)\cos(k_z)$

$$
\begin{aligned}
f^{\mu}_{ib} \longrightarrow\ & \chi_\Gamma(E)\left(f^0_{i_1 b}\hat{x}^0 + f^1_{i_1 b}\hat{x} + f^2_{i_1 b}\hat{y} + f^3_{i_1 b}\hat{z}\right) + \chi_\Gamma(C_2)\left(f^0_{i_2 b}\hat{x}^0 - f^1_{i_2 b}\hat{x} - f^2_{i_2 b}\hat{y} + f^3_{i_2 b}\hat{z}\right) \\
& + \chi_\Gamma(C_4^+)\left(f^0_{i_3 b}\hat{x}^0 + f^2_{i_3 b}\hat{x} - f^1_{i_3 b}\hat{y} + f^3_{i_3 b}\hat{z}\right) + \chi_\Gamma(C_4^-)\left(f^0_{i_4 b}\hat{x}^0 - f^2_{i_4 b}\hat{x} + f^1_{i_4 b}\hat{y} + f^3_{i_4 b}\hat{z}\right) \\
& + \chi_\Gamma(\sigma_x)\left(f^0_{i_5 b}\hat{x}^0 - f^1_{i_5 b}\hat{x} + f^2_{i_5 b}\hat{y} - f^3_{i_5 b}\hat{z}\right) + \chi_\Gamma(\sigma_y)\left(f^0_{i_6 b}\hat{x}^0 + f^1_{i_6 b}\hat{x} - f^2_{i_6 b}\hat{y} - f^3_{i_6 b}\hat{z}\right) \\
& + \chi_\Gamma(\sigma_a)\left(f^0_{i_7 b}\hat{x}^0 - f^1_{i_7 b}\hat{x} - f^2_{i_7 b}\hat{y} - f^3_{i_7 b}\hat{z}\right) + \chi_\Gamma(\sigma_b)\left(f^0_{i_8 b}\hat{x}^0 + f^2_{i_8 b}\hat{x} + f^1_{i_8 b}\hat{y} - f^3_{i_8 b}\hat{z}\right) \quad ,
\end{aligned}
\tag{3.4.46}
$$

where the characters of the irreducible representations of C_{4v} are given in (Table H.4). Taking the characters of the respective representations and transforming to k-space into account, we find the order parameters given in (Table 3.5). Here, we restrict the treat-

Table 3.5.: The point group C_{4v} with its five irreducible representations allows for five pairing functions. Since spin-orbit interaction is assumed to be present, the unit vectors $\hat{x}$, $\hat{y}$ and $\hat{z}$ represent the pseudospin structure of the two-particle states. Note, that combined transformation of all degrees of freedoms, i.e. momentum, band and pseudospin have to be performed in this classification. Since the point group C_{4v} does not contain the inversion operation, mixing of singlet and triplet components in a single order parameter is possible. The pseudospin basis states $\hat{x}^0$, $\hat{x}$, $\hat{y}$ and $\hat{z}$ are defined by (Equation 2.4.26).

mixed singlet/triplet				
irr. repr. Γ	$f^0_{\mathbf{k}b}$	$f^1_{\mathbf{k}b}$	$f^2_{\mathbf{k}b}$	$f^3_{\mathbf{k}b}$
A_1	$\hat{x}^0 f^{A_1}_{k_x k_y}$	$\hat{x} f^{E}_{k_x}$	$\hat{y} f^{E}_{k_y}$	
A_2	$\hat{x}^0 f^{A_2}_{k_x k_y}$	$\hat{x} f^{E}_{k_y}$	$-\hat{y} f^{E}_{k_x}$	
B_1	$\hat{x}^0 f^{B_1}_{k_x k_y}$	$\hat{x} f^{E}_{k_x}$	$-\hat{y} f^{E}_{k_y}$	
B_2	$\hat{x}^0 f^{B_2}_{k_x k_y}$	$\hat{x} f^{E}_{k_y}$	$\hat{y} f^{E}_{k_x}$	
E				$\hat{z} f^{E}_{k_x}, \hat{z} f^{E}_{k_y}$

ment to two-dimensional pairing functions, which means that only two-dimensional momentum functions will be involved. This is why the contributions to $\hat{z}$ components in the one-dimensional representations have to vanish. To acquire a more intuitive understanding of the states, we translate the superposition of singlet and triplet in the B_1 representation to a more transparent form, i.e.

$$\begin{aligned}\hat{x}^0 f^{B_1}_{k_x k_y} + \hat{x} f^{E}_{k_y} + \hat{y} f^{E}_{k_x} &= \hat{x}^0 \left(\cos(k_x) - \cos\left(k_y\right)\right) + \hat{x} \sin\left(k_y\right) + \hat{y} \sin(k_x) \\ &= \left(|\tilde{\uparrow}\tilde{\downarrow}\rangle - |\tilde{\downarrow}\tilde{\uparrow}\rangle\right)\left(\cos(k_x) - \cos\left(k_y\right)\right) - |\tilde{\uparrow}\tilde{\uparrow}\rangle\left(\sin(k_x) + i\sin\left(k_y\right)\right) + |\tilde{\downarrow}\tilde{\downarrow}\rangle\left(\sin(k_x) - i\sin\left(k_y\right)\right) \quad ,\end{aligned} \tag{3.4.47}$$

where we used the definition of the d-vector components (Equation 2.4.26). Note, that (Equation 3.4.47) is not a normalized state.

3.5. Particle-hole condensates

The *effective low-energy interaction*, whose properties were discussed in (Section 3.3), may not only give rise to superconducting Cooper pair states but also to particle-hole condensates like *charge-density wave* (*CDW*) and *spin-density wave* (*SDW*). In contrast to the particle-particle condensates, these states usually exhibit a lower degree of symmetry since they correspond to scattering processes described by the two-particle vertex with

finite momentum transfer, while the Cooper pairing partner states $|\mathbf{k}, \tilde{\sigma}\rangle, |-\mathbf{k}, \tilde{\sigma}'\rangle$ always have zero total momentum. In the framework of a *mean-field theory*, the particle-hole states correspond to the expectation value $\left\langle c^\dagger_{\mathbf{k}b\tilde{\sigma}} c_{\mathbf{k}+\mathbf{q}b\tilde{\sigma}'}\right\rangle$, which is characterized by the momentum transfer $\mathbf{q}$ that determines the real space structure of the particle-hole state.

3.5.1. Mean-field theory of particle-hole instabilities

Once more, our starting point is the two-particle vertex describing the low-energy effective two-particle interaction. In terms of fields and momentum/band/pseudospin basis, the two-particle vertex and its couplings corresponding to the *density-wave channel* are given by (see (Equation 3.3.1) and (Section 3.3.2))

$$\begin{aligned} U^{b_1\tilde{\sigma}_1 b_2\tilde{\sigma}_2 b_1'\tilde{\sigma}_1' b_2'\tilde{\sigma}_2'}_{\mathbf{k}_1\mathbf{k}_2\mathbf{k}_1'\mathbf{k}_2'}\, c^\dagger_{\mathbf{k}_1' b_1'\tilde{\sigma}_1'} c^\dagger_{\mathbf{k}_2' b_2'\tilde{\sigma}_2'} c_{\mathbf{k}_2 b_2\tilde{\sigma}_2} c_{\mathbf{k}_1 b_1\tilde{\sigma}_1}\Big|_{\substack{\mathbf{k}_1'=\mathbf{k}_1+\mathbf{k}_2-\mathbf{k}_2' \\ b_1'=b_1, b_2'=b_2}} \\ = U^{b\tilde{\sigma}_1 b'\tilde{\sigma}_2 b\tilde{\sigma}_1' b'\tilde{\sigma}_2'}_{\mathbf{k},\mathbf{k}'+\mathbf{q},\mathbf{k}+\mathbf{q},\mathbf{k}'}\, c^\dagger_{\mathbf{k}+\mathbf{q}b\tilde{\sigma}_1'} c^\dagger_{\mathbf{k}'b'\tilde{\sigma}_2'} c_{\mathbf{k}'+\mathbf{q}b'\tilde{\sigma}_2} c_{\mathbf{k}b\tilde{\sigma}_1} \quad . \end{aligned} \tag{3.5.1}$$

Similar to the (anomalous) expectation value of Cooper pairs in (Section 2.4), we define the mean-fields

$$g^{\mathbf{q}}_{\mathbf{k}b\tilde{\sigma}\tilde{\sigma}'} := \left\langle c^\dagger_{\mathbf{k}b\tilde{\sigma}} c_{\mathbf{k}+\mathbf{q}b\tilde{\sigma}'}\right\rangle \qquad \overline{g^{\mathbf{q}}_{\mathbf{k}b\tilde{\sigma}\tilde{\sigma}'}} = \left\langle c^\dagger_{\mathbf{k}+\mathbf{q}b\tilde{\sigma}} c_{\mathbf{k}b\tilde{\sigma}'}\right\rangle \quad , \tag{3.5.2}$$

and associated fluctuations $\delta^{\mathbf{q}}_{\mathbf{k}b\tilde{\sigma}\tilde{\sigma}'} := c^\dagger_{\mathbf{k}b\tilde{\sigma}} c_{\mathbf{k}+\mathbf{q}b\tilde{\sigma}'} - g^{\mathbf{q}}_{\mathbf{k}b\tilde{\sigma}\tilde{\sigma}'}$ and $\left(\delta^{\mathbf{q}}_{\mathbf{k}b}\right)^\dagger_{\tilde{\sigma}\tilde{\sigma}'} = c^\dagger_{\mathbf{k}+\mathbf{q}b\tilde{\sigma}} c_{\mathbf{k}b\tilde{\sigma}'} - \overline{g^{\mathbf{q}}_{\mathbf{k}b\tilde{\sigma}'\tilde{\sigma}}}$. By neglecting the terms quadratic in the fluctuations, one may approximate the quartic operator terms in the interaction (Equation 3.5.1) by

$$\begin{aligned} c^\dagger_{\mathbf{k}+\mathbf{q}b\tilde{\sigma}_1'} c^\dagger_{\mathbf{k}'b'\tilde{\sigma}_2'} c_{\mathbf{k}'+\mathbf{q}b'\tilde{\sigma}_2} c_{\mathbf{k}b\tilde{\sigma}_1} \approx -\overline{g^{\mathbf{q}}_{\mathbf{k}b\tilde{\sigma}_1\tilde{\sigma}_1'}} g^{\mathbf{q}}_{\mathbf{k}'b'\tilde{\sigma}_2'\tilde{\sigma}_2} + \overline{g^{\mathbf{q}}_{\mathbf{k}b\tilde{\sigma}_1\tilde{\sigma}_1'}} c^\dagger_{\mathbf{k}'b'\tilde{\sigma}_2'} c_{\mathbf{k}'+\mathbf{q}b'\tilde{\sigma}_2} \\ + g^{\mathbf{q}}_{\mathbf{k}'b'\tilde{\sigma}_2'\tilde{\sigma}_2} c^\dagger_{\mathbf{k}+\mathbf{q}b\tilde{\sigma}_1'} c_{\mathbf{k}b\tilde{\sigma}_1} \quad . \end{aligned} \tag{3.5.3}$$

Taking the non-interacting part $\mathcal{H}_0$ of the total Hamiltonian, characterized by the single-particle dispersion $\xi_{\mathbf{k}b\tilde{\sigma}}$ in pseudospin basis $\tilde{\sigma}$ into account, the mean-field Hamiltonian for particle-hole states with momentum transfer $\mathbf{q}$ yields

$$\mathcal{H}_{\mathrm{MF}} = \sum_{\mathbf{k}b\tilde{\sigma}} \xi_{\mathbf{k}b\tilde{\sigma}} c^\dagger_{\mathbf{k}b\tilde{\sigma}} c_{\mathbf{k}b\tilde{\sigma}} + \frac{1}{2} \sum_{\mathbf{k}b\tilde{\sigma}\tilde{\sigma}'} \overline{\Delta^{\mathbf{q}}_{\mathbf{k}b\tilde{\sigma}\tilde{\sigma}'}} c^\dagger_{\mathbf{k}b\tilde{\sigma}} c_{\mathbf{k}+\mathbf{q}b\tilde{\sigma}'} + \Delta^{\mathbf{q}}_{\mathbf{k}b\tilde{\sigma}\tilde{\sigma}'} c^\dagger_{\mathbf{k}+\mathbf{q}b\tilde{\sigma}'} c_{\mathbf{k}b\tilde{\sigma}} - \mathcal{M} \quad , \tag{3.5.4}$$

where the scalar term quadratic in mean-fields is given by $\mathcal{M} = \sum_{\substack{\mathbf{k},\mathbf{k}' \\ b,b'}} \sum_{\substack{\tilde{\sigma}_1,\tilde{\sigma}_2 \\ \tilde{\sigma}_1',\tilde{\sigma}_2'}} \overline{g^{\mathbf{q}}_{\mathbf{k}b\tilde{\sigma}_1\tilde{\sigma}_1'}} g^{\mathbf{q}}_{\mathbf{k}'b'\tilde{\sigma}_2'\tilde{\sigma}_2}$.

The *charge/pseudospin gap* is defined by the *gap equation*

$$\Delta^{\mathbf{q}}_{\mathbf{k}b\tilde{\sigma}_1\tilde{\sigma}'_1} := 2\sum_{\mathbf{k}'b'\tilde{\sigma}_2\tilde{\sigma}'_2} U^{b\tilde{\sigma}_1 b'\tilde{\sigma}_2 b\tilde{\sigma}'_1 b'\tilde{\sigma}'_2}_{\mathbf{k},\mathbf{k}'+\mathbf{q},\mathbf{k}+\mathbf{q},\mathbf{k}'} g^{\mathbf{q}}_{\mathbf{k}'b'\tilde{\sigma}'_2\tilde{\sigma}_2}$$
$$\text{and} \quad \overline{\Delta^{\mathbf{q}}_{\mathbf{k}b\tilde{\sigma}_1\tilde{\sigma}'_1}} = 2\sum_{\mathbf{k}'b'\tilde{\sigma}_2\tilde{\sigma}'_2} U^{b'\tilde{\sigma}'_2 b\tilde{\sigma}'_1 b'\tilde{\sigma}_2 b\tilde{\sigma}_1}_{\mathbf{k}',\mathbf{k}+\mathbf{q},\mathbf{k}'+\mathbf{q},\mathbf{k}} \overline{g^{\mathbf{q}}_{\mathbf{k}'b'\tilde{\sigma}'_2\tilde{\sigma}_2}} \quad , \tag{3.5.5}$$

that has to be solved self-consistently (cf. (Figure 2.6)) with respect to the expectation value $g^{\mathbf{q}}_{\mathbf{k}b\tilde{\sigma}\tilde{\sigma}'} = \mathrm{Tr}\left(c^\dagger_{\mathbf{k}b\tilde{\sigma}} c_{\mathbf{k}+\mathbf{q}b\tilde{\sigma}'} e^{\beta\mathcal{H}_{\mathrm{MF}}}\right) / \mathrm{Tr}\left(e^{\beta\mathcal{H}_{\mathrm{MF}}}\right)$, which feeds back into the density-wave mean-field Hamiltonian (Equation 3.5.4)

$$\mathcal{H}_{\mathrm{MF}} + \mathcal{M} = \frac{1}{2}\sum_{\mathbf{k}b\tilde{\sigma}\tilde{\sigma}'} \mathbf{C}^\dagger_{\mathbf{k}b\mathbf{q}} \begin{pmatrix} \xi_{\mathbf{k}b\tilde{\uparrow}} & 0 & \Delta^{\mathbf{q}}_{\mathbf{k}b\tilde{\uparrow}\tilde{\uparrow}} & \Delta^{\mathbf{q}}_{\mathbf{k}b\tilde{\downarrow}\tilde{\uparrow}} \\ 0 & \xi_{\mathbf{k}b\tilde{\downarrow}} & \Delta^{\mathbf{q}}_{\mathbf{k}b\tilde{\uparrow}\tilde{\downarrow}} & \Delta^{\mathbf{q}}_{\mathbf{k}b\tilde{\downarrow}\tilde{\downarrow}} \\ \overline{\Delta^{\mathbf{q}}_{\mathbf{k}b\tilde{\uparrow}\tilde{\uparrow}}} & \overline{\Delta^{\mathbf{q}}_{\mathbf{k}b\tilde{\uparrow}\tilde{\downarrow}}} & \xi_{\mathbf{k}+\mathbf{q}b\tilde{\uparrow}} & 0 \\ \overline{\Delta^{\mathbf{q}}_{\mathbf{k}b\tilde{\downarrow}\tilde{\uparrow}}} & \overline{\Delta^{\mathbf{q}}_{\mathbf{k}b\tilde{\downarrow}\tilde{\downarrow}}} & 0 & \xi_{\mathbf{k}+\mathbf{q}b\tilde{\downarrow}} \end{pmatrix} \mathbf{C}_{\mathbf{k}b\mathbf{q}} \quad , \tag{3.5.6}$$

with the particle-hole *Nambu spinor* for momentum transfer $\mathbf{q}$ (cf. [RRM07])

$$\mathbf{C}^\dagger_{\mathbf{k}b\mathbf{q}} := \left(c^\dagger_{\mathbf{k}b\tilde{\uparrow}}, c^\dagger_{\mathbf{k}b\tilde{\downarrow}}, c^\dagger_{\mathbf{k}+\mathbf{q}b\tilde{\uparrow}}, c^\dagger_{\mathbf{k}+\mathbf{q}b\tilde{\downarrow}}\right)^T \quad . \tag{3.5.7}$$

Note that - despite the notation - the single-particle dispersion $\xi_{\mathbf{k}b\tilde{\sigma}}$ must be independent of the pseudospin index. If it isn't, the spectrum will already be non-degenerate in the normal state and we have to resort to a different basis to solve the gap equation with respect to particular band indices b. Therefore, we may denote the single-particle dispersion in matrix form by $\xi_{\mathbf{k}b} = \mathrm{diag}(\xi_{\mathbf{k}b\tilde{\uparrow}}, \xi_{\mathbf{k}b\tilde{\downarrow}})$. The eigenvalues of (Equation 3.5.6) can be calculated analytically by exploiting the commutation of $\xi_{\mathbf{k}b}$ with $\Delta^{\mathbf{q}}_{\mathbf{k}b\tilde{\sigma}\tilde{\sigma}'}$ and are given by (cf. (Equation 2.4.17))

$$E^{\mathbf{q}}_{\mathbf{k}b} = \frac{\xi_{\mathbf{k}b} + \xi_{\mathbf{k}+\mathbf{q}b}}{2} \pm \sqrt{\left(\frac{\xi_{\mathbf{k}b} - \xi_{\mathbf{k}+\mathbf{q}b}}{2}\right)^2 + \frac{\mathrm{Tr}\left(\Delta^{\mathbf{q}}_{\mathbf{k}b}\right)^\dagger \Delta^{\mathbf{q}}_{\mathbf{k}b}}{2} \pm \sqrt{\left(\frac{\mathrm{Tr}\left(\Delta^{\mathbf{q}}_{\mathbf{k}b}\right)^\dagger \Delta^{\mathbf{q}}_{\mathbf{k}b}}{2}\right)^2 - \det\left(\left(\Delta^{\mathbf{q}}_{\mathbf{k}b}\right)^\dagger \Delta^{\mathbf{q}}_{\mathbf{k}b}\right)}} \quad . \tag{3.5.8}$$

Assuming a *unitary charge/spin gap* with $\left(\Delta^{\mathbf{q}}_{\mathbf{k}b}\right)^\dagger \Delta^{\mathbf{q}}_{\mathbf{k}b} \propto \sigma_0$, the eigenvalue expression for the mean-field Hamiltonian simplifies to (cf. [Ebe+16])

$$E^{\mathbf{q}}_{\mathbf{k}b} = \frac{\xi_{\mathbf{k}b} + \xi_{\mathbf{k}+\mathbf{q}b}}{2} \pm \sqrt{\left(\frac{\xi_{\mathbf{k}b} - \xi_{\mathbf{k}+\mathbf{q}b}}{2}\right)^2 + \frac{\mathrm{Tr}\left(\Delta^{\mathbf{q}}_{\mathbf{k}b}\right)^\dagger \Delta^{\mathbf{q}}_{\mathbf{k}b}}{2}} \quad . \tag{3.5.9}$$

Spin/charge order that is characterized by a momentum transfer $\mathbf{q}$ that satisfies $2\mathbf{q} = \mathbf{G}$, where $\mathbf{G}$ is a reciprocal lattice vectors is called *commensurate order*. In contrast, if the momentum transfer $\mathbf{q}$ is not related to a reciprocal vector by an integer, we talk about *incommensurate order*. The matrix elements of the gap $\Delta^{\mathbf{q}}_{\mathbf{k}b}$ in terms of pseudospin can be parameterized by

$$\Delta^{\mathbf{q}}_{\mathbf{k}b\tilde{\sigma}\tilde{\sigma}'} \stackrel{!}{=} \left(s^{\mathbf{q}\mu}_{\mathbf{k}b}\sigma_\mu\right)_{\tilde{\sigma}\tilde{\sigma}'} \quad \Leftrightarrow \quad \begin{array}{ll} s^{\mathbf{q}0}_{\mathbf{k}b} = \frac{\Delta^{\mathbf{q}}_{\mathbf{k}b\tilde{\uparrow}\tilde{\uparrow}} + \Delta^{\mathbf{q}}_{\mathbf{k}b\tilde{\downarrow}\tilde{\downarrow}}}{2} & s^{\mathbf{q}x}_{\mathbf{k}b} = \frac{\Delta^{\mathbf{q}}_{\mathbf{k}b\tilde{\uparrow}\tilde{\downarrow}} + \Delta^{\mathbf{q}}_{\mathbf{k}b\tilde{\downarrow}\tilde{\uparrow}}}{2} \\ s^{\mathbf{q}y}_{\mathbf{k}b} = \frac{-\Delta^{\mathbf{q}}_{\mathbf{k}b\tilde{\uparrow}\tilde{\downarrow}} + \Delta^{\mathbf{q}}_{\mathbf{k}b\tilde{\downarrow}\tilde{\uparrow}}}{2i} & s^{\mathbf{q}z}_{\mathbf{k}b} = \frac{\Delta^{\mathbf{q}}_{\mathbf{k}b\tilde{\uparrow}\tilde{\uparrow}} - \Delta^{\mathbf{q}}_{\mathbf{k}b\tilde{\downarrow}\tilde{\downarrow}}}{2} \end{array} \quad . \tag{3.5.10}$$

$s^{\mathbf{q}0}_{\mathbf{k}b}$ and $s^{\mathbf{q}x,y,z}_{\mathbf{k}b}$ are sometimes called the *singlet* and *triplet density-wave* states [Nay00]. In case of SU(2)-symmetry, they correspond to the conventional *charge-density wave* (*CDW*) and *spin-density wave* (*SDW*) [GC10]. Shifting the expectation value (Equation 3.5.2) by $\mathbf{q}$ provides the requirement $g^{\mathbf{q}}_{\mathbf{k}+\mathbf{q}b\tilde{\sigma}\tilde{\sigma}'} = \left\langle c^\dagger_{\mathbf{k}+\mathbf{q}b\tilde{\sigma}} c_{\mathbf{k}+2\mathbf{q}b\tilde{\sigma}'}\right\rangle = \left\langle c^\dagger_{\mathbf{k}+\mathbf{q}b\tilde{\sigma}} c_{\mathbf{k}b\tilde{\sigma}'}\right\rangle = \overline{g^{\mathbf{q}}_{\mathbf{k}b\tilde{\sigma}\tilde{\sigma}'}}$ for commensurate particle-hole states. Hence, commensurate particle-hole states must satisfy $g^{\mathbf{q}}_{\mathbf{k}+\mathbf{q}b\tilde{\sigma}\tilde{\sigma}'} = \overline{g^{\mathbf{q}}_{\mathbf{k}b\tilde{\sigma}\tilde{\sigma}'}}$. Consequently, commensurate states must eventually be real or purely imaginary (depending on the actual formfactor), while an incommensurate state may feature any phase [Voj09]. In absence of spin-orbit coupling, the states $\Delta^{\mathbf{q}}_{\mathbf{k}b\tilde{\sigma}\tilde{\sigma}'}$ may be factorized into spin and momentum part, which is, however, not allowed in our general case, that implies coupling of spin and spatial degrees of freedom [NJK91]. In contrast to the particle-particle states $\left\langle c^\dagger_{\mathbf{k}b\tilde{\sigma}} c^\dagger_{-\mathbf{k}b\tilde{\sigma}'}\right\rangle$ in (Section 3.4), that are essentially determined and restricted by *Fermi statistics*, while establishing a one-to-one correspondence between pseudospin structure and momentum dependency, the particle-hole states $\left\langle c^\dagger_{\mathbf{k}b\tilde{\sigma}} c_{\mathbf{k}+\mathbf{q}b\tilde{\sigma}'}\right\rangle$ are now longer governed by Fermi statistics (cf. [Nay00]) and may well be comprised of an odd momentum dependency in the singlet and an even momentum dependency in the triplet part (in presence of SU(2) and inversion symmetry) [Cha02; GC10].

3.5.2. Construction of particle-hole basis states

According to (Equation 3.5.1) the relevant couplings in the *density-wave channel* are given by (switching to a basis in terms of fermionic fields $\phi_{\mathbf{k}b\tilde{\sigma}}$)

$$U^{b\tilde{\sigma}_1 b'\tilde{\sigma}_2 b\tilde{\sigma}'_1 b'\tilde{\sigma}'_2}_{\mathbf{k},\mathbf{k}'+\mathbf{q},\mathbf{k}+\mathbf{q},\mathbf{k}'} \bar{\phi}_{\mathbf{k}+\mathbf{q}b\tilde{\sigma}'_1} \bar{\phi}_{\mathbf{k}'b'\tilde{\sigma}'_2} \phi_{\mathbf{k}'+\mathbf{q}b'\tilde{\sigma}_2} \phi_{\mathbf{k}b\tilde{\sigma}_1} \quad . \tag{3.5.11}$$

Analogously to the definition of particle-particle states (Equation 3.4.25), we define the bilinear in the fields

$$Q^{\mathbf{q}\mu}_{\mathbf{k}b} = \left(\sigma_\mu\right)_{\tilde{\sigma}\tilde{\sigma}'} \bar{\phi}_{\mathbf{k}b\tilde{\sigma}} \phi_{\mathbf{k}+\mathbf{q}b\tilde{\sigma}'} \qquad \overline{Q^{\mathbf{q}\mu}_{\mathbf{k}b}} = \left(\sigma_\mu\right)_{\tilde{\sigma}\tilde{\sigma}'} \bar{\phi}_{\mathbf{k}+\mathbf{q}b\tilde{\sigma}} \phi_{\mathbf{k}b\tilde{\sigma}'} \quad , \tag{3.5.12}$$

with the Pauli matrices $\sigma_\mu \in \{\sigma_0, \sigma_x, \sigma_y, \sigma_z\}$. Again, it turns out to be helpful to inves-

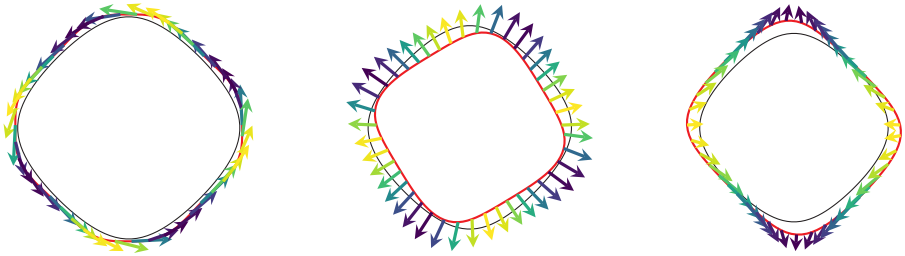

(a) (b) (c)

Figure 3.5.: The charge/spin order on a tetragonal lattice governed by D_{4h} symmetry is in presence of spin-orbit coupling characterized by the superposition of charge order, resulting in a shift of the Fermi surface, and spin order, that features a k-dependent spin expectation value around the Fermi surface. The shown charge/spin orderings correspond to A_{1g} in (Figure 3.5a), A_{2g} in (Figure 3.5a) and B_{2g} in (Figure 3.5a) irreducible representations as given in (Table 3.6). While the black line shows the normal state Fermi surface, the red line represents the shifted Fermi surface of the ordered state. The color map indicates the z-components of the spin expectation value.

tigate the symmetries of this entity. Under *inversion*, *time-reversal* and *rotation* the bilinear (Equation 3.5.12) behaves according to

$$\text{inversion} \qquad Q^{\mathbf{q}\mu}_{\mathbf{k}b} \xrightarrow{\hat{P}} Q^{\mathbf{q}\mu}_{-\mathbf{k}b} \tag{3.5.13a}$$

$$\text{time-reversal} \qquad Q^{\mathbf{q}\mu}_{\mathbf{k}b} \xrightarrow{\hat{\Theta}} g^{\mu\nu}\overline{Q^{\mathbf{q}\nu}_{-\mathbf{k}b}} \tag{3.5.13b}$$

$$\text{rotation} \qquad Q^{\mathbf{q}\mu}_{\mathbf{k}b} \xrightarrow{\hat{R}} \mathcal{D}^{\mu\nu}_g Q^{\mathbf{q}\nu}_{\mathcal{R}(\hat{n},\varphi)\mathbf{k}b} \quad , \tag{3.5.13c}$$

where $g^{\mu\nu} = \mathrm{diag}(+1,-1,-1,-1)$ and $\mathcal{D}^{\mu\nu}_g = \mathrm{diag}(1,\mathcal{R}(\hat{n},\varphi))$ with $\mathcal{R}(\hat{n},\varphi) \in \mathbb{R}^{3\times3}$ being the SO(3) rotation representation in real space (cf. (Equation 2.4.39)). Again, we assume that the rotation must affect both spatial and pseudospin degrees of freedom since the spin is "frozen" to the lattice due to spin-orbit interaction. The bilinears (Equation 3.5.12) are used to parametrize the reduced two-particle vertex in the particle-hole channel (Equation 3.5.11) by

$$U^{b\tilde{\sigma}_1 b'\tilde{\sigma}_2 b\tilde{\sigma}'_1 b'\tilde{\sigma}'_2}_{\mathbf{k},\mathbf{k}'+\mathbf{q},\mathbf{k}+\mathbf{q},\mathbf{k}'} \bar{\phi}_{\mathbf{k}+\mathbf{q}b\tilde{\sigma}'_1}\bar{\phi}_{\mathbf{k}'b'\tilde{\sigma}'_2}\phi_{\mathbf{k}'+\mathbf{q}b'\tilde{\sigma}_2}\phi_{\mathbf{k}b\tilde{\sigma}_1} = U^{\mathbf{q}bb'\mu\nu}_{\mathbf{k}\mathbf{k}'}\,\overline{Q^{\mathbf{q}\mu}_{\mathbf{k}b}}Q^{\mathbf{q}\nu}_{\mathbf{k}'b'} \quad , \tag{3.5.14}$$

where μ parametrizes $\tilde{\sigma}_1$, $\tilde{\sigma}'_1$ and ν accounts for $\tilde{\sigma}_2$, $\tilde{\sigma}'_2$. Although less obvious than in the particle-particle case, $U^{\mathbf{q}bb'\mu\nu}_{\mathbf{k}\mathbf{k}'}$ is Hermitian and may therefore be expanded in terms of eigenmodes by

$$U^{\mathbf{q}bb'\mu\nu}_{\mathbf{k}\mathbf{k}'} = \sum_n \xi_n f^{\mathbf{q}n}_{\mathbf{k}b\mu} \left(f^{\mathbf{q}n}_{\mathbf{k}'b'\nu}\right)^\dagger \quad , \tag{3.5.15}$$

with eigenvalues ξ_n and eigenvectors $f^{\mathbf{q}n}_{\mathbf{k}b\mu}$. Every eigenvector may be decomposed into its singlet/charge and triplet/pseudospin components by $f^{\mathbf{q}}_{\mathbf{k}b} = \hat{x}^0 f^{\mathbf{q}}_{\mathbf{k}b0} + \hat{x} f^{\mathbf{q}}_{\mathbf{k}bx} + \hat{y} f^{\mathbf{q}}_{\mathbf{k}by} + \hat{z} f^{\mathbf{q}}_{\mathbf{k}bz}$. The structure of $U^{\mathbf{q}bb'\mu\nu}_{\mathbf{k}\mathbf{k}'}$ in absence/presence of SU(2)-symmetry and inversion symmetry can be most easily investigated by expressing its elements in terms of the coupling of the reduced two-particle vertex in the particle-hole channel. This is done by collecting all matrix elements μ, ν that contribute to a specific pseudospin sector of the right-hand side in (Equation 3.5.14) (cf. to particle-particle case in appendix F). As a reference, we state some exemplary elements and their relation to the particle-hole couplings:

$$U^{\mathbf{q}bb'00}_{\mathbf{k}\mathbf{k}'} = \frac{U^{b\uparrow b'\uparrow b\uparrow b'\uparrow}_{\mathbf{k},\mathbf{k}'+\mathbf{q},\mathbf{k}+\mathbf{q},\mathbf{k}'} + U^{b\uparrow b'\downarrow b\downarrow b'\uparrow}_{\mathbf{k},\mathbf{k}'+\mathbf{q},\mathbf{k}+\mathbf{q},\mathbf{k}'} + U^{b\downarrow b'\uparrow b\uparrow b'\downarrow}_{\mathbf{k},\mathbf{k}'+\mathbf{q},\mathbf{k}+\mathbf{q},\mathbf{k}'} + U^{b\downarrow b'\downarrow b\downarrow b'\downarrow}_{\mathbf{k},\mathbf{k}'+\mathbf{q},\mathbf{k}+\mathbf{q},\mathbf{k}'}}{4} \tag{3.5.16a}$$

$$U^{\mathbf{q}bb'33}_{\mathbf{k}\mathbf{k}'} = \frac{U^{b\uparrow b'\uparrow b\uparrow b'\uparrow}_{\mathbf{k},\mathbf{k}'+\mathbf{q},\mathbf{k}+\mathbf{q},\mathbf{k}'} - U^{b\uparrow b'\downarrow b\downarrow b'\uparrow}_{\mathbf{k},\mathbf{k}'+\mathbf{q},\mathbf{k}+\mathbf{q},\mathbf{k}'} - U^{b\downarrow b'\uparrow b\uparrow b'\downarrow}_{\mathbf{k},\mathbf{k}'+\mathbf{q},\mathbf{k}+\mathbf{q},\mathbf{k}'} + U^{b\downarrow b'\downarrow b\downarrow b'\downarrow}_{\mathbf{k},\mathbf{k}'+\mathbf{q},\mathbf{k}+\mathbf{q},\mathbf{k}'}}{4} \tag{3.5.16b}$$

$$U^{\mathbf{q}bb'03}_{\mathbf{k}\mathbf{k}'} = \frac{U^{b\uparrow b'\uparrow b\uparrow b'\uparrow}_{\mathbf{k},\mathbf{k}'+\mathbf{q},\mathbf{k}+\mathbf{q},\mathbf{k}'} - U^{b\uparrow b'\downarrow b\downarrow b'\uparrow}_{\mathbf{k},\mathbf{k}'+\mathbf{q},\mathbf{k}+\mathbf{q},\mathbf{k}'} + U^{b\downarrow b'\uparrow b\uparrow b'\downarrow}_{\mathbf{k},\mathbf{k}'+\mathbf{q},\mathbf{k}+\mathbf{q},\mathbf{k}'} - U^{b\downarrow b'\downarrow b\downarrow b'\downarrow}_{\mathbf{k},\mathbf{k}'+\mathbf{q},\mathbf{k}+\mathbf{q},\mathbf{k}'}}{4} \tag{3.5.16c}$$

$$U^{\mathbf{q}bb'12}_{\mathbf{k}\mathbf{k}'} = \frac{-U^{b\uparrow b'\uparrow b\downarrow b'\downarrow}_{\mathbf{k},\mathbf{k}'+\mathbf{q},\mathbf{k}+\mathbf{q},\mathbf{k}'} + U^{b\uparrow b'\downarrow b\uparrow b'\downarrow}_{\mathbf{k},\mathbf{k}'+\mathbf{q},\mathbf{k}+\mathbf{q},\mathbf{k}'} - U^{b\downarrow b'\uparrow b\downarrow b'\uparrow}_{\mathbf{k},\mathbf{k}'+\mathbf{q},\mathbf{k}+\mathbf{q},\mathbf{k}'} + U^{b\downarrow b'\downarrow b\uparrow b'\uparrow}_{\mathbf{k},\mathbf{k}'+\mathbf{q},\mathbf{k}+\mathbf{q},\mathbf{k}'}}{4i} \quad . \tag{3.5.16d}$$

Assuming full SU(2)-symmetry and letting the pseudospin degree of freedom become the "natural" spin, which is accounted for by the relation (Equation 3.3.19)

$$U^{\sigma_1\sigma_2\sigma_1'\sigma_2'}_{\alpha_1\alpha_2\alpha_1'\alpha_2'} = V_{\alpha_1\alpha_2\alpha_1'\alpha_2'}\delta_{\sigma_1\sigma_1'}\delta_{\sigma_2\sigma_2'} - V_{\alpha_2\alpha_1\alpha_1'\alpha_2'}\delta_{\sigma_1\sigma_2'}\delta_{\sigma_2\sigma_1'} \quad , \tag{3.5.17}$$

we find

$$U^{\mathbf{q}bb'00}_{\mathbf{k}\mathbf{k}'} = \frac{1}{2}V^{bb'bb'}_{\mathbf{k},\mathbf{k}'+\mathbf{q},\mathbf{k}+\mathbf{q},\mathbf{k}'} - V^{b'bbb'}_{\mathbf{k}'+\mathbf{q},\mathbf{k},\mathbf{k}+\mathbf{q},\mathbf{k}'} \qquad U^{\mathbf{q}bb'33}_{\mathbf{k}\mathbf{k}'} = \frac{1}{2}V^{bb'bb'}_{\mathbf{k},\mathbf{k}'+\mathbf{q},\mathbf{k}+\mathbf{q},\mathbf{k}'} = U^{\mathbf{q}bb'11}_{\mathbf{k}\mathbf{k}'} = U^{\mathbf{q}bb'22}_{\mathbf{k}\mathbf{k}'} \quad , \tag{3.5.18}$$

while all other matrix elements $U^{\mathbf{q}bb'\mu\nu}_{\mathbf{k}\mathbf{k}'}$ with $\mu \neq \nu$ vanish. Hence, while SU(2)-symmetry suppresses finite elements with $\mu = 0$ and $\nu = 1, 2, 3$, i.e. *singlet/triplet mixing*, the presence of spin-orbit coupling is sufficient to introduce *mixing of charge and spin order*. At the end of the previous section, it was already mentioned that particle-hole states

are, in contrast to the particle-particle states, not restricted by a definite parity of their singlet/triplet part. However, in order to preserve inversion symmetry, all finite singlet and triplet components (in particular, in a mixed state due to spin-orbit coupling) have to have the same (either odd or even) parity. This becomes apparent from (Equation 3.5.15) by considering a single eigenmode and requiring $U^{\mathbf{q}bb'\mu\nu}_{\mathbf{k}\mathbf{k}'}$ to be invariant under spatial inversion. The loss of inversion symmetry (in addition to finite spin-orbit interaction) further enables the mixing of odd and even parity eigenmodes in both singlet and triplet components. In order to further investigate the possible charge-/spin-order-parameters and in particular the transformation behavior of the eigenmodes $f^{\mathbf{q}n}_{\mathbf{k}b\mu}$, we limit our considerations to *commensurate order* with $2\mathbf{q} = \mathbf{G}$. For instance, possible (in-plane) $\mathbf{q}$-vectors on the tetragonal lattice with point group $\mathrm{D_{4h}}$ are given by $\mathbf{q} = (\pi, \pi)$ and $\mathbf{q} = (\pi, 0)$. While $\mathbf{q} = (\pi, \pi)$ is invariant with respect to all operations of $\mathrm{D_{4h}}$ up to a reciprocal lattice vector, i.e. $\mathbf{q} = (\pi, \pi) \xrightarrow{g} \mathbf{q}' = \mathbf{q} + \mathbf{G}\ \forall g \in \mathrm{D_{4h}}$, $\mathbf{q} = (\pi, 0)$ breaks the set of symmetry operations down to $\mathrm{D_{2h}}$ since $\mathbf{q} = (\pi, 0) \xrightarrow{g} \mathbf{q}' = \mathbf{q} + \mathbf{G}\ \forall g \in \mathrm{D_{2h}}$. Here, $\mathrm{D_{4h}}$ and $\mathrm{D_{2h}}$ are called the *group of the wave-vector* $\mathbf{q} = (\pi, \pi)$ and $\mathbf{q} = (\pi, 0)$, respectively [DDJ08, Chap. 10.3.2]. Hence, the eigenmodes $f^{\mathbf{q}n}_{\mathbf{k}b\mu}$ transform according to any *irreducible representation* of the group of the wave vector $\mathbf{q}$. The possible charge-/spin order-parameters associated to $\mathbf{q} = (\pi, \pi)$ on the tetragonal lattice with $\mathrm{D_{4h}}$-symmetry are given in (Table 3.6). In order to visualize some of these order parameters, we take a simple Hubbard Hamiltonian on the square lattice with $\xi_{\mathbf{k}\tilde{\sigma}} = -2t\left(\cos(k_x) + \cos\left(k_y\right)\right) - 4t' \cos(k_x)\cos\left(k_y\right) - \mu$ ($\mu = -1.4t$ and $t' = -0.03t$) and introduce a charge/spin gap $\Delta^{\mathbf{q}}_{\mathbf{k}b\tilde{\sigma}\tilde{\sigma}'}$, i.e.

$$\mathcal{H}_{\mathrm{MF}} + \mathcal{M} = \sum_{\mathbf{k}b\tilde{\sigma}} \xi_{\mathbf{k}b\tilde{\sigma}} c^\dagger_{\mathbf{k}b\tilde{\sigma}} c_{\mathbf{k}b\tilde{\sigma}} + \frac{1}{2} \sum_{\mathbf{k}b\tilde{\sigma}\tilde{\sigma}'} \overline{\Delta^{\mathbf{q}}_{\mathbf{k}b\tilde{\sigma}\tilde{\sigma}'}} c^\dagger_{\mathbf{k}b\tilde{\sigma}} c_{\mathbf{k}+\mathbf{q}b\tilde{\sigma}'} + \Delta^{\mathbf{q}}_{\mathbf{k}b\tilde{\sigma}\tilde{\sigma}'} c^\dagger_{\mathbf{k}+\mathbf{q}b\tilde{\sigma}'} c_{\mathbf{k}b\tilde{\sigma}} \quad , \tag{3.5.19}$$

that is, for instance, associated to the $\mathrm{B_{1g}}$ representation

$$\Delta^{\mathbf{q}}_{\mathbf{k}b\tilde{\sigma}\tilde{\sigma}'} \propto \left(\cos(k_x) - \cos\left(k_y\right)\right) \sigma^0_{\tilde{\sigma}\tilde{\sigma}'} + \ldots + \sin(k_x)\sin\left(k_y\right)\sigma^z_{\tilde{\sigma}\tilde{\sigma}'} \quad , \tag{3.5.20}$$

In (Figure 3.5), we see that the resulting Fermi surface is k-dependently shifted against the normal state Fermi surface and the spin expectation value rotates along the Fermi surface.

Summary and preview

In this chapter we explored the vast range of possible spin-orbit Hamiltonians featuring either centrosymmetric or non-centrosymmetric spin-orbit interaction by means of the invariant expansion. We discussed the symmetries and transformation behavior of the resulting single-particle states and two-particle vertices and introduced the pseudospin

basis and helical spin degrees of freedom. In particular, the choice of the single-particle basis turned out to be essential for the reasonable definition of effective two-particle vertices. Based on the properly defined two-particle interaction, we investigated the mean-field theories for interactions in pseudospin and helical basis. The structure of the allowed order parameters and gap functions that intertwine spatial and spin degrees of freedom were derived. The following chapter will introduce the formal basics and techniques to set up the *perturbative renormalization group* and *functional renormalization group* in terms of functional path integrals. We will derive the second order perturbative expansion as basic tool for the derivation of the effective two-particle interaction in the weak-coupling limit and the *flow equation* of the two-particle vertex in the framework of functional renormalization that enables us to explore the effective two-particle quantities for finite interactions as well. Finally, we propose advanced schemes that employ the previously discussed symmetries to pave the way towards high momentum resolution and computational efficiency.

Table 3.6.: Since the group of the wave vector $\mathbf{q} = (\pi, \pi)$ is D_{4h}, there are charge-/spin order-parameters corresponding to ten irreducible representations. Due to finite spin-orbit interaction, the unit vectors $\hat{x}$, $\hat{y}$ and $\hat{z}$ represent the pseudospin structure of the two-particle states and only combined transformation of all degrees of freedoms, i.e. momentum, band and pseudospin have to be performed in this classification. For the notation of components we refer to (Equation 3.5.15) Note, that mixing of charge- and spin-ordering only occurs for finite spin-orbit coupling. This classification of order parameters applies to $\mathbf{q} \to (0,0)$, as well. The required basis functions are given in (Table H.7). If inversion symmetry is broken and $D_{4h} \to C_{4v}$, possible states are formed by combining even and odd states from the left and right column of the same row to comprise the corresponding irreducible representation of C_{4v}. For example, the B_1 representation may be associated to the state $\hat{z} f_{\mathbf{k}}^{B_{2g}} + \hat{x}^0 f_{\mathbf{k}}^{B_{1u}}$.

	charge/spin ordering			
irr. repr. Γ	$f^0_{\mathbf{k}b}$	$f^1_{\mathbf{k}b}$	$f^2_{\mathbf{k}b}$	$f^3_{\mathbf{k}b}$
A_{1g}	$\hat{x}^0 f_{\mathbf{k}}^{A_{1g}}$	$\hat{x} f_{k_x k_z}^{E_g}$	$\hat{y} f_{k_y k_z}^{E_g}$	$\hat{z} f_{\mathbf{k}}^{A_{2g}}$
A_{2g}	$\hat{x}^0 f_{\mathbf{k}}^{A_{2g}}$	$\hat{x} f_{k_y k_z}^{E_g}$	$-\hat{y} f_{k_x k_z}^{E_g}$	$\hat{z} f_{\mathbf{k}}^{A_{1g}}$
B_{1g}	$\hat{x}^0 f_{\mathbf{k}}^{B_{1g}}$	$\hat{x} f_{k_x k_z}^{E_g}$	$-\hat{y} f_{k_y k_z}^{E_g}$	$\hat{z} f_{\mathbf{k}}^{B_{2g}}$
B_{2g}	$\hat{x}^0 f_{\mathbf{k}}^{B_{2g}}$	$\hat{x} f_{k_y k_z}^{E_g}$	$\hat{y} f_{k_x k_z}^{E_g}$	$\hat{z} f_{\mathbf{k}}^{B_{1g}}$
E_g	$\hat{x}^0 f_{k_x k_z}^{E_g}, \hat{x}^0 f_{k_y k_z}^{E_g}$	$\hat{x} f_{\pi k_z}^{E_u}$	$\hat{y} f_{\pi k_z}^{E_u}$	$\hat{z} f_{k_x k_z}^{E_g}, \hat{z} f_{k_x k_z}^{E_g}$
A_{1u}	$\hat{x}^0 f_{\mathbf{k}}^{A_{1u}}$	$\hat{x} f_{k_x k_z}^{E_u}$	$\hat{y} f_{k_y k_z}^{E_u}$	$\hat{z} f_{\mathbf{k}}^{A_{2u}}$
A_{2u}	$\hat{x}^0 f_{\mathbf{k}}^{A_{2u}}$	$\hat{x} f_{k_y k_z}^{E_g}$	$-\hat{y} f_{k_x k_z}^{E_g}$	$\hat{z} f_{\mathbf{k}}^{A_{1u}}$
B_{1u}	$\hat{x}^0 f_{\mathbf{k}}^{B_{1u}}$	$\hat{x} f_{k_x k_z}^{E_g}$	$-\hat{y} f_{k_y k_z}^{E_g}$	$\hat{z} f_{\mathbf{k}}^{B_{2u}}$
B_{2u}	$\hat{x}^0 f_{\mathbf{k}}^{B_{2u}}$	$\hat{x} f_{k_y k_z}^{E_g}$	$\hat{y} f_{k_x k_z}^{E_g}$	$\hat{z} f_{\mathbf{k}}^{B_{1u}}$
E_u	$\hat{x}^0 f_{k_x k_z}^{E_u}, \hat{x}^0 f_{k_y k_z}^{E_u}$	$\hat{x} f_{\pi k_z}^{E_g}$	$\hat{y} f_{\pi k_z}^{E_g}$	$\hat{z} f_{k_x k_z}^{E_u}, \hat{z} f_{k_x k_z}^{E_u}$

4. Generating functionals and quantum many-body perturbation theory

All information about a quantum many-body system in thermodynamic equilibrium described by Hamiltonian $\mathcal{H}$ with a fixed average number of particles and a fixed average energy is hidden in the associated *partition function* of the *grand-canonical ensemble*, which is given by [Hua63; Tho13]

$$\mathcal{Z} = \operatorname{Tr} e^{-\beta\mathcal{H}} = \operatorname{Tr} e^{-\beta(\mathcal{H}_0+\mathcal{H}_I)} \quad . \tag{4.0.1}$$

The trace refers to the sum over all possible microstates and the temperature of the system is determined by $\beta = \frac{1}{k_B T}$ with $k_B \approx 1.38 \times 10^{-23}\,\mathrm{J\,K^{-1}}$ being the *Boltzmann constant*. The total Hamiltonian $\mathcal{H}$ is split into the non-interacting (single-particle) part $\mathcal{H}_0$ and the interacting part $\mathcal{H}_I$:

$$\mathcal{H} = \mathcal{H}_0 + \mathcal{H}_I = \sum_{\alpha,\alpha'} \underbrace{(t_{\alpha\alpha'} - \mu\delta_{\alpha\alpha'})}_{=h_{\alpha\alpha'}} c^\dagger_\alpha c_{\alpha'} + \sum_{\substack{\alpha_1,\alpha_2 \\ \alpha_1',\alpha_2'}} U_{\alpha_1,\alpha_2,\alpha_1',\alpha_2'}\, c^\dagger_{\alpha_1} c^\dagger_{\alpha_2} c_{\alpha_2'} c_{\alpha_1'} \quad . \tag{4.0.2}$$

Unfortunately, for an interacting system, the partition function is generally inaccessible since it is too hard to calculate. Henceforth, one has to rely on approximations to deduce properties of the interacting system from the partition function. One of the most frequently used approximations is based on the assumption of weak interactions and an expansion of the exponential in terms of the interacting part.

4.1. Fermionic functional integral formalism

The trace in (Equation 4.0.1) can be evaluated by means of a complete set of (fermionic) *Fock space* states $|n\rangle \in \oplus_{n=0}^{\infty} \mathcal{F}_n$, where $\mathcal{F}_n$ is the antisymmetrized n-particle Hilbert space. Employing these states in the partition function, we find

$$\mathcal{Z} = \operatorname{Tr} e^{-\beta\mathcal{H}} = \sum_n \langle n|\, e^{-\beta\mathcal{H}}\, |n\rangle \quad . \tag{4.1.1}$$

Since $|n\rangle$ contains any number of particles it is not an eigenstate of the Hamiltonian $\mathcal{H}$, in general. In order to compute the partition function as a functional integral, we

have to make use of a basis that simultaneously diagonalizes the creation and annihilation operators of the Hamiltonian $\mathcal{H}$ (Equation 4.0.2). The *fermionic coherent states* are perfectly suited to serve this purpose and are defined by [NO88a]

$$|\psi\rangle = \exp\left(-\sum_{\alpha} \psi_\alpha c_\alpha^\dagger\right)|0\rangle \quad . \tag{4.1.2}$$

The sum runs over all single-particle states α and the components ψ_α represent *Grassmann numbers*. Note, that the coherent state (Equation 4.1.2) may contain any number of particles including the vacuum state $|0\rangle$. The coherent state $|\psi\rangle$ is an eigenstate of the annihilation operator c_α, because of $c_\alpha|\psi\rangle = \psi_\alpha|\psi\rangle$ with the eigenvalues being the Grassmann fields ψ_α. In contrast, the creation operator satisfies the adjoint equation $\langle\psi| c_\alpha^\dagger = \langle\psi|\bar{\psi}_\alpha$. The coherent states feature a closure relation, i.e. they can be used to form a resolution of identity:

$$\mathbb{1} = \int \prod_{\alpha} \mathrm{d}\bar{\psi}_\alpha \mathrm{d}\psi_\alpha e^{-\sum_\alpha \bar{\psi}_\alpha \psi_\alpha} |\psi\rangle\langle\psi| \quad . \tag{4.1.3}$$

Here, the integral sign has the meaning of a linear mapping without any analogy to a Riemann integral. Inserting the closure relation of coherent states into the partition function in terms of Fock states (Equation 4.1.1) results in

$$\mathcal{Z} = \sum_n \langle n| \int \prod_{\alpha} \mathrm{d}\bar{\psi}_\alpha \mathrm{d}\psi_\alpha e^{-\sum_\alpha \bar{\psi}_\alpha \psi_\alpha} |\psi\rangle\langle\psi| e^{-\beta\mathcal{H}} |n\rangle \quad . \tag{4.1.4}$$

While the exponentials commute with $\langle n|\psi\rangle$, the inner products of Fock states and coherent states do not. It can be shown that $\langle n|\psi\rangle\langle\psi|n\rangle$ can be brought into the form $\langle -\psi|n\rangle\langle n|\psi\rangle$, where the new state $\langle -\psi| = \langle 0| e^{-\sum_\alpha \bar{\psi}_\alpha c_\alpha}$ arises from the anticommuting property of the Grassmann numbers. By exploiting the closure relation in Fock space to get rid of the $|n\rangle$ states, we end up with

$$\mathcal{Z} = \int \prod_{\alpha} \mathrm{d}\bar{\psi}_\alpha \mathrm{d}\psi_\alpha e^{-\sum_\alpha \bar{\psi}_\alpha \psi_\alpha} \langle -\psi| e^{-\beta\mathcal{H}} |\psi\rangle \quad . \tag{4.1.5}$$

Since $e^{-\beta\mathcal{H}}$ resembles the *time-evolution operator* $e^{-i\mathcal{H}/\hbar t}$, we introduce the *imaginary time* parameter τ by means of the *Wick rotation* $\tau := i\,t/\hbar$ [Wic54], which may vary in the domain $\tau \in [0, \beta]$. We adapt the idea of Feyman's path integral [Fey48; Fey49] by dividing the interval $\tau \in [0, \beta]$ into N equally spaced slices of width $\delta\tau := \frac{\beta}{N}$ and using $e^{-\beta\mathcal{H}} = \lim_{N\to\infty}\left(e^{-\frac{\beta}{N}\mathcal{H}}\right)^N$. After inserting N more closure relations (Equation 4.1.3) in between these N factors, we assume *normal ordering* in the Hamiltonian terms $\mathcal{H}$ to exploit the property of the coherent states being the eigenstates of the operators $c_\alpha^\dagger, c_\alpha$. Un-

fortunately, normal ordering will introduce an error $O((\beta/N)^2)$ due to the mixed terms that arise in second order of the expansion of $e^{-\frac{\beta}{N}\mathcal{H}}$ [FHS05; CD97; AHM08]. However, in the limit $N \to \infty$ this error is negligible. Note, that the Grassmann fields of the N closure relations acquire an additional index depending on which time slice they're associated to. In particular, the Grassmann fields are labeled with indices $j = 0, 1, 2, \ldots, N-1$, where the "initial" and "final" coherent states $\langle -\psi|$ and $|\psi\rangle$ are related and correspond to the indices $\psi = \psi^N$ and $-\psi = -\psi^N = \psi^0$. To proceed, we need the inner product of two coherent states $|\psi\rangle$ and $|\psi'\rangle$, which is given by $\langle\psi|\psi'\rangle = e^{\sum_\alpha \bar{\psi}_\alpha \psi'_\alpha}$ and is used to evaluate the overlap of the coherent states associated to consecutive time slices. By assembling all time slices, calculating their overlaps and employing the eigenvalue equations of the creation/annihilation operators of the Hamiltonian, we obtain the expression

$$\mathcal{Z} = \lim_{N\to\infty} \prod_{j=0}^{N-1} \int \prod_\alpha \mathrm{d}\bar{\psi}_\alpha^j \mathrm{d}\psi_\alpha^j e^{-\delta\tau \sum_{j=0}^{N-1} \left(\mathcal{H}(\bar{\psi}_\alpha^j, \psi_\alpha^{j+1}) + \frac{1}{\delta\tau} \sum_\alpha \bar{\psi}_\alpha^j \left(\psi_\alpha^{j+1} - \psi_\alpha^j \right) \right)} \quad . \tag{4.1.6}$$

The Hamiltonian $\mathcal{H}$ is now written in terms of Grassmann fields instead of second quantized operators. (Equation 4.1.6) shows that $\mathcal{Z}$ is calculated by sampling over all possible states for any field ψ_α^j at some particular time slice j. This process is illustrated by (Figure 4.1). By introducing the symbolic notation $\frac{\psi_\alpha^{j+1} - \psi_\alpha^j}{\delta\tau} := \partial_\tau \psi_\alpha^{j+1}$ and taking the limit $N \to \infty$, the fields ψ_α^j can be perceived as a function of τ and the exponent in (Equation 4.1.6) can be expressed by a Riemann integral. Therefore, we end up with the partition function (cf. [AS10])

$$\begin{aligned} \mathcal{Z} &= \int_{\psi(0) = -\psi(\beta)} \mathcal{D}[\bar{\psi}, \psi]\, e^{-S[\bar{\psi}, \psi]} \quad \text{with} \quad \mathcal{D}[\bar{\psi}, \psi] = \lim_{N\to\infty} \prod_{j=0}^{N-1} \int \prod_\alpha \mathrm{d}\bar{\psi}_\alpha^j \mathrm{d}\psi_\alpha^j \\ \text{and} \quad S[\bar{\psi}, \psi] &= \int_0^\beta \mathrm{d}\tau \left[\sum_\alpha \left(\bar{\psi}_\alpha(\tau) \partial_\tau \psi_\alpha(\tau) \right) + \mathcal{H}(\bar{\psi}_{\alpha'}(\tau), \psi_\alpha(\tau)) \right] \quad , \end{aligned} \tag{4.1.7}$$

with the action $S[\bar{\psi}, \psi]$. Due to the structure of the path integral the Grassmann fields in the first term of the action always involve the same single-particle state α, while the fields in the Hamiltonian $\mathcal{H}$ may differ. Hence, the Hamiltonian doesn't have to be represented in the basis which diagonalizes the single-particle term since the creation/annihilation operators simply "extract" the matching fields from the coherent states. Instead of using the domain of imaginary time, we can equally well switch to the representation

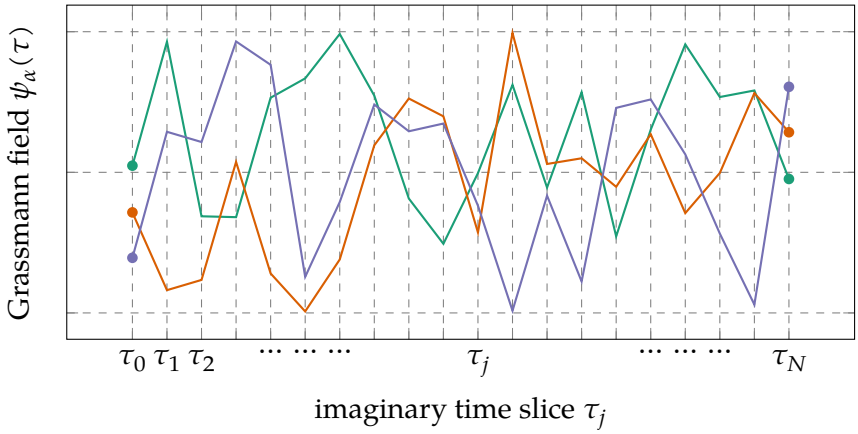

Figure 4.1.: The fermionic Grassmann fields along the imaginary time axis from $\tau = 0$ to $\tau = \beta$ have to be antiperiodic, $\psi(\tau_0 = 0) = -\psi(\tau_N = \beta)$ and are generally neither continuous nor differentiable with respect to the imaginary time parameter τ. Here, we show three different exemplary and randomly chosen paths. Note, that this illustration incorrectly assumes that a Grassmann field is (in some way) representable by a real number.

in frequency space by performing the transformation [Mat55]

$$\psi_\alpha(\tau) = \frac{1}{\sqrt{\beta}} \sum_n \psi_{\alpha n} e^{i\omega_n \tau} \qquad \psi_{\alpha n} = \frac{1}{\sqrt{\beta}} \int_0^\beta \mathrm{d}\tau \psi_\alpha(\tau) e^{-i\omega_n \tau} \tag{4.1.8a}$$

$$\bar{\psi}_\alpha(\tau) = \frac{1}{\sqrt{\beta}} \sum_n \bar{\psi}_{\alpha n} e^{-i\omega_n \tau} \qquad \bar{\psi}_{\alpha n} = \frac{1}{\sqrt{\beta}} \int_0^\beta \mathrm{d}\tau \bar{\psi}_\alpha(\tau) e^{i\omega_n \tau} \quad , \tag{4.1.8b}$$

with *Matsubara* frequencies $\omega_n = \frac{(2n+1)\pi}{\beta}$ due to the antisymmetry constraint $\psi(0) = -\psi(\beta)$. Plugging this representation into (Equation 4.1.7) we find that the "partial derivative" term results in $\frac{e^{-i\omega_n \delta\tau} - 1}{\delta\tau} \approx \frac{1 - i\omega_n \delta\tau - 1}{\delta\tau} = -i\omega_n$ up to first order. The imaginary time integral then implicitly states energy conservation by $\int_0^\beta \mathrm{d}\tau e^{-i(\omega_{n'} - \omega_n)\tau} = \beta\delta(\omega_{n'} - \omega_n)$ and $\int_0^\beta \mathrm{d}\tau e^{-i(\omega_{n'_1} + \omega_{n'_2} - \omega_{n_1} - \omega_{n_2})\tau} = \beta\delta(\omega_{n'_1} + \omega_{n'_2} - \omega_{n_1} - \omega_{n_2})$. Assuming a Hamiltonian with single-particle term $h_{\alpha\alpha'}$ and interaction $V_{\alpha_1\alpha_2\alpha'_1\alpha'_2}$ (Equation 4.0.2),

the entire path integral is given by

$$\mathcal{Z} = \int \mathcal{D}[\bar{\psi},\psi]\, e^{-S[\bar{\psi},\psi]} \quad \text{where} \quad \mathcal{D}[\bar{\psi},\psi] = \lim_{N\to\infty} \prod_{n=0}^{N} \prod_{\alpha,\alpha'} \mathrm{d}\bar{\psi}_{\alpha n} \mathrm{d}\psi_{\alpha n} \tag{4.1.9a}$$

$$\text{and} \quad S[\bar{\psi},\psi] = \sum_{\alpha,\alpha'} \sum_{n} \bar{\psi}_{\alpha' n} \left(-i\omega_n \delta_{\alpha\alpha'} + h_{\alpha'\alpha}\right) \psi_{\alpha n} + \frac{1}{\beta} \sum_{\substack{\alpha_1,\alpha_2 \\ \alpha_1',\alpha_2'}} \sum_{n_1,n_2} V_{\alpha_1\alpha_2\alpha_1'\alpha_2'} \bar{\psi}_{\alpha_1' n_1'} \bar{\psi}_{\alpha_2' n_2'} \psi_{\alpha_2 n_2} \psi_{\alpha_1 n_1} \quad . \tag{4.1.9b}$$

The Jacobian of the transformation to frequency representation is unity [Sha94b]. Note, that we omitted the factor $e^{-i\omega_n \delta\tau}$ in the quadratic and $e^{-i(\omega_{n_1}+\omega_{n_2})\delta\tau}$ in the quartic term of the action, which occur due to the fact that the fields ψ_α are evaluated at infinitesimal later imaginary time than $\bar{\psi}_\alpha$. These factors will, of course, cancel in the limit $N \to \infty$ but may, however, become important if the path integral suffers from convergence issues (cf. [Sha94b, Section III. C]). Note, that there is some arbitrariness to the definition of the fields in Matsubara representation. Another popular choice for the fields, in contrast to (Equation 4.1.8a) and (Equation 4.1.8b), is given by shifting the normalization entirely to the summation resulting in $\psi_\alpha(\tau) = \frac{1}{\beta}\sum_n \psi_{\alpha n} e^{i\omega_n \tau}$ and $\psi_{\alpha n} = \int_0^\beta \mathrm{d}\tau \psi_\alpha(\tau) e^{-i\omega_n \tau}$. As a consequence, both non-interacting and interacting part of the action require a temperature dependent normalization which is $\frac{1}{\beta}$ for the non-interacting and $\frac{1}{\beta^3}$ for the interacting action (in contrast to (Equation 4.1.9b)).

4.2. Generating functionals

In the previous section, we derived the coherent state path integral formulation of the partition function $\mathcal{Z}$ that featured an action of the form

$$S[\bar{\psi},\psi] = S_0[\bar{\psi},\psi] + S_I[\bar{\psi},\psi] \quad , \tag{4.2.1}$$

with the non-interacting part

$$S_0[\bar{\psi},\psi] = \sum_{\alpha,\alpha'} \sum_{n} \bar{\psi}_{\alpha' n} \left(-i\omega_n \delta_{\alpha\alpha'} + h_{\alpha'\alpha}\right) \psi_{\alpha n} \coloneqq \left(\bar{\psi}, G_0^{-1}\psi\right) \quad , \tag{4.2.2}$$

and the interacting part

$$S_I[\bar{\psi},\psi] = \frac{1}{\beta}\sum_{\substack{\alpha_1,\alpha_2\\ \alpha_1',\alpha_2'}}\sum_{\substack{n_1,n_2\\ n_1',n_2'}} V_{\alpha_1\alpha_2\alpha_1'\alpha_2'}\bar{\psi}_{\alpha_1' n_1'}\bar{\psi}_{\alpha_2' n_2'}\psi_{\alpha_2 n_2}\psi_{\alpha_1 n_1} \quad . \tag{4.2.3}$$

We assumed that both single-particle Hamiltonian $h_{\alpha'\alpha}$ and interaction $V_{\alpha_1\alpha_2\alpha_1'\alpha_2'}$ are independent of frequency. The notation $(\ldots,\ldots)$ represents the fermionic bilinear form $(\bar{\psi},\psi) = \int_\alpha \bar{\psi}_\alpha\psi_\alpha$, where $\int_\alpha$ is the integral/sum over appropriate quantum numbers [SH01]. The *free propagator* G_0 is defined by its inversion and given by $G_0(i\omega_n,\alpha,\alpha') = (-i\omega_n\delta_{\alpha\alpha'} + h_{\alpha'\alpha})^{-1}$. Going to the basis $\bar{\phi}_{\tilde{\alpha}n} = \bar{\psi}_{\alpha n}U^\dagger_{\tilde{\alpha}\alpha}$, $\phi_{\tilde{\alpha}n} = U_{\tilde{\alpha}\alpha}\psi_{\alpha n}$ (with $U^\dagger_{\tilde{\alpha}\alpha}U_{\tilde{\alpha}\alpha} = \mathbb{1}$) that diagonalizes the single-particle term, the free propagator can be written as

$$G_0(i\omega_n,\tilde{\alpha},\tilde{\alpha}') = \frac{1}{-i\omega_n + \xi_{\tilde{\alpha}}}\delta_{\tilde{\alpha}\tilde{\alpha}'} \quad \text{with} \quad \xi_{\tilde{\alpha}}\delta_{\tilde{\alpha}\tilde{\alpha}'} = U_{\tilde{\alpha}'\alpha'}h_{\alpha'\alpha}U^\dagger_{\tilde{\alpha}\alpha} \quad . \tag{4.2.4}$$

In order to compute *correlation functions*, we make use of several kinds of *generating functionals*. Among the commonly used generating functionals are the generating functionals $\mathcal{G}$ and $\mathcal{G}_c$ of the disconnected and connected Green functions, the generating functional $\mathcal{U}$ of amputated connected Green functions (also known as effective interaction [Sal99]) and the effective action Γ, which generates *one-particle irreducible vertex* functions. A generating functional is defined by introducing additional *source fields* into the partition function (Equation 4.1.9a). By deriving with respect to these source fields, one can produce any correlation function. The generating functional of disconnected Green functions is simply

$$\mathcal{G}[\bar{\eta},\eta] = \frac{1}{\mathcal{Z}}\int \mathcal{D}[\bar{\psi},\psi]\, e^{-S[\bar{\psi},\psi]-(\bar{\eta},\psi)-(\bar{\psi},\eta)} \quad , \tag{4.2.5}$$

where $\bar{\eta}$, η are the source fields, which are coupled to the "sampled" fields $\bar{\psi}$, ψ by the additional terms $(\bar{\eta},\psi)$ and $(\bar{\psi},\eta)$. The functional integral is normalized with the interacting partition function $\mathcal{Z} = \int \mathcal{D}[\bar{\psi},\psi]\, e^{-S[\bar{\psi},\psi]}$. (Equation 4.2.5) is employed to generate n-particle disconnected Green functions $G^{(n)}$ by taking functional derivatives with respect to the source fields [NO88a]

$$\begin{aligned} G^{(2n)}\left(\alpha_1',\ldots,\alpha_n';\alpha_1,\ldots,\alpha_n\right) &= (-1)^n\left\langle \psi_{\alpha_1'}\ldots\psi_{\alpha_n'}\bar{\psi}_{\alpha_n}\ldots\bar{\psi}_{\alpha_1}\right\rangle \\ &= \frac{\delta^{2n}\mathcal{G}[\bar{\eta},\eta]}{\delta\bar{\eta}_{\alpha_1'}\ldots\delta\bar{\eta}_{\alpha_n'}\delta\eta_{\alpha_n}\ldots\delta\eta_{\alpha_1}}\Big|_{\eta=\bar{\eta}=0} \quad . \end{aligned} \tag{4.2.6}$$

The n prefactors of (-1) originate from anticommuting Grassmann fields and functional derivative operators, i.e. $\delta_\eta(\bar{\psi},\eta) = -\bar{\psi}$. Taking higher order correlation functions of (Equation 4.2.6), it becomes apparent that these are comprised of disconnected parts. The *linked cluster theorem* states that the connected parts of $G^{(2n)}$ are obtained by

collecting terms that are proportional to n [NO88a]. This requires the generating functional of connected Green functions $\mathcal{G}_c[\bar{\eta}, \eta]$ to be defined as

$$\mathcal{G}_c[\bar{\eta}, \eta] = \ln\left[\frac{\mathcal{Z}}{\mathcal{Z}_0}\mathcal{G}[\bar{\eta}, \eta]\right] \quad , \tag{4.2.7}$$

with $\mathcal{Z}_0 = \int \mathcal{D}[\bar{\psi}, \psi] e^{-S_0[\bar{\psi}, \psi]}$ being the non-interacting partition function. The generating functionals of disconnected and connected Green functions serve as a prerequisite for the definition of the effective action Γ, which is defined in terms of $\mathcal{G}_c$ and given by [PS10]

$$\Gamma[\bar{\phi}, \phi] = -\mathcal{G}_c[\bar{\eta}, \eta] - (\bar{\phi}, \eta) - (\bar{\eta}, \phi) + (\bar{\phi}, G_0^{-1}\phi) \quad . \tag{4.2.8}$$

The effective action depends on the average fields $\bar{\phi}$ and ϕ, which are

$$\phi = \langle\psi\rangle_{\eta,\bar{\eta}} = -\frac{\delta\mathcal{G}_c[\bar{\eta}, \eta]}{\delta\bar{\eta}} \qquad \bar{\phi} = \langle\bar{\psi}\rangle_{\eta,\bar{\eta}} = \frac{\delta\mathcal{G}_c[\bar{\eta}, \eta]}{\delta\eta} \tag{4.2.9}$$

The notation $\langle\ldots\rangle_{\eta,\bar{\eta}}$ indicates an expectation value that is *not* obtained by setting the source fields to zero after the functional derivative but by keeping them finite. (Equation 4.2.8) and (Equation 4.2.9) show that the definition of the effective action $\Gamma[\bar{\phi}, \phi]$ amounts to the Legendre transform of the generating functional of the connected Green functions $\mathcal{G}_c[\bar{\eta}, \eta]$. The former source fields η, $\bar{\eta}$ now depend on the average fields $\bar{\phi}$, ϕ. Their dependency $\bar{\eta} = \bar{\eta}(\phi)$ and $\eta = \eta(\bar{\phi})$ is determined by inversion of (Equation 4.2.9). The one-particle irreducible vertex functions are straightforwardly given by

$$\gamma^{(2n)}\left(\alpha_1', \ldots, \alpha_n'; \alpha_1, \ldots, \alpha_n\right) = \left.\frac{\delta^{(2n)}\Gamma[\bar{\phi}, \phi]}{\delta\bar{\phi}_{\alpha_1'} \ldots \delta\bar{\phi}_{\alpha_n'}\delta\phi_{\alpha_n} \ldots \delta\phi_{\alpha_1}}\right|_{\bar{\phi}=\phi=0} \tag{4.2.10}$$

The set of *flow equations* that are derived in (Chapter 6) are the ones for the one-particle irreducible vertex functions, which are entirely given in terms of the effective action (Equation 4.2.8) [Met+12a]. As a useful ingredient for the formulation of this flow equation, we derive the *reciprocity relations* and the *tree expansion*, which relate certain functional derivatives of the generating functional of connected Green functions to functional derivatives of the effective action [KBS10]. The first derivative of the effective action (Equation 4.2.8) with respect to the field ϕ_α results in

$$\frac{\delta\Gamma\left[\bar{\phi},\phi\right]}{\delta\phi_\alpha} = -\int_\beta \frac{\delta\mathcal{G}_c\left[\bar{\eta},\eta\right]}{\delta\bar{\eta}_\beta}\frac{\delta\bar{\eta}_\beta}{\delta\phi_\alpha} - \int_\beta \frac{\delta\mathcal{G}_c\left[\bar{\eta},\eta\right]}{\delta\eta_\beta}\frac{\delta\eta_\beta}{\delta\phi_\alpha} - \int_\beta \bar{\phi}_\beta\left(-\frac{\delta\eta_\beta}{\delta\phi_\alpha}\right)$$
$$- \int_\beta \frac{\delta\bar{\eta}_\beta}{\delta\phi_\alpha}\phi_\beta - \int_\beta \bar{\eta}_\beta \underbrace{\left(-\frac{\delta\phi_\beta}{\delta\phi_\alpha}\right)}_{=\delta(\beta-\alpha)} + \int_\beta\int_\gamma \bar{\phi}_\beta \left(G_0^{-1}\right)_{\beta\gamma} \underbrace{\left(-\frac{\delta\phi_\gamma}{\delta\phi_\alpha}\right)}_{=\delta(\gamma-\alpha)} \quad . \tag{4.2.11}$$

Employing the definition (Equation 4.2.9) of the fields, we see that the first four terms cancel. The analogous derivative with respect to the adjoint field $\bar{\phi}_\alpha$ completes the *reciprocity relations* [NO88b]

$$\frac{\delta\Gamma\left[\bar{\phi},\phi\right]}{\delta\phi} = \bar{\eta} - \left(G_0^{-1}\right)^T\bar{\phi} \qquad \frac{\delta\Gamma\left[\bar{\phi},\phi\right]}{\delta\bar{\phi}} = -\eta + G_0^{-1}\phi \tag{4.2.12}$$

To find the lowest order tree expansion, we employ the identities $\delta(\alpha-\beta) = \frac{\delta\phi_\alpha}{\delta\phi_\beta}$, $0 = \frac{\delta\bar{\phi}_\alpha}{\delta\phi_\beta}$, the definition of fields (Equation 4.2.9) and the Legendre correspondence between $\mathcal{G}_c\left[\bar{\eta},\eta\right]$ and the effective action. The resulting second functional derivatives can be expressed in matrix form by (cf. [Met+12b])

$$\int_\gamma \underbrace{\begin{pmatrix} \frac{\delta^2\mathcal{G}_c}{\delta\bar{\eta}_\gamma\delta\eta_\alpha} & -\frac{\delta^2\mathcal{G}_c}{\delta\eta_\gamma\delta\eta_\alpha} \\ -\frac{\delta^2\mathcal{G}_c}{\delta\bar{\eta}_\gamma\delta\bar{\eta}_\alpha} & \frac{\delta^2\mathcal{G}_c}{\delta\eta_\gamma\delta\bar{\eta}_\alpha}\end{pmatrix}}_{:=G_c^{(2)}} \underbrace{\begin{pmatrix} \frac{\delta^2\Gamma}{\delta\bar{\phi}_\beta\delta\phi_\gamma} + \left(G_0^{-1}\right)_{\beta\gamma} & \frac{\delta^2\Gamma}{\delta\phi_\beta\delta\phi_\gamma} \\ \frac{\delta^2\Gamma}{\delta\bar{\phi}_\beta\delta\bar{\phi}_\gamma} & \frac{\delta^2\Gamma}{\delta\phi_\beta\delta\bar{\phi}_\gamma} - \left(G_0^{-1}\right)^T_{\beta\gamma}\end{pmatrix}}_{:=\boldsymbol{\gamma}^{(2)}} = \mathbb{1}\cdot\delta\left(\alpha-\beta\right) \quad , \tag{4.2.13}$$

which shows i.a. that the two-leg one-particle irreducible vertex function amounts to the negative of the irreducible self-energy.

4.3. Berezin integrals and Wick's theorem

The n-particle correlation functions (Equation 4.2.6) we encountered in the previous section can in general not be computed directly since the interacting partition function $\mathcal{Z}$ is unknown. Therefore, we have to rely on perturbative expansions of the partition function in order to calculate these correlation functions approximately (see (Section 4.4)). As an essential ingredient of these perturbative expansion, we will encounter *non-interacting* expectation values involving any number of fields, which have the form

$$\left\langle \psi_{\alpha_1'} \ldots \psi_{\alpha_n'} \bar{\psi}_{\alpha_n} \ldots \bar{\psi}_{\alpha_1} \right\rangle_0 \quad \text{with} \quad \langle \ldots \rangle = \frac{1}{\mathcal{Z}_0}\int \mathcal{D}\left[\bar{\psi},\psi\right] \ldots e^{-S_0[\bar{\psi},\psi]} \quad , \tag{4.3.1}$$

and can be calculated analytically. Taking the functional integral measure (Equation 4.1.9a) and the definition of the free action (Equation 4.1.9b) into account, the integral is given by

$$\int \mathcal{D}[\bar{\psi},\psi]\, e^{-S_0[\bar{\psi},\psi]} = \lim_{N\to\infty} \prod_{n=0}^{N} \prod_{\alpha,\alpha'} \int \mathrm{d}\bar{\psi}_{\alpha,n} \mathrm{d}\psi_{\alpha,n} e^{-\sum_{\alpha,\alpha'} \sum_n \bar{\psi}_{\alpha' n} G_0^{-1}(i\omega_n,\alpha',\alpha)\psi_{\alpha n}} \quad , \tag{4.3.2}$$

which is an infinite product of integrals of the form

$$\int \mathrm{d}\bar{\psi}\mathrm{d}\psi e^{-a\bar{\psi}\psi} = \int \mathrm{d}\bar{\psi}\mathrm{d}\psi\ (1 - a\bar{\psi}\psi) = -a \int \mathrm{d}\bar{\psi}\mathrm{d}\psi\ (-\psi\bar{\psi}) = a \quad \text{with} \quad a \in \mathbb{C} \quad . \tag{4.3.3}$$

We used $\int \mathrm{d}\psi\, \psi = 1$ and $\int \mathrm{d}\psi\, 1 = 0$ [Ber66; MS10a; Zin05] and the additional minus sign originates from the anticommutation of Grassmann fields and their differentials. The generalization of the *Berezin integral* to a set of fields $\psi = (\psi_1, \psi_2, \dots, \psi_N)$, $\bar{\psi} = (\bar{\psi}_1, \bar{\psi}_2, \dots, \bar{\psi}_N)$ and $A \in \mathbb{C}^{N\times N}$ is (cf. [Str14])

$$\prod_{n=1}^{N} \int \mathrm{d}\bar{\psi}_n \mathrm{d}\psi_n\, e^{-\sum_{ij}^{N} \bar{\psi}_i A_{ij} \psi_j} = \det A \quad . \tag{4.3.4}$$

Note, that in this case the expansion of the exponential does not terminate at linear but at N-th order. This is because at n-th order we have terms of $2n$ fields and there are $2N$ different Grassmann fields available. Therefore, at N-th order every field appears exactly once in the finite terms, while at $N+1$-th order some fields must appear twice in every term, which therefore vanish. Furthermore, only the terms that feature every field exactly once survive the integration. The structure of the coefficients A_{ij} resembles the *Laplacian determinant expansion* [AW05]. For instance, for $N = 2$ we find

$$\begin{aligned} e^{-\sum_{ij}^{N=2} \bar{\psi}_i A_{ij} \psi_j} &= 1 - \bar{\psi}_1 A_{11} \psi_1 - \bar{\psi}_1 A_{12} \psi_2 - \bar{\psi}_2 A_{21} \psi_1 - \bar{\psi}_2 A_{22} \psi_2 \\ &\quad + \frac{1}{2}\, \bar{\psi}_1 \psi_1 \bar{\psi}_2 \psi_2\, 2\,(A_{11}A_{22} - A_{21}A_{12}) \quad . \end{aligned} \tag{4.3.5}$$

Next, we have to consider additional linear terms in the exponent to take care of the source fields necessary to produce non-vacuum expectation values. Hence, we now have the Berezin integral

$$\prod_{n=1}^{N} \int \mathrm{d}\bar{\psi}_n \mathrm{d}\psi_n\, e^{-\sum_{ij}^{N} \bar{\psi}_i A_{ij} \psi_j + \bar{\psi}_i \eta_i + \bar{\eta}_i \psi_i} \quad \text{with} \quad . \tag{4.3.6}$$

Since the Berezin integral exhibits translation invariance, we can easily solve this integral by a shift of variables [Wip09]. First, we introduce the additional term $\sum_{ij} \bar{\eta}_i A^{-1}_{ij} \eta_j$, which transforms the exponent into

$$\sum_{ij}^{N} \bar{\psi}_i A_{ij} \psi_j + \bar{\psi}_i \eta_i + \bar{\eta}_i \psi_i + \bar{\eta}_i A^{-1}_{ij} \eta_j - \bar{\eta}_i A^{-1}_{ij} \eta_j = \sum_{ij}^{N} \left(\bar{\psi} - \bar{\eta} A^{-1}\right)_i A_{ij} \left(\psi - A^{-1}\eta\right)_j - \bar{\eta}_i A^{-1}_{ij} \eta_j \quad .$$

The Jacobian for the new variables $\bar{\psi} - \bar{\eta}A^{-1}$ and $\psi - A^{-1}\eta$ is unity. Therefore, we can simply rename the fields to be integrated, employ (Equation 4.3.4) and find

$$\prod_{n=1}^{N} \int \mathrm{d}\bar{\psi}_n \mathrm{d}\psi_n \, e^{-\sum_{ij}^{N} \bar{\psi}_i A_{ij} \psi_j + \bar{\psi}_i \eta_i + \bar{\eta}_i \psi_i} = \det A \, e^{-\sum_{ij}^{N} \bar{\eta}_i A^{-1}_{ij} \eta_j} \quad . \tag{4.3.7}$$

Now, we take the limit $N \to \infty$ and resort to the notation for inner products introduced in (Section 4.2), resulting in

$$\int \mathcal{D}[\bar{\psi}, \psi] \; e^{-(\bar{\psi}, A\psi) + (\bar{\psi}, \eta) + (\bar{\eta}, \psi)} = \det A \, e^{(\bar{\eta}, A^{-1}\eta)} \quad . \tag{4.3.8}$$

This integral represents the origin of all non-interacting fermionic correlation functions. We give it a try by ditching some source fields $\bar{\eta}$, η by several functional derivatives on both sides of (Equation 4.3.8) and setting the source fields to zero afterwards. Any odd number of functional derivatives with respect to $\bar{\eta}$, η will produce zero. For an even number, for instance, 2, we obtain

$$\begin{aligned} &\frac{\delta^2}{\delta\bar{\eta}_\alpha \delta\eta_{\alpha'}} \int \mathcal{D}[\bar{\psi}, \psi] \; e^{-(\bar{\psi}, A\psi) + (\bar{\psi}, \eta) + (\bar{\eta}, \psi)} \Big|_{\bar{\eta}=\eta=0} = \frac{\delta^2}{\delta\bar{\eta}_\alpha \delta\eta_{\alpha'}} \det A \, e^{(\bar{\eta}, A^{-1}\eta)} \Big|_{\bar{\eta}=\eta=0} \\ \Leftrightarrow &\int \mathcal{D}[\bar{\psi}, \psi] \; e^{-(\bar{\psi}, A\psi)} \bar{\psi}_{\alpha'} \psi_\alpha = \det A \, A^{-1}_{\alpha', \alpha} \quad . \end{aligned} \tag{4.3.9}$$

Note, that in this notation the *functional derivative* acts as

$$\frac{\delta}{\delta\eta_\alpha} (\bar{\psi}, \eta) = \frac{\delta}{\delta\eta_\alpha} \int_{\alpha'} \bar{\psi}_{\alpha'} \eta_{\alpha'} = -\int_{\alpha'} \bar{\psi}_{\alpha'} \underbrace{\frac{\delta\eta_{\alpha'}}{\delta\eta_\alpha}}_{\delta(\alpha - \alpha')} = -\bar{\psi}_\alpha \quad . \tag{4.3.10}$$

The generalization of (Equation 4.3.9) to an arbitrary (but even) number of fields $\bar{\psi}_{\alpha'}$, ψ_α involves a sum of terms given by elements of A^{-1}, whose sign is determined by the necessary permutations of functional derivatives and features all distinct pairs of the fields $\bar{\psi}_{\alpha'}$, ψ_α. Getting back to (Equation 4.3.1), we have the result of *Wick's theorem* [Wic50]

$$\left\langle \psi_{\alpha'_1} \dots \psi_{\alpha'_n} \bar{\psi}_{\alpha_n} \dots \bar{\psi}_{\alpha_1} \right\rangle_0 = \sum_{\text{all pairs}} (-1)^{n_{\mathcal{P}}} \left\langle \psi_{\alpha'_{\mathcal{P}(1)}} \bar{\psi}_{\alpha_{\mathcal{P}(1)}} \right\rangle_0 \dots \left\langle \psi_{\alpha'_{\mathcal{P}(n)}} \bar{\psi}_{\alpha_{\mathcal{P}(n)}} \right\rangle_0 \quad , \quad (4.3.11)$$

where the sign is determined by the number of permutations of anticommuting fields (anticommutations).

4.4. Perturbation theory

The starting point for perturbative calculations of correlation functions are the generating functionals in (Section 4.2), which are defined in terms of the functional integral partition function $\mathcal{Z}$. For instance, the generating functional of disconnected Green functions (Equation 4.2.5)

$$\mathcal{G}[\bar{\eta}, \eta] = \frac{1}{\mathcal{Z}} \int \mathcal{D}[\bar{\psi}, \psi] \, e^{-S_0[\bar{\psi},\psi] - S_I[\bar{\psi},\psi] - (\bar{\eta},\psi) - (\bar{\psi},\eta)} \quad , \quad (4.4.1)$$

basically consists of the interacting partition function $\mathcal{Z}$ and features the external sources $\bar{\eta}$, η coupled to the fields $\bar{\psi}, \psi$. Before we proceed, we will (Equation 4.1.9b) and introduce a more general and more convenient notation for the non-interacting and interacting action. The free action is given by

$$S_0[\bar{\psi}, \psi] = \int_{(K,\alpha,\alpha')} \left(G_0^{-1}(K) \right)_{\alpha\alpha'} \bar{\psi}_{K\alpha} \psi_{K\alpha'} \quad , \quad (4.4.2)$$

including the single-particle propagator

$$(G_0(K))^{-1}_{\alpha\alpha'} = -i\omega_n \delta_{\alpha\alpha'} + h_{\alpha'\alpha}(\mathbf{k}) \quad . \quad (4.4.3)$$

Here, we defined the multiindex $K = (i\omega_n, \mathbf{k})$ denoting both Matsubara frequency $i\omega_n$ and momentum $\mathbf{k}$. In correspondence with (Section 3.3), any remaining quantum numbers like sublattice, orbital and spin $\alpha = (s, o, \sigma)$ are hidden in the multiindex α. We assume $h_{\alpha'\alpha}$ to be independent of frequency. The interacting action is taken to consist of a two-particle interaction, only, which is

$$S_I[\bar{\psi}, \psi] = \frac{1}{\beta} \int_{\substack{(K_1,\alpha_1),(K_2,\alpha_2) \\ (K'_1,\alpha'_1),(K'_2,\alpha'_2)}} \Gamma(K_1, K_2, K'_1, K'_2)_{\alpha_1\alpha_2,\alpha'_1\alpha'_2} \, \bar{\psi}_{K'_1\alpha'_1} \bar{\psi}_{K'_2\alpha'_2} \psi_{K_2\alpha_2} \psi_{K_1\alpha_1} \quad . \quad (4.4.4)$$

Every integral $\int_{(K,\alpha)}$ indicates the summation $(i\omega_n, s, o, \sigma)$ and integration $(\mathbf{k})$ of appropriate quantum numbers and is normalized by (cf. (Equation 4.1.8a) and (Equation 4.1.8b))

$$\int_{(K,\alpha)} = \sum_{\omega_n} \frac{1}{\Omega} \int_{\mathbf{k}\in\Omega} \sum_{s} \sum_{o} \sum_{\sigma} \quad , \tag{4.4.5}$$

where Ω denotes the volume of the 1st Brillouin zone. Since the only correlation functions, which can be evaluated exactly are the non-interacting ones, we rely on an expansion of the exponential of the interacting part of the action. Hence, the partition function is expressed as

$$\mathcal{Z} = \int \mathcal{D}[\bar{\psi},\psi]\, e^{-S[\bar{\psi},\psi]} = \int \mathcal{D}[\bar{\psi},\psi]\, e^{-S_0[\bar{\psi},\psi]} e^{-S_I[\bar{\psi},\psi]} = \mathcal{Z}_0 \left\langle e^{-S_I[\bar{\psi},\psi]} \right\rangle_0 \quad , \tag{4.4.6}$$

where we used the definition of the non-interacting expectation value (Equation 4.3.1). The perturbation expansion amounts to a functional Taylor expansion of the exponential in terms of the interacting action

$$\frac{\mathcal{Z}}{\mathcal{Z}_0} = \left\langle \sum_{\nu=0}^{\infty} \frac{(-1)^\nu}{\nu!} \left(S_I[\bar{\psi},\psi]\right)^\nu \right\rangle_0 \quad . \tag{4.4.7}$$

Before we check out the first few orders of the series by plugging in the action (Equation 4.4.4), the indices of $\Gamma(K_1,K_2,K_1',K_2')_{\alpha_1\alpha_2\alpha_1'\alpha_2'}$ are reduced to $\Gamma_{\alpha_1\alpha_2\alpha_1'\alpha_2'}$ for the sake of simplicity. Up to second order in S_I, (Equation 4.4.7) is given by

$$\begin{aligned}\frac{\mathcal{Z}}{\mathcal{Z}_0} = \langle 1\rangle_0 &- \frac{1}{\beta} \int_{\substack{\alpha_1,\alpha_2\\ \alpha_1',\alpha_2'}} \Gamma_{\alpha_1\alpha_2\alpha_1'\alpha_2'} \left\langle \bar{\psi}_{\alpha_1'} \bar{\psi}_{\alpha_2'} \psi_{\alpha_2} \psi_{\alpha_1} \right\rangle_0 \\ &+ \frac{1}{2\beta^2} \int_{\substack{\alpha_1,\alpha_2\\ \alpha_1',\alpha_2'}} \int_{\substack{\alpha_3,\alpha_4\\ \alpha_3',\alpha_4'}} \Gamma_{\alpha_1\alpha_2\alpha_1'\alpha_2'} \Gamma_{\alpha_3\alpha_4\alpha_3'\alpha_4'} \left\langle \bar{\psi}_{\alpha_1'} \bar{\psi}_{\alpha_2'} \psi_{\alpha_2} \psi_{\alpha_1} \bar{\psi}_{\alpha_3'} \bar{\psi}_{\alpha_4'} \psi_{\alpha_4} \psi_{\alpha_3} \right\rangle_0 + O(\beta^{-3}) \quad .\end{aligned} \tag{4.4.8}$$

By virtue of *Wick's theorem* (Equation 4.3.11), the non-interacting averages are evaluated to yield all possible contractions of the four and eight fields, respectively. In first order, we find

$$\left\langle \bar{\psi}_{\alpha_1'} \bar{\psi}_{\alpha_2'} \psi_{\alpha_2} \psi_{\alpha_1} \right\rangle_0 = \left\langle \bar{\psi}_{\alpha_2'} \psi_{\alpha_2} \right\rangle_0 \left\langle \bar{\psi}_{\alpha_1'} \psi_{\alpha_1} \right\rangle_0 - \left\langle \bar{\psi}_{\alpha_1'} \psi_{\alpha_2} \right\rangle_0 \left\langle \bar{\psi}_{\alpha_2'} \psi_{\alpha_1} \right\rangle_0 \quad . \tag{4.4.9}$$

The contractions of the second order term including eight fields result in $4! = 24$ terms, which are given by

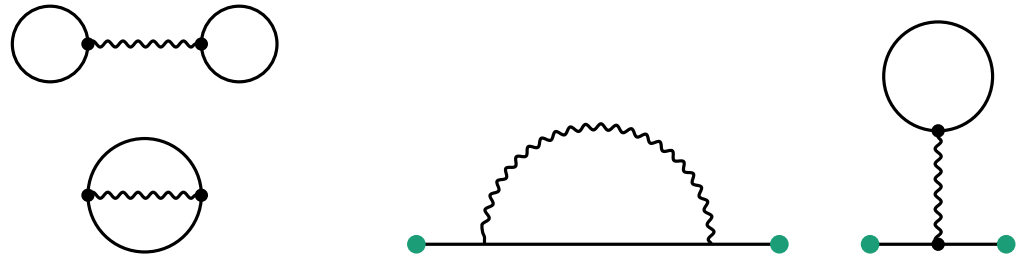

(a) (b)

Figure 4.2.: The two vacuum diagrams in (Figure 4.2a) correspond to the first order contributions to the perturbative expansion of the partition function. Here, the wavy line represents the two-particle interaction $\Gamma_{\alpha_1\alpha_2\alpha_1'\alpha_2'}$ and all solid lines are free fermionic propagators. All external legs are indicated by colored dots. The expansion of the 2-point function in first order features two connected and irreducible diagrams, given in (Figure 4.2b) (cf. [AGD12, Sec. 3 p.113]).

$$\begin{aligned}\left\langle \bar{\psi}_{\alpha_1'}\bar{\psi}_{\alpha_2'}\bar{\psi}_{\alpha_3'}\bar{\psi}_{\alpha_4'}\psi_{\alpha_2}\psi_{\alpha_1}\psi_{\alpha_3}\psi_{\alpha_4}\right\rangle_0 &= \left\langle \bar{\psi}_{\alpha_4'}\psi_{\alpha_2}\right\rangle_0\left\langle \bar{\psi}_{\alpha_3'}\psi_{\alpha_1}\right\rangle_0\left\langle \bar{\psi}_{\alpha_2'}\psi_{\alpha_3}\right\rangle_0\left\langle \bar{\psi}_{\alpha_1'}\psi_{\alpha_4}\right\rangle_0 \\ &\quad - \left\langle \bar{\psi}_{\alpha_3'}\psi_{\alpha_2}\right\rangle_0\left\langle \bar{\psi}_{\alpha_4'}\psi_{\alpha_1}\right\rangle_0\left\langle \bar{\psi}_{\alpha_2'}\psi_{\alpha_3}\right\rangle_0\left\langle \bar{\psi}_{\alpha_1'}\psi_{\alpha_4}\right\rangle_0 \\ &\quad + \ldots \quad \text{22 more terms} \quad \ldots \quad . \end{aligned} \tag{4.4.10}$$

Taking (Equation 4.3.9) into account, we find that the expectation values involving two fields are matrix elements of the free propagator G_0, i.e.

$$\langle \bar{\psi}_{\alpha'}\psi_{\alpha}\rangle_0 = \frac{1}{Z_0}\int \mathcal{D}[\bar{\psi},\psi]\,\bar{\psi}_{\alpha'}\psi_{\alpha}e^{-S_0[\bar{\psi},\psi]} = \left(G_0(K)\right)_{\alpha'\alpha} \quad . \tag{4.4.11}$$

To go beyond the *vacuum diagrams*, we employ the generating functional of disconnected Green functions (Equation 4.2.5) to generate the 2-point (disconnected) Green function and its expansion:

$$G^{(2)}\left(\mu_1',\mu_1\right) = -\left\langle \psi_{\mu_1'}\bar{\psi}_{\mu_1}\right\rangle = \frac{1}{Z}\int \mathcal{D}[\bar{\psi},\psi]\,\psi_{\mu_1'}\bar{\psi}_{\mu_1}e^{-S[\bar{\psi},\psi]} = \frac{Z_0}{Z}\left\langle \psi_{\mu_1'}\bar{\psi}_{\mu_1}e^{-S_I[\bar{\psi},\psi]}\right\rangle_0 \quad , \tag{4.4.12}$$

Up to linear order of the expansion we find the following contributions:

$$\frac{Z_0}{Z}\left\langle \psi_{\mu_1'}\bar{\psi}_{\mu_1}e^{-S_I[\bar{\psi},\psi]}\right\rangle_0 = \frac{Z_0}{Z}\left(\left\langle \psi_{\mu_1'}\bar{\psi}_{\mu_1}\right\rangle_0 - \frac{1}{\beta}\int_{\substack{\alpha_1,\alpha_2\\ \alpha_1',\alpha_2'}} \Gamma_{\alpha_1,\alpha_2,\alpha_1',\alpha_2'}\left\langle \psi_{\mu_1'}\bar{\psi}_{\mu_1}\bar{\psi}_{\alpha_1'}\bar{\psi}_{\alpha_2'}\psi_{\alpha_2}\psi_{\alpha_1}\right\rangle_0 + \dots\right)$$

$$= \frac{Z_0}{Z}\Bigg(\left(G_0(K)\right)_{\mu_1',\mu_1} - \frac{1}{\beta}\int_{\substack{\alpha_1,\alpha_2\\ \alpha_1',\alpha_2'}} \Gamma_{\alpha_1,\alpha_2,\alpha_1',\alpha_2'}\Big(\left\langle \bar{\psi}_{\mu_1'}\psi_{\mu_1}\right\rangle_0\left\langle \bar{\psi}_{\alpha_1'}\psi_{\alpha_1}\right\rangle_0\left\langle \bar{\psi}_{\alpha_2'}\psi_{\alpha_2}\right\rangle_0$$
$$-\left\langle \bar{\psi}_{\mu_1'}\psi_{\alpha_2}\right\rangle_0\left\langle \bar{\psi}_{\alpha_1'}\psi_{\alpha_1}\right\rangle_0\left\langle \bar{\psi}_{\alpha_2'}\psi_{\mu_1}\right\rangle_0 + \dots 4 \text{ more terms} \dots\Big)\Bigg) \quad . \tag{4.4.13}$$

The six terms in linear order comprise two disconnected and four connected diagrams. However, taking the prefactor $\frac{Z_0}{Z}$ and its expansion in terms of vacuum diagrams into account, it turns out that all disconnected parts are canceled. The connected diagrams can be further divided into *reducible* and *irreducible* ones, where the irreducible diagrams - produced by means of the *effective action* - *cannot* be separated into two parts by cutting a single propagator line [AGD12; Kle16]. The diagrammatic representation of first order vacuum graphs and connected (and irreducible) parts of the 2-point function are shown in (Figure 4.2).

Summary and preview

This chapter introduced the formalism of the fermionic functional path integral, the concept of generating functionals and the perturbative techniques required to tackle quantum many-body Hamiltonians by means of the perturbative and, in particular, the functional renormalization group. In order to properly define the fermionic path integral, we made use of Grassmann fields and fermionic coherent states. Based on the path integral formulation of the partition function in imaginary time, we defined the generating functionals of the disconnected and connected Green functions, as well as the effective action, which is used to produce one-particle irreducible vertex functions. We recapitulated Wick's theorem as an essential ingredient for the evaluation of all terms and diagrams appearing in the perturbative expansion. The next chapter about the perturbative renormalization group motivates the Cooper instability from a diagrammatic point of view and shows how to deal with the corresponding logarithmic divergence of the particle-particle bubble by introducing a cutoff into the theory.

5. Perturbative renormalization group

In (Chapter 2), it was already mentioned, that the superconducting state is impossible to obtain by means of perturbation theory. However, we skipped the details of how and why the perturbative expansion eventually breaks down when approaching the superconducting phase, which is what we will catch up on in the following chapter. At any order, the perturbative expansion of the two-particle vertex (cf. (Section 4.4)) involves diagrams, which have a ladder-like structure and are shown in (Figure 5.1). The selection of these diagrams is justified if they represent (eventually for some particular momentum channel of the two-particle vertex) the dominant contribution to the two-particle vertex, which indeed turns out to be the case for external legs carrying opposite momentum and spin. The divergence of this series indicates onset of the *Cooper instability* and the breakdown of perturbation theory. The sum inside the bracket of the second equality in (Figure 5.1), which corresponds to the irreducible part of the two-particle vertex, can be evaluated as *geometric series*. Assuming the most simple one-band model with spin rotation invariance, the bare interaction V_0 and employing the rules for the graphical representation of propagators and vertices stated in (Section 4.4) we can write the sum as (cf. (Equation 5.1.14))

$$\begin{aligned} U^{\text{Ladd}}_{\mathbf{k}\mathbf{k}'} &= 1 + \int_{i\omega,\mathbf{q}} G_0(i\omega,\mathbf{q}) V_0 G_0(-i\omega,-\mathbf{q}) \\ &\quad + \int_{i\omega,\mathbf{q}} \int_{i\omega',\mathbf{q}'} G_0(i\omega,\mathbf{q}) V_0 G_0(-i\omega,-\mathbf{q}) G_0(i\omega',\mathbf{q}') V_0 G_0(-i\omega',-\mathbf{q}') + \dots \\ &= \frac{1}{1 - V_0 \int_{i\omega,\mathbf{q}} G_0(i\omega,\mathbf{q}) G_0(-i\omega,-\mathbf{q})} \quad , \end{aligned} \tag{5.0.1}$$

where we attached the momenta $\mathbf{k}$, $-\mathbf{k}$ and $-\mathbf{k}'$, $\mathbf{k}'$ to the external legs. Using (Equation 4.4.3) for a single band $G_0(i\omega,\mathbf{q}) = (i\omega_n + \xi_{\mathbf{q}})^{-1}$ with single-particle dispersion $\xi_{\mathbf{q}}$ we find a logarithmic divergence $\propto \log(\beta W)$ for zero temperature ($\beta = (k_B T)^{-1}$) upon performing the momentum integration, where W represents the upper band edge of the dispersion $\xi_{\mathbf{q}}$. At the critical temperature, perturbation theory breaks down, which means that one cannot obtain the superconducting state by perturbative expansion to any finite order and that it is not adiabatically connected to the (non-interacting limit) of the Fermi liquid. Similar subtleties occur in the single-particle properties [Mat12, Chap. 15.4].

To avoid running into the logarithmic divergence of particle-particle terms in the perturbation series, one can introduce an infrared cutoff Ω_0 and treat the residual degrees of freedom below the cutoff by means of a renormalization group procedure. Hence,

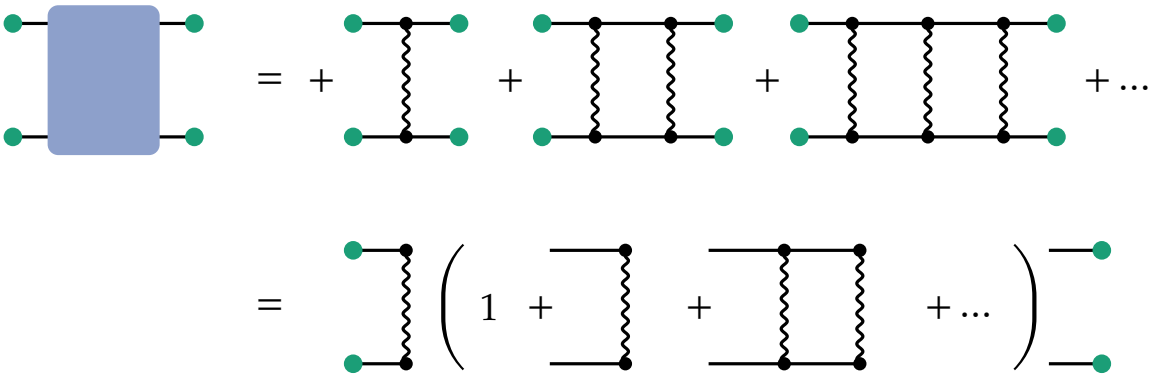

Figure 5.1.: The perturbative expansion of the irreducible two-particle vertex involves - among many others - types of diagrams that have *ladder-like* structure. These diagrams drive the Cooper instability and their sum eventually diverges at the critical temperature.

the perturbative renormalization group method consists of two steps (cf. [RKS10])

1. All modes outside a narrow range of energies specified by infrared cutoff Ω_0 about the Fermi energy are integrated out perturbatively resulting in an effective interaction at energy Ω_0.
2. The remaining low-energy modes are treated using the *logarithmic RG technique*, which thereby identifies the leading superconducting order in the Cooper instability

This procedure can be viewed as a generalization of the *Kohn-Luttinger effect* [KL65] described in (Section 2.3), where the evaluation of the Lindhard function revealed the generation of an attractive effective interaction in non-zero angular momentum channels from bare repulsive interactions. Although the combination of these two procedures has first been systematically worked out by Raghu and Kivelson [RKS10; RK11; Rag+12], similar approaches have already been used some time ago [Hlu99]. More recently, this methodology has been extended to take the effects of multiple bands [RKK10b; Cho+13], atomic spin-orbit coupling [SRS14; Sca16] and inversion symmetry breaking [VW11; WV14] into account.

The first section of the chapter will set up the general formalism for a second order perturbation theory of the two-particle vertex and present the resulting effective interaction for SU(2)-invariant and SU(2)-broken Hamiltonian with or without inversion symmetry. Simplifying the result to the example of the single-band Hubbard, we evaluate the particle-particle loops explicitly to find the logarithmic divergence discussed above and to properly define the infrared cutoff. The second section introduces the logarithmic renormalization group, that makes use logarithmic divergence and identifies the dominant pairing channel by calculating the renormalization group flow of the non-zero angular momentum channels in the effective Cooper pair interaction. Finally, the

last section tries to compare the results of the perturbative renormalization group with the methodology of the random phase approximation by working out the similarities and differences between the two methods.

5.1. Perturbative expansion of the irreducible two-particle vertex

The first step of the perturbative renormalization group procedure is to identify and calculate the perturbative corrections to the one-particle irreducible (1PI) two-particle vertex $U_{\alpha_1\alpha_2\alpha_1'\alpha_2'}$ (up to second order). To find these perturbative corrections we consider the 4-point function

$$\left\langle \bar{\psi}_\mu \bar{\psi}_\nu \psi_\kappa \psi_\lambda \right\rangle = \frac{\delta^4 \mathcal{G}\left[\bar{\eta}, \eta\right]}{\delta\bar{\eta}_\kappa \delta\bar{\eta}_\lambda \delta\eta_\mu \delta\eta_\nu}\bigg|_{\eta=\bar{\eta}=0} \quad , \tag{5.1.1}$$

where the expectation value is the fully interacting one, which is generated by the functional $\mathcal{G}\left[\bar{\eta}, \eta\right]$ (Equation 4.2.6). The source fields η, $\bar{\eta}$ have to be set to zero after performing the functional derivative. In more detail, the 4-point function is given by the functional integral

$$\left\langle \bar{\psi}_\mu \bar{\psi}_\nu \psi_\kappa \psi_\lambda \right\rangle = \frac{1}{\mathcal{Z}} \int \mathcal{D}\left[\bar{\psi}, \psi\right] \bar{\psi}_\mu \bar{\psi}_\nu \psi_\kappa \psi_\lambda e^{-S\left[\bar{\psi}, \psi\right]} \quad , \tag{5.1.2}$$

with $\mathcal{Z}$being the interacting partition function. The action $S\left[\bar{\psi}, \psi\right]$ (cf. (Equation 4.4.2) and (Equation 4.4.4)) is defined by

$$\begin{aligned} S\left[\bar{\psi}, \psi\right] = S_0\left[\bar{\psi}, \psi\right] + S_I\left[\bar{\psi}, \psi\right] = & \int_{(K,\alpha,\alpha')} \left(G_0^{-1}(K)\right)_{\alpha\alpha'} \bar{\psi}_{K\alpha} \psi_{K\alpha'} \\ & + \frac{1}{\beta} \int_{\substack{(K_1,\alpha_1),(K_2,\alpha_2) \\ (K_1',\alpha_1'),(K_2',\alpha_2')}} \Gamma(K_1, K_2, K_1', K_2')_{\alpha_1\alpha_2,\alpha_1'\alpha_2'} \, \bar{\psi}_{K_1'\alpha_1'} \bar{\psi}_{K_2'\alpha_2'} \psi_{K_2\alpha_2} \psi_{K_1\alpha_1} \quad , \end{aligned} \tag{5.1.3}$$

with the multiindex $K = (i\omega_n, K)$ comprising Matsubara frequency and momentum. Here, $G_0^{-1}(K)$ specifies the inverse free propagator given by (Equation 4.4.3)

$$\left(G_0(K)\right)^{-1}_{\alpha\alpha'} = -i\omega_n \delta_{\alpha\alpha'} + h_{\alpha'\alpha}(\mathbf{k}) \quad . \tag{5.1.4}$$

Exactly like in (Section 4.4), the perturbative series is given by calculating the non-interaction average of the four fields and the exponential of the interacting part of the action, which is

$$\frac{1}{Z}\int \mathcal{D}[\bar{\psi},\psi]\,\bar{\psi}_\mu\bar{\psi}_\nu\psi_\kappa\psi_\lambda e^{-S[\bar{\psi},\psi]} = \frac{Z_0}{Z}\left\langle \bar{\psi}_\mu\bar{\psi}_\nu\psi_\kappa\psi_\lambda e^{-S_I[\bar{\psi},\psi]}\right\rangle_0 \quad . \tag{5.1.5}$$

Since we don't intend to perform any resummation of an infinite series, in contrast to what we will do in (Section 5.4) in the context of the *random phase approximation* (*RPA*), we are content with the first few orders of the expansion. For the sake of brevity, we hide both particle indices $(K,\alpha) \to \alpha$ in a single one and up to third order we find

$$\begin{aligned}
\left\langle \bar{\psi}_\mu\bar{\psi}_\nu\psi_\kappa\psi_\lambda e^{-S_I[\bar{\psi},\psi]}\right\rangle_0 \approx{}& \left\langle \bar{\psi}_\mu\bar{\psi}_\nu\psi_\kappa\psi_\lambda\right\rangle_0 - \frac{1}{\beta}\int_{\substack{\mu_1,\nu_1\\ \kappa_1,\lambda_1}} \Gamma_{\mu_1\nu_1\kappa_1\lambda_1}\left\langle \bar{\psi}_\mu\bar{\psi}_\nu\psi_\kappa\psi_\lambda\bar{\psi}_{\mu_1}\bar{\psi}_{\nu_1}\psi_{\kappa_1}\psi_{\lambda_1}\right\rangle_0 \\
&+ \frac{1}{2\beta^2}\int_{\substack{\mu_1,\nu_1\\ \kappa_1,\lambda_1}}\int_{\substack{\mu_2,\nu_2\\ \kappa_2,\lambda_2}} \Gamma_{\mu_1\nu_1\kappa_1\lambda_1}\Gamma_{\mu_2\nu_2\kappa_2\lambda_2}\left\langle \bar{\psi}_\mu\bar{\psi}_\nu\psi_\kappa\psi_\lambda\bar{\psi}_{\mu_1}\bar{\psi}_{\nu_1}\psi_{\kappa_1}\psi_{\lambda_1}\bar{\psi}_{\mu_2}\bar{\psi}_{\nu_2}\psi_{\kappa_2}\psi_{\lambda_2}\right\rangle_0 \\
&- \frac{1}{6\beta^3}\int_{\substack{\mu_1,\nu_1\\ \kappa_1,\lambda_1}}\int_{\substack{\mu_2,\nu_2\\ \kappa_2,\lambda_2}}\int_{\substack{\mu_3,\nu_3\\ \kappa_3,\lambda_3}} \Gamma_{\mu_1\nu_1\kappa_1\lambda_1}\Gamma_{\mu_2\nu_2\kappa_2\lambda_2}\Gamma_{\mu_3\nu_3\kappa_3\lambda_3} \\
&\quad\times\left\langle \bar{\psi}_\mu\bar{\psi}_\nu\psi_\kappa\psi_\lambda\bar{\psi}_{\mu_1}\bar{\psi}_{\nu_1}\psi_{\kappa_1}\psi_{\lambda_1}\bar{\psi}_{\mu_2}\bar{\psi}_{\nu_2}\psi_{\kappa_2}\psi_{\lambda_2}\bar{\psi}_{\mu_3}\bar{\psi}_{\nu_3}\psi_{\kappa_3}\psi_{\lambda_3}\right\rangle_0 + O\left(\beta^{-4}\right) \quad .
\end{aligned} \tag{5.1.6}$$

Employing *Wick's theorem* in (Section 4.3) to the non-interacting correlation functions, we find that the number of contractions quickly increases from zeroth up to third order. Only expectation values with the same number of ψ and $\bar{\psi}$ fields provide a finite contribution, because we assume absence of *spontaneous symmetry breaking*. In fact, there are two contractions in zeroth order, 24 in first order, 720 in second order and 40 320 in third order. Fortunately, these numbers comprise all disconnected, connected, reducible and irreducible diagrams, while we are only interested in the connected and irreducible ones. The disconnected ones are canceled by the prefactor $\frac{Z_0}{Z}$ in (Equation 5.1.5), whose expansion was discussed in (Section 4.4). The number of disconnected, connected, reducible and irreducible diagrams is given in (Table 5.1). Here, we will focus on the second order of the expansion, denoted by $\delta\Gamma^{(2)}_{\mu\nu\kappa\lambda}$, that features five inequivalent diagrams out of 80 irreducible terms, which all have the same weight. Note, that these terms correspond to connected Green functions (cf. (Section 4.2)) and we have to remove the propagators at the (four) external legs to find the irreducible vertex part. The irreducible vertices of the five terms in second order are hence given by

$$\begin{aligned}
\delta\Gamma^{(2)}_{\mu\nu\kappa\lambda} ={}& \frac{1}{\beta}\int_{\substack{\mu',\nu'\\ \kappa',\lambda'}} (G_0)_{\mu'\kappa'}(G_0)_{\nu'\lambda'}\Big(\Gamma_{\mu\nu\kappa'\lambda'}\Gamma_{\mu'\nu'\kappa\lambda} + \Gamma_{\mu\mu'\lambda'\kappa}\Gamma_{\nu'\nu\lambda\kappa'} \\
&+\Gamma_{\mu\nu'\kappa'\lambda}\Gamma_{\mu'\nu\lambda'\kappa} + \Gamma_{\mu\nu'\lambda\kappa'}\Gamma_{\mu'\nu\kappa\lambda'} - \Gamma_{\mu\mu'\kappa\lambda'}\Gamma_{\nu'\nu\lambda\kappa'}\Big) \quad .
\end{aligned} \tag{5.1.7}$$

The different signs of the terms originate from the number of anticommutations necessary to get the required arrangement of fields in (Equation 5.1.6). Their diagrammatic

Table 5.1.: Although the number of contractions increases like $(2n)!$ with order n of the expansion of the two-particle vertex, the number of inequivalent irreducible diagrams is manageable. The number of spinful diagrams is even lower than the spinless version since the bare spinful two-particle interaction exhibits a higher degree of symmetry. In particular, the spinless two-particle interaction is symmetric only with respect to exchange of both pairs of fields at a time, i.e. $\Gamma_{\nu_1\mu_1\kappa_1\lambda_1} = \Gamma_{\mu_1\nu_1\lambda_1\kappa_1}$. In contrast, the spinful vertex features the fermionic antisymmetry relations, like i.a. $\Gamma_{\nu_1\mu_1\kappa_1\lambda_1} = -\Gamma_{\mu_1\nu_1\kappa_1\lambda_1}$.

order n	total	disconnected	connected			
			reducible	irreducible		
				total	inequivalent	
					spinless	spinful
0	2	2	0	0	0	0
1	24	20	0	4	1	1
2	720	512	128	80	5	3

representation is given in (Figure 5.2) and the order in which they appear corresponds to the order of terms in (Equation 5.1.7). The visual representation reveals that the first term in (Equation 5.1.7) is the *particle-particle* contribution while the second to fifth terms are the *particle-hole* terms. All five diagrams have the same weight and hence contribute to the second order correction with the same absolute prefactor. So far, we didn't assume any particular properties or symmetries of the pair interaction $\Gamma_{\mu\nu\kappa\lambda}$. Since we are interested in spinful, fermionic models, we a assume a pair interaction that satisfies (cf. (Equation 3.3.4) and [AGD12, Sec. 13, p. 115])

$$U_{\mu\nu\kappa\lambda} = -U_{\nu\mu\kappa\lambda} = -U_{\mu\nu\lambda\kappa} = +U_{\nu\mu\lambda\kappa} \quad . \tag{5.1.8}$$

Inserting this pair interaction into the second order perturbative correction (Equation 5.1.7) by substituting $\Gamma_{\mu\nu\kappa\lambda}$ with $U_{\mu\nu\kappa\lambda}$, we find for the terms inside the bracket

$$\begin{aligned} &U_{\mu\nu\kappa'\lambda'}U_{\mu'\nu'\kappa\lambda} + U_{\mu\mu'\lambda'\kappa}U_{\nu'\nu\lambda\kappa'} + U_{\mu\nu'\kappa'\lambda}U_{\mu'\nu\lambda'\kappa} + U_{\mu\nu'\lambda\kappa'}U_{\mu'\nu\kappa\lambda'} - U_{\mu\mu'\kappa\lambda'}U_{\nu'\nu\lambda\kappa'} \\ &\quad = U_{\mu\nu\kappa'\lambda'}U_{\mu'\nu'\kappa\lambda} + 2U_{\mu\mu'\kappa\lambda'}U_{\nu\nu'\lambda\kappa'} - 2U_{\mu\nu'\lambda\kappa'}U_{\nu\mu'\kappa\lambda'} \quad . \end{aligned} \tag{5.1.9}$$

In the first line we employed the antisymmetry (Equation 5.1.8) to the first interaction of the third term, such that it coincides with the second term, and to the second interaction of the fifth term, such that it equals the fourth term. Henceforth, the second order perturbative correction for a spinful fermionic pair-interaction yields (cf. [Sha94a; BBD03])

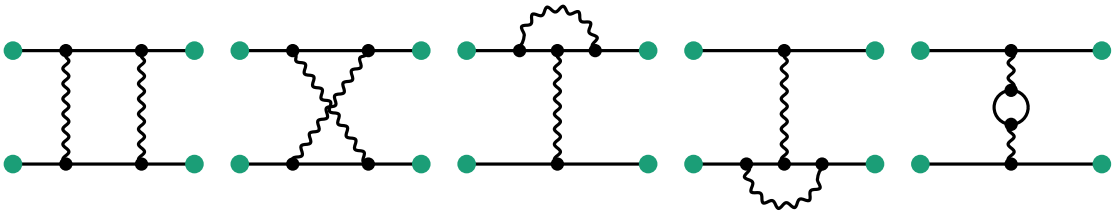

Figure 5.2.: There are five diagrams, which contribute to the second order perturbation expansion of the two-particle vertex (Equation 5.1.7). Note, that all five diagrams have the same weight, i.e. they contribute with the same (absolute value of the) prefactor. These five diagrams correspond to the perturbative expansion of a SU(2)-invariant bare pair interaction (cf. (Equation 5.2.1)).

$$\delta U^{(2)}_{\mu\nu\kappa\lambda} = \frac{1}{\beta} \sum_{\substack{\mu',\nu' \\ \kappa',\lambda'}} (G_0)_{\mu'\kappa'} (G_0)_{\nu'\lambda'} \left(\frac{1}{2} U_{\mu\nu\kappa'\lambda'} U_{\mu'\nu'\kappa\lambda} - U_{\mu\nu'\lambda\kappa'} U_{\nu\mu'\kappa\lambda'} + U_{\mu\mu'\kappa\lambda'} U_{\nu\nu'\lambda\kappa'} \right) \quad . \tag{5.1.10}$$

The diagrammatic representation of the spinful perturbative correction is given in (Figure 5.3b). Some of the literature refers to these contributions as *BCS*, *ZS′* and *ZS* terms [Sha94a; WV14]. Note, that $\delta U^{(2)}_{\mu\nu\kappa\lambda}$ must fulfill the antisymmetry relations (Equation 5.1.8) as well. In order to evaluate the perturbative correction $\delta U^{(2)}_{\mu\nu\kappa\lambda}$, several steps are necessary. First of all, we reimplement the full index structure by substitution of all indices according to $\alpha \to (K, \alpha) = (i\omega, \mathbf{k}, \alpha)$ (cf. (Equation 5.1.3)). Next, we focus on the free propagators $(G_0)_{\mu'\kappa'}$ and $(G_0)_{\nu'\lambda'}$ given by (Equation 5.1.4). To be able to conveniently calculate the integrals over the inner propagators - the *loop integrals* - we change to a basis, where the propagators assume diagonal a form in all indices. The representation of propagators *and* pair-interaction $U_{\mu\nu\kappa\lambda}$ in the new basis is found by means of a unitary transformation of the fields (cf. (Equation 3.3.33a) and (Equation 3.3.33b))

$$\phi_{\mathbf{k}\tilde{\alpha}} := \sum_{\alpha} U^{\tilde{\alpha}\alpha}_{\mathbf{k}} \psi_{\mathbf{k}\alpha} \qquad \bar{\phi}_{\mathbf{k}\tilde{\alpha}} := \sum_{\alpha} \bar{\psi}_{\mathbf{k}\alpha} \overline{U}^{\alpha\tilde{\alpha}}_{\mathbf{k}} \quad , \tag{5.1.11a}$$

with $U^{\tilde{\alpha}\alpha}_{\mathbf{k}}$ being the eigenvectors of $h_{\alpha'\alpha}(\mathbf{k})$ (cf. (Equation 5.1.4)). The collective indices α in orbital and $\tilde{\alpha}$ in band space may feature such indices as sublattice, orbital, spin and band, pseudospin and helicity (cf. (Section 3.3.1) and (Section 3.3.2)). We use the notation

$$\xi_{\mathbf{k}\tilde{\alpha}} = U^{\tilde{\alpha}\alpha'}_{\mathbf{k}} h_{\alpha'\alpha}(\mathbf{k}) \left(U^{\tilde{\alpha}\alpha}_{\mathbf{k}} \right)^{\dagger} \quad , \tag{5.1.12}$$

where $\xi_{\mathbf{k}\tilde{\alpha}}$ is diagonal and corresponds to the single-particle spectrum. Henceforth,

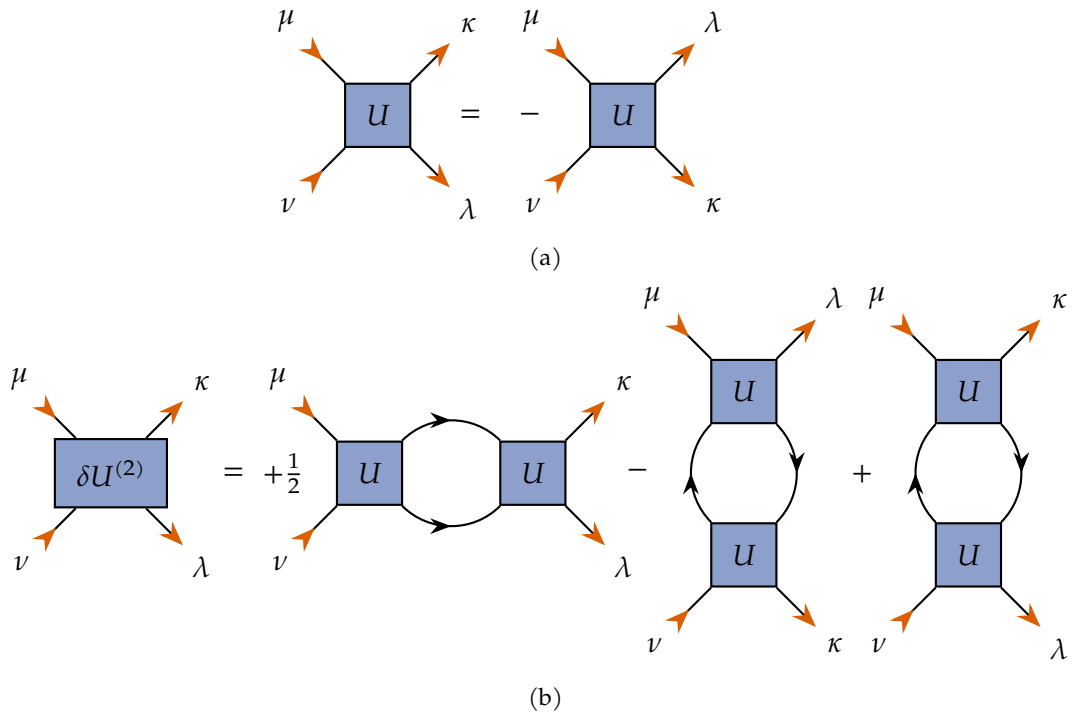

Figure 5.3.: The fermionic spinful pair interaction is antisymmetric with respect to exchange of the ingoing or outgoing particle indices, which is reflected by its diagram in (Figure 5.3a). The spinful fermionic bare pair interaction reduces the number of diagrams that contribute to the perturbative correction to the 1PI two-particle vertex in second order to three diagrams, which consist of one particle-particle and two particle-hole terms (Figure 5.3b). Note, that the antisymmetry of $\delta U^{(2)}$ is ensured by the opposite signs of direct and crossed particle-hole terms.

the propagators are, in diagonal form, given by

$$\left(G_0(i\omega, \mathbf{k})\right)_{\tilde{\alpha}} = \frac{1}{-i\omega_n + \xi_{\mathbf{k}\tilde{\alpha}}} \quad . \tag{5.1.13}$$

At this point, we are left with two integrals only in (Equation 5.1.10), because the propagators introduce $\delta_{\mu'\kappa'}$ and $\delta_{\nu'\lambda'}$ due to their diagonal form. We assume the bare interaction $U_{\mu\nu\kappa\lambda}$ to be independent of frequency and fix the external legs of the vertices at zero frequency by $i\omega_\mu = 0 = i\omega_\nu = i\omega_\kappa = i\omega_\lambda$. However, an scattering process at any order represented by $\delta U^{(2)}_{\mu\nu\kappa\lambda}$ or $U_{\mu\nu\kappa\lambda}$ must be subject to energy/frequency conservation. This has profound consequences for the propagators and results in important differences for particle-particle terms in contrast to particle-hole terms. The frequency balance for the particle-particle term (the first term) in (Equation 5.1.10) is summarized by $i\omega_\mu + i\omega_\nu = 0 = i\omega_{\kappa'} + i\omega_{\lambda'}$ resulting in $i\omega_{\kappa'} = -i\omega_{\lambda'}$ and $i\omega_{\mu'} + i\omega_{\nu'} = 0 = i\omega_\kappa + i\omega_\lambda$

resulting in $i\omega_{\mu'} = -i\omega_{\nu'}$. Since the propagators require $\delta_{\mu'\kappa'}$ and $\delta_{\nu'\lambda'}$, we are left with a single frequency $i\omega$ in the loop integrals with opposite sign in both propagators, i.e. $i\omega_{\mu'} = -i\omega_{\nu'}$. Analogous considerations apply to the particle-hole terms resulting, however, in a single frequency with same sign in both propagators, i.e. $i\omega_{\mu'} = i\omega_{\nu'}$. Finally, any vertex must obey *momentum conservation*, which results in characteristic momentum transfers for every diagram and a single momentum integration for the loop integrals. For instance, the particle-particle term features the momentum transfer $\mathbf{k} := \mathbf{k}_{\kappa'} = \mathbf{k}_\mu + \mathbf{k}_\nu - \mathbf{k}_{\lambda'}$, while the particle-hole terms have $\mathbf{k} := \mathbf{k}_{\mu'} = \mathbf{k}_\kappa - \mathbf{k}_\nu + \mathbf{k}_{\nu'}$ and $\mathbf{k} := \mathbf{k}_{\mu'} = \mathbf{k}_\kappa - \mathbf{k}_\mu + \mathbf{k}_{\nu'}$ respectively. Employing these preparations, we end up with the second order correction (Equation 5.1.10) that looks like

$$\begin{aligned}\left(\delta U^{(2)}\right)^{\tilde{\alpha}_1\tilde{\alpha}_2\tilde{\alpha}'_1\tilde{\alpha}'_2}_{\mathbf{k}_1\mathbf{k}_2\mathbf{k}'_1\mathbf{k}'_2} = \frac{1}{\beta}\sum_{i\omega_n}\sum_{\tilde{\alpha},\tilde{\alpha}'}\int\frac{\mathrm{d}\mathbf{k}}{\Omega}\Bigg(&\frac{1}{2}\frac{U^{\tilde{\alpha}_1\tilde{\alpha}_2\tilde{\alpha}\tilde{\alpha}'}_{\mathbf{k}_1,\mathbf{k}_2,\mathbf{k}_1+\mathbf{k}_2-\mathbf{k},\mathbf{k}}U^{\tilde{\alpha}\tilde{\alpha}'\tilde{\alpha}'_1\tilde{\alpha}'_2}_{\mathbf{k}_1+\mathbf{k}_2-\mathbf{k},\mathbf{k},\mathbf{k}'_1,\mathbf{k}'_2}}{(i\omega_n+\xi_{\mathbf{k}_1+\mathbf{k}_2-\mathbf{k}\tilde{\alpha}})(-i\omega_n+\xi_{\mathbf{k}\tilde{\alpha}'})}\\ &-\frac{U^{\tilde{\alpha}_1\tilde{\alpha}\tilde{\alpha}'_2\tilde{\alpha}'}_{\mathbf{k}_1,\mathbf{k},\mathbf{k}'_2,\mathbf{k}_1-\mathbf{k}'_2+\mathbf{k}}U^{\tilde{\alpha}_2\tilde{\alpha}'\tilde{\alpha}'_1\tilde{\alpha}}_{\mathbf{k}_2,\mathbf{k}_1-\mathbf{k}'_2+\mathbf{k},\mathbf{k}'_1,\mathbf{k}}}{(-i\omega_n+\xi_{\mathbf{k}_1-\mathbf{k}'_2+\mathbf{k}\tilde{\alpha}'})(-i\omega_n+\xi_{\mathbf{k}\tilde{\alpha}})}+\frac{U^{\tilde{\alpha}_1\tilde{\alpha}'\tilde{\alpha}'_1\tilde{\alpha}}_{\mathbf{k}_1,-\mathbf{k}_1+\mathbf{k}'_1+\mathbf{k},\mathbf{k}'_1,\mathbf{k}}U^{\tilde{\alpha}_2\tilde{\alpha}\tilde{\alpha}'_2\tilde{\alpha}'}_{\mathbf{k}_2,\mathbf{k},\mathbf{k}'_2,-\mathbf{k}_1+\mathbf{k}'_1+\mathbf{k}}}{(-i\omega_n+\xi_{-\mathbf{k}_1+\mathbf{k}'_1+\mathbf{k}\tilde{\alpha}'})(-i\omega_n+\xi_{\mathbf{k}\tilde{\alpha}})}\Bigg)\end{aligned}\quad , \tag{5.1.14}$$

where the indices $\tilde{\alpha}$ and $\tilde{\alpha}'$ sum over any band, pseudospin or helicity indices. Assuming the orbital/spin interaction $U^{\alpha_1\alpha_2\alpha'_1\alpha'_2}_{\mathbf{k}_1,\mathbf{k}_2,\mathbf{k}'_1,\mathbf{k}'_2}$, the bare interaction in band space is given by

$$U^{\tilde{\alpha}_1\tilde{\alpha}_2\tilde{\alpha}'_1\tilde{\alpha}'_2}_{\mathbf{k}_1,\mathbf{k}_2,\mathbf{k}'_2,\mathbf{k}'_2} = \sum_{\substack{\alpha_1\alpha_2\\ \alpha'_1,\alpha'_2}}\overline{u}^{\tilde{\alpha}_1\alpha_1}_{\mathbf{k}_1}\overline{u}^{\tilde{\alpha}_2\alpha_2}_{\mathbf{k}_2}U^{\alpha_1\alpha_2\alpha'_1\alpha'_2}_{\mathbf{k}_1,\mathbf{k}_2,\mathbf{k}'_1,\mathbf{k}'_2}u^{\alpha'_2\tilde{\alpha}'_2}_{\mathbf{k}'_2}u^{\alpha'_1\tilde{\alpha}'_1}_{\mathbf{k}'_1} \quad , \tag{5.1.15}$$

with $u^{\tilde{\alpha}\alpha}_{\mathbf{k}}$ being the eigenvectors of $h_{\alpha'\alpha}(\mathbf{k})$. The Matsubara sums with fermionic frequencies $\omega_n = \frac{(2n+1)\pi}{\beta}$ (see (Equation 4.1.8b)) are evaluated by means of contour inte-

gration (cf. e.g. [AS10, Chap. 4.2][BF04, Chap. 15.2]) and give [1]

$$\frac{1}{\beta}\sum_{i\omega_n}\frac{1}{(i\omega_n+\xi_{\mathbf{q}-\mathbf{k}\tilde{\alpha}})(-i\omega_n+\xi_{\mathbf{k}\tilde{\alpha}'})}=\frac{\tanh\left(\beta\xi_{\mathbf{q}-\mathbf{k}\tilde{\alpha}}/2\right)+\tanh\left(\beta\xi_{\mathbf{k}\tilde{\alpha}'}/2\right)}{2\left(\xi_{\mathbf{q}-\mathbf{k}\tilde{\alpha}}+\xi_{\mathbf{k}\tilde{\alpha}'}\right)}=\frac{f(-\beta\xi_{\mathbf{q}-\mathbf{k}\tilde{\alpha}})-f(\beta\xi_{\mathbf{k}\tilde{\alpha}'})}{\xi_{\mathbf{q}-\mathbf{k}\tilde{\alpha}}+\xi_{\mathbf{k}\tilde{\alpha}'}} \tag{5.1.17a}$$

$$\frac{1}{\beta}\sum_{i\omega_n}\frac{1}{(-i\omega_n+\xi_{\mathbf{q}+\mathbf{k}\tilde{\alpha}})(-i\omega_n+\xi_{\mathbf{k}\tilde{\alpha}'})}=\frac{\tanh\left(\beta\xi_{\mathbf{q}+\mathbf{k}\tilde{\alpha}}/2\right)-\tanh\left(\beta\xi_{\mathbf{k}\tilde{\alpha}'}/2\right)}{2\left(\xi_{\mathbf{k}\tilde{\alpha}'}-\xi_{\mathbf{q}+\mathbf{k}\tilde{\alpha}}\right)}=\frac{f(\beta\xi_{\mathbf{k}\tilde{\alpha}'})-f(\beta\xi_{\mathbf{q}+\mathbf{k}\tilde{\alpha}})}{\xi_{\mathbf{k}\tilde{\alpha}'}-\xi_{\mathbf{q}+\mathbf{k}\tilde{\alpha}}} \quad , \tag{5.1.17b}$$

for the particle-particle and particle-hole loops, respectively. In a renormalization group sense, the effective interaction in the Cooper channel is the only *relevant* interaction and the only generic instability of the *Fermi liquid* in the weak-coupling limit. Analogously to the discussions in (Section 3.4.1) and (Section 3.4.2), we have to distinguish the case of degenerate Fermi surfaces characterized by *pseudospin* degree of freedom from the case of a Fermi surface labeled by *helicity*, which simplifies the structure of pairing states in the weak-coupling limit. The Cooper vertex in terms of pseudospin indices is given by (cf. (Equation 3.4.12))

$$U^{bb'\tilde{\sigma}_1\tilde{\sigma}_2\tilde{\sigma}_1'\tilde{\sigma}_2'}_{\mathbf{k}\mathbf{k}'}:=U^{b\tilde{\sigma}_1 b\tilde{\sigma}_2 b'\tilde{\sigma}_1' b'\tilde{\sigma}_2'}_{\mathbf{k},-\mathbf{k},\mathbf{k}',-\mathbf{k}'} \quad , \tag{5.1.18}$$

and its second order perturbative correction (Equation 5.1.14) reduces to

$$\left(\delta U^{(2)}_{pp}\right)^{bb'\tilde{\sigma}_1\tilde{\sigma}_2\tilde{\sigma}_1'\tilde{\sigma}_2'}_{\mathbf{k}\mathbf{k}'}=\sum_{m\tilde{\tau}\tilde{\tau}'}\int\frac{\mathrm{d}\mathbf{q}}{\Omega}\left(\frac{1}{2}U^{b\tilde{\sigma}_1 b\tilde{\sigma}_2 m\tilde{\tau}m\tilde{\tau}'}_{\mathbf{k},-\mathbf{k},-\mathbf{q},\mathbf{q}}U^{m\tilde{\tau}m\tilde{\tau}'b'\tilde{\sigma}_1' b'\tilde{\sigma}_2'}_{-\mathbf{q},\mathbf{q},\mathbf{k}',-\mathbf{k}'}\frac{f(-\beta\xi_{-\mathbf{q}m\tilde{\tau}})-f(\beta\xi_{\mathbf{q}m\tilde{\tau}'})}{\xi_{-\mathbf{q}m\tilde{\tau}}+\xi_{\mathbf{q}m\tilde{\tau}'}}\right) \tag{5.1.19a}$$

$$\left(\delta U^{(2)}_{dph}\right)^{bb'\tilde{\sigma}_1\tilde{\sigma}_2\tilde{\sigma}_1'\tilde{\sigma}_2'}_{\mathbf{k}\mathbf{k}'}=-\sum_{m\tilde{\tau}m'\tilde{\tau}'}\int\frac{\mathrm{d}\mathbf{q}}{\Omega}\left(U^{b\tilde{\sigma}_1 m\tilde{\tau}b'\tilde{\sigma}_2' m'\tilde{\tau}'}_{\mathbf{k},\mathbf{q},-\mathbf{k}',\mathbf{k}+\mathbf{k}'+\mathbf{q}}U^{b\tilde{\sigma}_2 m'\tilde{\tau}'b'\tilde{\sigma}_1' m\tilde{\tau}}_{-\mathbf{k},\mathbf{k}+\mathbf{k}'+\mathbf{q},\mathbf{k}',\mathbf{q}}\frac{f(\beta\xi_{\mathbf{k}+\mathbf{k}'+\mathbf{q}m'\tilde{\tau}'})-f(\beta\xi_{\mathbf{q}m\tilde{\tau}})}{\xi_{\mathbf{k}+\mathbf{k}'+\mathbf{q}m'\tilde{\tau}'}-\xi_{\mathbf{q}m\tilde{\tau}}}\right) \tag{5.1.19b}$$

$$\left(\delta U^{(2)}_{cph}\right)^{bb'\tilde{\sigma}_1\tilde{\sigma}_2\tilde{\sigma}_1'\tilde{\sigma}_2'}_{\mathbf{k}\mathbf{k}'}=\sum_{m\tilde{\tau}m'\tilde{\tau}'}\int\frac{\mathrm{d}\mathbf{q}}{\Omega}\left(U^{b\tilde{\sigma}_1 m'\tilde{\tau}'b'\tilde{\sigma}_1' m\tilde{\tau}}_{\mathbf{k},-\mathbf{k}+\mathbf{k}'+\mathbf{q},\mathbf{k}',\mathbf{q}}U^{b\tilde{\sigma}_2 m\tilde{\tau}b'\tilde{\sigma}_2' m'\tilde{\tau}'}_{-\mathbf{k},\mathbf{q},-\mathbf{k}',-\mathbf{k}+\mathbf{k}'+\mathbf{q}}\frac{f(\beta\xi_{-\mathbf{k}+\mathbf{k}'+\mathbf{q}m'\tilde{\tau}'})-f(\beta\xi_{\mathbf{q}m\tilde{\tau}})}{\xi_{-\mathbf{k}+\mathbf{k}'+\mathbf{q}m'\tilde{\tau}'}-\xi_{\mathbf{q}m\tilde{\tau}}}\right) \quad , \tag{5.1.19c}$$

with m, m' and $\tilde{\tau}$, $\tilde{\tau}'$ being the "inner" band indices and pseudospin states, respectively, associated to the propagators. While the pseudospin indices $\tilde{\tau}$, $\tilde{\tau}'$ attached to the

[1] The tangens hyperbolicus $\tanh(x)$ is related to the Fermi-Dirac function $f(x)$ by

$$\tanh\left(\frac{x}{2}\right)=\frac{e^{\frac{x}{2}}-e^{-\frac{x}{2}}}{e^{\frac{x}{2}}+e^{-\frac{x}{2}}}=\frac{e^{\frac{x}{2}}+e^{-\frac{x}{2}}-2e^{-\frac{x}{2}}}{e^{\frac{x}{2}}+e^{-\frac{x}{2}}}=1-\frac{2}{1+e^{x}}=1-2f(x) \quad , \tag{5.1.16}$$

which satisfies $f(-x)=1-f(x)$.

band energies $\xi_{\mathbf{k}}$ of the propagator sum may be omitted because of pseudospin degeneracy, the pseudospin indices attached to the vertex functions play an important role in describing the correct pseudospin structure of the resulting pairing states. Note the formal similarity to the multiband extension in [Cho+13, III.B.]. Let's proceed to the case of helicity based vertex functions and non-degenerate Fermi surfaces. The Cooper channel in terms of helicities is determined by (cf. (Section 3.4.2))

$$U^{b\lambda b'\lambda'}_{\mathbf{k}\mathbf{k}'} \coloneqq U^{b\lambda b\lambda b'\lambda' b'\lambda'}_{\mathbf{k},-\mathbf{k},\mathbf{k}',-\mathbf{k}'} \quad , \tag{5.1.20}$$

where, in contrast to the pseudospin case, the structure in the spin degree of freedom is restricted by the requirement of equal-energy pairing. In this case, (Equation 5.1.14) reduces to the three contributions

$$\left(\delta U^{(2)}_{pp}\right)^{b\lambda b'\lambda'}_{\mathbf{k}\mathbf{k}'} = \sum_{m\kappa} \int \frac{\mathrm{d}\mathbf{q}}{\Omega} \left(\frac{1}{2} U^{b\lambda b\lambda m\kappa m\kappa}_{\mathbf{k},-\mathbf{k},-\mathbf{q},\mathbf{q}} U^{m\kappa m\kappa b'\lambda' b'\lambda'}_{-\mathbf{q},\mathbf{q},\mathbf{k}',-\mathbf{k}'} \frac{f(-\beta\xi_{-\mathbf{q}m\kappa}) - f(\beta\xi_{\mathbf{q}m\kappa})}{\xi_{-\mathbf{q}m\kappa} + \xi_{\mathbf{q}m\kappa}} \right) \tag{5.1.21a}$$

$$\left(\delta U^{(2)}_{dph}\right)^{b\lambda b'\lambda'}_{\mathbf{k}\mathbf{k}'} = -\sum_{m\kappa m'\kappa'} \int \frac{\mathrm{d}\mathbf{q}}{\Omega} \left(U^{b\lambda m\kappa b'\lambda' m'\kappa'}_{\mathbf{k},\mathbf{q},-\mathbf{k}',\mathbf{k}+\mathbf{k}'+\mathbf{q}} U^{b\lambda m'\kappa' b'\lambda' m\kappa}_{-\mathbf{k},\mathbf{k}+\mathbf{k}'+\mathbf{q},\mathbf{k}',\mathbf{q}} \frac{f(\beta\xi_{\mathbf{k}+\mathbf{k}'+\mathbf{q}m'\kappa'}) - f(\beta\xi_{\mathbf{q}m\kappa})}{\xi_{\mathbf{k}+\mathbf{k}'+\mathbf{q}m'\kappa'} - \xi_{\mathbf{q}m\kappa}} \right) \tag{5.1.21b}$$

$$\left(\delta U^{(2)}_{cph}\right)^{b\lambda b'\lambda'}_{\mathbf{k}\mathbf{k}'} = \sum_{m\kappa m'\kappa'} \int \frac{\mathrm{d}\mathbf{q}}{\Omega} \left(U^{b\lambda m'\kappa' b'\lambda' m\kappa}_{\mathbf{k},-\mathbf{k}+\mathbf{k}'+\mathbf{q},\mathbf{k}',\mathbf{q}} U^{b\lambda m\kappa b'\lambda' m'\kappa'}_{-\mathbf{k},\mathbf{q},\mathbf{k}',-\mathbf{k}+\mathbf{k}'+\mathbf{q}} \frac{f(\beta\xi_{-\mathbf{k}+\mathbf{k}'+\mathbf{q}m'\kappa'}) - f(\beta\xi_{\mathbf{q}m\kappa})}{\xi_{-\mathbf{k}+\mathbf{k}'+\mathbf{q}m'\kappa'} - \xi_{\mathbf{q}m\kappa}} \right) \quad , \tag{5.1.21c}$$

for the particle-particle, direct particle-hole and crossed particle-hole diagrams. In contrast to the particle-hole channels with momentum transfers $\mathbf{k}' - \mathbf{k}$ and $\mathbf{k} - \mathbf{k}'$, the particle-particle channel features zero momentum transfer. Here, the indices m, m' and κ, κ' denote the inner bands and helicities. So far, we used the most general fermionic pair interaction allowed with respect to the restrictions given in (Section 3.3.2). In the next section, we will limit our considerations to the case of SU(2)-invariant interactions and see how (Equation 5.1.14) and be simplified. Furthermore, we only treated the second order of the perturbative expansion, while ignoring the first order completely. In the next section, we will also discuss what the influence of the first order on the superconducting order is and under what circumstances it can be neglected.

5.2. Effective vertex for (non-local) Coulomb interaction

According to (Section 3.3) a spinful SU(2)-invariant two-particle vertex in orbital-spin space can be written by

$$U_{\mu\nu\kappa\lambda} = V_{\mu\nu\kappa\lambda}\delta_{\sigma_\mu\sigma_\kappa}\delta_{\sigma_\nu\sigma_\lambda} - V_{\mu\nu\lambda\kappa}\delta_{\sigma_\mu\sigma_\lambda}\delta_{\sigma_\nu\sigma_\kappa} \quad . \tag{5.2.1}$$

where $V_{\mu\nu\kappa\lambda} = V_{\nu\mu\lambda\kappa}$ and the multiindices attached to V are implied to lack spin dependency in contrast to the ones of U. The spin symmetry results in a free propagator (Equation 5.1.4), which is diagonal in spin space, i.e. $G_0(i\omega, \mathbf{k})_{\mu\nu} \propto \delta_{\mu\nu}$. Inserting (Equation 5.2.1) into the expansion (Equation 5.1.10), we find two sets of terms/diagrams corresponding to the two spin sectors given by the spin combinations in (Equation 5.2.1). Both sets of equations, each including five terms (one particle-particle and four particle-hole contributions) are equivalent to each other and to the general expansion (Equation 5.1.7). They represent the second order perturbative expansion of a SU(2)-invariant bare interaction. Let's assume a SU(2)-invariant (non-local) Coulomb repulsion in a single-orbital model. The corresponding interacting part of the Hamiltonian is

$$\mathcal{H}_I = U_0 \sum_i n_{i\uparrow} n_{i\downarrow} + \frac{U_1}{2} \sum_{\langle i \neq j \rangle} \sum_{\sigma,\sigma'} n_{i\sigma} n_{j\sigma'} \quad , \tag{5.2.2}$$

with the occupation number operator $n_{i\sigma} = c^\dagger_{i\sigma} c_{i\sigma}$. The parameters U_0 and U_1 determine the strength of on-site and nearest neighbor repulsion, respectively. Hence, the antisymmetrized bare pair interaction is fully characterized by its momentum and spin dependency. For instance, on the two dimensional square lattice with lattice constant a it is given by

$$\begin{aligned} U^{\sigma_1\sigma_2\sigma_1'\sigma_2'}_{\mathbf{k}_1\mathbf{k}_2\mathbf{k}_1'\mathbf{k}_2'} =& U_0 \left(\delta_{\sigma_1\sigma_1'}\delta_{\sigma_2\sigma_2'} - \delta_{\sigma_1\sigma_2'}\delta_{\sigma_2\sigma_1'}\right) \\ &+ U_1 \Big[\Big(\cos\big((\mathbf{k}_2 - \mathbf{k}_2')_x a\big) + \cos\Big((\mathbf{k}_2 - \mathbf{k}_2')_y a\Big)\Big) \delta_{\sigma_1\sigma_1'}\delta_{\sigma_2\sigma_2'} \\ &\quad - \Big(\cos\big((\mathbf{k}_1 - \mathbf{k}_2')_x a\big) + \cos\Big((\mathbf{k}_1 - \mathbf{k}_2')_y a\Big)\Big) \delta_{\sigma_1\sigma_2'}\delta_{\sigma_2\sigma_1'} \Big] \quad , \end{aligned} \tag{5.2.3}$$

and satisfies all the requirements developed in (Section 3.3.1), where momentum conservation $\mathbf{k}_1 + \mathbf{k}_2 = \mathbf{k}_1' + \mathbf{k}_2'$ is implied. The effective vertex in pseudospin basis comprised of (Equation 5.1.19a), (Equation 5.1.19b) and (Equation 5.1.19c) can be further simplified to account for the SU(2)-invariant Coulomb interaction (Equation 5.2.3) in a single-band model. Setting $U_1 = 0$ and only taking the on-site repulsion U_0 into account, we find that only the particle-particle and direct particle-hole terms contribute, while the crossed particle-hole diagram vanishes due to the given spin structure. Henceforth, we find (cf. [RKS10, Section II.])

$$\left(\delta U^{(2)}_{pp}\right)^{\uparrow\downarrow\uparrow\downarrow}_{\mathbf{k}\mathbf{k}'} = U_0^2 \int \frac{\mathrm{d}\mathbf{q}}{\Omega} \frac{f(-\beta\xi_{-\mathbf{q}}) - f(\beta\xi_{\mathbf{q}})}{\xi_{-\mathbf{q}} + \xi_{\mathbf{q}}} \qquad \left(\delta U^{(2)}_{dph}\right)^{\uparrow\downarrow\uparrow\downarrow}_{\mathbf{k}\mathbf{k}'} = -U_0^2 \int \frac{\mathrm{d}\mathbf{q}}{\Omega} \frac{f(\beta\xi_{\mathbf{k}+\mathbf{k}'+\mathbf{q}}) - f(\beta\xi_{\mathbf{q}})}{\xi_{\mathbf{k}+\mathbf{k}'+\mathbf{q}} - \xi_{\mathbf{q}}} \quad . \tag{5.2.4}$$

where the resulting momentum structure of the effective vertex exclusively arises from the progatator terms. Due to the presence of SU(2)-invariance, we only considered a single spin sector, which can be used to generate all others. The sum over spins contributed a factor of two to the particle-particle term. Obviously, the particle-particle contribution is a constant with respect to $\mathbf{k}$ and $\mathbf{k}'$ and further evaluation of the term reproduces the logarithmic divergence for temperature $T \to 0$, we introduced at the beginning of the chapter by means of particle-particle ladders. In particular, by assuming inversion symmetry of the single-particle spectrum, $\xi_{-\mathbf{q}} = \xi_{\mathbf{q}}$, the particle-particle term can be written as

$$\int \frac{\mathrm{d}\mathbf{q}}{\Omega} \frac{f(-\beta\xi_{-\mathbf{q}}) - f(\beta\xi_{\mathbf{q}})}{\xi_{-\mathbf{q}} + \xi_{\mathbf{q}}} = \int \frac{\mathrm{d}\mathbf{q}}{\Omega} \frac{\tanh\left(\beta\xi_{\mathbf{q}}/2\right)}{2\xi_{\mathbf{q}}} \approx \int_{1/\beta}^{W} \mathrm{d}\xi \, \frac{\rho(\xi)}{\xi} \approx \rho(0) \log\left(\beta W\right) \quad , \tag{5.2.5}$$

where we introduced the density of states $\rho(\xi)$ and the upper band edge W of the dispersion ξ, which was assumed to be particle-hole symmetric. The integrand in (Equation 5.2.5) $\tanh\left(\beta\xi_{\mathbf{q}}/2\right)/(2\xi_{\mathbf{q}})$ is symmetric about the energy axis and features a peak at zero energy that scales according to $\beta/4$ and eventually diverges for zero temperature, resulting in the logarithmic divergence. Although the general case of (Equation 5.1.19a) involves an integral featuring the k-dependent eigenvectors (Equation 5.1.15), that can only be integrated numerically, the logarithmic divergence at zero temperature is, however, not spoiled by these factors. Summarizing the result of the perturbative expansion of the two-particle vertex up to second order in the antiparallel spin channel for bare on-site Coulomb repulsion, we have

$$(\delta U)^{\uparrow\downarrow\uparrow\downarrow}_{\mathbf{k}\mathbf{k}'} \approx U_0 + U_0^2 \left(\rho(0) \log\left(\beta W\right) + \chi(\mathbf{k} + \mathbf{k}')\right) \quad . \tag{5.2.6}$$

where we abbreviated the *susceptibility*

$$\chi(\mathbf{k}) := -\int \frac{\mathrm{d}\mathbf{q}}{\Omega} \frac{f(\beta\xi_{\mathbf{k}+\mathbf{q}}) - f(\beta\xi_{\mathbf{q}})}{\xi_{\mathbf{k}+\mathbf{q}} - \xi_{\mathbf{q}}} \overset{\mathbf{k}\to 0}{=} -\int \frac{\mathrm{d}\mathbf{q}}{\Omega} \underbrace{\lim_{\beta\to 0} \frac{\mathrm{d}f(\beta\xi)}{\mathrm{d}\xi}}_{=-\delta(\xi)} = \rho(0) \quad . \tag{5.2.7}$$

The *susceptibility* is a positive definite quantity, since in the zero temperature limit $\beta \to \infty$ and for zero momentum transfer $\mathbf{q} \to 0$ it reduces to the non-interacting density of states $\rho(0)$ at the Fermi level. The parallel spin channel doesn't have the bare U_0 but contributions from both particle-hole terms, which give (neglecting the particle-particle part)

$$(\delta U)^{\uparrow\uparrow\uparrow\uparrow}_{\mathbf{k}\mathbf{k}'} \approx U_0^2 \left(\chi(\mathbf{k} + \mathbf{k}') - \chi(\mathbf{k}' - \mathbf{k})\right) \quad . \tag{5.2.8}$$

The result (Equation 5.2.6) can be used to find the singlet and triplet part of the effective Cooper channel by either symmetrization (antisymmetrization) in momentum space or antisymmetrization (symmetrization) in spin space. Hence, we find $\delta U^{SGT} = U + U_0^2 \left(\chi(\mathbf{k}+\mathbf{k}') + \chi(\mathbf{k}'-\mathbf{k})\right)$ and $\delta U^{TPT} = U_0^2 \left(\chi(\mathbf{k}+\mathbf{k}') - \chi(\mathbf{k}'-\mathbf{k})\right)$, where the triplet part corresponds to the parallel spin channel (cf. (Section 5.4)). Within the range of weak-interaction strength U_0, where the perturbative expansion is valid, the (short range) first order contribution will be much larger than the second order, which may be comprised of attractive channels. Only in the strong coupling limit $U_0 \geq 1$, where the perturbative expansion becomes invalid, the second order contribution will overcome the bare repulsion (see [AK11]). However, assuming a strongly-screened bare interaction, the second order term may well contribute to an overall attractive long-range channel. Furthermore, since the on-site interaction is constant in k-space, the non-local second order contribution may well generate a pairing state with finite angular momentum since the constant interaction of the first order is projected out in any channel with finite angular momentum, even if the second order attraction is much weaker. More technically, a Cooper vertex $\delta U^{(2)}_{\mathbf{k}\mathbf{k}'}$ comprised of both repulsive first-order and (weaker) attractive second order parts, may still feature bound states by choosing an angular momentum channel, which is part of the kernel (null space) of the vertex part associated to the repulsive channel(s). Hence, if the first order bare interaction contributes a non s-wave like repulsion, one has to take it into account and perform a careful analysis of the balance between both first and second order. To get rid of the restriction of a local bare interaction, we take the second term in (Equation 5.2.3) associated to a finite nearest neighbor interaction $U_1 > 0$ into account. On the one hand, the nearest neighbor interaction produces a non-local first order contribution, which suppresses the pairing states corresponding to basis functions and associated angular momentum channels, the bare interaction is comprised of. As a result, the inclusion of the long-range interaction may promote former subleading channels of the Cooper vertex to represent the leading instability (cf. [Rag+12]). On the other hand, the k-dependent bare interaction allows, even in the presence of SU(2)-symmetry for more contributing terms in the perturbative expansion. In particular, $U_1 > 0$ generates a finite contribution in the direct particle-hole channel (Equation 5.1.19b). As a matter of fact, perturbation theory alone cannot reproduce the superconducting state and associated properties. In order to deal with the logarithmic divergence (Equation 5.2.5), an energy cutoff is introduced and only degrees of freedom above this cutoff are taken into account in the perturbative expansion. In the next section, we will work out how to deal with the residual degrees of freedom in the vicinity of the Fermi surface by integrating them out by means of a renormalization group treatment. Finally, we note the special case of a logarithmic divergence that arises in the particle-hole channel channels as well. In case of a single-particle spectrum that features $\xi_{\mathbf{k}+\mathbf{k}'+\mathbf{q}} = -\xi_{\mathbf{q}}$ in (Equation 5.2.4), the crossed particle-hole term will resemble the integral and the log-divergence of the particle-particle term [BBD03]. This represents the basis for concept of the *parquet* renormalization group [MC13]. In particular, this case occurs in the iron pnictides where the momentum transfer connects particle and hole pockets with opposite energies [CEE08; Chu12].

5.3. Logarithmic renormalization

The residual low-energy degrees of freedom below the cutoff Λ_0 are treated by means of a (logarithmic) renormalization group flow in the spirit of [Pol92; Sha94a]. The starting point of this procedure is the effective two-particle vertex generated in the first step by means of the perturbation expansion in (Section 5.1). First of all, we have to properly define the cutoff Λ_0. The cutoff is supposed to avoid the infrared singularity caused by the particle-particle ladders (Equation 5.2.5), while at the same time being small enough so that only a narrow range of residual energies about the Fermi surface remains, in order to be able to safely linearize the single-particle dispersion in the vicinity of the Fermi level. The lower bound for the cutoff is determined by the log-divergence by assuming that the particle-particle ladder grows to be of order one at the point where the two-particle vertex is significantly affected, i.e. $U_0^2\, \rho(0) \log\left((\Lambda_0^l)^{-1} W\right) \approx 1$. The upper bound has to ensure that the remaining degrees of freedom lie within an energy shell much smaller than the bandwidth W of the single-particle spectrum, i.e. $\Lambda_0^u \approx U_0^2/W$. Summarizing the above, we find for the valid range of the cutoff the condition (cf. [RKS10, Sec. IV.])

$$\Lambda_0^l = W e^{-\frac{1}{U_0^2\, \rho(0)}} \quad \ll \quad \Lambda_0 \quad \ll \quad \frac{U_0^2}{W} = \Lambda_0^u \quad . \tag{5.3.1}$$

In contrast to Λ_0^l and Λ_0^u, which are related to physical energy scales, the actual cutoff Λ_0 is not and represents a purely mathematical tool. Hence, the starting point of the renormalization group flow can be summarized by an *effective* action (unrelated to the generating functional of the effective action) in terms of Grassmann fields $\bar{\psi}$, ψ associated to energy scale Λ_0, which includes the effective two-particle vertex in the Cooper channel and the corresponding quadratic term of the theory:

$$\begin{aligned} S\left[\bar{\psi}, \psi\right] = & \int_{(K,\alpha)} \left(i\omega_n - v^F_{\mathbf{k}\alpha} k\right) \bar{\psi}_{K\alpha} \psi_{K\alpha} \\ & + \quad \frac{1}{\beta} \int_{\substack{(K_1,\alpha_1),(K_2,\alpha_2) \\ (K_1',\alpha_1'),(K_2',\alpha_2')}} \Gamma^{\Lambda_0}(K_1, K_2, K_1', K_2')_{\alpha_1\alpha_2,\alpha_1'\alpha_2'}\, \bar{\psi}_{K_1'\alpha_1'} \bar{\psi}_{K_2'\alpha_2'} \psi_{K_2\alpha_2} \psi_{K_1\alpha_1} \quad , \end{aligned} \tag{5.3.2}$$

where $K = (i\omega_n, \mathbf{k})$ is the combined Matsubara and momentum index. The effective two-particle vertex Γ^{Λ_0} associated to Λ_0 is given by (Equation 5.1.14). The single-particle spectrum $\xi_{\mathbf{k}\alpha} = \varepsilon_{\mathbf{k}\alpha} - \mu \approx v^F_{\mathbf{k}\alpha} k$ is linearized in the vicinity of the Fermi surface with Fermi velocity $v^F_{\mathbf{k},\alpha}$ and the parameter k, which is measured relative to the Fermi momentum. The fields are separated by the cutoff Λ into "fast" and "slow" modes and likewise the non-interacting part of the action by setting [KBS10]

$$S\left[\bar{\psi}, \psi\right] = S_0\left[\bar{\psi}_>, \psi_>\right] + S_0\left[\bar{\psi}_<, \psi_<\right] + S_I\left[\bar{\psi}, \psi\right] \quad , \tag{5.3.3}$$

while the interacting part mixes both fast and slow modes. The corresponding functional integral can now be written as [Sha94a]

$$\mathcal{Z} = \int \mathcal{D}[\bar{\psi}, \psi] \, e^{-S[\bar{\psi},\psi]} = \int \mathcal{D}[\bar{\psi}_<, \psi_<] \int \mathcal{D}[\bar{\psi}_>, \psi_>] \, e^{-S_0[\bar{\psi}_<,\psi_<] - S_0[\bar{\psi}_<,\psi_<] - S_I[\bar{\psi}_<,\psi_<]} \quad . \tag{5.3.4}$$

The functional integral over the fast modes is easily evaluated to obtain

$$\begin{aligned} \mathcal{Z} &= \int \mathcal{D}[\bar{\psi}_<, \psi_<] \, e^{-S_0[\bar{\psi}_<,\psi_<]} \int \mathcal{D}[\bar{\psi}_>, \psi_>] \, e^{-S_0[\bar{\psi}_<,\psi_<] - S_I[\bar{\psi}_<,\psi_<]} \\ &= \int \mathcal{D}[\bar{\psi}_<, \psi_<] \, e^{-S_0[\bar{\psi}_<,\psi_<]} \mathcal{Z}_{0>} \left\langle e^{-S_I[\bar{\psi}_<,\psi_<]} \right\rangle_{0>} := \int \mathcal{D}[\bar{\psi}_<, \psi_<] \, e^{-S_{eff}[\bar{\psi}_<,\psi_<]} \quad , \end{aligned} \tag{5.3.5}$$

where $\mathcal{Z}_{0>}$ is the non-interacting partition function of fast modes and we defined the effective action $S_{eff}[\bar{\psi}_<, \psi_<]$ associated to the slow modes. Note, that even for an e.g. k-independent bare interaction, the integration of fast modes may in general produces an effective action of slow modes that is momentum dependent and involves all orders. The change of the effective action due to the integration of fast modes may be calculated perturbatively and generates for the two-particle vertex in second order the same diagrams that were already encountered in the context of "conventional" perturbation theory (Section 5.1). However, in contrast, to the previous case, the integration is restricted by the cutoff and confined to modes in a small shell around the Fermi level. It can be shown that only the particle-particle (BCS) diagram (cf. (Equation 5.1.10)) contributes to the renormalization flow [Sha94a]. Using the linearized spectrum, the *flow equation* in the particle-particle channel can be expressed by [RKS10]

$$\frac{\mathrm{d}\left(\delta U^{(2)}_{pp}\right)_{\mathbf{k}\mathbf{k}'}}{\mathrm{d}l} = -\left(\rho(0)\bar{v}^F\right)^2 \int_\Lambda^{\Lambda 0} \frac{\mathrm{d}q}{S_F} \frac{\left(\delta U^{(2)}_{pp}\right)_{\mathbf{k}\mathbf{q}}}{\sqrt{v^F_{\mathbf{k}} v^F_{\mathbf{q}}}} \frac{\left(\delta U^{(2)}_{pp}\right)_{\mathbf{q}\mathbf{k}'}}{\sqrt{v^F_{\mathbf{q}} v^F_{\mathbf{k}'}}} \quad , \tag{5.3.6}$$

with the flow parameter $l := \log \frac{\Lambda_0}{\Lambda}$. For a numerically more convenient calculation and notation we define the normalized matrix

$$g_{\mathbf{k}\mathbf{k}'} := \rho(0) \sqrt{\frac{\bar{v}^F}{v^F_{\mathbf{k}}}} \left(\delta U^{(2)}_{pp}\right)_{\mathbf{k}\mathbf{k}'} \sqrt{\frac{\bar{v}^F}{v^F_{\mathbf{k}'}}} \quad , \tag{5.3.7}$$

with $v^F_{\mathbf{k}} = |\nabla_{\mathbf{k}} \xi_{\mathbf{k}}|$ being the Fermi velocity of a particular Fermi sheet at the respective k-point and $\bar{v}^F$ being averaged Fermi velocity of the specific Fermi sheet. Since the Cooper vertex $\left(\delta U^{(2)}_{pp}\right)_{\mathbf{k}\mathbf{k}'}$ is a symmetric and Hermitian matrix we can easily write it in terms of its normalized eigenbasis. Each eigenvector corresponds to an angular momentum state

and a basis function associated to some irreducible representation of the underlying lattice. Using the eigenbasis of the Cooper channel, we see that every eigenvalue ζ_n renormalizes independently by

$$\frac{\mathrm{d}\zeta_n}{\mathrm{d}l} = -\zeta_n^2 \qquad \zeta_n(l) = \frac{\zeta_n^0}{1+\zeta_n^0 l} \quad . \tag{5.3.8}$$

with ζ_n^0 being the n-th unrenormalized eigenvalue. The eigenvalue, which first grows to be of order one, determines the symmetry of the Cooper instability. The flow equation of eigenvalues shows that a positive initial coupling ζ_n^0 flows down to zero (*irrelevant*) and an initial negative ζ_n^0 is *relevant* with respect to the renormalization flow .

5.4. Random phase approximation and spin fluctuations

While the *perturbative renormalization* took *all* diagrams up to second order in the weak-coupling limit into account, one might as well consider particular kinds of diagrams up to infinite order and thereby overcome the restriction of weak-coupling. One way of doing this is usually called the *random phase approximation* (*RPA*) [BS66]. Here, we consider it briefly due to its formal similarity to the perturbative renormalization and its use as a benchmark. Let's go back to the perturbative expansion of the two-particle vertex in (Equation 5.1.6), which produces (in case of an SU(2)-invariant bare interaction) five diagrams in second order as shown in (Figure 5.2). Later, we found that for the on-site Coulomb interaction only the first and second diagrams contribute to the effective two-particle vertex with antiparallel spins (cf. (Equation 5.2.4)). Instead of stopping in second order of the expansion, we now include the diagrams of these two types up to infinite order. The first few diagrams in these series are sketched in (Figure 5.4). For both the singlet and triplet part of the two-particle vertex these diagrams may be summed up by means of a geometric series analogously to the *particle-particle ladders* in (Figure 5.1). The opposite (antiparallel) spin Cooper channel of the effective two-particle vertex can be expressed by (cf. [BK08])

$$\left(U^{RPA}\right)^{\uparrow\downarrow\uparrow\downarrow}_{\mathbf{k}\mathbf{k}'} = U_0 + \frac{U_0^2\chi(\mathbf{k}+\mathbf{k}')}{1-U_0\chi(\mathbf{k}+\mathbf{k}')} + \frac{U_0^3\chi^2(\mathbf{k}-\mathbf{k}')}{1-U_0^2\chi^2(\mathbf{k}-\mathbf{k}')} \quad , \tag{5.4.1}$$

with the on-site Coulomb interaction U_0 (cf. (Equation 5.2.3)) and the non-interacting susceptibility (Equation 5.2.7). The equal (parallel) spin part has only the "bubble" terms, which result in

$$\left(U^{RPA}\right)^{\uparrow\uparrow\uparrow\uparrow}_{\mathbf{k}\mathbf{k}'} = -\frac{U_0^2\chi(\mathbf{k}-\mathbf{k}')}{1-U_0^2\chi^2(\mathbf{k}-\mathbf{k}')} \quad . \tag{5.4.2}$$

These results may be more conveniently expressed by defining the *RPA charge-/spin-susceptibilities* $\chi^c = \chi/(1+\chi)$ and $\chi^s = \chi/(1-\chi)$, respectively. With these, the effective two-particle vertex in antiparallel and parallel spin channels is given by (cf. [HKM11])

$$\left(U^{RPA}\right)^{\uparrow\downarrow\uparrow\downarrow}_{\mathbf{k}\mathbf{k}'} = U_0 + U_0^2\left(\chi^s(\mathbf{k}+\mathbf{k}') + \frac{1}{2}\chi^s(\mathbf{k}-\mathbf{k}') - \frac{1}{2}\chi^c(\mathbf{k}-\mathbf{k}')\right) \quad , \tag{5.4.3}$$

and

$$\left(U^{RPA}\right)^{\uparrow\uparrow\uparrow\uparrow}_{\mathbf{k}\mathbf{k}'} = -U_0^2\left(\chi^s(\mathbf{k}-\mathbf{k}') + \frac{1}{2}\chi^c(\mathbf{k}-\mathbf{k}')\right) \quad . \tag{5.4.4}$$

The singlet and triplet parts of the effective two-particle interaction are then determined via $\left(U^{RPA}_{SGT}\right)_{\mathbf{k}\mathbf{k}'} = \frac{2\left(U^{RPA}\right)^{\uparrow\downarrow\uparrow\downarrow}_{\mathbf{k}\mathbf{k}'} - \left(U^{RPA}\right)^{\uparrow\uparrow\uparrow\uparrow}_{\mathbf{k}\mathbf{k}'}}{2}$ and $\left(U^{RPA}_{TPT}\right)_{\mathbf{k}\mathbf{k}'} = \frac{\left(U^{RPA}\right)^{\uparrow\uparrow\uparrow\uparrow}_{\mathbf{k}\mathbf{k}'}}{2}$. The pairing strength is evaluated by integration of the eigenmodes of singlet and triplet vertices along the Fermi surface. Multi-orbital extensions of the RPA-approximation for the treatment of superconductivity require the formulation of the RPA vertices in terms of orbital matrices and the inclusion of additional diagrams. This has been extensively worked out for the iron-pnictides in two [Gra+09; Mai+11a; Mai+11b; Alt+16] and even three spatial dimensions [Gra+10; Wan+13b; Kre+13]. The inclusion of spin-orbit coupling has been achieved only recently [Kor17; Nis+17; Zha+17].

Summary and preview

This chapter introduced the perturbative renormalization group for multi-orbital systems including any kind of spin-orbit interaction. This kind of perturbative renormalization group is comprised of two steps. The first involves the perturbative expansion of the (spinful) two-particle vertex up to second order in the bare (repulsive) interaction, which generates a momentum dependent effective interaction. During the second step this effective interaction generated during the first step is employed as the input to a logarithmic renormalization group flow and only takes the modes within a small energy window in the vicinity of the Fermi level into account. Since the perturbative step requires the limitation to infinitesimal interaction strength, we consider the comparison to the random phase approximation as a method that remedies this shortcoming by infinite resummation of particular types of diagrams. While the random phase approximation appears to be numerically well-controlled, it suffers, in contrast to the perturbative renormalization group, from its limited applicability due to the selection of types of diagrams. The next chapter is devoted to the functional renormalization group as a method, which incorporates the advantages of the perturbative renormalization by cosidering all diagrams and it is at the same time extending the analysis to weak but finite interaction strength.

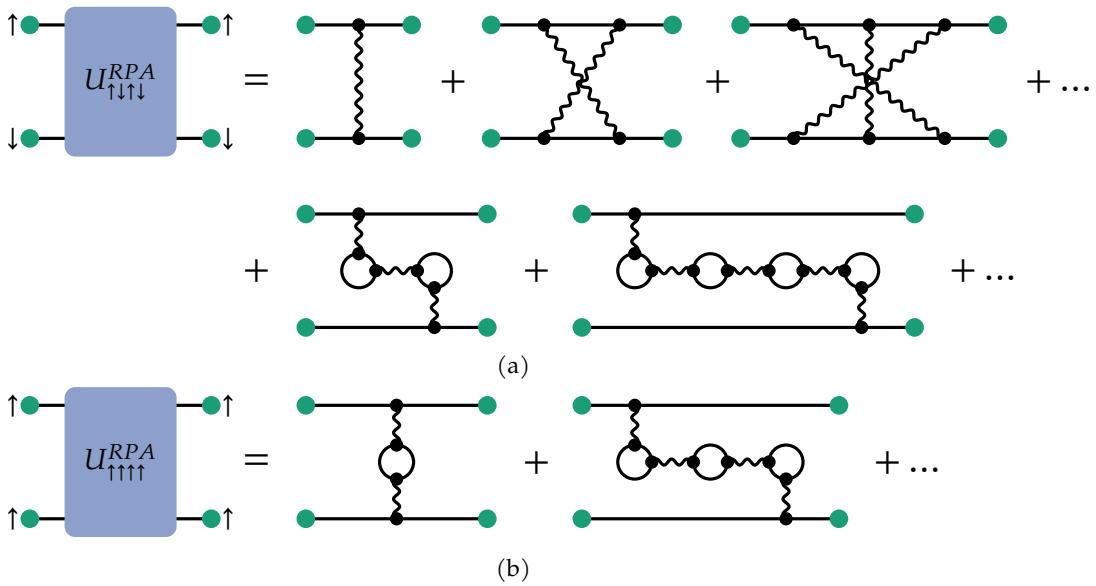

Figure 5.4.: The random phase approximation in a single-orbital model includes "bubble" and "ladder" type diagrams up to infinite order. Apart from the first order represented by the bare interaction, the singlet part features both "bubble" and "ladder" type diagrams. The "bubble" diagrams only appear in every even order. In contrast, in the triplet part only the "bubble" diagrams contribute and they only do in every even order.

6. Functional renormalization group

The functional renormalization group is one of the (modern) implementations of Wilson's renormalization group idea [Wil71c; Wil71d] among the *Migdal-Kadanoff real space RG* [Mig76; Kad76], the *momentum space RG* [WK74], the *numerical RG* [Wil75] and the *density-matrix renormalization group* (*DMRG*) [Whi92; Sch05a]. The common feature of all these versions of the renormalization group is the concept of iterative integration of all degrees of freedom that appear in the partition function describing the system under consideration. A single iteration is comprised of the *decimation step* (*mode elimination*) and the *rescaling* of momenta and fields . A key step towards the development of the functional renormalization group was the realization that the decimation step may be carried out in an infinitesimal way, thereby enabling the description of the effective action's change in terms of a functional differential equation [WH73]. In this chapter, we introduce and derive the flow equation of the effective action based on the corresponding generating functional supplemented by a cutoff dependent free propagator. The straightforward integration of this flow equation turns out to be unfeasible. Henceforth, by an expansion of the effective action in term of fields, particular n-particle correlation functions and their associated flow equations are derived. We are interested in the first two orders of the expansion which provide the flow equations of the self-energy and the irreducible two-particle vertex. The spinful flow equation of the two-particle vertex is parameterized in a way that allows for a convenient and numerically stable implementation.

6.1. Cutoff schemes and temperature flow

The functional renormalization group is based on the idea of calculating the partition function and generating functionals, respectively in an iterative way. To this end, a *cutoff function* is introduced which separates "fast" (high-energy) from "slow" (low-energy) modes and is characterized by the *cutoff-scale* Λ, defining the boundary between both. The cutoff function Θ_Λ is supposed to suppress all modes below Λ and keep all modes above unmodified. In the limit $\Lambda \to \infty$ the theory (and therefore the generating functional) is expected to be trivial and therefore exactly solvable. By reducing the cutoff Λ, the original theory and corresponding solution is (in principle) eventually obtained in the limit $\Lambda \to 0$. Starting from the limit $\Lambda \to \infty$, the change of the generating functional - when reducing the cutoff by an infinitesimal amount $\mathrm{d}\Lambda$ - can be described by a (nonlinear) functional differential equation. While these functional flow equations can be derived for any generating functional, we focus on the generating functional of the *effective action* which turns out to provide the most convenient initial condition for $\Lambda \to \infty$.

First of all, we have to introduce the cutoff dependency into the effective action, which is done by modifying the free propagator $G_0(K)$ to incorporate the scale dependency on Λ. In a more formal way, the modified free propagator $G_0^\Lambda(K)$ is required to satisfy (cf. [KBS10, Chap. 7.1])

$$G_0^\Lambda(K) = \begin{cases} 0 & \Lambda \to \infty \\ G_0^\Lambda(K) & \Lambda \quad \text{finite} \\ G_0(K) & \Lambda \to 0 \end{cases} \tag{6.1.1}$$

The cutoff function itself can be implemented in a variety of ways. On the one hand, one distinguishes between a *multiplicative cutoff function* C_Λ and an *additive cutoff function* (*regulator*) R_Λ which are introduced into the free propagator and the inverse free propagator, respectively (cf.[KBS10, Chap. 7.1]):

$$G_0^\Lambda := G_0 C_\Lambda \qquad \left(G_0^\Lambda\right)^{-1} := (G_0)^{-1} - R_\Lambda \quad . \tag{6.1.2}$$

On the other hand, cutoff functions can be realized in i.a. energy, temperature and frequency space. Although the most obvious way to separate fast from slow modes in energy space is by means of the *Heaviside step function* as the cutoff function, this should generally be avoided since the sharp cutoff leads to technical complications in the flow equations which involve the scale derivative of the cutoff function, resulting in a Dirac delta function. A *smooth* cutoff function Θ_Λ^ϵ is characterized not only by the scale Λ but also by the width ϵ of the step. For example, a multiplicative smooth cutoff function in energy space ξ and its derivative with respect to Λ are given by [Hon+01; GHM08]

$$\Theta_\Lambda^\epsilon(\xi) = 1 - \frac{1}{e^{(|\xi|-\Lambda)/(\epsilon\Lambda)}+1} \qquad \frac{\mathrm{d}}{\mathrm{d}\Lambda}\Theta_\Lambda^\epsilon(\xi) = \left(\Theta_\Lambda^\epsilon(\xi)-1\right)\Theta_\Lambda^\epsilon(\xi)\frac{|\xi|}{\epsilon\Lambda^2} \quad , \tag{6.1.3}$$

resulting in the associated modified Gaussian propagator $G_0^\Lambda(K) = \Theta_\Lambda^\epsilon(\xi) G_0(K)$, where the implicit dependency of the single-particle energy $\xi_{\mathbf{k}}$ on momentum $\mathbf{k}$ is implied. The smooth cutoff in energy space and its derivative with respect to the cutoff scale are illustrated in (Figure 6.1). Later, we may also require the derivative of the inverse of the cutoff function with respect to the cutoff parameter, which is given by

$$\frac{\mathrm{d}}{\mathrm{d}\Lambda}\left(\Theta_\Lambda^\epsilon(\xi)\right)^{-1} = -\frac{1}{\left(\Theta_\Lambda^\epsilon(\xi)\right)^2}\partial_\Lambda\Theta_\Lambda^\epsilon(\xi) = \frac{1-\Theta_\Lambda^\epsilon(\xi)}{\Theta_\Lambda^\epsilon(\xi)}\frac{|\xi|}{\epsilon\Lambda^2} \quad , \tag{6.1.4}$$

For the applications in (Part II) we will mainly make use of a temperature cutoff, which, however, does not comply to any of the above scheme categories of a cutoff or regulator cutoff. An energy/momentum cutoff like (Equation 6.1.3) artificially suppresses ferromagnetism since it excludes small momentum transfers until shortly before the

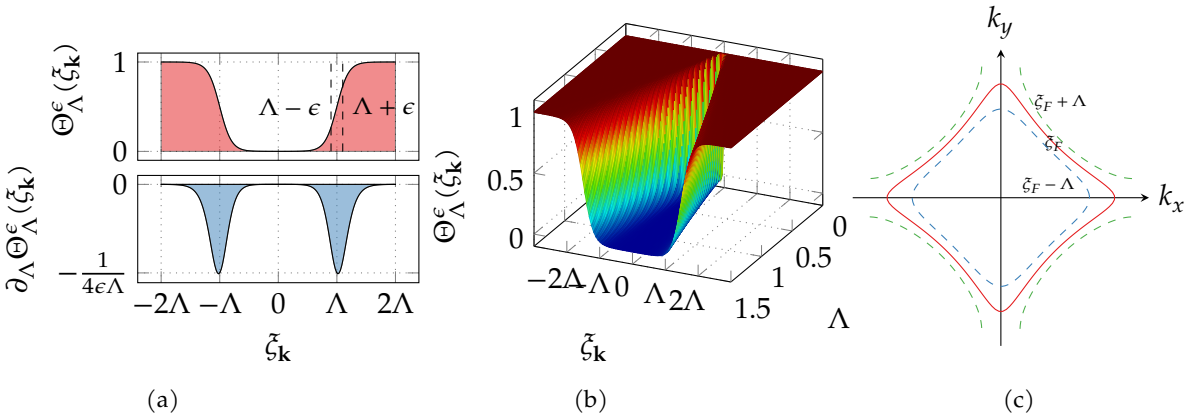

(a) (b) (c)

Figure 6.1.: (Figure 6.1a) The smooth cutoff function in energy space features a broadened step function of width ϵ. The derivative of the cutoff function with respect to the cutoff scale, which appears in the flow equations, scales reciprocal to the stepwidth Λ. (Figure 6.1b) The dependence of the cutoff function on energy and cutoff scale shows that the sign of its derivative with respect to the cutoff scale must be negative. (Figure 6.1c) The Fermi surface of the single-band Hubbard model $\xi_{\mathbf{k}} = -2t(\cos(k_x)+\cos(k_y))-4t'\cos(k_x)\cos(k_y)-\mu$ with $t = 1.0$, $t' = -0.25$ and $\mu = -1.1$) is shown in solid red, while the upper and lower limits of the region of k-space enclosed by the cutoff Λ, which has to be integrated out, are shown in dashed green and blue.

very end of the renormalization flow, which may even be not reached due to the divergence of another channel. In order to circumvent these issues, one may introduce the temperature T or the thermodynamic β, respectively, as the scale parameter [HS01]. Unfortunately, introducing the temperature as flow parameter, results in a renormalization group scheme, which does not allow for a separation of slow and fast modes but still for some intuitive interpretation of the flow parameter (see (Figure 6.2)). Before we can introduce the *temperature flow* parameter, we have to identify all temperature dependencies in the action (Equation 4.2.1). Apparently, only the interaction term incorporates a temperature-dependence in its prefactor $\frac{1}{\beta}$ (Equation 4.2.3). Defining the new Grassmann fields

$$\psi_\alpha \to \phi_\alpha = \beta^{1/4}\psi_\alpha \qquad \text{and} \qquad \bar{\psi}_\alpha \to \bar{\phi}_\alpha = \beta^{1/4}\bar{\psi}_\alpha \quad , \tag{6.1.5}$$

by a (temperature-dependent) rescaling of the fields, we can shift the temperature dependency from the interacting part to the non-interacting part. Note, that this transformation may look different depending on the original definition of fields in Matsubara representation (Equation 4.1.8a) and (Equation 4.1.8b). Hence, we obtain the action in terms of the rescaled fields

$$S\left[\bar{\phi},\phi\right] = \beta^{1/2}\int_{\alpha,\alpha'}\bar{\phi}_{\alpha'}\left(-i\omega\delta_{\alpha\alpha'}+h_{\alpha'\alpha}\right)\phi_{\alpha}+\int_{\substack{\alpha_1,\alpha_2\\ \alpha_1',\alpha_2'}}V_{\alpha_1\alpha_2\alpha_1'\alpha_2'}\bar{\phi}_{\alpha_1'}\bar{\phi}_{\alpha_2'}\phi_{\alpha_2}\phi_{\alpha_1} \quad , \quad (6.1.6)$$

with the (inverse) scale dependent Gaussian propagator

$$\left(G_0^{\Lambda}\right)^{-1}_{\alpha\alpha'} = \beta^{1/2}\left(-i\omega\delta_{\alpha\alpha'}+h_{\alpha'\alpha}\right) \qquad \left(G_0^{\Lambda}\right)_{\alpha\alpha'} = \beta^{-1/2}\left(-i\omega\delta_{\alpha\alpha'}+h_{\alpha'\alpha}\right)^{-1} \quad . \quad (6.1.7)$$

Using β as a flow parameter only partially satisfies the requirement (Equation 6.1.1) of the scale-dependent free propagator since $\lim_{\beta\to\infty}\left(G_0^{\Lambda=\beta}\right) = 0$ but $\lim_{\beta\to 0}\left(G_0^{\Lambda=\beta}\right) \neq G_0$. Fortunately, for the definition of the proper initial condition of the effective action only the limit $\beta \to \infty$ is important, as we will see at the end of (Section 6.2.2). Finally, we mention the *frequency cutoff* or Ω-scheme that is realized by a multiplicative cutoff function of the form [HS09]

$$C_{\Lambda}(\omega_n) = \frac{\omega_n^2}{\omega_n^2+\Lambda^2} \quad , \quad (6.1.8)$$

satisfying $\lim_{\Lambda\to\infty} C_{\Lambda}(\omega_n) = 0$ and $\lim_{\Lambda\to 0} C_{\Lambda}(\omega_n) = 1$. However, for the derivation of the flow equation the concrete implementation of the cutoff function does not matter yet and it is sufficient to assume that the Gaussian propagator features a parameter Λ, which incorporates a scale dependency resulting in proper boundary condition.

6.2. Fermionic functional flow equations

By means of the modified Gaussian propagator in (Equation 6.1.1) we introduce a cut-off/scale dependency into the (non-interacting) action

$$S\left[\bar{\phi},\phi\right] \to S^{\Lambda}\left[\bar{\phi},\phi\right] = S_0^{\Lambda}\left[\bar{\psi},\psi\right] + S_I\left[\bar{\psi},\psi\right] = \left(\bar{\psi},(G_0^{\Lambda})^{-1}\psi\right) + S_I\left[\bar{\psi},\psi\right] \quad , \quad (6.2.1)$$

the (non-interacting) partition function $\mathcal{Z}_{(0)} \to \mathcal{Z}_{(0)}^{\Lambda}$ and thereby into any generating functional like i.a. the generating functional of (dis)connected Green functions or the effective interaction. However, because of its useful and physical initial condition we focus on the generating functional of the one-particle irreducible vertex functions, the effective action Γ (cf. (Chapter 4)). Unfortunately, before we start to derive the flow equation of the effective action, we have to find the flow equation of the generating functional of connected Green functions, since the flow equation of the effective action turns out to depend on it.

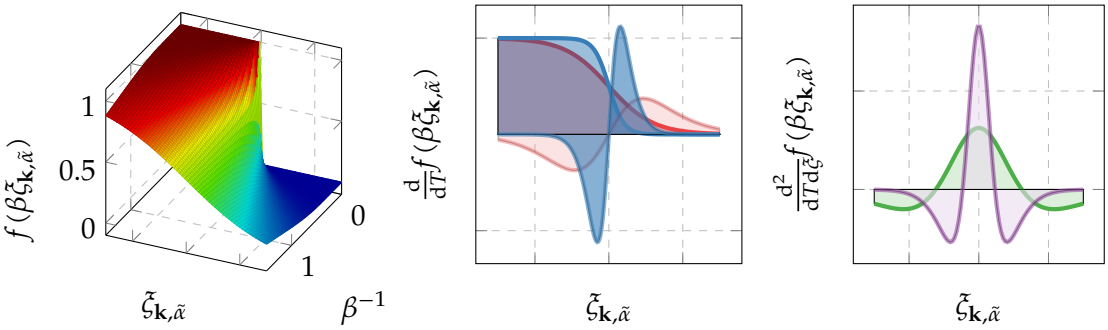

(a) (b) (c)

Figure 6.2.: The Fermi-Dirac function (Figure 6.2a) itself can be used as a regulator, where the temperature derivative determines the modes that are integrated out during a renormalization group step specified by some temperature (Figure 6.2b). Reducing the temperature, only modes inside an increasingly narrow shell around the Fermi surface contribute to the renormalization flow. If the band energies occurring in the loop integral are degenerate, the loop integrand is most conveniently expressed as the two-fold derivative of the Fermi-Dirac function with respect to temperature and energy.

6.2.1. Flow equation of the generating functional of (dis)connected Green functions

Imposing the scale dependency on the generating functional of disconnected Green functions (Equation 4.2.5), we find

$$\mathcal{G}^{\Lambda}[\bar{\eta},\eta] = \frac{1}{\mathcal{Z}^{\Lambda}} \int \mathcal{D}[\bar{\psi},\psi]\, e^{-S^{\Lambda}[\bar{\psi},\psi]-(\bar{\eta},\psi)-(\bar{\psi},\eta)} \quad , \tag{6.2.2}$$

with the scale dependency Λ entering through the interacting partition function $\mathcal{Z}^{\Lambda}$ and the action S^{Λ}. The total derivative of $\mathcal{G}^{\Lambda}$ with respect to the cutoff Λ is

$$\begin{aligned}
\frac{\mathrm{d}}{\mathrm{d}\Lambda}\mathcal{G}^{\Lambda}[\bar{\eta},\eta] =& -\frac{1}{(\mathcal{Z}^{\Lambda})^2}\left(\frac{\mathrm{d}\mathcal{Z}^{\Lambda}}{\mathrm{d}\Lambda}\right)\int \mathcal{D}[\bar{\psi},\psi]\, e^{-S_{\Lambda}[\bar{\psi},\psi]-(\bar{\eta},\psi)-(\bar{\psi},\eta)} \\
&+ \frac{1}{\mathcal{Z}^{\Lambda}}\int \mathcal{D}[\bar{\psi},\psi]\left(\bar{\psi}, \frac{\mathrm{d}(G_0^{\Lambda})^{-1}}{\mathrm{d}\Lambda}\psi\right) e^{-S^{\Lambda}[\bar{\psi},\psi]-(\bar{\eta},\psi)-(\bar{\psi},\eta)} \\
=& -\frac{1}{(\mathcal{Z}^{\Lambda})^2}\left(\frac{\mathrm{d}\mathcal{Z}^{\Lambda}}{\mathrm{d}\Lambda}\right)\int \mathcal{D}[\bar{\psi},\psi]\, e^{-S^{\Lambda}[\bar{\psi},\psi]-(\bar{\eta},\psi)-(\bar{\psi},\eta)} \\
&+ \frac{1}{\mathcal{Z}^{\Lambda}}\int \mathcal{D}[\bar{\psi},\psi]\left(\frac{\delta}{\delta\eta}, \frac{\mathrm{d}(G_0^{\Lambda})^{-1}}{\mathrm{d}\Lambda}\left(-\frac{\delta}{\delta\bar{\eta}}\right)\right) e^{-S^{\Lambda}[\bar{\psi},\psi]-(\bar{\eta},\psi)-(\bar{\psi},\eta)} \quad ,
\end{aligned} \tag{6.2.3}$$

where in the second equality we substituted the fields $\bar{\psi}$, ψ by functional derivatives with respect to the source fields $\bar{\eta}$, η. The expression is simplified by recollecting the terms making up the generating functional of disconnected Green functions, itself. In the next step, we decompose the fermionic bilinear into its integral form and evaluate the functional derivatives with respect to the source fields. As a result we obtain

$$\begin{aligned}
\frac{\mathrm{d}}{\mathrm{d}\Lambda}\mathcal{G}^{\Lambda}\left[\bar{\eta},\eta\right] &= -\frac{1}{\mathcal{Z}^{\Lambda}}\left(\frac{\mathrm{d}\mathcal{Z}^{\Lambda}}{\mathrm{d}\Lambda}\right)\mathcal{G}^{\Lambda}\left[\bar{\eta},\eta\right] - \left(\frac{\delta}{\delta\eta},\frac{\mathrm{d}(G_0^{\Lambda})^{-1}}{\mathrm{d}\Lambda}\frac{\delta}{\delta\bar{\eta}}\right)\mathcal{G}^{\Lambda}\left[\bar{\eta},\eta\right] \\
&= -\left(\frac{\mathrm{d}}{\mathrm{d}\Lambda}\ln\mathcal{Z}^{\Lambda}\right)\mathcal{G}^{\Lambda}\left[\bar{\eta},\eta\right] - \int_{\alpha}\int_{\beta}\left(\frac{\delta}{\delta\eta_{\alpha}}\left(\frac{\mathrm{d}(G_0^{\Lambda})^{-1}}{\mathrm{d}\Lambda}\right)_{\alpha,\beta}\frac{\delta}{\delta\bar{\eta}_{\beta}}\right)\mathcal{G}^{\Lambda}\left[\bar{\eta},\eta\right] \\
&= -\left(\frac{\mathrm{d}}{\mathrm{d}\Lambda}\ln\mathcal{Z}_{\Lambda}\right)\mathcal{G}^{\Lambda}\left[\bar{\eta},\eta\right] - \int_{\alpha}\int_{\beta}\left(\frac{\mathrm{d}(G_0^{\Lambda})^{-1}}{\mathrm{d}\Lambda}\right)_{\alpha,\beta}\left(\frac{\delta^2\mathcal{G}^{\Lambda}\left[\bar{\eta},\eta\right]}{\delta\eta\delta\bar{\eta}}\right)_{\alpha,\beta} \\
&= -\left(\frac{\mathrm{d}}{\mathrm{d}\Lambda}\ln\mathcal{Z}^{\Lambda}\right)\mathcal{G}^{\Lambda}\left[\bar{\eta},\eta\right] - \int_{\alpha}\left(\frac{\mathrm{d}(G_0^{\Lambda})^{-1}}{\mathrm{d}\Lambda}\left(\frac{\delta^2\mathcal{G}^{\Lambda}\left[\bar{\eta},\eta\right]}{\delta\eta\delta\bar{\eta}}\right)^{T}\right)_{\alpha,\alpha} \\
&= -\left(\frac{\mathrm{d}}{\mathrm{d}\Lambda}\ln\mathcal{Z}^{\Lambda}\right)\mathcal{G}^{\Lambda}\left[\bar{\eta},\eta\right] - \mathrm{Tr}\left[\frac{\mathrm{d}(G_0^{\Lambda})^{-1}}{\mathrm{d}\Lambda}\left(\frac{\delta^2\mathcal{G}_{\Lambda}\left[\bar{\eta},\eta\right]}{\delta\eta\delta\bar{\eta}}\right)^{T}\right] \quad . \qquad (6.2.4)
\end{aligned}$$

Here, we introduced the notation of the trace Tr referring to the integration over diagonal elements in superfield space α. Henceforth, the flow equation of the generating functional of disconnected Green functions can be summarized by (cf. [KBS10, Chap. 7.2] [Met+12b])

$$\frac{\mathrm{d}}{\mathrm{d}\Lambda}\mathcal{G}^{\Lambda}\left[\bar{\eta},\eta\right] = -\left(\frac{\mathrm{d}}{\mathrm{d}\Lambda}\ln\mathcal{Z}^{\Lambda}\right)\mathcal{G}_{\Lambda}\left[\bar{\eta},\eta\right] - \mathrm{Tr}\left[\frac{\mathrm{d}(G_0^{\Lambda})^{-1}}{\mathrm{d}\Lambda}\left(\frac{\delta^2\mathcal{G}_{\Lambda}\left[\bar{\eta},\eta\right]}{\delta\eta\delta\bar{\eta}}\right)^{T}\right] \quad . \qquad (6.2.5)$$

Let's proceed to the flow equation of the generating functional of connected Green functions $\mathcal{G}_c^{\Lambda}$ defined in (Equation 4.2.7), which becomes

$$\mathcal{G}_c^{\Lambda}\left[\bar{\eta},\eta\right] = \ln\left[\frac{\mathcal{Z}^{\Lambda}}{\mathcal{Z}_0^{\Lambda}}\mathcal{G}^{\Lambda}\left[\bar{\eta},\eta\right]\right] \quad , \qquad (6.2.6)$$

when imposing all cutoff dependencies. The total derivative of $\mathcal{G}_c^{\Lambda}$ with respect to Λ results in

$$\begin{aligned}\frac{\mathrm{d}}{\mathrm{d}\Lambda}\mathcal{G}_c^\Lambda[\bar\eta,\eta] &= \frac{\mathcal{Z}_0^\Lambda}{\mathcal{Z}^\Lambda\mathcal{G}^\Lambda[\bar\eta,\eta]}\frac{\mathrm{d}}{\mathrm{d}\Lambda}\left(\frac{\mathcal{Z}^\Lambda}{\mathcal{Z}_0^\Lambda}\mathcal{G}^\Lambda[\bar\eta,\eta]\right)\\ &= \frac{\mathcal{Z}_0^\Lambda}{\mathcal{Z}^\Lambda\mathcal{G}^\Lambda[\bar\eta,\eta]}\frac{\mathrm{d}}{\mathrm{d}\Lambda}\left(\frac{1}{\mathcal{Z}_0^\Lambda}\int\mathcal{D}[\bar\psi,\psi]\,e^{-S^\Lambda[\bar\psi,\psi]-(\bar\eta,\psi)-(\bar\psi,\eta)}\right)\\ &= \frac{\mathcal{Z}_0^\Lambda}{\mathcal{Z}^\Lambda\mathcal{G}^\Lambda[\bar\eta,\eta]}\left(-\frac{1}{(\mathcal{Z}_0^\Lambda)^2}\left(\frac{\mathrm{d}\mathcal{Z}_0^\Lambda}{\mathrm{d}\Lambda}\right)\int\mathcal{D}[\bar\psi,\psi]\,e^{-S^\Lambda[\bar\psi,\psi]-(\bar\eta,\psi)-(\bar\psi,\eta)}\right.\\ &\quad\left.+\frac{1}{\mathcal{Z}_0^\Lambda}\int\mathcal{D}[\bar\psi,\psi]\left(\bar\psi,\frac{\mathrm{d}(G_0^\Lambda)^{-1}}{\mathrm{d}\Lambda}\psi\right)e^{-S^\Lambda[\bar\psi,\psi]-(\bar\eta,\psi)-(\bar\psi,\eta)}\right)\quad. \end{aligned}\tag{6.2.7}$$

Again, we employ the functional derivatives with respect to the source fields $\bar\eta$, η to substitute the fields $\bar\psi$, ψ, pull the derivatives out of the integration and reassemble the generating functional $\mathcal{G}^\Lambda$. Hence, we obtain

$$\frac{\mathrm{d}}{\mathrm{d}\Lambda}\mathcal{G}_c^\Lambda[\bar\eta,\eta] = \frac{1}{\mathcal{Z}^\Lambda\mathcal{G}^\Lambda[\bar\eta,\eta]}\left(-\left(\frac{\mathrm{d}}{\mathrm{d}\Lambda}\ln\mathcal{Z}_0^\Lambda\right)-\left(\frac{\delta}{\delta\eta},\frac{\mathrm{d}(G_0^\Lambda)^{-1}}{\mathrm{d}\Lambda}\frac{\delta}{\delta\bar\eta}\right)\right)\mathcal{Z}^\Lambda\mathcal{G}^\Lambda[\bar\eta,\eta]\quad,\tag{6.2.8}$$

where we used $\frac{\delta}{\delta\eta}(\bar\psi,\eta) = -\bar\psi$ to get the correct sign of the second term. The term $\mathcal{Z}^\Lambda\mathcal{G}^\Lambda[\bar\eta,\eta]$ involving the interacting partition function and the generating functional of disconnected Green functions can be expressed by the non-interacting partition function $\mathcal{Z}_0^\Lambda$ and the generating functional of connected Green functions $\mathcal{G}_c^\Lambda$. Inverting (Equation 6.2.6) provides $\mathcal{Z}^\Lambda\mathcal{G}^\Lambda[\bar\eta,\eta] = \mathcal{Z}_0^\Lambda e^{\mathcal{G}_c^\Lambda[\bar\eta,\eta]}$. Inserting this relation into (Equation 6.2.8), we find

$$\frac{\mathrm{d}}{\mathrm{d}\Lambda}\mathcal{G}_c^\Lambda[\bar\eta,\eta] = -\left(\frac{\mathrm{d}}{\mathrm{d}\Lambda}\ln\mathcal{Z}_0^\Lambda\right)-e^{-\mathcal{G}_c^\Lambda[\bar\eta,\eta]}\left(\frac{\delta}{\delta\eta},\frac{\mathrm{d}(G_0^\Lambda)^{-1}}{\mathrm{d}\Lambda}\frac{\delta}{\delta\bar\eta}\right)e^{\mathcal{G}_c^\Lambda[\bar\eta,\eta]}\quad,\tag{6.2.9}$$

where the non-interacting partition function is canceled since it is independent of the source fields $\bar\eta$, η. Performing the functional derivatives with respect to these fields produces two terms that are given by

$$\begin{aligned}e^{-\mathcal{G}_c^\Lambda[\bar\eta,\eta]}\left(\frac{\delta}{\delta\eta},\frac{\mathrm{d}(G_0^\Lambda)^{-1}}{\mathrm{d}\Lambda}\frac{\delta}{\delta\bar\eta}\right)e^{\mathcal{G}_c^\Lambda[\bar\eta,\eta]} &= e^{-\mathcal{G}_c^\Lambda[\bar\eta,\eta]}\left(\frac{\delta}{\delta\eta},\frac{\mathrm{d}(G_0^\Lambda)^{-1}}{\mathrm{d}\Lambda}\frac{\delta\mathcal{G}_c^\Lambda[\bar\eta,\eta]}{\delta\bar\eta}\right)e^{\mathcal{G}_c^\Lambda[\bar\eta,\eta]}\\ &= \left(\frac{\delta\mathcal{G}_c^\Lambda[\bar\eta,\eta]}{\delta\eta},\frac{\mathrm{d}(G_0^\Lambda)^{-1}}{\mathrm{d}\Lambda}\frac{\delta\mathcal{G}_c^\Lambda[\bar\eta,\eta]}{\delta\bar\eta}\right)+\int_\alpha\int_\beta\left(\frac{\mathrm{d}(G_0^\Lambda)^{-1}}{\mathrm{d}\Lambda}\right)_{\alpha,\beta}\frac{\delta\mathcal{G}_c^\Lambda[\bar\eta,\eta]}{\delta\eta_\alpha\delta\bar\eta_\beta}\quad,\end{aligned}\tag{6.2.10}$$

where the integral arises from the decomposition of the fermionic bilinear and the

matrix property of the inverse Gaussian propagator. The second derivative of the generating functional $\mathcal{G}_c^\Lambda$ with respect to the source fields can be written as the superfield matrix of second functional derivatives. By using the transposed of the superfield matrix, the second integral becomes implicit and the second term may be expressed as the trace over superfield space. Hence, we obtain (cf. [KBS10, Chap. 7.2]

$$\frac{\mathrm{d}}{\mathrm{d}\Lambda}\mathcal{G}_c^\Lambda[\bar{\eta},\eta] = -\left(\frac{\mathrm{d}}{\mathrm{d}\Lambda}\ln\mathcal{Z}_0^\Lambda\right) - \left(\frac{\delta\mathcal{G}_c^\Lambda[\bar{\eta},\eta]}{\delta\eta}, \frac{\mathrm{d}(G_0^\Lambda)^{-1}}{\mathrm{d}\Lambda}\frac{\delta\mathcal{G}_c^\Lambda[\bar{\eta},\eta]}{\delta\bar{\eta}}\right) - \mathrm{Tr}\left[\frac{\mathrm{d}(G_0^\Lambda)^{-1}}{\mathrm{d}\Lambda}\left(\frac{\delta\mathcal{G}_c^\Lambda[\bar{\eta},\eta]}{\delta\eta\delta\bar{\eta}}\right)^T\right] \tag{6.2.11}$$

It can be shown that the derivative of the non-interacting partition function with respect to the cutoff can be expressed by the Gaussian propagators only, i.e. [1]

$$\frac{\mathrm{d}}{\mathrm{d}\Lambda}\ln\mathcal{Z}_0^\Lambda = \mathrm{Tr}\left[\frac{\mathrm{d}(G_0^\Lambda)^{-1}}{\mathrm{d}\Lambda}G_0^\Lambda\right] \quad , \tag{6.2.13}$$

which inserted into (Equation 6.2.11) yields the flow equation of the generating functional of connected Green functions, which is given by

$$\begin{aligned}\frac{\mathrm{d}}{\mathrm{d}\Lambda}\mathcal{G}_c^\Lambda[\bar{\eta},\eta] = &-\mathrm{Tr}\left[\frac{\mathrm{d}(G_0^\Lambda)^{-1}}{\mathrm{d}\Lambda}G_0^\Lambda\right] - \left(\frac{\delta\mathcal{G}_c^\Lambda[\bar{\eta},\eta]}{\delta\eta}, \frac{\mathrm{d}(G_0^\Lambda)^{-1}}{\mathrm{d}\Lambda}\frac{\delta\mathcal{G}_c^\Lambda[\bar{\eta},\eta]}{\delta\bar{\eta}}\right) \\ &- \mathrm{Tr}\left[\frac{\mathrm{d}(G_0^\Lambda)^{-1}}{\mathrm{d}\Lambda}\left(\frac{\delta\mathcal{G}_c^\Lambda[\bar{\eta},\eta]}{\delta\eta\delta\bar{\eta}}\right)^T\right] \quad .\end{aligned} \tag{6.2.14}$$

On the one hand, this flow equation is disadvantageous since it produces connected Green functions in contrast to irreducible vertex functions and on the other hand features an unphysical boundary condition for $\Lambda \to \infty$, which results in an ill-defined initial value problem. However, the flow equation (Equation 6.2.14) turns out to be essential for the derivation of the effective action's flow equation.

[1] The scale derivative of the non-interacting partition function $\frac{\mathrm{d}}{\mathrm{d}\Lambda}\ln\mathcal{Z}_0^\Lambda = \frac{1}{\mathcal{Z}_0^\Lambda}\frac{\mathrm{d}}{\mathrm{d}\Lambda}\mathcal{Z}_0^\Lambda$ is calculated by introducing source terms into the functional integral of $\mathcal{Z}_0^\Lambda$ to be able to employ the "source trick", once more, i.e

$$\begin{aligned}\frac{1}{\mathcal{Z}_0^\Lambda}\frac{\mathrm{d}}{\mathrm{d}\Lambda}\mathcal{Z}_0^\Lambda &= \frac{1}{\mathcal{Z}_0^\Lambda}\int\mathcal{D}[\bar{\psi},\psi]\left(\bar{\psi}, \frac{\mathrm{d}(G_0^\Lambda)^{-1}}{\mathrm{d}\Lambda}\psi\right)e^{-\left(\bar{\psi},(G_0^\Lambda)^{-1}\psi\right)-(\bar{\eta},\psi)-(\bar{\psi},\eta)}\Big|_{\eta=\bar{\eta}=0} \\ &= -\left(\frac{\delta}{\delta\eta}, \frac{\mathrm{d}(G_0^\Lambda)^{-1}}{\mathrm{d}\Lambda}\frac{\delta}{\delta\bar{\eta}}\right)\frac{1}{\mathcal{Z}_0^\Lambda}\int\mathcal{D}[\bar{\psi},\psi]\,e^{-\left(\bar{\psi},(G_0^\Lambda)^{-1}\psi\right)-(\bar{\eta},\psi)-(\bar{\psi},\eta)}\Big|_{\eta=\bar{\eta}=0}\end{aligned} \tag{6.2.12}$$

Using the shift $\psi \to \psi + G_{0,\Lambda}\eta$ and $\bar{\psi} \to \bar{\psi} + G_{0,\Lambda}^T\bar{\eta}$ in the integrating fields, they are decoupled from the source fields and the integration produces $\mathcal{Z}_0^\Lambda e^{-\left(\bar{\eta},G_0^\Lambda\eta\right)}$ canceling the non-interacting partition function. Performing the two-fold functional derivative with respect to the source fields and setting them to zero afterwards, yields the desired result.

6.2.2. Flow equation of the effective action

The effective action with scale dependency acquired by including the modified free propagator is given by (see (Equation 4.2.8))

$$\Gamma^{\Lambda}\left[\bar{\phi},\phi\right] = -\mathcal{G}_c^{\Lambda}\left[\bar{\eta},\eta\right] - \left(\bar{\phi},\eta_{\Lambda}\right) - \left(\bar{\eta}_{\Lambda},\phi\right) + \left(\bar{\phi},(G_0^{\Lambda})^{-1}\phi\right) \quad . \tag{6.2.15}$$

The fields $\bar{\eta}$, η are the source fields that were introduced by the definition of the generating functional of disconnected Green functions (Equation 4.2.5). Here, we have to discriminate between these cutoff independent source fields $\bar{\eta}$, η and the fields $\bar{\eta}_{\Lambda}$, η_{Λ} with cutoff dependency arising from the inversion of the definition of "average" fields $\phi = -\frac{\delta \mathcal{G}_c^{\Lambda}[\bar{\eta},\eta]}{\delta\bar{\eta}}$ and $\bar{\phi} = \frac{\delta \mathcal{G}_c^{\Lambda}[\bar{\eta},\eta]}{\delta\eta}$ given in (Equation 4.2.9). Note, that the fields $\bar{\phi}$, ϕ in terms of which the effective action is defined are taken to be cutoff independent. In order to find the flow equation of the effective action, we simply compute the total derivative of Γ^{Λ} with respect to Λ, i.e.

$$\begin{aligned}
\frac{\mathrm{d}}{\mathrm{d}\Lambda}\Gamma^{\Lambda}\left[\bar{\phi},\phi\right] &= -\frac{\mathrm{d}\mathcal{G}_c^{\Lambda}\left[\bar{\eta},\eta\right]}{\mathrm{d}\Lambda} - \left(\bar{\phi},\frac{\mathrm{d}\eta_{\Lambda}}{\mathrm{d}\Lambda}\right) - \left(\frac{\mathrm{d}\bar{\eta}_{\Lambda}}{\mathrm{d}\Lambda},\phi\right) + \left(\bar{\phi},\frac{\mathrm{d}(G_0^{\Lambda})^{-1}}{\mathrm{d}\Lambda}\phi\right) \\
&= -\left(\frac{\mathrm{d}\bar{\eta}_{\Lambda}}{\mathrm{d}\Lambda},\frac{\delta\mathcal{G}_c^{\Lambda}\left[\bar{\eta},\eta\right]}{\delta\bar{\eta}_{\Lambda}}\right) - \left(\frac{\mathrm{d}\eta_{\Lambda}}{\mathrm{d}\Lambda},\frac{\delta\mathcal{G}_c^{\Lambda}\left[\bar{\eta},\eta\right]}{\delta\eta_{\Lambda}}\right) - \frac{\mathrm{d}\mathcal{G}_c^{\Lambda}\left[\bar{\eta},\eta\right]}{\mathrm{d}\Lambda}\Big|_{\eta=\bar{\eta}=\text{const}} \\
&\quad - \left(\bar{\phi},\frac{\mathrm{d}\eta_{\Lambda}}{\mathrm{d}\Lambda}\right) - \left(\frac{\mathrm{d}\bar{\eta}_{\Lambda}}{\mathrm{d}\Lambda},\phi\right) + \left(\bar{\phi},\frac{\mathrm{d}(G_0^{\Lambda})^{-1}}{\mathrm{d}\Lambda}\phi\right)
\end{aligned} \tag{6.2.16}$$

The second line contains the terms that originate from the derivative of the generating functional $\mathcal{G}_c^{\Lambda}$ with respect to the cutoff. On the one hand, $\mathcal{G}_c^{\Lambda}$ is scale dependent through the fields $\bar{\eta}_{\Lambda}$, η_{Λ} and on the other hand may feature an explicit scale dependency. To correctly write down the derivative of $\mathcal{G}_c^{\Lambda}$ with respect to the implicit scale dependency through the fields, one has to resolve the ambiguity of the chain rule for Grassmann numbers [2]. The derivative (Equation 6.2.16) may be simplified by inserting the definition of the average fields (Equation 4.2.9). This causes the first and fifth and second and fourth terms to cancel, where we have to take into account that $(\phi,\psi) = -(\phi,\psi)$ for two Grassmann fields ϕ, ψ. Hence, we are left with the derivative

[2] The chain rule for Grassmann numbers and functionals of Grassmann fields requires the inner derivatives to be placed prior to the outer derivatives [Med06]. The order of inner and outer derivative of a Grassmann function(al) can be fixed by looking at a simple functional like e.g. $F(\bar{\eta}(\Lambda),\eta(\Lambda)) = f(\Lambda)\bar{\eta}(\Lambda)\eta(\Lambda)$ with $f(\Lambda)\in\mathbb{C}$ and Grassmann fields $\bar{\eta}(\Lambda),\eta(\Lambda)$. The total derivative of $F(\bar{\eta}(\Lambda),\eta(\Lambda))$ with respect to Λ produces three terms as given by the product rule, which are

$$\frac{\mathrm{d}F}{\mathrm{d}\Lambda} = \frac{\mathrm{d}f(\Lambda)}{\mathrm{d}\Lambda}\bar{\eta}(\Lambda)\eta(\Lambda) + f(\Lambda)\frac{\mathrm{d}\bar{\eta}}{\mathrm{d}\Lambda}\eta(\Lambda) + f(\Lambda)\bar{\eta}(\Lambda)\frac{\mathrm{d}\eta}{\mathrm{d}\Lambda} = \frac{\mathrm{d}\bar{\eta}}{\mathrm{d}\Lambda}\frac{\delta F}{\delta\bar{\eta}} - \frac{\delta F}{\delta\eta}\frac{\mathrm{d}\eta}{\mathrm{d}\Lambda} + \frac{\delta F}{\delta\Lambda}\Big|_{\bar{\eta}_{\Lambda},\eta_{\Lambda}=\text{const.}} \quad ,$$

which shows that the inner derivatives must be placed in front as a consequence of the anticommutation of derivative operators with respect to Grassmann fields and Grassmann fields itself.

of the generating functional of connected Green functions and the term involving the inverse free propagator $(G_0^\Lambda)^{-1}$. To further evaluate the expression we need the flow equation of the generating functional of connected Green functions, given by (Equation 6.2.14). Plugging it into (Equation 6.2.16), yields

$$\begin{aligned}\frac{\mathrm{d}}{\mathrm{d}\Lambda}\Gamma^\Lambda\left[\bar{\phi},\phi\right] = &\left(\bar{\phi},\frac{\mathrm{d}(G_0^\Lambda)^{-1}}{\mathrm{d}\Lambda}\phi\right) + \mathrm{Tr}\left[\frac{\mathrm{d}(G_0^\Lambda)^{-1}}{\mathrm{d}\Lambda}G_0^\Lambda\right] \\ &+ \left(\frac{\delta\mathcal{G}_c^\Lambda\left[\bar{\eta},\eta\right]}{\delta\eta},\frac{\mathrm{d}(G_0^\Lambda)^{-1}}{\mathrm{d}\Lambda}\frac{\delta\mathcal{G}_c^\Lambda\left[\bar{\eta},\eta\right]}{\delta\bar{\eta}}\right) + \mathrm{Tr}\left[\frac{\mathrm{d}(G_0^\Lambda)^{-1}}{\mathrm{d}\Lambda}\left(\frac{\delta^2\mathcal{G}_c^\Lambda\left[\bar{\eta},\eta\right]}{\delta\eta\delta\bar{\eta}}\right)^T\right] .\end{aligned} \tag{6.2.17}$$

Whne inserting the definition of the fields $\bar{\phi}$, ϕ (Equation 4.2.9), the first and third terms cancel. Similar to (Equation 6.2.14), we prefer a flow equation, which features a right hand side that depends on the generating functional itself. Hence, we have to express the second derivative of the generating functional of connected Green functions in terms of the effective action. This can be achieved by means of the "reciprocity relation" (Equation 4.2.13), which states that the second functional derivative of the generating functional of connected Green functions equals the inverse of the matrix of the effective action's second functional derivative. Henceforth, the derivative and therefore the *flow equation of the effective action* yields

$$\frac{\mathrm{d}}{\mathrm{d}\Lambda}\Gamma^\Lambda\left[\bar{\phi},\phi\right] = \mathrm{Tr}\left[\frac{\mathrm{d}(G_0^\Lambda)^{-1}}{\mathrm{d}\Lambda}G_0^\Lambda\right] - \mathrm{Tr}\left[\frac{\mathrm{d}(G_0^\Lambda)^{-1}}{\mathrm{d}\Lambda}\left(\boldsymbol{\gamma}^{(2)}\right)_{11}^{-1}\right] . \tag{6.2.18}$$

To be able to formulate a well-defined initial value problem, we have to find the initial condition of the effective action, i.e. the limit of the effective action for infinite cutoff scale. It can be shown (by means of the generating functional of the effective interaction) that (cf. [Met+12b])

$$\lim_{\Lambda\to\infty}\Gamma_\Lambda\left[\bar{\phi},\phi\right] = S_I\left[\bar{\phi},\phi\right] \tag{6.2.19}$$

the effective action reduces to the bare interaction for $\Lambda\to\infty$. A more intuitive way to understand this result is given by the fact that in a perturbative expansion of the effective action and its vertex functions in the limit of infinity cutoff scale, $\lim_{\Lambda\to\infty}\gamma_\Lambda^{(2n)}$, the only term that does not vanish must be the bare two-particle vertex, since all non-interacting degrees of freedom are turned off by the modified Gaussian propagator [Hed+04].

6.3. Hierarchy of flow equations

The previous section introduced and derived the flow equations of the generating functional of (dis)connected Green functions and the effective action, which also provides a well-defined initial value problem due to its physically meaningful behavior in the limit of an infinite cutoff scale $\Lambda \to \infty$. Unfortunately, the flow equation (Equation 6.2.18) represents a complicated functional integro-differential equation, which poses a both analytically and numerically unfeasible problem. Hence, we have to rely on approximative solutions of the flow equation. Here, we employ an *expansion in the fields* to approximate the flow equation. The expansion of the effective action (Equation 4.2.8) in terms of its fields ϕ, $\bar{\phi}$ is given by [Med06]

$$\begin{aligned}\Gamma^{\Lambda}\left[\bar{\phi},\phi\right] &= \sum_{k=0}^{\infty} \frac{(-1)^k}{(k!)^2} \int_{\substack{\alpha_1,\ldots,\alpha_k;\\ \alpha_1',\ldots,\alpha_k'}} \gamma_{\Lambda}^{(2k)}\left(\alpha_1',\ldots,\alpha_k',\alpha_1,\ldots,\alpha_k\right) \bar{\phi}_{\alpha_1'}\ldots\bar{\phi}_{\alpha_k'}\phi_{\alpha_k}\ldots\phi_{\alpha_1} \\ &= \gamma_{\Lambda}^{(0)} - \int_{\alpha_1,\alpha_1'} \gamma_{\Lambda}^{(2)}\left(\alpha_1',\alpha_1\right)\bar{\phi}_{\alpha_1'}\phi_{\alpha_1} + \frac{1}{4}\int_{\substack{\alpha_1,\alpha_2,\\ \alpha_1',\alpha_2'}} \gamma_{\Lambda}^{(4)}\left(\alpha_1',\alpha_2',\alpha_1,\alpha_2\right)\bar{\phi}_{\alpha_1'}\bar{\phi}_{\alpha_2'}\phi_{\alpha_2}\phi_{\alpha_1} + \ldots \quad ,\end{aligned} \tag{6.3.1}$$

where the coefficients are represented by the irreducible k-particle vertex functions defined in (Equation 4.2.10). While the left hand side of the flow equation (Equation 6.2.18) can be expanded straightforwardly, the right hand side requires some further treatment, because the effective action is hidden in the diagonal element of the inversion of the matrix of second functional derivatives $\boldsymbol{\gamma}^{(2)}$, which is given by (Equation 4.2.13) (including its scale dependency)

$$\boldsymbol{\gamma}^{(2)} = \begin{pmatrix} \frac{\delta^2\Gamma^{\Lambda}}{\delta\bar{\phi}\delta\phi} + (G^{\Lambda})^{-1} + \Sigma^{\Lambda} & \frac{\delta^2\Gamma}{\delta\phi\delta\phi} \\ \frac{\delta^2\Gamma}{\delta\bar{\phi}\delta\bar{\phi}} & \frac{\delta^2\Gamma^{\Lambda}}{\delta\phi\delta\bar{\phi}} - \left((G^{\Lambda})^{-1} + \Sigma^{\Lambda}\right)^T \end{pmatrix} \quad , \tag{6.3.2}$$

where we used the *Dyson equation* $(G^{\Lambda})^{-1} = (G_0^{\Lambda})^{-1} - \Sigma^{\Lambda}$ to express the scale dependent free propagator in terms of the full propagator and the self-energy [FW71]. The matrix of second functional derivatives is recast and separated into a field independent and field dependent part by

$$\begin{aligned}\boldsymbol{\gamma}^{(2)} &= \begin{pmatrix} G^{\Lambda})^{-1} & 0 \\ 0 & -\left(G^{\Lambda})^{-1}\right)^{T} \end{pmatrix} + \begin{pmatrix} \mathcal{M}_{\bar{\phi},\phi} & \frac{\delta^2\Gamma^{\Lambda}}{\delta\phi\delta\phi} \\ \frac{\delta^2\Gamma^{\Lambda}}{\delta\bar{\phi}\delta\bar{\phi}} & -\mathcal{M}^{T}_{\bar{\phi},\phi} \end{pmatrix} \\ &= \begin{pmatrix} (G^{\Lambda})^{-1} & 0 \\ 0 & -\left((G^{\Lambda})^{-1}\right)^{T} \end{pmatrix} \cdot \underbrace{\left(\mathbb{1} - \underbrace{\begin{pmatrix} -G^{\Lambda} & 0 \\ 0 & (G^{\Lambda})^{T} \end{pmatrix} \begin{pmatrix} \mathcal{M}_{\bar{\phi},\phi} & \frac{\delta^2\Gamma^{\Lambda}}{\delta\phi\delta\phi} \\ \frac{\delta^2\Gamma^{\Lambda}}{\delta\bar{\phi}\delta\bar{\phi}} & -\mathcal{M}^{T}_{\bar{\phi},\phi} \end{pmatrix}}_{:=\rho} \right)}_{:=\tilde{\boldsymbol{\gamma}}^{(2)}} \quad , \end{aligned} \tag{6.3.3}$$

where we defined the new matrix

$$\mathcal{M}_{\bar{\phi},\phi} = \frac{\delta^2\Gamma^{\Lambda}}{\delta\bar{\phi}\delta\phi} + \Sigma^{\Lambda}(\bar{\phi},\phi) = \frac{\delta^2\Gamma^{\Lambda}}{\delta\bar{\phi}\delta\phi} - \gamma^{(2)}(\bar{\phi},\phi) \quad , \tag{6.3.4}$$

and used the fact that the self-energy equals the negative of the two-leg irreducible vertex function $\gamma^{(2)}$ (cf. (Equation 4.2.13)). Apparently, by using the form and definitions in (Equation 6.3.3), the inverse of the matrix of second derivatives is given by

$$\left(\boldsymbol{\gamma}^{(2)}\right)^{-1} = \left(\tilde{\boldsymbol{\gamma}}^{(2)}\right)^{-1} \cdot \begin{pmatrix} G^{\Lambda} & 0 \\ 0 & -(G^{\Lambda})^{T} \end{pmatrix} \quad , \tag{6.3.5}$$

since the inverse of a product $A = B \cdot C$ of two matrices is $A^{-1} = (B \cdot C)^{-1} = C^{-1} \cdot B^{-1}$. In contrast to the inverse of $\boldsymbol{\gamma}^{(2)}$, the inverse of $\tilde{\boldsymbol{\gamma}}^{(2)} = 1 - \rho$ can be calculated by means of an expansion as a *geometric series*, i.e. [Ste98]

$$(\mathbb{1} - \rho)^{-1} = \sum_{k=0}^{\infty} \rho^k = \mathbb{1} + \rho + \rho^2 + O\left(\rho^3\right) \quad , \tag{6.3.6}$$

where

$$\rho = \begin{pmatrix} -G^{\Lambda}\mathcal{M}_{\bar{\phi},\phi} & -G^{\Lambda}\frac{\delta^2\Gamma^{\Lambda}}{\delta\phi\delta\phi} \\ (G^{\Lambda})^{T}\frac{\delta^2\Gamma^{\Lambda}}{\delta\bar{\phi}\delta\bar{\phi}} & -(G^{\Lambda})^{T}\mathcal{M}^{T}_{\bar{\phi},\phi} \end{pmatrix} \quad . \tag{6.3.7}$$

Up to second order in ρ the upper diagonal element of the inverse of the matrix of second functional derivatives is therefore given by

$$\left(\boldsymbol{\gamma}^{(2)}\right)^{-1}_{11} = \left(1 - G^\Lambda \mathcal{M}_{\bar{\phi},\phi} + G^\Lambda \mathcal{M}_{\bar{\phi},\phi} G^\Lambda \mathcal{M}_{\bar{\phi},\phi} - G^\Lambda \frac{\delta^2\Gamma^\Lambda}{\delta\phi\delta\phi}(G^\Lambda)^T \frac{\delta^2\Gamma^\Lambda}{\delta\bar{\phi}\delta\bar{\phi}} + O\left(\rho^3\right)\right) G^\Lambda \quad , \tag{6.3.8}$$

Since we are ultimately interested in the terms that arise on the left hand and right hand side of the flow equation in a particular order of the expansion in terms of the fields, we have to gain some insight into the expansion of $\mathcal{M}_{\bar{\phi},\phi}$ and $\frac{\delta^2\Gamma^\Lambda}{\delta\phi\delta\phi}$, $\frac{\delta^2\Gamma^\Lambda}{\delta\bar{\phi}\delta\bar{\phi}}$, which are the only terms on the right hand side incorporating any field dependency. Up to third order, all three of them contain only terms, which are quadratic or quartic in the fields. In particular, the first two orders of $\mathcal{M}_{\bar{\phi},\phi}$ are (cf. (Equation 6.3.4))

$$\begin{aligned}\mathcal{M}_{\bar{\phi}_{\beta'_1},\phi_{\beta_1}} = \frac{\delta^2\Gamma^\Lambda}{\delta\bar{\phi}_{\beta'_1}\delta\phi_{\beta_1}} - \gamma^{(2)}(\bar{\phi}_{\beta'_1},\phi_{\beta_1}) = -\int_{\alpha_1,\alpha'_1} \gamma^{(4)}_\Lambda\left(\alpha'_1,\beta'_1,\alpha_1,\beta_1\right)\bar{\phi}_{\alpha'_1}\phi_{\alpha_1} \\ + \frac{1}{4}\int_{\substack{\alpha_1,\alpha_2,\\ \alpha'_1,\alpha'_2}} \gamma^{(6)}_\Lambda\left(\alpha'_1,\alpha'_2,\beta'_1,\alpha_1,\alpha_2,\beta_1\right)\bar{\phi}_{\alpha'_1}\bar{\phi}_{\alpha'_2}\phi_{\alpha_2}\phi_{\alpha_1} + \ldots \quad ,\end{aligned} \tag{6.3.9}$$

since the two-particle irreducible vertex is canceled. The factorial in the denominator of the prefactor in (Equation 6.3.1) is partly canceled by the multiplicities of terms generated by the two-fold functional derivative. More precisely, two functional derivatives produce $\binom{k}{1}^2$ terms at order k, which, however, turn out to be equivalent, when anticommuting and renaming the appropriate fields. The two fold derivatives of the effective action originating from the off-diagonal terms in ρ yield (up to second order)

$$\begin{aligned}\frac{\delta^2\Gamma^\Lambda[\bar{\phi},\phi]}{\delta\bar{\phi}_{\beta'_1}\delta\bar{\phi}_{\beta'_2}} = -\frac{1}{2}\int_{\alpha_1,\alpha_2} \gamma^{(4)}_\Lambda\left(\beta'_1,\beta'_2,\alpha_1,\alpha_2\right)\phi_{\alpha_2}\phi_{\alpha_1} \\ + \frac{1}{6}\int_{\substack{\alpha_1,\alpha_2,\\ \alpha_3,\alpha'_1}} \gamma^{(6)}_\Lambda\left(\alpha'_1,\beta'_1,\beta'_2,\alpha_1,\alpha_2,\alpha_3\right)\bar{\phi}_{\alpha'_1}\phi_{\alpha_3}\phi_{\alpha_2}\phi_{\alpha_1} + \ldots \quad ,\end{aligned} \tag{6.3.10}$$

and

$$\begin{aligned}\frac{\delta^2\Gamma^\Lambda[\bar{\phi},\phi]}{\delta\phi_{\beta_1}\delta\phi_{\beta_2}} = +\frac{1}{2}\int_{\alpha'_1,\alpha'_2} \gamma^{(4)}_\Lambda\left(\alpha'_1,\alpha'_2,\beta_1,\beta_2\right)\bar{\phi}_{\alpha'_1}\bar{\phi}_{\alpha'_2} \\ - \frac{1}{6}\int_{\substack{\alpha_1,\alpha'_1,\\ \alpha'_2,\alpha'_3}} \gamma^{(6)}_\Lambda\left(\alpha'_1,\alpha'_2,\alpha'_3,\alpha_1,\beta_1,\beta_2\right)\bar{\phi}_{\alpha'_1}\bar{\phi}_{\alpha'_2}\bar{\phi}_{\alpha'_3}\phi_{\alpha_1} + \ldots \quad ,\end{aligned} \tag{6.3.11}$$

since the two-fold functional derivative of the effective action with respect to fields of the same "kind" will remove the one-particle vertex. We have now prepared all prerequisites needed to determine the flow equations associated to the first few order of

the expansion in the fields of the flow equation of the effective action (Equation 6.2.18). Starting with the zeroth order vertex $\gamma_\Lambda^{(0)}$ representing the interaction correction to the free energy, we find the flow equation (cf. [Kop01])

$$\frac{\mathrm{d}}{\mathrm{d}\Lambda}\gamma_\Lambda^{(0)} = \mathrm{Tr}\left[\frac{\mathrm{d}(G_0^\Lambda)^{-1}}{\mathrm{d}\Lambda}G_0^\Lambda\right] - \mathrm{Tr}\left[\frac{\mathrm{d}(G_0^\Lambda)^{-1}}{\mathrm{d}\Lambda}G^\Lambda\right] = \mathrm{Tr}\left[\frac{\mathrm{d}(G_0^\Lambda)^{-1}}{\mathrm{d}\Lambda}\left(G_0^\Lambda - G^\Lambda\right)\right] \quad , \tag{6.3.12}$$

which produces a renormalization flow, which is characterized by the difference between the free Gaussian G_0^Λ and the full propagator G^Λ. Note, that the flow equation may be formally integrated since the vertex function $\gamma_\Lambda^{(0)}$ does not appear on the right hand side. Besides, this is the only flow equation of the entire hierarchy of flow equations that contains the first term of the right hand side of (Equation 6.2.18), since only the second term features field dependent contributions.

6.3.1. Self-energy

The flow equations of all higher order vertex functions are obtained by comparing the coefficients associated to the terms with the corresponding number of fields on the left and right hand side of (Equation 6.2.18). The flow equation of the single-particle vertex $\gamma_\Lambda^{(2)}\left(\alpha_1', \alpha_1\right)$ - the negative of the self-energy - is hidden in the terms being quadratic in the fields. Referring to (Equation 6.3.8) and (Equation 6.3.9), we find that only the two-particle vertex $\gamma_\Lambda^{(4)}$ contributes to the right hand side. More precisely, we obtain

$$-\frac{\mathrm{d}}{\mathrm{d}\Lambda}\gamma_\Lambda^{(2)}\left(\alpha_1', \alpha_1\right)\bar{\phi}_{\alpha_1'}\phi_{\alpha_1} + \ldots = -\,\mathrm{Tr}\left[\frac{\mathrm{d}(G_0^\Lambda)^{-1}}{\mathrm{d}\Lambda}\left(-G^\Lambda M_{\bar{\phi},\phi}G^\Lambda\right)\right] \quad , \tag{6.3.13}$$

where $+\ldots$ indicates that higher order terms may be present on the right hand side. In (Section 6.2.1) we introduced Tr as the short-hand notation for the integration over diagonal terms. Recovering the integration of the trace (and one more "inner" integration), employing its cyclic invariance in order to shift the second full propagator in front and neglecting the fields, we find the flow equation of the single-particle vertex to be

$$\begin{aligned}\frac{\mathrm{d}}{\mathrm{d}\Lambda}\gamma_\Lambda^{(2)}\left(\alpha_1', \alpha_1\right) &= \int_{\beta_1', \beta_1}\left(G^\Lambda\frac{\mathrm{d}(G_0^\Lambda)^{-1}}{\mathrm{d}\Lambda}G^\Lambda\right)_{\beta_1', \beta_1}\gamma_\Lambda^{(4)}\left(\alpha_1', \beta_1', \alpha_1, \beta_1\right) \\ &= \int_{\beta_1', \beta_1} S^\Lambda\left(\beta_1', \beta_1\right)\gamma_\Lambda^{(4)}\left(\alpha_1', \beta_1', \alpha_1, \beta_1\right) \quad ,\end{aligned} \tag{6.3.14}$$

where we defined the *single-scale propagator* S^Λ by [SH01]

$$S^{\Lambda} := G^{\Lambda} \frac{\mathrm{d}(G_0^{\Lambda})^{-1}}{\mathrm{d}\Lambda} G^{\Lambda} \quad . \tag{6.3.15}$$

The diagrammatic representation of (Equation 6.3.14) shown in (Figure 6.3a) bears close pictorial similarity to the *Hartree term* in first order perturbation theory but is mathematically very different due to the occurrence of the single-scale propagator. In the presence of SU(2) symmetry the propagator terms must be diagonal in spin space, $S^{\Lambda} \propto \sigma_0$, and the two-particle vertex is given by (cf. (Equation 3.3.19))

$$\gamma_{\Lambda}^{(4)}\left(\alpha_1', \sigma_1', \alpha_2', \sigma_2', \alpha_1, \sigma_1, \alpha_2, \sigma_2\right) = g^{\Lambda}_{\alpha_1\alpha_2\alpha_1'\alpha_2'} \delta_{\sigma_1\sigma_1'} \delta_{\sigma_2\sigma_2'} - g^{\Lambda}_{\alpha_2\alpha_1\alpha_1'\alpha_2'} \delta_{\sigma_1\sigma_2'} \delta_{\sigma_2\sigma_1'} \quad , \tag{6.3.16}$$

where the multiindices on the right hand side are redefined to lack the spin degree of freedom. Inserting this relation and the diagonal single-scale propagator into (Equation 6.3.14) leads to the spinless SU(2)-invariant flow equation (cf. [UH12, Sec.II],[Met+12b, Eq.(109)])

$$\frac{\mathrm{d}}{\mathrm{d}\Lambda} s^{\Lambda}_{\alpha_1', \alpha_1} = \int_{\beta_1', \beta_1} S^{\Lambda}\left(\beta_1', \beta_1\right) \left[2\, g^{\Lambda}_{\alpha_1\beta_2\alpha_1'\beta_2'} - g^{\Lambda}_{\beta_2\alpha_1\alpha_1'\beta_2'}\right] \quad , \tag{6.3.17}$$

where we defined the spinless single-particle vertex by $s^{\Lambda}_{\alpha_1', \alpha_1} \delta_{\sigma_1, \sigma_1'} := \gamma^{(2)}_{\Lambda}\left(\alpha_1', \alpha_1\right)$. The diagrammatic illustration of (Equation 6.3.17) is given in (Figure 6.3b). Remember, that the single-particle vertex actually equals the negative of the self-energy Σ^{Λ} (cf. (Equation 4.2.13)).

6.3.2. Irreducible two-particle vertex

The quantity, which directly governs the properties of possible particle-particle and particle-hole instabilities is the effective irreducible two-particle vertex. The low-energy effective two-particle vertex is calculated via its flow equation, that is derived by taking the second, third and fourth orders of the expansion (Equation 6.3.8) into account and inserting them into (Equation 6.2.18). We find the following expression that contributes to terms quartic in the fields:

$$\begin{aligned} &\frac{\mathrm{d}}{\mathrm{d}\Lambda} \frac{1}{4} \int_{\substack{\alpha_1, \alpha_2, \\ \alpha_1', \alpha_2'}} \gamma_{\Lambda}^{(4)}\left(\alpha_1', \alpha_2', \alpha_1, \alpha_2\right) \bar{\phi}_{\alpha_1'} \bar{\phi}_{\alpha_2'} \phi_{\alpha_2} \phi_{\alpha_1} + \ldots \\ &= -\operatorname{Tr}\left[\frac{\mathrm{d}(G_0^{\Lambda})^{-1}}{\mathrm{d}\Lambda}\left(-G^{\Lambda} M_{\bar{\phi},\phi} + G^{\Lambda} M_{\bar{\phi},\phi} G^{\Lambda} M_{\bar{\phi},\phi} - G^{\Lambda} \frac{\delta^2 \Gamma^{\Lambda}}{\delta\phi\delta\phi} (G^{\Lambda})^T \frac{\delta^2 \Gamma^{\Lambda}}{\delta\bar{\phi}\delta\bar{\phi}}\right) G^{\Lambda}\right] \quad . \end{aligned} \tag{6.3.18}$$

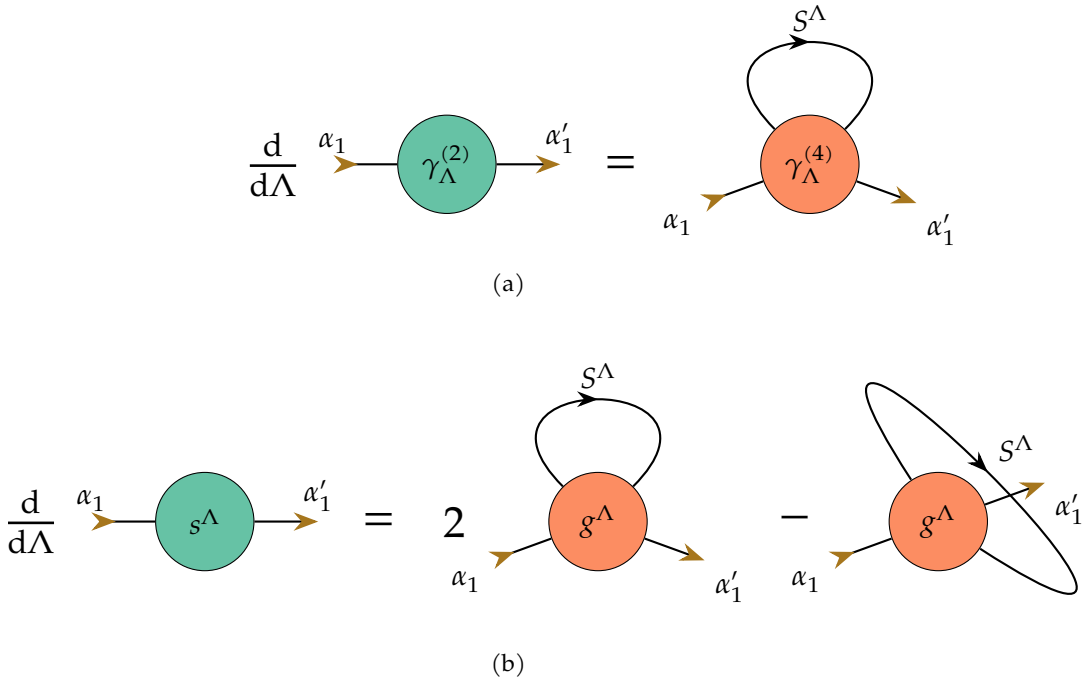

Figure 6.3.: The flow equation of the irreducible spinful single-particle vertex $\gamma_\Lambda^{(2)}$ - the negative of the self-energy Σ_Λ - has only one contribution from the irreducible two-particle vertex. The SU(2)-invariant version of the flow equation features two terms with opposite sign and different weighting factors.

The first term incorporates the three-particle vertex $\gamma_\Lambda^{(6)}$ in (Equation 6.3.9) contributing a term quartic in the fields, while the second term on the left hand side of (Equation 6.3.18) features the product of two two-particle vertices with "mixed" fields. Similar, the third term hosts the product of two two-particle vertices with "anomalous" field terms originating from (Equation 6.3.10) and (Equation 6.3.11). By employing the cyclic invariance of the trace in (Equation 6.3.18) we find that each term features one full propagator G^Λ and one single-scale propagator S^Λ. Comparing and collecting the coefficients of all terms quartic in the fields on the left and right hand side of (Equation 6.3.18), results in

$$\begin{aligned}\frac{\mathrm{d}}{\mathrm{d}\Lambda}\gamma_\Lambda^{(4)}\left(\alpha_1',\alpha_2',\alpha_1,\alpha_2\right) &= \int_{\beta_1',\beta_1} S^\Lambda\left(\beta_1',\beta_1\right)\gamma_\Lambda^{(6)}\left(\alpha_1',\alpha_2',\beta_1',\alpha_1,\alpha_2,\beta_1\right)\\ &- 4\int_{\substack{\beta_1,\beta_2,\\ \beta_1',\beta_2'}} S^\Lambda\left(\beta_1',\beta_2\right)G^\Lambda\left(\beta_2',\beta_1\right)\gamma_\Lambda^{(4)}\left(\alpha_1',\beta_1',\alpha_1,\beta_1\right)\gamma_\Lambda^{(4)}\left(\alpha_2',\beta_2',\alpha_2,\beta_2\right)\\ &+ \int_{\substack{\beta_1,\beta_2,\\ \beta_1',\beta_2'}} S^\Lambda\left(\beta_1',\beta_1\right)G^\Lambda\left(\beta_2',\beta_2\right)\gamma_\Lambda^{(4)}\left(\alpha_1',\alpha_2',\beta_1,\beta_2\right)\gamma_\Lambda^{(4)}\left(\beta_1',\beta_2',\alpha_1,\alpha_2\right) \quad . \quad (6.3.19)\end{aligned}$$

In the last term, we used that $G^{\Lambda}\left(\beta_2', \beta_2\right)^T = G^{\Lambda}\left(\beta_2, \beta_2'\right) = -G^{\Lambda}\left(\beta_2', \beta_2\right)$. Note, that we require the two-particle vertex on the left hand side of the flow equation to satisfy all constraints and symmetries discussed in (Section 3.3), which is, in particular, antisymmetry and self-adjointness. Hence, the problem with (Equation 6.3.18) is that, in contrast to the left hand side with $\gamma_{\Lambda}^{(4)}\left(\alpha_1', \alpha_2', \alpha_1, \alpha_2\right)$, the right hand side is obviously not antisymmetric with respect to exchange of primed or unprimed indices because of the second term. However, by splitting up the second term into two parts, exchanging appropriate pairs of indices and adjusting the sign in the second one, the antisymmetry can be restored [KB01; Sal99]. The terms including two two-particle vertices each, require an additional propagator term with exchanged "inner" indices. Henceforth, the flow equation becomes (cf. [KBS10, Chap.10.2.2] and [Sch+16; Sch+17])

$$\begin{aligned}\frac{\mathrm{d}}{\mathrm{d}\Lambda}\gamma_{\Lambda}^{(4)}\left(\alpha_1', \alpha_2', \alpha_1, \alpha_2\right) &= \int_{\beta_1', \beta_1} S^{\Lambda}\left(\beta_1', \beta_1\right)\gamma_{\Lambda}^{(6)}\left(\alpha_1', \alpha_2', \beta_1', \alpha_1, \alpha_2, \beta_1\right) \\ &+ \int_{\substack{\beta_1, \beta_2, \\ \beta_1', \beta_2'}} \left[S^{\Lambda}\left(\beta_1', \beta_1\right) G^{\Lambda}\left(\beta_2', \beta_2\right) + {}^{\beta_1 \leftrightarrow \beta_2}_{\beta_1' \leftrightarrow \beta_2'}\right] \times \Bigg[\frac{1}{2}\gamma_{\Lambda}^{(4)}\left(\alpha_1', \alpha_2', \beta_1, \beta_2\right)\gamma_{\Lambda}^{(4)}\left(\beta_1', \beta_2', \alpha_1, \alpha_2\right) \\ &- \gamma_{\Lambda}^{(4)}\left(\alpha_1', \beta_1', \alpha_1, \beta_2\right)\gamma_{\Lambda}^{(4)}\left(\alpha_2', \beta_2', \alpha_2, \beta_1\right) + \gamma_{\Lambda}^{(4)}\left(\alpha_1', \beta_1', \alpha_2, \beta_2\right)\gamma_{\Lambda}^{(4)}\left(\alpha_2', \beta_2', \alpha_1, \beta_1\right)\Bigg] .\end{aligned} \tag{6.3.20}$$

This flow equation shows, that there are - apart from the three-particle particle term - three contributions of the irreducible two-particle vertex to the renormalization flow of the two-particle vertex. The first term corresponds to the particle-particle channel (BCS) and the second and third terms represent the direct and crossed particle-hole channels (ZS and ZS') [Met+12a; HM00a]. The diagrammatics of the flow equation (Equation 6.3.20) are illustrated in (Figure 6.4).

Starting from the self-energy and the irreducible two-particle vertex, the derivation of flow equations can be continued up to any irreducible $2n$-particle vertex to obtain an infinite hierarchy of flow equations, since exactly like the flow equations of the self-energy, which features input from the two-particle vertex, and the two-particle vertex, which is influenced by the three-particle vertex, any $2n$-particle vertex is associated to a flow equation that includes the contribution of an $2(n+1)$-particle vertex. Because the calculation of the entire hierarchy of flow equations is obviously not feasible, we have to truncate the interdependencies at some order by setting the vertex function $\gamma_{\Lambda}^{(n+2)}$ in the flow equation of $\gamma_{\Lambda}^{(n)}$ to $\gamma_{\Lambda\to\infty}^{(n+2)}$. Since this truncation is usually done on the level of the two-particle vertex, this amounts to the negligence of the contribution of the three-particle vertex in the flow equation of the two-particle vertex. This approximation may be justified by the fact that effective irreducible vertex functions of the order $n \geq 6$ can be classified as irrelevant due to power counting arguments [Met+12a]. However, the truncation will result in the violation of *Ward identities* [Kat04]. In order to provide a self-contained presentation of the flow equations and full correspondence with perturbative renormalization (Chapter 5), we also show how the spinless flow equation for

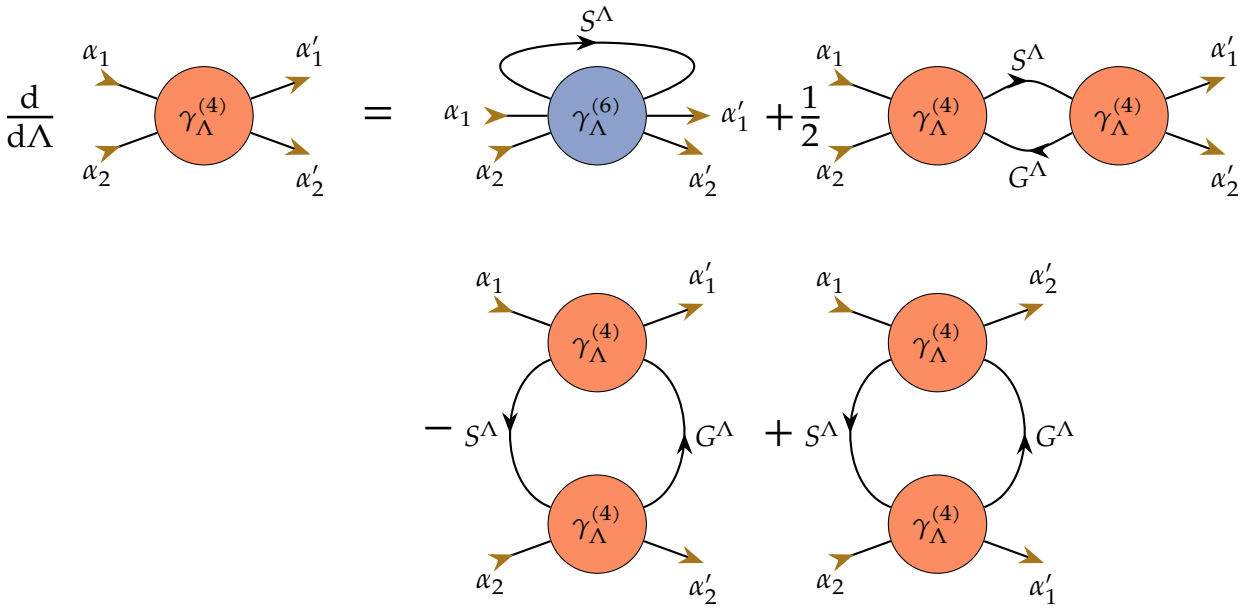

Figure 6.4.: The flow equation of the irreducible spinful two-particle vertex $\gamma_\Lambda^{(4)}$ has - apart from a term involving the three-particle vertex - one particle-particle contribution (BCS) and two particle-hole terms (ZS and ZS') including the irreducible two-particle vertex. Note, that the diagrams including the two-particle vertices are topologically equivalent to (Figure 5.3b).

SU(2)-symmetric models arises from (Equation 6.3.20). Here, we neglected the three-particle vertex contribution in the first place. Analogously to (Equation 6.3.16) we use the structure (Equation 3.3.19) of the fully SU(2)-invariant two-particle vertex:

$$\gamma_\Lambda^{(4)}\left(\alpha_1', \sigma_1', \alpha_2', \sigma_2', \alpha_1, \sigma_1, \alpha_2, \sigma_2\right) = g^\Lambda_{\alpha_1\alpha_2\alpha_1'\alpha_2'}\delta_{\sigma_1\sigma_1'}\delta_{\sigma_2\sigma_2'} - g^\Lambda_{\alpha_2\alpha_1\alpha_1'\alpha_2'}\delta_{\sigma_1\sigma_2'}\delta_{\sigma_2\sigma_1'} \quad , \tag{6.3.21}$$

with $\{\sigma_1, \sigma_2, \sigma_1', \sigma_2'\}$ being the spin indices and $\{\alpha_1, \alpha_2, \alpha_1', \alpha_2'\}$ being the multiindices representing all remaining quantum numbers. Like before the new coupling function g^Λ is symmetric with respect to exchange of both primed and unprimed indices at once and therefore satisfies $g^\Lambda_{\alpha_1\alpha_2\alpha_1'\alpha_2'} = g^\Lambda_{\alpha_2\alpha_1\alpha_2'\alpha_1'}$ (cf. (Equation 3.3.21)). Inserting the two-particle vertex (Equation 6.3.21) into (Equation 6.3.20) produces two terms on the left hand side and twelve terms on the right hand side of the flow equation. The terms on the right hand feature products of four Kronecker deltas each and may be simplified by performing the spin summation of the loop integrals. Note that the propagator terms are proportional to the identity in spin space. For instance, in the particle-particle and direct particle-hole terms, we encounter the following identities (the inner spin summations are denoted by τ_1, τ_2)

$$\sum_{\tau_1,\tau_2}\begin{cases}\delta_{\sigma_1\tau_1}\delta_{\sigma_2\tau_2}\delta_{\sigma_1'\tau_1}\delta_{\sigma_2'\tau_2}=\delta_{\sigma_1\sigma_1'}\delta_{\sigma_2\sigma_2'}\\ -\delta_{\sigma_1\tau_1}\delta_{\sigma_2\tau_2}\delta_{\sigma_1'\tau_2}\delta_{\sigma_2'\tau_1}=-\delta_{\sigma_1\sigma_2'}\delta_{\sigma_2\sigma_1'}\\ -\delta_{\sigma_1\tau_2}\delta_{\sigma_2\tau_1}\delta_{\sigma_1'\tau_1}\delta_{\sigma_2'\tau_2}=-\delta_{\sigma_1\sigma_2'}\delta_{\sigma_2\sigma_1'}\\ \delta_{\sigma_1\tau_2}\delta_{\sigma_2\tau_1}\delta_{\sigma_1'\tau_2}\delta_{\sigma_2'\tau_1}=\delta_{\sigma_1\sigma_1'}\delta_{\sigma_2\sigma_2'}\end{cases}\qquad \sum_{\tau_1,\tau_2}\begin{cases}\delta_{\sigma_1\sigma_1'}\delta_{\tau_1\tau_2}\delta_{\sigma_2\sigma_2'}\delta_{\tau_1\tau_2}=2\delta_{\sigma_1\sigma_1'}\delta_{\sigma_2\sigma_2'}\\ -\delta_{\sigma_1\sigma_1'}\delta_{\tau_1\tau_2}\delta_{\sigma_2\tau_1}\delta_{\sigma_2'\tau_2}=-\delta_{\sigma_1\sigma_1'}\delta_{\sigma_2\sigma_2'}\\ -\delta_{\sigma_1\tau_1}\delta_{\sigma_1'\tau_2}\delta_{\sigma_2\sigma_2'}\delta_{\tau_1\tau_2}=-\delta_{\sigma_1\sigma_1'}\delta_{\sigma_2\sigma_2'}\\ \delta_{\sigma_1\tau_1}\delta_{\sigma_1'\tau_2}\delta_{\sigma_2\tau_1}\delta_{\sigma_2'\tau_2}=\delta_{\sigma_1\sigma_2}\delta_{\sigma_1'\sigma_2'}\end{cases}$$

The ensemble of these Kronecker deltas separates the spinful flow equation into two sectors corresponding to the ones defined by the left hand side of the flow equation (Equation 6.3.21), which are completely decoupled. Henceforth, we compare coefficients in terms of the two kinds of Kronecker identities and find two equivalent sets of spinless flow equations, each of which is made up of two particle-particle and four particle-hole terms. Collecting the terms corresponding to e.g. the $\delta_{\sigma_1\sigma_1'}\delta_{\sigma_2\sigma_2'}$ spin sector, we find the spinless SU(2)-invariant flow equation of the irreducible two-particle vertex to be (cf. [KBS10, Chap.10.2.3], [PHT13], [Met+12b, Eq.(110)-(112)])

$$\begin{aligned}\frac{\mathrm{d}}{\mathrm{d}\Lambda}g^{\Lambda}_{\alpha_1\alpha_2\alpha_1'\alpha_2'} = \int_{\substack{\beta_1,\beta_2,\\ \beta_1',\beta_2'}}\Big[S^{\Lambda}\left(\beta_1',\beta_1\right)G^{\Lambda}\left(\beta_2',\beta_2\right)+{}^{\beta_1\leftrightarrow\beta_2}_{\beta_1'\leftrightarrow\beta_2'}\Big]\Big[g^{\Lambda}_{\alpha_1\alpha_2\beta_1'\beta_2'}g^{\Lambda}_{\beta_1\beta_2\alpha_1'\alpha_2'}\\ -2g^{\Lambda}_{\alpha_1\beta_2\alpha_1'\beta_1'}g^{\Lambda}_{\alpha_2\beta_1\alpha_2'\beta_2'}+g^{\Lambda}_{\alpha_1\beta_2\alpha_1'\beta_1'}g^{\Lambda}_{\beta_1\alpha_2\alpha_2'\beta_2'}+g^{\Lambda}_{\beta_2\alpha_1\alpha_1'\beta_1'}g^{\Lambda}_{\alpha_2\beta_1\alpha_2'\beta_2'}+g^{\Lambda}_{\beta_2\alpha_2\alpha_1'\beta_1'}g^{\Lambda}_{\beta_1\alpha_1\alpha_2'\beta_2'}\Big]\end{aligned}\quad, \tag{6.3.22}$$

where all multiindices $\{\alpha_1,\alpha_2,\alpha_1',\alpha_2'\}$ are taken to lack the spin degree of freedom. The diagrammatic representation of this flow equation corresponds to the diagrams in (Figure 5.2). Finally, we want to shortly comment on the numerical evaluation of loop integrals. To this end, we first note that (exactly like in (Section 5.1)) the vertex functions are taken to be frequency independent by projecting all external fields to zero Matsubara frequency $i\omega = 0$. Employing frequency and momentum conservation for all two-particle vertex functions, this results in individual restrictions for the propagator terms $S^{\Lambda}\left(\beta_1',\beta_1\right)G^{\Lambda}\left(\beta_2',\beta_2\right)$ associated to the particle-particle and particle-hole contributions of the flow equation. Note, that these considerations are independent of using the spinful (Equation 6.3.20) or spinless (Equation 6.3.22) flow equation. In the following, we resort to the combined frequency-momentum notation $K = (i\omega, \mathbf{k})$. On the one hand, the particle-particle term in the flow equation $g^{\Lambda}_{\alpha_1\alpha_2\beta_1'\beta_2'}g^{\Lambda}_{\beta_1\beta_2\alpha_1'\alpha_2'}$ gives $K_{\alpha_1}+K_{\alpha_2}=K_{\beta_1'}+K_{\beta_2'}$ with $\Rightarrow K_{\beta_2'}=K_{\alpha_1}+K_{\alpha_2}-K_{\beta_1'}$. On the other hand, for the particle-hole term(s) $g^{\Lambda}_{\alpha_1\beta_2\alpha_1'\beta_1'}g^{\Lambda}_{\alpha_2\beta_1\alpha_2'\beta_2'}$ we find $K_{\alpha_1}+K_{\beta_2}=K_{\alpha_1'}+K_{\beta_1'}$ with $\Rightarrow K_{\beta_2}=K_{\alpha_1'}-K_{\alpha_1}+K_{\beta_1'}$. Henceforth, the propagators in band basis can be written as (using the propagator (Equation 4.2.4), the single-scale propagator (Equation 6.3.15), the regulator cutoff function and its derivative (Equation 6.1.4))

$$S^{\Lambda}\left(\beta_1', \beta_1\right) G^{\Lambda}\left(\beta_2', \beta_2\right) \delta_{\beta_1'\beta_1} \delta_{\beta_2'\beta_2} = \frac{\frac{\mathrm{d}}{\mathrm{d}\Lambda} C_{\Lambda}(\xi_{\beta_1 \mathbf{k}})}{-i\omega_n + \xi_{\beta_1 \mathbf{k}}} \frac{C_{\Lambda}(\xi_{\beta_2 \mathbf{k}_{\alpha_1} + \mathbf{k}_{\alpha_2} - \mathbf{k}_{\beta_1}})}{i\omega_n + \xi_{\beta_2 \mathbf{k}_{\alpha_1} + \mathbf{k}_{\alpha_2} - \mathbf{k}_{\beta_1}}} \quad , \tag{6.3.23}$$

for the particle-particle term and

$$S^{\Lambda}\left(\beta_1', \beta_1\right) G^{\Lambda}\left(\beta_2', \beta_2\right) \delta_{\beta_1'\beta_1} \delta_{\beta_2'\beta_2} = \frac{\frac{\mathrm{d}}{\mathrm{d}\Lambda} C_{\Lambda}(\xi_{\beta_1 \mathbf{k}})}{-i\omega_n + \xi_{\beta_1 \mathbf{k}}} \frac{C_{\Lambda}(\xi_{\beta_2 \mathbf{k}_{\alpha_1'} - \mathbf{k}_{\alpha_1} + \mathbf{k}_{\beta_1'}})}{-i\omega_n + \xi_{\beta_2 \mathbf{k}_{\alpha_1'} - \mathbf{k}_{\alpha_1} + \mathbf{k}_{\beta_1'}}} \quad , \tag{6.3.24}$$

for the (direct) particle-hole term with momentum transfer, where the self-energy contribution to the full propagator G^{Λ} was neglected. When assuming the vertex functions to be frequency independent, the Matsubara summation can be performed analytically with the result given in (Equation 5.1.17a) for the particle-particle and (Equation 5.1.17b) for the particle-hole terms. Using an energy/momentum cutoff like (Equation 6.1.3), the particle-particle and particle-hole loops in the flow equations are obtained in terms of

$$\begin{aligned} &\frac{1}{\beta} \sum_{i\omega_n} \left[S^{\Lambda}\left(\beta_1', \beta_1\right) G^{\Lambda}\left(\beta_2', \beta_2\right) + \substack{\beta_1 \leftrightarrow \beta_2 \\ \beta_1' \leftrightarrow \beta_2'} \right] \delta_{\beta_1'\beta_1} \delta_{\beta_2'\beta_2} \\ &\qquad = \begin{cases} \frac{\mathrm{d}}{\mathrm{d}\Lambda} \left(C_{\Lambda}(\xi_{\beta_1 \mathbf{k}}) C_{\Lambda}(\xi_{\beta_2 \mathbf{q} - \mathbf{k}_{\beta_1}}) \right) \frac{f(-\beta\xi_{\beta_1 \mathbf{k}}) - f(\beta\xi_{\beta_2 \mathbf{q} - \mathbf{k}_{\beta_1}})}{\xi_{\beta_1 \mathbf{k}} + \xi_{\beta_2 \mathbf{q} - \mathbf{k}_{\beta_1}}} & \text{particle-particle} \\ \frac{\mathrm{d}}{\mathrm{d}\Lambda} \left(C_{\Lambda}(\xi_{\beta_1 \mathbf{k}}) C_{\Lambda}(\xi_{\beta_2 \mathbf{q} + \mathbf{k}_{\beta_1}}) \right) \frac{f(+\beta\xi_{\beta_1 \mathbf{k}}) - f(\beta\xi_{\beta_2 \mathbf{q} + \mathbf{k}_{\beta_1}})}{\xi_{\beta_1 \mathbf{k}} - \xi_{\beta_2 \mathbf{q} - \mathbf{k}_{\beta_1}}} & \text{particle-hole} \end{cases} , \end{aligned} \tag{6.3.25}$$

where the momentum transfer $\mathbf{q}$ is given by $\mathbf{q} = \mathbf{k}_{\alpha_1} + \mathbf{k}_{\alpha_2}$ for the particle-particle, by $\mathbf{q} = \mathbf{k}_{\alpha_1'} - \mathbf{k}_{\alpha_1}$ for the direct particle-hole and by $\mathbf{q} = \mathbf{k}_{\alpha_1'} - \mathbf{k}_{\alpha_2}$ for the crossed particle-hole terms. In case of a *temperature flow* the free propagator in band basis is given by $\left(G_0^{\Lambda}\right)_{\mathbf{k}\alpha} = \beta^{-1/2} \left(-i\omega + \xi_{\mathbf{k}\alpha}\right)^{-1}$ (Equation 6.1.7). The scale derivative of the inverse free propagator is

$$\frac{\mathrm{d}(G_0^{\Lambda})^{-1}}{\mathrm{d}\Lambda} = \frac{\mathrm{d}}{\mathrm{d}\Lambda} \left[\beta^{1/2} \left(-i\omega_n + \xi_{\mathbf{k}\alpha}\right) \right] \overset{\omega_n = \frac{(2n+1)\pi}{\beta}}{\overset{\downarrow}{=}} = \frac{1}{2} \beta^{-1/2} \left(i\omega_n + \xi_{\mathbf{k}\alpha}\right) \quad , \tag{6.3.26}$$

where the derivative is performed with respect to $\Lambda = \beta$. Hence, the full propagator (by means of $G^{\Lambda} = \left(G_0^{\Lambda} - \Sigma^{\Lambda}\right)^{-1}$) and the single-scale propagator are

$$G^{\Lambda}(K,\alpha) = \frac{\beta^{-1/2}}{-i\omega + \xi_{\mathbf{k}\alpha}} \qquad S^{\Lambda}(K,\alpha) = G^{\Lambda}\frac{\mathrm{d}(G_0^{\Lambda})^{-1}}{\mathrm{d}\Lambda}G^{\Lambda} = \frac{\beta^{-3/2}}{2}\frac{i\omega_n + \xi_{\mathbf{k}\alpha}}{(-i\omega_n + \xi_{\mathbf{k}\alpha})^2} \quad , \tag{6.3.27}$$

where the self-energy contribution Σ^{Λ} was neglected. Therefore, the loop terms in the temperature flow scheme are

$$\begin{aligned}
&\frac{1}{\beta}\sum_{i\omega_n}\left[S^{\Lambda}\left(\beta_1',\beta_1\right)G^{\Lambda}\left(\beta_2',\beta_2\right) + {}^{\beta_1\leftrightarrow\beta_2}_{\beta_1'\leftrightarrow\beta_2'}\right]\delta_{\beta_1'\beta_1}\delta_{\beta_2'\beta_2} \\
&\quad = \frac{1}{\beta}\sum_{i\omega_n}\left[\frac{\beta^{-2}}{2}\frac{i\omega_n + \xi_{\mathbf{k}\beta_1}}{(-i\omega_n + \xi_{\mathbf{k}\beta_1})^2(\pm i\omega_n + \xi_{\mathbf{q}\mp\mathbf{k}\beta_2})} + \frac{-i\omega_n + \xi_{\mathbf{k}\beta_2}}{(-i\omega_n + \xi_{\mathbf{k}\beta_1})(\pm i\omega_n + \xi_{\mathbf{q}\mp\mathbf{k}\beta_2})^2}\right] \\
&\quad = \frac{1}{\beta}\sum_{i\omega_n}\frac{1}{\beta^2}\frac{-\omega_n^2 + \xi_{\mathbf{k}\beta_1}\xi_{\mathbf{q}\mp\mathbf{k}\beta_2}}{(-i\omega_n + \xi_{\mathbf{k}\beta_1})^2(\pm i\omega_n + \xi_{\mathbf{q}\mp\mathbf{k}\beta_2})^2} \quad ,
\end{aligned} \tag{6.3.28}$$

where the $\pm$ applies for the particle-particle and particle-hole case, respectively. The expression in the last line can be conveniently simplified by means of a derivative with respect to the flow parameter by [3]

$$\frac{1}{\beta}\sum_{i\omega_n}\frac{1}{\beta^2}\frac{-\omega_n^2 + \xi_{\mathbf{k}\beta_1}\xi_{\mathbf{q}\mp\mathbf{k}\beta_2}}{(-i\omega_n + \xi_{\mathbf{k}\beta_1})^2(\pm i\omega_n + \xi_{\mathbf{q}\mp\mathbf{k}\beta_2})^2} = \frac{1}{\beta}\sum_{i\omega_n}\frac{\mathrm{d}}{\mathrm{d}\beta}\left[\frac{1}{\beta}\frac{1}{(-i\omega_n + \xi_{\mathbf{k}\beta_1})}\frac{1}{(\pm i\omega_n + \xi_{\mathbf{q}\mp\mathbf{k}\beta_2})}\right] \quad . \tag{6.3.30}$$

After exchanging the summation and the derivative, the Matsubara sum can be performed with the well-known result (cf. (Equation 5.1.17a) and (Equation 5.1.17b))

$$\frac{1}{\beta}\sum_{i\omega_n}\left[S^{\Lambda}\left(\beta_1',\beta_1\right)G^{\Lambda}\left(\beta_2',\beta_2\right) + {}^{\beta_1\leftrightarrow\beta_2}_{\beta_1'\leftrightarrow\beta_2'}\right]\delta_{\beta_1'\beta_1}\delta_{\beta_2'\beta_2} = \frac{\mathrm{d}}{\mathrm{d}\beta}\frac{f(\mp\beta\xi_{\mathbf{k}\beta_1}) - f(\beta\xi_{\mathbf{q}\mp\mathbf{k}\beta_2})}{\xi_{\mathbf{k}\beta_1} \pm \xi_{\mathbf{q}\mp\mathbf{k}\beta_2}} \quad . \tag{6.3.31}$$

This final form of the loops in the framework of the temperature flow scheme provides the most transparent analogy to the perturbative renormalization group. More precisely, the loops of functional renormalization in the temperature flow scheme (Equation 6.3.31) and the loops of perturbative renormalization ((Equation 5.1.17a) and (Equa-

[3] The derivative of the propagator product with respect to the flow parameter β is

$$\frac{\mathrm{d}}{\mathrm{d}\beta}\left[\frac{1}{\beta}\frac{1}{(-i\omega_n + \xi)}\frac{1}{(\pm i\omega_n + \xi')}\right] = \frac{1}{\beta^2}\frac{\omega_n^2 - \xi\xi'}{(-i\omega_n + \xi)^2(\pm i\omega_n + \xi')^2} \quad , \tag{6.3.29}$$

where we used $\frac{\mathrm{d}}{\mathrm{d}\Lambda}i\omega_n = -i\omega_n/\beta$.

tion 5.1.17b)) only differ in the preceding temperature derivative.

6.4. Parameterization of the flow equation

The flow equations presented in the preceding section can be formulated in a numerically more efficient way by taking the constraints and symmetries given in (Section 3.3) into account. Here, we limit our considerations to the irreducible two-particle vertex. Apart from that, there are numerous more symmetries and resulting interdependencies in the two-particle vertex due to time-reversal and point group operation, which can, however, only be exploited numerically.

6.4.1. Parametrization of the two-particle vertex

The antisymmetry and self-adjointness of the irreducible two-particle vertex have been shown to reduce the number of independent spin-sectors from sixteen to six (cf. (Equation 3.3.6)). These considerations enable us to rewrite the spinful flow equation (Equation 6.3.20) in terms of these six spinless tensors, named $\{A, B, C, D, E, F\}$. This parametrization of the flow equation effectively suppresses the spin degree of freedom by implicitly performing the spin summation in the first place. Since we work in band basis, both full and single-scale propagators are assumed to be diagonal. Hence, the spin summation of the loop integral is limited to four terms only for each of the diagrams. By inserting the parametrization (Equation 3.3.6) into the spinful flow-equation (Equation 6.3.20), we find six coupled flow equations, i.e. one for each of the independent spin sectors $\{A, B, C, D, E, F\}$. Here, we only give the expressions for the flow equation of tensors A and B. The flow equation of A depends on A, B, C, D only, and is given by

$$\begin{aligned}
\frac{\mathrm{d}}{\mathrm{d}\Lambda} A_{\alpha_1\alpha_2\alpha_1'\alpha_2'} &= \int_{\beta_1,\beta_2} \left[S^\Lambda_{\beta_1} G^\Lambda_{\beta_2} + S^\Lambda_{\beta_2} G^\Lambda_{\beta_1} \right] \\
&\times \Bigg[\frac{1}{2} \Big(A_{\alpha_1\alpha_2\beta_1\beta_2} A_{\beta_1\beta_2\alpha_1'\alpha_2'} + B_{\alpha_1\alpha_2\beta_1\beta_2} \overline{B_{\alpha_1'\alpha_2'\beta_1\beta_2}} - B_{\alpha_1\alpha_2\beta_2\beta_1} \overline{B_{\alpha_1'\alpha_2'\beta_1\beta_2}} \\
&+ C_{\alpha_1\alpha_2\beta_1\beta_2} \overline{C_{\alpha_1'\alpha_2'\beta_1\beta_2}} \Big) - \Big(A_{\alpha_1\beta_2\alpha_1'\beta_1} A_{\alpha_2\beta_1\alpha_2'\beta_2} + \overline{B_{\alpha_1'\beta_1\alpha_1\beta_2}} B_{\alpha_2\beta_1\alpha_2'\beta_2} \\
&+ B_{\alpha_1\beta_2\alpha_1'\beta_1} \overline{B_{\alpha_2'\beta_2\alpha_2\beta_1}} + D_{\alpha_1\beta_2\alpha_1'\beta_1} D_{\alpha_2\beta_1\alpha_2'\beta_2} \Big) + \Big(A_{\alpha_1\beta_1\alpha_2'\beta_2} A_{\alpha_2\beta_2\alpha_1'\beta_1} \\
&+ B_{\alpha_1\beta_1\alpha_2'\beta_2} \overline{B_{\alpha_1'\beta_1\alpha_2\beta_2}} + \overline{B_{\alpha_2'\beta_2\alpha_1\beta_1}} B_{\alpha_2\beta_2\alpha_1'\beta_1} + D_{\alpha_1\beta_1\alpha_2'\beta_2} D_{\alpha_2\beta_2\alpha_1'\beta_1} \Big) \Bigg] \quad . \qquad (6.4.1)
\end{aligned}$$

In contrast, the flow equation of B depends on the five tensors A, B, C, D, E and appears to be

$$\begin{aligned}
\frac{\mathrm{d}}{\mathrm{d}\Lambda} B_{\alpha_1\alpha_2\alpha_1'\alpha_2'} &= \int_{\beta_1,\beta_2} \left[S^{\Lambda}_{\beta_1} G^{\Lambda}_{\beta_2} + S^{\Lambda}_{\beta_2} G^{\Lambda}_{\beta_1} \right] \\
&\times \Bigg[\frac{1}{2} \Big(A_{\alpha_1\alpha_2\beta_1\beta_2} B_{\beta_1\beta_2\alpha_1'\alpha_2'} + B_{\alpha_1\alpha_2\beta_1\beta_2} D_{\beta_1\beta_2\alpha_1'\alpha_2'} - B_{\alpha_1\alpha_2\beta_2\beta_1} D_{\beta_1\beta_2\alpha_2'\alpha_1'} \\
&+ C_{\alpha_1\alpha_2\beta_1\beta_2} \overline{E_{\alpha_1'\alpha_2'\beta_1\beta_2}} \Big) - \Big(- A_{\alpha_1\beta_2\alpha_1'\beta_1} B_{\alpha_2\beta_1\beta_2\alpha_2'} + \overline{B_{\alpha_1'\beta_1\alpha_1\beta_2}} C_{\alpha_2\beta_1\alpha_2'\beta_2} \\
&- B_{\alpha_1\beta_2\alpha_1'\beta_1} D_{\alpha_2\beta_1\beta_2\alpha_2'} + D_{\alpha_1\beta_2\alpha_1'\beta_1} E_{\alpha_2\beta_1\alpha_2'\beta_2} \Big) + \Big(- B_{\alpha_1\beta_1\beta_2\alpha_2'} A_{\alpha_2\beta_2\alpha_1'\beta_1} \\
&+ C_{\alpha_1\beta_1\alpha_2'\beta_2} \overline{B_{\alpha_1'\beta_1\alpha_2\beta_2}} + D_{\alpha_1\beta_1\beta_2\alpha_2'} B_{\alpha_2\beta_2\beta_1\alpha_1'} + E_{\alpha_1\beta_1\alpha_2'\beta_2} D_{\alpha_2\beta_2\alpha_1'\beta_1} \Big) \Bigg] \quad . \qquad (6.4.2)
\end{aligned}$$

Both flow equations don't involve any explicit spin degree of freedom anymore, since the six tensors represent the full spin structure of the two-particle interaction and the spin summation of the spinful flow equation was already taken care of. The remaining four flow equations for $\{C, D, E, F\}$ can be derived analogously.

Summary and preview

This chapter introduced the functional renormalization group based on the generating functional of the effective action. After introducing the cutoff dependency into the free propagator and deriving the flow equation of the effective action, we used the expansion of the effective action in terms of fields to obtain an infinite hierarchy of coupled flow equations. In particular, we are interested in the flow equations at first and second order, i.e. the (spinful) flow equations of the self-energy and the irreducible two-particle vertex. We discussed the mathematical details necessary for the numerical implementation of these flow equations. Based on the considerations of the symmetries of the two-particle vertex in (Section 3.3) we gave a parametrization of the flow equation of the two-particle vertex that allows for a numerically efficient calculation of all spin-sectors, while avoiding the inclusion of any redundant couplings.

Part II.

Applications

7. Methodological benchmarking by means of toy models

In the first part of this thesis we introduced the methodological novelties and concepts for perturbative ((Chapter 5)) and functional renormalization group ((Chapter 6)) approaches to fermionic systems with broken SU(2) spin symmetry, for instance with sizeable spin-orbit interaction. Furthermore, the developed methods are well-suited to deal with additional broken symmetries. In particular, these computational tools enable us to perform renormalization group calculations in absence of spacial inversion symmetry *or* time-reversal symmetry. In (Chapter 3) we discussed and derived the possible results and allowed quantum states, which may occur in these system, from a symmetry point of view. The second part of this thesis will employ these methods to physically interesting systems that are subject to current research interest. The first of these being the oxide-heterostructure represented by $LaAlO_3/SrTiO_3$, which features broken spacial inversion symmetry and Rashba interaction. The second one is the intriguing matter of strontium ruthenate, which will be introduced by a three-orbital Hamiltonian including centrosymmetric spin-orbit coupling. However, before we dive into these (realistic) models, we proceed by making sure that in the limit of vanishing spin-orbit interaction and zero magnetic field the developed computational tools reproduce the phases and quantum states of well-known toy models, which serve as a reference for the reliability of the proposed methods.

7.1. Hubbard model on the two-dimensional square lattice

The *Hubbard model* has been around for already more than fifty years [Hub63] and represents one of the simplest models for interacting correlated electrons. Nevertheless, it has been shown to exhibit metal-insulator transitions, (high-temperature) superconductivity and (antiferro-)magnetism [LeB+15]. The (extended) repulsive Hubbard model on the square lattice is defined by

$$\mathcal{H}_0 = -t_{ij} \sum_{i,j\sigma} \left(c^\dagger_{i\sigma} c_{j\sigma} + \text{h.c.} \right) - \mu \sum_{i\sigma} c^\dagger_{i\sigma} c_{j\sigma} + U \sum_i n_{i\uparrow} n_{i\downarrow} + V \sum_{\langle ij \rangle \sigma\sigma'} n_{i\sigma} n_{j\sigma'} \quad . \tag{7.1.1}$$

with on-site Coulomb repulsion $U > 0$, nearest neighbour interaction $V > 0$ and the number operator $n_{i\sigma} = c^\dagger_{i\sigma} c_{i\sigma}$. The non-interacting band structure and Fermi surface of the Hamiltonian (Equation 7.1.1) on the square lattice are shown in (Figure 7.1a) for two sets of parameters given by nearest neighbor $t = 1.0\,\text{eV}$ and next nearest neighbour

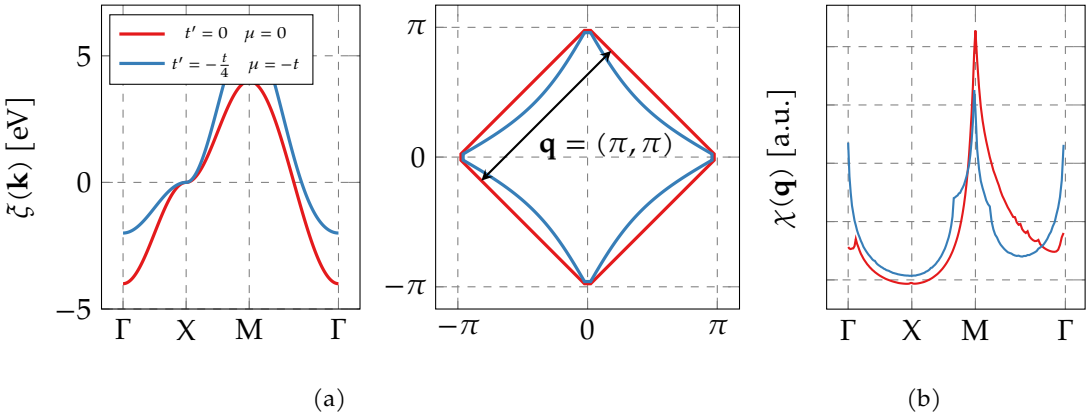

(a) (b)

Figure 7.1.: The band structure and Fermi surface of the single-orbital Hubbard model given by (Equation 7.1.1) for the two sets of parameters $t' = 0t, -0.25t$ and the chemical potential $\mu = 0t, -1.0t$. The bare susceptibility $\chi(\mathbf{q})$ is strongly enhanced for fluctuations with momentum transfer $\mathbf{q} = (\pi, \pi)^T$.

hopping $t' = 0t, -0.25t$ and the chemical potential $\mu = 0t, -1.0t$. For the first parameter set $t' = 0$ and $\mu = 0$, the Fermi surface is perfectly nested with respect to the momentum transfer $\mathbf{q} = (\pi, \pi)^T$ and the band structure shows particle-hole symmetry. The finite next nearest neighbour hopping $t' = -0.25t$ and the shift in the chemical potential destroys the perfect nesting by slightly warping the Fermi surface. In (Figure 7.1b) we plotted the bare susceptibility $\chi(\mathbf{q})$ defined in (Equation 5.2.7). For both sets of parameters, the susceptibility is strongly enhanced at the M point corresponding to $\mathbf{q} = (\pi, \pi)^T$ fluctuations, which is a consequence of the (almost) perfect nesting of the Fermi surface and the van-Hove singularity in the density of states at zero energy $\xi(\mathbf{k}) = 0$.

7.1.1. Antiferromagnetic fluctuations and d-wave superconductivity

Judging from (Figure 7.1b) and the bare susceptibility, we can expect *antiferromagnetic fluctuations* with ordering vector $\mathbf{q} = (\pi, \pi)^T$ to be strong in the single-band Hubbard model near half-filling. Indeed, the half-filled Hubbard model has been shown to order antiferromagnetically already on the mean-field level [KU75]. To go beyond the mean-field approximation, we employ the perturbative renormalization group approach in (Chapter 5). However, the perturbative method ceases to be exact when approaching half-filling due to the strong particle-hole fluctuations. Hence it is only valid away from the perfectly nested case with the van-Hove singularity at the Fermi level. Consequently, we use the perturbative method to calculate the phase diagram with respect to electron filling n and nearest neighbor interaction V for sizeable chemical potential $\mu > 0$ of the extended Hubbard model (Equation 7.1.1) to avoid half-filling. The phase diagram (Figure 7.2a) is dominated by singlet d-wave pairing states with symmetry representations B_{1g} and B_{2g}. While the symmetry protected nodes of B_{2g} are located along the main axis', i.e. $k_x = 0$ and k_y, the B_{1g} representation features nodes along the diagonals

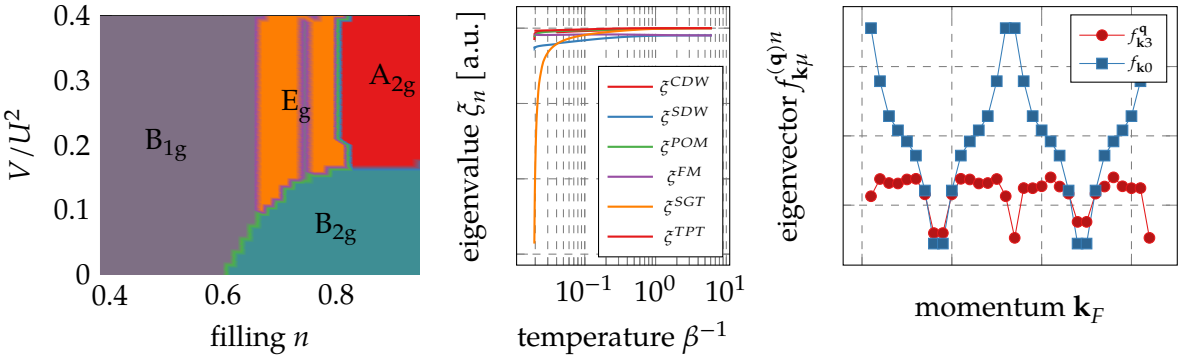

(a) (b)

Figure 7.2.: (Figure 7.2a) shows the phase diagram of the single-band Hubbard model (Equation 7.1.1) with respect to the electron filling n and nearest neighbor interaction V. It is qualitatively similar to the phase diagram of [Hlu99] and the transition between B_{2g} and B_{2g} along the axis of n agrees quantitatively with [Rag+12]. In (Figure 7.2b), the functional renormalization group flow for $\mu = -t$ and $t' = -0.25t$ exhibits the singlet pairing instability with B_{1g} symmetry and the associated order parameters $f^{\mathbf{q}}_{\mathbf{k}3}$ and $f_{\mathbf{k}0}$ (plotted along the Fermi surface given by discrete Fermi points $\mathbf{k}^i_F$) of the spin-density wave with ordering vector $\mathbf{q} = (\pi, \pi)$ and the singlet pairing (cf. notation in (Section 3.5) and (Section 3.4)).

with $k_x = \pm k_y$. By shifting its anti-nodal regime towards the van-Hove singularity at X, the B_{1g} pairing state gains condensation energy. To approach the half-filled case, we make use of the functional renormalization group in (Chapter 6). The functional renormalization group flow of the eigenvalues of various kinds of particle-hole and pairing channels and associated order parameters is given in (Figure 7.2b). By analyzing the harmonic content of the gap functions in (Figure 7.2b) for $\mu = -t$ and $t' = -0.25t$, we find that the B_{1g} state is mostly comprised of short range first nearest neighbor pairing and has a small contribution from longer range third nearest neighbor pairing described by the order parameter:

$$d^0_{\mathbf{k}} = \Delta_1 \left(\cos(k_x) - \cos\left(k_y\right)\right) + \Delta_1 \left(\cos(2k_x) - \cos\left(2k_y\right)\right) \quad , \tag{7.1.2}$$

where Δ_1, Δ_3 specify the overall and relative gap magnitudes with $|\Delta_1| \approx 2|\Delta_3|$. The required lattice harmonics are given in appendix H. The interplay and competition between antiferromagnetism and d-wave superconductivity in the Hubbard model near half-filling have been investigated extensively and appear to be an established result [ZS98; HM00b].

7.2. Chiral superconductivity on the honeycomb lattice

Since the first experimental realization of graphene about a decade ago [Nov+05], the community has been showing immense interest in this hexagonal honeycomb structure made of carbon atoms. Besides having extraordinary mechanical properties, the graphene sheets feature an exotic dispersion relation of the electrons at the K-points of the Brillouin zone reminiscent of relativistic massless Dirac particles [GM07; Gei09]. An illustration of the honeycomb lattice structure with sublattices A, B and basis vectors $\mathbf{a}_1 = \frac{a}{2}\left(3, \sqrt{3}\right)^T$ and $\mathbf{a}_2 = \frac{a}{2}\left(3, -\sqrt{3}\right)^T$ is provided in (Figure 7.3a). In order to derive a simple tight-binding model for a perfectly plane graphene sheet, we assume rotationally invariant p_z orbitals that make up the electronic states at the Fermi surface. Taking only first nearest neighbor hoppings into account, we find the non-interacting tight-binding Hamiltonian:

$$\mathcal{H}_0 = \sum_{\mathbf{k},\sigma} \left(c^\dagger_{\mathbf{k}A\sigma}, c^\dagger_{\mathbf{k}B\sigma}\right)^T \begin{pmatrix} t_2 h_2(\mathbf{k}) - \mu & t_1 h_1(\mathbf{k}) \\ t_1 \bar{h}_1(\mathbf{k}) & t_2 h_2(\mathbf{k}) - \mu \end{pmatrix} \begin{pmatrix} c_{\mathbf{k}A\sigma} \\ c_{\mathbf{k}B\sigma} \end{pmatrix} \quad , \tag{7.2.1}$$

where $c^\dagger_{\mathbf{k}A(B)\sigma}$, $c_{\mathbf{k}A(B)\sigma}$ creates (annihilates) an electron on sublattice A (B) and μ is the chemical potential. The momentum dependency is given by

$$h_1(\mathbf{k}) = e^{-ik_x} + 2e^{ik_x/2}\cos\left(k_y\sqrt{3}/2\right) \quad \text{and} \tag{7.2.2}$$

$$h_2(\mathbf{k}) = \cos\left(\sqrt{3}k_y\right) + \cos\left((3k_x + \sqrt{3}k_y)/2\right) + \cos\left((3k_x - \sqrt{3}k_y)/2\right) \quad , \tag{7.2.3}$$

where the lattice constant was set to unity $a = 1$. For second nearest neighbor hopping being zero $t_2 = 0$ the single-particle spectrum and the eigenstates of (Equation 7.2.1) can be calculated analytically. The eigenvalues are given by

$$\xi_\pm(\mathbf{k}) = \pm\sqrt{|h_1(\mathbf{k})|^2} = \pm\sqrt{1 + 4\cos\left(k_y\sqrt{3}/2\right)\cos\left(k_x\,3/2\right) + 4\cos^2\left(k_y\sqrt{3}/2\right)} \quad , \tag{7.2.4}$$

and they are plotted along the high symmetry points of the Brillouin zone in (Figure 7.3b). The eigenstates show that the "orbital weight" of a Bloch state is equally distributed among both sublattices, i.e.

$$\mathbf{u}_\pm(\mathbf{k}) = \begin{pmatrix} \frac{h_1(\mathbf{k})}{\xi_\pm(\mathbf{k})}\alpha \\ \alpha \end{pmatrix} = \frac{1}{\sqrt{2}}\begin{pmatrix} \pm e^{i\phi(\mathbf{k})/2} \\ e^{-i\phi(\mathbf{k})/2} \end{pmatrix} \quad , \quad \alpha \in \mathbb{C} \quad , \tag{7.2.5}$$

with α being the normalization constant, which may carry any phase. In the second

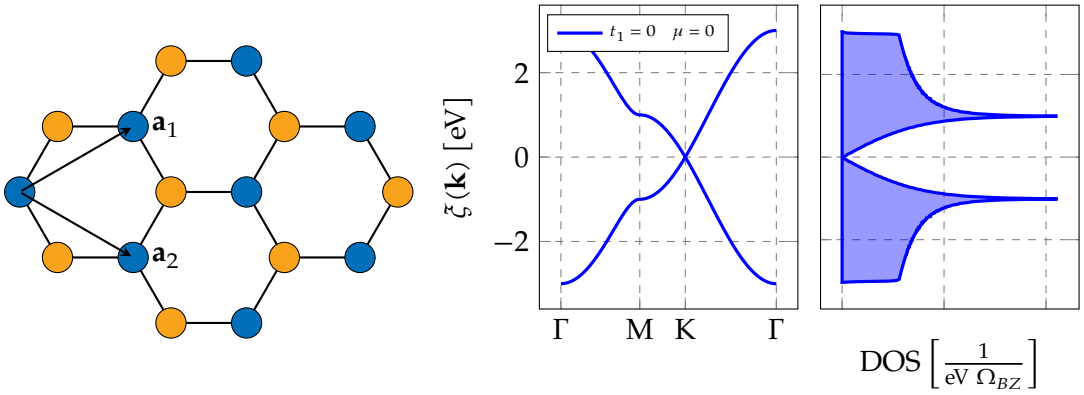

(a) (b)

Figure 7.3.: (Figure 7.3a) illustrates the structure of the honeycomb lattice with basis vectors $\mathbf{a}_1 = \frac{a}{2}(3, \sqrt{3})^T$ and $\mathbf{a}_2 = \frac{a}{2}(3, -\sqrt{3})^T$ and sublattices A and B. The band structure (Figure 7.3b) is characterized by the *Dirac cone* at the Fermi surface. In its vicinity the dispersion can be approximated by $\xi_{\mathbf{k}} \approx v_F^{\perp} k_{\perp} + v_F^{\parallel} k_{\parallel}$ with the Fermi velocities $v_F^{\perp}$ and $v_F^{\parallel}$ perpendicular and parallel to the Fermi surface. The density of states is zero at the Dirac point and increases linearly in its vicinity.

equality we defined the phase $\phi(\mathbf{k})$ by $h_1(\mathbf{k}) = \xi_{\pm}(\mathbf{k}) e^{i\phi(\mathbf{k})/2}$ and chose $\alpha = \frac{1}{\sqrt{2}} e^{-i\phi(\mathbf{k})/2}$. Although both sublattices contribute the same "weight" to any Bloch state, the eigenstate components feature a relative phase between both sublattice parts. Note, that this relative phase is the origin of the non-zero *Berry phase* in *graphene* [Zha+05; XCN10a; PM11].

7.2.1. Singlet pairing in the E_{2g} representation

The structure of the eigenstates (Equation 7.2.5) has profound consequences on the momentum dependency of the bare interaction in band basis. To obtain the band representation (Equation 5.1.15) of a on-site interaction U_0, we employ the transformations (Equation 3.3.33a) and (Equation 3.3.33b). However, taking higher order hoppings in (Equation 7.2.1) into account, will result in a Hamiltonian whose eigenstates can in general not be represented analytically. This poses a numerical challenge with respect to the phases of Bloch states. To render the resulting order parameters associated to instabilities of the renormalization group flow gauge-invariant, we either have to fix a particular gauge (cf. (Figure 3.2) and discussion in (Section 3.2)), which results in eigenstates, which coincide with the analytically given states for hopping parameters $t_n = 0$, $\forall n > 1$ (cf. appendix E), or we have to rely on pairing between *time-reversal* and *inversion symmetry* partner states as explained in (Section 3.4). The interacting Hamiltonian with on-site repulsion U_0 and nearest neighbor interaction U_1 between electrons on sublattices A and B is:

$$\mathcal{H}_I = U_0 \sum_i n_{i\uparrow} n_{i\downarrow} + U_1 \sum_{\langle ij \rangle} \sum_{\sigma\sigma'} n_{i\sigma} n_{j\sigma'} \quad , \tag{7.2.6}$$

with $n_{i\sigma} = c^\dagger_{i\sigma} c_{i\sigma}$. Note, that while the on-site interaction U_0 requires antiparallel spins, the longer-range interaction U_1 may have finite contributions in both antiparallel and parallel interaction matrix elements, which becomes important for the proper setup of the spinful antisymmetric two-particle vertex (cf. appendix G). However, in this subsection we limit our considerations to the spinless interaction. Henceforth, the bare (spinless) two-particle vertex in band basis for an on-site interaction U_0 is determined by (using the notation given in (Equation 3.3.19))

$$\begin{aligned} V_{\mathbf{k}_1 b_1 \mathbf{k}_2 b_2 \mathbf{k}'_1 b'_1 \mathbf{k}'_2 b'_2} &= \sum_{\alpha_i} \bar{u}^{b_1 \alpha_1}_{\mathbf{k}_1} \bar{u}^{b_2 \alpha_2}_{\mathbf{k}_2} V_{\mathbf{k}_1 \alpha_1 \mathbf{k}_2 \alpha_2 \mathbf{k}'_1 \alpha'_1 \mathbf{k}'_2 \alpha'_2} u^{b'_2 \alpha'_2}_{\mathbf{k}'_2} u^{b'_1 \alpha'_1}_{\mathbf{k}'_1} \\ &= U_0 \sum_{\alpha} \bar{u}^{b_1 \alpha}_{\mathbf{k}_1} \bar{u}^{b_2 \alpha}_{\mathbf{k}_2} u^{b'_2 \alpha}_{\mathbf{k}'_2} u^{b'_1 \alpha}_{\mathbf{k}'_1} \quad , \end{aligned} \tag{7.2.7}$$

where we substituted the notation $\pm$ in (Equation 7.2.5) with appropriate band indices $b = \pm$ and used the summation over all four pairs of A, B sublattice indices with $\alpha_i \in \{A_i, B_i\} \forall i \in \{1, 2, 3, 4\}$. The simplification of the transformation in the second line is due to the on-site interaction having the same sublattice index associated to any of the four fermionic fields. Inserting the eigenstates (Equation 7.2.5) into (Equation 7.2.7), we find that the remaining two terms contributing to the vertex in band space are complex conjugated to each other. As a result, the momentum dependency of the two-particle interaction in band space is described by $\cos\left((-\phi(\mathbf{k}_1 - \phi(\mathbf{k}_2) + \phi(\mathbf{k}'_1) + \phi(\mathbf{k}'_2)/2\right)$ and $\sin(\ldots)$ for the upper and lower band, respectively. Consequently, the two-particle vertex in band space for on-site interaction and only nearest neighbor hopping must always be real for "properly gauged" eigenstates. As a second indicator for a proper band basis, we note that the Cooper channel of the vertex turns out to be momentum independent on the mean-field level since the phase $\phi(\mathbf{k})$ satisfies $\phi(-\mathbf{k}) = -\phi(\mathbf{k})$ due to $h_1(-\mathbf{k}) = \bar{h_1}(\mathbf{k})$. The renormalization group flow for the bare interaction (Equation 7.2.7) and corresponding Fermi surface topology for the setup $\mu = -1.2t_1$ and $t_2 = 0$ are shown in (Figure 7.4). While the perfect nesting condition of the Fermi surface and the van-Hove singularity at the Fermi level will give rise to a spin-density wave with ordering vector $\mathbf{q} = (\pi, \pi/\sqrt{3})^T$, a shift in the electron filling that destroys the perfect nesting of the Fermi surface will promote the singlet pairing in the two-dimensional E_2 representation of the hexagonal point group to be the leading instability. The harmonic analysis of the associated gap function given in the right part of (Figure 7.4) reveals that it is mostly comprised of first and third nearest neighbor pairing. Since the two eigenvectors associated to basis functions are degenerate, any superposition of both can be realized. Mean-field theory shows that a complex superposition with relative $e^{\pm i\pi/2}$ will maximize the condensation energy. The "chiral" $d+id$ singlet pairing state has been proposed in several works, that made use of various renormalization group schemes

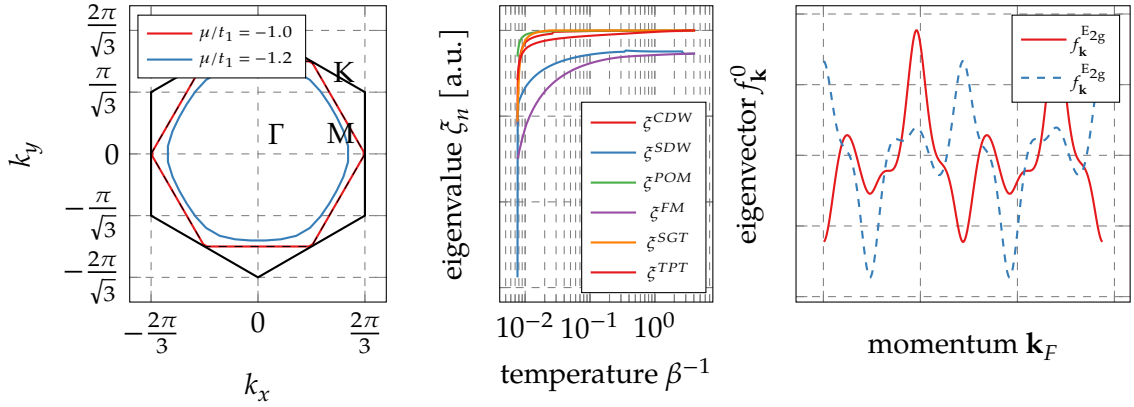

Figure 7.4.: The Fermi surface for $\mu = -t_1$ and $t_2 = 0$ is perfectly nested and promotes a spin-density wave instability with momentum transfer $\mathbf{q} = (\pi, \pi/\sqrt{3})^T$. However, deforming the Fermi surface to get rid of the nesting condition by shifting the electron filling ($\mu = -1.2t_1$) will enhance the singlet pairing channel and eventually result in an instability with the symmetry of the E_{2g} representation of the hexagonal point group.

[NLC12; NC12; Kie+12].

Summary and preview

In this chapter we established the connection between our spinful renormalization group framework of perturbative and functional kind with previous work in the field by means of toy models. We firstly took the single-band Hubbard model to reproduce well-known results at and away from half-filling. We found that the perturbative renormalization group scheme cannot be employed directly at half-filling due to the perfect nesting condition, the van-Hove singularity at the Fermi level and the resulting strong particle-hole fluctuations. However, since the functional renormalization group scheme takes both particle-particle and particle-hole channels into account, we are able to fill this gap. This shows that the perturbative and functional renormalization group schemes represent a symbiotic set of methods. Furthermore, we employed the functional renormalization group scheme to competing instabilities of the Hubbard model on the honeycomb lattice and found the chiral superconducting instabilities widely known as $d + id$ state. In the next chapter, we will make use of further capabilities of our renormalization group schemes by taking finite noncentrosymmetric spin-orbit coupling terms into account. As a physical interesting example, we show how topological superconducting may arise in the oxide heterostructure of $LaAlO_3/SrTiO_3$.

8. Topological superconductivity in oxide heterostructures

As a first step into the realm of spin-orbit physics we consider the oxide-heterostructure of $LaAlO_3/SrTiO_3$. The research in $LaAlO_3/SrTiO_3$ is part of an exciting new field of condensed matter research in complex oxide interfaces [MS10b]. It is based on the discovery that a well-defined interface made up of (otherwise insulating) oxides can give rise to an electron gas with astonishing properties like i.a. high mobility [OH04]. The diversity of this new field of research is driven by the complex interplay between spin, lattice, charge and orbital degrees of freedom [Zub+11] and results in unusual behavior of electronic, (ferro-)magnetic, magnetoelectric and superconducting properties [Li+11]. Here, we are interested in the superconductivity in the $LaAlO_3/SrTiO_3$ oxide heterostructure featuring a critical temperature of $T_C \approx 200\,\mathrm{mK}$ [Rey+07]. Obviously, the most striking difference of the two-dimensional electron gas at the heterostructure interface to any bulk system is the broken inversion symmetry, which allows for an admixture of singlet and triplet pairing states (cf. (Section 3.4.2)). Concerning the nature of the pairing state, there have been proposals for a mixed singlet-triplet state with d_{xy} and $(p_x \pm ip_y)$-wave symmetry (given in pseudospin basis) [Yad+09] based on Eliashberg theory and a s_{++} versus s_{+-} state (given in helical basis) with same or alternating sign on the spin-split Fermi surfaces [SS15].

8.1. Electronic properties

The two-dimensional electron gas at the heterointerface of $LaAlO_3/SrTiO_3$ is constituted by the $SrTiO_3$ layer and its usually empty $3d_{xy}$, $3d_{xz}$ and $3d_{yz}$ orbitals (t_{2g}) states of Ti^{4+} that are occupied by the charge carriers from the $LaAlO_3$ film [OH04; San+11]. We describe the single-particle properties in the orbital o, o' (and spin σ, σ') degrees of freedom by the Hamiltonian

$$\mathcal{H}_0 = \sum_{\mathbf{k}} \sum_{oo'\sigma\sigma'} a^\dagger_{\mathbf{k}o'\sigma'} \left(h_{\mathbf{k}oo'}\right)_{\sigma\sigma'} a_{\mathbf{k}o\sigma} \quad , \tag{8.1.1}$$

where $a^\dagger_{\mathbf{k}o\sigma}$ and $a_{\mathbf{k}o\sigma}$ create and annihilate an electron in orbital o with crystal momentum $\mathbf{k}$ and spin projection quantum number σ. Magnetotransport and magnetoconductance measurements suggest that the d_{xz} and d_{yz} orbitals play an important role in contributing to and hosting superconductivity in the interface. Therefore, we focus on the description of an effective non-interacting Hamiltonian in these orbitals, which

is comprised of a spinless orbital term and a term that features both centro- and non-centrosymmetric spin-orbit coupling:

$$h_{\mathbf{k}} = h^0_{\mathbf{k}} + h^{\mathrm{SOC}}_{\mathbf{k}} \quad . \tag{8.1.2}$$

The matrix elements of the d_{xz} and d_{yz} orbital degrees of freedom in $h_{\mathbf{k}oo'}$ must be consistent with C_{4v} symmetry and time-reversal symmetry. Up to second order in momentum, they are given by

$$h^0_{\mathbf{k}} = \begin{pmatrix} \xi_{A1}(\mathbf{k}) + \xi'_{A1}(\mathbf{k}) - \mu & \xi_{B2}(\mathbf{k}) \\ \xi_{B2}(\mathbf{k}) & \xi_{A1}(\mathbf{k}) + \xi'_{A1}(\mathbf{k}) - \mu \end{pmatrix} \otimes \sigma_0 \quad , \tag{8.1.3}$$

with the Pauli matrix σ_0 representing identity in spin space. The dispersion relations are defined by

$$\xi_{A1}(\mathbf{k}) = t_1 \left(\cos(k_x) + \cos\left(k_y\right)\right) \tag{8.1.4}$$

$$\xi'_{A1}(\mathbf{k}) = t_2 \left(\sin^2(k_x) + \sin^2(k_y)\right) \tag{8.1.5}$$

$$\xi_{B2}(\mathbf{k}) = t_3 \sin(k_x) \sin\left(k_y\right) \quad , \tag{8.1.6}$$

and where the subscripts describe the irreducible representations, the dispersions are associated to. The phenomenological parameters that were chosen to closely match the experimental data and ab-initio calculation of [Kin+14][ZTH13] are given by (in eV) $t_1 = 0.31$, $t_2 = 0.0032$, $t_3 = 0.1432$, $\mu = 0.0004$. The spin-orbit part is composed of an atomic (centrosymmetric) term $\tau_y \otimes \sigma_z$ and a Rashba-Dresselhaus term (up to first order) due to the broken inversion symmetry: (cf. (Section 3.1))

$$\begin{aligned} h^{\mathrm{SOC}}_{\mathbf{k}} = \alpha_C \tau_y \otimes \sigma_z + \alpha_R \sin(k_x) \tau_0 \otimes \sigma_y - \alpha_R \sin\left(k_y\right) \tau_0 \otimes \sigma_x \\ - \alpha_R \sin(k_x) \tau_x \otimes \sigma_x + \alpha_R \sin\left(k_y\right) \tau_x \otimes \sigma_y \\ - \alpha_R \sin(k_x) \tau_z \otimes \sigma_y - \alpha_R \sin\left(k_y\right) \tau_z \otimes \sigma_x \quad . \end{aligned} \tag{8.1.7}$$

While $\sigma_{x,y,z}$ denotes the Pauli matrices in spin space, $\tau_{x,y,z}$ represent the Pauli matrices in d_{xz}, d_{yz} orbital space. The parameters specifying the strength of spin-orbit interactions are (in eV) $\alpha_C = 0.0108$ and $\alpha_R = 0.0016$. The resulting two-dimensional band structure and related properties are shown in (Section 8.1). The upper band does not produce any Fermi sheet, while the Fermi surface of the lower band has a small cloverleaf-like shape centered around the Γ-point. As the starting point for the renormalization group procedure, we assume an interacting Hamiltonian, which includes intra- and interorbital density-density interaction:

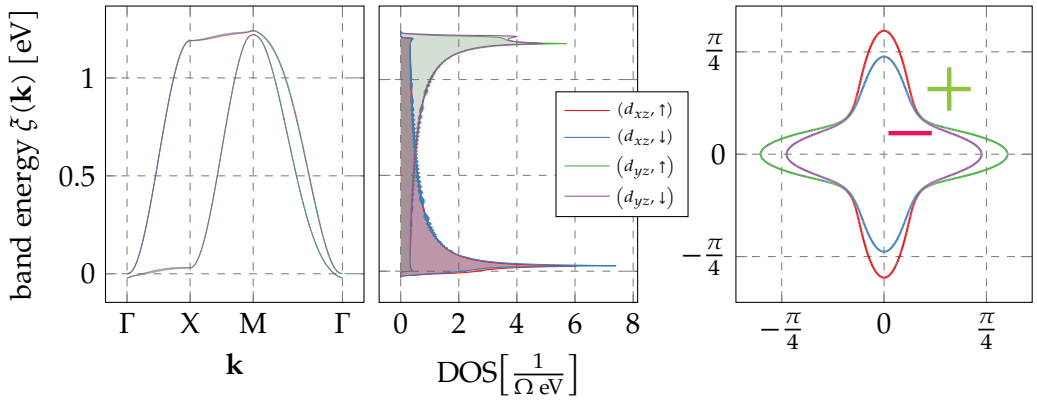

Figure 8.1.: The two-dimensional band structure that results from equation ((Equation 8.1.2)) features only one band which intersects with the Fermi level. Although there is only one Fermi sheet the two orbital character of the band structure is revealed in the non-trivial orbital and spin character of the states along the Fermi surface. The color code indicates the orbital and spin content of a particular band. The density of states shows a very prominent peak slightly above the Fermi level. The resulting Fermi surface has a cloverleaf like shape and covers only a tiny part of the Brillouin zone. Note, that only a fraction of the Brillouin zone is shown.

$$\mathcal{H}_I = \sum_i \sum_o U_1\, n_{io\uparrow} n_{io\downarrow} + \frac{1}{2} \sum_i \sum_{o \neq o'} \sum_{\sigma,\sigma'} U_2\, n_{io\sigma} n_{io'\sigma'} \quad , \tag{8.1.8}$$

where the indices o and o' again denote the orbitals d_{xz} and d_{yz}. The parameters U_1 and U_2 specify the interaction strength of the intra- and interorbital terms among these two orbitals. Since the spin-orbit coupling term $h^{SOC}_{\mathbf{k}}$ introduces spin off-diagonal terms into the non-interacting Hamiltonian, the new basis that diagonalizes (Equation 8.1.2) does not only superpose different orbitals but also different spin degrees of freedom. The new quasiparticle basis is characterized by band index b and helicity $\lambda = \pm$ [BS12]. The corresponding operators $b^\dagger_{\mathbf{k}b\lambda}$ ($b_{\mathbf{k}b\lambda}$) which create (annihilate) a quasiparticle with crystal momentum $\mathbf{k}$ in band b with helicity λ are defined by the eigenstates $u_{\mathbf{k}b\lambda}$ of (Equation 8.1.1), and are given by the unitary transformation

$$b_{\mathbf{k}b\lambda} = u_{\mathbf{k}b\lambda,o\sigma} a_{\mathbf{k}o\sigma} \qquad b^\dagger_{\mathbf{k}b\lambda} = a^\dagger_{\mathbf{k}o\sigma} \overline{u}_{\mathbf{k}o\sigma,b\lambda} \quad , \tag{8.1.9}$$

where the sum over repeated indices is implicit. Hence, they fulfill the eigenvalues equation $h_{\mathbf{k}} u_{\mathbf{k}b\lambda} = \xi_{\mathbf{k}b\lambda} u_{\mathbf{k}b\lambda}$ with $\xi_{\mathbf{k}b\lambda}$ being the eigenvalues or band energies.

Table 8.1.: The character table of the two dimensional point group C_{4v} contains four one- and one two-dimensional irreducible representations. In the absence of inversion symmetry and the pairing of time-reversal partners, the representation E is forbidden since all pairing states in the helical basis must have even parity.

	E	$2C_{4z}$	C_{2z}	2σ	$2\sigma_d$
A_1	+1	+1	+1	+1	+1
A_2	+1	+1	+1	-1	-1
B_1	+1	-1	+1	+1	-1
B_2	+1	-1	+1	-1	+1

8.2. Nodal versus nodeless gap and singlet-triplet mixing

To generate the renormalization group flow, we employed the spinful flow equation (Equation 6.3.20) (with the contribution from the three-particle vertex being discarded) and evaluated the eigenmodes of the Cooper channel (Equation 3.4.29). The initial condition of the flow equation is required to be the bare interaction and is provided by the two-particle interaction (Equation 8.1.8) in helical basis. The (functional) renormalization group flow of the Cooper channel's eigenvalues ξ^n for U_1 =1.0 eV and $U_2 = 0$ is shown in (Figure 8.2a). The eigenstate of the leading (most negative) eigenvalue may be characterized by the irreducible A_1 representation (s-wave) of the corresponding point group C_{4v}. The subleading instabilities can be associated to B_1, B_2 and A_2 representations. The absence of any eigenstate that transforms according to the irreducible E representation is not a coincidence but required by time-reversal symmetry and fermionic anticommutation rules (as discussed in (Section 3.4.2)). The remaining symmetry-allowed irreducible representations of the point group and their characters are listed in (Table 8.1). (Figure 8.2b) plots the momentum dependency of the pairing states along the Fermi pockets associated to the helicities $\lambda = \pm$, where $\lambda = +$ labels the outer pocket and $\lambda = -$ the inner one. The plot shows the two leading instability eigenvectors with A_1 and B_1 symmetry. The peculiar feature of the pairing eigenstates is their sign change between the spin-split Fermi pockets. According to the analysis in (Section 3.4.2) the corresponding pairing state in pseudospin representation has mainly of triplet character. This sign change not only implies the main triplet character of the pairing state but also topologically non-trivial properties [Smi+17a]. In two dimensions, this property is described by the *topological index* for time-reversal invariant non-centrosymmetric superconductors defined by [SF09; Sam15; QHZ10]

$$N_{2D} = \prod_s \left[\operatorname{sgn} \Delta_s\right]^{m_s} \quad , \tag{8.2.1}$$

where the product is over all (well-separated) Fermi sheets with index s and m_s is

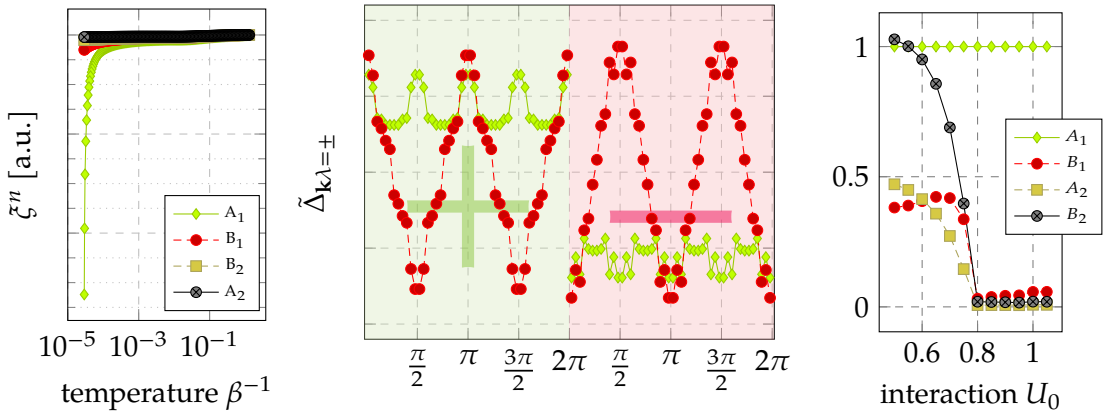

(a) (b) (c)

Figure 8.2.: The flow of the Cooper channel's eigenvalues in (Figure 8.2a) show that the eigenmode with A_1 representation is the leading instability for U_1 =1.0 eV and $U_2 = 0$. In (Figure 8.2b), we show the momentum dependency along the two spin-split Fermi sheets of the eigenstates corresponding to the two largest eigenvalues, i.e. A_1, B_1. The left and right half of the plot correspond to the outer + and inner − Fermi pockets as labeled in (Section 8.1). Apparently, both A_1 and B_1 pairing states are of similar shape on both pockets but feature opposite signs on two spin-split Fermi sheets. According to the analysis in (Section 3.4.2) the corresponding pairing state in pseudospin representation is mainly of triplet character. The plot in (Figure 8.2c) shows the change of the eigenvalues relative to the eigenvalue associated to A_1 as a function of interorbital interaction strength. Hence, when decreasing the interorbital interaction, the strength of the B_2 representation increases until there's a transition from "extended" s-wave to "extendend" d-wave in the weak-coupling limit.

the number of time-reversal invariant points enclosed by the respective Fermi pocket. However, even the nodal pairing instability corresponding to B_1 and B_2 turn out to be associated to topological invariants [SR11; SBT12] describing different types of edge states. We observe a strong "extended" s-wave instability for an interorbital interaction of the order of the bandwidth W. When reducing the interaction strength, the d-waves states associated to B_1 and B_2 become more important relative to the s-wave (cf. (Figure 8.2c)). Finally, in the (weak-couling) limit $U_1 << W$, the d-wave state B_1 with nodes located along the main axis' is the leading pairing instability.

Summary and preview

In this chapter we entered the realm of spin-orbit physics by investigating the pairing instabilities in the $LaAlO_3/SrTiO_3$ oxide heterostructure by means of a simple two-orbital d_{xz}, d_{yz} model. The renormalization group flow has to be performed in the helical spin band basis. The associated pairing functions turn out to be all even parity, i.e. described by the one-dimensional representations of the point group C_{4v}. For interorbital interactions of the order of the bandwidth, the leading instability appears to be a fully gap

"s-wave" given by the A_1 representation. However, by reducing the interaction strength, we find a transition from the fully gap A_1 state to a nodal B_2 pairing state. The peculiar feature of both of these pairing states is their sign change between the both Fermi pockets labeled by helicity $\lambda = \pm$. This sign change implies a non-trivial topological invariant for both the nodal as well as the nodeless pairing state. In the next and last chapter, we investigate the properties of the superconducting gap function in Sr_2RuO_4 .

9. The curious case of Strontium Ruthenate

The physics of strontium ruthenate (Sr_2RuO_4) has been puzzling condensed-matter experimentalists as well as theorists for more than twenty years [Mae+94]. The very core of the confusion generated by contradicting experimental results on Sr_2RuO_4 over the past two decades is the debate over the nature and symmetry of its *superconducting order parameter* [Mac+17]. Early proposals suggested an odd parity *chiral spin triplet* state [RS95], which was later supported by experimental results of muon spin rotation (μSR) [Luk+98] and polar Kerr effect [Xia+06] measurements with evidence for a time-reversal symmetry breaking pairing state. However, this chiral "$p + ip$" state results in the existence of edge currents, which, unfortunately, have never been observed so far despite extensive efforts [Kir+07; Cur+14]. Possible order parameters may be derived from the tetragonal symmetry of crystal of strontium ruthenate (see (Figure 9.1a)) and the associated point group D_{4h}. However, the superconducting state in Sr_2RuO_4 develops out of a normal state with properties, which are consistent with Fermi liquid parameters [Ber+03]. Moreover, resistivity measurements in the normal state show a highly anisotropic behavior with an interlayer to in-plane resistivity ratio $\rho_c/\rho_{ab} \approx 850$ at 2.0 K [Mae+94] and the Fermi surface of Sr_2RuO_4 is quasi two-dimensional and shows only a weak dispersion along the c-axis [Mae+97]. Both the enlarged spatial separation between layers (cf. caption of (Figure 9.1)) and the strong anisotropy in electronic and transport properties have been taken as indicators to rule out pairing states that require finite interlayer coupling [Sig+99]. In particular, these pairing states are associated to the even two-dimensional irreducible representation E_g (see (Table H.6)). Nevertheless, some theoretical works (i.a. [ZM05]) make use of exactly this irreducible representation - called *chiral spin singlet* - since it is equally well consistent with the phase shifts observed in *Josephson junction* experiments [Nel+04]. More recently, temperature-dependent heat capacity measurements suggest the existence of vertical line nodes in the order parameter [Has+17].

When discussing possible superconducting order parameters in Sr_2RuO_4 we have to distinguish two scenarios: The limit of zero spin-orbit interaction where spatial and spin degrees of freedom are decoupled and the limit of strong spin-orbit coupling, which intertwines orbital and spin degrees of freedoms (cf. (Section 2.4.4)). For instance, the possible order parameters in the odd E_u representation of D_{4h} are six fold degenerate for zero spin-orbit interaction and split into four one-dimensional and one two-dimensional representations in the presence of strong spin-orbit coupling (Equation 2.4.42). The role and importance of spin-orbit coupling in Sr_2RuO_4 has been emphasized both from a theoretical [NS00] and from an experimental [Vee+14] point of view.

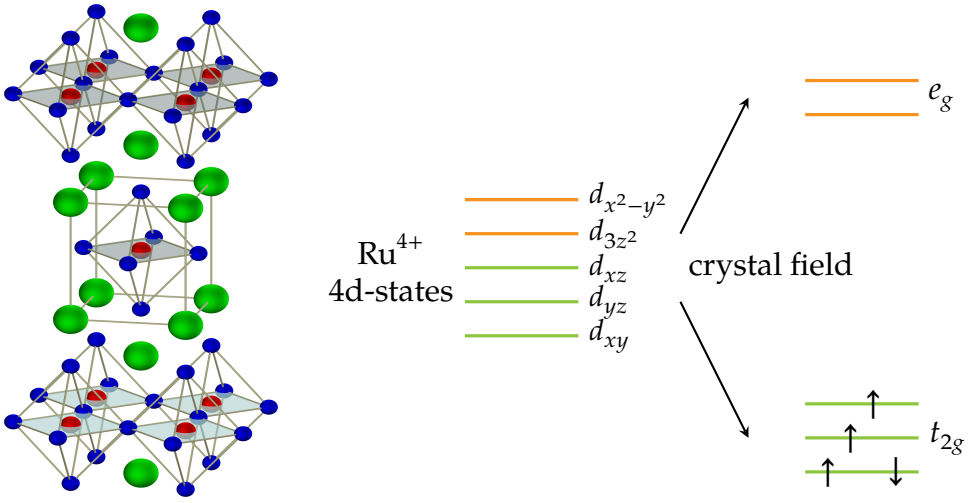

Figure 9.1.: The crystal of strontium ruthenate forms a layered perovskite structure, exactly like La_2CuO_4, which is the parent compound of the high-T_c superconductors (Figure 9.1a). The ions are represented in the colors green (Sr), red (Ru) and blue (O). The RuO_2 layers are separated by two layers of SrO that are shifted by half a lattice constant relative to each other along the horizontal plane. Thus, the Ru-atoms are enclosed in octahedra of O atoms. The crystal is characterized by two lattice constants: The in plane constants are $a = b = 3.87\,\text{Å}$ and the lattice constant along the c-direction is $c = 12.74\,\text{Å}$ [WL93] at 300 K. The influence of the octahedral crystal field splits the 4d-states of Ru^{4+} into the low-lying t_{2g} and the unoccupied e_g states (see (Figure 9.1b)).

Previous numerical studies of the superconducting instabilities in Sr_2RuO_4 in the weak-coupling limit without [RKK10a] and with [SRS14; Sca] spin-orbit coupling have provided important insights concerning the question, if the order parameter is mainly located on the quasi one-dimensional or two-dimensional Fermi sheets. While renormalization group calculations for finite interactions suggest the quasi two-dimensional γ band to host the superconducting state [Wan+13a], weak-coupling calculations [RKK10a] suggest the pairing to arise from the quasi one-dimensional α and β bands.

9.1. Ab-initio and single-particle properties

A generic three-orbital model of the low-energy electronic structure of Sr_2RuO_4 that involves the t_{2g}-orbitals of the Ru^{4+} ions, namely the d_{xz}, d_{yz} and d_{xy} orbitals, is given by

$$\mathcal{H}_0 = \sum_i \sum_{o\,o'} \sum_{\sigma\,\sigma'} h^{oo'}_{\sigma\sigma'}\, a^\dagger_{io\sigma} a_{io'\sigma'} \quad , \quad h^{oo'}_{\sigma\sigma'} \in \mathbb{C}^{6\times 6} \quad . \tag{9.1.1}$$

The indices refer to the lattice site (i), the orbital (o,o') and the spin (σ,σ') degree of freedom. Hence, the operators $a^\dagger_{io\sigma}$ ($a_{io\sigma}$) create (annihilate) an electron on site i in orbital o with spin σ, respectively. The spin was included to incorporate spin-orbit coupling at a later stage. The orbital index is ordered according to $\left(d_{xz}, d_{yz}, d_{xy}\right) \triangleq (1,2,3)$. For the time being we assume matrix elements that are diagonal in spin space and take only orbital-dependent hoppings into account. The matrix elements of the non-interacting Hamiltonian in orbital space are obtained by considering the symmetries of the lattice and the t_{2g} orbitals (see appendix A). The most generic matrix elements and their momentum dependencies are [PK12]

$$h^{oo'}_{\sigma\sigma'} = \begin{pmatrix} \xi_{xz}(\mathbf{k}) & \eta(\mathbf{k}) & 0 \\ \eta(\mathbf{k}) & \xi_{yz}(\mathbf{k}) & 0 \\ 0 & 0 & \xi_{xy}(\mathbf{k}) \end{pmatrix} \otimes \mathbb{1}_{2\times 2} \quad , \tag{9.1.2}$$

with their dispersions defined by ($\mathbf{k} = (k_x, k_y)$)

$$\begin{aligned} \xi_{xz}(\mathbf{k}) &= -2\left(t_1 \cos(k_x) + t_2 \cos\left(k_y\right)\right) \\ \xi_{yz}(\mathbf{k}) &= -2\left(t_2 \cos(k_x) + t_1 \cos\left(k_y\right)\right) \\ \xi_{xy}(\mathbf{k}) &= -2\, t_3 \left(\cos(k_x) + \cos\left(k_y\right)\right) \\ &\quad - 4\, t_4 \cos(k_x)\cos\left(k_y\right) - 2\, t_5 \left(\cos(2k_x) + \cos\left(2k_y\right)\right) \\ \eta(\mathbf{k}) &= -4\, t_6 \sin(k_x)\sin\left(k_y\right) \quad . \end{aligned} \tag{9.1.3}$$

Estimates for the corresponding overlap integrals resulting in the hopping parameters t_i are given in (Table 9.1), which were derived from i.a. LDA calculations, dHvA measurements and ARPES data. Since spin-orbit coupling is suggested to be an essential ingredient to the unconventional properties of Sr_2RuO_4 , we include the on-site term $\mathcal{H}_{SOC} = \lambda \sum_i \mathbf{L}_i \cdot \mathbf{S}_i$ into the single-particle Hamiltonian. The matrix elements of $\mathcal{H}_{SOC}$ term may be evaluated in terms of the combined orbital/spin basis, e.g. $\left\langle a^\dagger_{xz,\sigma} \middle| \lambda\, \mathbf{L}\cdot\mathbf{S} | a^\dagger_{yz,\sigma} \right\rangle$ and provide (cf. appendix B and [NS00])

$$\mathcal{H}_{SOC} = \frac{i\lambda}{2} \sum_{\mathbf{k}} \sum_{l,m,n} \epsilon_{lmn} \sum_{\sigma,\sigma'} \sigma^n_{\sigma\sigma'} a^\dagger_{\mathbf{k}l\sigma} a_{\mathbf{k}m\sigma'} = \sum_{\mathbf{k}} \frac{i\lambda}{2}\, \mathbf{a}^\dagger_{\mathbf{k}} \begin{pmatrix} 0 & -\sigma_z & \sigma_x \\ \sigma_z & 0 & -\sigma_y \\ -\sigma_x & \sigma_y & 0 \end{pmatrix} \mathbf{a}_{\mathbf{k}} \quad , \tag{9.1.4}$$

with the orbital indices l, m. In the first equality we used the orbital ordering $(1,2,3) =$

Table 9.1.: The hopping parameters of the single particle Hamiltonian (Equation 9.1.2) were derived from the fit of the model (Equation 9.1.3) to ARPES data [Zab+12]. However, this data only provides the renormalized quasiparticle band structure and experiments determining the shape and topology of the Fermi sheets (dHvA) only suggest the relative strengths of the hopping parameters but not the bare bandwidth. Therefore, we rely on LDA calculations and multiband quasiparticle calculations based on perturbation theory and dynamical mean-field methods to fix the absolute bandwidth of about 3.5 eV [MS97; LL00; Mra+11]. All parameter are given in units of eV.

[eV]	t_1	t_2	t_3	t_4	t_5	t_6	μ	λ
	0.6042	0.0667	0.3375	0.1625	0.0208	0.0583	−0.5083	0.1333

(yz, xz, xy), where ϵ_{lmn} is the total antisymmetric Levi-Civita symbol. In contrast, in the second equality we introduced the basis

$$\mathbf{a}_{\mathbf{k}}^{\dagger} = \left(a_{xz\uparrow}^{\dagger},\, a_{xz\downarrow}^{\dagger},\, a_{yz\uparrow}^{\dagger},\, a_{yz\downarrow}^{\dagger},\, a_{xy\uparrow}^{\dagger},\, a_{xy\downarrow}^{\dagger} \right) \quad . \tag{9.1.5}$$

Based on these prerequisites we are able to write down the entire single particle term of the three orbital model including atomic spin-orbit coupling, which is given by $\mathcal{H} = \mathcal{H}_0 + \mathcal{H}_{SOC}$. Any higher order non-local centrosymmetric spin-orbit terms may be incorporated into the Hamiltonian by considering the combined symmetry groups of orbital, momentum and spin spaces as discussed in (Section 3.1). The electronic properties that arise from this Hamiltonian are shown in (Figure 9.2). In (Figure 9.2a) we illustrate the shift of the Fermi surface sheet due to increasing spin-orbit interaction strength. Apparently, spin-orbit coupling has the largest influence on the α Fermi pocket at the M-point. The band structure in (Figure 9.2b) features spin-orbit interaction and shows the orbital weight of the associated eigenstates for the three bands. On the one hand, the α and β-bands are comprised of mixed d_{xz} and d_{yz} orbital content depending on the momentum. On the other hand, the γ is exclusively made up of d_{xy} orbital states. This result changes when turning on spin-orbit interaction by introducing mixed d_{xz} and d_{yz} orbital weight into the γ band as well.

9.2. Quasi one- versus two-dimensional superconductivity

In order to find the bare two-particle interaction representing the starting point of any renormalization group calculation, we turn to the interacting part of the Hamiltonian of the three-orbital model. To this end, we consider only on-site (momentum independent) interaction. The multi-orbital character of the Hamiltonian is taken into account by considering intra-orbital, inter-orbital interaction, Hund's rule coupling and pair hopping processes. Although we use a SU(2)-spin symmetry breaking single-

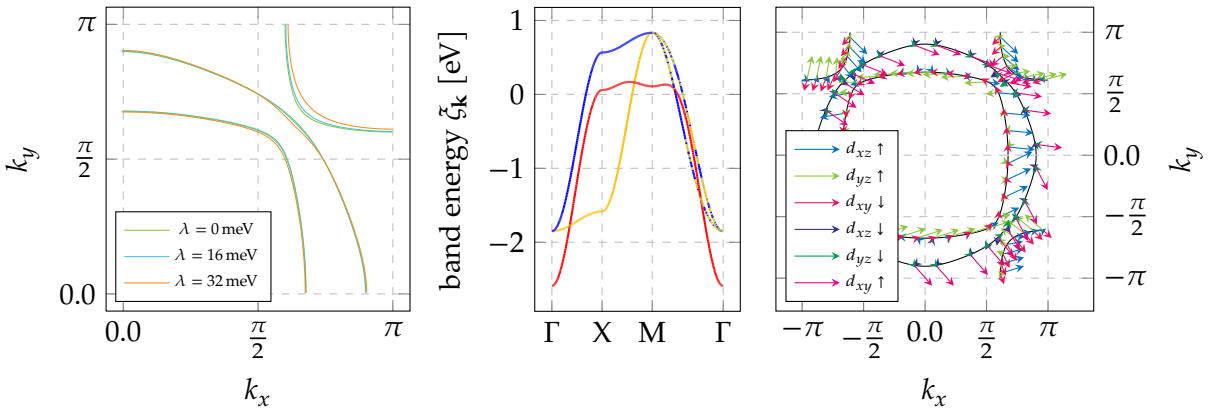

(a) (b) (c)

Figure 9.2.: The influence of spin-orbit coupling on the Fermi surface is illustrated in (Figure 9.2a). Apparently, the electron pocket at M associated to the α-band experiences the largest shift. The non-interacting band structure with zero spin-orbit coupling shows three bands ((Figure 9.2b)). The color code indicates the orbital content of the bands. While α and β bands have mixed d_{xz}, d_{yz}-orbital weight, the γ band is made up of d_{xy}-orbital states only. In contrast, spin-orbit interaction introduces mixed orbital content of opposite spin states into the states of the γ Fermi surface. (Figure 9.2c) exhibits the properly defined - taking the adiabatic pseudospin and "smooth gauge" into account - eigenstates along the Fermi sheets.

particle Hamiltonian (Equation 9.1.4), we assume the interacting part of the Hamiltonian to be spin rotation invariant. The implications and subtleties of spinful interacting multi-orbital Hamiltonians regarding the numerical implementation are discussed in appendix G. These arise from the requirement of total antisymmetric with respect to particle exchange for fermionic interactions. The multi-d-orbital Hamiltonian is adapted from a *Kanamori Hamiltonian* and can be written as (cf. [GMM12])

$$\begin{aligned}\mathcal{H}_I = \sum_i \Bigg[& U_{\text{intra}} \sum_l n_{l\uparrow} n_{l\downarrow} + U_{\text{inter}} \sum_{l\neq m} n_{l\uparrow} n_{m\downarrow} + (U_{\text{inter}} - J) \sum_{l\neq m} \sum_\sigma n_{l\sigma} n_{m\sigma} \\ & - J_{\text{Hund}} \sum_{l\neq m} a^\dagger_{l\uparrow} a^\dagger_{m\downarrow} a_{m\uparrow} a_{l\downarrow} + J_{\text{Pair}} \sum_{l\neq m} a^\dagger_{l\uparrow} a^\dagger_{l\downarrow} a_{m\uparrow} a_{m\downarrow} \Bigg] \quad . \end{aligned} \tag{9.2.1}$$

A set of reasonable interaction parameters for (Equation 9.2.1) can be obtained by means of *constrained RPA* calculations. The literature provides several sets of these parameters that tend to slightly differ. Some of them are given in (Table 9.2). The exact output of these calculations actually gives orbital-dependent values for the interaction. However, what we are interested in are the *fixed points* of the renormalization group flow and therefore these details are usually negligible. Before we can start to calculate the renormalization group flow, we have to find the representation of the interacting

Table 9.2.: The interaction parameters of multi-orbital Hamiltonians can be obtained by *constrained RPA* calculations [MA08]. The parameters were adapted from [Mra+11; VJB12] for the case of $U(1)_C \otimes SU(2)_S \otimes SO(3)_O$ symmetry and $J = J_H = J_P$ resulting in $U_{\text{inter}} = U_{\text{intra}} - 2J$ [Sug12]. Besides, we list some a set of parameters that were used in the literature for the interacting Hamiltonian of Sr_2RuO_4 .

[eV]	U_{intra}	U_{inter}	J_{Hund}	J_{Pair}	Ref.
	2.3	1.5	0.4	0.4	[Mra+11]
	2.56	1.94	0.26	0.26	[VJB12]
	3.2	1.3	0.3	0.3	[Wan+13a]

Hamiltonian in band-pseudospin basis. To this end, the definition of the eigenstates of the non-interacting part of the Hamiltonian is crucial regarding the proper pseudospin and definition and "gauge". Alternatively, one can rely on the pairing of time-reversal and inversion symmetry partners (as discussed in (Section 3.4)), which, however, is obviously not applicable for the investigation of particle-hole instabilities in the context of the functional renormalization group.

The phase diagram of the three orbital Hamiltonian of Sr_2RuO_4 with respect to interorbital interaction and Hund's rule coupling is given in (Figure 9.3). The phase diagram comprises a large section with odd parity triplet pairing (TPT) with eigenstates that transform according to the E_u representation of the point group. The opposite side of the phase diagram is dominated by different particle-particle and particle-hole instabilities, which comprise even parity singlet pairing and ferromagnetic tendencies. The fact that Hund's rule promotes ferromagnetic instabilities can already be understood on a mean-field level by considering the energetically favored states with parallel spin orientation due to Hund's coupling. Regarding the pairing instabilities, we see that the singlet pairing (SGT) transforms like a B_{1g} representation is located on the γ band. In contrast, the large portion of triplet pairing in the phase diagram is dominated by gap functions, which are located on the quasi one-dimensional α and β bands. Performing an harmonic analysis of the triplet state, we find that the pair wave function is dominated by longer range second nearest neighbor pairing. Taking the degeneracy of the two-dimensional irreducible representation E_u into account, we can describe the triplet state in terms of the d-vector

$$\mathbf{d}_{\mathbf{k}b} = \left(\sin(k_x)\cos\left(k_y\right) + e^{i\varphi}\sin\left(k_y\right)\cos(k_x)\right)\hat{z} \quad , \tag{9.2.2}$$

where we projected on the $k_z = 0$. By considering a renormalized mean-field theory for this triplet state, we find that the phase $e^{i\varphi} = i$ will maximize the condensation energy associated to the Bogoliubov-de Gennes quasiparticle spectrum.

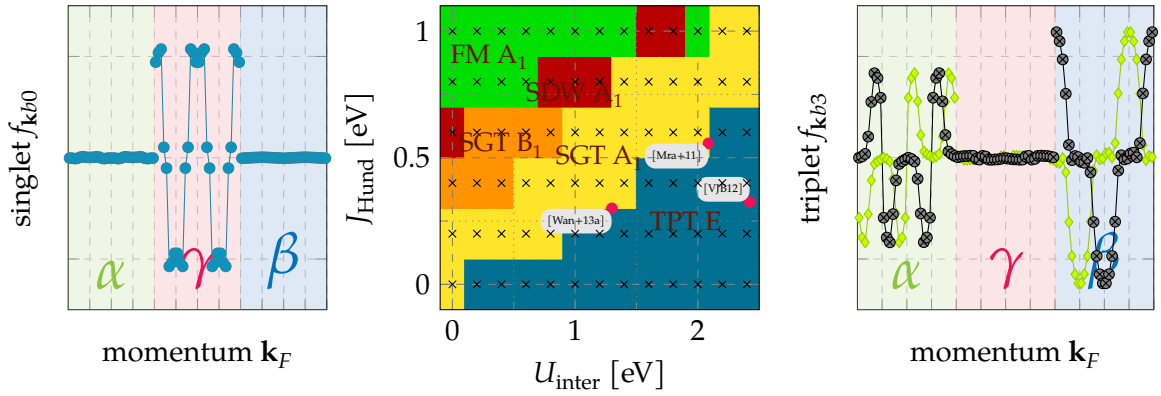

Figure 9.3.: The phase diagram of three-orbital Hamiltonian zero spin-orbit coupling with respect to interorbital interaction U_{inter} and Hund's rule coupling J_{Hund} exhibits are large portion of odd parity triplet pairing (TPT). The abbreviations represent ferromagnetic (FM), antiferromagnetic (SDW), singlet pairing (SGT) and triplet pairing (TPT) instabilities. The pair hopping parameter is fixed by $J_{\text{Pair}} = J_{\text{Hund}}$ while the intraorbital interaction U_{intra} is given by 3.2 eV at all data points. The sets of interaction parameter given in the literature are mainly located in the triplet pairing section of the phase diagram. The shown triplet pairing function (right) is located at $U_{\text{inter}} = 1.8$, $J_{\text{Hund}} = 0.2$ in the phase diagram and the singlet pairing function (left) corresponds to the flow at $U_{\text{inter}} = 0.2$, $J_{\text{Hund}} = 0.4$.

Summary

This chapter dealt with the problem of the superconducting order parameter in Sr_2RuO_4 and discussed the role of spin-orbit coupling for the intricate pairing state in this material. We introduced a generic three-orbital model in terms of d_{xz},d_{yz},d_{xy}-states for the low lying t_{2g} multiplet of the Ru^{4+} ions. The single-particle Hamiltonian and the resulting electronic properties were adjusted to the results of ab-initio electronic structure calculations and the experimentally determined Fermi surface topology. We made use of a set of interaction parameters for a multi-orbital Kanamori-Hamiltonian, that are adapted from the literature and based on the constrained RPA method to find screened interaction values. This Kanamori Hamiltonian was used as the starting point for a the functional renormalization group (see (Chapter 6)) flow based on three-orbital model of Sr_2RuO_4 . We found a rich phase diagram with respect to interorbital interactions and Hund's rule coupling made up of singlet and triplet pairing as well as ferromagnetic states. However, the interaction parameters found in the literature all coincide with points in the phase diagram where the competing orders are dominated by odd parity triplet pairing located on the quasi one-dimensional α and β Fermi sheets. To overcome the strict and unnatural separation of order parameters being hosted by either the γ or α and β bands, the influence of spin-orbit coupling must be taken into account.

10. Summary and outlook

The development of numerical approaches to unconventional and topological superconductivity in strongly correlated systems of itinerant fermions with substantial spin-orbit interaction has been the major objective of this thesis. These methods are based on a combination of functional and perturbative renormalization group approaches.

In (Chapter 2), we motivated the concept of Cooper pairing and reviewed the basics of BCS-theory. In contrast to traditional BCS-theory, which is based on a phonon-driven attractive effective interaction, the Kohn-Luttinger effect has a purely electronic nature and is able to establish pairing in higher angular momentum channels $L > 0$. Consequently, we worked out a generalized BCS-theory for any spin and angular momentum channel that is characterized by the interplay between spin and spatial symmetries. As a convenient description of this theory, we introduced the d-vector formalism.

The (Chapter 3) served as the starting point to mean-field theories beyond SU(2)-symmetric effective two-particle interactions. The first section provided an exhaustive derivation and classification of various types of spin-orbit interaction in both centro- and non-centrosymmetric systems. This derivation is mainly based on the concept of the invariant expansion. As a result, we found spin-orbit Hamiltonians for multi-d-orbital models on the tetragonal lattice and square lattice. Among these Hamiltonians we obtained atomic and non-local $\mathbf{L} \cdot \mathbf{S}$ couplings as well as Rashba and Dresselhaus terms in multi-orbital models. To be able to deal with these Hamiltonians numerically, we discussed the proper choice of a pseudospin basis and the implications of the "gauge-freedom" of Bloch states. The third section analyzed the key symmetries of the spinful two-particle vertex in orbital and band basis. There are four types of important continuous and discrete transformations that were taken into account: SU(2)-rotations, time-reversal, spatial inversion and point-group operations. The presence or absence of the associated symmetries has important implications on the structure of the two-particle vertex. In orbital space we worked out the relationship between the spinful and spinless vertices. In band space, we further distinguished between the pseudospin basis and the helical basis depending on the presence or absence of spatial inversion symmetry. The two-particle vertex in band space was the central object of the instability analysis of the effective action in terms of mean-field theories since we limited the treatment to equal energy pairing. In the fourth section and in the context of generalized Cooper pairing with broken spin symmetry, the equivalence of pairing between time-reversal and inversion symmetry partners states and Bloch states with "smooth" gauge was emphasized. The mean-field theories for Cooper pairing in a pseudospin and a helical basis showed that, while pairing in a pseudospin basis is still characterized by means of sin-

glet and triplet states, Cooper pairs in a helical basis can exhibit singlet triplet mixing. Analogously to the particle-particle instabilities, the corresponding particle-hole condensates were shown to feature mixing of charge- and spin density-wave states already in the presence of spin-orbit coupling and inversion symmetry. The absence of inversion symmetry further allows for the superposition of states associated to irreducible representations with even and odd symmetries.

The (Chapter 4) served as a reminder and setup of the fermionic functional integral formalism for the quantum-many body partition function in terms of Grassmann fields. The notation and formalism of the partition function were established to introduce the generating functionals that were required in the following chapters. The connection to the perturbative expansion of the partition function and correlation functions was given and evaluated by means of Wick's theorem.

The perturbative renormalization group in (Chapter 5) uses the perturbative expansion of the irreducible two-particle vertex to generate an effective two-particle interaction, which is fed into a logarithmic renormalization group scheme in order to investigate the dominant instabilities. We state the relevant diagrammatic contributions to the perturbative two-particle vertex both for spinful and spinless interactions. We briefly draw the connection to the random phase approximation.

Finally, the functional renormalization group method was introduced in (Chapter 6) based on the modified Gaussian propagator with cutoff or scale dependency. The modified single-particle propagator is inserted into the generating functionals to yield scale dependent functionals. By calculating the total derivative of the generating functionals with respect to the cutoff, we obtained a set of flow equations. The flow equations for the self-energy and the irreducible two-particle vertex were explicitly derived by means of an expansion in the fields and the truncation of all three particle contributions. In the framework of the temperature flow renormalization group scheme, the close connection to the perturbative renormalization was worked out, which can be easily exploited in the numerical context in order to obtain an efficient implementation.

To establish the methodological novelties and check the numerical stability of our implementation, two types of well-known toy models with established results were considered in (Chapter 7).

The application to oxide-heterostructures in the form of $LaAlO_3/SrTiO_3$ in (Chapter 8) revealed the possibility of topological superconductivity in the form of an "extended" s-wave state, which amounts to a fully gapped order parameter with opposite signs on the two spin split Fermi sheets originating from the strong Rashba coupling in the presence of inversion symmetry breaking. This state corresponds to an order parameter with dominant triplet contribution. In the weak-coupling limit, we find a similar but "extended" nodal d-wave state.

In (Chapter 9), the intriguing matter of strontium ruthenate Sr_2RuO_4 was discussed. Based on the well-established three-orbital model of the t_{2g} states, we found triplet pairing on the quasi-one-dimensional bands and singlet d-wave pairing on the γ-sheet depending on the set of multi-orbital interaction. However, taking the results of available c-RPA calculations into account, the interaction setup appears to be close to the one, which produces the triplet pairing on the quasi-one-dimensional bands.

Although this thesis already put a main focus on the methodological development, there are a variety of open issues, which should be considered in future work. First of all, in order to reliably access the discussed exotic particle-hole condensates, a continuous and point-group symmetry conserving momentum discretization of the vertex functions is essential. Furthermore, the frequency dependency of vertex functions and the renormalization of the self-energy should be included in order to enable a systematic comparison with other quantum many-body approaches like RPA. The applications discussed in this thesis can, of course, only cover a certain portion of the full potential of the functional and perturbative renormalization group schemes for multi-orbital systems with spin-orbit interaction. Among other interesting candidate systems, we mention the heavier nuclei cousins of graphene, called Xenes, with substantial (in-plane) Rashba interaction (on a substrate) and the five orbital pnictide models, for which the influence of atomic spin-orbit coupling has been discussed lately. Therefore, the presented methodological development promises to provide many useful insights into spin-orbit physics of correlated electrons and awaits future applications.

Part III.

Appendices

A. Construction of SU(2)-symmetric d-orbital Hamiltonians

Most of the strongly correlated systems that are studied i.a. in the context of high-temperature superconductors and transition metal-oxides have states at the Fermi level that posses 3d or 4d-orbital character [Eme93] [Vol12] (cf. (Chapter 8) and (Chapter 9)). The general (analytical) construction of these bands may be done by considering the symmetries of the underlying lattice and the orbitals themselves. The *d*-orbitals are the eigenstates of the $l = 2$ angular momentum operator $\hat{\mathbf{L}}$. The Lie algebra associated to the angular momentum is given by [Lie88; Pau65]

$$\left[\hat{L}_i, \hat{L}_j\right] = i\epsilon_{ijk}\hat{L}_k \quad , \tag{A.0.1}$$

with the *generators* $\hat{L}_i$ $i \in \{1, 2, 3\}$ and the *structure constant* ϵ_{ijk}. First of all, we have to determine the representation of the generators for the $l = 2$ case, where we have $\hat{L}_i \in \mathbb{C}^{(2l+1)\times(2l+1)}$, i.e. $\hat{L}_i \in \mathbb{C}^{5\times5}$. Their matrix elements are most conveniently found by exploiting the action of $\hat{L}_z$ and $\hat{L}_\pm := \hat{L}_x \pm i\hat{L}_y$ on the eigenstates $|l, m\rangle$ of the $\hat{\mathbf{L}}^2$ and $\hat{L}_z$ operators, i.e. [Bal98, Chap. 7]

$$L_z|l, m\rangle = m|l, m\rangle \quad \text{and} \quad L_\pm|l, m\rangle = \sqrt{l(l+1) - m(m\pm1)}\,|l, m\pm1\rangle \quad . \tag{A.0.2}$$

Henceforth, for $l = 2$ and the basis $\mathbf{l}^\dagger := \left(a^\dagger_{-2}, a^\dagger_{-1}, a^\dagger_0, a^\dagger_{+1}, a^\dagger_{+2}\right)^T$ we find the matrices

$$\hat{L}_z = \begin{pmatrix} -2 & & & & \\ & -1 & & & \\ & & 0 & & \\ & & & +1 & \\ & & & & +2 \end{pmatrix} \quad \text{and} \quad \hat{L}_\pm = \begin{pmatrix} 0 & (2) & & & \\ 2 & 0 & (\sqrt{6}) & & \\ & \sqrt{6} & 0 & (\sqrt{6}) & \\ & & \sqrt{6} & 0 & (2) \\ & & & 2 & 0 \end{pmatrix} \quad , \tag{A.0.3}$$

while the other two generators are consequently given by $\hat{L}_x = \frac{\hat{L}_+ + \hat{L}_-}{2}$ and $\hat{L}_y = \frac{\hat{L}_+ - \hat{L}_-}{2i}$. Note, that $\hat{L}^2 = \hat{L}_x^2 + \hat{L}_y^2 + \hat{L}_z^2 \propto \mathbb{1}$ is the Casimir operator of the corresponding space, which has to commute with any operator of that space. Since we don't want to work in the $|l, m\rangle$ basis but in the most commonly used basis of real orbitals, we employ linear combinations of the $|l, m\rangle$ states that amount to the unitary transformation

$$U_d = \frac{1}{\sqrt{2}} \begin{pmatrix} 0 & 1 & 0 & -1 & 0 \\ 0 & -i & 0 & -i & 0 \\ i & 0 & 0 & 0 & -i \\ 1 & 0 & 0 & 0 & 1 \\ 0 & 0 & -\sqrt{2} & 0 & 0 \end{pmatrix} \quad , \tag{A.0.4}$$

with $U_d^\dagger U_d = \mathbb{1}$ that results in the orbital basis

$$\mathbf{d}^\dagger := \left(a^\dagger_{d_{xz}}, a^\dagger_{d_{yz}}, a^\dagger_{d_{xy}}, a^\dagger_{d_{x^2-y^2}}, a^\dagger_{d_{z^2}} \right)^T \quad . \tag{A.0.5}$$

with $\mathbf{d} = U_d \mathbf{l}$. The generators transform according to $\hat{L}_i \to \hat{L}'_i = U_d \hat{L}_i U_d^\dagger$. In the new basis (and the old one) we can express any SO(3) transformation of the orbitals by means of the *exponential parametrization* and the generators by $e^{-i\hat{\mathbf{L}}\hat{n}\varphi}$ [Geo99]. In particular, a rotation about the z-axis is given by

$$e^{-iL'_z\varphi} = \begin{pmatrix} \cos(\varphi) & -\sin(\varphi) & 0 & 0 & 0 \\ \sin(\varphi) & \cos(\varphi) & 0 & 0 & 0 \\ 0 & 0 & \cos(2\varphi) & -\sin(2\varphi) & 0 \\ 0 & 0 & \sin(2\varphi) & \cos(2\varphi) & 0 \\ 0 & 0 & 0 & 0 & 1 \end{pmatrix} \quad . \tag{A.0.6}$$

We see that in the new basis the orbitals form invariant subspaces with respect to rotations about the z-axis. On the one hand, the d_{xz} and d_{yz} orbitals transform into each other and on the other hand the d_{xy} and $d_{x^2-y^2}$ orbitals stay among themselves while the d_{z^2} doesn't hook up with anyone.

A.1. Four-fold symmetry groups D_{4h} and C_{4v}

A lot of the strongly correlated 3d/4d orbital systems are found in compounds comprised of i.a. transition metals that form a perovskite structure. Hence, we will assume a four-fold symmetry (with inversion) corresponding to the point group D_{4h} that is comprised of sixteen elements given in appendix H. The representation of the four-fold rotation about the z-axis and the reflections in the (x,z), (y,z), $(x=y,z)$, $(x=-y,z)$ and (x,y) planes is

$$
\begin{aligned}
e^{-iL'_z\varphi_i} &= \begin{pmatrix} \cos(\varphi_i) & -\sin(\varphi_i) & 0 & 0 & 0 \\ \sin(\varphi_i) & \cos(\varphi_i) & 0 & 0 & 0 \\ 0 & 0 & 1 & 0 & 0 \\ 0 & 0 & 0 & 1 & 0 \\ 0 & 0 & 0 & 0 & 1 \end{pmatrix} \quad \varphi_i \in \left\{0, \frac{\pi}{2}, \pi, \frac{3\pi}{2}\right\} \\
e^{-iL'_{y,x}\pi} &= \mathrm{diag}(\pm 1, \mp 1, -1, 1, 1) \\
e^{-i\frac{L'_x \mp L'_y}{\sqrt{2}}\pi} &= \begin{pmatrix} 0 & \pm 1 \\ \pm 1 & 0 \end{pmatrix} \oplus \mathrm{diag}(1, -1, 1) \\
e^{-iL'_z\pi} &= \mathrm{diag}(-1, -1, 1, 1, 1) \quad .
\end{aligned} \tag{A.1.1}
$$

Note that a reflection is comprised of an inversion followed by a rotation by π about the normal vector of the plane of reflection [Mer98, Chap. 17, p. 440]. However, since angular momentum is a pseudovector (axial vector), the representation of the inversion is the identity operation. The matrix representations for the remaining elements of $\mathrm{D_{4h}}$ may be inferred from (Equation A.1.1) and the multiplication (Table H.2). (Table A.1) provides the explicit transformation behavior of all orbitals under $\mathrm{D_{4h}}$. We already noted the invariant subspaces of orbitals with respect to the rotations. This is true as well for all reflections and (improper) rotations of $\mathrm{D_{4h}} \subset \mathrm{SO}(3)$. The transformation behavior of the d-orbitals under D_{4h} is summarized in (Table A.1). Checking out all the representations, we finally see that the matrices of orbital transformation $\mathcal{L}_{l=2}^{\mathrm{D_{4h}}}$ are comprised of four irreducible representations:

$$
\mathcal{L}_{l=2}^{\mathrm{D_{4h}}} = \mathrm{E_g} \oplus \mathrm{B_{2g}} \oplus \mathrm{B_{1g}} \oplus \mathrm{A_{1g}} \quad . \tag{A.1.2}
$$

Note, that we may only have even representations due to the angular momentum being $l = 2$ in d-orbitals. In general, we have the parity $(-1)^l$ for orbital angular momentum [Bal98, Chap. 13, p. 372]. In order to derive a non-interacting, phenomenological Hamiltonian in orbital space, we make use of the *invariant expansion* (*theory of invariants*) [BP74]. The 5×5 Hamiltonian $\mathcal{H}(\mathbf{k})$ in orbital basis (Equation A.0.5) is required to satisfy [Win03, Chap. 2.5]:

$$
\mathcal{L}(g)\mathcal{H}(\mathbf{k})\mathcal{L}^\dagger(g) \stackrel{!}{=} \mathcal{H}(\mathcal{P}\left(g^{-1}\right)\mathbf{k}) \quad , \tag{A.1.3}
$$

with $\mathcal{L}(g)$ and $\mathcal{P}$ being the representations of g in orbital and three dimensional momentum space, respectively. Due to (Equation A.1.2) that reflects the fact that certain orbital subspaces don't mix, we can write

$$
\mathcal{L}_{\Gamma_i}(g)\mathcal{H}_{\Gamma_i,\Gamma_j}(\mathbf{k})\mathcal{L}^\dagger_{\Gamma_j}(g) \stackrel{!}{=} \mathcal{H}_{\Gamma_i,\Gamma_j}(\mathcal{P}\left(g^{-1}\right)\mathbf{k}) \quad , \tag{A.1.4}
$$

where the Hamiltonian block $\mathcal{H}_{\Gamma_i,\Gamma_j} \in \mathbb{C}^{\dim(\Gamma_i)\times\dim(\Gamma_j)}$ is characterized by the irreducible representations Γ_i and Γ_j. Every block of the Hamiltonian may be expanded in terms of matrices $X \in \mathbb{C}^{\dim(\Gamma_i)\times\dim(\Gamma_j)}$ and basis functions (of $\mathbf{k}$) that transform according to the irreducible representations of D_{4h} that are contained in the product representation $\Gamma_i \otimes \Gamma_j$ [TRR79]. Here, we also require the basis functions $f(\mathbf{k})$ to satisfy $f(\mathbf{k}+\mathbf{G}) = f(\mathbf{k})$ where $\mathbf{G}$ is a reciprocal lattice vector. The illustration of the beforementioned is

$$\mathcal{H}(\mathbf{k}) = \mathbf{d}^\dagger \begin{bmatrix} \mathcal{H}_{E_g\otimes E_g} & \mathcal{H}_{E_g\otimes B_{2g}} & \mathcal{H}_{E_g\otimes B_{1g}} & \mathcal{H}_{E_g\otimes A_{1g}} \\ \mathcal{H}_{B_{2g}\otimes E_g} & \mathcal{H}_{B_{2g}\otimes B_{2g}} & \mathcal{H}_{B_{2g}\otimes B_{1g}} & \mathcal{H}_{B_{2g}\otimes A_{1g}} \\ \mathcal{H}_{B_{1g}\otimes E_g} & \mathcal{H}_{B_{1g}\otimes B_{2g}} & \mathcal{H}_{B_{1g}\otimes B_{1g}} & \mathcal{H}_{B_{1g}\otimes A_{1g}} \\ \mathcal{H}_{A_{1g}\otimes E_g} & \mathcal{H}_{A_{1g}\otimes B_{2g}} & \mathcal{H}_{A_{1g}\otimes B_{1g}} & \mathcal{H}_{A_{1g}\otimes A_{1g}} \end{bmatrix} \mathbf{d} \quad . \tag{A.1.5}$$

The product representations can be disassembled according to [Gos]

$\otimes$	E_g	B_{2g}	B_{1g}	A_{1g}
E_g	$A_{1g} \oplus A_{2g} \oplus B_{1g} \oplus B_{2g}$	E_g	E_g	E_g
B_{2g}	E_g	A_{1g}	A_{2g}	B_{2g}
B_{1g}	E_g	A_{2g}	A_{1g}	B_{1g}
A_{1g}	E_g	B_{2g}	B_{1g}	A_{1g}

into irreducible representations of D_{4h}. Since all but the E_g representation are one-dimensional we only really have to care about the 2×2 block in the upper left of the Hamiltonian (Equation A.1.5). Therefore, we make the ansatz

$$\mathcal{H}_{E_g\otimes E_g} = f_{\Gamma_0}(\mathbf{k})\sigma_0 + f_{\Gamma_x}(\mathbf{k})\sigma_x + f_{\Gamma_y}(\mathbf{k})\sigma_y + f_{\Gamma_z}(\mathbf{k})\sigma_z \quad , \tag{A.1.6}$$

in terms of the Pauli matrices $\sigma_{0,x,y,z} \in \mathbb{C}^{2\times2}$ and the basis functions $f_{\Gamma_{0,x,y,z}}$ associated to a specific Pauli matrix but an unknown representation $\Gamma_{0,x,y,z}$. The transformation of the matrix elements associated to the d_{xz} and d_{yz} orbitals given in (Equation A.1.1) for all operations of C_{4v} is conveniently expressed in terms of Pauli matrices by

(d_{xz}, d_{yz})	E/i	C_2/σ_h	C_4^+/S_4^-	C_4^-/S_4^+	σ_x/C_y'	σ_y/C_y'	σ_a/C_b'	σ_b/C_a'
	σ_0	$-\sigma_0$	$i\sigma_y$	$-i\sigma_y$	σ_z	$-\sigma_z$	σ_x	$-\sigma_x$

making it easy to show that σ_0 transforms like A_{1g}, σ_x transforms like B_{2g}, σ_y transforms like A_{2g} and σ_z transforms like B_{1g}. We note, that the effect of the remaining eight operations of D_{4h} can also be obtained by considering that this block is governed by the E_g representation. Henceforth, we have the assignments $\Gamma_0 = A_{1g}$, $\Gamma_x = B_{2g}$, $\Gamma_y = A_{2g}$ and $\Gamma_z = B_{1g}$ for the basis functions $f_{\Gamma_{0,x,y,z}}(\mathbf{k})$. In the block comprised of the E_g and a

one-dimensional representation we don't have to care about any matrix X but only have to make sure that we use two linear independent basis functions for the two components of the block. In the blocks of single matrix elements we simply have to insert the associated basis function up to the desired order. An exemplary d-orbital Hamiltonian with phenomenological parameters and up to second nearest neighbor basis functions is given by (cf. [Gra+09; Gra+10, Appendix])

$$\mathcal{H}(\mathbf{k}) = \mathbf{d}^\dagger \begin{pmatrix} \zeta^{xz}_{\mathrm{A_{1g}}}(\mathbf{k}) + \zeta^{xz}_{\mathrm{B_{1g}}}(\mathbf{k}) & \zeta^{yz}_{\mathrm{B_{2g}}}(\mathbf{k}) - i\zeta^{yz}_{\mathrm{A_{2g}}}(\mathbf{k}) & \zeta^{xy}_{\mathrm{E_g}}(\mathbf{k}) & \zeta^{x^2-y^2}_{\mathrm{E_g}}(\mathbf{k}) & \zeta^{z^2}_{\mathrm{E_g}}(\mathbf{k}) \\ \zeta^{yz}_{\mathrm{B_{2g}}}(\mathbf{k}) + i\zeta^{yz}_{\mathrm{A_{2g}}}(\mathbf{k}) & \zeta^{yz}_{\mathrm{A_{1g}}}(\mathbf{k}) - \zeta^{xz}_{\mathrm{B_{1g}}}(\mathbf{k}) & \tilde{\zeta}^{xy}_{\mathrm{E_g}}(\mathbf{k}) & \tilde{\zeta}^{x^2-y^2}_{\mathrm{E_g}}(\mathbf{k}) & \tilde{\zeta}^{z^2}_{\mathrm{E_g}}(\mathbf{k}) \\ \zeta^{xy}_{\mathrm{E_g}}(\mathbf{k}) & \tilde{\zeta}^{xy}_{\mathrm{E_g}}(\mathbf{k}) & \zeta^{xy}_{\mathrm{A_{1g}}}(\mathbf{k}) & \zeta^{x^2-y^2}_{\mathrm{A_{2g}}}(\mathbf{k}) & \zeta^{z^2}_{\mathrm{B_{2g}}}(\mathbf{k}) \\ \zeta^{x^2-y^2}_{\mathrm{E_g}}(\mathbf{k}) & \tilde{\zeta}^{x^2-y^2}_{\mathrm{E_g}}(\mathbf{k}) & \zeta^{x^2-y^2}_{\mathrm{A_{2g}}}(\mathbf{k}) & \zeta^{x^2-y^2}_{\mathrm{A_{1g}}}(\mathbf{k}) & \zeta^{z^2}_{\mathrm{B_{1g}}}(\mathbf{k}) \\ \zeta^{z^2}_{\mathrm{E_g}}(\mathbf{k}) & \tilde{\zeta}^{z^2}_{\mathrm{E_g}}(\mathbf{k}) & \zeta^{z^2}_{\mathrm{B_{2g}}}(\mathbf{k}) & \zeta^{z^2}_{\mathrm{B_{1g}}}(\mathbf{k}) & \zeta^{z^2}_{\mathrm{A_{1g}}}(\mathbf{k}) \end{pmatrix} \mathbf{d} \quad , \tag{A.1.7}$$

with the matrix elements of the $\mathrm{E_g} \otimes \mathrm{E_g}$ block

$$\begin{aligned} \zeta^{xz/yz}_{\mathrm{A_{1g}}}(\mathbf{k}) &= \left(t^{xz/yz,1}_{\mathrm{A_{1g}}} \cos(k_x) + t^{yz/xz,1}_{\mathrm{A_{1g}}} \cos\left(k_y\right) + t^{xz,2}_{\mathrm{A_{1g}}} \cos(k_x) \cos\left(k_y\right) \right) \cos(k_z) \\ \zeta^{xz,1}_{\mathrm{B_{1g}}}(\mathbf{k}) &= t^{xz,1}_{\mathrm{B_{1g}}} \left(\cos(k_x) - \cos\left(k_y\right) \right) \cos(k_z) \\ \zeta^{yz}_{\mathrm{B_{2g}}}(\mathbf{k}) &= t^{yz,2}_{\mathrm{B_{2g}}} \sin(k_x) \sin\left(k_y\right) \cos(k_z) \\ \zeta^{yz}_{\mathrm{A_{2g}}}(\mathbf{k}) &= 0 \quad , \end{aligned} \tag{A.1.8}$$

the six matrix elements of the $\mathrm{E_g} \otimes \mathrm{B_{2g}}$ $\mathrm{B_{1g}}$, $\mathrm{A_{1g}}$ blocks (with $\alpha = xy$, $x^2 - y^2$ and z^2)

$$\begin{aligned} \zeta^{\alpha}_{\mathrm{E_g}}(\mathbf{k}) &= \left(t^{\alpha,1}_{\mathrm{E_g}} \sin(k_x) + t^{\alpha,2}_{\mathrm{E_g}} \sin(k_x) \cos\left(k_y\right) \right) \sin(k_z) \\ \tilde{\zeta}^{\alpha}_{\mathrm{E_g}}(\mathbf{k}) &= \left(t^{\alpha,1}_{\mathrm{E_g}} \sin\left(k_y\right) + t^{\alpha,2}_{\mathrm{E_g}} \sin\left(k_y\right) \cos(k_x) \right) \sin(k_z) \quad , \end{aligned} \tag{A.1.9}$$

and the nine matrix elements of the one-dimensional representation blocks

$$
\begin{aligned}
\zeta^{xy}_{\mathrm{A_{1g}}} &= \left(t^{xy,1}_{\mathrm{A_{1g}}}\left(\cos(k_x)+\cos\left(k_y\right)\right)+t^{xy,2}_{\mathrm{A_{1g}}}\cos(k_x)\cos\left(k_y\right)\right)\cos(k_z)\\
\zeta^{x^2-y^2}_{\mathrm{A_{2g}}} &= 0 \qquad \zeta^{z^2}_{\mathrm{B_{2g}}} = t^{z^2,2}_{\mathrm{B_{2g}}}\sin(k_x)\sin\left(k_y\right)\cos(k_z)\\
\zeta^{x^2-y^2}_{\mathrm{A_{1g}}} &= \left(t^{x^2-y^2,1}_{\mathrm{A_{1g}}}\left(\cos(k_x)+\cos\left(k_y\right)\right)+t^{x^2-y^2,2}_{\mathrm{A_{1g}}}\cos(k_x)\cos\left(k_y\right)\right)\cos(k_z)\\
\zeta^{z^2}_{\mathrm{B_{1g}}} &= t^{z^2,1}_{\mathrm{B_{1g}}}\left(\cos(k_x)-\cos\left(k_y\right)\right)\cos(k_z)\\
\zeta^{z^2}_{\mathrm{A_{1g}}} &= \left(t^{z^2,1}_{\mathrm{A_{1g}}}\left(\cos(k_x)+\cos\left(k_y\right)\right)+t^{z^2,2}_{\mathrm{A_{1g}}}\cos(k_x)\cos\left(k_y\right)\right)\cos(k_z) \quad . \qquad \text{(A.1.10)}
\end{aligned}
$$

where we used the basis functions of the $\mathrm{D_{4h}}$ and $\mathrm{C_{4v}}$ group in (Table H.7), respectively. Note, that Hermiticity was implied to reduce the number of matrix elements from twenty-five to fifteen. Furthermore, in the first nearest neighbor terms of $\mathrm{A_{1g}}$ on the diagonal associated to the xz and yz orbitals, we introduced different hopping parameters t for the k_x and k_y contributions since these are symmetric w.r.t. $k_x \leftrightarrow k_y$. A non-zero $\mathrm{A_{2g}}$ contribution is obtained only starting up from the fourth nearest neighbor terms. Furthermore, the Hamiltonian is obliged to obey *time-reversal symmetry* . For the present spinless case the time-reversal operation on the Hamiltonian is simply given by complex conjugation $\hat{\Theta} = \mathcal{K}$ and inversion of momentum $\mathbf{k} \to -\mathbf{k}$. Therefore, the condition for time-reversal symmetry is

$$
\Theta\mathcal{H}(\mathbf{k})\Theta^{-1} = \overline{\mathcal{H}(-\mathbf{k})} = \left(\mathcal{H}(-\mathbf{k})\right)^T \stackrel{!}{=} \mathcal{H}(\mathbf{k}) \quad , \qquad \text{(A.1.11)}
$$

where we exploited the Hermiticity of $\mathcal{H}(\mathbf{k})$. This restricts the diagonal elements of the Hamiltonian to be even in momentum, i.e. $\mathcal{H}_{ii}(-\mathbf{k}) = \mathcal{H}_{ii}(\mathbf{k})$, which is indeed the case in (Equation A.1.7) since all diagonal matrix elements are associated to the even representations $\mathrm{A_{1g}}$ and $\mathrm{B_{1g}}$. The off-diagonal elements $\mathcal{H}_{ij}(\mathbf{k})$ with $i \neq j$ are subject to the condition $\mathcal{H}_{ij}(-\mathbf{k}) = \mathcal{H}_{ji}(\mathbf{k})$ that forbids e.g. a non-zero $\mathrm{A_{2g}}$ contribution in the $\mathrm{E_g} \otimes \mathrm{E_g}$ block of (Equation A.1.7). Generically speaking, the off-diagonal elements must be either real and even in momentum or purely imaginary and odd in momentum. Finally, we want to know what the consequences of the breakdown of the inversion symmetry, i.e. $\mathrm{D_{4h}} \to \mathrm{C_{4v}}$ for the Hamiltonian (Equation A.1.7) are. First of all, if we imply inversion symmetry corresponding to the full $\mathrm{D_{4h}}$ group but want to consider a two-dimensional Hamiltonian $\mathcal{H} = \mathcal{H}(k_x, k_y)$ we have to get rid of k_z which results in basis functions of $\mathrm{E_g}$ that are odd instead of even in $\mathbf{k}$. Therefore, we have to set all matrix elements in (Equation A.1.9) to zero. To see this, consider the inversion i operation that leaves the orbitals invariant but introduces $\mathbf{k} \to -\mathbf{k} = (-k_x, -k_y, -k_z)$ into the basis functions resulting in a sign change for the $\mathrm{E_g}$ functions, if we don't explicitly include $\sin(k_z)$, which is obviously a contradiction of (Equation A.1.3). If we explicitly break inversion symmetry $z \to -z$, we can actually have non-zero (Equation A.1.9) but omit the z-component, of course. In this case, we have to prepend an imaginary $\pm i$ to the $\zeta^{\alpha}_{\mathrm{E_g}}(\mathbf{k})$ and $\tilde{\zeta}^{\alpha}_{\mathrm{E_g}}(\mathbf{k})$ elements to ensure time-reversal symmetry.

Table A.1.: The five d-orbitals, the Pauli matrices and their transformation behavior under all operations of the D_{4h} group are used to construct Hamiltonians that comply with the required symmetry. We divided the table into two parts where the first half corresponds to the operations of the subgroup C_{4v} and the second half introduces the group elements that exploit the three-dimensionality. The d_{z^2} orbital is invariant w.r.t. the entire group, i.e. it transforms according to the A_{1g} representation. The orbitals d_{xy} and $d_{x^2-y^2}$ behave like the B_{2g} and B_{1g} representations, respectively. Since the orbitals d_{xz} and d_{yz} do mix and have even parity (due to angular momentum $L = 2$) they must obviously transform according to E_g . The transformation of the Pauli matrices is to be understood as $\sigma_i \to \mathcal{S}(g)^\dagger \sigma_i \mathcal{S}(g)$ $g \in D_{4h}$ where $\mathcal{S}(g) = e^{-i\hat{n}\cdot\sigma\varphi/2}$. Like expected, the inversion is the only operation that leaves the Pauli matrices invariant since spin is a pseudovector. The irreducible representation for σ_z is A_{2g} and σ_x and σ_y behave like E_g .

D_{4h}	d_{xy}	d_{xz}	d_{yz}	$d_{x^2-y^2}$	d_{z^2}	σ_x	σ_y	σ_z
E	d_{xy}	d_{xz}	d_{yz}	$d_{x^2-y^2}$	d_{z^2}	σ_x	σ_y	σ_z
C_2	d_{xy}	$-d_{xz}$	$-d_{yz}$	$d_{x^2-y^2}$	d_{z^2}	$-\sigma_x$	$-\sigma_y$	σ_z
C_4^+	$-d_{xy}$	$-d_{yz}$	d_{xz}	$-d_{x^2-y^2}$	d_{z^2}	$-\sigma_y$	σ_x	σ_z
C_4^-	$-d_{xy}$	d_{yz}	$-d_{xz}$	$-d_{x^2-y^2}$	d_{z^2}	σ_y	$-\sigma_x$	σ_z
σ_x	$-d_{xy}$	d_{xz}	$-d_{yz}$	$d_{x^2-y^2}$	d_{z^2}	$-\sigma_x$	σ_y	$-\sigma_z$
σ_y	$-d_{xy}$	$-d_{xz}$	d_{yz}	$d_{x^2-y^2}$	d_{z^2}	σ_x	$-\sigma_y$	$-\sigma_z$
σ_a	d_{xy}	d_{yz}	d_{xz}	$-d_{x^2-y^2}$	d_{z^2}	$-\sigma_y$	$-\sigma_x$	$-\sigma_z$
σ_b	d_{xy}	$-d_{yz}$	$-d_{xz}$	$-d_{x^2-y^2}$	d_{z^2}	σ_y	σ_x	$-\sigma_z$
σ_h	d_{xy}	$-d_{xz}$	$-d_{yz}$	$d_{x^2-y^2}$	d_{z^2}	$-\sigma_x$	$-\sigma_y$	σ_z
i	d_{xy}	d_{xz}	d_{yz}	$d_{x^2-y^2}$	d_{z^2}	σ_x	σ_y	σ_z
S_4^+	$-d_{xy}$	d_{yz}	$-d_{xz}$	$-d_{x^2-y^2}$	d_{z^2}	σ_y	$-\sigma_x$	σ_z
S_4^-	$-d_{xy}$	$-d_{yz}$	d_{xz}	$-d_{x^2-y^2}$	d_{z^2}	$-\sigma_y$	σ_x	σ_z
C_x'	$-d_{xy}$	$-d_{xz}$	d_{yz}	$d_{x^2-y^2}$	d_{z^2}	σ_x	$-\sigma_y$	$-\sigma_z$
C_y'	$-d_{xy}$	d_{xz}	$-d_{yz}$	$d_{x^2-y^2}$	d_{z^2}	$-\sigma_x$	σ_y	$-\sigma_z$
C_a'	d_{xy}	$-d_{yz}$	$-d_{xz}$	$-d_{x^2-y^2}$	d_{z^2}	σ_y	σ_x	$-\sigma_z$
C_b'	d_{xy}	d_{yz}	d_{xz}	$-d_{x^2-y^2}$	d_{z^2}	$-\sigma_y$	$-\sigma_x$	$-\sigma_z$

B. L · S-coupling in p- and d-orbitals

The orbital basis that is used for the evaluation of the spin-orbit interaction operator must be the same as the one for the corresponding SU(2) -invariant tight-binding model. The matrix elements of the $\mathbf{L}\cdot\mathbf{S}$-operator are evaluated by considering the representation of this operator in terms of raising and lowering operators

$$\hat{L}_+ = \hat{L}_x + i\hat{L}_y \qquad \hat{L}_+ = \hat{L}_x - i\hat{L}_y \quad . \tag{B.0.1}$$

of the orbital angular momentum, i.e.

$$\mathbf{L}\cdot\mathbf{S} = \frac{1}{2}\left(\frac{L_+ + L_-}{2}\sigma_x + \frac{L_+ - L_-}{2i}\sigma_y + L_z\sigma_z\right) \quad . \tag{B.0.2}$$

The actions of the ladder operators and the L_z-operator on the eigenstates of the $\hat{L}_z$ operator are ($\hbar = 1$)

$$L_\pm \left|l,m\right\rangle = \sqrt{l(l+1) - m(m\pm 1)}\left|l,m\pm 1\right\rangle \quad \text{and} \quad L_z\left|l,m\right\rangle = m\left|l,m\right\rangle \quad . \tag{B.0.3}$$

This representation can be used to find the matrix elements of $\hat{\mathbf{L}}\cdot\hat{\mathbf{S}}$ by writing the different p- and d-orbitals in terms of the $\hat{L}_z$-eigenstates. These are plugged into expressions like e.g. $\langle p_x,\sigma|\,\mathbf{L}\cdot\mathbf{S}\,|p_x,\sigma\rangle$, $\langle p_x,\sigma|\,\mathbf{L}\cdot\mathbf{S}\,\big|p_y,\sigma\big\rangle$ for the p-orbitals. Since we are satisfied with a matrix representation in terms of Pauli matrices, we only have to employ the orbital angular momentum operator and leave the spins alone. In a numerical context (which seems almost obligatory for angular momentum $l \geq 2$) we may proceed as follows: first determine the operator $L_\pm$ and L_z that are $\in \mathbb{C}^{(2l+1)\times(2l+1)}$ in the $|l,m\rangle$ basis whose matrix elements are given above, set up the unitary transformation matrix $U_{l,m}$ that takes the $|l,m\rangle$ states and constructs superpositions of these to get the new basis, e.g. the p_x, p_y, etc. states (cf. (Equation B.1.3)), the new $L'_{x,y,z}$ are then obtained from the "intrinsic" operators by $L'_{x,y,z} = U_{l,m}L_{x,y,z}U^\dagger_{l,m}$, which results in the operator $\hat{\mathbf{L}}\cdot\hat{\mathbf{S}} \propto \sum_{i=x,y,z} L'_i \otimes \sigma_i$. Besides, the new basis in terms of linear combinations of $|l,m\rangle$ states is invariant w.r.t. *time-reversal*. This is due to the fact that $|l,m\rangle$ transforms according to $\hat{\Theta}\,|l,m\rangle = (-1)^m\,|l,-m\rangle$ [SN11, Chap. 4.4, p.276][Sha12, Chap. 12.5, p.337] under time-reversal and we used linear combinations that combine $+m$ and $-m$ making these states invariant w.r.t. time-reversal (also cf. appendix D). Note, that the $\mathbf{L}' = (L'_x, L'_y, L'_z)$ as generators of the group imply the orbitals's transformation behavior by means of the operator $e^{-i\hat{n}\mathbf{L}\varphi}$.

B.1. Angular momentum $L = 1$: p-orbitals

We choose the three p-orbitals states to be real in terms of the spherical harmonics $Y_{l=1}^{m=-1} \propto \sin\theta e^{-i\phi}$, $Y_{l=1}^{m=0} \propto \cos\theta$ and $Y_{l=1}^{m=1} \propto \sin\theta e^{+i\phi}$ (cf.[AW05; CS51]) and include the spin degree of freedom ($Y_{l=1}^{m=1}$ is denoted by $|l,m\rangle$) (cf. [Chr+15, Appendix B])

$$|p_x\rangle \otimes |\sigma\rangle = |p_x,\sigma\rangle = \frac{|1,-1,\sigma\rangle - |1,1,\sigma\rangle}{\sqrt{2}} \tag{B.1.1}$$

$$\left|p_y\right\rangle \otimes |\sigma\rangle = \left|p_y,\sigma\right\rangle = \frac{|1,-1,\sigma\rangle + |1,1,\sigma\rangle}{\sqrt{2}i} \tag{B.1.2}$$

$$|p_z\rangle \otimes |\sigma\rangle = |p_z,\sigma\rangle = |1,0,\sigma\rangle \quad , \tag{B.1.3}$$

corresponding to the unitary transformation and bases

$$U_p = \frac{1}{\sqrt{2}}\begin{pmatrix} 1 & 0 & -1 \\ -i & 0 & -i \\ 0 & 1 & 0 \end{pmatrix} \qquad \mathbf{p}^\dagger := \left(a_{p_x}^\dagger, a_{p_y}^\dagger, a_{p_z}^\dagger\right)^T \quad , \tag{B.1.4}$$

where we assume that the states are orthonormal. We note that this definition of orbitals implies their transformation behavior for rotations about the z-axis by its generator L_z, which is

$$e^{-iL_z\varphi} = \begin{pmatrix} \cos(\varphi) & -\sin(\varphi) & 0 \\ \sin(\varphi) & \cos(\varphi) & 0 \\ 0 & 0 & 1 \end{pmatrix} \quad . \tag{B.1.5}$$

Therefore, the p_x, p_y-orbitals transform into each other while th p_z is invariant. Looking at the representation of the p-orbitals and $\hat{\mathbf{L}}\cdot\hat{\mathbf{S}}$ (Equation B.0.2) we see that we can only get non-zero matrix elements in between different orbital states since both $\hat{L}_x$ and $\hat{L}_y$ change the magnetic quantum number by one and the $|p_x\rangle$, $\left|p_y\right\rangle$ contain magnetic quantum numbers that differ by two while the eigenvalue of $|p_z\rangle$ is zero. For example, we have

$$\begin{aligned}\left\langle p_x,\sigma\right|\mathbf{L}\cdot\mathbf{S}\left|p_y,\sigma\right\rangle &= \frac{\langle 1,1,\sigma| + \langle 1,-1,\sigma|}{\sqrt{2}}\left(\ldots + \frac{L_z\sigma_z}{2}\frac{|1,1,\sigma\rangle - |1,-1,\sigma\rangle}{\sqrt{2}i}\right) \\ &= \frac{1}{4i}\left(\langle 1,1,\sigma| + \langle 1,-1,\sigma|\right)\sigma_z\left(|1,1,\sigma\rangle + |1,-1,\sigma\rangle\right) = \frac{\sigma_z}{2i} \quad .\end{aligned} \tag{B.1.6}$$

Employing the basis $\mathbf{c}_{o,\sigma}^\dagger = (c_{p_x,\uparrow}^\dagger, c_{p_x,\downarrow}^\dagger, c_{p_y,\uparrow}^\dagger, c_{p_y,\downarrow}^\dagger, c_{p_z,\uparrow}^\dagger, c_{p_z,\downarrow}^\dagger)$, we can summarize the results by

$$\hat{\mathbf{L}} \cdot \hat{\mathbf{S}} = \frac{1}{2} \mathbf{c}^{\dagger}_{o,\sigma} \begin{pmatrix} 0 & -i\sigma_z & i\sigma_y \\ i\sigma_z & 0 & -i\sigma_x \\ -i\sigma_y & i\sigma_x & 0 \end{pmatrix} \mathbf{c}_{o,\sigma} \quad . \tag{B.1.7}$$

B.2. Angular momentum $L = 2$: d-orbitals

The same procedure can be applied for spin-orbit coupling in the five d-orbitals $d_{xz}, d_{yz}, d_{xy}, d_{x^2-y^2}, d_{z^2}$. Choosing a real orbital basis, we have (that complies to (Equation A.0.4))

$$|d_{xz}, \sigma\rangle = \frac{|2,-1,\sigma\rangle - |2,1,\sigma\rangle}{\sqrt{2}} \tag{B.2.1}$$

$$\left|d_{yz}, \sigma\right\rangle = \frac{|2,-1,\sigma\rangle + |2,1,\sigma\rangle}{\sqrt{2}i} \tag{B.2.2}$$

$$\left|d_{xy}, \sigma\right\rangle = -\frac{|2,-2,\sigma\rangle - |2,2,\sigma\rangle}{\sqrt{2}i} \tag{B.2.3}$$

$$\left|d_{x^2-y^2}, \sigma\right\rangle = \frac{|2,-2,\sigma\rangle + |2,2,\sigma\rangle}{\sqrt{2}} \tag{B.2.4}$$

$$|d_{z^2}, \sigma\rangle = -\,|2,0,\sigma\rangle \quad , \tag{B.2.5}$$

In the following, we employ the basis

$$\mathbf{c}^{\dagger}_{o,\sigma} = \left(c^{\dagger}_{d_{xz}}, c^{\dagger}_{d_{yz}}, c^{\dagger}_{d_{xy}}, c^{\dagger}_{d_{x^2-y^2}}, c^{\dagger}_{d_{z^2}}\right)^T \otimes \left(c^{\dagger}_{\uparrow}, c^{\dagger}_{\downarrow}\right)^T \quad , \tag{B.2.6}$$

and find the matrix elements of the $\hat{\mathbf{L}} \cdot \hat{\mathbf{S}}$- operator to be (cf. [Kon11, p. 25] [KGF10])

$$\hat{\mathbf{L}} \cdot \hat{\mathbf{S}} = \frac{1}{2} \mathbf{c}^{\dagger}_{o,\sigma} \begin{pmatrix} 0 & -i\sigma_z & -i\sigma_x & -i\sigma_y & -\sqrt{3}i\sigma_y \\ i\sigma_z & 0 & i\sigma_y & -i\sigma_x & \sqrt{3}i\sigma_x \\ i\sigma_x & -i\sigma_y & 0 & -2i\sigma_z & 0 \\ i\sigma_y & i\sigma_x & 2i\sigma_z & 0 & 0 \\ \sqrt{3}i\sigma_y & -\sqrt{3}i\sigma_x & 0 & 0 & 0 \end{pmatrix} \mathbf{c}_{o,\sigma} \quad . \tag{B.2.7}$$

Note that a non-interacting Hamiltonian $\mathcal{H}^0_{\mathbf{k}}$ including any $\hat{\mathbf{L}} \cdot \hat{\mathbf{S}}$ terms does neither break *time-reversal* $\hat{\Theta}$ nor *inversion symmetry* $\hat{I}$ since both $\hat{\mathbf{L}}$ and $\hat{\mathbf{S}}$ are odd under time reversal and both even under inversion. If we combine both of these symmetries, we see that the energy spectrum is doubly degenerate. More technically, we have

$$\left[\mathcal{H}^0_{\mathbf{k}}, \hat{\Theta}\right] = 0 \qquad \left[\mathcal{H}^0_{\mathbf{k}}, \hat{I}\right] = 0 \quad . \tag{B.2.8}$$

Consider the eigenvalue equation $\mathcal{H}^0_{\mathbf{k}} |\mathbf{k}, b, \sigma\rangle = \varepsilon_{\mathbf{k},b,\sigma} |\mathbf{k}, b, \sigma\rangle$ and the fact that time-reversal and inversion operation commute, i.e. $\left[\hat{\Theta}, \hat{I}\right] = 0$. The combined action of inversion and time-reversal on some eigenstate is $\hat{\Theta}\hat{I} |\mathbf{k}, \sigma\rangle = \hat{\Theta} |-\mathbf{k}, \sigma\rangle = |+\mathbf{k}, \bar{\sigma}\rangle$ where $\bar{\sigma}$ denotes the spin state opposite to σ. On the one hand, we have $\hat{\Theta}\hat{I}\mathcal{H}^0_{\mathbf{k}} |\mathbf{k}, \sigma\rangle = \mathcal{H}^0_{\mathbf{k}}\hat{\Theta}\hat{I} |\mathbf{k}, \sigma\rangle = \mathcal{H}^0_{\mathbf{k}} |+\mathbf{k}, \bar{\sigma}\rangle = \varepsilon_{\mathbf{k},b,\bar{\sigma}} |+\mathbf{k}, b, \bar{\sigma}\rangle$ and on the other hand $\hat{\Theta}\hat{I}\mathcal{H}^0_{\mathbf{k}} |\mathbf{k}, \sigma\rangle = \hat{\Theta}\hat{I}\varepsilon_{\mathbf{k},b,\sigma} |\mathbf{k}, \sigma\rangle = \varepsilon_{\mathbf{k},b,\sigma} |+\mathbf{k}, b, \bar{\sigma}\rangle$. Therefore, the eigenvalues must fulfill $\varepsilon_{\mathbf{k},b,\bar{\sigma}} = \varepsilon_{\mathbf{k},b,\sigma}$.

C. Non-local spin-orbit interaction

Here, we focus on the derivation of possible spin-orbit Hamiltonians for the five d-orbitals d_{xz}, d_{yz}, d_{xy}, $d_{x^2-y^2}$ and d_{z^2} on the tetragonal lattice corresponding to the point group D_{4h}. It is straightforward to determine the transformation behavior of the different orbitals. In particular, d_{xz} and d_{yz} transform according to the irreducible representation E_g, d_{xy} like B_{2g}, $d_{x^2-y^2}$ like B_{1g} and d_{z^2} like behaves like A_{1g}. For details see appendix A. The second ingredient is the transformation behavior of the Pauli matrices that is determined by $\sigma_i \to \mathcal{S}(g)^\dagger \sigma_i \mathcal{S}(g)$. To summarize, the Pauli matrices σ_x and σ_y transform like E_g and σ_z transforms like the A_{2g} irreducible representation of D_{4h}. This becomes apparent in (Table A.1). Note, that orbitals as well as Pauli matrices must transform according to *even* representations since they are both pseudovectors and are therefore invariant under spatial inversion. To construct the d-orbital spin-orbit interaction Hamiltonian, we employ the basis

$$\mathbf{a}^\dagger_{\mathbf{k},o,\sigma} = \left(a^\dagger_{\mathbf{k},d_{xz}}, a^\dagger_{\mathbf{k},d_{yz}}, a^\dagger_{\mathbf{k},d_{xy}}, a^\dagger_{\mathbf{k},d_{x^2-y^2}}, a^\dagger_{\mathbf{k},d_{z^2}}\right)^T \otimes \left(a^\dagger_\uparrow, a^\dagger_\downarrow\right)^T \quad . \tag{C.0.1}$$

In terms of this basis, the representation blocks that characterize the orbital's transformation behavior are given by

$$\mathcal{H}_0 = \mathbf{a}^\dagger_{\mathbf{k}} \begin{pmatrix} E_g \otimes E_g & E_g \otimes B_{2g} & E_g \otimes B_{1g} & E_g \otimes A_{1g} \\ B_{2g} \otimes E_g & B_{2g} \otimes B_{2g} & B_{2g} \otimes B_{1g} & B_{2g} \otimes A_{1g} \\ B_{1g} \otimes E_g & B_{1g} \otimes B_{2g} & B_{1g} \otimes B_{1g} & B_{1g} \otimes A_{1g} \\ A_{1g} \otimes E_g & A_{1g} \otimes B_{2g} & A_{1g} \otimes B_{1g} & A_{1g} \otimes A_{1g} \end{pmatrix} \mathbf{a}_{\mathbf{k}} \quad . \tag{C.0.2}$$

These product representations split up into the direct sums [Gos]:

$\otimes$	E_g	B_{2g}	B_{1g}	A_{1g}
E_g	$A_{1g} \oplus A_{2g} \oplus B_{1g} \oplus B_{2g}$	E_g	E_g	E_g
B_{2g}	E_g	A_{1g}	A_{2g}	B_{2g}
B_{1g}	E_g	A_{2g}	A_{1g}	B_{1g}
A_{1g}	E_g	B_{2g}	B_{1g}	A_{1g}

The lower right 3×3 block consists of one-dimensional representations, only. Firstly, we will focus on the upper left block involving the product of two E_g representations. The Pauli matrices are used to expand the matrix of the 2×2 orbital structure in this

block. In this context, we will label these Pauli matrices in d_{xz} and d_{yz} orbital-space by τ_0, τ_x, τ_y and τ_z. Considering the transformation of the d_{xz} and d_{yz} orbitals (cf. (Table A.1)), we can determine that τ_x transforms like B_{2g}, τ_y transforms like A_{2g}, τ_z transforms like B_{1g} and τ_0 obviously transforms like A_{1g}. The point group operations may be implemented by $\{E,C_2,C_4^+,C_4^-,\sigma_x,\sigma_y,\sigma_a,\sigma_b\} = \{\tau_0,-\tau_0,i\tau_y,-i\tau_y,\tau_z,-\tau_z,\tau_x,-\tau_x\}$. We note, that one may actually avoid the double group treatment in this context by dealing with the transformation properties of the Pauli matrices exclusively, instead of considering the transformation behavior of the actual states and spinors. This way, the additional minus signs related to the additional group elements given by $\bar{E}$ describing the more sophisticated transformation properties of the double group simply cancels.

C.1. Centrosymmetric spin-orbit coupling in d-orbitals

For the upper 2×2 block representing the d_{xz} and d_{yz} orbitals of the five-d-orbital Hamiltonian we found (Equation 3.1.40)

$$\mathcal{H}_{SOC}^{xz,yz} = \left(\cos\left(k_x\right) + \cos\left(k_y\right)\right)\tau_y \otimes \sigma_z \quad . \tag{C.1.1}$$

We proceed with the orbital sectors that involve the d_{xz} and d_{yz} times the d_{xy}, $d_{x^2-y^2}$ and d_{z^2} orbitals. They're all governed by the E_g representation. To get a one-dimensional representation in $\mathbf{k}$-space, spin space must be described by E_g, i.e. σ_x, σ_y, since $E_g \otimes E_g = A_{1g} \oplus A_{2g} \oplus B_{1g} \oplus B_{2g}$. In the d_{xz} and d_{yz} times d_{xy} matrix elements $\left(\sigma_x,\sigma_y\right)$ behave like B_1, $\left(\sigma_y,\sigma_x\right)$ like A_2, $\left(\sigma_x,-\sigma_y\right)$ like A_1 and $\left(\sigma_y,-\sigma_x\right)$ transforms according to B_2. In the d_{xz} and d_{yz} times $d_{x^2-y^2}$ matrix elements $\left(\sigma_x,\sigma_y\right)$ behave like B_2, $\left(\sigma_y,\sigma_x\right)$ like A_1, $\left(\sigma_x,-\sigma_y\right)$ like A_2 and $\left(\sigma_y,-\sigma_x\right)$ transforms according to B_1. At last, in the d_{xz} and d_{yz} times d_{z^2} matrix elements $\left(\sigma_x,\sigma_y\right)$ behave like A_2, $\left(\sigma_y,\sigma_x\right)$ like B_1, $\left(\sigma_x,-\sigma_y\right)$ like B_2 and $\left(\sigma_y,-\sigma_x\right)$ transform like A_1. If we only consider up to second order basis functions in momentum space, we can omit the A_2 contribution. The corresponding part of the orbital matrix is hence given by

$$\mathbf{M}^{\alpha\alpha'}(\mathbf{k}) = \begin{pmatrix} if^{A_1}(\mathbf{k})\hat{x} + if^{B_1}(\mathbf{k})\hat{x} + if^{B_2}(\mathbf{k})\hat{y} & -if^{A_1}(\mathbf{k})\hat{y} + if^{B_1}(\mathbf{k})\hat{y} - if^{B_2}(\mathbf{k})\hat{x} \\ if^{A_1}(\mathbf{k})\hat{y} + if^{B_1}(\mathbf{k})\hat{y} + if^{B_2}(\mathbf{k})\hat{x} & if^{A_1}(\mathbf{k})\hat{x} - if^{B_1}(\mathbf{k})\hat{x} + if^{B_2}(\mathbf{k})\hat{y} \\ if^{A_1}(\mathbf{k})\hat{y} + if^{B_1}(\mathbf{k})\hat{y} + if^{B_2}(\mathbf{k})\hat{x} & -if^{A_1}(\mathbf{k})\hat{x} + if^{B_1}(\mathbf{k})\hat{x} - if^{B_2}(\mathbf{k})\hat{y} \end{pmatrix} \quad , \tag{C.1.2}$$

where we used $f^{A_1}(\mathbf{k}) = \cos\left(k_x\right) + \cos\left(k_y\right)$, $f^{B_1}(\mathbf{k}) = \cos\left(k_x\right) - \cos\left(k_y\right)$ and $f^{B_2}(\mathbf{k}) = \sin\left(k_x\right)\sin\left(k_y\right)$. Lastly, we deal with the purely one-dimensional orbital sectors in the lower right part of the Hamiltonian and orbital matrix, respectively. As a consequence of the one-dimensional representation in the orbitals and the requirement of the even one-dimensional representations in $\mathbf{k}$-space, our only option for spin space is σ_z asso-

ciated to A_2. The $d_{xy} \times d_{x^2-y^2}$ matrix element is determined by $A_2 \otimes A_2 = A_1$, i.e. an A_1 representation basis function in $\mathbf{k}$-space. The $d_{xy} \times d_{z^2}$ matrix element is provided by $B_2 \otimes A_2 = B_1$. The $d_{yz} \times d_{z^2}$ matrix element determines the momentum space representation basis function to be $B_1 \otimes A_2 = B_2$. To summarize, this results in the d-orbital spin-orbit matrix being given in the basis (Equation C.0.1):

$$\mathbf{M}^{\alpha\alpha'}(\mathbf{k}) = \begin{pmatrix} 0 & -i\left(2-k_x^2-k_y^2\right)\hat{z} & 2i\left(1-k_x^2\right)\hat{x}+ik_xk_y\hat{y} & 2i\left(1-k_x^2\right)\hat{y}+ik_xk_y\hat{x} & 2i\left(1-k_x^2\right)\hat{y}+ik_xk_y\hat{x} \\ & 0 & -2i\left(1-k_y^2\right)\hat{y}-ik_xk_y\hat{x} & 2i\left(1-k_y^2\right)\hat{x}+ik_xk_y\hat{y} & 2i\left(1-k_y^2\right)\hat{x}-ik_xk_y\hat{y} \\ & & 0 & i\left(2-k_x^2-k_y^2\right)\hat{z} & -i\left(k_x^2-k_y^2\right)\hat{z} \\ & & & 0 & ik_xk_y\hat{z} \\ & & & & 0 \end{pmatrix}, \tag{C.1.3}$$

where we abbreviated $\cos(k_x) + \cos\left(k_y\right) \approx 2 - k_x^2 - k_y^2$, $\sin(k_x)\sin\left(k_y\right) \approx k_xk_y$ and $\cos(k_x) - \cos\left(k_y\right) \approx -k_x^2 + k_y^2$. The matrix elements of the left lower triangle are given by the requirement of antisymmetry $\mathbf{M}^{\alpha\alpha'}(\mathbf{k}) = -\mathbf{M}^{\alpha'\alpha}(\mathbf{k})$.

D. Time-reversal operation for single-particle terms

Consider the single particle Hamiltonian

$$\mathcal{H}_0 = \sum_{\mathbf{k}} \sum_{\alpha,\alpha'} \sum_{\sigma,\sigma'} h^{\sigma\sigma'}_{\alpha\alpha'}(\mathbf{k})\, c^\dagger_{\mathbf{k}\alpha'\sigma'} c_{\mathbf{k}\alpha\sigma} = \sum_{\mathbf{k}} \sum_{\alpha,\alpha'} \left(c^\dagger_{\mathbf{k}\alpha'\uparrow}, c^\dagger_{\mathbf{k}\alpha'\downarrow}\right)^T \begin{pmatrix} h^{\uparrow\uparrow}_{\alpha\alpha'}(\mathbf{k}) & h^{\uparrow\downarrow}_{\alpha\alpha'}(\mathbf{k}) \\ h^{\downarrow\uparrow}_{\alpha\alpha'}(\mathbf{k}) & h^{\downarrow\downarrow}_{\alpha\alpha'}(\mathbf{k}) \end{pmatrix} \begin{pmatrix} c_{\mathbf{k}\alpha\uparrow} \\ c_{\mathbf{k}\alpha\downarrow} \end{pmatrix} \quad , \tag{D.0.1}$$

with momentum $\mathbf{k}$, orbital indices α, α' and spins σ, σ'. The (antiunitary) time-reversal operator for spin-$\frac{1}{2}$ particles is given by $\hat{\Theta} = -i\sigma_y\hat{\mathcal{K}}$ with the inverse $\hat{\Theta}^{-1} = +i\sigma_y\hat{\mathcal{K}}$ where σ_y and $\mathcal{K}$ are the second Pauli matrix and the operator of complex conjugation, respectively [Wig12; SN11] [Sch05b, Chap. 11.4, p.228]. Assuming we work in a (real) orbital basis that is time-reversal invariant, we don't have to care about the orbital transformation, since the complex conjugation of matrix elements is already taken care of by $\hat{\Theta}$ (cf. appendix B). To find the time-reversal of (Equation D.0.1), it is convenient to use the transformation of creation and annihilation operators w.r.t. time-reversal, that is [1]

$$c^{(\dagger)}_{\mathbf{k}\alpha'\sigma'} \xrightarrow{\text{TR}} \hat{\Theta} c^{(\dagger)}_{\mathbf{k}\alpha'\sigma'} \hat{\Theta}^{-1} = \sum_\tau c^{(\dagger)}_{-\mathbf{k}\alpha'\tau} \hat{\Theta}_{\tau\sigma'} \quad . \tag{D.0.2}$$

Note, that the momentum is not affected by the operator itself and must be inverted "by hand". To see, that the time-reversed operator may be written as a sum over matrix elements of a single operator, we may best take a simple spin state [2] With these prerequisites the time-reversal of (Equation D.0.1) is

$$\hat{\Theta}\mathcal{H}_0\hat{\Theta}^{-1} = \sum_{\mathbf{k}} \sum_{\alpha,\alpha'} \sum_{\sigma,\sigma'} \hat{\Theta} h^{\sigma\sigma'}_{\alpha\alpha'}(\mathbf{k})\, c^\dagger_{\mathbf{k}\alpha'\sigma'} c_{\mathbf{k}\alpha\sigma} \hat{\Theta}^{-1} = \sum_{\mathbf{k}} \sum_{\alpha,\alpha'} \sum_{\sigma,\sigma'} \overline{h^{\sigma\sigma'}_{\alpha\alpha'}(\mathbf{k})}\, \hat{\Theta} c^\dagger_{\mathbf{k}\alpha'\sigma'} c_{\mathbf{k}\alpha\sigma} \hat{\Theta}^{-1} \quad , \tag{D.0.3}$$

[1] Consider the state $|\psi\rangle = c^{(\dagger)}|\phi\rangle$ which is generated by the action of $c^{(\dagger)}$ on some state $|\phi\rangle$. Using the time-reversal operator $\hat{\Theta}$ and its inverse $\hat{\Theta}^{-1}$, we have $|\psi\rangle = c^{(\dagger)}\hat{\Theta}^{-1}\hat{\Theta}|\phi\rangle$. The action of time-reversal on $|\psi\rangle$ is $\hat{\Theta}|\psi\rangle = \hat{\Theta}c^{(\dagger)}\hat{\Theta}^{-1}\hat{\Theta}|\phi\rangle$. Therefore, the operators must transform like $c^{(\dagger)} \to \hat{\Theta}c^{(\dagger)}\hat{\Theta}^{-1}$.

[2] Let $|\phi\rangle = \chi|\uparrow\rangle$ be a "pure" spin-up-state, that can also be expressed by $|\phi\rangle = \chi c^\dagger_\uparrow|0\rangle$. The effect of time-reversal is $\hat{\Theta}|\phi\rangle = -\overline{\chi}|\downarrow\rangle = -\overline{\chi}c^\dagger_\downarrow|0\rangle$. However, we can also transform the operator $c^\dagger_\uparrow \to \hat{\Theta}c^\dagger_\uparrow\hat{\Theta}^{-1}$ which results in $\hat{\Theta}|\phi\rangle = \overline{\chi}\hat{\Theta}c^\dagger_\uparrow\hat{\Theta}^{-1}|0\rangle$. Therefore, we must have $\hat{\Theta}c^\dagger_\uparrow\hat{\Theta}^{-1} = \sum_\sigma c^\dagger_\sigma\hat{\Theta}_{\sigma,\uparrow}$.

where we let the complex conjugation part $\hat{\mathcal{K}}$ of the operator from the left act on the matrix element of the Hamiltonian. The transformation of the operators can be evaluated by inserting an identity in terms of time-reversal operators $\hat{\Theta}^{-1}\hat{\Theta} = \sigma_0$ in between. Now, we can employ the property (Equation D.0.2) to find the transformed Hamiltonian

$$\hat{\Theta}\mathcal{H}_0\hat{\Theta}^{-1} = \sum_{\mathbf{k}}\sum_{\alpha,\alpha'}\sum_{\tau,\tau'} h^{\tau\tau'}_{\alpha\alpha'}(\mathbf{k})\, c^{\dagger}_{-\mathbf{k}\alpha'\tau'} c_{-\mathbf{k}\alpha\tau} \quad \text{with} \quad h^{\tau\tau'}_{\alpha\alpha'}(\mathbf{k}) = \sum_{\sigma,\sigma'} \overline{h^{\sigma\sigma'}_{\alpha\alpha'}(\mathbf{k})}\, \hat{\Theta}_{\tau\sigma}\hat{\Theta}^{-1}_{\sigma'\tau'} \quad . \tag{D.0.4}$$

Keeping the original basis with operators at $\mathbf{k}$ and transforming the matrix elements only (compare coefficients in terms of operators), we obtain

$$h^{\sigma\sigma'}_{\alpha\alpha'}(\mathbf{k}) \xrightarrow{\text{TR}} \begin{pmatrix} \overline{h^{\downarrow\downarrow}_{\alpha\alpha'}(-\mathbf{k})} & -\overline{h^{\downarrow\uparrow}_{\alpha\alpha'}(-\mathbf{k})} \\ -h^{\uparrow\downarrow}_{\alpha\alpha'}(-\mathbf{k}) & \overline{h^{\uparrow\uparrow}_{\alpha\alpha'}(-\mathbf{k})} \end{pmatrix} \quad . \tag{D.0.5}$$

Instead of the Hamiltonian, we often consider the non-interacting action S_0 (like e.g. in (Section 3.3), (Chapter 4) and (Chapter 6)) in terms of the Grassmann fields $\bar{\psi}$ and ψ:

$$S_0[\bar{\psi},\psi] = \sum_{\mathbf{k},i\omega_n}\sum_{\alpha,\alpha'}\sum_{\sigma,\sigma'} \bar{\psi}_{n\mathbf{k}\alpha'\sigma'}\left(i\omega - h^{\sigma\sigma'}_{\alpha\alpha'}(\mathbf{k})\right)\psi_{n\mathbf{k}\alpha\sigma} \quad . \tag{D.0.6}$$

In contrast to the creation/annihilation operators, the Grassmann fields are actually conjugated under time-reversal and transform according to (cf. [KBS10, chap. 6.3.2])

$$\begin{aligned} \psi_{\mathbf{k}\alpha\sigma} &\xrightarrow{\text{TR}} \hat{\Theta}\psi_{-\mathbf{k}\alpha\sigma} = \sum_{\tau}\left(-i\sigma_y\right)_{\sigma\tau}\bar{\psi}_{-\mathbf{k}\alpha\tau} \\ \bar{\psi}_{\mathbf{k}\alpha\sigma} &\xrightarrow{\text{TR}} \hat{\Theta}^{-1}\bar{\psi}_{-\mathbf{k}\alpha\sigma} = \sum_{\tau}\left(+i\sigma_y\right)_{\sigma\tau}\psi_{-\mathbf{k}\alpha\tau} = \sum_{\tau}\psi_{-\mathbf{k}\alpha\tau}\left(-i\sigma_y\right)_{\tau\sigma} \quad , \end{aligned} \tag{D.0.7}$$

where the conjugation of Grassmann fields, however, must not be taken as complex conjugation. Inserting the transformed fields into the non-interacting action (Equation D.0.6), yields

$$\begin{aligned} S_0[\bar{\psi},\psi] &\xrightarrow{\text{TR}} \sum_{\mathbf{k},\alpha,\alpha'}\sum_{\substack{\sigma,\sigma'\\ \tau,\tau'}} \psi_{-\mathbf{k}\alpha'\tau'}\left(-i\sigma_y\right)_{\tau'\sigma'}\left(i\omega - h^{\sigma\sigma'}_{\alpha\alpha'}(\mathbf{k})\right)\left(-i\sigma_y\right)_{\sigma\tau}\bar{\psi}_{-\mathbf{k}\alpha\tau} \\ &= \sum_{\mathbf{k},\alpha,\alpha'}\sum_{\tau,\tau'}\left[\sum_{\sigma,\sigma'}\left(-i\sigma_y\right)_{\tau'\sigma'}\left(i\omega - h^{\sigma\sigma'}_{\alpha\alpha'}(\mathbf{k})\right)\left(-i\sigma_y\right)_{\sigma\tau}\right](-\bar{\psi}_{-\mathbf{k}\alpha\tau}\psi_{-\mathbf{k}\alpha'\tau'}) \quad , \end{aligned} \tag{D.0.8}$$

where the anticommutation of Grassmann fields produces an additional minus sign.

The inner bracket evaluates to (neglecting the Matsubara frequency that does not transform, anyway)

$$\sum_{\sigma,\sigma'} \left(-i\sigma_y\right)_{\tau'\sigma'} h^{\sigma\sigma'}_{\alpha\alpha'}(\mathbf{k}) \left(-i\sigma_y\right)_{\sigma\tau} = \begin{pmatrix} -h^{\downarrow\downarrow}_{\alpha\alpha'}(\mathbf{k}) & h^{\downarrow\uparrow}_{\alpha\alpha'}(\mathbf{k}) \\ h^{\uparrow\downarrow}_{\alpha\alpha'}(\mathbf{k}) & -h^{\uparrow\uparrow}_{\alpha\alpha'}(\mathbf{k}) \end{pmatrix}_{\tau\tau'} \quad , \tag{D.0.9}$$

To obtain the final transformation behavior, we have to compare the basis in (Equation D.0.8) with the untransformed basis $\bar{\psi}_{\mathbf{k}\alpha'\sigma'}\psi_{\mathbf{k}\alpha\sigma}$ in (Equation D.0.6). To summarize, the orbital and spin indices are exchanged, the momentum is inverted to $-\mathbf{k}$ and we get a minus sign from the Grassmann fields. Therefore, the transformation of the matrix elements is given by

$$h^{\sigma,\sigma'}_{\alpha,\alpha'}(\mathbf{k}) \xrightarrow{\text{TR}} \begin{pmatrix} h^{\downarrow\downarrow}_{\alpha'\alpha}(-\mathbf{k}) & -h^{\uparrow\downarrow}_{\alpha'\alpha}(-\mathbf{k}) \\ -h^{\downarrow\uparrow}_{\alpha'\alpha}(-\mathbf{k}) & h^{\uparrow\uparrow}_{\alpha'\alpha}(-\mathbf{k}) \end{pmatrix}_{\sigma\sigma'} = \begin{pmatrix} \overline{h^{\downarrow\downarrow}_{\alpha\alpha'}(-\mathbf{k})} & \overline{-h^{\downarrow\uparrow}_{\alpha\alpha'}(\mathbf{k})} \\ -h^{\uparrow\downarrow}_{\alpha\alpha'}(-\mathbf{k}) & h^{\uparrow\uparrow}_{\alpha\alpha'}(-\mathbf{k}) \end{pmatrix}_{\sigma\sigma'} \quad , \tag{D.0.10}$$

where we made use of the Hermiticity of the Hamiltonian. We may also directly transform the matrix elements by

$$\begin{aligned} h^{\sigma\sigma'}_{\alpha\alpha'}(\mathbf{k}) \xrightarrow{\text{TR}} \hat{\Theta} h^{\sigma\sigma'}_{\alpha\alpha'}(\mathbf{k}) \hat{\Theta}^{-1} &= \left(-i\sigma_y \mathcal{K}\right) h^{\sigma\sigma'}_{\alpha\alpha'}(-\mathbf{k}) \left(+i\sigma_y \mathcal{K}\right) \\ &= \begin{pmatrix} \overline{h^{\downarrow\downarrow}_{\alpha\alpha'}}(-\mathbf{k}) & \overline{-h^{\downarrow\uparrow}_{\alpha\alpha'}}(-\mathbf{k}) \\ -h^{\uparrow\downarrow}_{\alpha\alpha'}(-\mathbf{k}) & h^{\uparrow\uparrow}_{\alpha\alpha'}(-\mathbf{k}) \end{pmatrix}_{\sigma\sigma'} \quad . \end{aligned} \tag{D.0.11}$$

Apparently, the result (Equation D.0.10) of the passive transformation is fully consistent with the one (Equation D.0.11) of the active transformation. Hence, the Grassmann fields enable us to perform the time-reversal operation as a passive as well as an active transformation. In contrast, by using creation/annihilation operators we're unable to disentangle the transformation of basis and matrix elements for time-reversal (which is in general true for any antiunitary (antilinear) transformation). In particular, in a numerical context, this is an essential result since we usually (have to) keep the basis while transforming the matrix elements. In particular, for higher-order vertex functions the passive (basis-) transformation turns out to be of extraordinary convenience. Furthermore, the time-reversal operation by means of transformation of fields is equally well applicable to off-diagonal or anomalous terms like the superconducting gap (cf. (Section 2.4.4)).

E. Local basis transformation and BCS-Theory

In (Section 3.2) it was shown how the Bloch states can be *uniquely* and *unambiguously* defined by requiring the components and phases of eigenstates of the single-particle Hamiltonian to be continuous and differentiable along any path through the Brillouin zone. In fact, this definition is only *unique* up to *global phase*. Here, we will discuss and comment on different choices of Bloch states and their restrictions regarding the investigation of the BCS ground state and its symmetry. The relevance of the phase of Bloch states was noted a long time ago in the context of *Wannier functions* [Koh59; Koh73] and this degree of freedom in the definition of Bloch states has been exploited ever since to obtain *maximally localized Wannier functions* [MV97; Mar+12]. The eigenstates of a single-particle Hamiltonian $\mathcal{H}_0$ in the presence of the potential $V(\mathbf{r})$ exhibiting the periodicity $V(\mathbf{r}+\mathbf{R})$ ($\mathbf{R}$ being a real space lattice vector) of the lattice are given by [Blo29]

$$\mathcal{H}_0\psi_{\mathbf{k}b\sigma} = \xi_{\mathbf{k}b\sigma}\psi_{\mathbf{k}b\sigma} \quad \text{where} \quad \psi_{\mathbf{k}b\sigma} = \psi_{\mathbf{k}b\sigma}(\mathbf{r}) = e^{i\mathbf{k}\mathbf{r}}\, u_{\mathbf{k}b}(\mathbf{r})\, \chi_\sigma \quad , \tag{E.0.1}$$

with crystal momentum $\mathbf{k}$, band index b, cell periodic function $u_{\mathbf{k}b}(\mathbf{r}) = u_{\mathbf{k}b}(\mathbf{r}+\mathbf{R})$ and spinor χ_σ. By means of the Bloch states (Equation E.0.1), we are able to construct *Wannier functions* given by [Wan37; HS75]

$$\phi_{\mathbf{R}b\sigma}(\mathbf{r}) = \frac{1}{\Omega_{BZ}}\int_{\mathrm{BZ}} \mathrm{d}\mathbf{k}\; e^{-i\mathbf{k}\mathbf{R}}\, \psi_{\mathbf{k}b\sigma}(\mathbf{r}) \quad \text{and} \quad \psi_{\mathbf{k}b\sigma}(\mathbf{r}) = \sum_{\mathbf{R}o} u_{\mathbf{k}bo} e^{i\mathbf{k}\mathbf{R}}\, \phi_{\mathbf{R}o\sigma}(\mathbf{r}) \quad . \tag{E.0.2}$$

that relate to the Bloch states by (inverse) Fourier transformation. Both Bloch and Wannier functions provide an equally valid description of the system. The Bloch functions exhibit a "gauge freedom" that amounts to the transformation

$$\psi_{\mathbf{k}b\sigma}(\mathbf{r}) \to e^{i\varphi_{b\sigma}(\mathbf{k})}\psi_{\mathbf{k}b\sigma}(\mathbf{r}) \quad \text{or} \quad u_{\mathbf{k}b}(\mathbf{r})\chi_\sigma \to \tilde{u}_{\mathbf{k}b}(\mathbf{r}) = e^{i\varphi_{b\sigma}(\mathbf{k})}u_{\mathbf{k}b}(\mathbf{r}) \quad , \tag{E.0.3}$$

with $\varphi_{b\sigma}(\mathbf{k}) \in \mathbb{R}$ being a real function periodic in reciprocal space. Note that this gauge freedom - although introduced in the Bloch states - equally affects the Wannier functions and their properties by (Equation E.0.2) but does not change the physical description and properties of the system. In particular, as long as we require the phase $\varphi_{b\sigma}(\mathbf{k})$ to be "smooth", which is to say $\nabla_{\mathbf{k}}\tilde{u}_{\mathbf{k}b}(\mathbf{r})$ is well-defined throughout the Brillouin zone, the Wannier functions are "well-localized" [Blo62][Mar+12, II A 1.]. Another

important aspect that arises in the context of the phases of Bloch states is the concept of the *Berry phase* [Ber84]. Although the Berry phase has a gauge-invariant formulation, a proper and "smooth" treatment of the Bloch phases is capable of revealing the Berry phase as well and may therefore serve as a double check for a suitable definition of Bloch states [Zak89; XCN10b]. So far, we only discussed the properties of Bloch functions and related quantities themselves without actually making use of the Bloch states as a basis for a transparent representation and convenient calculation of correlation functions in the context of i.a. RPA and FRG methods. Henceforth, it is of particular importance to distinguish between the dependency of Bloch and Wannier functions on their gauge and the corresponding *basis transformation*. In order to choose a suitable gauge to work with, we present two different basic recipes to fix the gauge freedom of the eigenstates of the single-particle Hamiltonian:

1. require the eigenstates to transform *trivially* under all point group operations
2. require all components of the eigenstates (including their phases) to evolve *continuously* through k-space

Looking at the first concept, let's first define what *trivially* is supposed to mean. Consider an eigenstate $\mathbf{u}_{\mathbf{k}}$ at $\mathbf{k}$, which is mapped to the corresponding eigenstate $\tilde{\mathbf{u}}_{\mathbf{k}'}$ at $\mathbf{k}' = \mathcal{P}(g)\mathbf{k}$ for an operation $g \in \mathcal{G}$, with $\mathcal{G}$ being the point group and $\mathcal{P}$ the representation of operation g in k-space. If the mapping can be written as $\tilde{\mathbf{u}}_{\mathbf{k}'} = \mathcal{D}(g)\mathbf{u}_{\mathbf{k}'}$ without employing any additional phase, where $\mathcal{D}(g)$ is the representation of g in the space of the single-particle Hamiltonian, the eigenstates are said to transform trivially. In contrast, if the eigenstates lack the trivial transformation behavior, they satisfy $\tilde{\mathbf{u}}_{\mathbf{k}'} = e^{i\phi_{\mathbf{k}}}\mathcal{D}(g)\mathbf{u}_{\mathbf{k}'}$, in general (which is sometimes called the "natural" and "non-natural" basis, see [MHW13]). Trying to implement a natural basis (trivial point group transformation behavior) in conjunction with a momentum independent representation $\mathcal{D}(g)$, inevitably leads to contradictions in the definition of basis states at special $\mathbf{k}$-points along lines (in two spatial dimension) and planes (in three spatial dimensions). This is due to $\mathcal{D}(g) \neq \mathbb{1}\ \forall g \in \{\mathcal{G}\backslash \mathrm{E}\}$ for $\mathbf{k}$ with $\mathbf{k} = \mathcal{P}(g)\mathbf{k}$.

Momentum dependent representation In (Section 3.1.2), (Section 3.3.1) and (Section 3.3.2), we consequently stuck to a (unique) single-particle basis in orbital-spin space, which gives rise to point group representation matrices $\mathcal{D}(g)$, that are momentum independent. This is motivated by finding representation matrices, which directly reflect the physical transformation behavior of the orbitals and the spin degree of freedom. However, we also could have introduced (local) representation matrices $\mathcal{D}_{\mathbf{k}}(g)$ parameterized by momentum $\mathbf{k}$ by requiring the single-particle Hamiltonian $\mathcal{H}_{0\mathbf{k}}$ in band basis - which is equivalent to the diagonal matrix containing the band dispersions - to transform trivially, assuming a suitable band labeling, i.e. (cf. (Equation 3.3.33a))

$$U_{\mathbf{k}}\mathcal{H}_{0\mathbf{k}}U_{\mathbf{k}}^{\dagger} = \mathrm{diag}(\xi_{\mathbf{k}1\tilde{\uparrow}}, \dots, \xi_{\mathbf{k}n\tilde{\downarrow}}) = U_{\mathcal{P}(g)\mathbf{k}}\mathcal{H}_{0\,\mathcal{P}(g)\mathbf{k}}U_{\mathcal{P}(g)\mathbf{k}}^{\dagger} \quad , \tag{E.0.4}$$

where the dimension of the Hamiltonian - given by the number of orbitals and sublattices - is n. The momentum dependent representation can be read off from (Equation E.0.4) by solving for $\mathcal{H}_{0\,\mathcal{P}(g)\mathbf{k}}$ in terms of $\mathcal{H}_{0\mathbf{k}}$, which gives

$$\mathcal{H}_{0\,\mathcal{P}(g)\mathbf{k}} = U^\dagger_{\mathcal{P}(g)\mathbf{k}} U_{\mathbf{k}} \mathcal{H}_{0\mathbf{k}} U^\dagger_{\mathbf{k}} U_{\mathcal{P}(g)\mathbf{k}} \equiv \mathcal{D}_{\mathbf{k}}(g) \mathcal{H}_{0\mathbf{k}} \mathcal{D}_{\mathbf{k}}(g)^\dagger \quad , \tag{E.0.5}$$

and defines the $\mathbf{k}$-dependent representation $\mathcal{D}_{\mathbf{k}}(g) = U^\dagger_{\mathcal{P}(g)\mathbf{k}} U_{\mathbf{k}}$ in orbital-spin space (cf. [MHW13, Sec. 5.2]). Assuming a trivial transformation behavior in band basis in (Equation 3.3.37), i.e. $\mathcal{B}_{\mathbf{k}}(g) = U_{\mathcal{P}(g^{-1})\mathbf{k}} \mathcal{D}(g) U^\dagger_{\mathbf{k}} = \mathbb{1}$ and solving for the representation matrix in orbital-spin space, leads to the equivalent result $\mathcal{D}(g) = \mathcal{D}_{\mathbf{k}}(g) = U^\dagger_{\mathcal{P}(g^{-1})\mathbf{k}} U_{\mathbf{k}}$. Using these $\mathbf{k}$-dependent representations will eliminate the inconsistencies in the definition of a natural basis, since $\mathcal{D}_{\mathbf{k}}(g) = U^\dagger_{\mathcal{P}(g)\mathbf{k}} U_{\mathbf{k}} = \mathbb{1}$ for all $\mathbf{k}$ with $\mathcal{P}(g)\mathbf{k} = \mathbf{k}$, at the price of introducing a basis with obscure transformation behavior that does not reflect the physical properties of orbital and spin degree of freedom.

Minimal two-orbital model for the pnictides To make our consideration regarding the phase of eigenstates more transparent, we employ a two-orbital model that is used in the context of the pnictides. It is defined in terms of d_{xz} and d_{yz}-orbital states and is given by [Rag+08] (cf. (Equation A.1.7))

$$\mathcal{H}_0 = \sum_{\mathbf{k}\sigma} \mathbf{c}^\dagger_{\mathbf{k}\sigma} \left[\zeta_{\mathrm{A_{1g}}}(\mathbf{k}) \tau_0 + \zeta_{\mathrm{B_{2g}}}(\mathbf{k}) \tau_x + \zeta_{\mathrm{B_{1g}}}(\mathbf{k}) \tau_z \right] \mathbf{c}_{\mathbf{k}\sigma} \quad , \quad \mathbf{c}^\dagger_{\mathbf{k}\sigma} = \begin{pmatrix} c^\dagger_{\mathbf{k}\ xz\ \sigma} \\ c^\dagger_{\mathbf{k}\ yz\ \sigma} \end{pmatrix}^T \quad , \tag{E.0.6}$$

where τ_0, τ_x and τ_z are the Pauli matrices in d_{xz} and d_{yz}-orbital space. The matrix elements and their dispersions are defined by

$$\begin{aligned} \zeta_{\mathrm{A_{1g}}}(\mathbf{k}) \pm \zeta_{\mathrm{B_{1g}}}(\mathbf{k}) &= -2t_{1,2} \cos(k_x) - 2t_{2,1} \cos\big(k_y\big) - 4t_3 \cos(k_x) \cos\big(k_y\big) - \mu \\ \zeta_{\mathrm{B_{2g}}}(\mathbf{k}) &= -4t_4 \sin(k_x) \sin\big(k_y\big) \quad , \end{aligned} \tag{E.0.7}$$

with the tight-binding parameters $t_1 = -1$, $t_2 = 1.3t_1$, $t_3 = t_4 = -0.85t_1$ and $\mu = 1.45t_1$. The resulting band structure, density of states and Fermi surface pockets are shown in (Figure E.1). The eigenmodes $\xi_{\mathbf{k}\pm}$ and $u_{\mathbf{k}\pm}$ of the single-particle Hamiltonian (Equation E.0.6) can be calculated analytically and are given by [1]

[1] The unitary transformation from orbital to band space is given by

$$U_{\mathbf{k}} = \begin{pmatrix} -\sqrt{\frac{1}{2} + \frac{\zeta_{\mathrm{B_{1g}}}(\mathbf{k})}{2|\zeta_{\mathbf{k}}|}} & \sqrt{\frac{1}{2} - \frac{\zeta_{\mathrm{B_{1g}}}(\mathbf{k})}{2|\zeta_{\mathbf{k}}|}} \\ \sqrt{\frac{1}{2} - \frac{\zeta_{\mathrm{B_{1g}}}(\mathbf{k})}{2|\zeta_{\mathbf{k}}|}} & \sqrt{\frac{1}{2} + \frac{\zeta_{\mathrm{B_{1g}}}(\mathbf{k})}{2|\zeta_{\mathbf{k}}|}} \end{pmatrix} \quad \text{and obeys} \quad U^\dagger_{\mathbf{k}} U_{\mathbf{k}} = \tau_0 \quad , \tag{E.0.8}$$

which is not affected by any k-dependent phase $e^{-i\phi_{\mathbf{k}}}$ multiplied to the first/second row (or both).

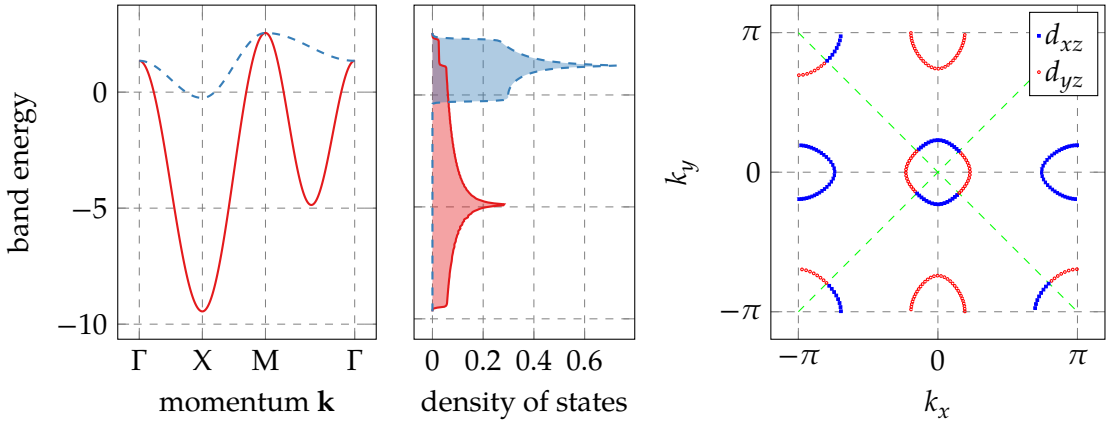

Figure E.1.: The single-particle spectrum of the two-orbital model of LaFeOAs features two bands, which give rise to two hole pockets at Γ and M and two electron pockets X and X′. The color and shape code indicates the dominant orbital weight - d_{xz} versus d_{yz} - of the Fermi surface states.

$$\xi_{\mathbf{k}\pm} = \zeta_{\mathrm{A_{1g}}}(\mathbf{k}) \pm |\zeta_{\mathbf{k}}| \qquad u_{\mathbf{k}\pm} = \left(\mp\sqrt{\frac{1}{2} \pm \frac{\zeta_{\mathrm{B_{1g}}}(\mathbf{k})}{2|\zeta_{\mathbf{k}}|}}, \sqrt{\frac{1}{2} \mp \frac{\zeta_{\mathrm{B_{1g}}}(\mathbf{k})}{2|\zeta_{\mathbf{k}}|}} \right)^T$$
$$\text{with} \quad |\zeta_{\mathbf{k}}| := \sqrt{\zeta^2_{\mathrm{B_{1g}}}(\mathbf{k}) + \zeta^2_{\mathrm{B_{2g}}}(\mathbf{k})} \quad , \tag{E.0.9}$$

Due to the analytic expression (Equation E.0.9) in terms of the matrix elements of the Hamiltonian that transform according to irreducible representations of $\mathrm{D_{4h}}$, the transformation behavior of the eigenstates is obvious. Under a rotation about the z-axis by $\frac{\pi}{2}$ the absolute values of the components of $u_{\mathbf{k}\pm}$ are exchanged. This is illustrated by (Figure E.1), where we can see that the dominant orbital weight is exchanged under this rotation on all pockets. Furthermore, the transition from dominant d_{xz} to d_{yz}-orbital weight and vice versa coincides with the line nodes of the $\mathrm{B_{1g}}$ representation basis functions along the diagonals with $k_x = k_y$. The normalized eigenstates still have a degree of freedom being the overall sign or any k-dependent phase $e^{-i\phi_{\mathbf{k}\pm}}$, i.e. the transformation $u_{\mathbf{k}\pm} \to e^{-i\phi_{\mathbf{k}\pm}} u_{\mathbf{k}\pm}$ obviously does not affect the considerations above and the property of $u_{\mathbf{k}\pm}$ being a normalized eigenvector of the Hamiltonian. By employing some **k**-dependent phase to the eigenvectors, one can generate an infinite number of different sets of eigenvectors. However, we are interested in the two particular choices for $\phi_{\mathbf{k}\pm}$ that will either let the eigenstates transform trivially under any point group operation of the underlying lattice or make the absolute values and phases of all eigenvector components change continuously along a closed path through **k**-space (except for single-particle Hamiltonians with topologically non-trivial properties). Both of these two sets of eigenstates are shown in the two right panels of (Figure E.2), while the left

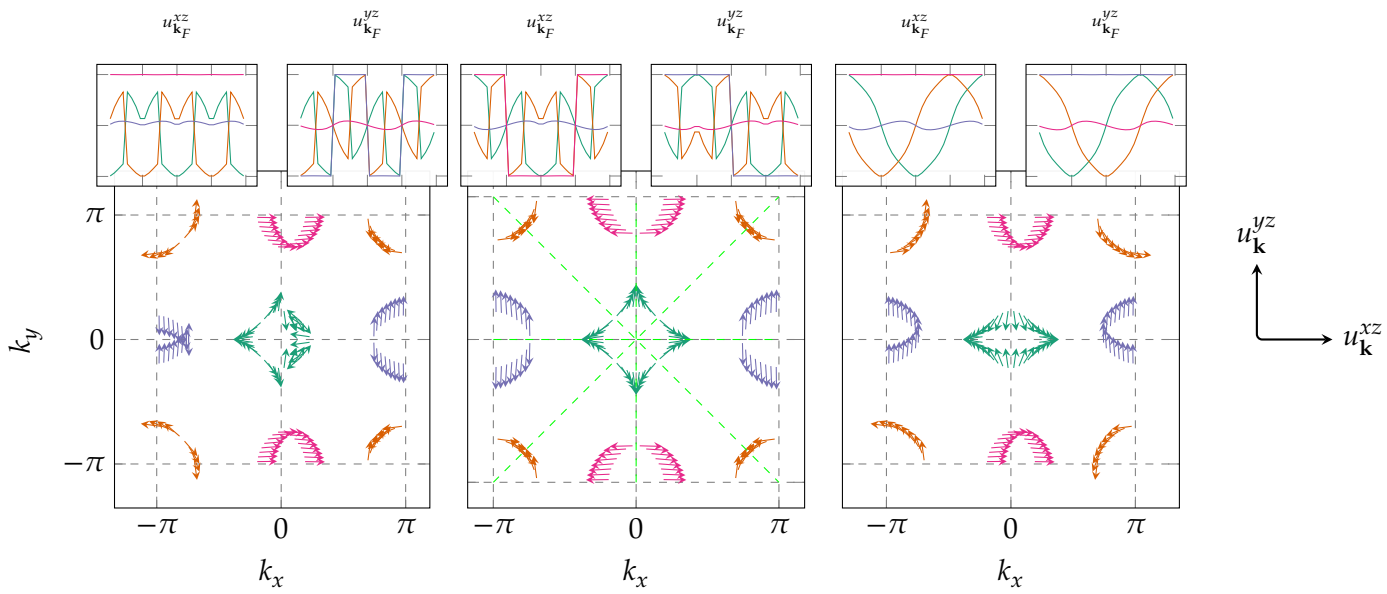

Figure E.2.: The phases of eigenstates of the Hamiltonian usually vary in a random and arbitrary way along the Fermi surface (left panel). Here, a single arrow represents one real eigenstate $\mathbf{u}_{\mathbf{k}\pm}$ and its d_{xz} and d_{yz} components along the k_x and k_y coordinates at the respective Fermi momentum. To find a more suitable "gauge" for the calculation of correlation functions, one can either employ point group symmetries to make the eigenvectors transform trivially ("natural basis" in center) or let them behave "smoothly" (right panel) along a closed path through the Brillouin zone. Note that, the "smooth" eigenstates on the right are the only set of eigenstates with $\nabla_{\mathbf{k}} u_{\mathbf{k}b}$ being well-defined for all $\mathbf{k} \in BZ$. The insets plot the $u^{xz}_{\mathbf{k}}$ and $u^{yz}_{\mathbf{k}}$ components of the eigenstates along the particular Fermi pockets.

one illustrates the usually random phases of eigenvectors as generated by numerics.

The eigenstates in the center represent the basis states that transform trivially under all point group operations (where we assumed the "physical" k-independent point group representations), i.e. $\mathbf{u}_{\mathbf{k}'} = \mathcal{D}(g)\mathbf{u}_{\mathbf{k}}$ with $\mathbf{k}' = \mathcal{P}(g)\mathbf{k}$ for an operation $g \in \mathcal{G}$, with $\mathcal{G}$ being the point group and $\mathcal{P}$ the representation of the operation g in k-space (cf. (Section 3.3.1)). For instance, the rotation by $\frac{\pi}{2}$ about the z-axis, denoted by $g = \mathrm{C}_4^+$ will transform the orbitals according to $d_{xz} \xrightarrow{\mathrm{C}_4^+} -d_{yz}$ and $d_{yz} \xrightarrow{\mathrm{C}_4^+} d_{xz}$. Therefore, we have the representation

$$\mathcal{D}(g = \mathrm{C}_4^+) = \begin{pmatrix} 0 & -1 \\ 1 & 0 \end{pmatrix} \quad , \tag{E.0.10}$$

in the space of the Hamiltonian. Furthermore, the reflection in the y-z-plane is represented by $\mathcal{D}(\sigma_y) = \mathrm{diag}(-1, 1)$. Applying the rotation by $\frac{\pi}{2}$ twice and the reflection

once, an eigenstate $u_{\mathbf{k}=(k_x,k_y)\pm} = (u^{xz}, u^{yz})_{\mathbf{k}\pm}$ transforms to $(-u^{xz}, -u^{yz})_{(-k_x,-k_y)\pm}$ and $(-u^{xz}, u^{yz})_{(-k_x,k_y)\pm}$, respectively. However, for a momentum in the limit of $k_y \to 0$ both operations map to $\mathbf{k}' = (-k_x, 0)$, which results in a contradicting definition of the eigenstate at $\mathbf{k}'$. By considering all other operations and the multiplication table of the point group, we can see that the requirement of trivially transforming eigenstates necessarily leads to inconsistencies (more specifically discontinuities) along all high-symmetry lines, which are indicated by the dashed green lines in (Figure E.2). Even worse, taking into account the actual three dimensional point group reflecting the symmetry of the Hamiltonian, which is D_{4h} and considering the reflection in the x-y-plane that maps both orbitals xz and yz to its negative, the inconsistent definition of all states in the x-y-plane becomes apparent.

Extended $s^{\pm}$ versus s-wave in the iron pnictides To appreciate the consequences of a "wrong" basis choice, we make use of the widely accepted $s_{\pm}$-wave, which is believed to be the pairing symmetry in the pnictides [Maz10]. Its lowest order harmonic in k-space corresponds to the second order harmonic of A_{1g} and is $f^{s_\pm}(\mathbf{k}) = \cos(k_x)\cos\left(k_y\right)$. Hence, for a Fermi surface like (Figure E.2) it corresponds to nodeless gaps on all pockets, since the nodes of $f^{s_\pm}$ do not intersect with any Fermi sheet, but with opposite signs for pockets around Γ and M versus pockets around X and X$'$. According to the analysis of order parameters in (Section 3.4.1) the *relevant interaction* responsible for the formation of $s_{\pm}$ pairing is given by (cf. eg. [Tho+11a; Tho+11b])

$$V_{\mathbf{k}_F\mathbf{k}'_F}\, c^\dagger_{\mathbf{k}_F\uparrow} c^\dagger_{-\mathbf{k}_F\downarrow} c_{-\mathbf{k}'_F\uparrow} c_{\mathbf{k}'_F\downarrow} = f^{s_\pm}_{\mathbf{k}_F} \left(f^{s_\pm}_{\mathbf{k}'_F}\right)^\dagger\, c^\dagger_{\mathbf{k}_F\uparrow} c^\dagger_{-\mathbf{k}_F\downarrow} c_{-\mathbf{k}'_F\uparrow} c_{\mathbf{k}'_F\downarrow} \quad . \tag{E.0.11}$$

Note, that compared to the formalism introduced in (Chapter 3) the two band indices of the basis states were omitted in favor of a more transparent notation, by simply having twice the number of momentum states for the single band index. Furthermore, all basis states are restricted to the Fermi surface denoted by the subscript F. Let's assume the basis operators in (Equation E.0.11) are the basis states corresponding to the "smooth" basis of the right panel in (Figure E.2). We setup the basis transformation

$$c^\dagger_{\mathbf{k}_F} \to e^{i\phi_\mathbf{k}} c^\dagger_{\mathbf{k}_F} := \tilde{c}^\dagger_{\mathbf{k}_F} \qquad c_{\mathbf{k}_F} \to e^{-i\phi_\mathbf{k}} c_{\mathbf{k}_F} := \tilde{c}_{\mathbf{k}_F} \qquad \text{with} \quad \phi_\mathbf{k} = \frac{1 - \operatorname{sgn}\left(\cos(k_x)\cos\left(k_y\right)\right)}{2}\pi \quad , \tag{E.0.12}$$

which brings the "smooth" basis $c^\dagger_{\mathbf{k}_F}$ to the new basis $\tilde{c}^\dagger_{\mathbf{k}_F}$. Inserting the new operators (Equation E.0.12) in (Equation E.0.11) will yield the order parameter to be of s-wave symmetry. While, it is, of course, invalid to change the basis at will, the example shows that an arbitrary choice of basis will eventually result in a wrong pairing symmetry.

Free energy of the BCS-Hamiltonian Consider a Hamiltonian in basis $c^\dagger_{\mathbf{k}b\tilde{\sigma}}$ with single-particle dispersion $\xi_{\mathbf{k}b\tilde{\sigma}}$ and effective interaction $U^{b,\tilde{\sigma}_1,b,\tilde{\sigma}_2,b',\tilde{\sigma}'_1,b',\tilde{\sigma}'_2}_{\mathbf{k},-\mathbf{k},\mathbf{k}',-\mathbf{k}'}$, i.e.

$$\mathcal{H} = \sum_{\mathbf{k}b\tilde{\sigma}} \xi_{\mathbf{k}b\tilde{\sigma}} c^\dagger_{\mathbf{k}b\tilde{\sigma}} c_{\mathbf{k}b\tilde{\sigma}} + \sum_{\mathbf{k}\mathbf{k}'} \sum_{bb'} \sum_{\substack{\tilde{\sigma}_1\tilde{\sigma}_2 \\ \tilde{\sigma}'_1\tilde{\sigma}'_2}} U^{b,\tilde{\sigma}_1,b,\tilde{\sigma}_2,b',\tilde{\sigma}'_1,b',\tilde{\sigma}'_2}_{\mathbf{k},-\mathbf{k},\mathbf{k}',-\mathbf{k}'} c^\dagger_{\mathbf{k}b\tilde{\sigma}_1} c^\dagger_{-\mathbf{k}b\tilde{\sigma}_2} c_{-\mathbf{k}'b'\tilde{\sigma}'_2} c_{\mathbf{k}'b'\tilde{\sigma}'_1} \quad . \tag{E.0.13}$$

Employing a mean-field theory with $f_{\mathbf{k}b\tilde{\sigma}\tilde{\sigma}'} = \langle c_{-\mathbf{k}b\tilde{\sigma}} c_{\mathbf{k}b\tilde{\sigma}'} \rangle$ according to (Equation 2.4.6) will result in the BCS-Hamiltonian

$$\mathcal{H}_{BCS} = \sum_{\mathbf{k},b,\tilde{\sigma}} \xi_{\mathbf{k}b\tilde{\sigma}}\, c^\dagger_{\mathbf{k}b\tilde{\sigma}} c_{\mathbf{k}b\tilde{\sigma}} + \frac{1}{2} \sum_{\mathbf{k},b} \sum_{\tilde{\sigma},\tilde{\sigma}'} \left(\overline{\Delta_{\mathbf{k}b\tilde{\sigma}'\tilde{\sigma}}}\, c_{-\mathbf{k}b\tilde{\sigma}} c_{\mathbf{k}b\tilde{\sigma}'} + \Delta_{\mathbf{k}b\tilde{\sigma}\tilde{\sigma}'}\, c^\dagger_{\mathbf{k}b\tilde{\sigma}} c^\dagger_{-\mathbf{k}b\tilde{\sigma}'} \right) + \mathcal{K} \quad , \tag{E.0.14}$$

with the definition

$$\Delta_{\mathbf{k}b\tilde{\sigma}_1\tilde{\sigma}_2} = 2 \sum_{\mathbf{k}',b'} \sum_{\tilde{\sigma}'_1,\tilde{\sigma}'_2} U^{b,\tilde{\sigma}_1,b,\tilde{\sigma}_2,b',\tilde{\sigma}'_1,b',\tilde{\sigma}'_2}_{\mathbf{k},-\mathbf{k},\mathbf{k}',-\mathbf{k}'} f_{\mathbf{k}'b'\tilde{\sigma}'_2\tilde{\sigma}'_1} \quad , \tag{E.0.15}$$

and the complex number

$$\mathcal{K} = - \sum_{\substack{\mathbf{k},b \\ \tilde{\sigma}_1,\tilde{\sigma}_2}} \sum_{\substack{\mathbf{k}',b' \\ \tilde{\sigma}'_1,\tilde{\sigma}'_2}} U^{b,\tilde{\sigma}_1,b,\tilde{\sigma}_2,b',\tilde{\sigma}'_1,b',\tilde{\sigma}'_2}_{\mathbf{k},-\mathbf{k},\mathbf{k}',-\mathbf{k}'} \overline{f_{\mathbf{k}b\tilde{\sigma}_2\tilde{\sigma}_1}} f_{\mathbf{k}'b'\tilde{\sigma}'_2\tilde{\sigma}'_1} \quad . \tag{E.0.16}$$

Consider the basis transformation

$$c^\dagger_{\mathbf{k}b\tilde{\sigma}} \to e^{i\phi_{\mathbf{k}b\tilde{\sigma}}} c^\dagger_{\mathbf{k}b\tilde{\sigma}} = \tilde{c}^\dagger_{\mathbf{k}b\tilde{\sigma}} \qquad \text{and} \qquad c_{\mathbf{k}b\tilde{\sigma}} \to e^{-i\phi_{\mathbf{k}b\tilde{\sigma}}} c_{\mathbf{k}b\tilde{\sigma}} = \tilde{c}_{\mathbf{k}b\tilde{\sigma}} \quad . \tag{E.0.17}$$

The transformation of (Equation E.0.13) to the new basis is most conveniently done by inserting appropriate terms like $1 = e^{-i\phi_{\mathbf{k}b\tilde{\sigma}}} e^{i\phi_{\mathbf{k}b\tilde{\sigma}}}$ into the Hamiltonian. While the total Hamiltonian must of course be invariant under this basis transformation, the k-dependence of the interaction generally changes, according to

$$\tilde{U}^{b,\tilde{\sigma}_1,b,\tilde{\sigma}_2,b',\tilde{\sigma}'_1,b',\tilde{\sigma}'_2}_{\mathbf{k},-\mathbf{k},\mathbf{k}',-\mathbf{k}'} = e^{-i\phi_{\mathbf{k}b\tilde{\sigma}_1} - i\phi_{-\mathbf{k}b\tilde{\sigma}_2}} U^{b,\tilde{\sigma}_1,b,\tilde{\sigma}_2,b',\tilde{\sigma}'_1,b',\tilde{\sigma}'_2}_{\mathbf{k},-\mathbf{k},\mathbf{k}',-\mathbf{k}'} e^{+i\phi_{\mathbf{k}'b'\tilde{\sigma}'_1} + i\phi_{-\mathbf{k}'b'\tilde{\sigma}'_2}} \quad , \tag{E.0.18}$$

with $\tilde{U}^{b,\tilde{\sigma}_1,b,\tilde{\sigma}_2,b',\tilde{\sigma}'_1,b',\tilde{\sigma}'_2}_{\mathbf{k},-\mathbf{k},\mathbf{k}',-\mathbf{k}'}$ being the interaction in the basis $\tilde{c}^\dagger_{\mathbf{k}b\tilde{\sigma}}$. Taking the transformation of the remaining entities into account, one finds that the gap equation (Equation E.0.15) is form-invariant under the basis transformation, while the gap itself transforms like

$$\Delta_{\mathbf{k}b\tilde{\sigma}_1\tilde{\sigma}_2} \to e^{-i\phi_{\mathbf{k}b\tilde{\sigma}_1}-i\phi_{-\mathbf{k}b\tilde{\sigma}_2}}\Delta_{\mathbf{k}b\tilde{\sigma}_1\tilde{\sigma}_2} = \tilde{\Delta}_{\mathbf{k}b\tilde{\sigma}_1\tilde{\sigma}_2} \quad . \tag{E.0.19}$$

Note, that this statement is *not* related to the lowering of the free energy by a complex superposition (introduction of a *relative* phase $e^{i\pi}$) of two degenerate gap functions to form a topologically non-trivial state [Che+10]. Let's have a look at the *free energy* of the BCS-Hamiltonian, which is given by

$$\mathcal{F} = \langle \mathcal{H}_{BCS} \rangle = \frac{\mathrm{Tr}\left(\mathcal{H}_{BCS} e^{-\beta \mathcal{H}_{BCS}}\right)}{\mathrm{Tr}\left(e^{-\beta \mathcal{H}_{BCS}}\right)} = -\frac{\partial}{\partial \beta} \ln \mathcal{Z} \quad \text{with} \quad \mathcal{Z} = \mathrm{Tr}\left(e^{-\beta \mathcal{H}_{BCS}}\right) \quad . \tag{E.0.20}$$

Evaluating the trace with respect to the eigenbasis (Equation 2.4.21) and the quasiparticle energies $E_{\mathbf{k}b}$ (Equation 2.4.19), we find

$$\mathcal{F} = -\beta^{-1} \sum_{\mathbf{k}b} \ln\left(1 + e^{-\beta E_{\mathbf{k}b}}\right) + \sum_{\mathbf{k}b} E_{\mathbf{k}b} + \mathcal{K} \quad . \tag{E.0.21}$$

While the quasiparticle energies $E_{\mathbf{k}b}$ must be gauge-invariant, i.e. invariant w.r.t. to the basis transformations, we have a closer look at the constant $\mathcal{K}$, which transforms under (Equation E.0.17) to

$$\begin{aligned} \mathcal{K} \to - \sum_{\substack{\mathbf{k},b \\ \tilde{\sigma}_1,\tilde{\sigma}_2}} \sum_{\substack{\mathbf{k}',b' \\ \tilde{\sigma}'_1,\tilde{\sigma}'_2}} & e^{-i\phi_{\mathbf{k}b\tilde{\sigma}_1}-i\phi_{-\mathbf{k}b\tilde{\sigma}_2}} U^{b,\tilde{\sigma}_1,b,\tilde{\sigma}_2,b',\tilde{\sigma}'_1,b',\tilde{\sigma}'_2}_{\mathbf{k},-\mathbf{k},\mathbf{k}',-\mathbf{k}'} e^{+i\phi_{\mathbf{k}'b'\tilde{\sigma}'_1}+i\phi_{-\mathbf{k}'b'\tilde{\sigma}'_2}} \\ & \times \overline{f_{\mathbf{k}b\tilde{\sigma}_2\tilde{\sigma}_1}} e^{i\phi_{\mathbf{k}b\tilde{\sigma}_2}+i\phi_{-\mathbf{k}b\tilde{\sigma}_1}} f_{\mathbf{k}'b'\tilde{\sigma}'_2\tilde{\sigma}'_1} e^{-i\phi_{-\mathbf{k}'b'\tilde{\sigma}'_2}+i\phi_{\mathbf{k}'b'\tilde{\sigma}'_1}} = \mathcal{K} \quad , \end{aligned} \tag{E.0.22}$$

and therefore appears to be "gauge-invariant" as well. Hence, all superconducting states and their associated BCS-Hamiltonians that arise from the basis transformation have the same free energy and cannot be distinguished.

F. Parametrization of Cooper channel interaction

According to (Equation 3.4.26), one can decompose the Cooper channel of a spinful two-particle interaction by

$$U^{bb'\tilde{\sigma}_1\tilde{\sigma}_2\tilde{\sigma}_1'\tilde{\sigma}_2'}_{\mathbf{k}\mathbf{k}'}\bar{\phi}_{\mathbf{k}'b'\tilde{\sigma}_1'}\bar{\phi}_{-\mathbf{k}'b'\tilde{\sigma}_2'}\phi_{-\mathbf{k}b\tilde{\sigma}_2}\phi_{\mathbf{k}b\tilde{\sigma}_1} = U^{bb'\mu\nu}_{\mathbf{k}\mathbf{k}'}\overline{P^{\mu}_{\mathbf{k}'b'}}P^{\nu}_{\mathbf{k}b} \quad , \tag{F.0.1}$$

with $\mu, \nu \in \{0, 1, 2, 3\}$ and the bilinear

$$P^{\mu}_{\mathbf{k}b} = \left(i\sigma_\mu\sigma_y\right)_{\tilde{\sigma}\tilde{\sigma}'}\phi_{-\mathbf{k}b\tilde{\sigma}}\phi_{\mathbf{k}b\tilde{\sigma}'} = \begin{pmatrix} \phi_{-\mathbf{k}b\tilde{\uparrow}}\phi_{\mathbf{k}b\tilde{\downarrow}} - \phi_{-\mathbf{k}b\tilde{\downarrow}}\phi_{\mathbf{k}b\tilde{\uparrow}} \\ -\phi_{-\mathbf{k}b\tilde{\uparrow}}\phi_{\mathbf{k}b\tilde{\uparrow}} + \phi_{-\mathbf{k}b\tilde{\downarrow}}\phi_{\mathbf{k}b\tilde{\downarrow}} \\ i\phi_{-\mathbf{k}b\tilde{\uparrow}}\phi_{\mathbf{k}b\tilde{\uparrow}} + i\phi_{-\mathbf{k}b\tilde{\downarrow}}\phi_{\mathbf{k}b\tilde{\downarrow}} \\ \phi_{-\mathbf{k}b\tilde{\uparrow}}\phi_{\mathbf{k}b\tilde{\downarrow}} + \phi_{-\mathbf{k}b\tilde{\downarrow}}\phi_{\mathbf{k}b\tilde{\uparrow}} \end{pmatrix}_{\mu} \quad . \tag{F.0.2}$$

This expansion is justified by the four Pauli matrices representing a *complete basis* of complex 2×2 space. We have $4 \times 4 \times 4 = 64$ terms on the right hand of (Equation F.0.1), while on the left hand side only $2^4 = 16$ different terms in pseudospin space occur. Hence, every vertex element on the left is related to four element on the right hand side. However, the linear system of equations is neither under- nor overdetermined but exactly balanced since there are sixteen degrees of freedom on either side. Note that the Hermiticity of the two-particle vertex ensures that $\left(U^{bb'\mu\nu}_{\mathbf{k}\mathbf{k}'}\right)^{\dagger} = U^{b'b\nu\mu}_{\mathbf{k}'\mathbf{k}}$. For instance, the definition of the bilinear (Equation F.0.2) suggests that the vertex element $U^{bb'\tilde{\uparrow}\tilde{\uparrow}\tilde{\uparrow}\tilde{\uparrow}}_{\mathbf{k}\mathbf{k}'}$ is connected to the elements $U^{bb'\mu\nu}_{\mathbf{k}\mathbf{k}'}$with $\mu, \nu \in \{1, 2\}$ only. In particular, by looking for all coefficients on the right hand side that are associated to the basis term $\bar{\phi}_{\mathbf{k}'b'\tilde{\uparrow}}\bar{\phi}_{-\mathbf{k}'b'\tilde{\uparrow}}\phi_{-\mathbf{k}b\tilde{\uparrow}}\phi_{\mathbf{k}b\tilde{\uparrow}}$, we find the relation

$$U^{bb'\tilde{\uparrow}\tilde{\uparrow}\tilde{\uparrow}\tilde{\uparrow}}_{\mathbf{k}\mathbf{k}'} = \left(U^{bb'11}_{\mathbf{k}\mathbf{k}'} - iU^{bb'12}_{\mathbf{k}\mathbf{k}'} + iU^{bb'21}_{\mathbf{k}\mathbf{k}'} + U^{bb'22}_{\mathbf{k}\mathbf{k}'}\right) \quad . \tag{F.0.3}$$

Analogous expressions for the elements $U^{bb'\tilde{\uparrow}\tilde{\uparrow}\tilde{\downarrow}\tilde{\downarrow}}_{\mathbf{k}\mathbf{k}'}$, $U^{bb'\tilde{\downarrow}\tilde{\downarrow}\tilde{\uparrow}\tilde{\uparrow}}_{\mathbf{k}\mathbf{k}'}$ and $U^{bb'\tilde{\downarrow}\tilde{\downarrow}\tilde{\downarrow}\tilde{\downarrow}}_{\mathbf{k}\mathbf{k}'}$ depending on $U^{bb'\mu\nu}_{\mathbf{k}\mathbf{k}'}$with $\mu, \nu \in \{1, 2\}$, exclusively, can be worked out straightforwardly. By inverting this linear system of four equations, we find expressions for $U^{bb'\mu\nu}_{\mathbf{k}\mathbf{k}'}$with $\mu, \nu \in \{1, 2\}$ in terms of the original vertex elements on the left hand side, e.g. we get

$$U^{bb'11}_{\mathbf{k}\mathbf{k}'} = \frac{U^{bb'\tilde{\uparrow}\tilde{\uparrow}\tilde{\uparrow}\tilde{\uparrow}}_{\mathbf{k}\mathbf{k}'} - U^{bb'\tilde{\uparrow}\tilde{\uparrow}\tilde{\downarrow}\tilde{\downarrow}}_{\mathbf{k}\mathbf{k}'} - U^{bb'\tilde{\downarrow}\tilde{\downarrow}\tilde{\uparrow}\tilde{\uparrow}}_{\mathbf{k}\mathbf{k}'} + U^{bb'\tilde{\downarrow}\tilde{\downarrow}\tilde{\downarrow}\tilde{\downarrow}}_{\mathbf{k}\mathbf{k}'}}{4} \quad . \tag{F.0.4}$$

The elements $U^{bb'12}_{\mathbf{k}\mathbf{k}'}$, $U^{bb'21}_{\mathbf{k}\mathbf{k}'}$ and $U^{bb'22}_{\mathbf{k}\mathbf{k}'}$ depend on the same vertex elements but involve different combinations of signs. The linear systems of equations for the remaining elements split up into three sets: $U^{bb'00}_{\mathbf{k}\mathbf{k}'}$, $U^{bb'03}_{\mathbf{k}\mathbf{k}'}$, $U^{bb'30}_{\mathbf{k}\mathbf{k}'}$ and $U^{bb'33}_{\mathbf{k}\mathbf{k}'}$ are determined by the four vertex elements $U^{bb'\tilde{\sigma}\bar{\tilde{\sigma}}\tilde{\sigma}\bar{\tilde{\sigma}}}_{\mathbf{k}\mathbf{k}'}$ and $U^{bb'\tilde{\sigma}\bar{\tilde{\sigma}}\bar{\tilde{\sigma}}\tilde{\sigma}}_{\mathbf{k}\mathbf{k}'}$ ($\bar{\tilde{\sigma}}$ is the opposite pseudospin state w.r.t. to $\tilde{\sigma}$) that involve an equal number of both $(\tilde{\uparrow},\tilde{\downarrow})$-pseudospin states, $U^{bb'01}_{\mathbf{k}\mathbf{k}'}$, $U^{bb'02}_{\mathbf{k}\mathbf{k}'}$, $U^{bb'31}_{\mathbf{k}\mathbf{k}'}$ and $U^{bb'32}_{\mathbf{k}\mathbf{k}'}$ are determined by the four vertex elements $U^{bb'\tilde{\sigma}\bar{\tilde{\sigma}}\tilde{\sigma}\tilde{\sigma}}_{\mathbf{k}\mathbf{k}'}$ and $U^{bb'\bar{\tilde{\sigma}}\tilde{\sigma}\tilde{\sigma}\tilde{\sigma}}_{\mathbf{k}\mathbf{k}'}$ that involve three equal pseudospin states, two of which are the primed indices and finally $U^{bb'10}_{\mathbf{k}\mathbf{k}'}$, $U^{bb'20}_{\mathbf{k}\mathbf{k}'}$, $U^{bb'13}_{\mathbf{k}\mathbf{k}'}$ and $U^{bb'23}_{\mathbf{k}\mathbf{k}'}$ are determined by the four vertex elements $U^{bb'\tilde{\sigma}\tilde{\sigma}\tilde{\sigma}\bar{\tilde{\sigma}}}_{\mathbf{k}\mathbf{k}'}$ and $U^{bb'\tilde{\sigma}\tilde{\sigma}\bar{\tilde{\sigma}}\tilde{\sigma}}_{\mathbf{k}\mathbf{k}'}$ that involve three equal pseudospin states, two of which are the unprimed indices. In particular, we have e.g.

$$\begin{aligned} U^{bb'03}_{\mathbf{k}\mathbf{k}'} &= \frac{U^{bb'\tilde{\uparrow}\tilde{\downarrow}\tilde{\uparrow}\tilde{\downarrow}}_{\mathbf{k}\mathbf{k}'} + U^{bb'\tilde{\uparrow}\tilde{\downarrow}\tilde{\downarrow}\tilde{\uparrow}}_{\mathbf{k}\mathbf{k}'} - U^{bb'\tilde{\downarrow}\tilde{\uparrow}\tilde{\downarrow}\tilde{\uparrow}}_{\mathbf{k}\mathbf{k}'} - U^{bb'\tilde{\downarrow}\tilde{\uparrow}\tilde{\uparrow}\tilde{\downarrow}}_{\mathbf{k}\mathbf{k}'}}{4} \\ U^{bb'20}_{\mathbf{k}\mathbf{k}'} &= \frac{U^{bb'\tilde{\uparrow}\tilde{\uparrow}\tilde{\uparrow}\tilde{\downarrow}}_{\mathbf{k}\mathbf{k}'} - U^{bb'\tilde{\uparrow}\tilde{\uparrow}\tilde{\downarrow}\tilde{\uparrow}}_{\mathbf{k}\mathbf{k}'} - U^{bb'\tilde{\downarrow}\tilde{\downarrow}\tilde{\downarrow}\tilde{\uparrow}}_{\mathbf{k}\mathbf{k}'} + U^{bb'\tilde{\downarrow}\tilde{\downarrow}\tilde{\uparrow}\tilde{\downarrow}}_{\mathbf{k}\mathbf{k}'}}{4i} \end{aligned} \quad . \tag{F.0.5}$$

Referring back to (Equation 3.3.48) that shows that spatial inversion symmetry requires the Cooper pair vertex to be invariant under exchange of both primed and unprimed pseudospin indices, we can check what happens with the newly parameterized vertex elements under spatial inversion. While we find that

$$U^{bb'11}_{\mathbf{k}\mathbf{k}'} \to U^{bb'11}_{-\mathbf{k}-\mathbf{k}'} = \frac{U^{bb'\tilde{\uparrow}\tilde{\uparrow}\tilde{\uparrow}\tilde{\uparrow}}_{\mathbf{k}\mathbf{k}'} - U^{bb'\tilde{\uparrow}\tilde{\uparrow}\tilde{\downarrow}\tilde{\downarrow}}_{\mathbf{k}\mathbf{k}'} - U^{bb'\tilde{\downarrow}\tilde{\downarrow}\tilde{\uparrow}\tilde{\uparrow}}_{\mathbf{k}\mathbf{k}'} + U^{bb'\tilde{\downarrow}\tilde{\downarrow}\tilde{\downarrow}\tilde{\downarrow}}_{\mathbf{k}\mathbf{k}'}}{4} = U^{bb'11}_{\mathbf{k}\mathbf{k}'} \quad , \tag{F.0.6}$$

is invariant under inversion anyway the terms that involve $\mu = 0$ and $\nu > 0$, like

$$U^{bb'03}_{\mathbf{k}\mathbf{k}'} \to U^{bb'03}_{-\mathbf{k}-\mathbf{k}'} = \frac{U^{bb'\tilde{\downarrow}\tilde{\uparrow}\tilde{\downarrow}\tilde{\uparrow}}_{\mathbf{k}\mathbf{k}'} + U^{bb'\tilde{\downarrow}\tilde{\uparrow}\tilde{\uparrow}\tilde{\downarrow}}_{\mathbf{k}\mathbf{k}'} - U^{bb'\tilde{\uparrow}\tilde{\downarrow}\tilde{\uparrow}\tilde{\downarrow}}_{\mathbf{k}\mathbf{k}'} - U^{bb'\tilde{\uparrow}\tilde{\downarrow}\tilde{\downarrow}\tilde{\uparrow}}_{\mathbf{k}\mathbf{k}'}}{4} = -U^{bb'03}_{\mathbf{k}\mathbf{k}'} = 0 \quad , \tag{F.0.7}$$

must actually vanish in presence of spatial inversion symmetry. Henceforth, in presence of spatial inversion symmetry the vertex $U^{bb'\mu\nu}_{\mathbf{k}\mathbf{k}'}$ must have the *block diagonal* structure

$$U^{bb'\mu\nu}_{\mathbf{k}\mathbf{k}'} = \left(\right)_{\mu\nu} ,$$

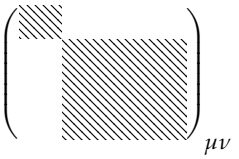

i.e. there is no mixing between singlet and triplet sectors, which becomes apparent from (Equation F.0.1) as well, by considering that its right hand side can be invariant under inversion only if both bilinears are either even or odd with respect to $\mathbf{k} \to -\mathbf{k}$.

G. Multi-orbital interactions

In multi-orbital systems with fermionic Coulomb repulsion, the interacting matrix elements can be modeled by a SU(2)-symmetric *Kanamori Hamiltonian* with five independent, local parameters (see [Kan63; GMM12])

$$\begin{aligned}\mathcal{H}_I = \sum_i \Big[U \sum_a n_{a\uparrow} n_{a\downarrow} + U' \sum_{a\neq b} n_{a\uparrow} n_{b\downarrow} + (U'-J) \sum_{a<b} \sum_\sigma n_{a\sigma} n_{b\sigma} \\ - J' \sum_{a\neq b} c^\dagger_{a\uparrow} c^\dagger_{b\downarrow} c_{b\uparrow} c_{a\downarrow} + J'' \sum_{a\neq b} c^\dagger_{a\uparrow} c^\dagger_{a\downarrow} c_{b\downarrow} c_{b\uparrow} \Big] \\ := \sum_i \sum_{\substack{a,b,\\ a',b'}} \sum_{\substack{\sigma_1,\sigma_2,\\ \sigma_1',\sigma_2'}} U_{a\sigma_1,b\sigma_2,a'\sigma_1'b'\sigma_2'} c^\dagger_{a'\sigma_1'} c^\dagger_{b'\sigma_2'} c_{b\sigma_2} c_{a\sigma_1} \quad . \end{aligned} \tag{G.0.1}$$

with lattice site index i, orbital indices a, b and spin indices σ, σ'. The electron number operator is defined by $n_{ia\sigma} = c^\dagger_{ia\sigma} c_{ia\sigma}$. Note, that if Hund's rule coupling is defined by $J\, \mathbf{S}_a \cdot \mathbf{S}_b$ with $\mathbf{S}_a = \sum_{\sigma,\sigma'} \boldsymbol{\sigma}_{\sigma\sigma'} c^\dagger_{a\sigma} c_{b\sigma'}$ being the spin operator, there's an "overlap" of matrix elements of interorbital interaction and Hund's rule coupling for parallel spins. In a numerical context, which makes use of the full spin-dependency of $\mathcal{H}_I$, we have to make sure that the interaction tensor $U_{a\sigma_1,b\sigma_2,a'\sigma_1'b'\sigma_2'}$ is antisymmetric under particle exchange as indicated by the fermionic operators $c^\dagger_{ia\sigma}$, $c_{ia\sigma}$. Due to the combination of orbital and spin degrees of freedom this requirement bears some intricacies. The interaction tensor for a *intraorbital interaction* U_{intra}, which is a density-density interaction of electrons in the same orbital, is simply given by (cf. (Equation 3.3.19))

$$U^{U_{\text{intra}}}_{a\sigma_1,b\sigma_2,a'\sigma_1'b'\sigma_2'} = U_{\text{intra}} \left(\delta_{\sigma_1\sigma_1'} \delta_{\sigma_2\sigma_2'} - \delta_{\sigma_1\sigma_2'} \delta_{\sigma_2\sigma_1'} \right) \delta_{aa'} \delta_{bb'} \delta_{ab} \quad . \tag{G.0.2}$$

In the language of (Equation 3.3.19), the spinless interaction V is simply $V^{U_{\text{intra}}}_{aba'b'} = U_{\text{intra}}$. However, for the *interorbital interaction* U_{inter}, the orbital structure has to be adapted. Choosing (any) two orbitals a, b the structure of the interaction tensor is

$$U^{U_{\text{inter}}}_{a\sigma_1,b\sigma_2,a'\sigma_1'b'\sigma_2'} = U_{\text{inter}} \left(-\delta_{\sigma_1\sigma_1'} \delta_{\sigma_2\sigma_2'} \delta_{aa'} \delta_{bb'} + \delta_{\sigma_1\sigma_2'} \delta_{\sigma_2\sigma_1'} \delta_{ab'} \delta_{ba'} \right) (1 - \delta_{ab}) \quad , \tag{G.0.3}$$

which amounts to the spinless interaction tensors $V^{U_{\text{inter}}}_{aba'b'} = -U_{\text{inter}} \delta_{aa'} \delta_{bb'} (1-\delta_{ab})$ and $V^{U_{\text{inter}}}_{aba'b'} = -U_{\text{inter}} \delta_{ab'} \delta_{ba'} (1-\delta_{ab})$. Both of them satisfy $V^{U_{\text{inter}}}_{aba'b'} = V^{U_{\text{inter}}}_{bab'a'}$, as required. Although we won't mention them explicitly, the same requirements apply to the remaining

types of interaction. To go beyond density-density interactions, we consider *Hund's rule coupling* corresponding to the (partly) third and fourth terms in the Kanamori Hamiltonian (Equation G.0.1). The associated tensor takes the form

$$U^{J_{\text{Hund}}}_{a\sigma_1,b\sigma_2,a'\sigma_1'b'\sigma_2'} = J_{\text{Hund}} \left(-\delta_{\sigma_1\sigma_1'}\delta_{\sigma_2\sigma_2'}\delta_{ab'}\delta_{ba'} + \delta_{\sigma_1\sigma_2'}\delta_{\sigma_2\sigma_1'}\delta_{aa'}\delta_{bb'}\right)(1-\delta_{ab}) \quad , \quad \text{(G.0.4)}$$

where we have to assume $J = J'$ in order to get a SU(2)-symmetric form of the interaction. Finally, the *pair hopping* interaction tensor is given by

$$U^{J_{\text{Pair}}}_{a\sigma_1,b\sigma_2,a'\sigma_1'b'\sigma_2'} = J_{\text{Pair}} \left(-\delta_{\sigma_1\sigma_1'}\delta_{\sigma_2\sigma_2'} + \delta_{\sigma_1\sigma_2'}\delta_{\sigma_2\sigma_1'}\right)\delta_{ab}\delta_{a'b'}(1-\delta_{aa'}) \quad . \quad \text{(G.0.5)}$$

To summarize, the total interaction tensor $U_{a\sigma_1,b\sigma_2,a'\sigma_1'b'\sigma_2'}$ for a two orbital system contains eight finite intraorbital matrix elements, sixteen interorbital and Hund's rule coupling matrix elements and eight pair hopping interaction matrix elements.

H. Point groups in two and three dimensions

As a reference for the definitions and notations of the point groups and their elements used in the main text, we recapitulate the basics of point groups C_{4v} and D_{4h} in two and three dimensions. To this end, we list the

- definition of point group elements
- multiplication table
- character table
- basis functions for irreducible representations

for each point group.

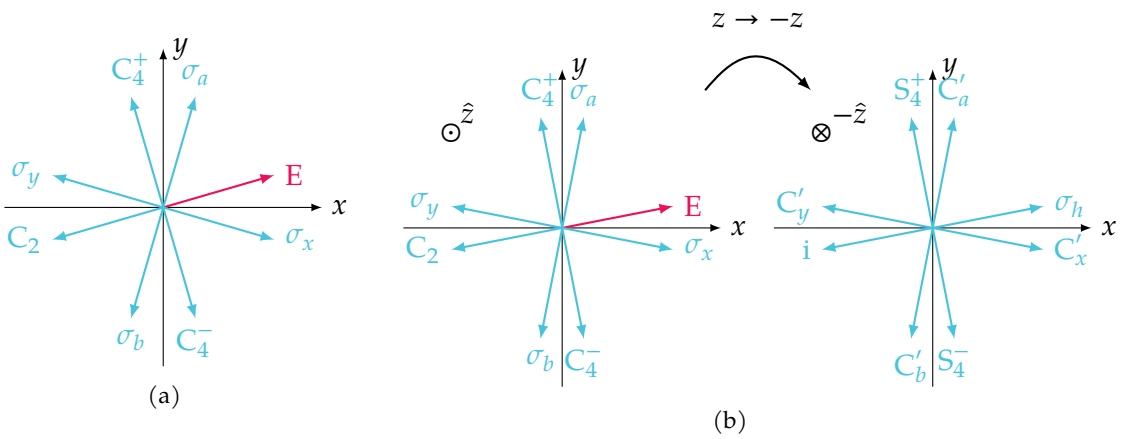

Figure H.1.: (Figure H.1a): The point group C_{4v} is made up of eight elements including four rotations and four reflections. (Figure H.1b): The point group D_{4h} is comprised of sixteen operations, eight of which are elements of the subgroup C_{4v}. The additional eight elements are obtained by multiplication of all C_{4v} elements with the reflection in the horizontal plane perpendicular to the z-axis. These additional elements are the reflection in the horizontal plane σ_h, the inversion i, the rotoreflections S_4^+ and S_4^- and the rotations about four different axis' in the x-y-plane C'_x, C'_y, C'_a and C'_b.

Table H.1.: The multiplication table of C_{4v} shows the products $g_1, g_2 \in C_{4v}$, $g_1 g_2 = g_3 \in C_{4v}$ of all point group elements. Apparently, the group is *non-Abelian*. Therefore, we defined the elements g_1 to be the ones in the column on the left.

	E	C_{4z}^+	C_{4z}^-	C_{2z}	σ_x	σ_y	σ_{da}	σ_{db}
E	E	C_{4z}^+	C_{4z}^-	C_{2z}	σ_x	σ_y	σ_{da}	σ_{db}
C_{4z}^+	C_{4z}^+	C_{2z}	E	C_{4z}^-	σ_{da}	σ_{db}	σ_y	σ_x
C_{4z}^-	C_{4z}^-	E	C_{2z}	C_{4z}^+	σ_{db}	σ_{da}	σ_x	σ_y
C_{2z}	C_{2z}	C_{4z}^-	C_{4z}^+	E	σ_y	σ_x	σ_{db}	σ_{da}
σ_x	σ_x	σ_{db}	σ_{da}	σ_y	E	C_{2z}	C_{4z}^-	C_{4z}^+
σ_y	σ_y	σ_{da}	σ_{db}	σ_x	C_{2z}	E	C_{4z}^+	C_{4z}^-
σ_{da}	σ_{da}	σ_x	σ_y	σ_{db}	C_{4z}^+	C_{4z}^-	E	C_{2z}
σ_{db}	σ_{db}	σ_y	σ_x	σ_{da}	C_{4z}^-	C_{4z}^+	C_{2z}	E

Table H.2.: The multiplication table of the point group D_{4h} shows that the group is constructed by the direct product of the group C_{4v} and the reflection in the horizontal plane, i.e. $D_{4h} = C_{4v} \otimes \sigma_h$.

D_{4h}	E	C_2	C_4^+	C_4^-	σ_x	σ_y	σ_a	σ_b	σ_h	i	S_4^+	S_4^-	C_x'	C_y'	C_a'	C_b'
E	E	C_2	C_4^+	C_4^-	σ_x	σ_y	σ_a	σ_b	σ_h	i	S_4^+	S_4^-	C_x'	C_y'	C_a'	C_b'
C_2	C_2	E	C_4^-	C_4^+	σ_y	σ_x	σ_b	σ_a	i	σ_h	S_4^-	S_4^+	C_y'	C_x'	C_b'	C_a'
C_4^+	C_4^+	C_4^-	C_2	E	σ_a	σ_b	σ_y	σ_x	S_4^+	S_4^-	i	σ_h	C_b'	C_a'	C_y'	C_x'
C_4^-	C_4^-	C_4^+	E	C_2	σ_b	σ_a	σ_x	σ_y	S_4^-	S_4^+	σ_h	i	C_a'	C_b'	C_x'	C_y'
σ_x	σ_x	σ_y	σ_b	σ_a	E	C_2	C_4^-	C_4^+	C_x'	C_y'	C_b'	C_a'	σ_h	i	S_4^-	S_4^+
σ_y	σ_y	σ_x	σ_a	σ_b	C_2	E	C_4^+	C_4^-	C_y'	C_x'	C_a'	C_b'	i	σ_h	S_4^+	S_4^-
σ_a	σ_a	σ_b	σ_x	σ_y	C_4^+	C_4^-	E	C_2	C_a'	C_b'	C_x'	C_y'	S_4^+	S_4^-	σ_h	i
σ_b	σ_b	σ_a	σ_y	σ_x	C_4^-	C_4^+	C_2	E	C_b'	C_a'	C_y'	C_x'	S_4^-	S_4^+	i	σ_h
σ_h	σ_h	i	S_4^+	S_4^-	C_x'	C_y'	C_a'	C_b'	E	C_2	C_4^+	C_4^-	σ_x	σ_y	σ_a	σ_b
i	i	σ_h	S_4^-	S_4^+	C_y'	C_x'	C_b'	C_a'	C_2	E	C_4^-	C_4^+	σ_y	σ_x	σ_b	σ_a
S_4^+	S_4^+	S_4^-	i	σ_h	C_a'	C_b'	C_y'	C_x'	C_4^+	C_4^-	C_2	E	σ_b	σ_a	σ_y	σ_x
S_4^-	S_4^-	S_4^+	σ_h	i	C_b'	C_a'	C_x'	C_y'	C_4^-	C_4^+	E	C_2	σ_a	σ_b	σ_x	σ_y
C_x'	C_x'	C_y'	C_b'	C_a'	σ_h	i	S_4^-	S_4^+	σ_x	σ_y	σ_b	σ_a	E	C_2	C_4^-	C_4^+
C_y'	C_y'	C_x'	C_a'	C_b'	i	σ_h	S_4^+	S_4^-	σ_y	σ_x	σ_a	σ_b	C_2	E	C_4^+	C_4^-
C_a'	C_a'	C_b'	C_x'	C_y'	S_4^+	S_4^-	σ_h	i	σ_a	σ_b	σ_x	σ_y	C_4^+	C_4^-	E	i
C_b'	C_b'	C_a'	C_y'	C_x'	S_4^-	S_4^+	i	σ_h	σ_b	σ_a	σ_y	σ_x	C_4^-	C_4^+	C_2	E

Table H.3.: By constructing all adjoint group elements, by evaluating $g_1, g_2 \in C_{4v}$, $g_1 \to g_2^\dagger g_1 g_2$ for all elements of C_{4v}, we find that there are five *classes* of the point group.

	E	C_{4z}^+	C_{4z}^-	C_{2z}	σ_x	σ_y	σ_{da}	σ_{db}
E	E	E	E	E	E	E	E	E
C_{4z}^+	C_{4z}^+	C_{4z}^+	C_{4z}^+	C_{4z}^+	C_{4z}^-	C_{4z}^-	C_{4z}^-	C_{4z}^-
C_{4z}^-	C_{4z}^-	C_{4z}^-	C_{4z}^-	C_{4z}^-	C_{4z}^+	C_{4z}^+	C_{4z}^+	C_{4z}^+
C_{2z}	C_{2z}	C_{2z}	C_{2z}	C_{2z}	C_{2z}	C_{2z}	C_{2z}	C_{2z}
σ_x	σ_x	σ_x	σ_y	σ_y	σ_x	σ_x	σ_y	σ_y
σ_y	σ_y	σ_y	σ_x	σ_x	σ_y	σ_y	σ_x	σ_x
σ_{da}	σ_{da}	σ_{da}	σ_{db}	σ_{db}	σ_{db}	σ_{db}	σ_{da}	σ_{da}
σ_{db}	σ_{db}	σ_{db}	σ_{da}	σ_{da}	σ_{da}	σ_{da}	σ_{db}	σ_{db}

Table H.4.: The character table of C_{4v} lists the five *irreducible representations*. There are four one-dimensional representations, namely A_1, A_2, B_1, B_2 and one two-dimensional representation given by E.

	E	$2C_{4z}$	C_{2z}	2σ	$2\sigma_d$
A_1	+1	+1	+1	+1	+1
A_2	+1	+1	+1	-1	-1
B_1	+1	-1	+1	+1	-1
B_2	+1	-1	+1	-1	+1
E	+2	+0	-2	0	0

Table H.5.: The basis functions of the square lattice for all irreducible representations of C_{4v} are constructed by considering all n-th nearest neighbor on the lattice and by employing all operations and associated characters (cf. (Figure 3.4b)).

	1st	2nd	3rd	4th
A_1	$\cos(x) + \cos(y)$	$\cos(x)\cos(y)$	$\cos(2x) + \cos(2y)$	$\cos(2x)\cos(y) + \cos(x)\cos(2y)$
A_2	0	0	0	$\sin(x)\sin(2y) - \sin(2x)\sin(y)$
B_1	$\cos(x) - \cos(y)$	0	$\cos(2x) - \cos(2y)$	$\cos(2x)\cos(y) - \cos(x)\cos(2y)$
B_2	0	$\sin(x)\sin(y)$	0	$\sin(x)\sin(2y) + \sin(2x)\sin(y)$
E	$\sin(x), \sin(y)$	$\sin(x)\cos(y)$,$\sin(y)\cos(x)$	$\sin(2x)$,$\sin(2y)$	$\sin(2x+y)$,$\sin(-x+2y)$

Table H.6.: The elements of D_{4h} are grouped into *ten classes*. Hence, the character table of the point group D_{4h} contains ten irreducible representations, which are distinguished by their *even* or *odd* parity.

D_{4h}	$\{E\}$	$\{C_2\}$	$\{C_4^+, C_4^-\}$	$\{\sigma_x, \sigma_y\}$	$\{\sigma_a, \sigma_b\}$	$\{\sigma_h\}$	$\{i\}$	$\{S_4^+, S_4^-\}$	$\{C_x', C_y'\}$	$\{C_a', C_b'\}$
A_{1g}	+1	+1	+1	+1	+1	+1	+1	+1	+1	+1
A_{2g}	+1	+1	+1	-1	-1	+1	+1	+1	-1	-1
B_{1g}	+1	+1	-1	+1	-1	+1	+1	-1	+1	-1
B_{2g}	+1	+1	-1	-1	+1	+1	+1	-1	-1	+1
E_g	+2	-2	0	0	0	-2	+2	0	0	0
A_{1u}	+1	+1	+1	-1	-1	-1	-1	-1	+1	+1
A_{2u}	+1	+1	+1	+1	+1	-1	-1	-1	-1	-1
B_{1u}	+1	+1	-1	-1	+1	-1	-1	+1	+1	-1
B_{2u}	+1	+1	-1	+1	-1	-1	-1	+1	-1	+1
E_u	+2	-2	0	0	0	+2	-2	0	0	0

Table H.7.: The n-th nearest neighbors basis functions, which transform according to any irreducible representation of the point group, are constructed by means of the character table,. Note, that these lattice harmonics may be constructed for up to an arbitrary number of nearest neighbors. However, particular lattice harmonics may vanish for a particular order n, e.g. there's no finite A_{2g} lattice harmonics for up to third nearest neighbors, while the B_{2g} function is zero for first nearest neighbors.

D_{4h}	1st NN	2nd NN
A_{1g}	$(\cos(x) + \cos(y))\cos(z)$	$\cos(x)\cos(y)\cos(z)$
A_{2g}	0	0
B_{1g}	$(\cos(x) - \cos(y))\cos(z)$	0
B_{2g}	0	$\sin(x)\sin(y)\cos(z)$
E_g	$\sin(x)\sin(z), \sin(y)\sin(z)$	$\sin(x)\cos(y)\sin(z)$,$\sin(y)\cos(x)\sin(z)$
A_{1u}	0	0
A_{2u}	$(\cos(x) + \cos(y))\sin(z)$	$\cos(x)\cos(y)\sin(z)$
B_{1u}	0	$\sin(x)\sin(y)\sin(z)$
B_{2u}	$(\cos(x) - \cos(y))\sin(z)$	0
E_u	$\sin(x)\cos(z), \sin(y)\cos(z)$	$\sin(x)\cos(y)\cos(z)$,$\sin(y)\cos(x)\cos(z)$

Bibliography

Articles

[Wei07] Pierre Weiss. "L'hypothèse du champ moléculaire et la propriété ferromagnétique". In: *J. phys. theor. appl.* 6.1 (1907), pp. 661–690.
(Cit. on p. 20.).

[Onn11] H Kamerlingh Onnes. "The resistance of pure mercury at helium temperatures". In: *Commun. Phys. Lab. Univ. Leiden* 12.120 (1911), p. 1.
(Cit. on pp. 2, 4.).

[Sch26] Erwin Schrödinger. "Quantisierung als eigenwertproblem". In: *Annalen der physik* 385.13 (1926), pp. 437–490.
(Cit. on p. 4.).

[Fer27] E Fermi. "Application of statistical gas methods to electronic systems". In: *Atti accad. naz. Lincei* 6 (1927), pp. 602–607.
(Cit. on p. 4.).

[HL27] Walter Heitler and Fritz London. "Wechselwirkung neutraler Atome und homöopolare Bindung nach der Quantenmechanik". In: *Zeitschrift für Physik A Hadrons and Nuclei* 44.6 (1927), pp. 455–472.
(Cit. on p. 4.).

[Tho27] L. H. Thomas. "The calculation of atomic fields". In: *Mathematical Proceedings of the Cambridge Philosophical Society* 23.5 (1927), pp. 542–548. DOI: 10.1017/S0305004100011683.
(Cit. on p. 4.).

[Wey27] H Weyl. "Quantum mechanics and group theory". In: *Z. Phys.* 46 (1927), p. 1.
(Cit. on p. 1.).

[Mul28] Robert S Mulliken. "The assignment of quantum numbers for electrons in molecules. I". In: *Physical Review* 32.2 (1928), p. 186.
(Cit. on p. 4.).

[WR28] EE Witmer and L Rosenfeld. "Über die Beugung von de Broglieschen Wellen an Kristallgittern". In: *Zeitschrift für Physik A Hadrons and Nuclei* 48.7 (1928), pp. 530–540.
(Cit. on p. 49.).

[Bet29] Hans A. Bethe. "Termaufspaltung in Kristallen (Splitting of Terms in Crystals)". In: *Annalen der Physik* 3 (1929), pp. 133–206.
(Cit. on p. 40.).

[Blo29] Felix Bloch. "Über die quantenmechanik der elektronen in kristallgittern". In: *Zeitschrift für Physik A Hadrons and Nuclei* 52.7 (1929), pp. 555–600.
(Cit. on pp. 49, 213.).

[Foc30] V Fock. "Bemerkung zum virialsatz". In: *Zeitschrift für Physik* 63.11-12 (1930), pp. 855–858.
(Cit. on p. 47.).

[Wig32] Eugene Wigner. "Über die Operation der Zeitumkehr in der Quantenmechanik". In: *Nachrichten von der Gesellschaft der Wissenschaften zu Göttingen, Mathematisch-Physikalische Klasse* 1932 (1932), pp. 546–559.
(Cit. on pp. 52, 85.).

[MO33] Walther Meissner and Robert Ochsenfeld. "Ein neuer Effekt bei Eintritt der Supraleitfähigkeit". In: *Naturwissenschaften* 21.44 (1933), pp. 787–788.
(Cit. on p. 13.).

[GC34] CJ Gorter and H Casimir. "On supraconductivity I". In: *Physica* 1.1-6 (1934), pp. 306–320.
(Cit. on p. 13.).

[Dir36] Paul AM Dirac. "Relativistic wave equations". In: *Proceedings of the Royal Society of London. Series A, Mathematical and Physical Sciences* 155.886 (1936), pp. 447–459.
(Cit. on p. 45.).

[Lan37a] Lev Davidovich Landau. "On the theory of phase transitions. I." In: *Zh. Eksp. Teor. Fiz.* 11 (1937), p. 19.
(Cit. on p. 1.).

[Lan37b] Lev Davidovich Landau. "On the theory of phase transitions. II." In: *Zh. Eksp. Teor. Fiz.* 11 (1937), p. 627.
(Cit. on p. 1.).

[Wan37] Gregory H. Wannier. "The Structure of Electronic Excitation Levels in Insulating Crystals". In: *Phys. Rev.* 52 (3 Aug. 1937), pp. 191–197. DOI: 10.1103/PhysRev.52.191. URL: https://link.aps.org/doi/10.1103/PhysRev.52.191.
(Cit. on p. 213.).

[FP39] Markus Fierz and Wolfgang Pauli. "On relativistic wave equations for particles of arbitrary spin in an electromagnetic field". In: *Proceedings of the Royal Society of London. Series A, Mathematical and Physical Sciences* (1939), pp. 211–232.
(Cit. on p. 45.).

[Hol41] Erik Holmberg. "On the Clustering Tendencies among the Nebulae. II. a Study of Encounters Between Laboratory Models of Stellar Systems by a New Integration Procedure." In: *The Astrophysical Journal* 94 (1941), p. 385.
(Cit. on p. 5.).

[Fey48] R. P. Feynman. "Space-Time Approach to Non-Relativistic Quantum Mechanics". In: *Rev. Mod. Phys.* 20 (2 Apr. 1948), pp. 367–387. DOI: 10.1103/RevModPhys.20.367. URL: http://link.aps.org/doi/10.1103/RevModPhys.20.367.
(Cit. on p. 108.).

[Fey49] R. P. Feynman. "Space-Time Approach to Quantum Electrodynamics". In: *Phys. Rev.* 76 (6 Sept. 1949), pp. 769–789. DOI: 10.1103/PhysRev.76.769. URL: http://link.aps.org/doi/10.1103/PhysRev.76.769.
(Cit. on p. 108.).

[Frö50] H. Fröhlich. "Theory of the Superconducting State. I. The Ground State at the Absolute Zero of Temperature". In: *Phys. Rev.* 79 (5 Sept. 1950), pp. 845–856. DOI: 10.1103/PhysRev.79.845. URL: https://link.aps.org/doi/10.1103/PhysRev.79.845.
(Cit. on p. 18.).

[GL50] Vitalii L Ginzburg and Lev D Landau. "On the theory of superconductivity". In: *Zh. eksp. teor. Fiz* 20.1064-1082 (1950), p. 35.
(Cit. on p. 13.).

[Gin50] VL Ginzburg. "Zh. VL Ginzburg and LD Landau". In: *Zh. Eksp. Teor. Fiz* 20 (1950), p. 1064.
(Cit. on p. 1.).

[Max50] Emanuel Maxwell. "Isotope Effect in the Superconductivity of Mercury". In: *Phys. Rev.* 78 (4 May 1950), pp. 477–477. DOI: 10.1103/PhysRev.78.477. URL: https://link.aps.org/doi/10.1103/PhysRev.78.477.
(Cit. on p. 13.).

[Rey+50] C. A. Reynolds et al. "Superconductivity of Isotopes of Mercury". In: *Phys. Rev.* 78 (4 May 1950), pp. 487–487. DOI: 10.1103/PhysRev.78.487. URL: https://link.aps.org/doi/10.1103/PhysRev.78.487.
(Cit. on p. 13.).

[Sho50] W Shockley. "Energy band structures in semiconductors". In: *Physical Review* 78.2 (1950), p. 173.
(Cit. on p. 48.).

[Wic50] G. C. Wick. "The Evaluation of the Collision Matrix". In: *Phys. Rev.* 80 (2 Oct. 1950), pp. 268–272. DOI: 10.1103/PhysRev.80.268. URL: http://link.aps.org/doi/10.1103/PhysRev.80.268.
(Cit. on p. 116.).

[PB53] D Pines and D Bohm. "A collective description of electron interaction: III Columb interactions in degenerate gas". In: *Phys. Rev* 92 (1953), pp. 609–625.
(Cit. on p. 6.).

[Cor+54] WS Corak et al. "Exponential temperature dependence of the electronic specific heat of superconducting vanadium". In: *Physical Review* 96.5 (1954), p. 1442.
(Cit. on p. 13.).

[Ell54] RJ Elliott. "Spin-Orbit Coupling in Band Theory—Character Tables for Some" Double" Space Groups". In: *Physical Review* 96.2 (1954), p. 280.
(Cit. on p. 45.).

[Lin54] J Lindhard. "J. Lindhard, Kgl. Danske Videnskab. Selskab, Mat.-Fys. Medd. 28, No. 8 (1954)". In: *Kgl. Danske Videnskab. Selskab, Mat.-Fys. Medd.* 28 (1954).
(Cit. on p. 27.).

[Wic54] G. C. Wick. "Properties of Bethe-Salpeter Wave Functions". In: *Phys. Rev.* 96 (4 Nov. 1954), pp. 1124–1134. DOI: 10.1103/PhysRev.96.1124. URL: https://link.aps.org/doi/10.1103/PhysRev.96.1124.
(Cit. on p. 108.).

[BP55] John Bardeen and David Pines. "Electron-Phonon Interaction in Metals". In: *Phys. Rev.* 99 (4 Aug. 1955), pp. 1140–1150. DOI: 10.1103/PhysRev.99.1140. URL: https://link.aps.org/doi/10.1103/PhysRev.99.1140.
(Cit. on p. 18.).

[Dre55] Gene Dresselhaus. "Spin-orbit coupling effects in zinc blende structures". In: *Physical Review* 100.2 (1955), p. 580.
(Cit. on p. 45.).

[DKK55] Gene Dresselhaus, AF Kip, and Charles Kittel. "Cyclotron resonance of electrons and holes in silicon and germanium crystals". In: *Physical Review* 98.2 (1955), p. 368.
(Cit. on pp. 48, 49.).

[LK55] Joaquin M Luttinger and Walter Kohn. "Motion of electrons and holes in perturbed periodic fields". In: *Physical Review* 97.4 (1955), p. 869.
(Cit. on pp. 49, 55.).

[Mat55] Takeo Matsubara. "A new approach to quantum-statistical mechanics". In: *Progress of theoretical physics* 14.4 (1955), pp. 351–378.
(Cit. on p. 110.).

[Coo56] Leon N Cooper. "Bound electron pairs in a degenerate Fermi gas". In: *Physical Review* 104.4 (1956), p. 1189.
(Cit. on p. 13.).

[Kan56] Evan O Kane. "Energy band structure in p-type germanium and silicon". In: *Journal of Physics and Chemistry of Solids* 1.1-2 (1956), pp. 82–99.
(Cit. on pp. 48, 49.).

[Lut56] JM Luttinger. "Quantum theory of cyclotron resonance in semiconductors: General theory". In: *Physical Review* 102.4 (1956), p. 1030.
(Cit. on pp. 49, 55.).

[BCS57] John Bardeen, Leon N Cooper, and John Robert Schrieffer. "Theory of superconductivity". In: *Physical Review* 108.5 (1957), p. 1175.
(Cit. on pp. 3, 4, 13, 18, 20.).

[Fey57] R. P. Feynman. "Superfluidity and Superconductivity". In: *Rev. Mod. Phys.* 29 (2 Apr. 1957), pp. 205–212. DOI: 10.1103/RevModPhys.29.205. URL: https://link.aps.org/doi/10.1103/RevModPhys.29.205.
(Cit. on p. 13.).

[GB57] Murray Gell-Mann and Keith A Brueckner. "Correlation energy of an electron gas at high density". In: *Physical Review* 106.2 (1957), p. 364.
(Cit. on p. 6.).

[Kan57] Evan O Kane. "Band structure of indium antimonide". In: *Journal of Physics and Chemistry of Solids* 1.4 (1957), pp. 249–261.
(Cit. on pp. 48, 50.).

[Lan57] LD Landau. "The theory of a Fermi liquid". In: *Soviet Physics Jetp-Ussr* 3.6 (1957), pp. 920–925.
(Cit. on p. 1.).

[And58a] P. W. Anderson. "Random-Phase Approximation in the Theory of Superconductivity". In: *Phys. Rev.* 112 (6 Dec. 1958), pp. 1900–1916. DOI: 10.1103/PhysRev.112.1900. URL: https://link.aps.org/doi/10.1103/PhysRev.112.1900.
(Cit. on p. 6.).

[And58b] Philip W Anderson. "Random-phase approximation in the theory of superconductivity". In: *Physical Review* 112.6 (1958), p. 1900.
(Cit. on p. 20.).

[Mig58] AB Migdal. "Interaction between electrons and lattice vibrations in a normal metal". In: *Sov. Phys. JETP* 7.6 (1958), pp. 996–1001.
(Cit. on pp. 18, 19.).

[And59] P.W. Anderson. "Theory of dirty superconductors". In: *Journal of Physics and Chemistry of Solids* 11.1 (1959), pp. 26–30. ISSN: 0022-3697. DOI: https://doi.org/10.1016/0022-3697(59)90036-8. URL: http://www.sciencedirect.com/science/article/pii/0022369759900368.
(Cit. on p. 90.).

[Gor59] Lev Petrovich Gor'kov. "Microscopic derivation of the Ginzburg-Landau equations in the theory of superconductivity". In: *Sov. Phys. JETP* 9.6 (1959), pp. 1364–1367.
(Cit. on p. 1.).

[Koh59] W. Kohn. "Analytic Properties of Bloch Waves and Wannier Functions". In: *Phys. Rev.* 115 (4 Aug. 1959), pp. 809–821. DOI: 10.1103/PhysRev.115.809. URL: https://link.aps.org/doi/10.1103/PhysRev.115.809.
(Cit. on p. 213.).

[Eli60] GM Eliashberg. "Interactions between electrons and lattice vibrations in a superconductor". In: *Sov. Phys. JETP* 11.3 (1960), pp. 696–702.
(Cit. on pp. 3, 18.).

[Nam60] Yoichiro Nambu. "Quasi-particles and gauge invariance in the theory of superconductivity". In: *Physical Review* 117.3 (1960), p. 648.
(Cit. on p. 20.).

[AM61] Philip W Anderson and Pierre Morel. "Generalized Bardeen-Cooper-Schrieffer states and the proposed low-temperature phase of liquid He 3". In: *Physical Review* 123.6 (1961), p. 1911.
(Cit. on pp. 17, 19.).

[MA62] P. Morel and P. W. Anderson. "Calculation of the Superconducting State Parameters with Retarded Electron-Phonon Interaction". In: *Phys. Rev.* 125 (4 Feb. 1962), pp. 1263–1271. DOI: 10.1103/PhysRev.125.1263. URL: https://link.aps.org/doi/10.1103/PhysRev.125.1263.
(Cit. on p. 26.).

[BW63] R Balian and NR Werthamer. "Superconductivity with pairs in a relative p wave". In: *Physical review* 131.4 (1963), p. 1553.
(Cit. on pp. 3, 36.).

[Hua63] Kerson Huang. "Statistical Mechanics, John Wily & Sons". In: *New York* (1963).
(Cit. on p. 107.).

[Hub63] John Hubbard. "Electron correlations in narrow energy bands". In: *Proc. R. Soc. Lond. A* 276.1365 (1963), pp. 238–257.
(Cit. on p. 165.).

[Kan63] Junjiro Kanamori. "Electron correlation and ferromagnetism of transition metals". In: *Progress of Theoretical Physics* 30.3 (1963), pp. 275–289.
(Cit. on p. 225.).

[HK64] Pierre Hohenberg and Walter Kohn. "Inhomogeneous electron gas". In: *Physical review* 136.3B (1964), B864.
(Cit. on p. 5.).

[Hed65] Lars Hedin. "New Method for Calculating the One-Particle Green's Function with Application to the Electron-Gas Problem". In: *Phys. Rev.* 139 (3A Aug. 1965), A796–A823. DOI: 10.1103/PhysRev.139.A796. URL: https://link.aps.org/doi/10.1103/PhysRev.139.A796.
(Cit. on p. 5.).

[KL65] W Kohn and JM Luttinger. "New mechanism for superconductivity". In: *Physical Review Letters* 15.12 (1965), p. 524.
(Cit. on pp. 4, 6, 26, 122.).

[KS65] Walter Kohn and Lu Jeu Sham. "Self-consistent equations including exchange and correlation effects". In: *Physical review* 140.4A (1965), A1133.
(Cit. on p. 5.).

[BS66] N. F. Berk and J. R. Schrieffer. "Effect of Ferromagnetic Spin Correlations on Superconductivity". In: *Phys. Rev. Lett.* 17 (8 Aug. 1966), pp. 433–435. DOI: 10.1103/PhysRevLett.17.433. URL: https://link.aps.org/doi/10.1103/PhysRevLett.17.433.
(Cit. on pp. 6, 136.).

[Kan66] EO Kane. "The k·p method". In: *Semiconductors and semimetals* 1 (1966), pp. 75–100.
(Cit. on pp. 48, 49.).

[SSW66] D. J. Scalapino, J. R. Schrieffer, and J. W. Wilkins. "Strong-Coupling Superconductivity. I". In: *Phys. Rev.* 148 (1 Aug. 1966), pp. 263–279. DOI: 10.1103/PhysRev.148.263. URL: https://link.aps.org/doi/10.1103/PhysRev.148.263.
(Cit. on p. 3.).

[McM68] W. L. McMillan. "Transition Temperature of Strong-Coupled Superconductors". In: *Phys. Rev.* 167 (2 Mar. 1968), pp. 331–344. DOI: 10.1103/PhysRev.167.331. URL: https://link.aps.org/doi/10.1103/PhysRev.167.331.
(Cit. on p. 3.).

[Pee70] PJE Peebles. "Structure of the coma cluster of galaxies". In: *The Astronomical Journal* 75 (1970), p. 13.
(Cit. on p. 5.).

[Wil71a] Kenneth G Wilson. "Renormalization group and critical phenomena. I. Renormalization group and the Kadanoff scaling picture". In: *Physical review B* 4.9 (1971), p. 3174.
(Cit. on pp. 6, 13.).

[Wil71b] Kenneth G Wilson. "Renormalization group and critical phenomena. II. Phase-space cell analysis of critical behavior". In: *Physical Review B* 4.9 (1971), p. 3184.
(Cit. on pp. 6, 13.).

[Wil71c] Kenneth G. Wilson. "Renormalization Group and Critical Phenomena. I. Renormalization Group and the Kadanoff Scaling Picture". In: *Phys. Rev. B* 4 (9 Nov. 1971), pp. 3174–3183. DOI: 10.1103/PhysRevB.4.3174. URL: https://link.aps.org/doi/10.1103/PhysRevB.4.3174.
(Cit. on p. 139.).

[Wil71d] Kenneth G. Wilson. "Renormalization Group and Critical Phenomena. II. Phase-Space Cell Analysis of Critical Behavior". In: *Phys. Rev. B* 4 (9 Nov. 1971), pp. 3184–3205. DOI: 10.1103/PhysRevB.4.3184. URL: https://link.aps.org/doi/10.1103/PhysRevB.4.3184.
(Cit. on p. 139.).

[Koh73] W. Kohn. "Construction of Wannier Functions and Applications to Energy Bands". In: *Phys. Rev. B* 7 (10 May 1973), pp. 4388–4398. DOI: 10.1103/PhysRevB.7.4388. URL: https://link.aps.org/doi/10.1103/PhysRevB.7.4388.
(Cit. on p. 213.).

[OS73] Konrad Osterwalder and Robert Schrader. "Axioms for Euclidean Green's functions". In: *Communications in mathematical physics* 31.2 (1973), pp. 83–112.
(Cit. on p. 69.).

[WH73] Franz J Wegner and Anthony Houghton. "Renormalization group equation for critical phenomena". In: *Physical Review A* 8.1 (1973), p. 401.
(Cit. on p. 139.).

[Ber74] VL Berezinskii. "New model of the anisotropic phase of superfluid He3". In: *Jetp Lett* 20.9 (1974), pp. 287–289.
(Cit. on pp. 3, 37.).

[PS74] William H Press and Paul Schechter. "Formation of galaxies and clusters of galaxies by self-similar gravitational condensation". In: *The Astrophysical Journal* 187 (1974), pp. 425–438.
(Cit. on p. 5.).

[WK74] Kenneth G Wilson and John Kogut. "The renormalization group and the ϵ expansion". In: *Physics Reports* 12.2 (1974), pp. 75–199.
(Cit. on pp. 4, 6, 13, 139.).

[HS75] W. Hanke and L. J. Sham. "Local-field and excitonic effects in the optical spectrum of a covalent crystal". In: *Phys. Rev. B* 12 (10 Nov. 1975), pp. 4501–4511. DOI: 10.1103/PhysRevB.12.4501. URL: https://link.aps.org/doi/10.1103/PhysRevB.12.4501.
(Cit. on p. 213.).

[KU75] Kenn Kubo and Mamoru Uchinami. "The Antiferromagnetic Ground State of a Half-Filled Hubbard Model". In: *Progress of Theoretical Physics* 54.5 (1975), pp. 1289–1298.
(Cit. on p. 166.).

[Leg75] Anthony J Leggett. "A theoretical description of the new phases of liquid He 3". In: *Reviews of Modern Physics* 47.2 (1975), p. 331.
(Cit. on p. 16.).

[Wil75] Kenneth G Wilson. "The renormalization group: Critical phenomena and the Kondo problem". In: *Reviews of modern physics* 47.4 (1975), p. 773.
(Cit. on p. 139.).

[Kad76] LP Kadanoff. "LP Kadanoff, Ann. Phys.(NY) 100, 359 (1976)." In: *Ann. Phys.(NY)* 100 (1976), p. 359.
(Cit. on p. 139.).

[Kal76] Hubert Kalf. "The virial theorem in relativistic quantum mechanics". In: *Journal of Functional Analysis* 21.4 (1976), pp. 389–396.
(Cit. on p. 47.).

[Mig76] A. A. Migdal. "Phase transitions in gauge and spin-lattice systems". In: *Soviet Journal of Experimental and Theoretical Physics* 42 (1976), p. 743.
(Cit. on p. 139.).

[Whi76] Simon DM White. "The dynamics of rich clusters of galaxies". In: *Monthly Notices of the Royal Astronomical Society* 177.3 (1976), pp. 717–733.
(Cit. on p. 5.).

[TRR79] H-R Trebin, U Rössler, and R Ranvaud. "Quantum resonances in the valence bands of zinc-blende semiconductors. I. Theoretical aspects". In: *Physical Review B* 20.2 (1979), p. 686.
(Cit. on pp. 49, 55, 196.).

[Mic80] Louis Michel. "Symmetry defects and broken symmetry. Configurations hidden symmetry". In: *Reviews of Modern Physics* 52.3 (1980), p. 617.
(Cit. on p. 1.).

[Kan82] Evan O Kane. "Energy band theory". In: *Handbook on semiconductors* 1 (1982), pp. 193–217.
(Cit. on p. 48.).

[And84a] P. W. Anderson. "Structure of "triplet" superconducting energy gaps". In: *Phys. Rev. B* 30 (7 Oct. 1984), pp. 4000–4002. DOI: 10.1103/PhysRevB.30.4000. URL: https://link.aps.org/doi/10.1103/PhysRevB.30.4000.
(Cit. on pp. 43, 83.).

[And84c] PW Anderson. "Structure of" triplet" superconducting energy gaps". In: *Physical Review B* 30.7 (1984), p. 4000.
(Cit. on p. 90.).

[Ber84] Michael V Berry. "Quantal phase factors accompanying adiabatic changes". In: *Proceedings of the Royal Society of London. A. Mathematical and Physical Sciences* 392.1802 (1984), pp. 45–57.
(Cit. on p. 214.).

[BR84a] Yu A Bychkov and É I Rashba. "Properties of a 2D electron gas with lifted spectral degeneracy". In: *JETP lett* 39.2 (1984), p. 78.
(Cit. on pp. 45, 59.).

[BR84b] Yu A Bychkov and Emmanuel I Rashba. "Oscillatory effects and the magnetic susceptibility of carriers in inversion layers". In: *Journal of physics C: Solid state physics* 17.33 (1984), p. 6039.
(Cit. on p. 59.).

[Ste84] G. R. Stewart. "Heavy-fermion systems". In: *Rev. Mod. Phys.* 56 (4 Oct. 1984), pp. 755–787. DOI: 10.1103/RevModPhys.56.755. URL: https://link.aps.org/doi/10.1103/RevModPhys.56.755.
(Cit. on p. 3.).

[VG84] GE Volovik and LP Gor'kov. "An unusual superconductivity in UBe13". In: *JETP lett* 39.12 (1984), pp. 550–553.
(Cit. on p. 45.).

[App85] Andrew W Appel. "An efficient program for many-body simulation". In: *SIAM Journal on Scientific and Statistical Computing* 6.1 (1985), pp. 85–103.
(Cit. on p. 5.).

[Arf85] G Arfken. "Mathematical Methods for Physicists 3rd edn (Orlando, FL: Academic)". In: (1985).
(Cit. on p. 15.).

[Blo85] E. I. Blount. "Symmetry properties of triplet superconductors". In: *Phys. Rev. B* 32 (5 Sept. 1985), pp. 2935–2944. DOI: 10.1103/PhysRevB.32.2935. URL: https://link.aps.org/doi/10.1103/PhysRevB.32.2935.
(Cit. on pp. 67, 92.).

[UR85] K Ueda and TM Rice. "p-wave superconductivity in cubic metals". In: *Physical Review B* 31.11 (1985), p. 7114.
(Cit. on p. 63.).

[VG85] G. E. Volovik and L. P. Gor'kov. "Superconducting classes in heavy-fermion systems". In: *Zh. Eksp. Teor. Fiz.* 88 (1985), pp. 1412–1428. URL: http://www.jetp.ac.ru/cgi-bin/dn/e_061_04_0843.pdf.
(Cit. on p. 1.).

[BM86] J George Bednorz and K Alex Müller. "Possible highTc superconductivity in the Ba- La- Cu- O system". In: *Zeitschrift für Physik B Condensed Matter* 64.2 (1986), pp. 189–193.
(Cit. on p. 3.).

[BMT87] J Georg Bednorz, K Alex Muller, and Masaaki Takashige. "Superconductivity in alkaline earth-substituted lanthanum copper oxide". In: *Science* 236 (1987), pp. 73–76.
(Cit. on p. 3.).

[Gor87] LP Gor'kov. "Superconductivity in Heavy-Fermion Systems". In: *Sov. Sci. Rev. A. Phys* 9.1 (1987).
(Cit. on p. 3.).

[BM88] J Georg Bednorz and K Alex Müller. "Perovskite-type oxides—The new approach to high-T c superconductivity". In: *Reviews of Modern Physics* 60.3 (1988), p. 585.
(Cit. on p. 3.).

[Hal88] F Duncan M Haldane. "Model for a quantum Hall effect without Landau levels: Condensed-matter realization of the" parity anomaly"". In: *Physical Review Letters* 61.18 (1988), p. 2015.
(Cit. on p. 45.).

[Inu+88] Masahiko Inui et al. "Coexistence of antiferromagnetism and superconductivity in a mean-field theory of high-T_c superconductors". In: *Phys. Rev. B* 37 (4 Feb. 1988), pp. 2320–2323. DOI: 10.1103/PhysRevB.37.2320. URL: https://link.aps.org/doi/10.1103/PhysRevB.37.2320.
(Cit. on p. 6.).

[OGK88] L. N. Oliveira, E. K. U. Gross, and W. Kohn. "Density-Functional Theory for Superconductors". In: *Phys. Rev. Lett.* 60 (23 June 1988), pp. 2430–2433. DOI: 10.1103/PhysRevLett.60.2430. URL: https://link.aps.org/doi/10.1103/PhysRevLett.60.2430.
(Cit. on p. 5.).

[RS88] EI Rashba and E Ya Sherman. "Spin-orbital band splitting in symmetric quantum wells". In: *Physics Letters A* 129.3 (1988), pp. 175–179.
(Cit. on p. 45.).

[BSW89] N. E. Bickers, D. J. Scalapino, and S. R. White. "Conserving Approximations for Strongly Correlated Electron Systems: Bethe-Salpeter Equation and Dynamics for the Two-Dimensional Hubbard Model". In: *Phys. Rev. Lett.* 62 (8 Feb. 1989), pp. 961–964. DOI: 10.1103/PhysRevLett.62.961. URL: https://link.aps.org/doi/10.1103/PhysRevLett.62.961.
(Cit. on p. 6.).

[Whi+89a] S. R. White et al. "Attractive and repulsive pairing interaction vertices for the two-dimensional Hubbard model". In: *Phys. Rev. B* 39 (1 Jan. 1989), pp. 839–842. DOI: 10.1103/PhysRevB.39.839. URL: https://link.aps.org/doi/10.1103/PhysRevB.39.839.
(Cit. on p. 6.).

[Whi+89b] S. R. White et al. "Numerical study of the two-dimensional Hubbard model". In: *Phys. Rev. B* 40 (1 July 1989), pp. 506–516. DOI: 10.1103/PhysRevB.40.506. URL: https://link.aps.org/doi/10.1103/PhysRevB.40.506.
(Cit. on p. 6.).

[Zak89] J. Zak. "Berry's phase for energy bands in solids". In: *Phys. Rev. Lett.* 62 (23 June 1989), pp. 2747–2750. DOI: 10.1103/PhysRevLett.62.2747. URL: https://link.aps.org/doi/10.1103/PhysRevLett.62.2747.
(Cit. on p. 214.).

[Ann90] James F. Annett. "Symmetry of the order parameter for high-temperature superconductivity". In: *Advances in Physics* 39.2 (1990), pp. 83–126. DOI: 10.1080/00018739000101481.
(Cit. on p. 6.).

[NJK91] A A Nersesyan, G I Japaridze, and I G Kimeridze. "Low-temperature magnetic properties of a two-dimensional spin nematic state". In: *Journal of Physics: Condensed Matter* 3.19 (1991), p. 3353. URL: http://stacks.iop.org/0953-8984/3/i=19/a=014.
(Cit. on p. 101.).

[Sca+91] R. T. Scalettar et al. "Antiferromagnetic, charge-transfer, and pairing correlations in the three-band Hubbard model". In: *Phys. Rev. B* 44 (2 July 1991), pp. 770–781. DOI: 10.1103/PhysRevB.44.770. URL: https://link.aps.org/doi/10.1103/PhysRevB.44.770.
(Cit. on p. 6.).

[SU91] Manfred Sigrist and Kazuo Ueda. "Phenomenological theory of unconventional superconductivity". In: *Reviews of Modern physics* 63.2 (1991), p. 239.
(Cit. on pp. 35, 42, 88.).

[Ani+92] V. I. Anisimov et al. "Spin bags, polarons, and impurity potentials in $La_{2-x}Sr_xCuO_4$ from first principles". In: *Phys. Rev. Lett.* 68 (3 Jan. 1992), pp. 345–348. DOI: 10.1103/PhysRevLett.68.345. URL: https://link.aps.org/doi/10.1103/PhysRevLett.68.345.
(Cit. on p. 5.).

[Mol92] Anders Pape Moller. "Female swallow preference for symmetrical male sexual ornaments". In: *Nature* 357.6375 (1992), p. 238.
(Cit. on p. 1.).

[Pol92] J. Polchinski. "Effective Field Theory and the Fermi Surface". In: *ArXiv High Energy Physics - Theory e-prints* (Oct. 1992). eprint: hep-th/9210046.
(Cit. on pp. 6, 134.).

[Whi92] Steven R White. "Density matrix formulation for quantum renormalization groups". In: *Physical review letters* 69.19 (1992), p. 2863.
(Cit. on p. 139.).

[Chu93] Andrey V. Chubukov. "Kohn-Luttinger effect and the instability of a two-dimensional repulsive Fermi liquid at T=0". In: *Phys. Rev. B* 48 (2 July 1993), pp. 1097–1104. DOI: 10.1103/PhysRevB.48.1097. URL: https://link.aps.org/doi/10.1103/PhysRevB.48.1097.
(Cit. on p. 28.).

[WL93] L. Walz and F. Lichtenberg. "Refinement of the structure of Sr_2RuO_4 with 100 and 295 K X-ray data". In: *Acta Crystallographica Section C* 49.7 (July 1993), pp. 1268–1270. DOI: 10.1107/S0108270192013143. URL: http://dx.doi.org/10.1107/S0108270192013143.
(Cit. on p. 180.).

[EA+94] Magnus Enquist, Anthony Arak, et al. "Symmetry, beauty and evolution". In: *Nature* 372.6502 (1994), pp. 169–172.
(Cit. on p. 1.).

[Mae+94] Y Maeno et al. "Superconductivity in a layered perovskite without copper". In: *Nature* 372.6506 (1994), pp. 532–534.
(Cit. on pp. 3, 179.).

[MS94] KSVP Mineev and KV Samokhin. "Helical phases in superconductors". In: *Zh. Eksp. Teor. Fiz* 105 (1994), pp. 747–763.
(Cit. on pp. 1, 83.).

[Sha94a] R. Shankar. "Renormalization-group approach to interacting fermions". In: *Rev. Mod. Phys.* 66 (1 Jan. 1994), pp. 129–192. DOI: 10.1103/RevModPhys.66.129. URL: https://link.aps.org/doi/10.1103/RevModPhys.66.129.
(Cit. on pp. 6, 125, 126, 134, 135.).

[Sha94b] R. Shankar. "Renormalization-group approach to interacting fermions". In: *Reviews of Modern Physics* 66 (Jan. 1994), pp. 129–192. DOI: 10.1103/RevModPhys.66.129. eprint: arXiv:cond-mat/9307009.
(Cit. on p. 111.).

[RS95] TM Rice and M Sigrist. "Sr2RuO4: an electronic analogue of 3He?" In: *Journal of Physics: Condensed Matter* 7.47 (1995), p. L643.
(Cit. on p. 179.).

[CG97] K Capelle and EKU Gross. "Density functional theory for triplet superconductors". In: *International journal of quantum chemistry* 61.2 (1997), pp. 325–332.
(Cit. on p. 5.).

[Mae+97] Yoshiteru Maeno et al. "Two-dimensional Fermi liquid behavior of the superconductor Sr_2RuO_4". In: *Journal of the Physical Society of Japan* 66.5 (1997), pp. 1405–1408.
(Cit. on p. 179.).

[MV97] Nicola Marzari and David Vanderbilt. "Maximally localized generalized Wannier functions for composite energy bands". In: *Phys. Rev. B* 56 (20 Nov. 1997), pp. 12847–12865. DOI: 10.1103/PhysRevB.56.12847. URL: https://link.aps.org/doi/10.1103/PhysRevB.56.12847.
(Cit. on p. 213.).

[MS97] I. I. Mazin and David J. Singh. "Ferromagnetic Spin Fluctuation Induced Superconductivity in Sr_2RuO_4". In: *Phys. Rev. Lett.* 79 (4 July 1997), pp. 733–736. DOI: 10.1103/PhysRevLett.79.733. URL: http://link.aps.org/doi/10.1103/PhysRevLett.79.733.
(Cit. on p. 182.).

[Ish+98] K Ishida et al. "Spin-triplet superconductivity in Sr2RuO4 identified by 17O Knight shift". In: *Nature* 396.6712 (1998), p. 658.
(Cit. on p. 3.).

[Luk+98] GM Luke et al. "Time-reversal symmetry-breaking superconductivity in Sr2RuO4". In: *Nature* 394 (1998), pp. 558–561.
(Cit. on pp. 3, 179.).

[ZS98] D Zanchi and HJ Schulz. "Weakly correlated electrons on a square lattice: A renormalization group theory". In: *EPL (Europhysics Letters)* 44.2 (1998), p. 235.
(Cit. on p. 167.).

[AKA99] Ryotaro Arita, Kazuhiko Kuroki, and Hideo Aoki. "Spin-fluctuation exchange study of superconductivity in two- and three-dimensional single-band Hubbard models". In: *Phys. Rev. B* 60 (21 Dec. 1999), pp. 14585–14588. DOI: 10.1103/PhysRevB.60.14585. URL: https://link.aps.org/doi/10.1103/PhysRevB.60.14585.
(Cit. on p. 6.).

[Hed99] Lars Hedin. "On correlation effects in electron spectroscopies and the GW approximation". In: *Journal of Physics: Condensed Matter* 11.42 (1999), R489.
(Cit. on p. 5.).

[Hlu99] Richard Hlubina. "Phase diagram of the weak-coupling two-dimensional t- t′ Hubbard model at low and intermediate electron density". In: *Physical Review B* 59.14 (1999), p. 9600.
(Cit. on pp. 122, 167.).

[Koh99] Walter Kohn. "Nobel Lecture: Electronic structure of matter—wave functions and density functionals". In: *Reviews of Modern Physics* 71.5 (1999), p. 1253.
(Cit. on p. 5.).

[Sig+99] M. Sigrist et al. "Phenomenology of the superconducting state in Sr2RuO4". In: *Physica C: Superconductivity* 317-318 (1999), pp. 134–141. ISSN: 0921-4534. DOI: https://doi.org/10.1016/S0921-4534(99)00053-2. URL: http://www.sciencedirect.com/science/article/pii/S0921453499000532.
(Cit. on pp. 97, 179.).

[HM00a] C. J. Halboth and W. Metzner. "Renormalization-group analysis of the two-dimensional Hubbard model". In: *Phys. Rev. B* 61 (Mar. 2000), pp. 7364–7377. DOI: 10.1103/PhysRevB.61.7364. eprint: arXiv:cond-mat/9908471.
(Cit. on p. 155.).

[HM00b] Christoph J Halboth and Walter Metzner. "d-wave superconductivity and Pomeranchuk instability in the two-dimensional Hubbard model". In: *Physical review letters* 85.24 (2000), p. 5162.
(Cit. on p. 167.).

[LL00] A Liebsch and A Lichtenstein. "Photoemission Quasiparticle Spectra of Sr_2RuO_4". In: *Physical review letters* 84.7 (2000), p. 1591.
(Cit. on p. 182.).

[Nay00] Chetan Nayak. "Density-wave states of nonzero angular momentum". In: *Phys. Rev. B* 62 (8 Aug. 2000), pp. 4880–4889. DOI: 10.1103/PhysRevB.62.4880. URL: https://link.aps.org/doi/10.1103/PhysRevB.62.4880.
(Cit. on pp. 43, 101.).

[NS00] K. K. Ng and M. Sigrist. "The role of spin-orbit coupling for the superconducting state in Sr_2RuO_4". In: *EPL (Europhysics Letters)* 49 (Feb. 2000), pp. 473–479. DOI: 10.1209/epl/i2000-00173-x. eprint: cond-mat/9911325.
(Cit. on pp. 43, 179, 181.).

[Sil00] John R Silvester. "Determinants of block matrices". In: *The Mathematical Gazette* 84.501 (2000), pp. 460–467.
(Cit. on p. 34.).

[ZS00] D Zanchi and HJ Schulz. "Weakly correlated electrons on a square lattice: Renormalization-group theory". In: *Physical Review B* 61.20 (2000), p. 13609.
(Cit. on pp. 4, 6.).

[Fou+01] W. M. C. Foulkes et al. "Quantum Monte Carlo simulations of solids". In: *Rev. Mod. Phys.* 73 (1 Jan. 2001), pp. 33–83. DOI: 10.1103/RevModPhys.73.33. URL: https://link.aps.org/doi/10.1103/RevModPhys.73.33.
(Cit. on p. 5.).

[GR01] Lev P Gor'kov and Emmanuel I Rashba. "Superconducting 2D system with lifted spin degeneracy: mixed singlet-triplet state". In: *Physical Review Letters* 87.3 (2001), p. 037004.
(Cit. on p. 45.).

[Hon+01] C. Honerkamp et al. "Breakdown of the Landau-Fermi liquid in two dimensions due to umklapp scattering". In: *Phys. Rev. B* 63 (3 Jan. 2001), p. 035109. DOI: 10.1103/PhysRevB.63.035109. URL: https://link.aps.org/doi/10.1103/PhysRevB.63.035109.
(Cit. on p. 140.).

[HS01] Carsten Honerkamp and Manfred Salmhofer. "Temperature-flow renormalization group and the competition between superconductivity and ferromagnetism". In: *Phys. Rev. B* 64 (18 Oct. 2001), p. 184516. DOI: 10.1103/PhysRevB.64.184516. URL: http://link.aps.org/doi/10.1103/

PhysRevB.64.184516.
(Cit. on pp. 6, 141.).

[Kop01] P. Kopietz. "Two-loop β-function from the exact renormalization group". In: *Nuclear Physics B* 595 (Feb. 2001), pp. 493–518. DOI: 10.1016/S0550-3213(00)00680-5. eprint: arXiv:hep-th/0007128.
(Cit. on p. 152.).

[KB01] P. Kopietz and T. Busche. "Exact renormalization group flow equations for nonrelativistic fermions: Scaling toward the Fermi surface". In: *Phys. Rev. B* 64.15, 155101 (Oct. 2001), p. 155101. DOI: 10.1103/PhysRevB.64.155101. eprint: arXiv:cond-mat/0103633.
(Cit. on p. 155.).

[SH01] Manfred Salmhofer and Carsten Honerkamp. "Fermionic Renormalization Group Flows: Technique and Theory". In: *Progress of Theoretical Physics* 105.1 (2001), pp. 1–35. DOI: 10.1143/PTP.105.1. eprint: http://ptp.oxfordjournals.org/content/105/1/1.full.pdf+html. URL: http://ptp.oxfordjournals.org/content/105/1/1.abstract.
(Cit. on pp. 112, 152.).

[SYW01] Volker Springel, Naoki Yoshida, and Simon DM White. "GADGET: a code for collisionless and gasdynamical cosmological simulations". In: *New Astronomy* 6.2 (2001), pp. 79–117.
(Cit. on p. 5.).

[Cha02] Sudip Chakravarty. "Theory of the d-density wave from a vertex model and its implications". In: *Phys. Rev. B* 66 (22 Dec. 2002), p. 224505. DOI: 10.1103/PhysRevB.66.224505. URL: https://link.aps.org/doi/10.1103/PhysRevB.66.224505.
(Cit. on p. 101.).

[ORR02] Giovanni Onida, Lucia Reining, and Angel Rubio. "Electronic excitations: density-functional versus many-body Green's-function approaches". In: *Rev. Mod. Phys.* 74 (2 June 2002), pp. 601–659. DOI: 10.1103/RevModPhys.74.601. URL: https://link.aps.org/doi/10.1103/RevModPhys.74.601.
(Cit. on p. 5.).

[Wen02a] Xiao-Gang Wen. "Quantum order: a quantum entanglement of many particles". In: *Physics Letters A* 300.2 (2002), pp. 175–181.
(Cit. on p. 1.).

[Wen02b] Xiao-Gang Wen. "Quantum orders and symmetric spin liquids". In: *Physical Review B* 65.16 (2002), p. 165113.
(Cit. on p. 1.).

[Ber+03] C Bergemann et al. "Quasi-two-dimensional Fermi liquid properties of the unconventional superconductor Sr_2RuO_4". In: *advances in Physics* 52.7 (2003), pp. 639–725.
(Cit. on p. 179.).

[BAG03] S Biermann, F Aryasetiawan, and A Georges. "First-Principles Approach to the Electronic Structure of Strongly Correlated Systems: Combining the G W Approximation and Dynamical Mean-Field Theory". In: *Physical review letters* 90.8 (2003), p. 086402.
(Cit. on p. 5.).

[BBD03] Benedikt Binz, Dionys Baeriswyl, and Benoıt Douçot. "Weakly interacting electrons and the renormalization group". In: *Annalen der Physik* 12.11-12 (2003), pp. 704–736.
(Cit. on pp. 125, 133.).

[Win03] Roland Winkler. "Origin of Spin–Orbit Coupling Effects". In: *Spin–Orbit Coupling Effects in Two-Dimensional Electron and Hole Systems* (2003), pp. 61–68.
(Cit. on pp. 45, 49, 55, 195.).

[Hed+04] R Hedden et al. "A functional renormalization group approach to zero-dimensional interacting systems". In: *Journal of Physics: Condensed Matter* 16.29 (2004), p. 5279. URL: http://stacks.iop.org/0953-8984/16/i=29/a=019.
(Cit. on p. 148.).

[Kat04] A. A. Katanin. "Fulfillment of Ward identities in the functional renormalization group approach". In: *Phys. Rev. B* 70 (11 Sept. 2004), p. 115109. DOI: 10.1103/PhysRevB.70.115109. URL: https://link.aps.org/doi/10.1103/PhysRevB.70.115109.
(Cit. on p. 155.).

[KV04] Gabriel Kotliar and Dieter Vollhardt. "Strongly Correlated Materials: Insights From Dynamical Mean-Field Theory". In: *Physics Today* 57.3 (2004), pp. 53–59. DOI: 10.1063/1.1712502. eprint: https://doi.org/10.1063/1.1712502. URL: https://doi.org/10.1063/1.1712502.
(Cit. on p. 5.).

[Lat+04] NN Lathiotakis et al. "Density functional theory for superconductors". In: *International journal of quantum chemistry* 99.5 (2004), pp. 790–797.
(Cit. on p. 5.).

[Nel+04] KD Nelson et al. "Odd-parity superconductivity in Sr2RuO4". In: *Science* 306.5699 (2004), pp. 1151–1154.
(Cit. on p. 179.).

[OH04] A Ohtomo and HY Hwang. "A high-mobility electron gas at the LaAlO3/SrTiO3 heterointerface". In: *Nature* 427.6973 (2004), pp. 423–426.
(Cit. on p. 173.).

[SZB04] KV Samokhin, ES Zijlstra, and SK Bose. "CePt 3 Si: An unconventional superconductor without inversion center". In: *Physical Review B* 69.9 (2004), p. 094514.
(Cit. on p. 92.).

[SC04] IA Sergienko and SH Curnoe. "Order parameter in superconductors with nondegenerate bands". In: *Physical Review B* 70.21 (2004), p. 214510.
(Cit. on pp. 65, 67, 91.).

[WZ04] Congjun Wu and Shou-Cheng Zhang. "Dynamic Generation of Spin-Orbit Coupling". In: *Phys. Rev. Lett.* 93 (3 July 2004), p. 036403. DOI: 10.1103/PhysRevLett.93.036403. URL: https://link.aps.org/doi/10.1103/PhysRevLett.93.036403.
(Cit. on p. 48.).

[KM05a] C. L. Kane and E. J. Mele. "Quantum Spin Hall Effect in Graphene". In: *Phys. Rev. Lett.* 95 (22 Nov. 2005), p. 226801. DOI: 10.1103/PhysRevLett.95.226801. URL: http://link.aps.org/doi/10.1103/PhysRevLett.95.226801.
(Cit. on p. 50.).

[KM05b] Charles L Kane and Eugene J Mele. "Quantum spin Hall effect in graphene". In: *Physical review letters* 95.22 (2005), p. 226801.
(Cit. on p. 45.).

[Lüd+05] M Lüders et al. "Ab initio theory of superconductivity. I. Density functional formalism and approximate functionals". In: *Physical Review B* 72.2 (2005), p. 024545.
(Cit. on p. 5.).

[Mar+05] MAL Marques et al. "Ab initio theory of superconductivity. II. Application to elemental metals". In: *Physical Review B* 72.2 (2005), p. 024546.
(Cit. on p. 5.).

[MYO05] Masahito Mochizuki, Youichi Yanase, and Masao Ogata. "Ferromagnetic Fluctuation and Possible Triplet Superconductivity in Na x CoO 2· y H 2 O: Fluctuation-Exchange Study of the Multiorbital Hubbard Model". In: *Physical review letters* 94.14 (2005), p. 147005.
(Cit. on p. 6.).

[Nov+05] Kostya S Novoselov et al. "Two-dimensional gas of massless Dirac fermions in graphene". In: *nature* 438.7065 (2005), p. 197.
(Cit. on p. 168.).

[Sch05a] Ulrich Schollwöck. "The density-matrix renormalization group". In: *Reviews of modern physics* 77.1 (2005), p. 259.
(Cit. on p. 139.).

[Sig05] Manfred Sigrist. "Review on the Chiral p-Wave Phase of Sr2RuO4". In: *Progress of Theoretical Physics Supplement* 160.Supplement 1 (2005), pp. 1–14.
(Cit. on p. 43.).

[SG05] George E Simion and Gabriele F Giuliani. "Friedel oscillations in a Fermi liquid". In: *Physical Review B* 72.4 (2005), p. 045127.
(Cit. on p. 28.).

[Spr05] Volker Springel. "The cosmological simulation code GADGET-2". In: *Monthly notices of the royal astronomical society* 364.4 (2005), pp. 1105–1134.
(Cit. on p. 5.).

[Spr+05] Volker Springel et al. "Simulations of the formation, evolution and clustering of galaxies and quasars". In: (2005).
(Cit. on p. 5.).

[ZM05] Igor Žuti ć and Igor Mazin. "Phase-Sensitive Tests of the Pairing State Symmetry in Sr_2RuO_4". In: *Phys. Rev. Lett.* 95 (21 Nov. 2005), p. 217004. DOI: 10.1103/PhysRevLett.95.217004. URL: https://link.aps.org/doi/10.1103/PhysRevLett.95.217004.
(Cit. on pp. 97, 179.).

[Zha+05] Yuanbo Zhang et al. "Experimental observation of the quantum Hall effect and Berry's phase in graphene". In: *nature* 438.7065 (2005), p. 201.
(Cit. on p. 169.).

[BHZ06] B. Andrei Bernevig, Taylor L. Hughes, and Shou-Cheng Zhang. "Quantum Spin Hall Effect and Topological Phase Transition in HgTe Quantum Wells". In: *Science* 314.5806 (2006), pp. 1757–1761. ISSN: 0036-8075. DOI: 10.1126/science.1133734. eprint: http://science.sciencemag.org/content/314/5806/1757.full.pdf. URL: http://science.sciencemag.org/content/314/5806/1757.
(Cit. on p. 48.).

[Kot+06] Gabriel Kotliar et al. "Electronic structure calculations with dynamical mean-field theory". In: *Reviews of Modern Physics* 78.3 (2006), p. 865.
(Cit. on p. 5.).

[Min+06] Hongki Min et al. "Intrinsic and Rashba spin-orbit interactions in graphene sheets". In: *Phys. Rev. B* 74 (16 Oct. 2006), p. 165310. DOI: 10.1103/PhysRevB.74.165310. URL: https://link.aps.org/doi/10.1103/PhysRevB.74.165310.
(Cit. on p. 50.).

[Rho06] Gillian Rhodes. "The evolutionary psychology of facial beauty". In: *Annu. Rev. Psychol.* 57 (2006), pp. 199–226.
(Cit. on p. 1.).

[Tym06] Dmitri Tymoczko. "The Geometry of Musical Chords". In: *Science* 313.5783 (2006), pp. 72–74. ISSN: 0036-8075. DOI: 10.1126/science.1126287. eprint: http://science.sciencemag.org/content/313/5783/72.full.pdf. URL: http://science.sciencemag.org/content/313/5783/72.
(Cit. on p. 1.).

[Xia+06] Jing Xia et al. "High resolution polar Kerr effect measurements of Sr 2 RuO 4: evidence for broken time-reversal symmetry in the superconducting state". In: *Physical review letters* 97.16 (2006), p. 167002.
(Cit. on p. 179.).

[Fab+07] Jaroslav Fabian et al. "Semiconductor spintronics". In: *arXiv preprint arXiv:0711.1461* (2007).
(Cit. on p. 60.).

[GM07] Andrey K Geim and Allan H MacDonald. "Graphene: exploring carbon flatland". In: *Physics today* 60.8 (2007).
(Cit. on p. 168.).

[Hel07a] K Held. "Electronic structure calculations using dynamical mean field theory". In: *Advances in physics* 56.6 (2007), pp. 829–926.
(Cit. on p. 5.).

[Hel07b] K. Held. "Electronic structure calculations using dynamical mean field theory". In: *Advances in Physics* 56.6 (2007), pp. 829–926. DOI: 10.1080/00018730701619647. eprint: https://doi.org/10.1080/00018730701619647. URL: https://doi.org/10.1080/00018730701619647.
(Cit. on p. 5.).

[Kir+07] JR Kirtley et al. "Upper limit on spontaneous supercurrents in Sr 2 Ru O 4". In: *Physical Review B* 76.1 (2007), p. 014526.
(Cit. on p. 179.).

[Kön+07] Markus König et al. "Quantum spin Hall insulator state in HgTe quantum wells". In: *Science* 318.5851 (2007), pp. 766–770.
(Cit. on p. 3.).

[RRM07] J. Reiss, D. Rohe, and W. Metzner. "Renormalized mean-field analysis of antiferromagnetism and *d*-wave superconductivity in the two-dimensional Hubbard model". In: *Phys. Rev. B* 75 (7 Feb. 2007), p. 075110. DOI: 10.1103/PhysRevB.75.075110. URL: http://link.aps.org/doi/10.1103/PhysRevB.75.075110.
(Cit. on p. 100.).

[Rey+07] Nicolas Reyren et al. "Superconducting interfaces between insulating oxides". In: *Science* 317.5842 (2007), pp. 1196–1199.
(Cit. on p. 173.).

[Wet07] C. Wetterich. "Bosonic effective action for interacting fermions". In: *Phys. Rev. B* 75 (8 Feb. 2007), p. 085102. DOI: 10.1103/PhysRevB.75.085102. URL: https://link.aps.org/doi/10.1103/PhysRevB.75.085102.
(Cit. on p. 69.).

[CEE08] A. V. Chubukov, D. V. Efremov, and I. Eremin. "Magnetism, superconductivity, and pairing symmetry in iron-based superconductors". In: *Phys. Rev. B* 78 (13 Oct. 2008), p. 134512. DOI: 10.1103/PhysRevB.78.134512. URL: https://link.aps.org/doi/10.1103/PhysRevB.78.134512.
(Cit. on p. 133.).

[GHM08] R Gersch, C Honerkamp, and W Metzner. "Superconductivity in the attractive Hubbard model: functional renormalization group analysis". In: *New Journal of Physics* 10.4 (2008), p. 045003. URL: http://stacks.iop.org/1367-2630/10/i=4/a=045003.
(Cit. on p. 140.).

[HKT08] Karsten Held, Andrey A Katanin, and Alessandro Toschi. "Dynamical vertex approximationan introduction". In: *Progress of Theoretical Physics Supplement* 176 (2008), pp. 117–133.
(Cit. on p. 7.).

[Kam+08] Yoichi Kamihara et al. "Iron-based layered superconductor La [O1-x F x] FeAs (x= 0.05- 0.12) with T c= 26 K". In: *Journal of the American Chemical Society* 130.11 (2008), pp. 3296–3297.
(Cit. on p. 3.).

[Kot+08] Hisashi Kotegawa et al. "Evidence for unconventional superconductivity in arsenic-free iron-based superconductor FeSe: a 77Se-NMR study". In: *Journal of the Physical Society of Japan* 77.11 (2008), pp. 113703–113703.
(Cit. on p. 3.).

[MA08] Takashi Miyake and F Aryasetiawan. "Screened Coulomb interaction in the maximally localized Wannier basis". In: *Physical Review B* 77.8 (2008), p. 085122.
(Cit. on p. 184.).

[Rag+08] S. Raghu et al. "Minimal two-band model of the superconducting iron oxypnictides". In: *Phys. Rev. B* 77 (22 June 2008), p. 220503. DOI: 10.1103/PhysRevB.77.220503. URL: https://link.aps.org/doi/10.1103/PhysRevB.77.220503.
(Cit. on p. 215.).

[Gei09] A. K. Geim. "Graphene: Status and Prospects". In: *Science* 324.5934 (2009), pp. 1530–1534. ISSN: 0036-8075. DOI: 10.1126/science.1158877. eprint: http://science.sciencemag.org/content/324/5934/1530.full.pdf. URL: http://science.sciencemag.org/content/324/5934/1530.
(Cit. on p. 168.).

[Gmi+09] M Gmitra et al. "Spin-orbit fields in ferromagnetic metal/semiconductor junctions". In: *arXiv preprint arXiv:0907.4149* (2009).
(Cit. on pp. 54, 59.).

[Gra+09] S Graser et al. "Near-degeneracy of several pairing channels in multiorbital models for the Fe pnictides". In: *New Journal of Physics* 11.2, 025016 (Feb. 2009), p. 025016. DOI: 10.1088/1367-2630/11/2/025016. arXiv: 0812.0343 [cond-mat.supr-con].
(Cit. on pp. 137, 197.).

[HS09] C. Husemann and M. Salmhofer. "Efficient parametrization of the vertex function, Ω scheme, and the t, t' Hubbard model at van Hove filling". In: *Phys. Rev. B* 79 (19 May 2009), p. 195125. DOI: 10.1103/PhysRevB.79.195125. URL: https://link.aps.org/doi/10.1103/PhysRevB.79.195125.
(Cit. on p. 142.).

[Qi+09] Xiao-Liang Qi et al. "Time-reversal-invariant topological superconductors and superfluids in two and three dimensions". In: *Physical review letters* 102.18 (2009), p. 187001.
(Cit. on pp. 3, 4.).

[Sam09] KV Samokhin. "Spin–orbit coupling and semiclassical electron dynamics in noncentrosymmetric metals". In: *Annals of Physics* 324.11 (2009), pp. 2385–2407.
(Cit. on pp. 50, 51, 58.).

[SF09] Masatoshi Sato and Satoshi Fujimoto. "Topological phases of noncentrosymmetric superconductors: Edge states, Majorana fermions, and non-Abelian statistics". In: *Physical Review B* 79.9 (2009), p. 094504.
(Cit. on p. 176.).

[Voj09] Matthias Vojta. "Lattice symmetry breaking in cuprate superconductors: stripes, nematics, and superconductivity". In: *Advances in Physics* 58.6 (2009), pp. 699–820.
(Cit. on p. 101.).

[Yad+09] Keiji Yada et al. "Electrically controlled superconducting states at the heterointerface SrTiO 3/LaAlO 3". In: *Physical Review B* 80.14 (2009), p. 140509.
(Cit. on p. 173.).

[Che+10] Meng Cheng et al. "Stable topological superconductivity in a family of two-dimensional fermion models". In: *Phys. Rev. B* 81 (2 Jan. 2010), p. 024504. DOI: 10.1103/PhysRevB.81.024504. URL: https://link.aps.org/doi/10.1103/PhysRevB.81.024504.
(Cit. on p. 220.).

[EM10] Andreas Eberlein and Walter Metzner. "Parametrization of Nambu Vertex in a Singlet Superconductor". In: *Progress of Theoretical Physics* 124.3 (2010), pp. 471–491. DOI: 10.1143/PTP.124.471. eprint: /oup/backfile/content_public/journal/ptp/124/3/10.1143/ptp.124.471/2/124-3-471.pdf. URL: http://dx.doi.org/10.1143/PTP.124.471.
(Cit. on p. 70.).

[GC10] David Garcia-Aldea and Sudip Chakravarty. "Singlet versus triplet particle-hole condensates in quantum oscillations in cuprates". In: *Phys. Rev. B* 82 (18 Nov. 2010), p. 184526. DOI: 10.1103/PhysRevB.82.184526. URL: https://link.aps.org/doi/10.1103/PhysRevB.82.184526.
(Cit. on pp. 43, 101.).

[Gra+10] S. Graser et al. "Spin fluctuations and superconductivity in a three-dimensional tight-binding model for $BaFe_2As_2$". In: *Phys. Rev. B* 81 (21 June 2010), p. 214503. DOI: 10.1103/PhysRevB.81.214503. URL: https://link.aps.org/doi/10.1103/PhysRevB.81.214503.
(Cit. on pp. 6, 137, 197.).

[HK10] M Zahid Hasan and Charles L Kane. "Colloquium: topological insulators". In: *Reviews of Modern Physics* 82.4 (2010), p. 3045.
(Cit. on p. 65.).

[KGF10] Sergej Konschuh, Martin Gmitra, and Jaroslav Fabian. "Tight-binding theory of the spin-orbit coupling in graphene". In: *Physical Review B* 82.24 (2010), p. 245412.
(Cit. on p. 203.).

[MC10] Saurabh Maiti and Andrey V. Chubukov. "Renormalization group flow, competing phases, and the structure of superconducting gap in multiband models of iron-based superconductors". In: *Phys. Rev. B* 82 (21 Dec. 2010), p. 214515. DOI: 10.1103/PhysRevB.82.214515. URL: https://link.aps.org/doi/10.1103/PhysRevB.82.214515.
(Cit. on p. 7.).

[MS10b] Jochen Mannhart and DG Schlom. "Oxide interfaces—an opportunity for electronics". In: *Science* 327.5973 (2010), pp. 1607–1611.
(Cit. on p. 173.).

[Maz10] Igor I Mazin. "Superconductivity gets an iron boost". In: *Nature* 464.7286 (2010), p. 183.
(Cit. on p. 218.).

[QHZ10] Xiao-Liang Qi, Taylor L Hughes, and Shou-Cheng Zhang. "Topological invariants for the Fermi surface of a time-reversal-invariant superconductor". In: *Physical Review B* 81.13 (2010), p. 134508.
(Cit. on p. 176.).

[QZ10] Xiao-Liang Qi and Shou-Cheng Zhang. "The quantum spin Hall effect and topological insulators". In: *arXiv preprint arXiv:1001.1602* (2010).
(Cit. on pp. 48, 49.).

[RKK10a] S. Raghu, A. Kapitulnik, and S. A. Kivelson. "Hidden Quasi-One-Dimensional Superconductivity in Sr_2RuO_4". In: *Phys. Rev. Lett.* 105 (13 Sept. 2010), p. 136401. DOI: 10.1103/PhysRevLett.105.136401. URL: http://link.aps.org/doi/10.1103/PhysRevLett.105.136401.
(Cit. on p. 180.).

[RKK10b] S Raghu, A Kapitulnik, and SA Kivelson. "Hidden quasi-one-dimensional superconductivity in Sr_2RuO_4". In: *Physical review letters* 105.13 (2010), p. 136401.
(Cit. on p. 122.).

[RKS10] S Raghu, SA Kivelson, and DJ Scalapino. "Superconductivity in the repulsive Hubbard model: An asymptotically exact weak-coupling solution". In: *Physical Review B* 81.22 (2010), p. 224505.
(Cit. on pp. 6, 122, 131, 134, 135.).

[RW10] Johannes Reuther and Peter Wölfle. "J 1- J 2 frustrated two-dimensional Heisenberg model: Random phase approximation and functional renormalization group". In: *Physical Review B* 81.14 (2010), p. 144410.
(Cit. on p. 10.).

[San10] Conrad Sanderson. "Armadillo: An open source C++ linear algebra library for fast prototyping and computationally intensive experiments". In: (2010).
(Cit. on p. 66.).

[Sch10] J. Schmalian. "Failed Theories of Superconductivity". In: *Modern Physics Letters B* 24 (2010), pp. 2679–2691. DOI: 10.1142/S0217984910025280. arXiv: 1008.0447.
(Cit. on p. 13.).

[WZ10] R Winkler and U Zülicke. "Invariant expansion for the trigonal band structure of graphene". In: *Physical Review B* 82.24 (2010), p. 245313.
(Cit. on p. 49.).

[XCN10a] Di Xiao, Ming-Che Chang, and Qian Niu. "Berry phase effects on electronic properties". In: *Reviews of modern physics* 82.3 (2010), p. 1959.
(Cit. on p. 169.).

[XCN10b] Di Xiao, Ming-Che Chang, and Qian Niu. "Berry phase effects on electronic properties". In: *Rev. Mod. Phys.* 82 (3 July 2010), pp. 1959–2007. DOI: 10.1103/RevModPhys.82.1959. URL: https://link.aps.org/doi/10.1103/RevModPhys.82.1959.
(Cit. on p. 214.).

[AK11] AS Alexandrov and VV Kabanov. "Unconventional high-temperature superconductivity from repulsive interactions: Theoretical constraints". In: *Physical review letters* 106.13 (2011), p. 136403.
(Cit. on p. 133.).

[HKM11] P J Hirschfeld, M M Korshunov, and I I Mazin. "Gap symmetry and structure of Fe-based superconductors". In: *Reports on Progress in Physics* 74.12 (2011), p. 124508. URL: http://stacks.iop.org/0034-4885/74/i=12/a=124508.
(Cit. on p. 137.).

[Li+11] Lu Li et al. "Coexistence of magnetic order and two-dimensional superconductivity at LaAlO3/SrTiO3 interfaces". In: *Nature physics* 7.10 (2011), pp. 762–766.
(Cit. on p. 173.).

[LJY11] Cheng-Cheng Liu, Hua Jiang, and Yugui Yao. "Low-energy effective Hamiltonian involving spin-orbit coupling in silicene and two-dimensional germanium and tin". In: *Physical Review B* 84.19 (2011), p. 195430.
(Cit. on p. 45.).

[Mai+11a] T. A. Maier et al. "*d*-wave pairing from spin fluctuations in the $K_xFe_{2-y}Se_2$ superconductors". In: *Phys. Rev. B* 83 (10 Mar. 2011), p. 100515. DOI: 10.1103/PhysRevB.83.100515. URL: http://link.aps.org/doi/10.1103/PhysRevB.83.100515.
(Cit. on p. 137.).

[Mai+11b] TA Maier et al. "d-wave pairing from spin fluctuations in the K x Fe 2- y Se 2 superconductors". In: *Physical Review B* 83.10 (2011), p. 100515.
(Cit. on pp. 6, 137.).

[MM11] Paolo Marconcini and Massimo Macucci. "The kp method and its application to graphene, carbon nanotubes and graphene nanoribbons: the Dirac equation". In: *arXiv preprint arXiv:1105.1351* (2011).
(Cit. on p. 49.).

[Mih11] B. Mihaila. "Lindhard function of a d-dimensional Fermi gas". In: *ArXiv e-prints* (Nov. 2011). arXiv: 1111.5337 [cond-mat.quant-gas].
(Cit. on p. 27.).

[Mra+11] Jernej Mravlje et al. "Coherence-Incoherence Crossover and the Mass-Renormalization Puzzles in Sr_2RuO_4". In: *Phys. Rev. Lett.* 106 (9 Mar. 2011), p. 096401. DOI: 10.1103/PhysRevLett.106.096401. URL: http://link.aps.org/doi/10.1103/PhysRevLett.106.096401.
(Cit. on pp. 182, 184, 185.).

[PM11] Cheol-Hwan Park and Nicola Marzari. "Berry phase and pseudospin winding number in bilayer graphene". In: *Physical Review B* 84.20 (2011), p. 205440.
(Cit. on p. 169.).

[RK11] S Raghu and SA Kivelson. "Superconductivity from repulsive interactions in the two-dimensional electron gas". In: *Physical Review B* 83.9 (2011), p. 094518.
(Cit. on p. 122.).

[RT11] Johannes Reuther and Ronny Thomale. "Functional renormalization group for the anisotropic triangular antiferromagnet". In: *Physical Review B* 83.2 (2011), p. 024402.
(Cit. on p. 10.).

[Sam11] Kirill V. Samokhin. "Unconventional Superconductivity in a Nutshell". In: *La Physique Au Canada* 67.2 (Juin 2011). URL: http://www.physics.brocku.ca/Courses/5P73/PiC67.pdf.
(Cit. on p. 36.).

[San+11] AF Santander-Syro et al. "Two-dimensional electron gas with universal subbands at the surface of SrTiO3". In: *Nature* 469.7329 (2011), pp. 189–193.
(Cit. on p. 173.).

[SR11] Andreas P Schnyder and Shinsei Ryu. "Topological phases and surface flat bands in superconductors without inversion symmetry". In: *Physical Review B* 84.6 (2011), p. 060504.
(Cit. on p. 177.).

[Tho+11a] Ronny Thomale et al. "Exotic d-wave superconducting state of strongly hole-doped K x Ba 1- x Fe 2 As 2". In: *Physical review letters* 107.11 (2011), p. 117001.
(Cit. on p. 218.).

[Tho+11b] Ronny Thomale et al. "Mechanism for explaining differences in the order parameters of FeAs-based and FeP-based pnictide superconductors". In: *Physical review letters* 106.18 (2011), p. 187003.
(Cit. on p. 218.).

[VW11] Oskar Vafek and Luyang Wang. "Spin-orbit coupling induced enhancement of superconductivity in a two-dimensional repulsive gas of fermions". In: *Physical Review B* 84.17 (2011), p. 172501.
(Cit. on p. 122.).

[Zub+11] Pavlo Zubko et al. "Interface physics in complex oxide heterostructures". In: *Annu. Rev. Condens. Matter Phys.* 2.1 (2011), pp. 141–165.
(Cit. on p. 173.).

[Chu12] Andrey Chubukov. "Pairing mechanism in Fe-based superconductors". In: *Annu. Rev. Condens. Matter Phys.* 3.1 (2012), pp. 57–92.
(Cit. on p. 133.).

[GMM12] Antoine Georges, Luca de' Medici, and Jernej Mravlje. "Strong electronic correlations from Hund's coupling". In: *arXiv preprint arXiv:1207.3033* (2012).
(Cit. on pp. 183, 225.).

[Kie+12] Maximilian L Kiesel et al. "Competing many-body instabilities and unconventional superconductivity in graphene". In: *Physical Review B* 86.2 (2012), p. 020507.
(Cit. on p. 171.).

[MH12] Stefan A Maier and Carsten Honerkamp. "Renormalization group flow for fermions into antiferromagnetically ordered phases: Method and mean-field models". In: *Physical Review B* 86.13 (2012), p. 134404.
(Cit. on p. 73.).

[Mar+12] Nicola Marzari et al. "Maximally localized Wannier functions: Theory and applications". In: *Rev. Mod. Phys.* 84 (4 Oct. 2012), pp. 1419–1475. DOI: 10.1103/RevModPhys.84.1419. URL: https://link.aps.org/doi/10.1103/RevModPhys.84.1419.
(Cit. on p. 213.).

[Met+12a] W. Metzner et al. "Functional renormalization group approach to correlated fermion systems". In: *Reviews of Modern Physics* 84 (Jan. 2012), pp. 299–352. DOI: 10.1103/RevModPhys.84.299. arXiv: 1105.5289 [cond-mat.str-el].
(Cit. on pp. 113, 155.).

[Met+12b] Walter Metzner et al. "Functional renormalization group approach to correlated fermion systems". In: *Rev. Mod. Phys.* 84 (1 Mar. 2012), pp. 299–352. DOI: 10.1103/RevModPhys.84.299. URL: http://link.aps.org/doi/10.1103/RevModPhys.84.299.
(Cit. on pp. 114, 144, 148, 153, 157.).

[NC12] Rahul Nandkishore and Andrey V Chubukov. "Interplay of superconductivity and spin-density-wave order in doped graphene". In: *Physical Review B* 86.11 (2012), p. 115426.
(Cit. on p. 171.).

[NLC12] Rahul Nandkishore, LS Levitov, and AV Chubukov. "Chiral superconductivity from repulsive interactions in doped graphene". In: *Nature Physics* 8.2 (2012), p. 158.
(Cit. on p. 171.).

[PK12] Christoph M Puetter and Hae-Young Kee. "Identifying spin-triplet pairing in spin-orbit coupled multi-band superconductors". In: *EPL (Europhysics Letters)* 98.2 (2012), p. 27010.
(Cit. on p. 181.).

[Rag+12] Srinivas Raghu et al. "Effects of longer-range interactions on unconventional superconductivity". In: *Physical Review B* 85.2 (2012), p. 024516.
(Cit. on pp. 122, 133, 167.).

[SBT12] Andreas P Schnyder, PMR Brydon, and Carsten Timm. "Types of topological surface states in nodal noncentrosymmetric superconductors". In: *Physical Review B* 85.2 (2012), p. 024522.
(Cit. on p. 177.).

[UH12] Stefan Uebelacker and Carsten Honerkamp. "Self-energy feedback and frequency-dependent interactions in the functional renormalization group flow for the two-dimensional Hubbard model". In: *Phys. Rev. B* 86 (23 Dec. 2012), p. 235140. DOI: 10.1103/PhysRevB.86.235140. URL: https://link.aps.org/doi/10.1103/PhysRevB.86.235140.
(Cit. on p. 153.).

[VJB12] Loïg Vaugier, Hong Jiang, and Silke Biermann. "Hubbard *U* and Hund exchange *J* in transition metal oxides: Screening versus localization trends from constrained random phase approximation". In: *Phys. Rev. B* 86 (16 Oct. 2012), p. 165105. DOI: 10.1103/PhysRevB.86.165105. URL: http://link.aps.org/doi/10.1103/PhysRevB.86.165105.
(Cit. on pp. 184, 185.).

[Vol12] D. Vollhardt. "Dynamical mean-field theory for correlated electrons". In: *Annalen der Physik* 524.1 (2012), pp. 1–19. ISSN: 1521-3889. DOI: 10.1002/andp.201100250. URL: http://dx.doi.org/10.1002/andp.201100250.
(Cit. on p. 193.).

[Zab+12] V. B. Zabolotnyy et al. "Effective tight-binding model for renormalized band structure of Sr_2RuO_4". In: *ArXiv e-prints* (Dec. 2012). arXiv: 1212.3994 [cond-mat.str-el].
(Cit. on p. 182.).

[BB13] Annica M. Black-Schaffer and Alexander V. Balatsky. "Odd-frequency superconducting pairing in multiband superconductors". In: *Phys. Rev. B* 88 (10 Sept. 2013), p. 104514. DOI: 10.1103/PhysRevB.88.104514. URL: https://link.aps.org/doi/10.1103/PhysRevB.88.104514.
(Cit. on p. 37.).

[Cho+13] Weejee Cho et al. "Band structure effects on the superconductivity in Hubbard models". In: *Physical Review B* 88.6 (2013), p. 064505.
(Cit. on pp. 122, 130.).

[Fis13] Mark H Fischer. "Gap symmetry and stability analysis in the multi-orbital Fe-based superconductors". In: *New Journal of Physics* 15.7 (2013), p. 073006. URL: http://stacks.iop.org/1367-2630/15/i=7/a=073006.
(Cit. on p. 37.).

[GBT13] Florian Geissler, Jan Carl Budich, and Björn Trauzettel. "Group theoretical and topological analysis of the quantum spin Hall effect in silicene". In: *New Journal of Physics* 15.8 (2013), p. 085030.
(Cit. on p. 49.).

[Kre+13] A. Kreisel et al. "Spin fluctuations and superconductivity in $K_xFe_{2-y}Se_2$". In: *Phys. Rev. B* 88 (9 Sept. 2013), p. 094522. DOI: 10.1103/PhysRevB.88.094522. URL: https://link.aps.org/doi/10.1103/PhysRevB.88.094522.
(Cit. on p. 137.).

[MHW13] Stefan A. Maier, Carsten Honerkamp, and Qiang-Hua Wang. "Interplay between Point-Group Symmetries and the Choice of the Bloch Basis in Multiband Models". In: *Symmetry* 5.4 (2013), pp. 313–343. ISSN: 2073-8994. DOI: 10.3390/sym5040313. URL: http://www.mdpi.com/2073-8994/5/4/313.
(Cit. on pp. 65, 67, 214, 215.).

[PHT13] C. Platt, W. Hanke, and R. Thomale. "Functional renormalization group for multi-orbital Fermi surface instabilities". In: *Advances in Physics* 62.4-6 (2013), pp. 453–562. DOI: 10.1080/00018732.2013.862020.
(Cit. on p. 157.).

[Roh+13] G. Rohringer et al. "One-particle irreducible functional approach: A route to diagrammatic extensions of the dynamical mean-field theory". In: *Phys. Rev. B* 88 (11 Sept. 2013), p. 115112. DOI: 10.1103/PhysRevB.88.115112. URL: https://link.aps.org/doi/10.1103/PhysRevB.88.115112.
(Cit. on p. 7.).

[Umm13] Giovanni AC Ummarino. "13 Eliashberg Theory". In: *Emergent Phenomena in Correlated Matter: Autumn School Organized by the Forschungszentrum Jülich and the German Research School for Simulation Sciences at Forschungszentrum Jülich 23-27 September 2013; Lecture Notes of the Autumn School Correlated Electrons 2013* 3 (2013).
(Cit. on p. 3.).

[Wan+13a] QH Wang et al. "Theory of superconductivity in a three-orbital model of Sr_2RuO_4". In: *EPL (Europhysics Letters)* 104.1 (2013), p. 17013.
(Cit. on pp. 180, 184, 185.).

[Wan+13b] Y. Wang et al. "Superconducting gap in LiFeAs from three-dimensional spin-fluctuation pairing calculations". In: *Phys. Rev. B* 88 (17 Nov. 2013), p. 174516. DOI: 10.1103/PhysRevB.88.174516. URL: https://link.aps.org/doi/10.1103/PhysRevB.88.174516.
(Cit. on p. 137.).

[ZTH13] Zhicheng Zhong, Anna Tóth, and Karsten Held. "Theory of spin-orbit coupling at LaAlO 3/SrTiO 3 interfaces and SrTiO 3 surfaces". In: *Physical Review B* 87.16 (2013), p. 161102.
(Cit. on p. 174.).

[Cur+14] PJ Curran et al. "Search for spontaneous edge currents and vortex imaging in Sr 2 Ru O 4 mesostructures". In: *Physical Review B* 89.14 (2014), p. 144504.
(Cit. on p. 179.).

[Ebe14] Andreas Eberlein. "Functional renormalization group study of fluctuation effects in fermionic superfluids". In: *arXiv preprint arXiv:1407.7661* (2014).
(Cit. on pp. 69, 71.).

[Hel14] Karsten Held. "Dynamical Vertex Approximation". In: *arXiv preprint arXiv:1411.5191* (2014).
(Cit. on p. 7.).

[Kin+14] PDC King et al. "Quasiparticle dynamics and spin–orbital texture of the SrTiO3 two-dimensional electron gas". In: *Nature communications* 5 (2014).
(Cit. on p. 174.).

[MEH14] Stefan A Maier, Andreas Eberlein, and Carsten Honerkamp. "Functional renormalization group for commensurate antiferromagnets: Beyond the mean-field picture". In: *Physical Review B* 90.3 (2014), p. 035140.
(Cit. on p. 73.).

[SRS14] Thomas Scaffidi, Jesper C Romers, and Steven H Simon. "Pairing symmetry and dominant band in Sr 2 RuO 4". In: *Physical Review B* 89.22 (2014), p. 220510.
(Cit. on pp. 122, 180.).

[Tar+14] C. Taranto et al. "From Infinite to Two Dimensions through the Functional Renormalization Group". In: *Phys. Rev. Lett.* 112 (19 May 2014), p. 196402. DOI: 10.1103/PhysRevLett.112.196402. URL: https://link.aps.org/doi/10.1103/PhysRevLett.112.196402.
(Cit. on p. 7.).

[Vee+14] C. N. Veenstra et al. "Spin-Orbital Entanglement and the Breakdown of Singlets and Triplets in Sr_2RuO_4 Revealed by Spin- and Angle-Resolved Photoemission Spectroscopy". In: *Phys. Rev. Lett.* 112 (12 Mar. 2014), p. 127002. DOI: 10.1103/PhysRevLett.112.127002. URL: https://link.aps.org/doi/10.1103/PhysRevLett.112.127002.
(Cit. on p. 179.).

[WV14] Luyang Wang and Oskar Vafek. "Unconventional superconductivity in a two-dimensional repulsive gas of fermions with spin–orbit coupling". In: *Physica C: Superconductivity and its Applications* 497 (2014), pp. 6–18.
(Cit. on pp. 122, 126.).

[Yin+14] T. Ying et al. "Determinant quantum Monte Carlo study of *d*-wave pairing in the plaquette Hubbard hamiltonian". In: *Phys. Rev. B* 90 (7 Aug. 2014), p. 075121. DOI: 10.1103/PhysRevB.90.075121. URL: https://link.aps.org/doi/10.1103/PhysRevB.90.075121.
(Cit. on p. 6.).

[Yip14] Sungkit Yip. "Noncentrosymmetric superconductors". In: *Annu. Rev. Condens. Matter Phys.* 5.2 (2014), pp. 15–33.
(Cit. on p. 86.).

[ZLW14] Gu-Feng Zhang, Yi Li, and Congjun Wu. "Honeycomb lattice with multiorbital structure: Topological and quantum anomalous Hall insulators with large gaps". In: *Phys. Rev. B* 90 (7 Aug. 2014), p. 075114. DOI: 10.1103/PhysRevB.90.075114. URL: https://link.aps.org/doi/10.1103/PhysRevB.90.075114.
(Cit. on pp. 45, 49.).

[Chr+15] Morten H. Christensen et al. "Spin reorientation driven by the interplay between spin-orbit coupling and Hund's rule coupling in iron pnictides". In: *Phys. Rev. B* 92 (21 Dec. 2015), p. 214509. DOI: 10.1103/PhysRevB.92.214509. URL: https://link.aps.org/doi/10.1103/PhysRevB.92.

214509.
(Cit. on p. 202.).

[Fu15] Liang Fu. "Parity-breaking phases of spin-orbit-coupled metals with gyrotropic, ferroelectric, and multipolar orders". In: *Physical review letters* 115.2 (2015), p. 026401.
(Cit. on p. 67.).

[KF15] Vladyslav Kozii and Liang Fu. "Odd-parity superconductivity in the vicinity of inversion symmetry breaking in spin-orbit-coupled systems". In: *Physical review letters* 115.20 (2015), p. 207002.
(Cit. on p. 67.).

[LeB+15] J. P. F. LeBlanc et al. "Solutions of the Two-Dimensional Hubbard Model: Benchmarks and Results from a Wide Range of Numerical Algorithms". In: *Phys. Rev. X* 5 (4 Dec. 2015), p. 041041. DOI: 10.1103/PhysRevX.5.041041. URL: https://link.aps.org/doi/10.1103/PhysRevX.5.041041.
(Cit. on p. 165.).

[Sam15] KV Samokhin. "Symmetry and topology of two-dimensional noncentrosymmetric superconductors". In: *Physical Review B* 92.17 (2015), p. 174517.
(Cit. on p. 176.).

[SS15] Mathias S Scheurer and Jörg Schmalian. "Topological superconductivity and unconventional pairing in oxide interfaces". In: *Nature communications* 6 (2015).
(Cit. on p. 173.).

[Alt+16] Michaela Altmeyer et al. "Role of vertex corrections in the matrix formulation of the random phase approximation for the multiorbital Hubbard model". In: *Physical Review B* 94.21 (2016), p. 214515.
(Cit. on p. 137.).

[Ebe+16] Andreas Eberlein et al. "Fermi Surface Reconstruction and Drop in the Hall Number due to Spiral Antiferromagnetism in High-T_c Cuprates". In: *Phys. Rev. Lett.* 117 (18 Oct. 2016), p. 187001. DOI: 10.1103/PhysRevLett.117.187001. URL: https://link.aps.org/doi/10.1103/PhysRevLett.117.187001.
(Cit. on p. 100.).

[Hir16] Peter J Hirschfeld. "Using gap symmetry and structure to reveal the pairing mechanism in Fe-based superconductors". In: *Comptes Rendus Physique* 17.1 (2016), pp. 197–231.
(Cit. on p. 37.).

[Sch+16] G. A. H. Schober et al. "Functional renormalization and mean-field approach to multiband systems with spin-orbit coupling: Application to the Rashba model with attractive interaction". In: *Phys. Rev. B* 93 (11 Mar. 2016), p. 115111. DOI: 10.1103/PhysRevB.93.115111. URL: https://

link.aps.org/doi/10.1103/PhysRevB.93.115111.
(Cit. on p. 155.).

[Cla+17] Laura Classen et al. "Interplay between Magnetism, Superconductivity, and Orbital Order in 5-Pocket Model for Iron-Based Superconductors: Parquet Renormalization Group Study". In: *Phys. Rev. Lett.* 118 (3 Jan. 2017), p. 037001. DOI: 10.1103/PhysRevLett.118.037001. URL: https://link.aps.org/doi/10.1103/PhysRevLett.118.037001.
(Cit. on p. 7.).

[FS17] Peter Fulde and Hermann Stoll. "Dealing with the exponential wall in electronic structure calculations". In: *The Journal of Chemical Physics* 146.19 (2017), p. 194107. DOI: 10.1063/1.4983207. eprint: https://doi.org/10.1063/1.4983207. URL: https://doi.org/10.1063/1.4983207.
(Cit. on p. 5.).

[Has+17] Elena Hassinger et al. "Vertical Line Nodes in the Superconducting Gap Structure of Sr 2 RuO 4". In: *Physical Review X* 7.1 (2017), p. 011032.
(Cit. on p. 179.).

[KIF17] Denis Kochan, Susanne Irmer, and Jaroslav Fabian. "Model spin-orbit coupling Hamiltonians for graphene systems". In: *Physical Review B* 95.16 (2017), p. 165415.
(Cit. on p. 49.).

[Kor17] M. M. Korshunov. "Itinerant spin fluctuations in iron-based superconductors". In: *ArXiv e-prints* (Oct. 2017). arXiv: 1710.09888 [cond-mat.supr-con].
(Cit. on pp. 6, 137.).

[LB17] J. Linder and A. V. Balatsky. "Odd-frequency superconductivity". In: *ArXiv e-prints* (Sept. 2017). arXiv: 1709.03986 [cond-mat.supr-con].
(Cit. on p. 37.).

[Mac+17] Andrew P Mackenzie et al. "Even odder after twenty-three years: the superconducting order parameter puzzle of Sr 2 RuO 4". In: *npj Quantum Materials* 2.1 (2017), p. 40.
(Cit. on p. 179.).

[Nis+17] Kazutaka Nishiguchi et al. "Random phase approximation for superconducting states in multi-orbital Hubbard models with spin-orbit coupling". In: *Journal of Physics: Conference Series* 807.5 (2017), p. 052013. URL: http://stacks.iop.org/1742-6596/807/i=5/a=052013.
(Cit. on pp. 6, 137.).

[Sch+17] G. A. H. Schober et al. "Truncated unity functional renormalization group for multiband systems with spin-orbit coupling". In: *ArXiv e-prints* (Oct. 2017). arXiv: 1710.08830 [cond-mat.str-el].
(Cit. on p. 155.).

[Smi+17a] M Smidman et al. "Superconductivity and spin–orbit coupling in non-centrosymmetric materials: a review". In: *Reports on Progress in Physics* 80.3 (2017), p. 036501.
(Cit. on pp. 54, 86, 176.).

[Smi+17b] M Smidman et al. "Superconductivity and spin–orbit coupling in non-centrosymmetric materials: a review". In: *Reports on Progress in Physics* 80.3 (2017), p. 036501. URL: http://stacks.iop.org/0034-4885/80/i=3/a=036501.
(Cit. on p. 92.).

[Spr+17] Peter O Sprau et al. "Discovery of orbital-selective Cooper pairing in FeSe". In: *Science* 357.6346 (2017), pp. 75–80.
(Cit. on p. 3.).

[Xin+17] Rui-Qi Xing et al. "Competing instabilities, orbital ordering, and splitting of band degeneracies from a parquet renormalization group analysis of a four-pocket model for iron-based superconductors: Application to FeSe". In: *Phys. Rev. B* 95 (8 Feb. 2017), p. 085108. DOI: 10.1103/PhysRevB.95.085108. URL: https://link.aps.org/doi/10.1103/PhysRevB.95.085108.
(Cit. on p. 7.).

[Zha+17] L.-D. Zhang et al. "Superconducting pairing in Sr_2RuO_4 from weak to intermediate coupling". In: *ArXiv e-prints* (Sept. 2017). arXiv: 1710.00010 [cond-mat.supr-con].
(Cit. on p. 137.).

[Est+18] I. Esterlis et al. "Breakdown of the Migdal-Eliashberg theory: A determinant quantum Monte Carlo study". In: *Phys. Rev. B* 97 (14 Apr. 2018), p. 140501. DOI: 10.1103/PhysRevB.97.140501. URL: https://link.aps.org/doi/10.1103/PhysRevB.97.140501.
(Cit. on p. 6.).

[HY18] W. Huang and H. Yao. "Possible three-dimensional nematic odd-parity superconductivity in Sr_2RuO_4". In: *ArXiv e-prints* (Mar. 2018). arXiv: 1803.00371 [cond-mat.supr-con].
(Cit. on p. 97.).

[Kit+18] Motoharu Kitatani et al. "Why Tc is so low in high-Tc cuprates: importance of the dynamical vertex structure". In: *ArXiv e-prints* (Jan. 2018). arXiv: 1801.05991 [cond-mat.supr-con].
(Cit. on p. 7.).

[Mar+18] Antimo Marrazzo et al. "Prediction of a Large-Gap and Switchable Kane-Mele Quantum Spin Hall Insulator". In: *Phys. Rev. Lett.* 120 (11 Mar. 2018), p. 117701. DOI: 10.1103/PhysRevLett.120.117701. URL: https://link.aps.org/doi/10.1103/PhysRevLett.120.117701.
(Cit. on p. 45.).

Lecture Notes and Conference proceedings

[Dir28] Paul AM Dirac. "The quantum theory of the electron". In: *Proceedings of the Royal Society of London A: Mathematical, Physical and Engineering Sciences*. Vol. 117. 778. The Royal Society. 1928, pp. 610–624.
(Cit. on p. 45.).

[LL35] Fritz London and Heinz London. "The electromagnetic equations of the supraconductor". In: *Proceedings of the Royal Society of London A: Mathematical, Physical and Engineering Sciences*. Vol. 149. 866. The Royal Society. 1935, pp. 71–88.
(Cit. on p. 13.).

[Blo62] E.I. Blount. "Formalisms of Band Theory". In: ed. by Frederick Seitz and David Turnbull. Vol. 13. Solid State Physics. Academic Press, 1962, pp. 305–373. DOI: https://doi.org/10.1016/S0081-1947(08)60459-2. URL: http://www.sciencedirect.com/science/article/pii/S0081194708604592.
(Cit. on p. 213.).

[Pau65] Wolfgang Pauli. "Continuous groups in quantum mechanics". In: *Springer Tracts in Modern Physics, Volume 37*. Springer, 1965, pp. 85–104.
(Cit. on p. 193.).

[Pau88] Wolfgang Pauli. "Zur quantenmechanik des magnetischen elektrons". In: *Wolfgang Pauli*. Springer, 1988, pp. 282–305.
(Cit. on p. 36.).

[And+90] Edward Anderson et al. "LAPACK: A portable linear algebra library for high-performance computers". In: *Proceedings of the 1990 ACM/IEEE conference on Supercomputing*. IEEE Computer Society Press. 1990, pp. 2–11.
(Cit. on p. 66.).

[Geo04] A. Georges. "Strongly Correlated Electron Materials: Dynamical Mean-Field Theory and Electronic Structure". In: *American Institute of Physics Conference Series*. Ed. by A. Avella and F. Mancini. Vol. 715. American Institute of Physics Conference Series. Aug. 2004, pp. 3–74. DOI: 10.1063/1.1800733. eprint: cond-mat/0403123.
(Cit. on p. 5.).

[SAM05] Manfred Sigrist, Adolfo Avella, and Ferdinando Mancini. "Introduction to unconventional superconductivity". In: *AIP Conference Proceedings*. Vol. 789. 1. AIP. 2005, pp. 165–243.
(Cit. on pp. 34, 42, 88.).

[SAM09] Manfred Sigrist, Adolfo Avella, and Ferdinando Mancini. "Introduction to unconventional superconductivity in non-centrosymmetric metals". In: *AIP Conference Proceedings*. Vol. 1162. 1. AIP. 2009, pp. 55–96.
(Cit. on pp. 38, 58, 92.).

[MC13] Saurabh Maiti and Andrey V Chubukov. "Superconductivity from repulsive interaction". In: *AIP Conference Proceedings*. Vol. 1550. 1. AIP. 2013, pp. 3–73.
(Cit. on p. 133.).

[Str14] William O. Straub. "An elementary primer on Gaussian integrals". Pasadena, California 91104, 2014. URL: http://vixra.org/pdf/1404.0026v1.pdf.
(Cit. on p. 115.).

[Tim12] Carsten Timm. "Theory of Superconductivity". TU Dresden, 2011/2012. URL: https://www.physik.tu-dresden.de/~timm/personal/teaching/thsup_w11/Theory_of_Superconductivity.pdf.
(Cit. on p. 21.).

[Wip09] Andreas Wipf. "Path Integrals. Berezin integral". 5. Auflage. FS-Universität Jena, WS 2008,2009. URL: http://www.tpi.uni-jena.de/qfphysics/homepage/wipf/lectures/pfad/pfad10.pdf.
(Cit. on p. 116.).

Theses

[Gal05] Calin Galeriu. "k· p Theory of semiconductor nanostructures". PhD thesis. 2005.
(Cit. on p. 48.).

[Kon11] Sergej Konschuh. "Spin-orbit coupling effects: from graphene to graphite". PhD thesis. 2011.
(Cit. on p. 203.).

[MH14] Stefan Maier and Carsten Honerkamp. "Functional Renormalization-Group Approaches to Multiband Models and Antiferromagnetically Ordered Phases". PhD thesis. Hochschulbibliothek der Rheinisch-Westfälischen Technischen Hochschule Aachen, 2014.
(Cit. on p. 73.).

[Sca16] Thomas Scaffidi. "Unconventional superconductivity in strontium ruthenate". PhD thesis. University of Oxford, 2016.
(Cit. on p. 122.).

Online

[GJ+10] Gaël Guennebaud, Benoît Jacob, et al. *Eigen v3*. 2010.
(Cit. on p. 66.).

[Fra] FraSchelle. *Superconducting gap, temperature dependence: how to calculate this integral?* URL: https://physics.stackexchange.com/questions/54200/superconducting-gap-temperature-dependence-how-to-calculate-this-integral/65444#65444.
(Cit. on p. 26.).

[Gos] Jonathan Goss. *Point Group Symmetry*. URL: https://www.staff.ncl.ac.uk/j.p.goss/symmetry/D4h_lvm.html.
(Cit. on pp. 43, 196, 205.).

[Hir] P.J. Hirschfeld. *Introduction to unconventional superconductivity*. URL: http://users.physik.fu-berlin.de/~pelster/Koenigstein/hirschfeld1.pdf.
(Cit. on p. 37.).

[Zal] Edward N. Zalta. *The Modern History of Computing*. URL: https://plato.stanford.edu/entries/computing-history/.
(Cit. on p. 5.).

Books

[Bra66] Auguste Bravais. *Etudes cristallographiques*. Gauthier-Villars, 1866.
(Cit. on p. 49.).

[Lie88] Sophus Lie. *Theorie der transformationsgruppen*. Vol. 1. , 1888.
(Cit. on p. 193.).

[CS51] Edward Uhler Condon and George Hiram Shortley. *The theory of atomic spectra*. Cambridge University Press, 1951.
(Cit. on pp. 15, 202.).

[Ber66] F.A. Berezin. *The Method of Second Quantization*. New York: Academic Press, 1966.
(Cit. on p. 115.).

[Sch68] Leonard I Schiff. *Quantum Mechanics, International series in pure and applied physics*. McGraw-Hill, 1968.
(Cit. on p. 48.).

[FW71] A.L. Fetter and J.D. Walecka. *Quantum Theory of Many-particle Systems*. Dover Books on Physics Series. Dover Publications, Incorporated, 1971. ISBN: 9780486428277. URL: http://books.google.de/books?id=0wekf1s83b0C.
(Cit. on p. 149.).

[BP74] Gennadiĭ Levikovich Bir and Grigoriĭ Ezekielevich Pikus. *Symmetry and strain-induced effects in semiconductors*. Vol. 624. Wiley New York, 1974.
(Cit. on pp. 49, 55, 195.).

[Dir81] Paul Adrien Maurice Dirac. *The principles of quantum mechanics*. 27. Oxford university press, 1981.
(Cit. on p. 45.).

[And84b] Philip Warren Anderson. *Basic notions of condensed matter physics*. Benjamin-Cummings, 1984.
(Cit. on p. 29.).

[BB86] Ronald Newbold Bracewell and Ronald N Bracewell. *The Fourier transform and its applications*. Vol. 31999. McGraw-Hill New York, 1986.
(Cit. on p. 15.).

[NO88a] J.W. Negele and H. Orland. *Quantum Many-Particle Systems*. Redwood City, 1988.
(Cit. on pp. 108, 112, 113.).

[NO88b] John W Negele and Henri Orland. *Quantum many-particle systems*. Vol. 200. Addison-Wesley New York, 1988.
(Cit. on pp. 70, 114.).

[De 89] Pierre Gilles De Gennes. *Superconductivity of metals and alloys*. Addison-Wesley, 1989.
(Cit. on p. 19.).

[Eme93] Victor J Emery. *Correlated electron systems*. Vol. 9. World Scientific, 1993.
(Cit. on p. 193.).

[GG95] J. Gilbert and L. Gilbert. *Linear Algebra and Matrix Theory*. Acad. Press, 1995. ISBN: 9780122829703. URL: `http://books.google.de/books?id=9nzjIb0uWhQC`.
(Cit. on p. 89.).

[Edm96] A.R. Edmonds. *Angular Momentum in Quantum Mechanics*. Investigations in physics. Princeton University Press, 1996. ISBN: 9780691025896. URL: `https://books.google.de/books?id=0BSOg0oHhZ0C`.
(Cit. on p. 15.).

[Tin96] Michael Tinkham. *Introduction to superconductivity*. Courier Corporation, 1996.
(Cit. on pp. 25, 26.).

[CD97] Pierre Cartier and Cecile DeWitt-Morette. *A rigorous mathematical foundation of functional integration*. Springer, 1997, pp. 1–50.
(Cit. on p. 109.).

[Bal98] L.E. Ballentine. *Quantum Mechanics: A Modern Development*. World Scientific, 1998. ISBN: 9789810241056.
(Cit. on pp. 74, 83, 193, 195.).

[Mer98] E. Merzbacher. *Quantum Mechanics*. 3rd ed. John Wiley & Sons, 1998. ISBN: 9780471887027. URL: http://books.google.de/books?id=6Ja%5C_QgAACAAJ.
(Cit. on pp. 55, 195.).

[Ste98] G.W. Stewart. *Matrix Algorithms: Volume 1, Basic Decompositions*. Matrix Algorithms. Society for Industrial and Applied Mathematics, 1998. ISBN: 9780898714142. URL: http://books.google.de/books?id=XHOQ%5C_HU-85IC.
(Cit. on pp. 89, 150.).

[Geo99] Howard Georgi. *Lie algebras in particle physics: from isospin to unified theories*. Vol. 54. Westview press, 1999.
(Cit. on p. 194.).

[Jac99] J.D. Jackson. *Classical Electrodynamics, 3rd Edition*. John Wiley & Sons, Limited, 1999.
(Cit. on p. 16.).

[MS99] Vladimir P Mineev and K Samokhin. *Introduction to unconventional superconductivity*. CRC Press, 1999.
(Cit. on p. 15.).

[Sal99] M. Salmhofer. *Renormalization:* Texts and Monographs in Physics Series. Springer, 1999. ISBN: 9783540646662. URL: http://books.google.de/books?id=nAXncL7%5C_KrQC.
(Cit. on pp. 112, 155.).

[Mey00] C.D. Meyer. *Matrix analysis and applied linear algebra. Solutions manual*. Matrix Analysis and Applied Linear Algebra. Society for Industrial and Applied Mathematics, 2000. ISBN: 9780898714548. URL: http://books.google.de/books?id=m7W2748ynMcC.
(Cit. on p. 89.).

[GPS01] Herbert Goldstein, Charles Poole, and John Safko. *Classical Mechanics*. 3rd edition. Addison Wesley, 2001. ISBN: 9780201657029.
(Cit. on p. 14.).

[Nak03] Mikio Nakahara. *Geometry, topology and physics*. CRC Press, 2003.
(Cit. on p. 70.).

[BF04] Henrik Bruus and Karsten Flensberg. *Many-body quantum theory in condensed matter physics: an introduction*. Oxford University Press, 2004.
(Cit. on p. 129.).

[Pen04] Roger Penrose. *The road to reality: A complete guide to the physical universe*. Jonathan Cape, 2004.
(Cit. on p. 5.).

[San04] G. Sansone. *Orthogonal Functions*. Dover Books on Mathematics Series. Dover Publications, 2004. ISBN: 9780486438016. URL: https://books.google.de/books?id=oC8ibpmlTrMC.
(Cit. on p. 16.).

[Wen04] Xiao-Gang Wen. *Quantum field theory of many-body systems: from the origin of sound to an origin of light and electrons*. Oxford University Press on Demand, 2004.
(Cit. on pp. 1, 2, 5.).

[AW05] George B Arfken and Hans J Weber. *Mathematical methods for physicists international student edition*. Academic press, 2005.
(Cit. on pp. 115, 202.).

[FHS05] Richard Phillips Feynman, Albert R Hibbs, and Daniel F Styer. *Quantum mechanics and path integrals*. Courier Corporation, 2005.
(Cit. on p. 109.).

[FS05] Kristian Fossheim and Asle Sudbø. *Superconductivity: physics and applications*. John Wiley & Sons, 2005.
(Cit. on p. 3.).

[GV05] Gabriele Giuliani and Giovanni Vignale. *Quantum theory of the electron liquid*. Cambridge university press, 2005.
(Cit. on p. 27.).

[Sch05b] Franz Schwabl. *Advanced quantum mechanics*. Springer Science & Business Media, 2005.
(Cit. on pp. 39, 52, 70, 209.).

[Zin05] J. Zinn-Justin. *Path Integrals in Quantum Mechanics*. Oxford graduate texts in mathematics. Oxford University Press, USA, 2005. ISBN: 9780198566748. URL: http://books.google.de/books?id=N2B0QgAACAAJ.
(Cit. on p. 115.).

[Med06] Volker Meden. *Funktionale Renormierungsgruppe*. RWTH Aachen: Lecture Notes, Mar. 2006.
(Cit. on pp. 147, 149.).

[Gel07] Murray Gell-Mann. *Beauty and truth in physics*. TED, 2007.
(Cit. on p. 1.).

[Kar07] Mehran Kardar. *Statistical physics of fields*. Cambridge University Press, 2007.
(Cit. on p. 30.).

[AHM08] Sergio Albeverio, Rafael Høegh-Krohn, and Sonia Mazzucchi. *Mathematical theory of Feynman path integrals: an introduction*. Vol. 523. Springer Science & Business Media, 2008.
(Cit. on p. 109.).

[BK08] Karl-Heinz Bennemann and John B Ketterson. *Superconductivity: Volume 1: Conventional and Unconventional Superconductors Volume 2: Novel Superconductors*. Springer Science & Business Media, 2008.
(Cit. on p. 136.).

[DDJ08] S. Dresselhaus, G. Dresselhaus, and Ado Jorio. *Group Theory: Application to the Physics of Condensed Matter*. SpringerLink: Springer e-Books. Springer, 2008. ISBN: 9783540328971. URL: `http://books.google.de/books?id=sKaH8vrfmnQC`.
(Cit. on pp. 75, 104.).

[AS10] Alexander Altland and Ben D Simons. *Condensed matter field theory*. Cambridge University Press, 2010.
(Cit. on pp. 109, 129.).

[KBS10] Peter Kopietz, Lorenz Bartosch, and Florian Schütz. *Introduction to the functional renormalization group*. Springer, 2010.
(Cit. on pp. 6, 113, 134, 140, 144, 146, 155, 157, 210.).

[MS10a] Franz Mandl and Graham Shaw. *Quantum field theory*. 2nd. The Atrium, Southern Gate, Chichester, West Sussex, PO19 8SQ, United Kingdom: John Wiley and Sons, Ltd, 2010.
(Cit. on p. 115.).

[PS10] Lorenz Bartosch Peter Kopietz and Florian Schuetz. *Introduction to the Functional Renormalization Group*. Springer-Verlag, 2010.
(Cit. on p. 113.).

[Tym10] Dmitri Tymoczko. *A geometry of music: Harmony and counterpoint in the extended common practice*. Oxford University Press, 2010.
(Cit. on p. 1.).

[Ann11] J.F. Annett. *Supraleitung, Suprafluidität und Kondensate*. Oldenbourg Wissenschaftsverlag, 2011. ISBN: 9783486705409. URL: `http://books.google.de/books?id=6n97camoL1YC`.
(Cit. on p. 1.).

[Mah11] G.D. Mahan. *Condensed Matter in a Nutshell*. In a Nutshell. Princeton University Press, 2011. ISBN: 9780691140162. URL: `http://books.google.de/books?id=v3FVOH2XK4gC`.
(Cit. on p. 49.).

[SN11] Jun John Sakurai and Jim Napolitano. *Modern quantum mechanics*. Addison-Wesley, 2011.
(Cit. on pp. 39, 52, 70, 83, 85, 201, 209.).

[AGD12] Alekseĭ Alekseevich Abrikosov, Lev Petrovich Gorkov, and Igor Ekhielevich Dzyaloshinski. *Methods of quantum field theory in statistical physics*. Courier Corporation, 2012.
(Cit. on pp. 119, 120, 125.).

[BS12] Ernst Bauer and Manfred Sigrist. *Non-centrosymmetric superconductors: introduction and overview*. Vol. 847. Springer Science & Business Media, 2012.
(Cit. on pp. 54, 57, 175.).

[Ful12] Peter Fulde. *Correlated electrons in quantum matter*. World Scientific, 2012.
(Cit. on p. 4.).

[Mat12] R.D. Mattuck. *A Guide to Feynman Diagrams in the Many-Body Problem: Second Edition*. Dover Books on Physics. Dover Publications, 2012. ISBN: 9780486131641. URL: https://books.google.de/books?id=1P%5C_DAgAAQBAJ.
(Cit. on p. 121.).

[Maz12] Guerino Mazzola. *The topos of music: geometric logic of concepts, theory, and performance*. Birkhäuser, 2012.
(Cit. on p. 1.).

[Sha12] Ramamurti Shankar. *Principles of quantum mechanics*. Springer Science & Business Media, 2012.
(Cit. on pp. 46, 48, 201.).

[Sug12] S. Sugano. *Multiplets of Transition-Metal Ions in Crystals*. Elsevier Science, 2012. ISBN: 9780323154796. URL: https://books.google.de/books?id=8SbsjFx1MbwC.
(Cit. on p. 184.).

[Wei12] Mitchel Weissbluth. *Atoms and molecules*. Elsevier, 2012.
(Cit. on p. 36.).

[Wig12] Eugene Wigner. *Group theory: and its application to the quantum mechanics of atomic spectra*. Vol. 5. Elsevier, 2012.
(Cit. on pp. 1, 39, 52, 209.).

[BH13] B Andrei Bernevig and Taylor L Hughes. *Topological insulators and topological superconductors*. Princeton University Press, 2013.
(Cit. on pp. 64, 65.).

[Tho13] David J Thouless. *The quantum mechanics of many-body systems*. Courier Corporation, 2013.
(Cit. on pp. 4, 107.).

[Fos14] Kristian Fossheim. *Superconductivity: discoveries and discoverers: ten physics Nobel laureates tell their story*. Springer Science & Business Media, 2014.
(Cit. on p. 13.).

[Col15] P. Coleman. *Introduction to Many-Body Physics*. Cambridge University Press, 2015. ISBN: 9780521864886. URL: https://books.google.de/books?id=kcrZCgAAQBAJ.
(Cit. on p. 30.).

[Kle16] Hagen Kleinert. *Particles and quantum fields*. World Scientific, 2016.
(Cit. on p. 120.).

[Sca] Thomas Scaffidi. *Weak-Coupling Theory of Topological Superconductivity*. Springer. (Cit. on p. 180.).

Index